THE PHYSICAL REVIEW

VOLUME 91 Second Series NUMBER 1

JULY 1, 1953

Published for the

AMERICAN PHYSICAL SOCIETY

by the

AMERICAN INSTITUTE OF PHYSICS

LANCASTER, PA., AND NEW YORK, N. Y.

Manuscripts

Send manuscripts to S. [illegible] Brookhaven National Laboratory, [illegible] New York.

Each article submitted [illegible] of (a) textual material, i.e., [illegible] to be set in type, and (b) [illegible] graphs from which zinc etch[illegible] cuts will be made. Textual [illegible] of an abstract, the body of [illegible] material, references, and fi[illegible] this material must be in [illegible] (except mathematical expres[illegible] with wide margins (for edi[illegible] the printer) on a durable, wh[illegible] letter size. The original co[illegible] should be submitted.

For general style, spellings, [illegible] form, recent issues of this [illegible] consulted.

The prime requisite is that [illegible] clear to the typesetter, who is [illegible] nor a mathematician.

Abstracts

An abstract must accompa[illegible] should be adequate as an in[illegible] mary. As an index, it should [illegible] major and minor, concerning w[illegible] tion is presented. As a summ[illegible] the conclusions of the article [illegible] results of general interest.

Mathematical Expressions

All but the simplest mathe[illegible] should be carefully printed in [illegible] to distinguish between capit[illegible] Indicate clearly superscripts [illegible] inverted carets and carets, [illegible] complicated superscripts and [illegible] repetition of a complicated e[illegible] quoting it by some convenient [illegible] the margin Greek letters and [illegible] Use fractional exponents in[illegible] Use the solidus (/) for fracti[illegible] will save vertical space.

References

References should appear [illegible] listed consecutively, and ar[illegible]

[1] A. B. Smith, Phys. Rev. 41, 6[illegible]

[2] H. Lamb, *Hydrodynamics* (Cam[illegible] Cambridge, England, 1960), sixth [illegible]

Tables

All but the simplest tabula[illegible] be organized in tabular form [illegible]

[illegible] possible figures should [illegible] [illegible] of a column in the [illegible] [illegible] convenient reduction [illegible] [illegible] original drawings [illegible] [illegible] the line in general should [illegible] [illegible] and the lettering and symbols [illegible] [illegible] on the original that will [illegible] [illegible] be less than about [illegible] [illegible] If the reduction is 3:1, the original [illegible] [illegible] and less than 1/8 in. high. [illegible] [illegible] of making zinc etchings [illegible] [illegible] black and white photographs [illegible] [illegible] drawings must be in [illegible] [illegible] or tracing cloth. Coordinate [illegible] [illegible] but if used must be blue [illegible] [illegible] lines which are to appear [illegible] [illegible]

[illegible] should have maximum [illegible] [illegible] to use space efficiently [illegible] [illegible] particularly at the top or [illegible] [illegible] the black or other solution [illegible] [illegible] drawing or photograph, with [illegible] [illegible] and the figure number. [illegible] [illegible] numbered consecutively and [illegible] [illegible] position indicated in the margin of the [illegible] [illegible] Figure captions should be typed [illegible] [illegible] with the manuscript (but not [illegible] [illegible]

[illegible] and oval photographs.

[illegible] that each manuscript [illegible] [illegible] and [illegible] [illegible] are unavoidable, but [illegible] [illegible] extensive alterations after the article has [illegible] [illegible] in type will be charged to the author.

[illegible] and all correspondence concerning [illegible] [illegible] of publication should be addressed to the [illegible] Publication Manager, American [illegible] [illegible], 57 East 55 Street, New York 22, New [illegible]

THE PHYSICAL REVIEW

A journal of experimental and theoretical physics established by E. L. Nichols in 1893

VOLUME 91

Second Series

JULY 1–SEPTEMBER 15, 1953

Published for the

AMERICAN PHYSICAL SOCIETY

by the

AMERICAN INSTITUTE OF PHYSICS

Incorporated

THE PHYSICAL REVIEW

A journal of experimental and theoretical physics established by E. L. Nichols in 1893

Published by the American Institute of Physics for the

AMERICAN PHYSICAL SOCIETY

Officers

President

ENRICO FERMI
Institute for Nuclear Studies
University of Chicago
Chicago 37, Illinois

Vice-President

H. A. BETHE
Cornell University
Ithaca, New York

Secretary

K. K. DARROW
Bell Telephone Laboratories
Office:
Columbia University
New York 27, New York

Treasurer

G. B. PEGRAM
Columbia University
New York 27, New York

Local Secretary for the Pacific Coast

J. KAPLAN
University of California at Los Angeles
Los Angeles, California

Managing Editor

S. A. GOUDSMIT
Brookhaven National Laboratory
Upton, Long Island
New York

BOARD OF EDITORS

Editor

S. A. GOUDSMIT

Assistant Editor

S. PASTERNACK

Associate Editors

1951–1953	*1952–1954*	*1953–1955*
C. L. CRITCHFIELD	W. P. ALLIS	W. A. FOWLER
M. DEUTSCH	F. G. BRICKWEDDE	KENNETH GREISEN
M. GOLDHABER	W. B. FRETTER	CHARLES KITTEL
T. H. JOHNSON	CONYERS HERRING	R. E. MARSHAK
R. SERBER	H. W. LEVERENZ	W. K. H. PANOFSKY
C. H. TOWNES	ARNOLD NORDSIECK	V. F. WEISSKOPF

Manuscripts for publication should be submitted to S. A. GOUDSMIT, Brookhaven National Laboratory, Upton, Long Island, New York. The authors' institutions are requested to pay a publication charge of $15 per page which, if honored, entitles them to 100 free reprints. Instructions will be sent with galley proofs.

Proof and all correspondence concerning papers in the process of publication should be addressed to the Publication Manager, American Institute of Physics, 57 East 55 Street, New York 22, New York.

Subscription Price

United States and Canada $30.00
Elsewhere $32.00

Back Numbers[1]

Yearly back number rate when complete year is available:
Prior to 1949: $25.00
Thereafter: $33.00
Single copies: $3.00 each, prior to July, 1929;
$1.50 each, July, 1929–December, 1941;
$3.00 each, January, 1942–December, 1946;
$1.50 each, thereafter.
General index, 1893–1920: $4.00.

Subscriptions, renewals, and orders for back numbers should be addressed to the American Institute of Physics, 57 East 55 Street, New York 22, New York.

Changes of address in the case of members of the American Physical Society should be addressed to the Treasurer; in the case of other subscribers to the American Institute of Physics.

[1] For Series 1 inquire of Physics Department, Cornell University, Ithaca, New York.

The Physical Review is published semi-monthly at Prince and Lemon Streets, Lancaster, Pennsylvania.

Entered as second-class matter March 6, 1947, at the Post Office at Lancaster, Pennsylvania, under the Act of March 3, 1879.

Acceptance for mailing at special rate of postage provided for in paragraph (d-2), section 34.40, P. L. & R. of 1948, authorized January 27, 1933.

THE
PHYSICAL REVIEW

A journal of experimental and theoretical physics established by E. L. Nichols in 1893

SECOND SERIES, VOL. 91, NO. 1 JULY 1, 1953

Simultaneous Measurement of Ionization and Attachment Coefficients*

MELVIN A. HARRISON† AND RONALD GEBALLE
Department of Physics, University of Washington, Seattle, Washington
(Received March 4, 1953)

Measurements have been made of pre-breakdown currents in four gases: oxygen, air, freon-12 (CCl_2F_2), and CF_3SF_5. The behavior of these currents differs from that previously attributed to all gases in that semilogarithmic graphs of current against electrode separation at constant E/p exhibit initial curvature, being concave toward the electrode separation axis. At low E/p an apparent saturation is found. This behavior is interpreted as resulting from a reaction of dissociative attachment of the kind $AB+e=(AB^-)^* \approx A+B^-$. On this basis simultaneously determined values of the ionization and attachment coefficients can be deduced. In oxygen and air these parameters, when determined from separate experiments, show a somewhat anomalous behavior. The apparent anomalies are explained with the result that ionization is found to commence at lower, and attachment persist to higher values of E/p than previously suspected. In freon-12 and CF_3SF_5 it is found that the ionization coefficient is about an order of magnitude larger than reported for similar gases when no account is taken of possible attachment. The attachment coefficient is observed to be larger for halogen-containing molecules than for the same halogens when free. Cross sections for attachment are computed for oxygen and air. Dependence of the cross sections on mean electron energy is discussed with reference to energy scales in these two gases.

INTRODUCTION

WE have reported previously[1] on simultaneous measurements of the ionization and attachment coefficients in oxygen. Since that time two additional papers[2,3] describing measurements of attachment in oxygen have appeared, and we have extended our procedure to air, CCl_2F_2 (freon-12), and CF_3SF_5. It is the purpose of this paper to relate in more detail the method we have employed, to present our results in these gases, and to discuss these results in comparison with those of other workers.

Following Townsend[4] it has been generally assumed that the current in a pre-breakdown discharge between plane parallel electrodes is described for sufficiently small electrode separation by the familiar equation,

$$i=i_0e^{\alpha d}, \tag{1}$$

where i is the total current, i_0 the initial electron current at the cathode, d the electrode separation. The ionization coefficient α is the mean number of ionizations per cm in the field direction produced by electron collision. Although in complex gases more than one type of ionizing process may occur, no attempt has been made as yet to separate out the corresponding contributions to α. At large separations, as is well known,[5] significant deviations from Eq. (1) are observed. These are explained in terms of secondary ionizing processes which take place at the cathode or within the body of the gas. Such processes cause a more rapid increase of current with electrode separation than is indicated by Eq. (1) and are essential to the occurrence of breakdown.

In complex gases and in those containing electronegative atoms other reactions result from electron collision. Ions which are produced in such processes affect the density of current carriers in a manner quite different from the ionization processes described above. Many types of ion-producing reactions have been observed, principally through the use of mass spectrographs. At present we confine ourselves to three,

* Supported in part by the U. S. Office of Ordnance Research.
† Now at Seattle Pacific College, Seattle, Washington.
[1] R. Geballe and M. A. Harrison, Phys. Rev. **85**, 372 (1952).
[2] A. Doehring, Z. Naturforsch. **7a**, 253 (1952).
[3] P. Herreng, Cahiers phys. **38**, 7 (1952).
[4] J. S. Townsend, Nature **62**, 340 (1900).
[5] L. B. Loeb, *Fundamental Processes of Electrical Discharge in Gases* (John Wiley and Sons, Inc., New York, 1939), Chap. IX.

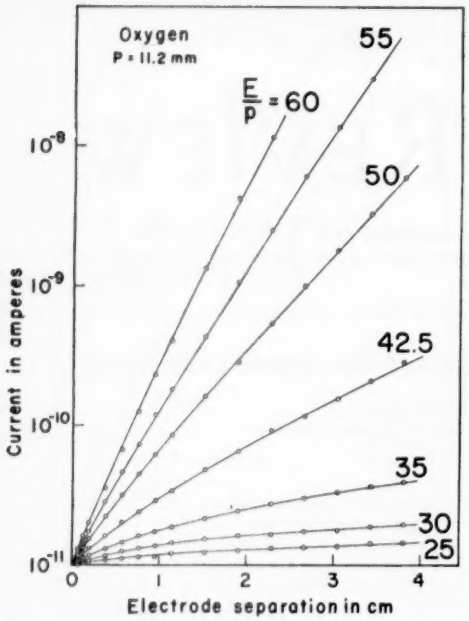

FIG. 1. Typical variation of $\ln i$ with d in oxygen at 11.2 mm pressure. Each curve gives the results of a run at constant E/p. Data are normalized to the same i_0. Solid curves are drawn from Eq. (5).

designated as follows:

(A) Direct attachment, $AB+e=AB^-$.

(B) Dissociative attachment, $AB+e=(AB^-)^*=A+B^-$.

(C) Dissociation into ions, $AB+e=A^++B^-+e$.

We assume that at a given value of mean electron energy, characterized by the experimental parameter E/p, where E is the field strength in volts/cm and p the pressure in mm of mercury, one of the reactions predominates and the others can be neglected. Furthermore we permit only those electrode separations which are small enough that secondary ionizing processes of the kind leading to breakdown have no appreciable effect. Focusing our attention on reactions of the types A and B, we describe the attachment process by a parameter η which we define in analogy to α as the mean number of attachments per cm of drift in the field direction. In order to find the current which flows when this process and ionization by collision occur simultaneously, we make use of equations of continuity as follows:

$$\partial n_e/\partial t+v_e\partial n_e/\partial x=\alpha v_e n_e-\eta v_e n_e, \quad (2)$$

$$\partial n_+/\partial t+v_+\partial n_+/\partial x=\alpha v_e n_e, \quad (3)$$

$$\partial n_-/\partial t+v_-\partial n_-/\partial x=\eta v_e n_e. \quad (4)$$

In these equations the subscripts e, $+$, and $-$ refer, respectively, to electrons, positive ions, and negative ions, while n means numerical density, and v stands for drift speed in the gas. The steady-state solution for the total current, with suitable boundary conditions, is found to be

$$i=i_0[\alpha/(\alpha-\eta)]\exp[(\alpha-\eta)d]-i_0\eta/(\alpha-\eta), \quad (5)$$

as previously given. When reaction C predominates, the appropriate equations have the solution

$$i=i_0[(\alpha+\lambda)/\alpha]\exp(\alpha d)-i_0\lambda/\alpha, \quad (6)$$

where λ is a coefficient describing the rate of reaction C in the same manner that η describes the rates of A and B. Solutions can be readily written down for situations in which reactions B and C occur together and in which secondary ionization processes described by the usual coefficient γ are present as well, but these are of no present concern.

Ordinarily α is measured by determining the slope of a semilogarithmic graph of i against d, on the assumption that Eq. (1) is correct.[4,6] Experimental evidence indicates that this is valid procedure for a large number of gases. It has also been applied to gases in which reactions of types A, B and C are known to occur.[7,8] Now semilogarithmic graphs of Eqs. (5) and (6) are distinctly nonlinear. However if α is much larger than η and/or λ, the deviation from linearity will be difficult

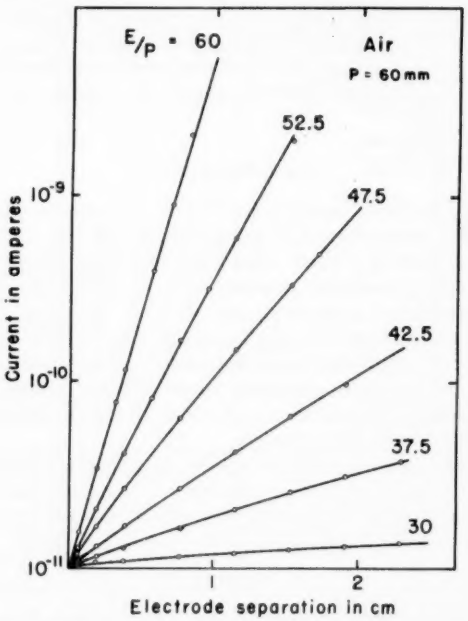

FIG. 2. Typical variation of $\ln i$ with d in air at 60 mm pressure with normalized i_0. Solid curves are drawn from Eq. (5). Multiplication is much greater than in oxygen because of the smaller attachment rate.

[6] Reference 5, Chap. VIII.

[7] B. M. Hochberg and E. J. Sandberg, Compt. rend. acad. sci. U.R.S.S. **53**, 511, (1946).

[8] K. Masch, Arch. Elektrotech. **26**, 587 (1932).

to observe. A similar difficulty occurs when the range of d is limited to large values, even if α is only slightly larger than η. In this event the additive terms in the equations are negligible, and the coefficient actually deduced will be $\alpha-\eta$. If d, because perhaps of instrumental limitations, is confined to small values (a few mm), the deviation again will be hardly apparent. The slope of a straight line drawn through the experimental points in this case will have no simple interpretation. It is apparent from this discussion that only if an extensive range of d is covered by experiment can the extent to which attachment and dissociation affect the discharge current be fully determined, and true values of the coefficients deduced.

APPARATUS AND PROCEDURE

The electrodes are polished copper disks 9 cm in diameter, with contoured edges. The anode is perforated at its center with about 400 holes within a circle of 2 cm diameter, and is rigidly mounted to the Pyrex vessel. A carefully made nut and screw with 40 threads per inch permit the cathode to be separated any distance between 0 and 4 cm through the agency of an iron armature which can be rotated by an external magnet. Ultraviolet light is admitted through a quartz window directly above the anode and falls normally on the cathode. The light intensity is monitored by a photocell; occasional adjustment of the load resistor is necessary to maintain sufficient constancy. The Pyrex vessel is made from a 5-liter flask and provides a minimum clearance of 4.5 cm. A coating of Dag on the interior wall of the vessel insures an equipotential boundary. Connection of this coating to a voltage divider permits adjustment of the wall potential. It was found possible to keep current diffusing to the wall less than 1 percent of the total even at the greatest electrode separation.

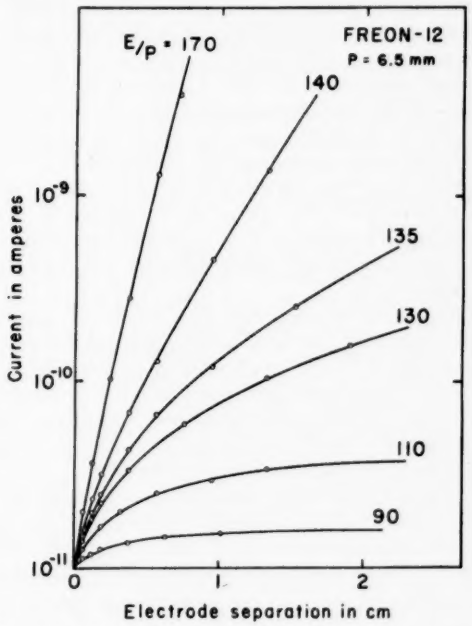

FIG. 3. Typical behavior of ln i in freon-12 at 6.5 mm pressure for various values of E/p. Solid curves are drawn from Eq. (5). Curvature is much more pronounced than in oxygen or air due to the very large attachment coefficient.

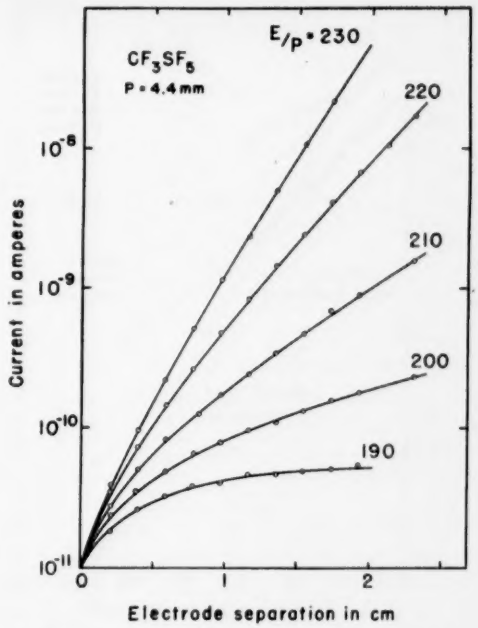

FIG. 4. Typical variation of ln$i$ with d in CF_3SF_5 at 4.4 mm pressure. Solid curves are drawn from Eq. (5). The saturation at low E/p is particularly apparent here.

The vessel and electrodes have been thoroughly cleaned and baked at temperatures exceeding 400°C in vacuum and an atmosphere of hydrogen for several hours whenever it appeared desirable. Occasionally when either the electrodes became visibly coated or the initial photocurrent was found to be smaller than normal, the electrodes were removed and mechanically cleaned, and the baking process was repeated. The apparatus has not been used unless a pressure of less than 10^{-5} mm of mercury could be maintained for several hours in the closed-off vessel.

In order to be sure that the effects to be reported were not instrumental, measurements were also made in two gases, hydrogen and nitrogen, which are free of any reactions involving ions except ionization by collision.[9-14] Semilogarithmic graphs of current were

[9] Mass spectrographic investigations have produced no evidence for the existence of N^- or N_2^- (see references 10 and 11). H^- has been reported in very small amounts (see references 12 to 14) but no estimates of the cross section for its formation are given. The present apparatus would have detected a process with a mean cross section of 10^{-21} cm^2.

[10] Tate, Smith, and Vaughan, Phys. Rev. **48**, 525 (1935).

[11] J. T. Tate and W. W. Lozier, Phys. Rev. **39**, 254 (1932).

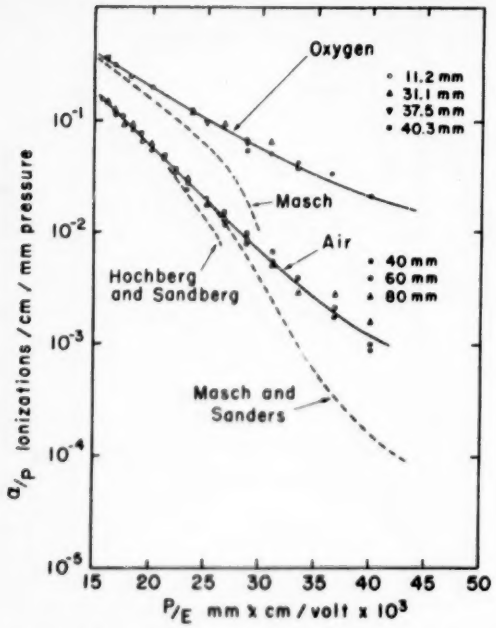

FIG. 5. Variation of ionization coefficient with p/E for oxygen and air. Solid curves are drawn by inspection through data of the present work. For a discussion of the other curves see text.

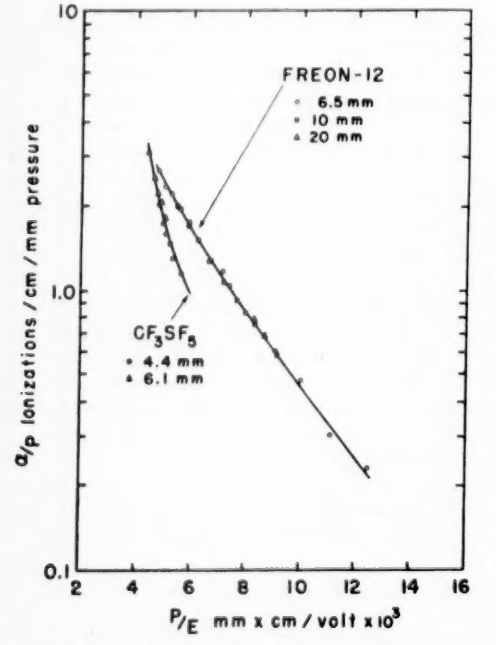

FIG. 6. Variation of ionization coefficient with p/E for freon-12 and CF_3SF_5. Solid curves are drawn by inspection through data of the present work. For discussion see the text.

[12] W. W. Lozier, Phys. Rev. **36**, 1417 (1930).
[13] H. D. Smyth and D. W. Mueller, Phys. Rev. **43**, 116 (1936).
[14] O. Tüxen, Z. Physik **103**, 463 (1936).

linear within the accuracy of the measurements, except that under certain conditions a slight concavity to the electrode separation axis was noted at separations less than three turns of the screw. This effect was found as well when the photocurrent was measured in vacuum. Similar observations have been reported[15] and explained in terms of the reflection of light back up through the holes in the anode. The effect seems definitely correlated with the degree of parallelism of the electrodes; when they are visibly nonparallel, no concavity is observed for these gases. It has been found possible to correct for this effect, utilizing the results of vacuum measurements. The correction is about 3 percent at one turn, 1 percent at three turns.

Attempts were made to obtain considerable purity of all the gases used. Hydrogen was admitted through a palladium thimble, and in addition other samples of tank hydrogen were passed slowly over hot copper and through a liquid nitrogen trap. Behavior of hydrogen treated in these various ways was identical. Nitrogen for use in measurements was generated by decomposition of NaN_3, and was passed through a liquid nitrogen trap. Oxygen was produced in three ways: by decomposition of HgO, $KMnO_4$, and MnO_2, with suitable liquid nitrogen traps to remove impurities. Again no difference among them could be detected. Air from outside the laboratory was filtered through a plug of glass wool and passed through a liquid nitrogen trap. Freon came from a commercial cylinder and was distilled in vacuum several times before admission from a trap cooled to the temperature of liquid nitrogen. CF_3SF_5 obtained from the Department of Chemistry[16] was purified in the same manner as freon. Gas pressures were measured with a mercury manometer. During all manipulations except admission of the last two gases a liquid nitrogen trap served as protection against mercury contamination. Subsequent checks indicated that no detectable contamination was admitted in these latter operations. Samples of all gases were changed frequently. At no time was there evidence that a gas had altered its properties while measurements were being made.

High voltage was supplied by a regulated negative supply, and was read with a calibrated resistor and a potentiometer. Ionization currents were passed through one of a set of calibrated resistors which were frequently checked against each other. The potential drop across the resistor in use was read with a Dolezalek electrometer. Electrode separations were determined by counting revolutions of the screw. Current measurements were made for varying separations at constant E/p. The gas was never permitted to break down. At sufficiently large E/p, when the electrode separation was increased to more than about 2 cm, a conditioning of the cathode

[15] A. A. Kruithoff and F. M. Penning, Physica **3**, 515 (1936).
[16] Gene A. Silvey and George H. Cady, J. Am. Chem. Soc. **72**, 3624 (1950). We wish to thank Dr. Silvey and Professor Cady for supplying this compound.

surface appeared to take place which affected the initial photocurrent. To eliminate this effect, measurements in this range of E/p were carried out at either reduced pressure or reduced light intensity.

DATA

Samples of data obtained in the gases are shown in Figs. 1 to 4. The solid curves in these figures are computed from Eq. (5). By a careful curve-fitting procedure values of α and η can be found from each curve. The procedure fails when at low E/p it is found that $\eta \gg \alpha$, and the current hardly rises above i_0. At high E/p the magnitudes of η and α are reversed, the curvature is slight, and while α can be determined with considerable accuracy, η cannot.

It can be seen that a straight line drawn through the points for separations of greater than one cm will pass reasonably close to all of them, and the deviations could be taken for experimental scatter. A straight line could

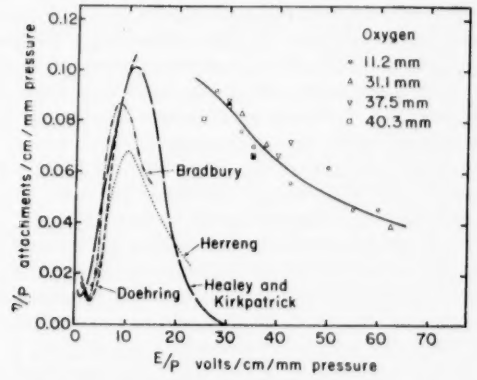

FIG. 7. Dependence of attachment coefficient on E/p for oxygen. Solid curve drawn by inspection through present data. Comparison data are given directly in reference 24 but have been computed from the results of references 2, 3, and 23 as discussed in the text.

similarly be drawn through the points, say, between 0.2 and 0.8 cm. Neither of these gives the correct α in the region of E/p where detectable curvature exists.

Data of this nature were taken in oxygen at pressures (measured at 20°C) from 11.2 to 40.3 mm; in air, from 40 to 80 mm; in freon-12, from 6.5 to 20 mm; and in CF_3SF_5, at 4.4 and 6.1 mm. During a run at constant E/p individual points, particularly those at small separations, were repeated to check their reproducibility. In each gas the range of E/p extended throughout the region of applicability of the method for these pressures.

RESULTS AND DISCUSSION

1. Measurement of α/p and η/p

Several factors have led us to base our analysis of the curves on Eq. (5) rather than Eq. (6). Important among them is the apparent saturation exhibited by

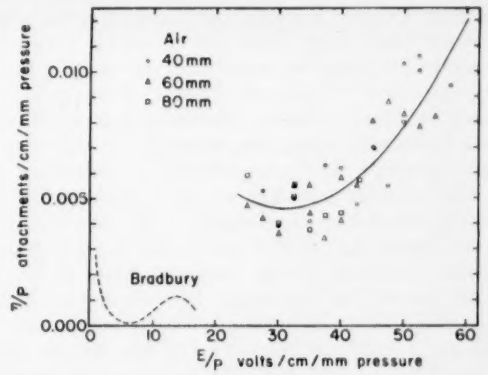

FIG. 8. Dependence of attachment coefficient on E/p for air. Solid curve again drawn by inspection. Scatter is greater than for oxygen because of the smaller curvature in Fig. 2. Comparison curve computed from the results of reference 23. The considerable difference in magnitude has as yet no explanation.

curves of Figs. 1 to 4. Such behavior is consistent only with the first of these equations. Furthermore in oxygen and in many complex gases it has been found that reactions of type B appear at electron energies of but a few volts,[17–20] whereas those of type C require more than ionization energy. Since dissociative attachment results from resonance capture of an electron, the cross section for this process can attain large values; e.g., a maximum of 10^{-16} cm^2 has been reported recently for SF_6.[20] Under conditions of the present experiments where ionization is just assuming a dominant role it seems quite unlikely that C should occur to an appreciable extent.

On this basis Fig. 5 shows values of α/p found for oxygen and air plotted against p/E. This scale of

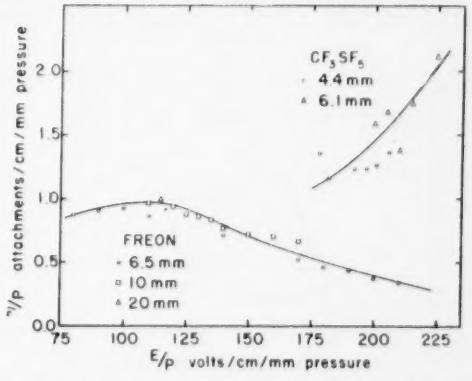

FIG. 9. Behavior of the attachment coefficient with E/p in freon-12 and CF_3SF_5. Curves are drawn by inspection. Scatter in the CF_3SF_5 is principally because these were the first data to be taken.

[17] W. W. Lozier, Phys. Rev. **46**, 268, (1934).
[18] R. F. Baker and J. T. Tate, Phys. Rev. **52**, 683 (1938).
[19] R. H. Vought, Phys. Rev. **71**, 93 (1947).
[20] A. J. Ahearn and N. B. Hannay, J. Chem. Phys. **21**, 119 (1953).

abscissas is chosen because it produces for many gases a nearly linear graph. The solid curves are drawn by inspection. Included for comparison are results of other investigations.[8,21,22] It should be noted that the measurements of Masch[8] and of Hochberg and Sandberg[22] were made with separations between 0.2 and 0.8 cm, while Sanders'[21] did not extend below one cm. The first of these authors remarked on the probable effect of attachment on his oxygen data but did not analyze it. In air, where the effect of attachment is considerably diluted, curvature of the semilogarithmic graphs is slight for all E/p. Agreement between results of the quite different measurements of Masch and Sanders in this gas is readily accounted for by this circumstance.

There are no published data with which to compare the curves of Fig. 6 directly. Hochberg and Sandberg[7] have given values of α/p in several complex gases containing electronegative atoms, measured with separations of less than one cm. In agreement with their work and consistent with the high dielectric strength of such gases we find the net electron multiplication to be appreciable only at values of E/p considerably larger than for simple gases. The magnitude of α/p however is larger by about one order than reported by these authors.

Figure 7 shows the behavior of the attachment coefficient deduced for oxygen, reported in part previously.[1] Included for comparison are results of earlier investigations[23,24] as well as two recent studies.[2,3] As not all of these authors presented their results in this form, it has been necessary to recalculate the coefficient making use of appropriate auxiliary data. In this form these curves represent as nearly as possible the original data, independent of computations involving drift and random speeds. Since their data up to the present have been interpreted only in the light of an attachment process, incipient electron production has appeared as a falling off of the attachment coefficient. It is in the region where α/p and η/p are of comparable magnitude that three of their curves exhibit a sharp decline.

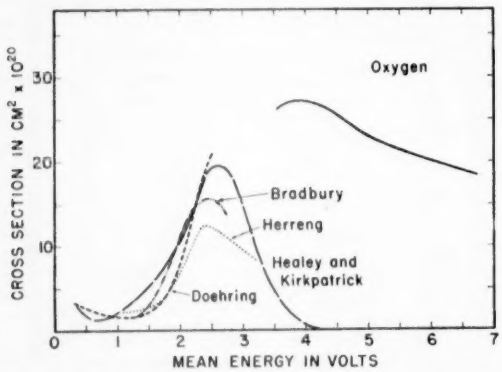

FIG. 10. Mean cross section for attachment in oxygen plotted against mean electron energy. All curves are calculated from those of Fig. 7 using the auxiliary data of reference 29.

Figure 8 presents the attachment coefficient in air and, for comparison, that deduced from Bradbury's paper.[23] It will be noted that the magnitude of the coefficient is considerably less than in oxygen. It is expected that it be less in approximately the ratio of the mole fractions of oxygen in the two gases, in other words, that the peak in air should be about 0.02 attachments per cm per mm. It seems reasonable that such a value would be attained at higher E/p than could be reached by the present apparatus. The positive slope over most of this curve as contrasted with the negative slope observed in oxygen is attributed to the differing energy scales of the two gases. Our data seem to indicate, within the precision of the method, a slight upturn below $E/p=30$. We are hesitant about the validity of this feature, particularly since the curve should in some manner join that of Bradbury. Whereas in oxygen, the coefficients measured in other researches rise to a magnitude comparable with that found in the present work, this is by no means true in air. For this we have as yet no explanation.

In Fig. 9 are given the attachment coefficients for freon-12 and CF_3SF_5 as functions of E/p. Their magnitudes are comparable with that reported for iodine,[25] and considerably larger than that found in chlorine[26] or expected for fluorine. The data in CF_3SF_5, which were taken early in the work show considerable scatter, and the curve is sketched only to indicate a possible behavior for this gas. The large magnitude of η/p in these substances might reflect the possibility for multiple reactions of type B. Here again it is apparent that the large probability for attachment could cause a serious underestimate of the rate of electron multiplication.

It is of some interest to point out that in the range of pressures employed no dependence on this parameter has been detected for any of the gases studied.

2. Dependence of Mean Cross Section on Mean Energy

In oxygen and in air it is possible to make further calculations. Auxiliary data exist from which the variation of mean cross section for negative ion production can be correlated with mean electron energy. The cross section is related to η/p by the equation $\sigma=(\eta/p)\times(v_e/c)(1/n_0)$, where n_0 is the number of molecules per cm³ at a pressure of one mm of mercury, v_e is the drift speed of the electrons, and c their mean speed of agitation. The mean energy is obtained from diffusion measurements in a manner due originally to Townsend.[27]

[21] F. H. Sanders, Phys. Rev. **41**, 667 (1932); **44**, 1020 (1933).
[22] B. M. Hochberg and E. J. Sandberg, J. Tech. Phys. (U.R.S.S.) **12**, 65 (1942).
[23] N. Bradbury, Phys. Rev. **44**, 883 (1933).
[24] R. H. Healey and J. W. Reed, *The Behavior of Slow Electrons in Gases* (Amalgamated Wireless, Sydney, 1941), p. 94.
[25] R. H. Healey, Phil. Mag. **26**, 940 (1938).
[26] V. W. Bailey and R. H. Healey, Phil. Mag. **19**, 725 (1935).

Several sets[24,27–30] of data of this kind in oxygen and air have been reported, with considerable discrepancy among them. The discrepancies are relatively unimportant in the calculation of cross sections, as only the ratio of the above speeds enters; hence the magnitudes of σ are probably correct in the two gases. As the energy scales (variation of mean energy with E/p) reported by these authors differ widely, it has been necessary to adopt one for each gas on an almost arbitrary basis. In the case of oxygen the data of Brose[29] have been used. Townsend and Tizard[27] present the most complete data for air, but the recent work of Huxley and Zaazou[30] is probably more reliable. Since the latter authors give no data for $E/p > 25$, an extrapolation has been made.

Results of these computations are given in Figs. 10 and 11, for the cross sections compiled from our results and, for comparison, the work of the other investigators. All curves have been plotted using values of η/p from Figs. 7 and 8 and with auxiliary data as indicated in the previous paragraph. In oxygen the maximum agrees in magnitude with the estimate of Massey, 80×10^{-20} cm^2 for the type B reaction, if one recalls that the present value is an average over the energy distribution. Since this author's estimate of the (unaveraged) cross section for the type C reaction is smaller by a factor of almost 4, additional weight is added to the reasons for adopting B as the principal process. The maxima in oxygen and air again should be nearly in the ratio 5:1, deviation from this value being caused by differing energy distributions. Present data are not inconsistent with this conclusion. The increase of cross section as the mean energy approaches thermal values has been attributed to a reaction of type A.[31–33] The

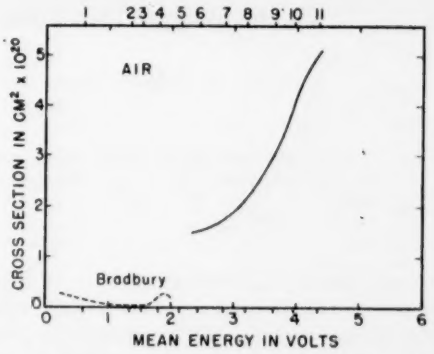

FIG. 11. Mean cross section for attachment in air plotted against mean electron energy. The scale at the bottom refers to the work of Townsend and Tizard. That at the top is due to Huxley and Zaazou, although energies above 6 volts are obtained by extrapolation.

peak found at somewhat higher energy by several workers (see Fig. 10) has been correlated with a level of the oxygen molecule at 1.62 volts.[23,34] Inelastic collisions at this energy, it has been suggested, return electrons to the very low energy region where they are captured by reaction A. Hagstrum[35] and others,[17] however, have shown that reaction B has an appearance potential of 6 volts and a peak probability at 8 volts. The previously mentioned estimate for the height of this peak (80×10^{-20} cm^2) provides sufficiently well for the presently observed maximum to indicate that dissociative attachment is responsible in large part for the observed behavior of the oxygen. Since the excitation function for the 1.62-volt level is presently unknown, the contribution of this "reflection" process cannot be estimated.

The authors wish to acknowledge helpful comments by interested friends, in particular those of Professor L. B. Loeb of the University of California.

[27] J. S. Townsend and H. T. Tizard, Proc. Roy. Soc. (London) **A87**, 357 (1912); **A88**, 336 (1913).
[28] J. S. Townsend and V. A. Bailey, Phil. Mag. **42**, 873 (1921).
[29] H. L. Brose, Phil. Mag. **50**, 536 (1925).
[30] L. G. H. Huxley and A. A. Zaazou, Proc. Roy. Soc. (London) **A196**, 402 (1949).
[31] F. Bloch and N. Bradbury, Phys. Rev. **48**, 689 (1935).
[32] M. Biondi, Phys. Rev. **84**, 1072 (1951).
[33] H. S. W. Massey, *Negative Ions* (Cambridge University Press, Cambridge, 1950), second edition, p. 72.
[34] D. R. Bates and H. S. W. Massey, Trans. Roy. Soc. (London) **A239**, 269 (1943).
[35] H. D. Hagstrum, Revs. Modern Phys. **23**, 185 (1951).

Conductivity of Thin Films in a Longitudinal Magnetic Field*

ERNEST KOENIGSBERG
Institute for Atomic Research, Iowa State College, Ames, Iowa
(Received February 26, 1953)

An integral expression for the electrical conductivity of thin films in a longitudinal magnetic field is derived by an analysis of free electron trajectories in the film. This is evaluated in the limit of strong magnetic fields.

IT is well known that a free electron moving in parallel electric and magnetic fields will follow a helical trajectory with the axis of the helix parallel to the field. The projection of an element of the helix in the plane normal to the axis is an arc of a circle. If ψ is the arc angle in the plane normal to the axis, then the arc length of the element of the helix is $r_0\psi$, where r_0 is the radius of curvature of the electron path in a plane normal to magnetic field $H(r_0=mvc/eH)$. The radius of curvature in the plane normal to the axis of the helix is $r=r_0\sin\delta$, where δ is the angle made by the electron velocity and the field direction.

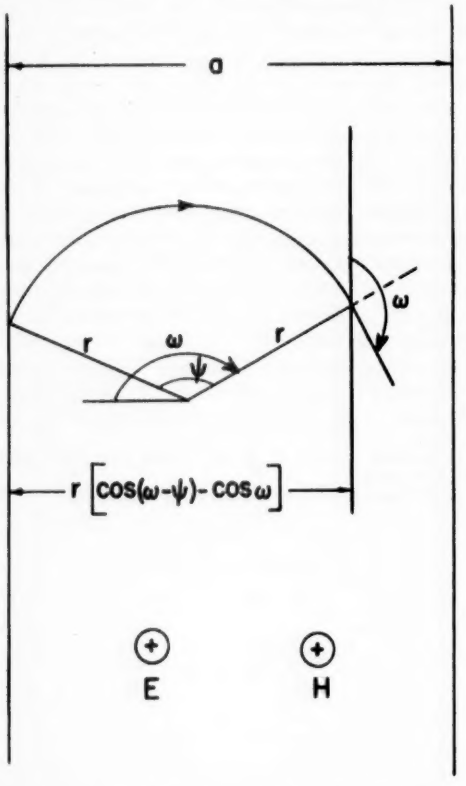

FIG. 1. Projection of an electron trajectory in the plane normal to the field direction, and geometric construction to obtain X; $0<\omega<\pi$.

Chambers[1] has shown that if one assumes diffuse scattering by the walls, the conductivity σ of a thin metal sample in a longitudinal magnetic field may be expressed by

$$\frac{\sigma}{\sigma_0}=1-\frac{3}{4\pi S}\int_S dS\int_0^{2\pi} d\omega\int_0^{\pi} d\delta\,\sin\delta\cos^2\delta e^{-\psi r_0/l}, \quad (1)$$

where σ_0 is the bulk conductivity, S is the cross-sectional area normal to the field direction, and l is the mean free path. ω is the angle between the projection of the velocity vector in the plane normal to the field and some fixed direction in that plane, dS is the differential cross-sectional area which includes the projection of the electron position in this plane, and ψ is the angle of arc in this plane which a trajectory has traversed since striking the wall and is, in general, a function of δ and ω as well as of position. The term to be integrated represents the effect of the shortened free path for those electrons which collide with the walls of the sample.

Chambers[1] evaluated Eq. (1) for thin *wires* in a longitudinal magnetic field by using geometric arguments. We use similar arguments for the conductivity of thin metal *films* in a longitudinal field.

For thin films dS/S can be replaced by $dX(r,\omega,\psi)/a$, where $X(r,\omega,\psi)$ is the perpendicular distance from the film wall to the electron position and a is the film thickness. Figure 1 shows the geometrical construction which gives $X=r[\cos(\omega-\psi)-\cos\omega]$. If the trajectory is shifted to the right, then, for a given ω, ψ increases; shifting the trajectory to the left will decrease ψ. By differentiation we obtain, for a given value of ω,

$$dS/S=dX/a=r\sin(\omega-\psi)d\psi/a. \quad (2)$$

By symmetry the scattering effects will be the same for both walls. We need only deal with one wall and multiply the integrand by two. Similarly we have symmetry for the effects of the polar angle δ, so we integrate between the limits zero and $\pi/2$ and multiply by two. Equation (1) then becomes

$$\frac{\sigma}{\sigma_0}=1-\frac{3r_0}{\pi a}\int_0^{\pi/2} d\delta\,\sin^2\delta\cos^2\delta A(\delta), \quad (3)$$

* Contribution No. 215 from the Institute for Atomic Research and Department of Physics, Iowa State College, Ames, Iowa. Work was performed in the Ames Laboratory of the U. S. Atomic Energy Commission.

[1] R. G. Chambers, Proc. Roy. Soc. (London) **A202**, 378 (1950).

where

$$A(\delta)=\int_0^{2\pi} d\omega \int_{\psi} d\psi \sin(\omega-\psi)e^{-\psi r_0/l}. \tag{3a}$$

To establish boundary conditions for the ψ-integration we distinguish two cases:

$$(1)\quad a\geq 2r=2r_0\sin\delta, \tag{4a}$$

$$(2)\quad a\leq 2r. \tag{4b}$$

Case (1)

The limits on ψ (for a given ω) are obtained by shifting the trajectories of Figs. 1 and 2 as far as possible to the right and to the left, keeping the endpoints of the trajectories within the walls. Thus for $0<\omega<\pi$ (see Fig. 1) we obtain the lower limit on ψ when the trajectory leaves the wall at an angle ω and the upper limit when the trajectory is tangent to the left wall. For $\pi<\omega<2\pi$ (Fig. 2) we obtain the lower limit when the trajectory returns to the left wall at an angle ω and the upper limit when the trajectory is tangent to the left wall. The limiting conditions are

$$\begin{aligned} &0<\psi<\omega && \text{for}\quad 0<\omega<\pi,\\ &2(\omega-\pi)<\psi<\omega && \text{for}\quad \pi<\omega<2\pi. \end{aligned} \tag{5}$$

Using the conditions (5) in Eq. (3a) we obtain

$$A(\delta)=\frac{l}{r_0}\left[2-\frac{l^2}{4r_0^2+l^2}(1+e^{-2\pi r_0/l})\right]. \tag{6}$$

Case (2)

This case has more complicated upper limiting values for ψ because some trajectories can strike both walls (without an intermediate collision). The possible values of ψ for a given ω are limited by the relations

$$\begin{aligned} &r[\cos(\omega-\psi)-\cos\omega]<a && \text{for}\quad 0<\omega<\pi,\\ &r[\cos(\omega-\psi)+1]<a && \text{for}\quad \pi<\omega<2\pi, \end{aligned}$$

as is evident from the figures. Unfortunately, we have not been able to express $A(\delta)$ in closed form for this case. $A(\delta)$ and the contribution of this case to the conductivity must be obtained by numerical integration.

If $a\geq 2r_0$, then the integrand is only the type discussed in Case 1. The conductivity, using Sondheimer's[2] notation, is then given by

$$\frac{\sigma}{\sigma_0}=1-\frac{3}{16\kappa}\left[2-\frac{\beta^2}{4\kappa^2+\beta^2}(1+e^{-2\pi\kappa/\beta})\right], \tag{7}$$

where $\kappa=a/l$ and $\beta=a/r_0(\beta\geq 2)$. In the limit $\kappa/\beta\gg 1$, Eq. (7) becomes

$$\sigma/\sigma_0=1-(3/8\kappa), \tag{8}$$

which is Fuchs'[3] result for thick films in zero magnetic field. If $\kappa/\beta\ll 1$, Eq. (7) becomes

$$\sigma/\sigma_0=1-(3\pi/8\beta), \tag{9}$$

independent of the ratio of film thickness to mean free path.

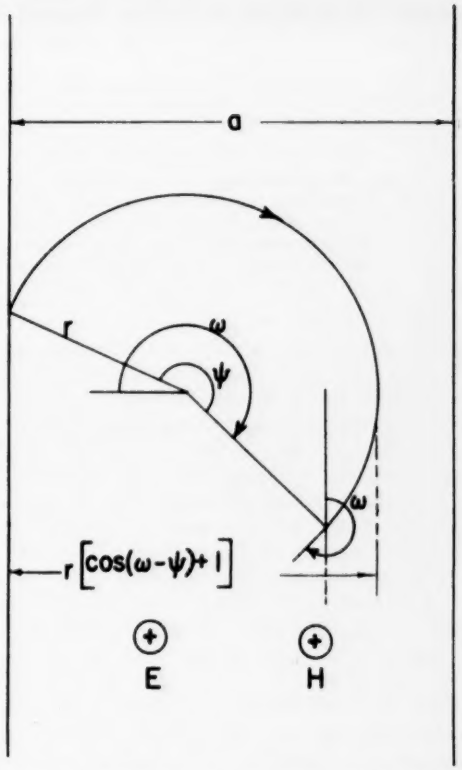

FIG. 2. Projection of an electron trajectory in the plane normal to the field direction; $\pi<\omega<2\pi$.

[2] E. H. Sondheimer, Advances in Phys. **1**, 1 (1952).

[3] K. Fuchs, Proc. Cambridge Phil. Soc. **34**, 100 (1938).

Angular Aberrations in Sector Shaped Electromagnetic Lenses for Focusing Beams of Charged Particles

EDGAR G. JOHNSON* AND ALFRED O. NIER
Department of Physics, University of Minnesota, Minneapolis, Minnesota
(Received March 13, 1953)

The general expression for the second-order angular aberration of sector shaped electromagnetic lenses consisting of superimposed uniform magnetic and radial electric fields used for the plane focusing of diverging beams of charged particles is derived. The result is applied to the special cases of pure magnetic and pure electric field lenses. The ion optics of a mass spectrometer employing sector electric and magnetic lenses in tandem and which has first-order velocity focusing and second-order angular focusing is obtained.

THE development of electronic techniques and the successful application of mass spectrometers to the measurement of isotopic abundances and gas analyses suggests that a mass spectrometer might be employed advantageously for the precision measurement of atomic masses. A properly designed instrument would have certain immediate advantages over existing mass spectrographs and could in time be developed to the point where it might far surpass these instruments.

An instrument employing magnetic deflection only cannot be employed for the precision determination of atomic masses. The spread in energy of ions from the ion sources limits the resolution. Also, the distribution in the energy spread depends upon the type of ion studied with ion fragments formed from molecules usually having an initial energy obtained in the dissociation process; thus they will be focused in the instrument with lower accelerating voltages than are the molecular ions, and a measurement of their position in the mass spectrum will not be an accurate measure of their mass. Hence, it is customary to employ combinations of electric and magnetic fields which will give double-focusing, i.e., which will focus ions having both a spread in energy and angle as they leave the ion source.

In a mass spectrograph a photographic plate is employed for detecting the ions. Compromises in design are often necessary in order to achieve approximate focusing over a region of the spectrum. Since in a mass spectrometer focusing is required at only one point, it should be possible to achieve a more exact focus.

The sector-shaped electromagnetic lenses usually used in the construction of mass spectrometers are those in which the mean ion beam enters and exits perpendicular to the field boundaries. The first-order ion optical properties of such lenses have been worked out by Herzog[1] and others. In the derivations, variations of the ion beam in mass, energy, distance from optical axis, and angular divergence are limited to sufficiently small percentages of the mean values so that squares, cross products, and higher order terms can be neglected in the treatment. The resolution of systems employing the optical properties is then limited by the effect of these second-order terms, chief of which is the second-order angular aberration. A completely general expression for this aberration is not available in the literature, although formulas applicable to a number of special cases are given by Henneberg,[2] Bruche and Scherzer,[3] and by Hutter.[4] These include all arrangements for pure magnetic lenses; but for pure electric lenses, or for combinations, only cases in which object and image distances are both zero are covered. In none of these special cases, nor in any of the double-focusing systems employing two of them in tandem, can the final second-order angular aberration be reduced to zero. In the next section we shall derive a more general expression for the second-order angular aberration, and in a following section we shall show that arrangements can be constructed in which the second-order angular aberration vanishes. An instrument having this property could employ a relatively large divergence angle and hence have good intensity without a loss in resolution.

DERIVATION OF SECOND-ORDER ANGULAR ABERRATION

To derive the expression for second-order angular aberration we shall, as Herzog did, write the equation of motion of a given charged particle as it approaches, passes through, and leaves an electromagnetic lens. Throughout the treatment the angle of divergence, α, will be considered large enough so that its square and terms proportional to its square will be significant. Variations in other quantities will be considered small enough that their squares and also all cross products can be neglected. The first and most lengthy step will be to find an equation of motion in the lens, or field space, which is accurate to the second order. The procedure will be to express all quantities, including the field intensity, in terms of the mean ion beam and its parameters; and in particular all variables will be expressed as fractional deviations from the mean values so that any power of these variables can be expressed as a convergent power series.

* Present address: Minnesota Mining and Manufacturing Company, St. Paul, Minnesota.

[1] G. Herzog, Z. Physik **89**, 447 (1934).

[2] W. Henneberg, Ann. Physik **19**, 335 (1934).

[3] E. Bruche and O. Scherzer, *Geometrische Electronenoptik* (Julius Springer, Berlin, 1934).

[4] R. G. E. Hutter, Phys. Rev. **67**, 248 (1945).

Consider a sector shaped field area of total angle Φ and coordinates r, ϕ for the particle and with object space and image space to the left and right, respectively, as in Fig. 1. There will be a homogeneous magnetic field of intensity B, perpendicular to the r, ϕ plane, and a cylindrical electric field of intensity $E=E_0r_0/r$, in the opposite direction to the radius vector. The values of B and E_0 must be such that the mean ion beam, consisting of ions of charge e, mass m_0, velocity v_0 and entering perpendicular to the field area at r_0, will describe a circle of radius r_0 and exit again perpendicular to the field boundary and along the optic axis.

If we consider f to be that fraction of the centripetal force produced by the electric field we have

$$f(m_0v_0^2/r_0)=eE_0, \tag{1a}$$

$$(1-f)(m_0v_0^2/r_0)=eBv_0, \tag{1b}$$

and we can express E_0 and B in terms of the mean ion beam parameters and the dimensionless field characteristic f. Thus $f=0$ for a pure magnetic field and $f=1$ for a pure electric field.

Now consider the motion of any given particle with charge e, mass m, and velocity v. Forces on the particle will have components along the unit radius vector $\mathbf{R}_1$, and the unit vector perpendicular to it, $\boldsymbol{\phi}_1$. There will be no forces perpendicular to the r, ϕ plane. The differential equation of motion is:

$$\begin{aligned} m[d^2r/dt^2-r(d\phi/dt)^2]\mathbf{R}_1 &+(1/r)(d/dt)[mr^2d\phi/dt]\boldsymbol{\phi}_1 \\ &=-(eE_0r_0/r)\mathbf{R}_1-e\mathbf{v}\times\mathbf{B} \\ &=-e[Brd\phi/dt+E_0r_0/r]\mathbf{R}_1 \\ &\quad +eB(dr/dt)\boldsymbol{\phi}_1. \end{aligned} \tag{2}$$

Equation (2) immediately gives two differential equations involving the time rate variation of r and ϕ. Since the equation involving ϕ can easily be integrated to

$$d\phi/dt=eB/2m+C/r^2, \tag{3}$$

where C is a constant of integration; and since

$$\begin{aligned} dr^2/dt^2=(d\phi/dt)^2(d^2r/d\phi^2) &\\ +(d\phi/dt)(dr/d\phi)^2(d/dr)(d\phi/dt), & \end{aligned} \tag{4}$$

it is possible to eliminate the time variable and obtain the differential equation of r as a function of ϕ. Before doing so let

$$r=r_0(1+\rho), \tag{5a}$$

where ρ will be a numeric representing the fractional deviation of r from the mean value r_0. If we also let:

$$m=m_0(1+\gamma), \tag{5b}$$

$$v=v_0(1+\beta), \tag{5c}$$

γ and β are also numerics representing the fractional deviations from the mean mass and mean velocity. The dependent variable ρ will be a function of its value at entry into the field area, of γ and β, and of the diverging angle α. If all these are zero ρ will also be zero and the particle will follow the optic axis. Since, in this derivation, α is to be an order of magnitude larger than the other independent variables, ρ and $d\rho/d\phi$ will both be considered roughly proportional to α so that only the cube and higher order terms in ρ and $d\rho/d\phi$ will be neglected. The squares and cross products of γ and β will be neglected.

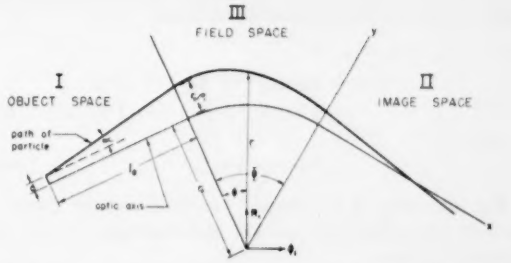

FIG. 1. Diagram showing path of a charged particle through a sector shaped electromagnetic lens. Particle is shown leaving object plane at a distance d from optic axis and at a diverging angle α.

Substitution of expressions (1a), (1b), (4), (5a), (5b), and (5c) into the coefficient of $\mathbf{R}_1$ in Eq. (2) will result in:

$$\begin{aligned} d^2\rho/d\phi^2-(2C/r_0^2)(d\rho/d\phi)^2(d\phi/dt)^{-1}(1+\rho)^{-3}-(1+\rho) &\\ =-(1+\gamma)^{-1}[(1-f)(v_0/r_0)(1+\rho)(d\phi/dt)^{-1} &\\ +f(v_0^2/r_0^2)(1+\rho)^{-1}(d\phi/dt)^{-2}]. & \end{aligned} \tag{6}$$

From Eq. (3) the constant C and therefore $d\phi/dt$ in general can be evaluated in terms of the angular velocity possessed by the particle at the time of entry into the field area. Using the subscript 1 to denote values at $\phi=0$,

$$(d\phi/dt)_1=(v_1\cos\alpha)/r_1=v_1(1-\tfrac{1}{2}\alpha^2)/[r_0(1+\rho_1)]. \tag{7}$$

A particle entering the field area at a point other than r_0 will undergo a change in energy because of the variation in potential in the cylindrical condenser. By equating energy terms we can solve for v_1 in terms of the initial velocity and the point of entry into the field area. We obtain:

$$C=[1+f-\rho_1{}^2-f^2\rho_1{}^2-\alpha^2+2\beta+\gamma-f\gamma]v_0r_0/2, \tag{8}$$

$$\begin{aligned} d\phi/dt=[1-\rho-f\rho+\tfrac{3}{2}\rho^2+\tfrac{3}{2}f\rho^2-\tfrac{1}{2}\rho_1{}^2 &\\ -\tfrac{1}{2}f^2\rho_1{}^2-\tfrac{1}{2}\alpha^2+\beta]v_0/r_0. & \end{aligned} \tag{9}$$

Substitution of (8) and (9) in (6) will finally result in an equation in which the mean values m_0, v_0, and r_0 will cancel out, and only the small fractional deviations ρ, ρ_1, α, β, and γ remain. These quantities can all be expanded in convergent power series, and by doing this and dropping all terms of higher than second order we

get a differential equation as follows:

$$d^2\rho/d\phi^2+(1+f^2)\rho-\delta = (1+f)(d\rho/d\phi)^2-\tfrac{1}{2}(1+f^2+4f^3)\rho^2 -\tfrac{1}{2}(1+f+f^2+f^3)\rho_1^2-\tfrac{1}{2}(1+f)\alpha^2, \quad (10)$$

where

$$\delta=\gamma+(1+f)\beta. \quad (10a)$$

The quantity δ represents variation in the particle other than those of position and direction in the ion optical system.

Exact solutions to this type of equation are not known; however, we are interested only in solutions that will satisfy it to a second-order approximation. To find these we can replace the second-order terms on the right by the square of the *first-order* solution and its derivative.

The only first-order terms are those on the left-hand side. When set equal to zero they constitute the differential equation used by Herzog.[1] The solution is straightforward and corresponds to the Gaussian dioptrics of the system. Calling the first-order solution ρ_g we have:

$$\rho_g(\phi)=a\sin((1+f^2)^{\frac{1}{2}}\phi)+b\cos((1+f^2)^{\frac{1}{2}}\phi) +\delta/(1+f^2). \quad (11)$$

a and b are the two constants of integration. The second-order approximation to Eq. (10) is then:

$$d^2\rho/d\phi^2+(1+f^2)\rho=(1+f)(d\rho_g/d\phi)^2 -\tfrac{1}{2}(1+f^2+4f^3)\rho_g^2-\tfrac{1}{2}(1+f+f^2+f^3)\rho_{g1}^2 -\tfrac{1}{2}(1+f)\alpha^2+\delta, \quad (12)$$

where the right-hand side is a function of ϕ alone.

General solutions to equations of type (12) are known, and it can be shown by the method of undetermined coefficients that a general solution to (12) is

$$\rho(\phi)=a\sin(\kappa\phi)+b\cos(\kappa\phi)+\delta/\kappa^2-\tfrac{1}{4}K_1(a^2+b^2) +\tfrac{1}{6}K_2ab\sin(2\kappa\phi)-(K_2/12)(a^2-b^2)\cos(2\kappa\phi), \quad (13)$$

where a and b are the two arbitrary constants of integration and κ, K_1, and K_2 are functions of the field characteristic f defined as

$$\kappa=(1+f^2)^{\frac{1}{2}}, \quad (14a)$$

$$K_1=(1+f^2+4f^3)/\kappa^2, \quad (14b)$$

$$K_2=(3+2f+3f^2+6f^3)/\kappa^2. \quad (14c)$$

The constants of integration are determined by the boundary conditions in the object space (see Fig. 1):

$$\rho(0)=(d+\alpha l_0)/r_0, \quad (15)$$

where d is the object ordinate and l_0 is the object distance; and

$$\rho'(0)=\alpha[1+\rho(0)], \quad (16)$$

since α is equal to the ratio of velocity components at the field boundary. Here the prime signifies derivation with respect to ϕ.

When (15) and (16) are carried out, it can be seen that both a and b contain terms proportional to the first power of α plus terms proportional to α^2. In addition, b also contains terms proportional to δ and d/r_0. We will assume that d/r_0 is a numeric of order equal to or greater than α^2, so that its square and cross product with α can be neglected. This restriction is not detrimental, since in practice object ordinates are either zero or the result of a second-order aberration of a previous system. The constants of integration are then easily evaluated as follows:

$$a=\alpha/\kappa-\alpha^2l_0(\tfrac{1}{3}K_2-1)/r_0\kappa, \quad (17a)$$

$$b=d/r_0-\delta/\kappa^2+\alpha l_0/r_0+\alpha^2(\tfrac{1}{4}K_1)(1/\kappa^2+l_0^2/r_0^2) +\alpha^2(K_2/12)(1/\kappa^2-l_0^2/r_0^2). \quad (17b)$$

We can now write an equation of motion for the particle in the image space II (see Fig. 1) with coordinates y and x:

$$y=r_0\rho(\Phi)+x\rho'(\Phi)[1-\rho(\Phi)], \quad (18)$$

where the coefficient of x is the divergence angle as the particle leaves the field area.

Performing operations indicated in (18) and using the above values for the constants of integration we obtain an equation of motion in the image space which can be divided into four groups of terms:

$$\begin{aligned} y=d\{&\cos(\kappa\Phi)-(\kappa x/r_0)\sin(\kappa\Phi)\} \\ &+(r_0\delta/\kappa^2)\{1-\cos(\kappa\Phi)+(\kappa x/r_0)\sin(\kappa\Phi)\} \\ &+\alpha\{(r_0/\kappa-\kappa x l_0/r_0)\sin(\kappa\Phi)+(l_0+x)\cos(\kappa\Phi)\} \\ &+\alpha^2\{[-(\tfrac{1}{3}K_2-1)l_0/\kappa-(3K_1+K_2)x/12\kappa \\ &-(3K_1-K_2)\kappa x l_0^2/12r_0^2]\sin(\kappa\Phi) \\ &+[(3K_1+K_2)r_0/12\kappa^2+(3K_1-K_2)l_0^2/12r_0 \\ &-(\tfrac{1}{3}K_2-1)xl_0/r_0]\cos(\kappa\Phi) \\ &+[K_2l_0/6\kappa+(\tfrac{1}{6}K_2-\tfrac{1}{2})(1/\kappa^2-l_0^2/r_0^2)\kappa x] \\ &\times\sin(2\kappa\Phi)+[(\tfrac{1}{3}K_2-1)xl_0/r_0-(1/\kappa^2 \\ &-l_0^2/r_0^2)r_0K_2/12]\cos(2\kappa\Phi) \\ &-[(1/\kappa^2+l_0^2/r_0^2)K_1r_0/4]\}. \end{aligned} \quad (19)$$

The largest contribution to this ordinate will, in general, be due to the terms containing the first power of α. Conditions under which the coefficient of α vanishes result in first-order focusing. We shall call all values of x for which this is true l_i, the image distance, and shall also define two new symbols for simplicity as follows: $n_0=l_0/r_0$, ratio of object distance to mean radius, and $n_i=l_i/r_0$, ratio of image distance to mean radius. We then have the well-known conditions for first-order focusing:

$$n_0n_i-1/\kappa^2=(1/\kappa)(n_0+n_i)\cot(\kappa\Phi). \quad (20)$$

Expression (19) without the terms containing α and with $x=l_i$ then becomes the image ordinate at a first-order focal point. The coefficient of d is the magnification M of the system, and the term containing δ is the

dispersion D due to the mass and/or velocity difference:

$$M=\cos(\kappa\Phi)-\kappa n_i\sin(\kappa\Phi), \quad (21)$$

$$D=(r_0\delta/\kappa^2)[1-\cos(\kappa\Phi)+\kappa n_i\sin(\kappa\Phi)]. \quad (22)$$

These equations are the same as found previously by Herzog.

The last group of terms in (19) represents the widening of the image due to the square of the diverging angle α and is thus the second-order angular aberration. It is a complicated function of the geometry of the system and of the field characteristic f [see Eqs. (14)]. The geometry of the system is represented by the field angle Φ and the object and image distances. The expression can be simplified if we define a quantity independent of Φ which will express the degree of asymmetry of the system, i.e., the relation between the object and image distances. We define z as:

$$z=\cos(\tan^{-1}(\kappa n_i))/\cos(\tan^{-1}(\kappa n_0)).^{5,6} \quad (23)$$

For symmetry $n_0=n_i$ and $z=1$. When $n_i=\infty$, $z=0$; when $n_0=\infty$, $z=\infty$. Then, in terms of z and Φ,

$$\kappa n_i=[1/z+\cos(\kappa\Phi)]/\sin(\kappa\Phi) \quad (24)$$

$$\kappa n_0=[z+\cos(\kappa\Phi)]/\sin(\kappa\Phi). \quad (25)$$

Upon substituting (24) and (25) into the last group of terms in (19), we obtain an expression for the second-order angular aberration which can be reduced by trigonometric manipulation to:

$$L=-\{K_3[(z+1)\csc^2(\kappa\Phi/2) + (z^2-z-1+1/z)\csc^2(\kappa\Phi)]+K_4[z^2+1/z]\}\alpha^2r_0. \quad (26)$$

Here L is used to denote the second-order angular aberration, and K_3 and K_4 are combinations of K_1 and K_2 such that $K_3=(f+5f^3)/[2(1+f^2)^2]$ and $K_4=(\frac{1}{2}-\frac{1}{4}f+\frac{1}{2}f^2-f^3)/(1+f^2)^2$. The magnification and dispersion are also simplified when expressed in terms of z.

$$M=-1/z, \quad (27)$$

$$D=r_0\delta(1+1/z)/\kappa^2. \quad (28)$$

Equations (26), (27), and (28) express the three most significant properties of sector shaped electromagnetic lenses of the type discussed here.

SPECIAL CASES

The manner in which the second-order angular aberration behaves with changes in any of the independent variables will be examined by considering some special cases.

First consider the aberration when Φ is an integral multiple of π/κ. It will be seen that Eq. (26) fails to yield finite answers. However, correct expressions for these cases can be derived from the last group of terms in Eq. (19). With the help of Eqs. (20), (24), and (25) it can be shown that when Φ is equal to $k\pi/\kappa$, where k is any integer, then z must equal $(-1)^{k+1}$ and n_0 is equal to $-n_i$. Thus, when k is odd,

$$L=-[3K_1+K_2+\kappa^2n_0^2(3K_1+3K_2-12)]\alpha^2r_0/6\kappa^2. \quad (29)$$

When k is even, $L=0$. Inspection of Eq. (28) shows that the dispersion D is also zero when k is even. Thus, whenever the field angle is an even multiple of π/κ, the system behaves in the same manner as the well-known 360° pure magnetic case.

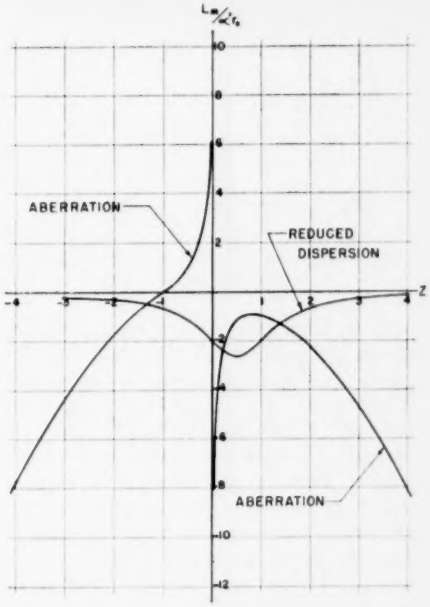

FIG. 2. Angular aberration L_m for pure magnetic sector lens as given by Eq. (30). The ordinate scale for reduced dispersion is the coefficient of δ/α^2 rather than the coefficient of α^2r_0 in Eq. (30).

Pure Magnetic Field

For a pure magnetic field f is equal to zero, $\kappa=1$, $K_3=0$, and $K_4=\frac{1}{2}$. Then (26) becomes

$$L_m=-[z^2+1/z]\alpha^2r_0/2. \quad (30)$$

This is the same expression as given by Bruche and Scherzer.[3] Figure 2 shows the variation of L_m with z. The second-order angular aberration has its minimum value in an asymmetrical analyzer for which $z=(0.5)^{\frac{1}{3}}=0.794$.

In mass spectrometers employing a sector magnetic field for making mass separations a quantity which is a better "figure of merit" for the resolving power than the dispersion is the "reduced dispersion." It is defined as the ratio of the dispersion to the angular aberration and is obtained by dividing Eq. (28) by (30). Its dependence on z is also plotted in Fig. 2. The maximum absolute value occurs when $z=\frac{1}{2}$. Thus a slightly asym-

[5] With the help of the focusing relationship (20) it can be shown that $\tan^{-1}(\kappa n_i)+\tan^{-1}(\kappa n_0)+\kappa\Phi=\pi$, which reduces to Barber's (reference 6) theorem for the pure magnetic case where $\kappa=1$.

[6] N. F. Barber, Proc. Leeds Phil. Soc. **2**, 427 (1933).

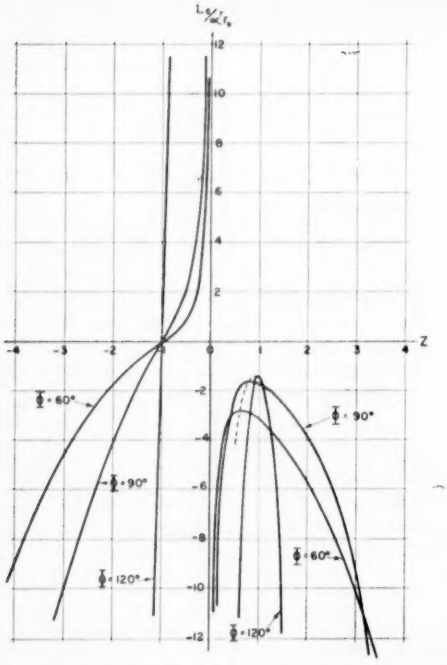

FIG. 3. Angular aberration L_a for pure electric sector lens as given by Eq. (31). Dotted curve shows loci of points of minimum aberration.

metrical analyzer, gives a reduced dispersion $\frac{1}{3}$ higher than the symmetrical analyzer used in most single focusing magnetic deflection mass spectrometers.

Pure Electric Field

For a pure electric field, f is equal to 1, $\kappa=\sqrt{2}$, $K_3=\frac{3}{4}$, and $K_4=-1/12$, and Eq. (26) becomes

$$L_e=-[(3/4)((z+1)\csc^2(\Phi/\sqrt{2}) + (z^2-z-1+1/z)\csc^2(\sqrt{2}\Phi))-(z^2+1/z)/12]\alpha^2r_0. \quad (31)$$

Unlike the pure magnetic case, the result depends upon the sector angle Φ of the cylindrical condenser, and the expression is more complicated algebraically. However, for any given value of Φ the same type of double branched curve as in the pure magnetic case can be expected. In Fig. 3 is plotted the angular aberration L_e as a function of z for three values of Φ.

As in the magnetic case, the lower right branch of the curve is the most interesting, as the other branch produces the trivial case at $z=-1$. In general the minimum absolute value of the aberration in the right-hand branch occurs for $z<1$. The dotted line traces the path of the minimum which can be seen to approach $-(4/3)\alpha^2r_0$ as Φ approaches $\pi/2^{\frac{1}{2}}$. Because of the indeterminacy discussed previously, the plot for $\Phi=\pi/2^{\frac{1}{2}}$ would be a semi-infinite line extending down $z=1$ from a value of $-4/3$.

Simple Symmetric Systems With Superimposed Electrostatic and Magnetic Fields

As an example of how the field characteristic f affects the angular aberration consider the symmetric case, i.e., $z=1$. Then from (26):

$$L=-[2K_3\csc^2(\kappa\Phi/2)+2K_4]\alpha^2r_0. \quad (32)$$

In Fig. 4 we have plotted the value of L for $f=1$, $\frac{1}{2}$, 0, $-\frac{1}{2}$, and -1. These five curves give us a general idea of the behavior of the aberration for symmetric cases as we vary the deflecting field from pure electric to pure magnetic, but with both tending to bend the ions in the same direction; and then on into the negative values of f, where the electric and magnetic fields oppose each other but the magnetic predominates.

We see that for the pure electric field the angular aberration has its minimum value of $-4\alpha^2r_0/3$ for the familiar[7] case, $\Phi=\pi/\sqrt{2}$, when the object and image are located at the boundary of the field. Also, it is seen that for small negative values of f there exist cases where the second-order angular aberration is zero. These cases are of limited interest in our consideration. In general they will not give energy focusing. Also the construction of cylindrical electric condensers of sufficient size to give a uniform field over the region where an ion beam may travel requires a rather large air gap in the magnet with the result that the cost of the magnet and associated power source may be considerable.

SYSTEMS EMPLOYING ELECTRIC AND MAGNETIC FIELDS IN TANDEM

A number of successful double focusing instruments have been constructed employing sector electric and magnetic deflecting fields in tandem. In these systems the image point of the electric field serves as the object point of the magnetic field; and they are so constructed that any small chromatic aberrations occurring in the electric lens are canceled by an equal but opposite aberration in the magnetic lens. The compound system then possesses velocity focusing as well as first-order divergence focusing. Such a compound system is illustrated in Fig. 5. It is especially true in these systems that the second-order angular aberration is the limiting factor in either resolution or intensity. For example, the instrument of Bainbridge and Jordan[8] consists of a $\pi/2^{\frac{1}{2}}$ electrostatic analyzer followed by a 60° symmetric magnetic analyzer. The angular aberration in the electrostatic image plane is $-(4/3)\alpha^2r_0$. Since the magnification of any symmetric magnetic system is -1, the $-(4/3)\alpha^2r_0$ will be subtracted from the $-\alpha^2r_0$ of the magnetic system leaving the net angular aberration as $+\frac{1}{3}\alpha^2r_0$. The instruments of Dempster[9] and Mattauch[10] have similar residual angular aberrations.

[7] A. L. Hughes and V. Rojansky, Phys. Rev. **34**, 284 (1929).
[8] K. T. Bainbridge and E. B. Jordan, Phys. Rev. **50**, 282 (1936).
[9] A. J. Dempster, Phys. Rev. **51**, 67 (1937).
[10] J. Mattauch, Phys. Rev. **50**, 617 (1936).

With the help of the more general formula for angular aberrations, (26), it can be shown that it is possible to construct instruments which possess both velocity focusing and second-order divergence focusing.

As noted in Fig. 5, the compound system contains eight geometrical parameters: Φ_e, r_e, l_{oe}, l_{ie}, Φ_m, r_m, l_{om}, and l_{im}. The subscript e refers to the electric system and m to the magnetic system. These are not all independent since the first-order focusing relationship (20) must be satisfied for both systems, and also any proportional change could be made on all the lengths involved without changing the characteristics of the system. Basically then, there are five independent variables. For mathematical work it is convenient to consider these as Φ_e, Φ_m, z_e, z_m and the ratio r_e/r_m. To obtain the desired results, two more conditions must be met by these parameters; the final first-order chromatic aberration must be zero and the final second-order angular aberration must also be zero. It is apparent that mathematical solutions will exist even though three of the five variables are arbitrarily specified.

For actual use solutions must be found which also satisfy a number of practical considerations. These are listed below:

1. All quantities must be real and all field angles must be positive.

2. The object and image distances for the electrostatic analyzer should be positive and greater than zero. Correction for the fringing field at entrance and exit can then be made using the calculations of Herzog.[11]

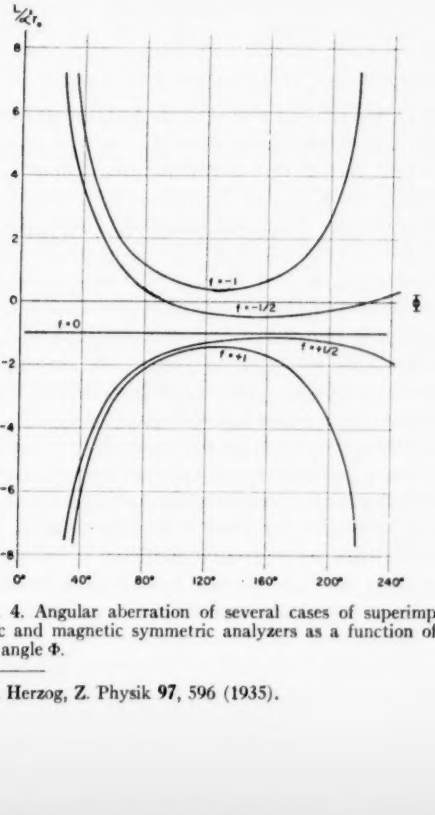

FIG. 4. Angular aberration of several cases of superimposed electric and magnetic symmetric analyzers as a function of the sector angle Φ.

[11] G. Herzog, Z. Physik **97**, 596 (1935).

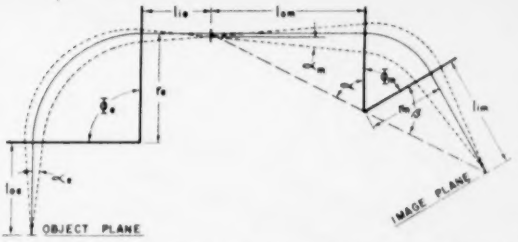

FIG. 5. Typical double focusing system employing electric and magnetic lenses in tandem.

3. The final image slit must be away from magnetic or electric fields so that it will be easy to use various kinds of detection systems for the ions, e.g., an electron multiplier of the Allen[12] type.

4. The ion source should be sufficiently removed from both the electric and magnetic analyzing fields that if an ion source magnet is used for collimating an electron beam in the source, its field will not affect the analyzers.

5. The magnetic field sector must be reasonably small, 90° or less, so that the cost of the magnet will not be unduly high.

6. The apparatus must not have unreasonable dimensional tolerances which would lead to exorbitant expense of construction.

To investigate cases where a combination of velocity focusing and second-order divergence focusing are possible, we will simply solve two simultaneous equations—the first being the velocity focusing condition, and the second the second-order divergence focusing condition.

These are:

$$M_m D_e + D_m = 0, \tag{33}$$

$$M_m L_e + L_m = 0. \tag{33a}$$

The dispersions symbolized by D_e and D_m are those suffered by an ion with the mean mass, m_0, but with a small velocity difference, β (see 5c). The equations can be solved by ordinary algebraic techniques and with the help of the following expressions from the preceding sections:

$$M_m = -1/z_m, \tag{27}$$

$$L_m = -(z_m^2 + 1/z_m)\alpha_m^2 r_m/2, \tag{30}$$

$$L_e = -\{9[(z_e+1)\csc^2(\Phi_e/\sqrt{2}) + (z_e^2 - z_e - 1 + 1/z_e)\csc^2(\sqrt{2}\Phi_e)] - [z_e^2 + 1/z_e]\}\alpha_e^2 r_e/12, \tag{31}$$

or

$$L_e \equiv -\alpha^2 r_e K_e \tag{34}$$

for simplicity. From (28), with $\delta = \beta$ and $\kappa = 1$,

$$D_m = r_m\beta(1 + 1/z_m). \tag{35}$$

[12] J. S. Allen, Phys. Rev. **55**, 966 (1939); Rev. Sci. Instr. **18**, 739 (1947).

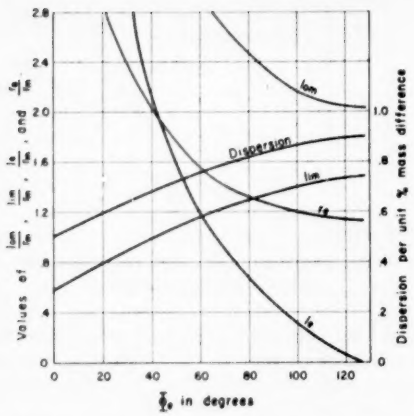

FIG. 6. Variation of ratios of l_{om}, l_{im}, l_e and r_e to r_m as a function of Φ_e for instruments which employ electric and magnetic sector fields in tandem and for which there is first order velocity and second order angle focusing. Figure also shows corresponding dispersion per r_m per percent of mass difference.

From (28), with $\delta=2\beta$ and $\kappa=\sqrt{2}$,

$$D_e=r_e\beta(1+1/z_e). \tag{36}$$

The square of the divergence angle of the mean beam as it enters the magnetic field, α_m^2, is of course the square of the diverging angle as it leaves the electric field—that is [see (16) and (18)],

$$\alpha_m^2=[\rho'(\Phi_e)]^2=z_e^2\alpha_e^2. \tag{37}$$

Thus in terms of the geometric parameters, Φ_e, Φ_m, z_e, z_m, and r_e/r_m, both (33) and (33a) can be satisfied if

$$z_m=\tfrac{1}{2}\pm[2K_e/(z_e^2+z_e)-\tfrac{3}{4}]^{\frac{1}{2}} \tag{38}$$

and

$$r_e/r_m=(1+z_m)/(1+1/z_e). \tag{39}$$

(39) is the velocity focusing condition which is the same as that derived by first-order theory. The quantity, $2K_e/(z_e^2+z_e)$, which we shall call A for convenience, is a function of Φ_e and z_e. Thus, whenever Φ_e and z_e are such that A is greater than $\frac{3}{4}$, there will be two real values of z_m, at least one of them positive, for which the second order angular aberration is zero. Φ_m, the magnetic field angle, does not enter into the mathematical conditions since, as noted earlier, the actual size of the angle does not influence the magnification, dispersion, or aberrations in a pure magnetic system. It does enter into the practical consideration, however. We shall now investigate the range of values possible in A with two objectives: (1) to find when $A>\frac{3}{4}$ and (2) to find the corresponding values of z_m. This second objective is of interest because of the manner in which the dispersive power of the instrument for a given percentage mass difference, γ, depends on z_m. From (28) with $\delta=\gamma$ and $\kappa=1$:

$$D=r_m\gamma(1+1/z_m). \tag{40}$$

Thus, the smallest possible value of z_m will produce a system with the largest dispersion. In terms of Φ_e and z_e,

$$A=3/2[(1/z_e)\csc^2\sqrt{2}\Phi_e/2+(1-1/z_e)^2\csc^2\sqrt{2}\Phi_e] -(1/6)(1-1/z_e+1/z_e^2). \tag{41}$$

It is evident that, at least for $z_e>0$, A can be easily made as large as desired by reducing the size of Φ_e, so that real values of z_m are assured.

Very small values of z_m could be had if the quantity A were near the value $\frac{3}{4}$. By holding Φ_e fixed and minimizing (41) with respect to z_e, we can find the minimum possible value of A, and the corresponding z_m as well as z_e for any given value of Φ_e. Table I shows minimum values of A and the corresponding values of z_e and z_m for values of Φ_e between 0 and $\pi/\sqrt{2}$ radians. This covers the entire range of possible values for $A_{\min}$ because of the manner in which Φ_e enters into (41). It can be seen that A is always greater than one, and that, therefore, second-order focusing can be achieved with some real and positive values of z_m for any values of Φ_e and z_e. Conversely, however, second-order focusing cannot be achieved in systems in which z_m is between 0 and 1. It can be seen that $A_{\min}$ is quite insensitive to changes in Φ_e. It approaches the value 1 as Φ_e approaches zero, which means very small negative values of z_m; however, when Φ_e is less than about 65°, values of z_e necessary for the minimum values of A are negative. Inspection of (25) will show that this would mean a negative value of the electric field object distance which violates our practical consideration No. 2.

TABLE I. Maximum dispersion mathematically obtainable for various values of Φ_e.

Φ_e	$A_{\min}$	z_e	z_m	Dispersion/$r_m\delta$
0°	1.000	−1.00		
20°	1.050	−1.092	−0.047, 1.047	−10.3, 0.978
40°	1.176	−1.568	−0.153, 1.153	− 2.77, 0.933
60°	1.311	−5.975	−0.249, 1.249	− 1.50, 0.900
80°	1.372	+2.643	−0.289, 1.289	− 1.23, 0.888
100°	1.362	+1.256	−0.282, 1.282	− 1.27, 0.890
120°	1.337	+1.014	−0.266, 1.266	− 1.38, 0.895
127°17′	1.333	+1.00	−0.264, 1.264	− 1.39, 0.896

Practical systems, in which the electric field angle Φ_e is less than 65° can, of course, be constructed. However, z_e must be positive and therefore the values of A will be greater than the minimums listed in Table I. Figure 6 illustrates how, for a given positive value of z_e, the geometric parameters of velocity focusing, second-order divergence focusing mass spectrometers vary with Φ_e. The value of z_e used is +1. Φ_m, the magnetic field angle, has been set at 60° for purposes of calculating values of l_{om} and l_{im}. Values of r_e/r_m and of the dispersion per unit percentage mass difference are independent of Φ_m. The value of r_m has been taken as unity. The value of the dispersion per unit percent mass difference is plotted as a "figure of merit" for the systems. It can

be seen to vary from 0.5 to nearly 0.9 as Φ_e approaches $180/\sqrt{2}$ degrees. The dispersion in a typical first-order divergence focusing, velocity focusing instrument such as that of Bainbridge and Jordan[8] is 1.0. It can also be seen that for Φ_e less than 60°, values of r_e, l_{oe}, l_{ie}, and l_{im} become prohibitively large. The best dispersion occurs for $\Phi_e=180/\sqrt{2}$ degrees. However, in this case l_{oe} is 0, so that practical location of ion source (or collector) is not possible. The range between $\Phi_e=60°$ and 120° seems the most practical.

The theory developed here has been used to design a mass spectrometer for precision mass determinations;[13] numerous measurements[14,15] have been made. For this instrument $\Phi_e=90°$ and $\Phi_m=60°$, r_e and r_m are 18.87 and 15.24 cm, respectively. l_{oe}, l_{ie}, l_{om}, and l_{im} are 6.61, 6.61, 34.77, and 20.73 cm, respectively.

[13] A. O. Nier and T. R. Roberts, Phys. Rev. **81**, 507 (1951).
[14] Collins, Nier, and Johnson, Phys. Rev. **84**, 717 (1951); **86**, 408 (1952).
[15] R. E. Halsted, Phys. Rev. **88**, 666 (1952).

PHYSICAL REVIEW VOLUME 91, NUMBER 1 JULY 1, 1953

The Specific Heat Discontinuity in Antiferromagnets and Ferrites*

LOUIS N. HOWARD† AND J. SAMUEL SMART
United States Naval Ordnance Laboratory, White Oak, Maryland
(Received March 24, 1953)

It is shown that, in a molecular field approximation, the internal energy and specific heat of a ferromagnet and antiferromagnet have the same form, regardless of the number of sets of neighbors whose interactions are considered and of the signs of the interactions. The Néel theory is used to derive an expression for the discontinuity in specific heat in ferrites at the Curie temperature. This discontinuity ΔC is in general smaller than it would be for a ferromagnet or antiferromagnet with the same number of atoms. Numerical calculations indicate that for most ferrites ΔC should decrease monotonically as nonmagnetic atoms are substituted for magnetic atoms on the A sites. On the other hand, if the nonmagnetic atoms go on the B sites, ΔC should pass through a maximum.

THE usual approximation of exchange interactions by a molecular field gives an expression

$$E=-\tfrac{1}{2}(NkT_c)3S_0(S_0+1)^{-1}\sigma^2 \tag{1}$$

for the internal energy of a ferromagnet. Here N is the total number of magnetic atoms, S_0 the spin quantum number of each atom, T_c the Curie temperature, and σ the reduced magnetization. The magnetic contribution to the specific heat of the material is then obtained by differentiating Eq. (1) with respect to T. It is found that at the Curie temperature the specific heat should have a discontinuity given by[1]

$$(\Delta C)_0=5Nk\,S_0(S_0+1)[(S_0+1)^2+S_0^2]^{-1}, \tag{2}$$

a result which depends only on S_0 and not on the molecular field or the Curie temperature.

It is easy to show that, for the same approximation, the same results obtain, regardless of the number of sets of neighbors whose interactions are considered and of the signs of these interactions if the magnetic atoms all occupy equivalent positions in the lattice. Thus Eqs. (1) and (2) hold for antiferromagnets as well as ferromagnets. Suppose we consider interactions of all sets of neighbors up to and including the ith. Then subdivide the original magnetic lattice into sublattices so that (a) all sublattices are equivalent under the group of translations of the original lattice, (b) each atom has only one kind of neighbors on any other sublattice, and (c) each atom has neither ith nor nearer neighbors on its own sublattice. Let the number of sublattices required be n. Then

$$E=-\tfrac{1}{2}(Ng\mu_B/n)\sum_{j=1}^{n}\mathbf{S}_j\cdot\mathbf{H}_j, \tag{3}$$

where $\mathbf{S}_j$ is the average net spin on the jth sublattice and $\mathbf{H}_j$ is the molecular field acting on atoms on the jth sublattice. We may write

$$\mathbf{H}_j=\sum_{k=1}^{n}\gamma_{jk}\mathbf{S}_k, \tag{4}$$

where $\gamma_{jk}\mathbf{S}_k$ is the internal field acting on an atom on the jth sublattice caused by its neighbors on the kth [$\gamma_{kk}=0$, from condition (c)]. Then Eq. (3) may be written in the form

$$E=-\tfrac{1}{2}(Ng\mu_B/n)\mathbf{S}'\boldsymbol{\gamma}\mathbf{S}, \tag{5}$$

where $\mathbf{S}$ is the column matrix with elements $\mathbf{S}_1, \cdots, \mathbf{S}_n$, $\mathbf{S}'$ is its transpose, and $\boldsymbol{\gamma}$ is the $n\times n$ matrix with elements γ_{jk}. Now if we use the result that the eigenvalues of $\boldsymbol{\gamma}$ are given by

$$\boldsymbol{\gamma}\mathbf{S}=3kT_c[g\mu_B S_0(S_0+1)]^{-1}\mathbf{S}, \tag{6}$$

* This work was supported in part by the U. S. Office of Naval Research.
† Now a National Science Foundation Fellow at Princeton University, Princeton, New Jersey.
[1] See, for instance, J. H. Van Vleck, *The Theory of Electric and Magnetic Susceptibilities* (Oxford University Press, London, 1932), p. 345.

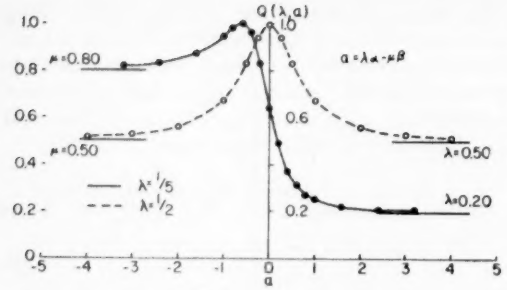

FIG. 1. Q as a function of a for $\lambda=\frac{1}{2}$ and $\frac{1}{5}$. In this and the following figures, the points indicate calculated, not experimental, values.

with $|\mathbf{S}_i|=|\mathbf{S}_j|$, then Eq. (1) follows immediately. There are of course n eigenvalues of $\boldsymbol{\gamma}$ but the largest eigenvalue and its corresponding eigenvector gives the Curie temperature and type of ordering which actually occurs. One additional point should be mentioned; ordinarily Eq. (6) is derived for the magnetization at or just below T_c, and it is perhaps not immediately obvious that it holds for all temperatures. However, we know that $|S_i|=|S_j|$ at all temperatures since the sublattices are equivalent; then if Eq. (6) holds just below T_c, it will hold in general.

It is of interest to see how Eqs. (1) and (2) are changed if the magnetic atoms occupy different classes of sites such that all sites of any one class are mutually equivalent, but any site in one class is not equivalent to any site in another class. The ferrites are probably the best-known example of such a case; here the magnetic atoms are situated on two types of crystallographic sites, usually called the A and B sites. We shall discuss this case explicitly, using the Néel theory[2] as a basis. Although the procedure described above is also applicable here with appropriate generalization, it seems preferable to use Néel's notation so that the results can be more easily compared with previous results of Néel's theory.

Let N like magnetic atoms be distributed among the A and B interstices of the spinel structure so that there are λN atoms on the A sites and μN atoms on the B sites. Néel assumes that the $A-B$ interaction is dominant and negative and that the $A-A$ and $B-B$ interactions may be either positive or negative. The molecular fields are written

$$\mathbf{H}_a=n_0(\alpha\mathbf{M}_a-\mathbf{M}_b), \quad H_b=n_0(-\mathbf{M}_a+\beta\mathbf{M}_b), \quad (7a, b)$$

where n_0 is defined as a positive quantity and α and β may be either positive or negative. The coefficients n_0, α, and β are defined for N magnetic atoms distributed as described above and are independent of whether or not there are other A and B sites occupied by nonmagnetic atoms. $\mathbf{M}_a$ and $\mathbf{M}_b$ are the magnetizations of the A and B sites, respectively, and are considered to have opposite signs. Then the internal energy is

$$E=-\tfrac{1}{2}(\mathbf{M}_a\cdot\mathbf{H}_a+\mathbf{M}_b\cdot\mathbf{H}_b)$$
$$=-\tfrac{1}{2}(Ng\mu_BS_0)^2n_0[\alpha\lambda^2\sigma_a^2-2\lambda\mu\boldsymbol{\sigma}_a\cdot\boldsymbol{\sigma}_b+\beta\mu^2\sigma_b^2]. \quad (8)$$

Here σ_a and σ_b are the reduced magnetizations of the two sites with $\boldsymbol{\sigma}_a=\mathbf{M}_a/(\lambda Ng\mu_BS_0)$ and $\boldsymbol{\sigma}_b=\mathbf{M}_b/(\mu Ng\mu_BS_0)$.

The temperature variation of σ_a and σ_b is given by the relations

$$\sigma_a=B(g\mu_BS_0|\mathbf{H}_a|/kT),$$
$$\sigma_b=B(g\mu_BS_0|\mathbf{H}_b|/kT), \quad (9a, b)$$

where B is the Brillouin function for spin S_0. To find the behavior of E near T_c, we may use the approximations for σ_a and σ_b developed by Néel:[3]

$$\sigma_a^2=\rho^2\sigma_b^2=F(S_0)\rho G(\lambda,\rho)(T_c-T)/T_c \quad (10)$$

for $(T_c-T)/T_c\ll 1$. Here

$$F(S_0)=(30/9)S_0^2\{(S_0+1)^2+S_0^2\}(S_0+1)^{-4}, \quad (11)$$

$$G(\lambda,\rho)=[\lambda\rho+\mu/\rho]/[\lambda\rho^2+\mu/\rho^2], \quad (12)$$

and ρ is the negative root of the equation

$$\lambda\rho^2+(\lambda\alpha-\mu\beta)\rho-\mu=0. \quad (13)$$

Combining Eqs. (8) and (10)–(13), we find after considerable algebra

$$\Delta C=(\Delta C)_0Q(\lambda,a), \quad (14)$$

where $a=\lambda\alpha-\mu\beta$ and

$$Q(\lambda,a)=\frac{2\lambda\mu[a^2+4\lambda\mu]}{a^2+2\lambda\mu+(\mu-\lambda)a[a^2+4\lambda\mu]^{\frac{1}{2}}}. \quad (15)$$

Thus the function $Q(\lambda, a)$ gives the ratio of ΔC for a ferrite to that for a ferromagnet or antiferromagnet with the same number of magnetic atoms. Note that it depends on the ratio of the molecular field coefficients but not on the coefficients themselves.

An investigation of the mathematical properties of

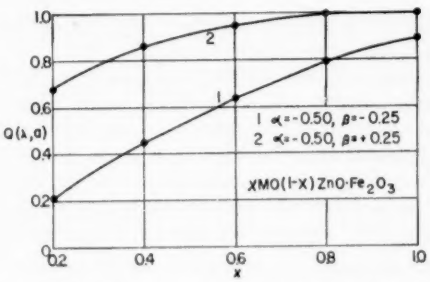

FIG. 2. Q as a function of x for mixed ferrites of the type $x\mathrm{MO}(1-x)\mathrm{ZnO}\cdot\mathrm{Fe_2O_3}$, where the Zn^{++} replaces magnetic atoms on the A sites.

[2] L. Néel, Ann. phys. **3**, 137 (1948).

[3] Reference 2, Appendix II.

$Q(\lambda, a)$ shows that $\lambda \leq Q \leq 1$ and that

$$\lim_{a\to\infty} Q=\lambda, \qquad \lim_{a\to-\infty} Q=\mu.$$

If $\alpha=\beta$, then Q is unchanged by interchange of λ and μ; if, in addition, $\lambda=\mu=\frac{1}{2}$, then $Q=1$. Both of these results are to be expected from physical considerations. Figure 1 shows Q as a function of a for $\lambda=\frac{1}{5}$ and $\lambda=\frac{1}{2}$. Most of the cases of practical interest fall between these two values of λ. It should be mentioned explicitly here that we are considering only the case where the ferrimagnetic arrangement has the highest Curie temperature and that our results do not apply if the doubly antiferromagnetic or triangular arrangements studied by Yafet and Kittel[4] have the highest Curie temperature.

Finally, we have in general

$$Q(\lambda, \lambda-\mu)=1. \tag{16}$$

The condition $a=\lambda-\mu$ is a very important one in the Néel theory.[5] It is just the condition that $|\mathbf{H}_a|=|\mathbf{H}_b|$ and $|\boldsymbol{\sigma}_a|=|\boldsymbol{\sigma}_b|$ for all temperatures. Then the curve of magnetization *vs* temperature exhibits an exact Brillouin behavior, and we get $Q=1$ as might be expected.

For most ferrites $|\mathbf{H}_a|>|\mathbf{H}_b|$ and Q is correspondingly less than unity. If α and β are determined by some independent method, such as analysis of the paramagnetic susceptibility data, then Eq. (14) may be compared with the experimental data on specific heats. However, there is no unique procedure for determining α and β from the susceptibility data and the results obtained by different methods differ considerably. This fact, coupled with the oversimplifications inherent in the Néel theory, make it evident that only an order of magnitude agreement should be expected. Comparisons were made with the data of McGuire and Howard[6] on Ferroxcube III and of Bochirol[7] on Ni and Co ferrite. The theoretical and experimental values agree to within 50 percent or less in each case.

[4] Y. Yafet and C. Kittel, Phys. Rev. **87**, 290 (1952).
[5] Reference 2, p. 155.
[6] T. R. McGuire and L. N. Howard, Phys. Rev. **78**, 342 (1950).
[7] L. Bochirol, Compt. rend. **232**, 1474 (1951).

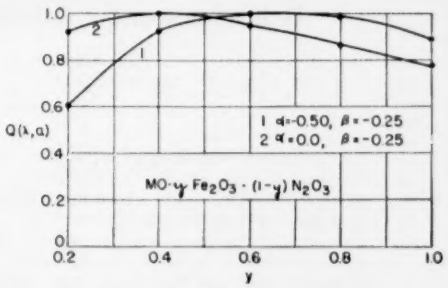

FIG. 3. Q as a function of y for mixed ferrites of the type $MO \cdot yFe_2O_3(1-y)N_2O_3$, where N is a nonmagnetic trivalent ion which replaces magnetic atoms on the B sites.

Equation (14) should be fairly reliable in predicting how ΔC varies in a series of related ferrites. As an example, we shall consider a series in which the magnetic atoms are gradually replaced by nonmagnetic ones. Figure 2 shows Q as a function of x for mixed ferrites of the form $x_{MO} \cdot (1-x)_{ZnO} \cdot Fe_2O_3$. Curves 1 and 2 are calculated for typical values of α and β with the assumptions that all of the Zn goes to the A sites and that α and β are independent of composition. It is to be noted that Q falls off monotonically with increasing Zn content. The interpretation of this effect is that $|\mathbf{H}_a| > |\mathbf{H}_b|$ for $x=0$ and that the substitution of nonmagnetic atoms for magnetic ones on the A sites further increases the inequality and diminishes Q still more.

On the other hand, if the nonmagnetic atoms go to the B sites, then the inequality should be lessened, so that Q increases and even passes through a maximum if Eq. (16) is satisfied for some intermediate composition. Figure 3 shows how Q varies as a function of composition when the Fe^{3+} ions are replaced by nonmagnetic ions N^{3+} which all go to the B sites. It is seen that a maximum does occur for the two sets of α and β chosen. A series in which such an effect might be expected is the nickel ferrite-aluminate series studied by Maxwell, Pickart, and Hall[8] and by Gorter and Herbschleb.[9]

[8] Maxwell, Pickart, and Hall, Bull. Am. Phys. Soc. **28**, No. 2, 8 (1953).
[9] E. W. Gorter (private communication).

Hall Effects of the Cobalt Nickel Alloys and of Armco Iron*†

SIMON FONER AND EMERSON M. PUGH
Carnegie Institute of Technology, Pittsburgh, Pennsylvania
(Received March 9, 1953)

Experimental investigations of the Hall effects in cobalt, the cobalt-nickel alloys, and Armco iron are described in detail. Precision measurements were made with magnetic fields up to 30 kilogauss in order to separate the ordinary and extraordinary effects. The ordinary effect in all the Co-Ni alloys was found to be negative and agreed within a factor of two with values expected from only 4*s* band conductivity. The ordinary effect in Armco iron was positive indicating hole conduction in the 3*d* band. The field parameter α was observed to be small and negative for most of the cobalt rich alloys, while it was positive for the nickel rich alloys and Armco iron. The limitations in the use of the simple two-band model for explaining the data are outlined. No explanation of α is given.

A. INTRODUCTION

IT has been shown by Stoner[1] that the number of 4*s* electrons/atom in Cu-Ni alloys at 0°K can be estimated from the saturation magnetization M_s, by using a simple band model. This simple band model has been extrapolated to Ni and Co and the Co-Ni alloys. Since it fits a large amount of magnetic data,[2] it has been widely accepted.[3] It is generally supposed that the 4*s* electrons in these metals are solely responsible for their electrical conductivity. Since ordinary Hall coefficients depend upon the number of conduction carriers, Hall measurements should check these predictions. One should expect fair agreement with measurements made at temperatures well below the Curie points of these metals.

Early Hall measurements on Fe, Co, and Ni, which were necessarily made at rather low magnetic fields, disagreed in order of magnitude with the predictions of this simple band picture and gave positive coefficients for Fe and Co. When the conduction is primarily electronic, negative coefficients are expected.

The work of Pugh and Lippert[4] on a number of ferromagnetic elements and alloys suggested that these discrepancies were attributable to internal magnetic fields, proportional to the intensity of magnetization, which were much larger than the measured fields. Studies of old data on nickel[5] indicated that if sufficient precision were available at high fields an ordinary Hall effect could be separated from the extraordinary low field value, previously reported. The ordinary coefficients obtained from these studies agreed reasonably well with the predictions of the simple band theory.

Recent measurements on Cu, Ni, and the Cu-Ni alloys[6] and on a nickel ferrite[7] have confirmed the earlier evidence[5] that the Hall potential difference E_H in ferromagnetic materials may be represented by the empirical formula

$$E_H=(H+4\pi\alpha M)R_0I/t, \tag{1}$$

where H = the magnetizing field, M = the intensity of magnetization, α = the field parameter, I = the total current in the rectangular plate sample, and t = the thickness of the sample.

If only the 4*s* band contributes to the conduction and if this band is nearly empty, the ordinary Hall coefficient, R_0, is given by

$$R_0=-1/Nn_sec, \tag{2}$$

where n_s = the number of 4*s* electrons/atom, N = the number of atoms/cc, and e and c are the electronic charge[8] and velocity of light, respectively. The measurements of Schindler and Pugh[6] on Cu, Ni, and their alloys showed that n_s from Eq. (2) agreed with the predictions of the simple band model to within a factor of 2. However, there were marked deviations from the expected values. For example, there was a large decrease in R_0 at Ni, which could be explained by assuming that there was some 3*d* band conduction.

Assuming that both the 3*d* band and 4*s* band contribute to the conduction, R_0 for the simple two-band model is given by

$$R_0=-\left\{\left(\frac{\sigma_s}{\sigma}\right)^2\frac{1}{n_s}\pm\left(\frac{\sigma_d}{\sigma}\right)^2\frac{1}{n_d}\right\}\Big/Nec, \tag{3}$$

where n_d is either the number of holes/atom in a nearly filled 3*d* band or the number of electrons/atom in a nearly empty 3*d* band; the minus sign being chosen with the former and the plus sign with the latter. The

* This research was supported by the U. S. Office of Naval Research.

† Submitted by one of the authors (SF) in partial fulfillment of the requirements for the degree of Doctor of Science at Carnegie Institute of Technology.

[1] E. C. Stoner, Phil. Mag. **15**, 1018 (1933).

[2] J. C. Slater, J. Appl. Phys. **8**, 385 (1937).

[3] F. Seitz, *Modern Theory of Solids* (McGraw-Hill Book Company, Inc., New York, 1940), pp. 434–436; R. M. Bozorth, *Ferromagnetism* (D. Van Nostrand Company, Inc., New York, 1951), pp. 434–442.

[4] E. M. Pugh, Phys. Rev. **36**, 1503 (1930); E. M. Pugh and T. W. Lippert, Phys. Rev. **42**, 709 (1932).

[5] Pugh, Rostoker, and Schindler, Phys. Rev. **80**, 688 (1950); N. Rostoker and E. Pugh, Phys. Rev. **82**, 125 (1951).

[6] A. I. Schindler and E. M. Pugh, Phys. Rev. **89**, 295 (1953).

[7] Simon Foner, Phys. Rev. **88**, 955 (1952).

[8] By convention, R_0 is defined as negative for electronic conduction, as in copper. Here the quantity e is the absolute value of the electronic charge.

total conductivity is designated by σ, and the conductivities of the 4*s* and 3*d* bands are designated by σ_s and σ_d, respectively. The coefficient R_0 approaches zero as hole conduction increases and would become positive, according to Eq. (3), when $\sigma_d^2/n_d > \sigma_s^2/n_s$. This explanation for the small negative value of R_0 in the nickel-rich Cu-Ni alloys seemed plausible because of the early work which suggested that the sign of the Hall effect in both Co and Fe was opposite to that in Ni and Cu.

The values obtained for R_0 in the Cu-Ni alloy series indicated that such measurements could give some insight into the electronic configurations in this transition group of elements and their alloys. Measurements needed to be extended through the Ni-Co alloys to Co and to Fe. However, to study these metals, it was necessary to employ larger magnetic fields and greater precision in measurements than had been available for the study of the Cu-Ni series of alloys.

B. MEASUREMENT PROCEDURE

For these measurements high sensitivity is important. The magnitude of E_H in Eq. (1) can be increased by decreasing t, but uncertainties in the determination of t decrease the accuracy when t is made too small. The samples[9] used, unless otherwise stated, were machined from cast ingots to 4.5 cm×2 cm×0.1 cm, annealed at 800°C in helium for two hours, then slowly cooled to room temperature. The sample holder was similar to that of Schindler and Pugh,[6] but pressure contacts between the sample and current electrodes were used.

In making Hall measurements on nonmagnetic materials with high resistivity, a number of systematic errors are eliminated or reduced[10] by using alternating currents and by reversing the magnetic field. However, with ferromagnetic metals, these procedures introduce more difficulties than they cure. For example, an alternating sample current induces stray potentials. This limits the sample current that can be employed profitably and thus reduces the accuracy of the measurements. Furthermore, it is difficult to attain with ac measurements the sensitivity of 2×10^{-9} volt attained here with the dc system. Therefore, a dc system has been adopted for these measurements.

A diagram of the measuring system is shown in Fig. 1. The appropriate potential (either from *c* and R_1, for the Hall emf, or from the appropriate thermocouple, for the Ettingshausen correction measurements) is fed to the Wenner potentiometer, 2, where it is balanced to the nearest 10^{-7} volt. The remaining difference potential ($<10^{-7}$ volt) is amplified by the breaker amplifier, 3,

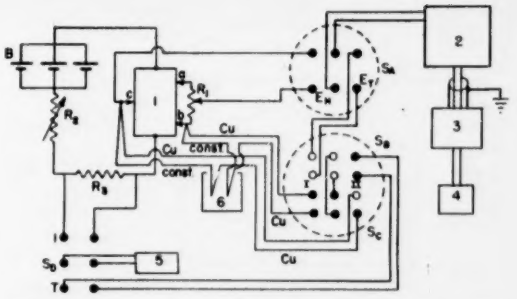

FIG. 1. Schematic diagram of dc measuring circuit: 1—sample, 2—Wenner potentiometer, 3—Liston-Folb model 10 breaker amplifier, 4—Esterline-Angus recorder, 5—portable Rubicon potentiometer, 6—ice bath; *a*, *b*, and *c*—copper probes (*a* and *b* are 4 mm apart), R_1—1Ω Micropot voltage divider, R_2—variable resistor, R_3—150-amp, 50-mv shunt, *B*—degaussing batteries, S_A, S_B, S_C—oil immersed switches.

and recorded by 4. This amplifier-recorder system is calibrated by making 10^{-7} volt changes with the Wenner potentiometer at short time intervals. Both the sample current and the temperature were measured while recording the Hall effect. In order to attain the desired sensitivity, complete electrical and thermal shielding was needed. Great care was required to avoid electrical leakage between the various elements, including the ground. Induced voltages in the measuring circuit caused by vibration or small magnetic field variations were reduced by rigidly mounting the lead wires in positions that minimized the effect of unavoidable loops in the measuring circuit. With these necessary precautions, a sensitivity of $\pm2\times10^{-9}$ volt was obtained.

The sample was mounted in the 1 in. gap between iron-cobalt poles of a new A. D. Little magnet. These poles were truncated cones, tapered from 11 in. diameter to $5\frac{3}{4}$ in. diameter. The magnetic field could be changed rapidly and reproducibly (1 part in 8000) in predetermined steps or reversed in direction by a current control system described elsewhere.[11] The field was uniform to 0.5 percent or better over a 1-in. diameter (covering the central region of the sample) for the fields used in this work. A small flux coil, mounted on the sample, in conjunction with a sensitive galvanometer arranged as a flux meter, was used to measure *B*.

Thermal stability was attained by turning on the sample current and magnet cooling system for about two hours before making measurements. A number of effects can produce temperature variations within the sample. The more important ones are the slow thermal drift of the magnet and the sample current supply system, hysteresis losses within the sample caused by changing the magnetic field, the magnetocaloric effect, and the Ettingshausen effect. The copper probes and the sample constituted a thermocouple so that any temperature variation within the sample superimposed

[9] The impurities in cobalt in percent by weight as analyzed by Westinghouse Research Laboratory are 0.52 Ni, 0.16 Fe, 0.04 Cu, 0.12 C, 0.07 Mn, and 0.01 S. The impurities in percent by weight in nickel as analyzed by the International Nickel Company were 0.12 Cu and 0.23 Co. The Armco iron was not analyzed but the nominal impurities are given as 0.015 C, 0.035 Mn, 0.025 S, 0.005 P, 0.003 Si, and traces of Cu and Ni. The compositions of the Co-Ni alloys were known to within 1 percent.

[10] E. M. Pell and R. L. Sproull, Rev. Sci. Instr. **23**, 548 (1952); J. J. Donoghue and W. P. Eatherly, Rev. Sci. Instr. **22**, 513 (1951).

[11] S. Foner, thesis, Carnegie Institute of Technology, June, 1952 (unpublished).

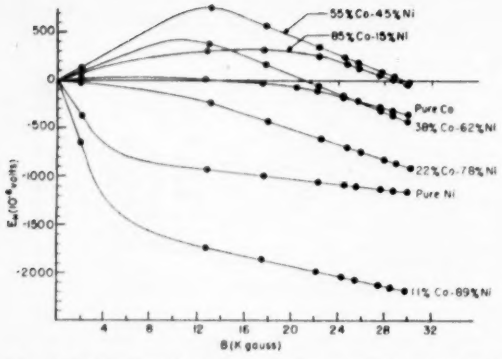

FIG. 2. Hall potential difference *versus* magnetic induction for the Co-Ni series of alloys normalized to $I=25.0$ amp, $t=0.1$ cm for temperatures from 9 to 13°C.

potentials on the Hall potential. The emf's caused by small thermal drifts were eliminated by observing the change in potential for incremental field changes and subtracting the potential drift (quite small) from the field dependent contributions. Using the copper constantan thermocouples (Fig. 1), the field dependent temperature variation at the probes (such as the Ettingshausen effect) could be measured to about 3×10^{-4}°C in spite of a fairly large thermal drift. If the Ettingshausen temperature change is measured with field reversals (at various fields) the magnetocaloric effect (already suppressed to a large extent by the thermal conduction of the current leads) is eliminated, since it does not reverse with field direction. The Ettingshausen correction for R_0 was less than 1 percent for all the metals studied, except Ni for which 2 percent correction was made. The Ettingshausen correction for α was 0.1 or less.

Nearly adiabatic boundary conditions were imposed by the method of measurement. For metals, it is usually assumed that the heat current, which is conducted along with the primary electric current, does not produce an appreciable temperature gradient along the direction of the primary electric current because of the high thermal conductivity. However, a small temperature gradient along the sample which reversed with reversal of the primary electric current, could be observed by the thermocouples at probes *b* and *c* in Fig. 1, which were placed about 2 mm apart along the length of the sample. The maximum temperature difference between probes *b* and *c* was 0.4°C for some of the Co-Ni alloys but was at least an order of magnitude smaller for pure Co and Armco iron. Calculations showed that the corrections to the Hall effect because of the transverse thermomagnetic effects, resulting from this temperature gradient, were negligible. A detailed consideration of the various electric and thermal effects and their boundary conditions has been given by Sommerfeld and Frank.[12]

[12] A. Sommerfeld and N. H. Frank, Revs. Modern Phys. **3**, 1 (1931).

C. EXPERIMENTAL PROCEDURE FOR REDUCING SYSTEMATIC ERROR

Usually Hall measurements are made by reversing the the applied magnetic field and observing the corresponding changes in potential so that any potentials which do not reverse with reversal of the applied field are experimentally eliminated. In principle such a procedure could be used here. However, with ferromagnetic metals, this procedure introduces several difficulties. Generally, in the ferromagnetic materials, the Hall potential changes rapidly at low fields and much more slowly at fields above saturation. High field data must be examined very accurately to obtain R_0 and α. Thus when the field reversal method is used for these measurements, large potentials are observed which must be subtracted from each other. Large errors are inherent in such procedures. Furthermore, large hysteresis and eddy current losses are encountered in ferromagnetic metals with field reversal, so that extraneous thermal effects are introduced which further limit the precision. Thus, the incremental method of measurement leads to much greater accuracy in R_0, especially, if the small field-dependent potentials which do not reverse with field reversal are eliminated by the procedure described in Sec. *D*.

Because of the small, extraneous potentials which depend on the field but do not reverse with it, the observed incremental potentials are different for different directions of the field; i.e., the observed slope of E_H *vs* B curve at high fields changes slightly when the field is reversed. Fortunately, these extraneous potentials are much less field dependent at high fields than at low fields. The errors caused by these potentials can be eliminated by averaging the ordinates of the curves obtained with the two field directions.

The origin of these small potentials is uncertain. They may be the result of field dependence of the resistivity of the sample (magnetoresistance) or to field dependence of the thermocouple constant of the circuit composed of the copper probes and the sample. While both effects must be present, tests indicate that the magnetoresistance effect is the most important.

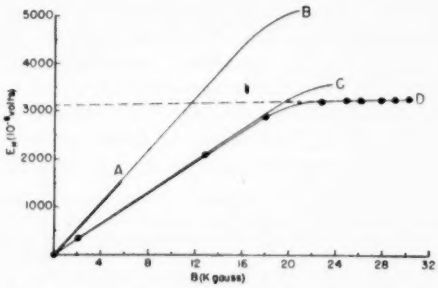

FIG. 3. Hall potential difference *versus* magnetic induction for Armco iron, curve *D* compared with curves *B* and *C* by Smith in 1910 and *A* by Unwin in 1921, all normalized to $I=25.0$ amp, $t=0.1$ cm at room temperatures (curve *D* at 13°C).

In practice, it is not feasible to change R_1 (Fig. 1) during a series of measurements. For this reason R_1 is positioned so that a small bias is applied to the measuring system to prevent drift from reversing the polarity of the potential applied to the potentiometer. This avoids the spurious potentials that would be introduced by a reversing switch in this circuit. Thus this bias depends upon the resistivity of the sample, which in turn depends upon the magnitude but not the direction of the field.

Several experiments were conducted to study this effect. They included reversing the direction of the primary current, changing the setting of R_1, and varying the magnitude and reversing the direction of the magnetic field. The dependence of this effect upon the material of the sample was also investigated. The results of all of these experiments could be satisfactorily explained by assuming a transverse magnetoresistance effect. Two extensive sets of data for the 11 percent Co–89 percent Ni sample were taken, one immediately after the other. The primary current direction was reversed for one of these sets and R_1 was carefully repositioned to obtain identical bias conditions. The positioning of the sample and leads was not disturbed. The two values of R_0 obtained agreed to within 0.1 percent. No difference in magnitude of this extraneous effect at high fields could be detected.

If the effect is attributable to a transverse magnetoresistance, it should be most noticeable near the Curie temperature. To test this, measurements were made on on a sample containing 70 percent Ni–30 percent Cu, whose Curie point is near room temperatures. As expected, the effect was larger than in any of the Co-Ni alloys.

D. EXPERIMENTAL RESULTS

The variations of Hall emf with magnetic induction, B, for a number of Co-Ni alloys, normalized to a current of 25.0 amp and a thickness of 0.100 cm (values near to the experimental ones), are shown in Fig. 2. All of the data presented in this paper were obtained by the following procedure. The changes of Hall emf with incremental changes in field were arithmetically averaged for three or more runs. The same procedure was then used for the field in the reverse direction and the results for the two field directions were averaged algebraically to obtain the experimental points. In this way, any potentials which did not reverse with field direction were eliminated. The differences in the slopes of the E_H *vs* B curves for opposite field directions above magnetic saturation were less than 1 percent for all the metals except Ni.

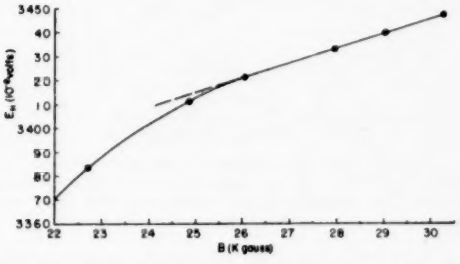

FIG. 4. Hall potential difference *versus* magnetic induction for Armco iron, showing the high field part of curve D in Fig. 3.

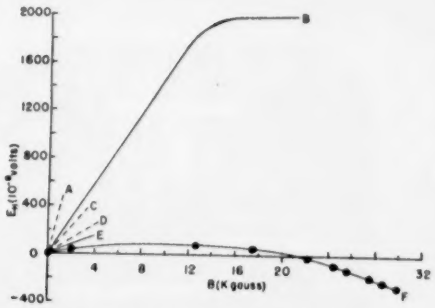

FIG. 5. Hall potential difference *versus* magnetic induction for cobalt at room temperature. Curves A and C by Ettingshausen and Nernst (1886), B by Smith (1910), D by Unwin (1921), and E by Zahn (1904), are compared with the new data F, all normalized to $I=25.0$ amp and $t=0.1$ cm.

The origin of coordinates for each of the E_H *vs* B curves was determined by observing the change in Hall emf for field reversals at some field well above magnetic saturation. The curves above saturation were straight lines within the accuracy of measurement for all of the ferromagnetic metals investigated.

No previous Hall data are available for the Co-Ni alloys, though early results on the elements Ni, Fe, and Co are available. The new data on Ni, shown in Fig. 2, agree well with older experiments at low fields and extend the results to higher fields.

The new data on Armco iron are shown by curve D in Fig. 3. Early results on iron also are plotted in Fig. 3 for comparison. Curve A[13] (which extends only to 6.3 kilogauss) and B[14] are not in good agreement with curves C[14] and D. This may be explained by the higher purity of the iron used in C and D. The high field portion of curve D is shown in Fig. 4. It is interesting to note that the iron was obviously not saturated below 26 kilogauss.

The rather large spread of the early low field data for cobalt is shown by the comparisons in Fig. 5. Unfortunately, the values of magnetic induction used in the early experiments are not available for curves A, C, or D. Curve E extends only to 4 kilogauss. The initial slopes of the curves in Fig. 5 are all positive, which explains why positive Hall coefficients for cobalt are found in the early literature. However, the new data taken up to high fields as shown by curve F in Fig. 5 demonstrates that the ordinary Hall coefficient

[13] F. Unwin, Proc. Roy. Soc. (Edinburgh) **41**, 44 (1921).
[14] A. W. Smith, Phys. Rev. **30**, 1 (1910).

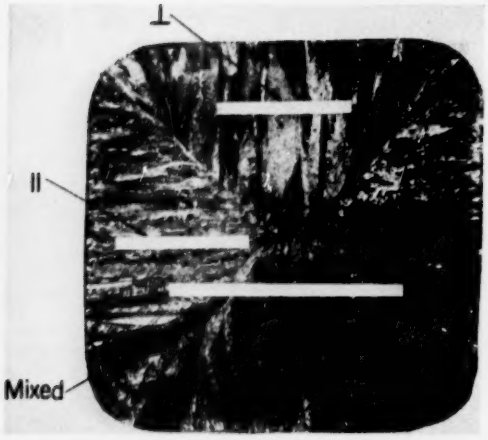

FIG. 6. Cross section of columnar cobalt ingot, etched to show the relative positions of samples used for the Hall effect measurements that are plotted in Fig. 7.

is negative in cobalt, a fact which certainly is not apparent from curve B.

The large discrepancies between the curves in Fig. 5 suggested the possibility that Hall effects in cobalt may be structure sensitive. When the cobalt ingot from which the sample was cut was etched and photomicrographed, the pronounced columnar structure shown in Fig. 6 was revealed. X-ray analysis of an unannealed section of this ingot indicated the presence of both cubic and hexagonal cobalt. Because of the sluggish phase transformation that takes place around 300°C, such mixtures are fairly common in cobalt. The direction perpendicular to the columnar axis was the (100) direction in the f.c.c. phase and the (10·1) direction in the h.c.p. phase. If the Hall effects are strongly structure sensitive, Hall measurements might be expected to vary with the orientation of the columnar axis. Accordingly, two differently oriented samples (designated ⊥ and ||, depending on the direction of the columnar axis with respect to the face of the sample) were cut from this ingot as shown in Fig. 6. The location from which the original sample was cut is indicated by the designation "mixed" in Fig. 6. While the original sample was annealed before the Hall measurements were made, the two new samples were left unannealed to preserve their orientations. The Hall measurements made on these three samples[15] at fields above 12 kilogauss are plotted in Fig. 7. Since the slopes of the three curves are nearly the same at high fields, R_0 is nearly the same for all. The small vertical displacement between the ⊥ and || curves indicate that α is only slightly dependent upon the orientation. The somewhat larger displacement of these two from the curve for the "mixed" crystal is apparently the result of the dependence of α on the state of anneal. Certainly differences in orientation cannot account for the large variations in the Hall effects indicated by the curves shown in Fig. 5.

It appears that the large spread of data in Fig. 5 must be attributed to the variability in the impurity content of the cobalt used. Analysis of the early papers of Ettingshausen and Nernst,[16] Smith,[14] Unwin,[13] and Zahn[17] show that they had great difficulties trying to procure pure cobalt. For example, the curves A and C were measured on two samples of what was believed to be the same material. In a private communication, A. W. Smith states that his Co undoubtedly contained impurities. Unwin and Zahn both attempted to produce electrolytic cobalt. The results of the latter two investigators (curves D and E) agree more closely with the results obtained here for cobalt[9] shown in curve F.

E. ANALYSIS OF DATA AND RESULTS

1. Methods of Analysis

The analysis of the data follows directly from the empirical formula. The Hall constant R may be defined by $R=(t/I)(\partial E_H/\partial B)$, and, from Eq. (1), substituting $H=B-4\pi M$,

$$R=\frac{t}{I}\frac{\partial E_H}{\partial B}=R_0\left[1+4\pi(\alpha-1)\frac{\partial M}{\partial B}\right], \qquad (4)$$

so that $R=R_0$ when $\partial M/\partial B=0$ or when $\alpha=1$. Therefore, when the temperature of the ferromagnetic metal is not too close to its Curie point, $\partial M/\partial B$ is so small, at high magnetic fields, that R may be considered equal to R_0. The slope of the straight line portion of the E_H vs B curve above saturation then can be used to calculate R_0. When M is a constant equal to M_s at high fields, α may be calculated in two independent

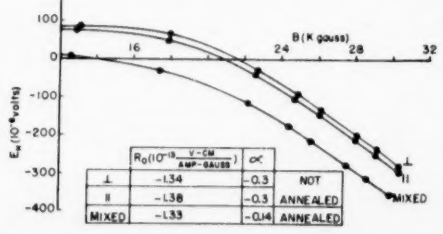

FIG. 7. Hall effect in differently oriented columnar cobalt samples compared with an annealed sample having a mixed orientation, all normalized to $I=25.0$ amp and $t=0.1$ cm at temperatures between 9 and 13°C.

[15] Notice that the temperature for mixed Co in Fig. 7 is lower than for that shown in Fig. 5. A limited range of temperatures from 8 to 25°C was used for these measurements. The absolute magnitude of the initial slope of the E_H vs B curves increased slightly with increasing temperature for all the Co-Ni alloys and Armco iron over this range. This temperature dependence agrees with Smith's data below the Curie temperature for iron, cobalt, and nickel and also with data of Lippert and Pugh on 70 percent Fe–30 percent Ni.

[16] H. Zahn, Ann. Physik **14**, 924 (1904), discusses the iron impurities in the samples used by Ettingshausen and Nernst.

[17] H. Zahn, Ann. Physik **14**, 886 (1904).

ways[7] as a test of the applicability of Eq. (1). Extrapolating the high field straight line back to the $B=0$ axis and substituting in Eq. (1), the intercept is $4\pi(\alpha-1)M_sR_0I/t$. Thus, without using the low field data, α can be determined if M_s is known. The second method uses the low field data. Equation (4) may be written as

$$\frac{\partial E_H}{\partial B}=\left[\alpha+(1-\alpha)\frac{1}{\mu}\right]\frac{R_0I}{t}, \tag{5}$$

where μ is the incremental permeability. At low fields $\mu\gg1$ and at high fields $\mu\cong1$, so that the ratio between the low and high field slopes determines α. Thus there are two independent methods for determining α when the E_H *vs* B curve is a straight line at high fields. In general, these two values of α will be equal only if Eq. (1) is applicable and if $\partial M/\partial B$ is negligible at the highest fields employed. Another method of calculating α (equivalent to the first method) is convenient for curves of the type shown in Fig. 8. Using Eq. (1) and extrapolating the straight line portion at high fields to the $E_H=0$ axis, where $B=B_0$,

$$\alpha=1-(B_0/4\pi M_s). \tag{6}$$

For this special type of curve a null detection method[18] can be used for determining α.

2. Verification of the Empirical Formulation

The values of α obtained from the ratio of the low and high field slopes in Fig. 2 are in good agreement with the values for α given in Fig. 9. The low field data were too limited for this to constitute a proof of the validity of Eq. (1), which here is presumed to have been established at low fields by experiments reported

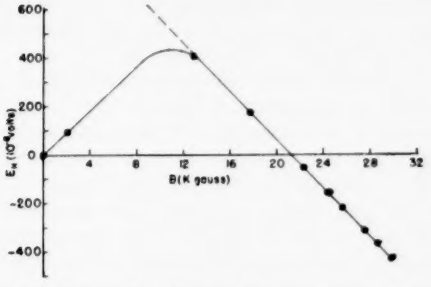

FIG. 8. Hall potential difference *versus* magnetic induction for 38 percent Co in Ni, normalized to $I=25.0$ amp and $t=0.1$ cm at 9°C.

[18] Ferromagnetic metals which show a behavior similar to that in Fig. 8 may be examined quite easily to determine α for the other transverse galvano- and thermomagnetic effects. If Eq. (1) applies to these transverse effects and if $M=M_s$ where the E_H *vs* B curve crosses the B axis, a null detection method can be used to obtain α very simply. By observing the change in the transverse potential or the transverse temperature difference with the reversal of various values of B until a null is obtained, B_0 can be determined. If M_s is known from an independent measurement, Eq. (4) gives the value of α.

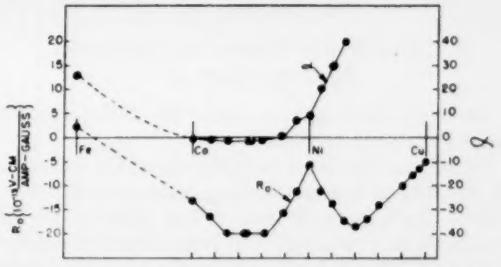

FIG. 9. Values of R_0 and α *vs* composition for elements and binary alloys from Fe to Cu.

previously.[4] A better check was found in the Armco iron data where the slopes could be determined more accurately; the initial slope from Fig. 3 and the final slope from Fig. 4. The value of α obtained from the intercept is 25.6 (using $4\pi M_s=21.6$ kilogauss) while that obtained from the ratio of slopes is 26.2. This excellent agreement indicates that Eq. (1) is valid and that sufficiently high fields were used to accurately determine R_0. Figure 4 illustrates the importance of making measurements at sufficiently high fields, for the E_H *vs* B curve does not become a straight line until 26 kilogauss has been exceeded. The point at 26 kilogauss is actually 4×10^{-9} volt below the straight line while the three points at higher fields deviate by less than 1×10^{-9} volt.

3. Results

The results obtained to date with the ferromagnetic elements and alloys, including those on the previously investigated Cu-Ni alloys,[6] are shown in Fig. 9. The values of R_0 were obtained from high field data assuming $R=R_0$ in Eq. (2). The values for α were obtained by extrapolating the high field straight line portion of the E_H *vs* B curve to the convenient E_H or B axis. Corrections[6] to R_0 should be made for the Cu-Ni alloys between 20 percent and 60 percent Cu because α was large and $\partial M/\partial B$ at room temperatures was not small enough to be neglected, since at room temperatures these alloys were too near to their Curie points. No such corrections were needed for the data on Ni-Co alloys. The Curie temperature of these alloys increases almost linearly from Ni to Co (Ni 358°C, Co 1115°C). Thus with measurements made at room temperatures, these alloys were far below their Curie points and $\partial M/\partial B$ could be neglected at high fields. Furthermore, from Fig. 9, α is quite small for the Co-Ni alloys. The combination of a small $\partial M/\partial B$ and a small α assures that $R=R_0$ to a high accuracy. Although the Curie temperature for Armco iron is high (770°C), its α is so high that a small correction of the order of 3 percent for R_0 would be required if $\partial M/\partial B\sim10^{-4}$. Since no data are available yet for Co-Fe alloys, the lines for α and R_0 are dashed between these two elements.

F. DISCUSSION

1. The Effective Number of Conduction Electrons/atom, n^*

Corrected values of R_0, α, and n^* for all the annealed samples are listed in Table I.

The n^* was calculated from Eq. (2) and is plotted in Fig. 10 along with the number, n_s, of 4*s* electrons/atom, inferred from magnetic data.[19] The value of n^* for Armco iron is -3.02 (i.e., 3.02 holes). For convenience in plotting Fig. 10 has not been extended to include this point. The data for the Cu-Ni alloys were obtained from the work of Schindler and Pugh.[6] The agreement between n^* and n_s within a factor of two from Cu to Co is as good as that found for most monovalent metals. Compared to the earlier results obtained at low fields for Ni, Co, and Fe, this agreement is remarkable. From this early data n^* was too low in Ni by a factor of 20, of the opposite sign and too low in Co by a factor of 10, and too low in Fe by a factor of 30.

2. The Field Parameter α

At present the quantity α is not well understood. Pugh and Rostoker[20] have recently discussed a number of proposals for explaining this quantity and have shown that none of them appear entirely satisfactory. It appears to be a much more complex quantity than R_0.

If α does represent an effective field term, it should be observed in other conduction phenomena. Smit[21] has used a similar effective field formulation for his low temperature magnetoresistance data on some ferromagnetic metals and finds $\alpha \sim 2$ for Ni and $\alpha \sim 1$ for Fe at liquid nitrogen temperature. This is in good agreement with $\alpha = 1.9$ for Ni obtained by Jan and Gijsman[22] from Hall measurements at this same temperature. They also measured the low field Hall effects for iron at low temperatures and thus determined the product $R_0\alpha$, but they were unable to obtain sufficiently high fields to determine R_0 separately. By using the value of R_0 determined here at room temperatures for Armco iron, an approximate value of α can be calculated from their data. The result, $\alpha = 1.3$, is again in good agreement with Smit's value of $\alpha \cong 1$ for Fe. This calculation assumes that in Fe the low temperature R_0 is close to that at room temperature, which may not be valid. For example, Jan and Gijsman found that R_0 in Ni at low temperatures was about half that at room temperature. These limited data do suggest that the effective field $H + 4\pi\alpha M$ in Eq. (1) may be the same quantity observed by Smit in his magnetoresistance measurements.

TABLE I. Corrected values of R_0, α, and n^* for the annealed samples.

Composition percent Co in Ni	$R_0\left(10^{-13}\frac{\text{v-cm}}{\text{amp-gauss}}\right)$	α	t(°C)	n^*
0	− 5.6	9.3	9	1.23
11	−11.3	7.3	8	0.61
22	−15.6	0.1	11	0.44
38	−19.9	−1.0	9	0.35
53	−19.6	−1.3	10	0.35
55	−19.5	−1.4	12	0.36
70	−19.6	−1.1	12	0.35
85	−16.4	−0.9	13	0.42
100	−13.3	−0.14	14	0.53
Armco iron	+ 2.45	25.6	13	−3.02

3. Two Band Model

Although the experimentally determined n^* shown in Fig. 10 agrees to within a factor of two with n_s, the deviations are too great to be accounted for by experimental error. The values of n_s plotted in Fig. 10 are taken from the two band model that has been used to account for the saturation magnetization of these metals. If the values of R_0 could be interpreted in terms of band models, Hall measurements would provide considerable information concerning the electronic structure of these bands.

It has been shown[5] that the high value of n^* in Ni can be accounted for by assuming that the 3*d* band also contributes to the conduction. Schindler and Pugh[6] point out that the low values of n^* they obtained for the alloys containing from 30 percent to 60 percent Cu in Ni should not be taken too seriously, since these alloys were measured[23] at temperatures near to or above their Curie points. Corrections[6] for the fact that $\partial M/\partial B \neq 0$ at high fields are in the right direction to improve the agreement with predicted values.

In comparing values of n^* with those of n_s, it is convenient to proceed to the left in Fig. 10 from 20 percent Cu in Ni toward Co. As Ni is approached the rise in n^* relative to n_s can be attributed to the increased conductivity in the 3*d* band caused by the increase in the number of holes. The decrease in n^* beyond Ni can then be attributed to the decrease in conductivity in the 3*d* band because of the decreasing mobility in this band as $\partial^2\epsilon(k)/\partial k^2$ approaches zero. One might then expect that, when n^* goes below n_s beyond 12 percent Co in Ni, the conduction in the 3*d* band changes to the electronic type. However, small amounts of electronic conduction in the 3*d* band would make n^* larger rather than smaller than n_s. Actually Eq. (3) will yield values of $n^* < n_s$ only for very large values of σ_d/σ. This becomes clear when Eq. (3) is written in terms of the ratio δ obtained by dividing the

[19] The value of M_s increases almost linearly from Ni to Co so that the number of holes in the *d* band, n_d, has been presumed to increase in the same manner in this range. Measurements of M_s at $H = 11.0$ and 18.0 K oersteds were made for the Co-Ni alloys at room temperature. The results agreed closely with those at $H = 10K$ oersteds, reported by O. Bloch, Arch. Sci. Phys. et Nat. **33**, 293 (1912), and are not included here.

[20] E. M. Pugh and N. Rostoker, Revs. Modern Phys. **25**, 151 (1953).

[21] J. Smit, Physica **16**, 612 (1951).

[22] J. P. Jan and H. M. Gijsman, Physica **18**, 339 (1952).

[23] Low temperature measurements on the Cu-Ni alloys are now in progress.

mobility in the 3*d* band by the mobility in the 4*s* band. When $\sigma_d/\sigma_s=\delta n_d/n_s$ is substituted into Eq. (3)

$$n^*=(n_s+\delta n_d)^2/(n_s\pm\delta^2 n_d), \tag{7}$$

where the negative sign applies to conduction by positive carriers and the plus sign applies to conduction by electrons in the 3*d* band. The conduction in the 4*s* band is assumed to be electronic in all cases, since in these metals this band can be considered nearly empty.

From Eq. (7) the value of n^* can be positive and less than n_s only if $\delta\gg1$. When $\delta=1$, $n^*=n_s+n_d$ for electronic 3*d* conduction and $n^*>n_s+n_d$ for positive carrier 3*d* conduction. With Eq. (3) it is very easy to account for values of n^* that are fairly large compared to n_s and impossible to account for values of n^* less than n_s, unless $\delta\gg1$, which seems improbable.

It must be concluded that the two band model, using Eqs. (3) and (7)[24] cannot account for the observed values of R_0 in these metals, with $n_s\geqq0.6$. If n_s could be assumed to be less than 0.35 per atom or could be assumed to decrease monotonically from near 0.6 at 60 percent Cu in Ni to near 0.2 or 0.3 at Fe, the experimental values for R_0 could be explained with the two band model, using Eqs. (3) and (7).

With either of these assumptions the data on R_0 can be explained as follows: The 3*d* band is divided into sub-bands. The top sub-band is filled to the inflexion point near 38 percent Co in Ni. From there on to pure Co the conduction in this 3*d* band becomes electronic as the sub-band is further depleted. Since R_0 is positive in Fe, the contribution to R_0 from the 3*d* band holes exceeds the contribution from the 4*s* electrons. This indicates that the next sub-band is being emptied. One objection to this explanation is that the choice of any value for n_s less than 0.6 makes it difficult to account for the saturation magnetization, unless one assumes some net polarization of the 4*s* electrons.‡

N. Rostoker has suggested that the approximation of a spherical Fermi surface used in these models may be at fault. For example, the value of n^* for copper is about 50 percent too high.[25] Detailed calculations of the band structure by N. Rostoker in collaboration with Walter Kohn are now in progress.

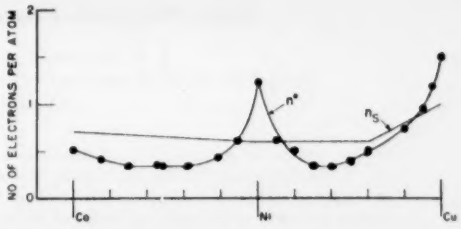

FIG. 10. Effective number of electrons, n^*, *vs* composition for elements and binary alloys from Co to Cu. The generally accepted values of n_s are plotted for comparison.

G. SUMMARY

Room temperature measurements of the ordinary Hall constant, R_0, and the field parameter, α, have been completed on Ni, Co, Fe and the Co-Ni alloy series. The sign of R_0 in Fe indicates conduction by positive carriers (3.0 holes/atom). For all of the other ferromagnetic metals studied here R_0 agrees to within a factor of two with the value predicted from the assumption that all of the conduction is electronic with from 0.6 to 0.7 electron/atom. This agreement is comparable to that of the previous work on Cu-Ni alloys. The detailed behavior of R_0 in these binary alloys from Cu through Ni to Co suggests varying amounts of conduction from the 3*d* band. However, this detailed behavior cannot be explained with a simple two band approximation without making one of two doubtful assumptions. To explain the data with this approximation, it must be assumed either that the mobility in the 3*d* band may be much greater than that in the 4*s* band or that the number of electrons/atom in the 4*s* band may be less than 0.35. Probably this band model is too simple and more exact calculations must be made to account for the data.

We are indebted to N. Rostoker for his very valuable aid and suggestions in numerous discussions and to J. E. Goldman, R. Smoluchowski, W. Kohn, and A. I. Schindler for their comments and criticisms. We are also indebted to R. W. Turner for the x-ray analysis of the columnar cobalt.

We are indebted to the U. S. Office of Naval Research for funds to carry on this research and to the Westinghouse Research Laboratories for supplying the samples.

[24] In deriving these equations, it is assumed that the bands are either nearly full or nearly empty. However, this is not a serious limitation if the 4*s* band can be considered nearly empty. The contribution to R_0 from the 3*d* band is relatively small in any case. When the 3*d* band is neither nearly full nor nearly empty (say about half full), its conductivity should be so low as to produce only a small effect.

‡ *Note added in proof.*—It is generally assumed that the *g* value in these ferromagnetic metals and alloys is equal to 2. Recent results of A. J. P. Meyer, Compt. rend. **235**, 1382 (1952) showed a spectroscopic *g* value of 2.20 which was independent of concentration up to 28 percent Cu in Ni. This would decrease the expected value of n_s by only 10 percent.

[25] At copper the 4*s* band is approximately half full. Therefore, the large value of n^* corresponding to a small value for R_0 may be merely evidence that the band cannot be considered nearly empty.

Some Magnetic Properties of Gadolinium Metal*

J. F. Elliott, S. Legvold, and F. H. Spedding
Institute for Atomic Research and Department of Physics, Iowa State College, Ames, Iowa

(Received February 26, 1953)

The saturation magnetization of gadolinium has been found to follow a $T^{\frac{1}{2}}$ law between 20–250°K. The saturation magnetization at absolute zero, determined by extrapolation is 253.6±0.9 cgs units, corresponding to 7.12 Bohr magnetons. The data fall considerably below the theoretical curve predicted by the Debye quantum modification of the Weiss theory of ferromagnetism for the ${}^8S_{7/2}$ state. Curie point determinations have also been made.

I. INTRODUCTION

THE ferromagnetic properties of metallic gadolinium were reported in 1935 by Urbain, Weiss, and Trombe,[1] and by Trombe.[2] The value of the absolute saturation magnetization was cited as 253.5 cgs units, and the Curie point as 16°C. The development of processes for the separation of pure rare earth salts[3] and for the preparation of the pure metals[4] at this laboratory has made it possible to pursue such measurements further.

Preliminary measurements were made using a ballistic method with the sample in the form of a torus.[5] Since there appeared to be certain discrepancies between these preliminary measurements and those reported by Trombe, it was deemed desirable to extend these measurements to higher fields. This paper is a report on the extension of the preliminary measurements.

II. EXPERIMENTAL PROCEDURE

The spectrographic analysis of the gadolinium metal used was as follows: Ca, detectable, but less than 200 ppm; Sm, detectable, but less than 600 ppm; Fe, Co, and other rare earths, not detected.

Curie point determinations were made with annealed and unannealed samples. Magnetic moment measurements were made on an annealed sample only. The samples were annealed for twenty-four hours at 400°C.

The magnet used in these measurements was a 20-kw Weiss type electromagnet which was constructed at this laboratory. This magnet has a 12-inch core which tapers to six-inch pole faces. It is capable of producing a 20-kilogauss field over a 1½-inch pole gap.

Magnetic moments were measured by a method similar to that suggested by Sucksmith.[6] The gradient of the electromagnet was calibrated using a sample of 99.99 percent pure iron, supplied by Johnson, Matthey and Company, Limited. The saturation magnetization at 20°C, for this sample, was taken to be 217.8 cgs units. The calibration was checked using a sample of nickel 99.97 percent pure and assuming a saturation value of 54.65 cgs units.

The calibration samples and the gadolinium were in the form of cylinders, 10 mm long and 1 mm in diameter. The magnetizing field was calculated using the expression

$$H = H_0 - NI, \tag{1}$$

where H = the magnetizing field, H_0 = the applied field, I = the magnetization per cm³, and N = the demagnetizing constant, taken to be 0.0875 for samples of the above aspect ratio.[7]

Two methods were used for the Curie point determination. In the preliminary measurements with the torus, the variation of magnetic moment with temperature was observed for a small constant field. The second method was to observe the variation of the spontaneous magnetization with temperature, using fields produced by the electromagnet, where the spontaneous magnetization was determined by the extrapolation technique of Weiss and Forrer.[8]

The cryogenic apparatus for the saturation magnetization measurements and the high field Curie point determinations consisted of a double Dewar. The inner Dewar contained the sample the temperature of which was controlled by a stream of helium gas. The outer Dewar contained a heat exchanger and a liquid bath. Helium gas was cooled in the exchanger, then mixed with a stream of warm helium before entering the inner Dewar. The temperature range from 39°–85°K was obtained with a hydrogen bath, from 85°–260°K with nitrogen, 200°–280°K with acetone and dry ice, 280°–310°K with ice water. The temperature was controlled to within a degree for saturation measurements and to within a quarter of a degree for Curie point determinations.

The temperature was measured by a copper-constantan thermocouple calibrated over the temperature range employed.

* Contribution No. 234 from the Institute for Atomic Research and Department of Physics, Iowa State College, Ames, Iowa. Work was performed in the Ames Laboratory of the U. S. Atomic Energy Commission.

[1] Urbain, Weiss, and Trombe, Compt. rend. **200**, 2132 (1935).
[2] F. Trombe, Ann. phys. **7**, 383 (1937).
[3] F. H. Spedding *et al.*, J. Am. Chem. Soc. **69**, 2812 (1947).
[4] F. H. Spedding and A. H. Daane, J. Am. Chem. Soc. **74**, 2783 (1952).
[5] Legvold, Spedding, Barson, and Elliott, Revs. Modern Phys. **25**, 129 (1953).
[6] W. Sucksmith, Proc. Roy. Soc. (London) **A170**, 551 (1939).
[7] See R. Bozorth, *Ferromagnetism* (D. Van Nostrand Company, Inc., 1951), pp. 846–849.
[8] P. Weiss and R. Forrer, Ann. phys. **5**, 153 (1926).

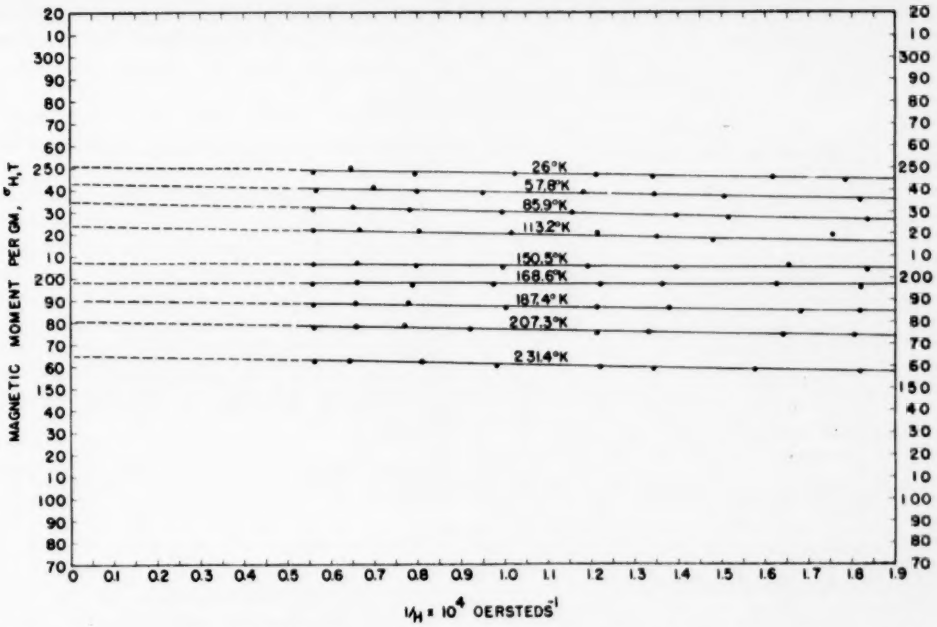

FIG. 1. Representative curves of the isothermal variation of magnetic moment of gadolinium as a function of $1/H$.

This apparatus was used throughout, except for the 20.4°K data. Here the sample was immersed directly in the hydrogen bath, and the necessary buoyancy corrections made.

III. RESULTS

Figure 1 shows several of the representative curves of the isothermal variation of the magnetic moment as a function of $1/H$. It was found that the variation, for magnetizing fields of 4000–18 000 oersteds over the temperature range of 20–253°K, is well represented by the expression

$$\sigma_{H,T}=\sigma_{s,T}(1-a/H), \tag{2}$$

where $\sigma_{H,T}$ = the magnetic moment per gram, $\sigma_{s,T}$ = the saturation moment per gram at T°K, H = the magnetizing field, and a = constant. The data were extrapolated to zero, using the method of least squares to find the saturation magnetization.

The values of the saturation magnetization, obtained by the above extrapolation, are plotted as a function of $T^{\frac{1}{2}}$ in Fig. 2(a). It may be observed that the data seem to agree quite well over the temperature range examined with an expression of the form,

$$\sigma_{s,T}=\sigma_{s,0}(1-bT^{\frac{1}{2}}), \tag{3}$$

where $\sigma_{s,0}$ = the absolute saturation magnetization, b = a constant, and T = absolute temperature. It may be further observed [Fig. 2(b)] that there appears to be some correlation between our data and the expression,

$$\sigma_{s,T}=\sigma_{s,0}(1-bT^{2}), \tag{4}$$

between 250°K and 130°K, but the data seem to fit the $T^{\frac{1}{2}}$ expression at least as well if not better than the T^{2} expression over this range. Consequently, the $T^{\frac{1}{2}}$ law is used over the entire range for determining the absolute saturation magnetic moment.

Using again the method of least squares, the value of the saturation magnetization at absolute zero was found to be 253.6±0.6 cgs units. This saturation moment corresponds to 7.12 Bohr magnetons.

In Fig. 3 the ratio of $\sigma_{s,T}/\sigma_{s,0}$ is plotted as a function of the ratio of T/θ, where θ is the Curie temperature. Several curves, obtained from the Debye quantum modification of the Weiss theory of ferromagnetism for various J values, are also shown. To make com-

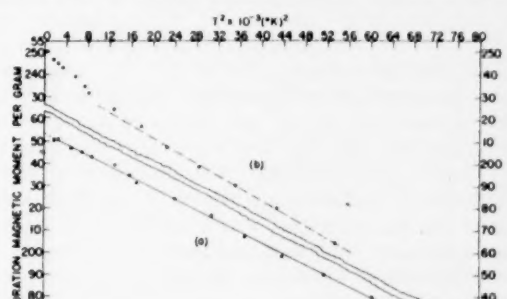

FIG. 2. (a) The saturation magnetic moment of gadolinium as a function of $T^{\frac{1}{2}}$; (b) of T^{2}.

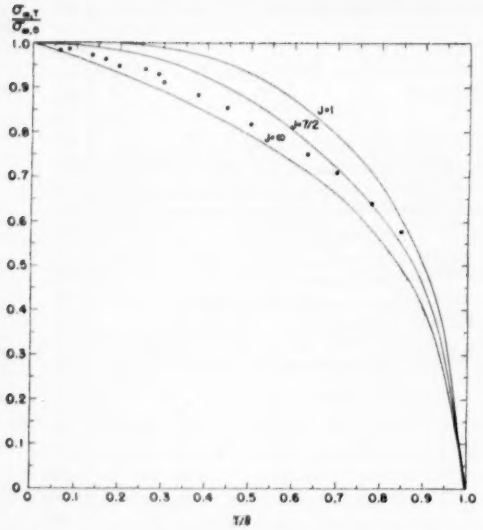

FIG. 3. The reduced magnetization curve for gadolinium; also, the theoretical curves for $J=1$, $J=7/2$ and $J=\infty$, from the Debye-Weiss quantum theory of ferromagnetism.

parison between experimental data and the Debye-Weiss theory, the ratio of $\sigma_{0,T}/\sigma_{0,0}$, where $\sigma_{0,T}$ is the spontaneous magnetization, should be plotted as a function of T/θ. However, our data indicate that the value of the spontaneous magnetization differs from the saturation magnetization by only a few percent, which would not change the location of the plotted points significantly.

The variation of the square of the spontaneous magnetization with temperature near the Curie point is shown in Fig. 4(b). The intersection of the extension of the nearly linear portion of this curve with the temperature axis was taken to be the Curie point, i.e., 17.7±0.3°C. In Fig. 4(a) the Curie point is determined from data obtained by the ballistic method using the torus and a small applied field (i.e., 23 oersteds) and was found to be 15.9±0.1°C.

IV. DISCUSSION OF RESULTS

Of particular interest is the fact that the value of the absolute saturation magnetization obtained by Trombe by extrapolation of a T^2 plot agrees exceedingly well with the value obtained here using an extrapolation of a $T^{\frac{3}{2}}$ plot. This discrepancy was obvious even in our preliminary measurements where, for instance, our value for the saturation magnetization at 77°K was some 4 percent lower than that obtained by Trombe.

Of interest also is the fact that the saturation magnetization of gadolinium follows a $T^{\frac{3}{2}}$ law over nearly its entire ferromagnetic range. Gadolinium thus seems to be peculiar in this respect as other ferromagnetics follow a $T^{\frac{3}{2}}$ law only at very low temperatures.

Our investigation also showed that gadolinium is not as magnetically "hard" as indicated by Trombe, although considerably "harder" than iron. The constant (a) in Eq. (2) is an indication of this "hardness" and has the value of about 170 from our data. This is to be compared with Trombe's value of 1250. This difference of "hardness" between our samples and Trombe's was also indicated by our preliminary measurements at low fields,[4] using the ballistic method.

The Curie point found by the ballistic method, Fig. 4(a), agrees quite well with Trombe's value, where he has defined the Curie point as the temperature at which ferromagnetism disappears in a small field. The Curie point is found to be some two degrees higher when it is defined as the temperature at which spontaneous magnetization disappears. The disagreement between the values of the Curie points does not seem unreasonable when the differences in their definitions are considered.

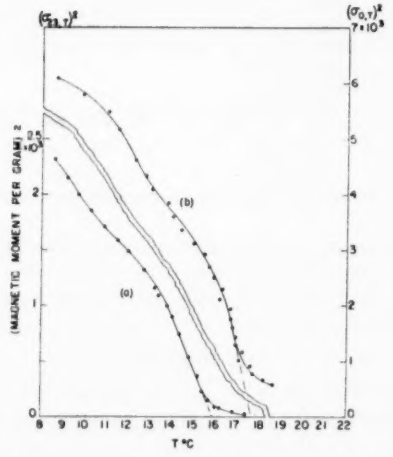

FIG. 4. (a) The Curie point of gadolinium using the ballistic method and an applied field of 23 oersteds. (b) The Curie point using spontaneous magnetization.

It was possible to repeat the data obtained by the ballistic method irrespective of whether the Curie point was approached from above or below, showing there was no temperature hystersis (within at least 0.1°) at the Curie point.

It may be observed that the absolute saturation magnetization is some 2 percent higher than would be predicted if only the spins of the $4f$ electrons contributed to the magnetization; this deviation is outside the experimental error. Also, the reduced magnetization data points fall far below the curve calculated for the ${}^8S_{7/2}$ spectrographic state using the Debye-Weiss theory of ferromagnetism. Had $\sigma_{0,T}$ data been used for this plot rather than $\sigma_{\infty,T}$ data, the experimental points would have been slightly lower than the points shown.

The authors wish to express their thanks to Jack Powell for preparing the rare earth salts and to A. H. Daane and Richard Barton for preparing the metal samples.

Matrix Elements of Spin-Spin Interaction*

FREDERICK R. INNES
University of Pennsylvania, Philadelphia, Pennsylvania
(Received February 13, 1953)

An expansion of the spin-spin interaction operator allows a derivation of matrix elements using the methods of Racah. Formulas are given for configurations involving two nonequivalent electrons and for n equivalent electrons. Extension of the results to other configurations may be made using known procedures.

I. INTRODUCTION

THE consideration of the Heisenberg spin-spin interaction operator[1] in problems of complex spectra has proved useful in explaining energy level structures showing deviations from the Landé interval rule. It has been recognized that there are appreciable spin-spin contributions in the spectra of light atoms.[2] More recently the work of Araki[3] and Trees[4] suggests that such contributions may be significant in the spectra of atoms of quite large atomic number.

Procedures for computing the matrix elements of this operator are available for both two-electron and equivalent electron configurations. Marvin[5] gave a treatment of the two-electron case using the method of one-electron eigenfunctions and computed elements involving s, p, and d electrons. Aller, Ufford, and Van Vleck[6] applied similar methods to the configuration $2p^3$ and pointed out limiting conditions on the number of nonvanishing coefficients which occur in the elements of the spin-spin and spin-other-orbit operators. More recently, Trees[4] generalized a relation given by Racah and used it to find the elements in d^n configurations. Araki[3] had already developed interval formulas using methods analogous in part to those of Trees and the present writer.

In a new formulation, the use of one-electron eigenfunctions should be avoided, since their use leads to cumbersome procedures for all but the simplest configurations. At the same time the structure of the operator should be explicitly shown, also to the end that treatment of different configurational problems is facilitated.

By expanding the interaction operator into a form such that the relations given by Racah[7] can be used to find the elements, both these objectives may be fulfilled. Thus the formulas developed below yield matrix elements directly in the *SLJM* scheme. They are expressed in terms of W coefficients and submatrix elements which are available, for the most part, in tabular form.[7,8] Direct indication is also given of those elements which are nonvanishing.

An additional point involving the nature of the present formulation arises in connection with the d^n configurations considered by Trees. The observation was made that the elements were diagonal with respect to the seniority number v.[9] The explanation of this circumstance is given in Sec. V below. Briefly stated, the spin-spin interaction breaks up into products of one-particle tensors of odd degree and these are known to be diagonal in v.

Extension of the general results to configurations other than ll' and l^n should follow along lines laid out in R-III Sec. 5 and Sec. 7. However, these applications have not been considered at this time.

For the configurations considered in the present paper, the matrix elements are found by direct use of Eqs. (10) and (12). These equations have been stated in quite general terms, since they find application in all the two-particle interactions of complex spectra. A short treatment of the electrostatic interaction has been included as an example of such an application.

II. THE SPIN-SPIN INTERACTION AS A SCALAR PRODUCT

Given two systems, i and j, a vector distance $\mathbf{r}_{ij}$ apart and characterized by spin-vectors $\mathbf{s}_i$ and $\mathbf{s}_j$, the Heisenberg spin-spin interaction, denoted by H_m^{II} (following Marvin[10]), is as follows:

$$H_m^{II} = -a^2 r_{ij}^{-5}\left[3(\mathbf{s}_i\cdot\mathbf{r}_{ij})(\mathbf{s}_j\cdot\mathbf{r}_{ij}) - (\mathbf{s}_i\cdot\mathbf{s}_j)r_{ij}^2\right] \quad (1)$$

in which $a=e\mu^{-1}c^{-1}$. This operator is of rank 2 in the spin and orbital parts separately, but a scalar in the product space. It may also be regarded as the scalar part of a double tensor[11] $\mathbf{T}^{(22)}$.

* Part of a dissertation to be submitted to the faculty of The Graduate School of the University of Pennsylvania in partial fulfillment of the requirements for the degree of Doctor of Philosophy.

[1] W. Heisenberg, Z. Physik **39**, 499 (1926); or E. U. Condon and G. H. Shortley, *The Theory of Atomic Spectra* (Cambridge University Press, Cambridge, 1951), 7?1. The symbol *TAS* is used in further references to this text.

[2] Discussion and references, *TAS* 7?.

[3] G. Araki, Prog. Theoret. Phys. **3**, 152 (1948); **3**, 262 (1948).

[4] R. E. Trees, Phys. Rev. **82**, 683 (1951).

[5] H. H. Marvin, Phys. Rev. **71**, 102 (1947).

[6] Aller, Ufford, and Van Vleck, Astrophys. J. **109**, 42 (1949).

[7] G. Racah, Phys. Rev. **61**, 186 (1942); **62**, 438 (1942); **63**, 367 (1943); **76**, 1352 (1949). These papers are denoted R-I, R-II, R-III, and R-IV, respectively.

[8] For tables of the Racah coefficients, see L. C. Biedenharn, Oak Ridge National Laboratory Report ORNL-1098, 1952 (unpublished).

[9] See reference 4, Eq. (10).

[10] See reference 5, Eq. (1) (discussion on p. 103). The symbol H_m^{II} is also used, in the course of the present work, in situations which imply a sum over n particles [see reference 4, Eq. (1)].

[11] E. Wigner, *Gruppentheorie* (Vieweg, Braunschweig, 1931), p. 295; also R-II Sec. 5. $\mathbf{T}^{(22)}$ is a two-particle operator. Its properties are discussed in reference 4, Sec. II.

The spin and orbital parts of this operator are separated when it is written as a scalar product. This is done in terms of two-particle irreducible tensor operators. A convenient way of defining these is through the vector-coupling formalism,

$$\{\mathbf{A}^{(k_1)}\mathbf{B}^{(k_2)}\}_Q^{(K)}=\sum_{q_1,q_2}(k_1k_2q_1q_2|KQ)A_{q_1}^{(k_1)}B_{q_2}^{(k_2)}, \quad (2)$$

comparable to *TAS* 14[3]1. The components of the rank 2 tensor operator compounded from two vectors are

$$\begin{aligned}\{\mathbf{A}\,\mathbf{B}\}_0^{(2)}&=6^{-\frac{1}{2}}(3A_0B_0-\mathbf{A}\cdot\mathbf{B}),\\ \{\mathbf{A}\,\mathbf{B}\}_{\pm1}^{(2)}&=2^{-\frac{1}{2}}(A_0B_{\pm1}+A_{\pm1}B_0), \quad (3)\\ \{\mathbf{A}\,\mathbf{B}\}_{\pm2}^{(2)}&=A_{\pm1}B_{\pm1}.\end{aligned}$$

The vector components are defined according to R-II(24).

The interaction operator takes the following form:

$$H_m^{II}=-3\sum_Q(-)^Q\{\mathbf{s}_i\mathbf{s}_j\}_Q^{(2)}\{\mathbf{R}\,\mathbf{R}\}_{-Q}^{(2)}, \quad (4)$$

in which Q assumes integer values from -2 to $+2$. The vector $\mathbf{R}=ar_{ij}^{-2\frac{1}{2}}\mathbf{r}_{ij}$. With minor changes, Eq. (4) may be found in Araki[3] or Trees[4] (among others).

Matrix elements of the spin operator in Eq. (4) are obtained immediately since the two vector arguments are separate in i and j. But the orbital part must be expanded before its elements can be found, just as in the case of the electrostatic interaction operator $e^2r_{ij}^{-1}$.

III. THE EXPANSION OF $\{\mathbf{R}\,\mathbf{R}\}^{(2)}$

The tensors $\mathbf{C}^{(k)}$ of R-II(46) are "radial" in type and the two-particle tensors $\{\mathbf{C}_i^{(k_1)}\mathbf{C}_j^{(k_2)}\}^{(K)}$ are suitable operators for the required expansion. However, in evaluating the expansion coefficients, it is convenient to use the two-particle orthonormal wave functions of *TAS* 14[3]1:

$$\begin{aligned}&\psi(k_1k_2KQ)\\ &\quad=(4\pi)^{-1}[(2k_1+1)(2k_2+1)]^{\frac{1}{2}}\{\mathbf{C}_i^{(k_1)}\mathbf{C}_j^{(k_2)}\}_Q^{(K)},\\ &\quad=\sum_{q_1,q_2}(k_1k_2q_1q_2|KQ)\phi_i(k_1q_1)\phi_j(k_2q_2). \quad (5)\end{aligned}$$

The ϕ-functions are spherical harmonics, defined as in *TAS* 4[3], that is, $\phi(kq)=\Theta(kq)\Phi(q)$. The vector $\mathbf{R}$, defined in Sec. II, may be written $R_q=ar_{ij}^{-2\frac{1}{2}}(4\pi/3)^{\frac{1}{2}}\times[r_i\phi_i(1q)-r_j\phi_j(1q)]$. After some reduction, the orbital operator is expressed as

$$\begin{aligned}\{\mathbf{R}\,\mathbf{R}\}_Q^{(2)}=4\pi\tfrac{1}{3}\sqrt{2}\,5^{-\frac{1}{2}}a^2r_{ij}^{-5}[&r_i^2\sqrt{3}\psi(202Q)\\ &-r_ir_j\sqrt{2}\,5^{\frac{1}{2}}\psi(112Q)+r_j^2\sqrt{3}\psi(022Q)]. \quad (6)\end{aligned}$$

The quantity r_{ij}^{-5} must be expanded in Legendre polynomials.[12] Setting $\rho=r_j/r_i$, and assuming $r_i>r_j$,

$$\begin{aligned}r_{ij}^{-5}=\tfrac{1}{3}[r_i(1-\rho^2)]^{-3}&\sum_p\rho^p(2p+1)\\ &\times[(2p+3)-(2p-1)\rho^2]P_p(\cos\omega). \quad (7)\end{aligned}$$

[12] E. J. Routh, Proc. London Math. Soc. **26**, Series 1, 481 (1895).

After inserting (7) in (6), an expansion in ψ-functions can be carried out. It has already been observed that only the coefficients $c_t=\int\{\mathbf{R}\,\mathbf{R}\}_Q^{(2)}\psi(t+2\ t2Q)d\tau_id\tau_j$ need be considered.[13] There are three non-vanishing integrals in the sum over p and these may be found by the use of R-II(45), (38). The final result is

$$\begin{aligned}\{\mathbf{R}\,\mathbf{R}\}_Q^{(2)}=4\pi\tfrac{1}{3}\sqrt{2}\,5^{-\frac{1}{2}}a^2r_i^{-3}&\sum_t(-)^t\rho^t\\ &\times[(t+2)(t+1\tfrac{1}{2})(t+1)]^{\frac{1}{2}}\psi(t+2\ t2Q), \quad (8a)\end{aligned}$$

and using Eq. (5),

$$\begin{aligned}\{\mathbf{R}\,\mathbf{R}\}_Q^{(2)}=6^{-1}5^{-\frac{1}{2}}a^2r_i^{-3}&\sum_t(-)^t\rho^t\\ &\times[(2t+5)!/(2t)!]^{\frac{1}{2}}\{\mathbf{C}_i^{(t+2)}\mathbf{C}_j^{(t)}\}_Q^{(2)}. \quad (8b)\end{aligned}$$

The operator appears as a generating function in Eq. (8a). This equation is thus one of the equations which may be used in deriving recurrence and other relations between ψ-functions.

IV. MATRIX ELEMENTS OF TWO-PARTICLE OPERATORS

The matrix elements of the general operator $\{\mathbf{T}_i^{(k_1)}\mathbf{Y}_j^{(k_2)}\}^{(k)}$ will next be considered. The nature of $\mathbf{T}^{(k_1)}$ and $\mathbf{Y}^{(k_2)}$ will be unrestricted except as implied by the subscripts i and j. In the j_1j_2jm scheme the elements are

$$\begin{aligned}&(j_1j_2jm|\{\mathbf{T}^{(k_1)}\mathbf{Y}^{(k_2)}\}_q^{(k)}|j_1'j_2'j'm')\\ &\quad=(-)^{k+q}(2k+1)^{\frac{1}{2}}\sum_{q_1,q_2}V(k_1k_2k;q_1q_2-q)\\ &\qquad\times\sum_{j''m''}(j_1j_2jm|T_{q_1}^{(k_1)}|j_1'j_2j''m'')\\ &\qquad\quad\times(j_1'j_2j''m''|Y_{q_2}^{(k_2)}|j_1'j_2'j'm'). \quad (9)\end{aligned}$$

Upon using in succession R-II(29), (41), (44a, b) with occasional use of R-II(19a, b), (40a, b), the following result is found:

$$\begin{aligned}&(j_1j_2jm|\{\mathbf{T}^{(k_1)}\mathbf{Y}^{(k_2)}\}_q^{(k)}|j_1'j_2'j'm')\\ &\quad=(-)^{k-j'+m}V(jj'k;-mm'q)\\ &\qquad\times[(2j+1)(2k+1)(2j'+1)]^{\frac{1}{2}}\\ &\qquad\times(j_1\|T^{(k_1)}\|j_1')(j_2\|Y^{(k_2)}\|j_2')\\ &\qquad\times\sum_{j''}(2j''+1)W(j_1jj_1'j'';j_2k_1)\\ &\qquad\times W(j_2j''j_2'j';j_1'k_2)W(k_1jk_2j';j''k). \quad (10)\end{aligned}$$

The submatrix element $(j_1j_2j\|\{\mathbf{T}^{(k_1)}\mathbf{Y}^{(k_2)}\}^{(k)}\|j_1'j_2'j')$ is given directly by R-II(29).

Equation (10) may be regarded as a generalization which includes as special cases R-II(29), (38), (44a, b). The sum over products of three W coefficients is, apart

[13] Reference 6, p. 47. Occasion is taken to note that a comparison of $\psi(t+2,t2Q)$ with the functions appearing in this reference discloses an error in the m dependence of the latter (to correct, read m' instead of $-m$ and also sum over m'). Conclusions of the reference are not affected by this correction.

from normalization, a type of unitary coefficient discussed by Fano.[14] The matrix element of the scalar product of two operators of the type given in Eq. (10) is given directly by R-II(38).

The matrix elements of a two-particle double tensor operator in the $l^n\alpha vSLJM$ scheme may be found by a procedure similar to that used in R-III Sec. 7. The operator is separated into two parts, which involve two-particle and one-particle tensors, respectively:

$$\sum_{i>j}\{\mathbf{s}_i^{(\kappa_1)}\mathbf{s}_j^{(\kappa_2)}\}^{(K)}\{\mathbf{T}_i^{(k_1)}\mathbf{Y}_j^{(k_2)}\}^{(K)}$$
$$=\tfrac{1}{2}[\sum_{i,j}\{\mathbf{s}_i^{(\kappa_1)}\mathbf{s}_j^{(\kappa_2)}\}^{(K)}\{\mathbf{T}_i^{(k_1)}\mathbf{Y}_j^{(k_2)}\}^{(K)}$$
$$-\sum_i(\mathbf{s}_i^{(\kappa_1)}\mathbf{s}_i^{(\kappa_2)})^{(K)}(\mathbf{T}_i^{(k_1)}\mathbf{Y}_i^{(k_2)})^{(K)}]. \quad (11)$$

Evaluation of the elements proceeds very much as in the case of Eq. (10). The result is most simply stated in terms of one-particle double tensors $\mathbf{U}^{(\kappa k)}$, which are related to the $\mathbf{V}^{(1k)}$ tensors of R-II(102b) by a submatrix element in the spin tensor, $\mathbf{V}^{(\kappa k)}=(s\|s^{(\kappa)}\|s)\mathbf{U}^{(\kappa k)}$. The element is

$$(l^n\alpha vSL\|\sum_{i>j}\{\mathbf{s}_i^{(\kappa_1)}\mathbf{s}_j^{(\kappa_2)}\}^{(K)}$$
$$\times\{\mathbf{T}_i^{(k_1)}\mathbf{Y}_j^{(k_2)}\}^{(K)}\|l^n\alpha'v'S'L')$$
$$=(-)^{\kappa_1+\kappa_2+k_1+k_2}\tfrac{1}{2}(2K+1)(s\|s^{(\kappa_1)}\|s)$$
$$\times(s\|s^{(\kappa_2)}\|s)(l\|T^{(k_1)}\|l)(l\|Y^{(k_2)}\|l)$$
$$\times[\sum_{\alpha''v''S''L''}(l^n\alpha vSL\|U^{(\kappa_1k_1)}\|l^n\alpha''v''S''L'')$$
$$\times(l^n\alpha''v''S''L''\|U^{(\kappa_2k_2)}\|l^n\alpha'v'S'L')$$
$$\times W(\kappa_1S\kappa_2S';S''K)W(k_1Lk_2L';L''K)$$
$$-(l^n\alpha vSL\|U^{(KK)}\|l^n\alpha'v'S'L')W(\kappa_1S\kappa_2S;SK)$$
$$\times W(k_1lk_2l;lK)]. \quad (12)$$

In this expression, as in (11) above, the spin ranks are restricted to the values 0 and 1 for one-particle tensors. It follows that for the spin-spin interaction the term involving $\mathbf{U}^{(KK)}$ in Eq. (12) will vanish. In the spin-other-orbit interaction, this term would not vanish, in general, since $K=1$ in this case. For the electrostatic interaction $\kappa_1=\kappa_2=K=0$, and the coefficient of F^k, expressed in terms of the $\mathbf{U}^{(k)}$ tensors of R-II(102a), is

$$f_k=\tfrac{1}{2}(l\|C^{(k)}\|l)^2[(2L+1)^{-1}\sum_{\alpha''v''L''}(-)^{L-L''}$$
$$\times(l^n\alpha vSL\|U^{(k)}\|l^n\alpha''v''SL'')$$
$$\times(l^n\alpha''v''SL''\|U^{(k)}\|l^n\alpha'v'SL)$$
$$-n(2l+1)^{-1}\delta(\alpha,\alpha')\delta(v,v')]; \quad (13)$$

since, formally, $\mathbf{U}^{(0k)}=(2S+1)^{\frac{1}{2}}(2s+1)^{-\frac{1}{2}}\mathbf{U}^{(k)}$.

[14] U. Fano, National Bureau of Standards Report 1214 (1951), Appendix D (unpublished). Related material and further references will be found in Biedenharn, Blatt, and Rose, Revs. Modern Phys. **24**, 249 (1952); L. C. Biedenharn, J. Math. Phys. **31**, 287 (1953).

Although most of the useful term values have already been made available, this formula is of use, in some instances, for their computation, e.g., in f^n configurations.[15] One advantage which it has over other formulations is that terms which are nondiagonal in v are found directly.[16]

V. THE MATRIX ELEMENTS OF THE SPIN-SPIN INTERACTION

Use of R-II(38) immediately yields

$$\langle SLJM|H_m^{II}|S'L'JM\rangle$$
$$=(-)^{S+L'-J}W(SLS'L';J2)\langle SL\|T^{(22)}\|S'L'\rangle. \quad (14)$$

Thus the J dependence is completely given by the phase factor and W coefficient[17] and is independent of the configurations of the wave functions.

For two-electron wave functions, not necessarily antisymmetric, the submatrix element is

$$(l_1l_2SL\|T^{(22)}\|l_1'l_2'S'L')$$
$$=-3(s_1s_2S\|\{\mathbf{s}_i\mathbf{s}_j\}^{(2)}\|s_1's_2'S')$$
$$\times(l_1l_2L\|\{\mathbf{R}\,\mathbf{R}\}^{(2)}\|l_1'l_2'L'). \quad (15)$$

Taking $s_1=s_2=s_1'=s_2'=\frac{1}{2}$, the spin part is fixed, since S and S' must both be unity. The value is $+\frac{1}{2}(5)^{\frac{1}{2}}$. Using Eq. (8b) and representing the radial integral as in reference 5, one finds that

$$(l_1l_2SL\|T^{(22)}\|l_1'l_2'SL')$$
$$=(-)^{L+L'+1}\,2(5)^{\frac{1}{2}}[(2L+1)(2L'+1)]^{\frac{1}{2}}$$
$$\times\sum_t(-)^t\,{}^2R^t[(2t+5)!/(2t)!]^{\frac{1}{2}}$$
$$\times(l_1\|C^{(t+2)}\|l_1')(l_2\|C^{(t)}\|l_2')$$
$$\times\sum_{L''}(2L''+1)W(l_1Ll_1'L'';l_2t+2)$$
$$\times W(l_2L''l_2'L';l_1't)W(t+2LtL';L''2). \quad (16)$$

The completely antisymmetrized matrix element will involve four elements of the above type, differing in the order of individual quantum numbers.[18] Such permutations involve phase factors in the two-particle wave functions [see R-I(6)]. In general, factors involving both spin and orbital quantum numbers will occur (e.g., in the case of the electrostatic interaction), but for the spin-spin interaction, the spin phase contri-

[15] The term values for f^4 are the subject of a forthcoming paper by E. F. Reilly. The procedure used is that of R-IV, with checks on the numerical work provided by Eq. (13).

[16] The parallel result is that of R-III (78), (79).

[17] See reference 4, Eqs. (2) and (3).

[18] As in reference 5, Eq. (2); *TAS* 7[4].

bution is zero. The final form will then be

$$(l_i l_j SL\|T^{(22)}\|l_i' l_j' SL') = \tfrac{1}{2}[(l_1 l_2 SL\|T^{(22)}\|l_1' l_2' SL') - (-)^{l_1+l_2-L}(l_2 l_1 SL\|T^{(22)}\|l_1' l_2' SL') + (-)^{l_1+l_2-L+l_1'+l_2'-L'}(l_2 l_1 SL\|T^{(22)}\|l_2' l_1' SL') - (-)^{l_1'+l_2'-L'}(l_1 l_2 SL\|T^{(22)}\|l_2' l_1' SL')]. \quad (17)$$

The formula found by inserting Eq. (17) in Eq. (14) is equivalent to the procedure of Marvin.[19] Specialization to the case in which $l_i = l_i'$ and $l_j = l_j'$ is immediate and the case of two equivalent electrons is handled by standard methods (*TAS* 6[8]).

In the $l^n \alpha v SLJM$ scheme, the matrix element follows from Eq. (12). The submatrix element which enters the coefficient of M^t is

$$(l^n \alpha v SL\|\mu_t\|l^n \alpha' v S'L') = -2(5)^{\frac{1}{2}}[(2t+5)!/(2t)!]^{\frac{1}{2}}(l\|C^{(t+2)}\|l)(l\|C^{(t)}\|l) \times \sum_{\alpha'' S'' L''} (l^n \alpha v SL\|V^{(1,t+2)}\|l^n \alpha'' v S'' L'') \times (l^n \alpha'' v S'' L''\|V^{(1,t)}\|l^n \alpha' v S'L') \times W(1S1S'; S''2) W(t+2LtL'; L''2), \quad (18)$$

in which $\mathfrak{y}_t$ is the angular part of $\mathbf{T}_t^{(22)}$ (for $\mathfrak{y}^t$, see reference 5, Table IV). The coefficient μ_0 assumes a simple form when the relation

$$(l^n \alpha v SL\|V^{(10)}\|l^n \alpha' v S'L') = [(2L+1)/(2l+1)]^{\frac{1}{2}}(S\|S\|S)\delta(\alpha SL, \alpha' S'L')$$

is used.[20]

The values of t are prescribed by the properties of $(l\|\dot{C}^{(t+2)}\|l)$. By R-II(50′), t is restricted to even numbers ranging from 0 to $2l-2$. The sum of the ranks of the tensors $\mathbf{V}^{(1k)}$ is thus an odd number. According to R-III Sec. 6.(6), these tensors are diagonal with respect to v. It follows that the coefficients μ_t are likewise diagonal, as observed by Trees.[9]

It may be further noted that while the diagonal spin-orbit matrix elements in l^{2l+1} configurations must vanish, since in $\mathbf{V}^{(11)}$ the sum of the ranks is even [R-II Sec. 6 and R-III(69b)], the same does not hold true for the spin-spin elements in which the tensors are of odd degree.

The author wishes to thank Dr. C. W. Ufford for suggesting this problem and for his advice and help during the course of the work. He is also much indebted to Dr. G. Racah and Dr. J. H. Van Vleck for their interest and for important observations and suggestions which they have made.

[19] Elements given by combining Eqs. (16), (14), and (17) differ by the phase factor $(-)^{L-L'}$ from those given in Table V of reference 5, if the given order of quantum numbers is used. This difference corresponds to the transposition of the element in Eq. (16).

[20] The resulting expression for μ_0 has been given by G. Racah (private letter to R. E. Trees). Other relations pertaining to the d^n configurations are given in the same letter. *Note added in proof.*—These relations have been derived by I. Talmi in a recent paper [Phys. Rev. **89**, 1065 (1953), Sec. III and Sec. IV]. Dependence of the matrix elements on the seniority number is also discussed (as in Sec. V of the present paper).

Correlation Energy in the Ground State of He I†

LOUIS C. GREEN, MARJORIE M. MULDER, AND PAUL C. MILNER*
Strawbridge Observatory, Haverford College, Haverford, Pennsylvania
(Received January 27, 1953)

With a view of examining the effects of configuration interaction in a simple case, the three term and six term expressions given by Hylleraas for the ground-state wave function of He I have been expanded in series of Legendre functions of the cosine of the angle between the two radius vectors. The coefficients in these expansions are functions of r_1 and r_2, the distances of the two electrons from the nucleus. The various component functions are presented, together with the coefficients with which these functions enter the expansions, and their contributions to the total energy. A discussion is given of the method of estimating the magnitude of the correlation, or configuration interaction, energy. Evidence is presented that the total correlation energy is at least $-0.129R_{\mathrm{He}}hc$ and may be even more negative. Of this amount it is estimated that $-0.056R_{\mathrm{He}}hc$ is associated with the radial part of the correlation energy, $-0.075R_{\mathrm{He}}hc$ with the angular part, and $+0.002R_{\mathrm{He}}hc$ with the mixed part.

THE importance of configuration interaction in atomic spectra has long been recognized,[1] and a number of calculations dealing with such interactions have been made.[2–6] In general, some improvement in term separations has been obtained when superposition was included but in the two most thorough treatments of such effects by self-consistent field methods, the work of Hartree[2] on O, O^+, and O^{++} and the work of Jucys[3] on C, the results were disappointing. It therefore seemed valuable to investigate the effects of configuration interaction by considering a relatively simple case in some detail. As a consequence in an earlier paper[5] two of the present authors together with others undertook the expansion of two of the Hylleraas wave functions for the $^1S_0$ ground state of He I in series of central field wave functions representing the various configurations.[7] In total five configurations were considered: $1s^2$, $1s2s$, $1s3s$, $2s^2$ and $2p^2$. The wave functions in each case were taken as symmetrized products of self-consistent field wave functions for the individual electrons. For the $1s^2$ and $1s2s$ configurations a second set of expansion coefficients was also calculated using analytic variationally determined wave functions. One of the results of this work was to show that for the self-consistent field wave functions the nonspherically symmetric $2p^2$ was the second largest contributor to the ground-state wave function among the configurations considered.

However, in this earlier work the coefficient of the $1s2s$ configuration was markedly different for the self-consistent field wave functions and for the analytic ones. It seemed entirely possible that the same might also be true for the $2p^2$ as well as the other excited configurations. This would mean in the case of the $2p^2$ that the angular dependence which would be found for the Hylleraas functions would depend on the particular kind of radial functions used in the expansion. This of course would not be true if a sufficiently large number of orthogonal functions were used so that they could be considered as forming a fair approximation to a complete set for the purpose in hand. However, to obtain such a set and to expand in terms of it might well be a heavy task.

To avoid this difficulty it was decided to use an expansion of the form[8]

$$\Psi_H{}^N=\sum_i C_i\Phi_i{}^N P_i{}^N \qquad (1)$$

where $\Psi_H{}^N$ is the normalized Hylleraas wave function, the $\Phi_i{}^N$'s are normalized functions [whose functional form is to be determined from Eq. (1)] of the distances r_1 and r_2 of the two electrons from the nucleus, and the $P_i{}^N$'s are the normalized Legendre functions of the various orders i of the cosine of the angle between the two radius vectors. More precisely, $\Psi_H{}^N$ is normalized with respect to integration over r_1, θ_1, and φ_1, the coordinates of the first electron, r_2 for the second electron, and θ and φ, the Euler angles specifying the direction of r_2 with respect to r_1. $\Phi_i{}^N$ is normalized with respect to integration over r_1, θ_1, φ_1, r_2, and φ. From Eq. (1) it then follows that $\Phi_i{}^N$ is given by the

† This work was supported in part by a U. S. Office of Naval Research contract administered by the University of Pennsylvania, and in part by a grant from the Research Corporation.
* Now at Princeton University, Princeton, New Jersey.
[1] E. U. Condon and G. H. Shortley, *The Theory of Atomic Spectra* (Cambridge University Press, Cambridge, 1935), Chap. XV.
[2] Hartree, Hartree, and Swirles, Trans. Roy. Soc. (London) **A238**, 229 (1939).
[3] A. Jucys (sometimes transliterated A. Yutsis), J. Exptl. Theoret. Phys. (U.S.S.R.) **19**, 565 (1949).
[4] For references to the earlier literature see reference 5 below. In addition one should mention A. Jucys and V. J. Kavetskis, Zhur. Eksptl. i Teort. Fiz. (U.S.S.R.) **21**, 1139 (1951); G. F. Koster, Phys. Rev. **86**, 148 (1952); J. Lennard-Jones and J. A. Pople, Phil. Mag. **43**, 581 (1952); A. Brickstock and J. A. Pople, Phil. Mag. **43**, 1090 (1952); N. Rosenzweig, Phys. Rev. **88**, 580 (1952).
[5] Green, Mulder, Ufford, Slaymaker, Krawitz, and Mertz, Phys. Rev. **85**, 65 (1952).
[6] G. R. Taylor and R. G. Parr, Proc. Natl. Acad. Sci. **38**, 154 (1952).
[7] The possibility of investigating configuration interaction in HeI in this manner was suggested to one of us (L.C.G.) by Dr. G. Breit.
[8] The value of an expansion in terms of Legendre functions was pointed out to two of us (L.C.G. and M.M.M.) by Dr. E. U. Condon.

expression

$$\Phi_i^N=\frac{1}{c_i}\int\Psi_H^N P_i^N\sin\theta d\theta, \tag{2}$$

and c_i by the expression

$$c_i=\left\{\int\left[\int\Psi_H^N P_i^N\sin\theta d\theta\right]^2 d\tau'\right\}^{\frac{1}{2}}, \tag{3}$$

where $d\tau'$ indicates the volume element with respect to r_1, θ_1, φ_1, r_2, and φ.

It is clear that the c_i's depend on the particular form which is used for Ψ_H^N. Therefore to obtain an indication of their stability for small variations in Ψ_H^N, expansions of the type given in Eq. (1) were carried out for both the three and the six constant expressions given by Hylleraas. The three term wave function has the form

$$\Psi_H^N=Ne^{-Zs}(1+a_1u+a_2t^2),$$

and the six term wave function the form

$$\Psi_H^N=Ne^{-Zs}(1+a_1u+a_2t^2+a_3s+a_4s^2+a_5u^2),$$

where $s=r_1+r_2$, $t=r_1-r_2$, and $u=r_{12}$, and the r's are expressed in atomic units. The values which were used for the constants in the three term expression were $N=1.321350$, $Z=1.816$, $a_1=0.30$, $a_2=0.13$, and in the six term expression $N=1.381890$, $Z=1.818$, $a_1=0.353$, $a_2=0.128$, $a_3=-0.101$, $a_4=0.033$, $a_5=-0.032$. The three term wave function gives $-5.80488\ R_{\mathrm{He}}hc$ for the energy and the six term one gives $-5.80648\ R_{\mathrm{He}}hc$. An empirical value for this quantity can be found by adding the ionization energies for He I and He II $(-1.80734\pm0.00014)\ R_{\mathrm{He}}hc$ and $-4.00018\ R_{\mathrm{He}}hc$, respectively, to give $(-5.80752\pm0.00014)\ R_{\mathrm{He}}hc$.[9] The two expressions are therefore quite similar and both give excellent values of the energy. Table I gives the values of the c_i's found in the two expansions. Column two gives the values of the c_i's in the expansion of the three term Hylleraas expression and column three the values in the expansion of the six term expression. The final line of the table gives the value of $\sum_i c_i^2$. If the expansions were complete and the normalization constants were exact, this sum should be one. The stability of the c_i's is indicated by the similarity of their values in the two expansions.

TABLE I. Values of c_i in the expansion $\Psi_H^N=\Sigma_i c_i\Phi_i^N P_i^N$.

	Three term $\Psi^N{}_H$	Six term $\Psi^N{}_H$
c_0	0.997535	0.997945
c_1	0.069227	0.062583
c_2	0.010398	0.012739
c_3	0.003528	0.004322
$\Sigma_i c_i^2$	0.999989	0.999991

[9] The values of the ionization energies and R_{He} in cm^{-1} were taken from Charlotte E. Moore, *Atomic Energy Levels*, National Bureau of Standards Circular 467 (U. S. Government Printing Office, Washington, D. C., 1949), pp. 4, 6.

The most interesting result which appears in Table I is the large contribution to the ground-state wave function of components which are not spherically symmetric. Thus the coefficients of the P_1^N, P_2^N, and P_3^N terms are approximately 7 percent, 1 percent and 0.4 percent of the coefficient of the P_0^N term.

From Eq. (2) one may find the form of the Φ_i^N's. For those associated with the three term expression one obtains

$$\Phi_0^N=\sqrt{2}N\frac{1}{c_0}e^{-Z(r_1+r_2)}\left\{1+\tfrac{1}{8}a_1r_>\left(\frac{r_<^2}{r_>^2}+3\right)+a_2(r_>-r_<)^2\right\},$$

and for $i=n>0$,

$$\Phi_n^N=\sqrt{2}N\frac{1}{c_n}e^{-Z(r_1+r_2)}\left\{\frac{a_1}{(2n+3)(2n+1)^{\frac{1}{2}}}\frac{r_<^n}{r_>^{n-1}}\times\left(\frac{r_<^2}{r_>^2}-\frac{2n+3}{2n-1}\right)\right\}$$

where $r_<$ is the lesser, and $r_>$ the greater, of r_1 and r_2. For the Φ_i^N's associated with the six-term expression one finds for $i=0$ and 1,

$$\Phi_0^N=\sqrt{2}N\frac{1}{c_0}e^{-Z(r_1+r_2)}\left\{1+\tfrac{1}{8}a_1r_>\left(\frac{r_<^2}{r_>^2}+3\right)+a_2(r_>-r_<)^2+a_3(r_1+r_2)+a_4(r_1+r_2)^2+a_5(r_1^2+r_2^2)\right\},$$

$$\Phi_1^N=\sqrt{2}N\frac{1}{c_1}e^{-Z(r_1+r_2)}\left\{\frac{a_1}{5\sqrt{3}}\left(\frac{r_<^3}{r_>^2}-5\right)-\frac{2a_5}{\sqrt{3}}r_1r_2\right\}.$$

The Φ_i^N's for $i>1$ for the three and six term expressions are identical except for the values of the c_i's, a_i's and N and Z.

It is interesting now to see how much the various angular components of the ground-state wave function contribute to the total energy of the state. Therefore we have listed in Table II for the three and six constant functions the contributions to the total energy of the various terms in the integral

$$E=\int\sum_i(c_i\Phi_i^N P_i^N)^*H\sum_i(c_i\Phi_i^N P_i^N)d\tau,$$

where $d\tau$ indicates the volume element with respect to all six variables.

The first column of Table II gives the various terms in the integrand, where (i) is written for $c_i\Phi_i^N P_i^N$. The second and fourth columns give the contributions to the energy in units of $R_{\mathrm{He}}hc$ of these terms for the cases of the three- and six-constant Hylleraas wave functions, respectively. The third and fifth columns give

TABLE II. Contributions to the total energy of the terms in $E=\int\Sigma_i(c_i\Phi_i{}^N P_i{}^N)^* H\Sigma_i(c_i\Phi_i{}^N P_i{}^N)d\tau$ in units of $R_{He}hc$.

Terms	3-constant Hylleraas wave function: Contributions of the terms	3-constant Hylleraas wave function: Contributions of the angular components of the wave function	6-constant Hylleraas wave function: Contributions of the terms	6-constant Hylleraas wave function: Contributions of the angular components of the wave function
$(0)^*H(0)$	−5.72823	−5.72823	−5.73371	−5.73371
$(1)^*H(1)$	+0.01700	−0.06992	+0.01921	−0.06527
$(1)^*H(0)+(0)^*H(1)$	−0.08692		−0.08448	
$(2)^*H(2)$	+0.00179	−0.00478	+0.00269	−0.00545
$(2)^*H(0)+(0)^*H(2)$	−0.00790		−0.00969	
$(2)^*H(1)+(1)^*H(2)$	+0.00133		+0.00155	
$(3)^*H(3)$	+0.00044	−0.00110	+0.00066	−0.00121
$(3)^*H(0)+(0)^*H(3)$	−0.00192		−0.00235	
$(3)^*H(1)+(1)^*H(3)$	+0.00030		+0.00035	
$(3)^*H(2)+(2)^*H(3)$	+0.00008		+0.00013	
Sum	−5.80403	−5.80403	−5.80564	−5.80564
$\int\Psi_H{}^{N*}H\Psi_H{}^N d\tau$	−5.80488		−5.80648	

the contributions of the various angular components of these wave functions to the energy if all of the angular components of lower order are also present. The next to last line of Table II gives the sum of the contributions to the energy of the first four angular components, and the final line gives the energy found by Hylleraas for the complete wave function.

An examination of Table II shows that the spherically symmetric term accounts for 98.7 percent of the total energy given by the three-constant wave function and for 98.8 percent of that given by the six-constant wave function. The addition of a cosine term allows one to pick up 91.2 percent and 89.7 percent of the remaining energy, respectively. The terms containing the second-order Legendre polynomial account for 71.0 percent and 72.6 percent of what then remains, and the terms containing the third-order Legendre polynomial account for 55.9 percent and 59.1 percent, respectively, of what is still left after the spherically symmetric component and the first two angular components have been included. The first four components together account for 99.9851 percent and 99.9855 percent, respectively, of the total energies given by the three-constant and six-constant wave functions.

A comparison of the results given in Tables I and II shows that the ratios of the contributions of the non-spherically symmetric components to those of the spherically symmetric ones are much larger for the wave function than for the energy. Thus the contributions of the $P_1{}^N$, $P_2{}^N$, and $P_3{}^N$ components to the energy are only 1.22 percent, 0.083 percent, and 0.019 percent of the contribution of the $P_0{}^N$ component in the case of the three constant wave function and only 1.14 percent, 0.095 percent, and 0.021 percent in the case of the six-constant function. The ratios of the contributions to the wave function of the $P_1{}^N$, $P_2{}^N$, and $P_3{}^N$ components to that of the $P_0{}^N$ component are therefore roughly 6, 13, and 19 times as large as the corresponding ratios of the contributions to the energy. This result emphasizes the difficulty of obtaining a high accuracy wave function by minimizing the energy.

One may use the data in Table II, together with the results of earlier work, to estimate the magnitude of the correlation energy, that is, the configuration interaction energy, and its component parts for the ground state of He I. The correlation energy is sometimes taken to be the difference between the experimental value of the energy and the energy as found by the Hartree-Fock procedure, without any consideration of configuration interaction. However, the correlation energy as computed in this way does not have the simple physical significance which one would like to associate with this term. We can see that this is the case by considering the physical situation which leads to the introduction of the concept of correlation energy. If a wave function is to take into account the repulsion between electrons and the consequent low probability that two of them will be found in the same small volume, it must be small whenever two electrons are close together. The Hartree and the Hartree-Fock wave functions are in general the only high accuracy wave functions available for complex atoms. Of these two types the Hartree-Fock wave functions are the superior since exchange effects are included in their derivation, and we shall limit our further discussion to functions of this type. However, Hartree-Fock functions are not necessarily small when two electrons are close together. They take the electron repulsion into account only in the average. As a result the energies obtained from such functions are higher than the observed energies because they include the positive repulsive potential energies from the increased electron interactions. It would therefore seem to be more meaningful physically to define the correlation energy (the configuration interaction energy) as the difference between the energy given by an exact solution of the Schrödinger equation for the particular problem and the energy given by the Hartree-Fock component in an expansion of the exact solution. This expansion of the exact solution is to be made in

terms of some orthonormal set of functions of which the Hartree-Fock function is the first member. The reasons for suggesting this definition will be presented in the following paragraph.

If we are to use this definition for the correlation energy, the method of computing this quantity which was mentioned first can yield only a lower limit and this limit, at least for the case of the ground state of He I, is considerably smaller than the true value. The reason for this is the following: To build an exact solution from a Hartree-Fock wave function it is necessary to superpose the Hartree-Fock solutions for other configurations or to include multiplicative functions of the r_{ij}'s. The energy found for such a solution would be lower than that found for the Hartree-Fock solution alone. However, the new wave function must be normalized, and the contribution of the Hartree-Fock component to the total energy will be less than if this component were the only one. Therefore the difference between the observed energy and the Hartree-Fock energy is a smaller quantity than the correlation energy as defined above. The proper procedure to determine this energy would be to find the difference between the energy given by the exact solution and the energy given by the Hartree-Fock component of the exact solution where the Hartree-Fock wave function is that of the configuration making the largest contribution to the energy of the state. To obtain the latter quantity one would multiply the ordinary Hartree-Fock energy by the square of the coefficient of the Hartree-Fock wave function in an expansion of the exact solution in terms of some orthonormal set of functions of which the Hartree-Fock function was the first member. Unfortunately, it will usually be the case that neither the exact solution nor any close approximation to it will be known. One may then take the experimental energy as the energy which would be given by an exact solution if one were known, but there would seem to be no way of determining the needed expansion coefficient. Under these circumstances one can only turn to the first method of estimating the correlation energy mentioned above, which assumes it to be the difference between the experimental and the Hartree-Fock energy, recognizing that this method yields only a lower limit.

Fortunately in the case of the ground state of He I the data are more complete. The three- and six-constant Hylleraas ground-state wave functions are both excellent approximations to the exact solution of the Schrödinger equation of the problem. The three-constant function gives the observed energy to better than 0.05 percent and the six-constant function to better than 0.02 percent. For this state the self-consistent field wave functions with and without exchange are identical and the energy has been found to be $-5.723\ R_{\mathrm{He}}hc$.[10] In addition, in earlier work[5] the three- and six-constant Hylleraas wave functions were expanded in terms of symmetrized products of self-consistent field wave functions, and the coefficients of the $1s^2$ configuration were found to be 0.99550 and 0.99606, respectively. The largest contribution which these wave functions can yield to the energy given by the Hylleraas expressions can therefore be found by multiplying the energy obtained using only these wave functions by the square of their expansion coefficients. This procedure gives $-5.672R_{\mathrm{He}}hc$ and $-5.678\ R_{\mathrm{He}}hc$ for the three- and six-term wave functions, respectively. However, the three-term Hylleraas expression yields an energy $0.003\ R_{\mathrm{He}}hc$ above the experimental value and the six-term expression an energy $0.001\ R_{\mathrm{He}}hc$ higher than the experimental. It is not clear what part of these differences between the Hylleraas and the experimental energies should be assigned to the correlation energy. If we assume that none of it should be so assigned, we obtain the smallest estimates of the size of the correlation energy, $-0.133\ R_{\mathrm{He}}hc$ and $-0.129\ R_{\mathrm{He}}hc$, respectively. These values are considerably larger than the value $-0.073\ R_{\mathrm{He}}hc$ found by Taylor and Parr.[6] The discrepancy is accounted for by their use of an older value of the Hartree-Fock energy[11] and by the fact that they did not employ an expansion coefficient to determine a correction factor, so that they took no cognizance, in the manner suggested above, of the reduction of this energy which would result if terms were included in the wave function to take account of the correlation in the position of the electrons.

In general, it is clear that the choice of the correction factor will depend on the particular approximation to the exact wave function which has been employed. Thus the coefficients of the $1s^2$ configuration in the expansions of the two Hylleraas functions were different. However, if one employs approximate wave functions which give good values of the energy and which are of sufficiently general form, the expansion coefficient of the $1s^2$ configuration should be relatively stable. It might seem that if the correlation energy is introduced by the addition of terms in the interelectron distances it would only be necessary to set the coefficients of such terms equal to zero to find the noncorrelation part of the energy. This is not the case, however, since when r_{ij} terms are introduced they will take up part of the average interelectron distance effect. Thus, in the case of the three-constant He I ground-state wave function, the contribution of the terms not involving the interelectron distance is only $-3.11084\ R_{\mathrm{He}}hc$.

It is interesting now to estimate what part of the total correlation energy is radial, what part angular, and what part may be classified as mixed. One may take the radial correlation energy for the ground state of He I as the difference between the contribution to the total energy from the purely radial terms of a wave function which gives a good value of the energy and contains both radial and angular terms and the Hartree-

[10] W. S. Wilson, Phys. Rev. 48, 536 (1935).

[11] H. Bethe, *Handbuch der Physik* (Julius Springer, Berlin, 1933), second edition, Vol. 24/1, p. 370.

Fock energy corrected as in the preceding paragraphs. Similarly the angular part of the correlation energy may be taken as the difference between the contribution from the Hartree-Fock component plus the nonspherically symmetric components and the corrected Hartree-Fock energy. Finally, the mixed part of the correlation energy may be taken as the contribution from the cross-product terms between those parts of the purely radial terms which do not belong to the Hartree-Fock wave function and the nonspherically symmetric terms. We should therefore take the difference between the energy given in Table II for the spherically symmetric component and the corrected Hartree-Fock energy as the radial correlation energy. This quantity is $-0.056\ R_{\mathrm{He}}hc$ for both the three- and six-term wave functions. It is not possible from the data at hand to compute a value strictly according to the tentative definition given above for the angular correlation energy. This results from the fact that, in calculating the contribution of the nonspherically symmetric components, the cross-product terms have been found using $\Phi_0{}^N$ instead of the Hartree-Fock part of $\Phi_0{}^N$. However, the correct calculation has been made for the cross product involving the first angular component $\Phi_1{}^N$ of the Hylleraas three-term expression, with the result that the value found was $-0.08896\ R_{\mathrm{He}}hc$ instead of $-0.08692\ R_{\mathrm{He}}hc$ as given in line 3 of Table II. This indicates, as was to be expected, that the mixed part of the correlation energy amounts to only a few percent of the radial and angular parts. If one accepts this result as applicable to the other angular components, which have not been specifically investigated, one would estimate the angular correlation energy as a few percent more than the difference between the energy given by one of the Hylleraas expressions and that given by its $\Phi_0{}^N$ component. The angular correlation energy is therefore probably a few percent more than $-0.077\ R_{\mathrm{He}}hc$ and $-0.073\ R_{\mathrm{He}}hc$, perhaps $-0.079\ R_{\mathrm{He}}hc$ and $-0.075\ R_{\mathrm{He}}hc$, for the three- and six-term wave functions, respectively. In accordance with this argument we estimate the mixed correlation energy very roughly as $+0.002\ R_{\mathrm{He}}hc$. These values for the parts of the correlation energy assume that the entire difference between the experimental ground-state energy and the values given by the Hylleraas functions should be attributed to that part of the energy which does not depend on the correlation of the positions of the electrons. Without this assumption the above values of the correlation energies would be slightly increased, but just how these small differences should be divided between the noncorrelation energy and the various parts of the correlation energy is not clear.

In summary the present work gives the results of the expansion of the three-term and the six-term expressions given by Hylleraas for the ground-state wave function of He I in series of normalized Legendre functions times normalized functions of r_1 and r_2. The coefficients in these expansions decrease with increasing order of the Legendre functions but not so rapidly as might have been expected. Thus the coefficient of the term involving the Legendre function of order one is 7 percent of the coefficient of the spherically symmetric term. The contribution of the various terms to the total energy falls off more rapidly. A definition of total correlation energy is suggested, and on the basis of this definition, the value of the total correlation energy is found to be at least $-0.129\ R_{\mathrm{He}}hc$ for the He I ground state. The total correlation energy is further divided into radial, angular, and mixed parts of estimated size $-0.056\ R_{\mathrm{He}}hc$, $-0.075\ R_{\mathrm{He}}hc$, and $+0.002\ R_{\mathrm{He}}hc$, respectively.

Mass Surfaces

ALEX E. S. GREEN* AND NICHOLAS A. ENGLER†
Department of Physics, University of Cincinnati, Cincinnati, Ohio
(Received December 18, 1952)

We examine in the light of recent experimental data smooth mass surfaces which may be placed in the form

$$M-A=\Delta_m(A)+J(A)[D-D_m(A)]^2,$$

where $\Delta_m(A)$, $D_m(A)$, and $J(A)$ are key functions which characterize the mass surface and $D=N-Z$ is the neutron excess. We here attempt to find an optimum set of key functions and to evaluate various semi-empirical key functions now in use.

In this study we introduce the reference key functions

$$\Delta_m(A)=(A-100)^2/100-64, \text{ (mMU)}$$
$$J(A)=25/A, \text{ (mMU)}$$

and

$$D_m(A)=0.4A^2/(A+200).$$

We use these reference functions in such a way as to effectively subject the data and various semi-empirical functions to microscopic examination, so that "fit" becomes immediately apparent. We note that most of the semi-empirical mass surfaces in current use give rise to large systematic errors in nuclear masses. The large errors are not inherent properties of the semi-empirical equation since a set of constants can be found which reduce these errors to within the range of uncertainty caused by shell effects.

1. A REFERENCE MASS SURFACE

NUCLEAR mass surfaces have been used in pure and applied nuclear physics for the following reasons: (1) They serve to systematize existing experimental information concerning nuclear masses and energies and thereby provide a succinct summary of a large quantity of information. (2) They provide a reasonable basis for predicting unknown nuclear masses and energies. (3) They serve as smooth base surfaces from which irregularities of the experimental mass surface may be charted permitting thereby a careful study of these irregularities. (4) They serve to test various statistical theories of the nucleus. In all but the last application the theoretical justification of the expression used for the nuclear surface is unimportant as compared to the accuracy and simplicity of the mathematical representation. Since the mass surfaces which have some direct theoretical foundations are rathe cumbersome to use and, as we shall see, quite inaccurate we have developed a simpler and more accurate reference surface. This reference surface is a member of the class of surfaces in which the mass decrement, $\Delta=M-A$, may be expressed in the form

$$\Delta=\Delta_m(A)+J(A)[D-D_m(A)]^2, \quad (1)$$

where $D=N-Z$ is the neutron excess and $\Delta_m(A)$, $D_m(A)$, and $J(A)$ are functions of the mass number. Mass data, beta-decay data, and various theoretical models of the nucleus suggest that, apart from shell and pairing discontinuities, a surface of this general form may be used as an approximate representation of nuclear mass decrements. The function $\Delta_m(A)$ fixes the depth of the valley of the mass surface. The term $J(A)[D-D_m(A)]^2$ is based upon the assumption that apart from the shell and pairing discontinuities isobaric sections of the mass surface are parabolas. $D_m(A)$ fixes the neutron excess of the vertex and $J(A)$ characterizes the width of the parabola. The parabolic (A, Z) surface corresponding to Eq. (1) may be obtained by letting $D=A-2Z$ and $D_m(A)=A-2Z_m(A)$.

For our reference mass surface we use for $A>10$ the simple key functions[1]

$$\Delta_m{}^r(A)=(A-100)^2/100-64, \text{ mMU} \quad (2)$$

$$J^r(A)=25/A, \text{ mMU} \quad (3)$$

and

$$D_m{}^r(A)=0.4A^2/(A+200). \quad (4)$$

Apart from accuracy, convenience and simplicity of computation were major considerations in our choice of

TABLE I. Key reference functions.

A	$\Delta_m{}^r(A)$ mMU	$J^r(A)$ mMU	$D_m{}^r(A)$	A	$\Delta_m{}^r(A)$ mMU	$J^r(A)$ mMU	$D_m{}^r(A)$
10	17.000	2.500	0.190	140	−48.000	0.179	23.059
20	0.000	1.250	0.727	150	−39.000	0.167	25.714
30	−15.000	0.833	1.565	160	−28.000	0.156	28.444
40	−28.000	0.625	2.667	170	−15.000	0.147	31.243
50	−39.000	0.500	4.000	180	−0.000	0.139	34.105
60	−48.000	0.417	5.538	190	17.000	0.132	37.026
70	−55.000	0.357	7.259	200	36.000	0.125	40.000
80	−60.000	0.312	9.143	210	57.000	0.119	43.024
90	−63.000	0.278	11.172	220	80.000	0.114	46.095
100	−64.000	0.250	13.333	230	105.000	0.109	49.209
110	−63.000	0.227	15.613	240	132.000	0.104	52.364
120	−60.000	0.208	18.000	250	161.000	0.100	55.555
130	−55.000	0.192	20.485				

* Now at the Department of Physics, Florida State University, Tallahassee, Florida.

† Now at the Department of Physics, University of Dayton, Dayton, Ohio.

[1] A. E. S. Green, Phys. Rev. **86**, 654 (1952). The tentative change of the constant in Eq. (2) from 62 to 64 was in response to a large change (8 mMU) in the heavy masses.

Eqs. (2)–(4). To show the order of magnitude of these functions, we give in Table I the values of these key functions for various mass numbers. Since $[D-D_m{}^r(A)]^2$ are usually numbers of the order of unity, we note if we compare $J^r(A)$ with $\Delta_m{}^r(A)$ that the latter is the dominant term in the expression for mass decrements. The over-all accuracy of $\Delta_m{}^r(A)$ will become apparent when we discuss Fig. 1 (see Sec. 3).

2. SEMI-EMPIRICAL MASS SURFACES

According to the well-known statistical theory of Weiszäcker[2] Bethe,[3] Bohr and Wheeler,[4] and others, nuclear energies may be represented by

$$E^w=-a_1A+a_2A^{\frac{2}{3}}+a_3(Z^2/A^{\frac{1}{3}})+a_4(N-Z)^2/4A. \quad (5)$$

While the constants a_1, a_2, a_3, and a_4 may be related to physically important parameters it is usual to relax the theoretical constraints and instead to adjust these constants to fit the experimental data. For this reason Eq. (5) is referred to as a semi-empirical. The equation for mass decrements corresponding to Eq. (5) expressed as a function of the mass number and the neutron excess is

$$\Delta^w=\tfrac{1}{2}(A+D)\Delta_n+\tfrac{1}{2}(A-D)\Delta_H-a_1A+a_2A^{\frac{2}{3}} +a_3(A-D)^2/4A^{\frac{1}{3}}+a_4D^2/4A, \quad (6)$$

where Δ_n and Δ_H are the mass decrements of the neutron and the hydrogen atom. We may place this expression in the form of Eq. (1) by finding the function $D_m(A)$ which gives the minimum of Δ^w for a fixed A and by substituting this expression into Eq. (6). They key functions so obtained are

$$\Delta_m{}^w(A)=-[a_1-(3\Delta_n+\Delta_H)/4]A +(a_4+\Delta_n-\Delta_H)D_m{}^w(A)/4+a_2A^{\frac{1}{3}}, \quad (7)$$

$$D_m{}^w(A)=A[\rho A^{\frac{1}{3}}-(\Delta_n-\Delta_H)/a_4]/(1+\rho A^{\frac{1}{3}}), \quad (8)$$

$$J^w(A)=(a_4/4A)(1+\rho A^{\frac{1}{3}}), \quad (9)$$

where $\rho=a_3/a_4$. In some treatments the Z in Eq. (5) is replaced by $Z(Z-1)$. The key functions then are

$$\Delta_m{}^w(A)=-[a_1-(3\Delta_n+\Delta_H)/4]A +(a_4+\Delta_n-\Delta_H)D_m{}^w(A)/4 +(a_2-a_3/4)A^{\frac{1}{3}}+a_3D_m{}^w(A)/4A^{\frac{1}{3}}, \quad (7')$$

$$D_m{}^w(A)=[\rho A^{\frac{1}{3}}(A-1)-(\Delta_n-\Delta_H)/a_4]/(1+\rho A^{\frac{1}{3}}). \quad (8')$$

$J^w(A)$ is unchanged. In Table II we list various sets of empirical constants which have appeared in the literature. Whenever they are known we have listed the proton and neutron mass decrements originally used in the adjustment of the empirical constants. The last set of constants is a tentative set arrived at in this paper. In the last column we indicate the equations to which these constants refer, and in the next to the last column we list the fission constant $2a_2/a_3$.

3. THE OPTIMUM MASS SURFACE

We shall now attempt to use the experimental data to evaluate a set of functions which within the class represented by Eq. (1) provide the optimum representation of this data. We shall denote these functions by the superscript letter o. Instead of attempting to evaluate this function directly we shall introduce a set of parameters which characterize the deviations of the optimum functions from our empirical functions. For this purpose we shall define R^o, Υ^o and r^o by

$$R^o=\Delta_m{}^o(A)-\Delta_m{}^r(A),$$

$$\Upsilon^o=D_m{}^o(A)-D_m{}^r(A), \quad (10)$$

and

$$r^o=J^o(A)/J^r(A). \quad (11)$$

In a similar way we may define three parameters R^w, Υ^w, and r^w to characterize the deviations of the Weiszäcker functions from our reference functions. These deviation functions may be computed for any set of semi-empirical constants.[5] We may now in principle use the experimental data to evaluate R^o, Υ^o, and r^o. The extents to which R^o deviates from 0, Υ^o deviates from 0, and r^o deviates from 1 measure the inaccuracy of our

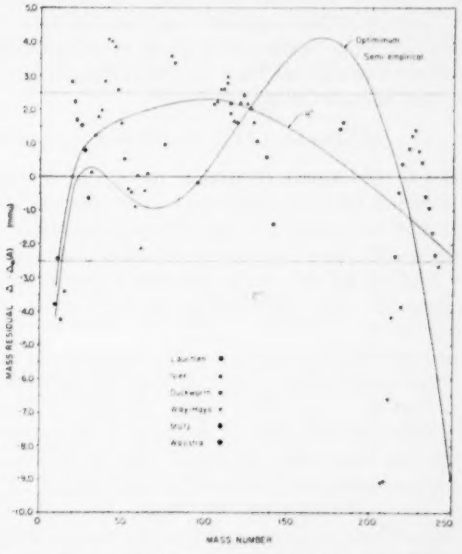

FIG. 1. Mass residuals for beta-stable odd-A nuclide vs mass number. R^o is our tentative, optimum, smooth residual. The optimum semi-empirical curve represents the residual for the semi-empirical equation arrived at in this paper. The base line represents our reference function $\Delta_m{}^r(A)$. Sources of experimental data are indicated by the symbols (see references 6–12).

[2] C. F. von Weiszäcker, Z. Physik **96**, 431 (1935).
[3] H. A. Bethe and R. F. Bacher, Revs. Modern Phys. **8**, 165 (1936).
[4] N. Bohr and J. A. Wheeler, Phys. Rev. **56**, 426 (1939).

[5] A preliminary report of this study of the semi-empirical equation was made at the March, 1952 meeting of the American Physical Society in Columbus, Ohio [N. Engler and A. E. S. Green, Phys. Rev. **86**, 654 (1952)].

TABLE II. Sets of empirical constants (in mMU).

Sym	Author	Ref	Δ_n	Δ_H	a_1	a_2	a_3	a_4	$2a_3/a_2$	Eqs.
I	Bethe	a	8.450	8.070	14.885	14.176	0.623	83.770	43.5	7, 8, 9
II	Fermi	b	8.930	8.123	15.04	14.0	0.627	83	44.7	7, 8, 9
III	Mattauch	c	8.945	8.131	15.74	16.5	0.647	88.24	51.0	7, 8, 9
IV	Feenberg	d	8.920	8.130	15.035	14.069	0.627	77.755	44.9	7', 8', 9
V	Pryce	e	8.930	8.123	15.089	15.035	0.655	84.199	45.9	7, 8, 9
VI	Metropolis	f	8.982	8.142	15.0825	14.0	0.627	82.970	44.7	7, 8, 9
VII	Fowler	g	8.930	8.132	16.432	17.989	0.741	96.872	48.6	7', 8', 9
VIII	This paper		8.982	8.142	16.720	18.500	0.750	100.00	49.3	7, 8, 9

[a] See reference 3.
[b] C. Goodman, *The Science and Engineering of Nuclear Power* (Addison Wesley Press, Cambridge, 1947), Chap. 2 by M. Deutsch.
[c] J. Mattauch and S. Flugge, *Introduction to Nuclear Physics* (Interscience Publishers, Inc., New York, 1946).
[d] E. Feenberg, Revs. Modern Phys. **19**, 239 (1947). This comprehensive article lists several sets of constants and goes deeply into the question of the variation of semi-empirical constants. The particular set referred to here is quoted by J. M. Blatt and V. F. Weisskopf, in *Theoretical Nuclear Physics* (John Wiley and Sons, Inc., New York, 1952).
[e] M. H. L. Pryce, Proc. Phys. Soc. (London) **63**, 692 (1950). The neutron and proton masses for 1950 were assumed here since they were not given in the paper.
[f] N. Metropolis and G. Reitweiser, *Table of Atomic Masses*, U. S. Atomic Energy Commission Report NP 1980, March, 1950 (unpublished).
[g] W. A. Fowler (unpublished) quoted on p. 11 of W. E. Siri, *Isotopic Tracers and Nuclear Radiations* (McGraw-Hill Book Company, Inc., New York, 1949).

reference functions. The extents to which R^o deviates from R^w, Υ^o deviates from Υ^w, and r^o deviates from r^w measure the inaccuracy of the semi-empirical function. By this procedure we shall in effect make microscopic examination of the data in relation to the analytical expressions which we are investigating.

4. THE DEVIATION FUNCTION R^o

If the experimental masses conform to Eq. (1), then $D-D_m{}^o(A)$ for the beta-stable odd mass nuclides should take on random values between ± 1 since if the neutron excess were more than one unit away from the valley for a particular set of isobars, beta-decay would produce a nuclide with less mass. Thus on the average the parabolic term contributes approximately

$$25([D-D_m{}^o(A)]^2)/A \approx 12.5/A, \qquad (12)$$

a quantity which may be ignored for $A>10$. We may therefore use the mass decrement values for the beta-stable odd nuclides to represent rather accurately the variation with mass number of the valley points of the mass surface. In Fig. 1 we plot the residuals of the experimental mass decrements for beta-stable odd nuclides *vs* A.

The experimental data used in Fig. 1 has for the most part been compiled from mass determinations reported since 1950 by Nier,[6] Duckworth,[7] Lauritsen,[8] Motz,[9] and their co-workers, and by Wapstra.[10] The sources of the data are indicated on the figure. For the very heavy nuclides we used a new mass table based upon the mass value for Pb^{208} reported by Hays, Richards, and Goudsmit[11] and the neutron and proton binding energies compiled by Way.[12] This set of masses runs about 8 mMU below the masses compiled by Stern.[13]

Examining Fig. 1, we see that the experimental residuals tend to fluctuate about the zero axis rather erratically. The smooth dotted curve indicated in Fig. 1 represents our tentative choice of R^o. Our effective scale (the distance between the two dashed lines is 5 mMU) is so large that we are here in a realm in which smooth curves may be chosen with considerable latitude. However, for our purposes here this latitude is essentially negligible. We note, first of all, that the deviations $R^o=\Delta-\Delta_m{}^r(A)$ are only of the order of a few millimass units and are quite small compared to the magnitude of the variation of decrements. (See column 2 Table I). Accordingly we may conclude that our reference function $\Delta_m{}^r(A)$ "fits" the experimental data quite well. In Fig. 2 we represent the residuals R^o by a series of dark circles and the residual $R^w=\Delta_m{}^w(A)-\Delta_m{}^r(A)$ for various semi-empirical equations by curved lines. To

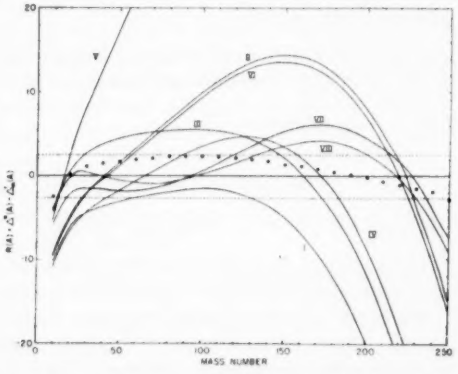

FIG. 2. Semi-empirical residuals *vs* mass number for various sets of semi-empirical constants. (See references in Table II.) I—Bethe; II—Fermi; III—Mattauch; IV—Feenberg; V—Pryce; VI—Metropolis; VII—Fowler; VIII—This paper. The small solid circles represent the estimated R^o from Fig. 1.

[6] Collins, Nier, and Johnson, Phys. Rev. **86**, 408 (1952); R. E. Halsted, Phys. Rev. **85**, 726 (1952); **88**, 666 (1952).
[7] Duckworth, Johnson, Kegley, Olson, Presont, Stanford, and Woodcock, Phys. Rev. **78**, 179, 479 (1950); **79**, 402 (1950); **81**, 286 (1951); **82**, 468 (1951); **83**, 1114 (1951); Nature **167**, 1025 (1951).
[8] Li, Whaling, Fowler, and Lauritsen, Phys. Rev. **83**, 512 (1951).
[9] H. T. Motz, Phys. Rev. **81**, 1061 (1951).
[10] A. H. Wapstra (private communications).
[11] Hays, Richards, and Goudsmit, Phys. Rev. **84**, 824 (1951); **85**, 1065 (1952).
[12] K. Way and M. Wood (private communication, 1951).
[13] M. O. Stern, Revs. Modern Phys. **21**, 316 (1949).

accommodate the computed deviations a much smaller scale is used (the distance between the two dashed lines again is 5 mMU). The large magnitude of some of the deviations may come as a shock to the reader. Since nuclear masses have not changed to this extent in recent years we must either conclude that the methods of adjustment used in these earlier studies were very sensitive to these changes in nuclear masses (particularly those of the neutron and proton) or else the adjustments were made to a limited portion of the mass surface. Of the surfaces which have appeared earlier in the literature Fowler's surface is the most accurate.

Our curve which is closest to R^o was obtained by an iterative process which started from Fermi's constants. We essentially retained Fermi's $D_m(A)$ but varied the constants by discrete steps so as to reduce to zero the departures at widely spaced mass numbers. The $\Delta_m{}^w(A)$ function so obtained was then plotted and the process repeated until R^w was in good agreement with R^o. Since unassessed shell effects make us somewhat uncertain as to the validity of our tentative R^o we did not go as far as is possible with our attempt to match R^w to R^o. However, we have already gone far enough to show that large systematic errors in absolute masses are not intrinsic to the semi-empirical equation but instead these errors can be reduced substantially by an adjustment of the constants. We note, however, that the constants we obtained are quite larger than those quoted earlier in the literature and represent further steps in the direction already taken by Fowler. Fowler's constants, however, are not strictly comparable with ours since he has used Eq. (7′).

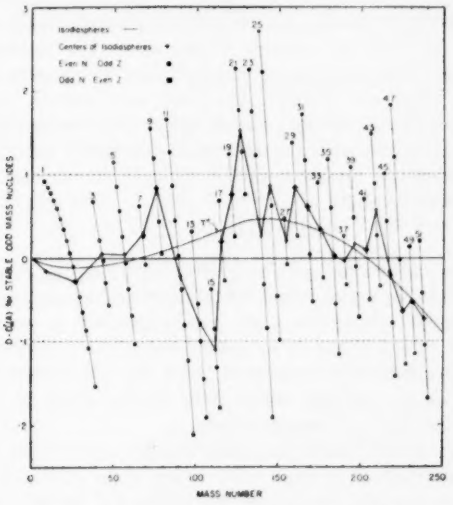

FIG. 3. $D-D_m{}^r(A)$ for beta-stable odd-A nuclides *vs* mass number. Υ^o locates our tentative optimum smooth line of beta-stability relative to our reference function. The base line represents our reference $D_m{}^r(A)$. Isodiaspheres are nuclides with equal neutron excess.

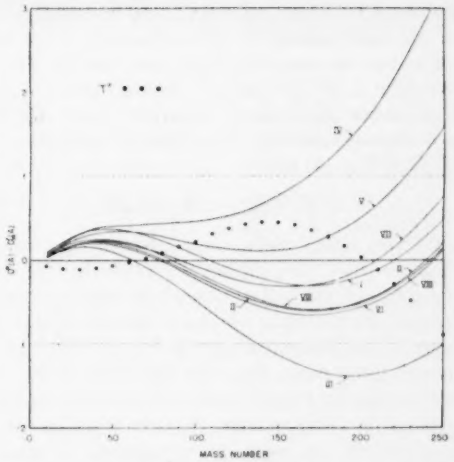

FIG. 4. Semi-empirical lines of beta-stability for various sets of semi-empirical constants. The solid circles are taken from the optimum smooth curve in Fig. 3.

5. THE FUNCTIONS $\Upsilon(A)$ AND $r(A)$

To determine the optimum $D_m{}^o(A)$ or $\Upsilon^o(A)$ we made use of the fact that according to Eq. (1) beta-stable odd mass nuclides should all have $D-D_m{}^o(A)$ values within ± 1. In Fig. 3 we have plotted $D-D_m{}^r(A)$ for all beta-stable odd nuclides. The jagged line joins the centers of the stable limits for various isodiaspheres. The larger discontinuities in this line undoubtedly are due to shell effects. Until these shell effects can be assessed quantitatively it is impossible to determine a precise Υ^o which represents the smooth line of beta-stability. However we have drawn a smooth curve which represents our tentative estimate of $\Upsilon^o(A)$. We could vary this curve in some places by as much as ± 0.2 unit without fear of contradicting the data. Unfortunately this uncertainty is a large fraction of the change in D (2 units) involved in beta-decay. Accordingly we must eventually fix Υ^o more precisely if we hope to make reliable estimates of the parabolic energy effect in beta-decay.

In Fig. 4 we show the Υ^w corresponding to various semi-empirical equations. We note that beyond the light nuclides these lines of least mass disagree with each other by distances which are much greater than 0.2 unit so that we can draw some conclusions from our tentative Υ^o despite its uncertainty. It would appear that Fermi's, Bethe's, Fowler's, and Metropolis' lines of least mass are more accurate than the others and are just about as good as our reference line. It also appears that all of the semi-empirical lines have the wrong general shape particularly in the very heavy region. Thus to match Υ^o it is necessary to allow ρ to vary rather than simply to make an adjustment of ρ. Using Fig. 4 the necessary variation of ρ can readily be determined. However, shell effects should first be precisely assessed before $\rho(A)$ is evaluated and interpreted.

The parabolic width ratio $r(A)$ may be evaluated for those odd mass isobars for which three or more mass values or two or more beta decay energies are known. For example, if M^-, M, and M^+ are the masses of three adjacent isobars which are β^- unstable, beta-stable, and β^+ or K capture unstable, it can readily be shown using Eq. (1) and Eq. (4) that

$$r=(M^-+M^+-2M_s)A/200. \quad (13)$$

In the very heavy region there are many instances in which more than three masses are available. For these cases a graphical method was found the most convenient to evaluate the parabolic width and hence r. The results of these calculations are shown in Fig. 5. The r values evaluated from mass data are represented by solid circles whereas the r values from beta-decay energies are represented by solid squares. Because these points are quite scattered we have not attempted to draw a smooth r^o curve. Also shown on this same graph are the r^w values corresponding to various semi-empirical equations. In view of the scattered nature of the experimental points we do not feel that any one of the analytical r^w including our $r=1$ has particular merit relative to the others. It is probable that experimental error and pairing effects[14] contributed to the scattering of r values.

6. OTHER APPLICATIONS OF THE REFERENCE FUNCTIONS

Another important application of our reference surface is to the organization and interpretation of the vast quantity of data concerning nuclear Q values. Let us consider a bombardment type reaction represented by the transformation

$$x(a,d)+X(A,D)\rightarrow X'(A',D')+x'(a',d'), \quad (14)$$

where x, X, X', and x' symbolize the incident, target, product and ejected nuclides, respectively. The Q value

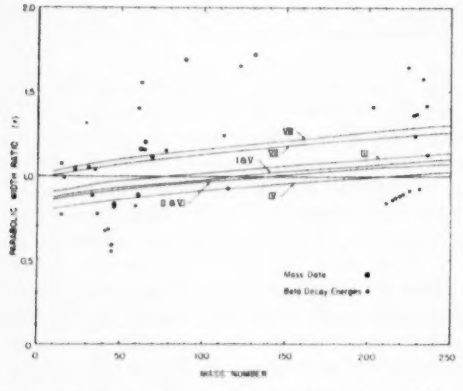

FIG. 5. Experimental and semi-empirical parabolic width ratios *vs* mass number. The horizontal line $r=1$ corresponds to our reference parabolic width function $J^r(A)$.

[14] C. D. Coryell and H. E. Suess, Phys. Rev. **86**, 609 (1952).

for this reaction in terms of the mass decrements of these nuclides is

$$Q=\delta+\Delta-\Delta'+\delta'. \quad (15)$$

Using Eq. (1) for the target and product nuclides and the experimental decrements for the very light nuclides, Q may be placed in the form

$$Q=Q_m(A)+Q_q \quad (16)$$

where

$$Q_m(A)=\delta-\delta'+\Delta_m(A)-\Delta_m(A'), \quad (17)$$

and

$$Q_q=J(A)[D-D_m(A)]^2-J(A')[D'-D_m(A')]^2. \quad (18)$$

Since $A'=A+a-a'$ we find, using Eq. (2), that for our reference function Eq. (17) becomes

$$Q_m{}^r(A)=\delta-\delta'+2(a-a')-(a-a')^2/100-2(a-a')A/100. \quad (19)$$

For reactions which produce a change in mass number from the target to the product nuclide this term usually makes the major contribution to the Q value. The great advantage of our reference surface with respect to the closely related semi-empirical surfaces is the simplicity of this expression for Q_m. The reader may convince himself of this advantage by deriving the general Q_m term corresponding to Eq. (7) or Eq. (7′). In Table III we tabulate the functions Q_m for most of the interesting bombardment reactions.[15] The table is so arranged that the function in each box is for a process in which the particle labeling the column is captured and the particle labeling the row is released. The constant term in each box is based upon the mass decrements for neutral light nuclides given by Li *et al.*[8] If these mass decrements change, the constants in Table III should be changed accordingly. Since Q_m is generally dominant, Table III may be used as a rough survey of nuclear reaction energies. For example, we note in accord with experience that reactions induced by deuterons, tritons, and helium-3 particles when gamma-rays, neutrons, protons, and alpha-particles are released are markedly exoergic.

For every experimental Q value let us define the residual Q value,

$$R(Q)=Q-Q_m{}^r(A). \quad (20)$$

These differences may be attributed primarily to discontinuities in the experimental mass surface and to the parabolic effect. Since the parabolic effect is usually small or else it can be estimated the Q value residuals, which can readily be computed with the aid of Table III, provide an excellent set of data for the study of discontinuities in the mass surface.

Residual Q values may also be used to facilitate the construction of a mass table based upon the latest Q values and beta-decay energies. Using Eq. (20) we note that

$$R\{Q[X(x,x')X']\}=R(X)-R(X'), \quad (21)$$

[15] We use the symbol χ to denote He^3.

TABLE III. $Q_m{}^r$ values in mMU. (The symbol χ denotes He^3.)

	γ	n	p	d	t	χ	α
γ	0	$10.972-0.02A$	$10.132-0.02A$	$18.695-0.04A$	$22.907-0.06A$	$22.887-0.06A$	$11.713-0.08A$
n	$-10.992+0.02A$	0	-0.840	$7.743-0.02A$	$11.975-0.04A$	$11.955-0.04A$	$0.801-0.06A$
p	$-10.152+0.02A$	0.840	0	$8.583-0.02A$	$12.815-0.04A$	$12.795-0.04A$	$1.641-0.06A$
d	$-18.775+0.04A$	$-7.763+0.02A$	$-8.603+0.02A$	0.000	$4.252-0.02A$	$4.232-0.02A$	$-6.902-0.04A$
t	$-23.087+0.06A$	$-12.055+0.04A$	$-12.895+0.04A$	$-4.272+0.02A$	0	-0.020	$-11.134-0.02A$
χ	$-23.067+0.06A$	$-12.035+0.04A$	$-12.875+0.04A$	$-4.252+0.02A$	0.020	0	$-11.114-0.02A$
α	$-12.033+0.08A$	$-0.981+0.06A$	$-1.821+0.06A$	$+6.822+0.04A$	$+11.114+0.02A$	$11.094+0.02A$	0
np	$-21.164+0.04A$	$-10.152+0.02A$	$-10.992+0.02A$	-2.389	$+1.863-0.02A$	$+1.843-0.02A$	$-9.291-0.04A$
nn	$-22.004+0.04A$	$-10.992+0.02A$	$-11.832+0.02A$	-3.229	$+1.023-0.02A$	$+1.003-0.02A$	$-10.131-0.04A$

where by definition

$$R(X)=\Delta-\Delta_m{}^r(A). \tag{22}$$

Thus we see that the residual Q values are related only to the masses of the target and product nuclides and not to the very light particles involved in the reaction. The residual Q-value data thus have the same significance as beta-decay energies, since for beta-decay energies

$$E_{\beta^-}=R(X)-R(X'), \tag{23}$$

and

$$E_{\beta^+}+2m_ec^2=R(X)-R(X'), \tag{24}$$

where E_{β^-} and E_{β^+} are the end point energies in β^- and β^+ decay. When sufficient Q value residuals and beta decay energies are known in a region we may solve for the mass residuals in terms of one known mass residual (say from a mass spectrographic determination). Using Eq. (22) we may readily convert these mass residuals into mass decrements. This was the procedure used in the construction of a new table of heavy masses[16] and it worked out quite well.

Applications of the reference functions to the study of fission, radioactive decay and other nuclear transformations are quite straightforward and will not be discussed here.

7. CONCLUSION

We have here made several applications of a set of reference functions [Eqs. (2)–(4)] for the purpose of examining semi-empirical mass surfaces in relation to the experimental data. We see from Fig. 2, Fig. 4, and Fig. 5 that each of these reference functions represent some sort of average of the semi-empirical functions, an average which is apparently more accurate than any of the semi-empirical functions. We have shown that most of the sets of semi-empirical constants quoted in the literature give rise to rather large systematic errors in nuclear masses. These large errors, however, are not inherent properties of the semi-empirical equation, since we have found a set which reduces these errors to within the range of uncertainty caused by shell effects. Our constants are substantially larger than those previously appearing in the literature, with the exception of the constants obtained by Fowler which are only slightly smaller than ours. It is interesting to note that of all the sets, only Fowler's and ours correspond to a fissionability constant close to the value 47.8 used by Bohr and Wheeler to predict photofission thresholds.

There is still good evidence which indicates that to fit the absolute mass surface and the line of beta-stability we must allow the semi-empirical constants to vary. However, until shell and pairing effects are quantitatively assessed such a study would probably not yield significant conclusions.

We have illustrated some applications of our reference functions to the organization and study of nuclear data.

We would like to express our appreciation to the many persons who have assisted in this study and in particular to acknowledge our indebtedness to Robert B. Minogue, John S. Nader, David F. Edwards, Rosalind Oppenheim, Nina J. Marucci, Richard Oswald, Lester Sollman, and Mrs. Walter Steiger.

We would also like to thank Drs. A. O. Nier, W. Whaling, N. Metropolis, K. Way, H. E. Duckworth, and A. H. Wapstra for sending us data prior to publication which were helpful in this study.

[16] J. S. Nader, Master's thesis, University of Cincinnati, 1952 (unpublished).

Discontinuities in the Nuclear Mass Surface

ALEX E. S. GREEN* AND DAVID F. EDWARDS
Department of Physics, University of Cincinnati, Cincinnati, Ohio
(Received December 18, 1952)

Proton and neutron binding energies are analyzed in such a way as to permit an approximate assessment of the effects associated with pairing and shell structure. We draw several interesting conclusions with respect to the accuracy of various theoretical expressions which have been proposed for the pairing effect. Our analysis of the data and considerations of an atomic model lead us to a simple approximate representation of a shell stabilizing correction to nuclear energies. This shell structure term accounts rather well for the observed departures from the general trends of beta-stability, nuclear masses, and nuclear Q values. Our shell correction suggests that much larger systematic variations in nuclear masses may be identified with shell structure effects than might previously have been suspected.

1. THE DATA AND THEIR INTERPRETATION

IT has been pointed out in the preceding paper[1] that nuclear mass decrements can be represented fairly accurately by the smooth function:

$$\Delta_m{}^r(A)=(A-100)^2/100-64, \text{ (mMU)}. \quad (1)$$

To facilitate the analysis of the discontinuities in the experimental mass surface, we have converted the experimental data into a set of mass residuals and reaction energy or Q-value residuals. The mass residual, in mMU, for a particular nuclide is here defined as

$$R=\Delta-\Delta_m{}^r(A), \quad (2)$$

where Δ is the experimental mass decrement ($\Delta=M-A$). The Q-value residual is defined [GE Eq. (20)] as:

$$R(Q)=Q-Q_m{}^r(A). \quad (3)$$

By referring the mass decrements and Q values to $\Delta_m{}^r(A)$ and $Q_m{}^r(A)$ instead of the complete reference functions, we greatly simplify the task of computing residuals. At the same time we still have the advantages of reference functions which are good approximations to the actual functions.

For studying shell and pairing discontinuities in the nuclear mass surface, we shall assume that the mass residuals may be represented by

$$R(N,Z)=S_{ij}(N,Z)+P(N,Z)+J^o[D-D_m{}^o(A)]^2. \quad (4)$$

The subscript i is used to denote a region of the mass surface lying between the planes defined by the magic neutron number N_u and N_l and the subscript j is used to denote a region lying between planes defined by the magic proton numbers Z_u and Z_l. (See Table II or Fig. 6.) $S_{ij}(N,Z)$ is assumed to embody the shell structure effect and $P(N,Z)$ is now used to represent the pairing effect. We shall assume that

$$\begin{aligned} &P(O,O)=H, \quad P(E,E)=-H, \\ &P(E,O)=p, \quad P(O,E)=n, \end{aligned} \quad (5)$$

where E and O denote the evenness or oddness of N or Z, respectively. We thus are adhering to the convention of referring masses to a surface which lies halfway between the even-even and odd-odd nuclear surfaces. We now allow, however, for the possible departures of the two odd mass surfaces from this intermediate surface. The parabolic term contains the optimum smooth functions for the line of stability and the parabolic width.

When both the target and product nuclides belong to the same zone, the Q-value residual is

$$\begin{aligned} R(Q)=S_{ij}(N,Z)-S_{ij}(N',Z')+P(N,Z) \\ -P'(N',Z')+J^o\theta^2-J^{o\prime}\theta'^2, \end{aligned} \quad (6)$$

where

$$\theta=D-D_m{}^o(A) \quad \text{and} \quad \theta'=D'-D_m{}^o(A').$$

Since the change in N, Z, and A are usually small compared to N, Z, and A we may express this equation approximately as

$$\begin{aligned} R(Q)\approx(n'-n)\partial S_{ij}/\partial N+(z'-z)\partial S_{ij}/\partial Z \\ +P-P'+J^o(\theta^2-\theta'^2), \end{aligned} \quad (7)$$

where n, n', z, and z' are the neutron and proton numbers of the incident and ejected particles. Thus apart from the spin and parabolic effect residual Q values are related to the partial derivatives of the shell function. The problem of opportioning the residual Q values to the four terms on the right side of Eq. (7) is complicated by the fact that these terms are frequently of the same order of magnitude. Fortunately by the judicious choice of data for study the problem becomes tractable.

2. NEUTRON AND PROTON BINDING ENERGIES

Neutron and proton binding energies furnish a good source of data for studying shell effects since in these cases either the first or second term in Eq. (7) vanishes. Neutron and proton binding energies may be obtained from

$$\begin{aligned} B_n(N,Z)=\Delta(N-1,Z)+\Delta_n-\Delta(N,Z) \\ =-Q[X(\gamma,n)X'] \end{aligned} \quad (8)$$

* Now at the Department of Physics, Florida State University, Tallahassee, Florida.

[1] A. E. S. Green and N. A. Engler, preceding paper [Phys. Rev. 91, 40 (1953)]; hereafter referred to as GE.

and

$$B_p(N,Z)=\Delta(N,Z-1)+\Delta_H-\Delta(N,Z)$$
$$=-Q[X(\gamma,p)X'] \quad (9)$$

To obtain the residual neutron binding energy we subtract $Q_m{}^r$ from both sides of Eq. (8). We find

$$R_n(N,Z)=B_n(N,Z)-B_n{}^r(A), \quad (10)$$

where $B_n{}^r(A)$ is the negative of the $Q_m{}^r(A)$ for the γ, n reaction. Using GE Eq. (17), it is simple to show that

$$R_n(N,Z)=R(N-1,Z)-R(N,Z). \quad (11)$$

Similiarly, for the residual proton binding energy,

$$R_p(N,Z)=B_p(N,Z)-B_p{}^r(A) \quad (12)$$
$$=R(N,Z-1)-R(N,Z). \quad (13)$$

$B_n{}^r(A)$ and $B_p{}^r(A)$ are reference functions found in Table III GE.

An extensive collection of neutron binding energies from (γ,n) thresholds, from the Q values of (n,γ) reactions, and (d,p) reactions, and from mass data is available.[2] However, few proton binding energies have been measured directly. The residual proton binding energies may be computed from (p,γ) reactions, (d,n) reactions and mass residual data using Eqs. (12) and (13) or else by the use of

$$R_p(N,Z)=R_n(N,Z)$$
$$+[R(N,Z-1)-R(N-1,Z)] \quad (14)$$

which follows from Eqs. (11) and (13). Since the difference between the mass residuals indicated in brackets is the same as the difference between masses this term may frequently be obtained from beta decay energies.

In view of Eqs. (8) and (9) we have, as special cases of Eq. (7),

$$R_n(N,Z)=-\partial S_{ij}/\partial N+P'-P+J^o(\theta'^2-\theta^2), \quad (15)$$

and

$$R_p(N,Z)=-\partial S_{ij}/\partial Z+P'-P+J^o(\theta'^2-\theta^2). \quad (16)$$

The parabolic term presents considerable difficulties. Not only is it a tedious term to compute but it is particularly sensitive to small fluctuations in the location of the valley. Since the shell effect is probably the main cause of fluctuations in the line of stability, we find ourselves in the situation of having to know the shell correction in order to evaluate the shell correction. Fortunately a successive approximation approach helps to resolve the difficulty. The approach which we adopted is based upon an attempt to minimize the parabolic term by selecting pairs of nuclides which have at least one β-stable member. Since the change in θ associated with the removal of a neutron or proton is of the order of $+1$ or -1, respectively, the difference of the squares may be expected to be a positive or negative number of the order of unity. Consequently the parabolic correction term is of the order of $25/A$, which is relatively small for medium and heavy nuclides although appreciable for light nuclides. Accordingly we must expect, particularly for small A, scattering of the points from any smooth curve which represents the shell and spin corrections.

[2] *Nuclear Data*, National Bureau of Standards, Circular 499 (U. S. Government Printing Office, Washington, D. C., 1950) and Supplements appearing in Nuclear Science Abstracts.

TABLE I. The pairing correction to binding energies.

	Neutron binding			Proton binding		
N, Z	$\tau\neq\pi+\nu$	$\tau=\pi+\nu$	$\pi=\nu=H$	$\tau\neq\pi+\nu$	$\tau=\pi+\nu$	$\pi=\nu=H$
E, E	ν	ν	H	π	π	H
O, O	$-\tau+\pi$	$-\nu$	$-H$	$-\tau+\nu$	$-\pi$	$-H$
E, O	$\tau-\pi$	ν	$+H$	$-\pi$	$-\pi$	$-H$
O, E	$-\nu$	$-\nu$	$-H$	$\tau-\nu$	$+\pi$	H

It has been pointed out that the pairing correction represents the additional energy due to unpaired nucleons. If the reference surface is taken as the *EE* surface, we may denote the additional energies of an *EO*, *OE*, or *OO* nuclide as π, ν, and τ, respectively. These are the same π and ν as used by Coryell and Suess.[3] To allow for the possible interaction of the odd proton and odd neutron, we have not restricted our τ to $\pi+\nu$. In Table I we show an analysis of the pairing correction for the binding energies of protons and neutrons as they depend upon the nuclear type given in column one. In columns 2 and 5 we indicate the pairing energy differences involved in these cases under the general assumption that the pairing energies take on the values 0, π, ν and τ. In columns 3 and 6 we indicate what these differences would be if $\tau=\pi+\nu$. In columns 4 and 7 we indicate what these differences would be if $\pi=\nu=\tau/2=H$.

Ignoring momentarily the parabolic and pairing corrections, the neutron and proton binding energy residuals [Eqs. (15) and (16)] are just the negatives of the partial derivatives of the shell structure term. On plots of R_n *vs* N and R_p *vs* Z the points corresponding to the nuclides should collect about the curves $-\partial S_{ij}/\partial N$ and $-\partial S_{ij}/\partial Z$, respectively. Taking into account the pairing term of Eq. (15) and (16) we would expect, if $\tau=\pi+\nu$, that the experimental points will be above or below $-\partial S_{ij}/\partial N$ and $-\partial S_{ij}/\partial Z$ by the distances given in columns 3 and 6 of Table I. Accordingly, the points on the R_n *vs* N plot should group in such a way that the curve $-\partial S_{ij}/\partial N$ would be half-way between the average distributions of the *EE*, *EO* group and the *OO*, *OE* group. Similiarly for the R_p *vs* Z plot, the average distribution curves for the *EE*, *OE* group and the *OO*, *EO* group should be equally spaced about the $-\partial S_{ij}/\partial Z$ curve. We must expect random scattering about these distribution curves because of the parabolic factor. The distance between these average distribution curves on the R_n and R_p plots is expected to be 2ν and 2π, respectively. On the other hand, if τ differs from $\pi+\nu$ we would in both cases find four curves spaced

[3] C. D. Coryell and H. E. Suess, Phys. Rev. **86**, 609 (1952).

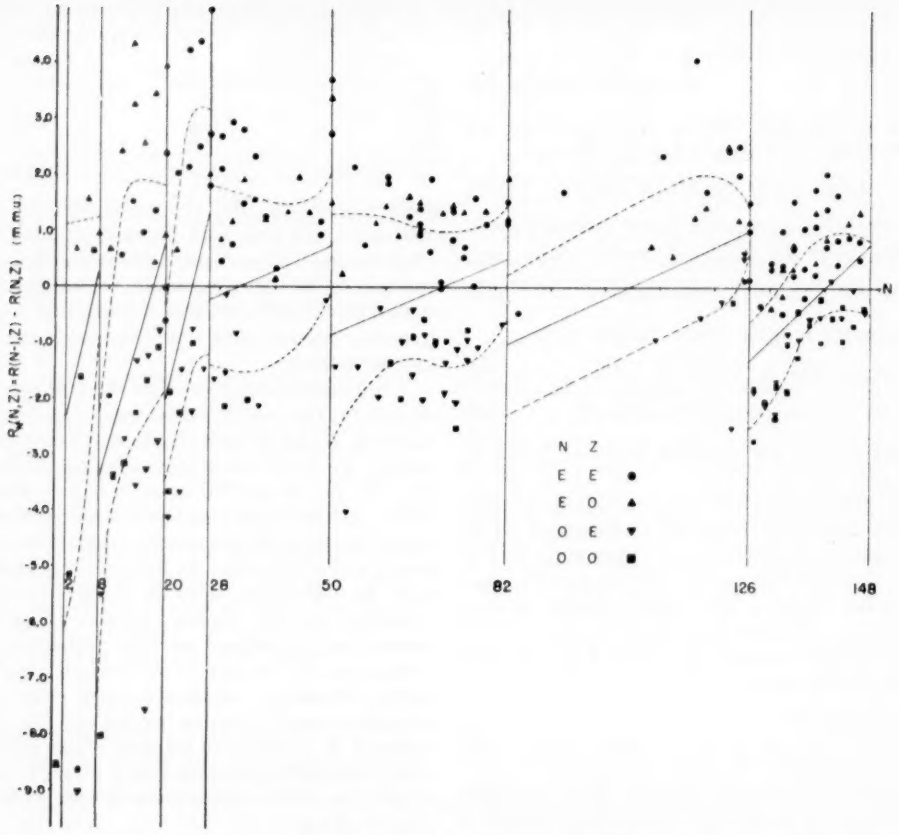

FIG. 1. The residual neutron binding energy *vs* neutron number. The points are designated as to the type, i.e., the evenness or oddness of the number of neutrons or protons. The grouping of the *EE* and *EO* types and the grouping of the *OO* and *OE* types can be seen. The dashed curves indicate the average distributions of these groups. The solid line represents our visual estimate of the best straight line representation of $-(\partial S_{ij}/\partial N)$. The $-(\partial S_{ij}/\partial N)$ which we use in Sec. 4 consists of a series of straight line segments running from -1 at the lower magic number to 1 at the upper magic number.

with respect to $-\partial S_{ij}/\partial N$ and $-\partial S_{ij}/\partial Z$ in accord with the columns 2 and 5 of Table I.

The neutron and proton binding energy residuals computed from recent experimental data[2] are shown in Figs. 1 and 2, respectively. To accommodate the computed residuals different vertical scales were used in Figs. 1 and 2.

3. THE PAIRING EFFECT

If we examine Figs. 1 and 2 we observe that to a large extent the grouping of types expected on the basis of the assumption that $\tau=\pi+\nu$, is fulfilled. In several instances significant departures seem to occur. The most noteworthy is in the region of A values between 230 and 240 where $\tau-(\pi+\nu)\approx 1$ mMU.

In Fig. 3 we have plotted pairing energies, experimental and empirical, as functions of the mass number. The corresponding N and Z numbers computed from the reference line of beta-stability $\{N_m{}^r(A)=\frac{1}{2}[A+D_m{}^r(A)]$, $Z_m{}^r(A)=\frac{1}{2}[A-D_m{}^r(A)]\}$ are also shown. The squares and the circles represent estimated values of π and ν, respectively, for five-unit intervals of N and Z. These values have been obtained from an analysis of the separation of the types in Fig. 1 and Fig. 2.

In Eq. (5) we take as a reference the surface which lies halfway between the *EE* and *OO* surfaces. For the case $\pi\neq\nu$ we may let $H=\frac{1}{2}(\pi+\nu)$. Various functions of A have been proposed for this pairing correction. In Fig. 3 we show three of these functions, $H_1(A)=140/A$,[4] $H_2(A)=36/A^{\frac{1}{2}}$,[5] and $H_3=10/A^{\frac{1}{2}}$.[6] Of these three the last appears to best follow the variation with A. The function $12/A^{\frac{1}{2}}$ is probably still better although it is somewhat smaller in the middle range than the experimental data indicate.

[4] S. Glasstone, *Source Book on Atomic Energy* (D. Van Nostrand Company, Inc., New York, 1950). The pairing function suggested by J. W. Blatt and V. F. Weisskopf in *Theoretical Nuclear Physics* (John Wiley and Sons, Inc., New York, 1952) is quite close to this one.

[5] E. Fermi (unpublished).

[6] A. E. S. Green, Phys. Rev. **86**, 654 (1952).

Mayer,[7] on the assumption of a delta-function attractive potential for the spin orbit coupling model, obtains formulas for the pairing energy which may be expressed as

$$\pi = -C(j_\pi + \tfrac{1}{2})/A \tag{17}$$

and

$$\nu = -C(j_\nu + \tfrac{1}{2})/A, \tag{18}$$

where j_π or j_ν is the total angular momentum of each proton or neutron in a given subshell and $C \sim 25$ Mev. These values of π and ν are also plotted in Fig. 3. π is represented by the dashed lines and ν by the dash-dot lines. We have based our j values on the spin orbit model as represented by the specific level scheme of Klinkenberg.[8] We have used only the average A for a particular subshell since according to Eqs. (17) and (18) the variation in π or ν within a subshell is small. For the moment we cannot say that Eqs. (17) and (18) are consistent with our experimental estimates of π and ν. The fact that Eqs. (17) and (18) are not inconsistent with the experimental values suggests that we must ultimately abandon efforts to represent the pairing effect by the simple functions of mass number which are in common use.

The values of $\pi - \nu$ as found from the circles shown in Fig. 3 are in agreement, on the whole, with the values given by Coryell.[9]

4. A REFERENCE SHELL CORRECTION

From the scattering of the points in Figs. 1 and 2 it is obvious that a variety of $-\partial S_{ij}/\partial N$ and $-\partial S_{ij}/\partial Z$

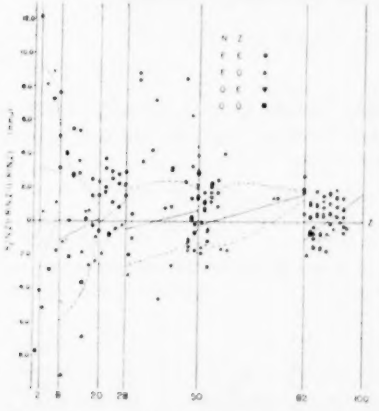

FIG. 2. The residual proton binding energy *vs* proton number. The points are designated as to the type, i.e., the evenness or oddness of the number of neutrons and protons. The grouping of the *EE* and *OE* types and the grouping of the *OO* and *EO* types can be seen. The dashed curves indicate the average distributions of these groups. The solid line represents our visual estimate of the best straight line representation of $-(\partial S_{ij}/\partial Z)$. The $-(\partial S_{ij}/\partial Z)$ which we use in Sec. 4 consists of a series of straight line segments running from -1 at the lower magic number to 1 at the upper magic number.

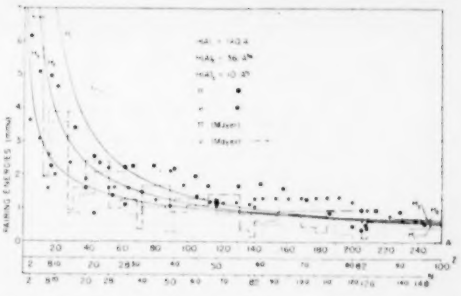

FIG. 3. The pairing energies of the last nucleon are plotted as a function of the mass number. The N and Z scales correspond to values which lie along our reference line of beta-stability. The experimental pairing energies (ν and π) as estimated from Figs. 1 and 2 are indicated by the solid circle and square, respectively. The pairing functions of mass number given by Glasstone, Fermi, and Green are represented by the solid curves.

curves may be chosen. To proceed further in our attempt to find a suitable representation of shell effects, we have elected to represent these curves by the series of straight line segments. This representation is not only suggested by the proton and neutron binding energy data but it is also suggested by the irregularities in the corresponding ionization energy data in the atomic case.[10] Accordingly, we shall assume that between any two major magic numbers we have

$$-\partial S_{ij}/\partial N = 2\alpha_i(N - N_i) \tag{19}$$

and

$$-\partial S_{ij}/\partial Z = 2\alpha_i(Z - Z_j), \tag{20}$$

where α_i and α_j are proportional to the slopes of these straight line segments and N_i and Z_j are constants which must be adjusted for each region. In effect we have chosen to represent the shell correction by the series of functions

$$S_{ij}(N, Z) = -\alpha_i(N - N_i)^2 - \alpha_j(Z - Z_j)^2 + k_{ij}. \tag{21}$$

Our shell function thus has the shape of an inverted cup with the peak value at N_i and Z_j, points which usually lie intermediate between the boundaries of the zone.[11] In Table II we list the values of α_i, N_i, α_j, and Z_j obtained from a visual adjustment of the straight line segments in Figs. 1 and 2.

Let us now consider the manner in which the addition of a shell term given by Eq. (21) alters a mass decrement surface which has the basic form

$$\Delta(A, D) = \Delta_m(A) + J[D - D_m(A)]^2. \tag{22}$$

Since the semi-empirical equation may be placed in this form our discussion is applicable to these equations as

[7] M. G. Mayer, Phys. Rev. **78**, 22 (1950).
[8] P. F. A. Klinkenberg, Revs. Modern Phys. **24**, 63 (1952).
[9] C. D. Coryell *Annual Reviews of Nuclear Science* (Annual Reviews, Inc., Stanford, 1953), Vol. II.

[10] See Fig. 6.3, H. E. White, *Introduction to Atomic Spectra* (McGraw-Hill Book Company, Inc., New York, 1934).
[11] A. H. Wapstra, Physica **18**, 83 (1952) has proposed a shell stabilizing term which is quite different from that proposed here. Our shell stabilizing term has the advantage of introducing sharp breaks in the line of betas-tability which is considered to be essential by Coryell (reference 9).

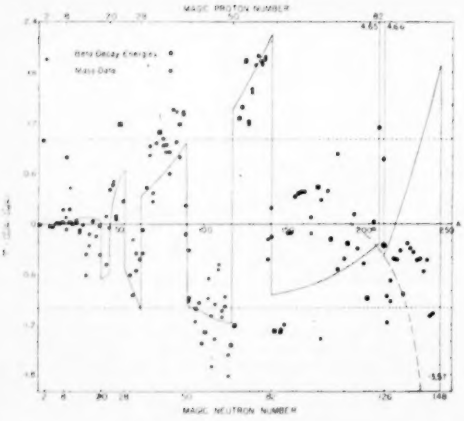

FIG. 4. Location of beta-stability point *vs* mass numbers. The circles and squares indicate the points computed on the basis of experimental data. The solid line represents the line of stability computed on the basis of our reference shell correction and our smooth reference line of beta-stability. The dashed line indicates the change in the smooth baseline apparently needed in the very heavy region.

well as to our reference equation. Letting

$$N=\tfrac{1}{2}(A+D_m+D-D_m)=N_m(A)+\tfrac{1}{2}(D-D_m), \quad (23)$$

and

$$Z=\tfrac{1}{2}(A-D_m-D+D_m)=Z_m(A)-\tfrac{1}{2}(D-D_m), \quad (24)$$

and inserting these into the sum of Eq. (21) and Eq. (22), we find it is possible to express the result in each zone in the form of Eq. (22) if we let

$$\Delta_m{}^{ij}(A)=\Delta_m(A)-\alpha_i[N_m(A)-N_i]^2 -\alpha_j[Z_m(A)-Z_j]^2+k_{ij}-\frac{1}{4J^{ij}(A)} \times\{\alpha_i[N_m(A)-N_i]-\alpha_j[Z_m(A)-Z_j]\}^2, \quad (25)$$

$$D_m{}^{ij}(A)=D_m(A)+[\alpha_i(N_m-N_i) -\alpha_j(Z_m-Z_j)]/2J^{ij}(A) \quad (26)$$

and

$$J^{ij}(A)=J(A)-(\alpha_i+\alpha_j)/4. \quad (27)$$

Rather than go further with the extensive set of empirical constants listed in Table II, we may without introducing considerable error replace these constants by the slightly different set:

$$\bar{\alpha}_i=(N_u-N_l)^{-1}\ \text{mMU}, \quad \bar{\alpha}_j=(Z_u-Z_l)^{-1}\ \text{mMU},$$
$$\bar{N}_i=(N_u+N_l)/2, \quad \bar{Z}_j=(Z_u+Z_l)/2, \quad (28)$$

where the subscripts u and l refer to the upper and lower magic numbers of the particular zone. In using these simple expressions for the parameters in our shell correction, we have exploited the latitude now available to us in view of the scattered data. Essentially we are representing the shell structure function by the expression:

$$S_{ij}(N,Z)=-\frac{1}{N_u-N_l}\left(N-\frac{N_u+N_l}{2}\right)^2 -\frac{1}{Z_u-Z_l}\left(Z-\frac{Z_u+Z_l}{2}\right)^2+k_{ij}. \quad (29)$$

This expression, which of course must be treated only as a first approximation, has the distinct advantage of requiring only one empirical constant for each zone other than the magic numbers themselves. Using our smooth reference functions, we shall now investigate the extent to which this reference shell function may account for effects attributed to shell structure. *Since our reference functions are "averages" of the semi-empirical functions much of this discussion pertains to these latter functions also.*

5. THE SHELL CORRECTION AND THE LINE OF BETA-STABILITY

In the preceding paper[1] (see Fig. 3), marked irregularities were noted in the function Υ which characterizes the deviations of the true line of stability from the reference function $D_m{}^r(A)$. To arrive at a more precise curve for Υ, we shall present the results of an analysis based upon beta decay energies and mass data rather than stability limits. Let $D_m{}^{ij}(A)$ denote the true minimum of an isobaric section at mass number A. If we ignore the π, ν difference the mass difference between adjacent odd mass isobaric nuclides is

$$M^*-M_s=J^{ij}(A)\{[D^*-D_m{}^{ij}(A)]^2 -[D_s-D_m{}^{ij}(A)]^2\}, \quad (30)$$

where the asterisk denotes a radionuclide and the subscript s the stable nuclide. Since $D^*=D_s\pm 2$, this becomes

$$M^*-M=4J^{ij}(A)\{1\pm[D-D_m{}^{ij}(A)]\} =\gamma^{ij}[1\pm(\theta-\Upsilon)]100/A, \quad (31)$$

TABLE II. Shell correction parameters.

i	N_l	N_u	α_i	$\bar{N}$	$\bar{\alpha}_i$	$\bar{N}$
1	0	2			0.300	1
2	2	8	0.22	7	0.1667	5
3	8	20	0.18	18	0.0834	14
4	20	28	0.22	25	0.125	24
5	28	50	0.023	33	0.0455	39
6	50	82	0.022	70	0.0312	66
7	82	126	0.023	104	0.02275	104
8	126	148	0.048	140	0.0455	137
j	Z_l	Z_u	α_j	Z	$\bar{\alpha}_j$	$\bar{Z}$
1	0	2			0.500	1
2	2	8			0.1667	5
3	8	20	0.05	19	0.0834	14
4	20	28	0.088	21	0.125	24
5	28	50	0.023	40	0.0455	39
6	50	82	0.030	53	0.0312	66
7	82	100	0.075	88	0.0555	91

where here

$$\theta = D - D_m{}^r(A) \tag{32}$$

and

$$\Upsilon = D_m{}^{ij}(A) - D_m{}^r(A). \tag{33}$$

If two mass differences are known we may set up two equations and solve Eq. (31) for r^{ij} and Υ for a given isobaric section. Unfortunately apart from the region of heavy nuclides there are only a few instances in which two mass differences are known for odd isobars. In order to make some use of the extensive data corresponding to odd mass isobars for which only one mass difference is known, we have for these cases as a reasonable first approximation let $r^{ij}=1$ (see GE, Fig. 5) and solved this one equation for Υ.

In Fig. 4 we show the location of the minimum mass points of odd mass nuclides which have been computed using a recent collection of beta decay energies (circles) and our set of mass values (squares). Also shown in Fig. 4 is the difference $\Upsilon = D_m{}^{ij} - D_m{}^r(A)$ computed using Eq. (26) and Eq. (28). It is clear from the plot that in the main the experimental points do fluctuate in accord with the predictions based upon our reference shell function. The agreement may be improved even further if in the very heavy region $D_m{}^r(A)$ were taken as the dotted curve indicated in Fig. 4.

6. SHELL CORRECTION AND THE NUCLEAR MASSES

The constants, k_{ij}, in Eq. (21) are still to be determined. Substituting S_{ij} from Eq. (21) into Eq. (4) we have

$$R(N,Z) = -\bar{\alpha}_i(N-\bar{N}_i)^2 - \bar{\alpha}_j(Z-\bar{Z}_j)^2 + k_{ij} + J^o\theta^{o2} + P. \tag{34}$$

For odd-mass beta-stable nuclides the pairing term and parabolic term will be small so that the constants, k_{ij}, can be evaluated approximately by substituting the data appropriate for these nuclides. Using the values of $\bar{\alpha}_i$, $\bar{\alpha}_j$, $\bar{N}_i$, and $\bar{Z}_j$ from Table II as well as a table of $R(N,Z)$ values computed from recent mass data we have calculated the various k_{ij} values. In this computation we have noted that for a particular zone, i.e., a specific i and j, the computed value of k_{ij} varied somewhat. The k_{ij} at shell edges derivated the greatest from the average; accordingly, values of $R(N,Z)$ for either magic N or magic Z or both were not included in the final computation of k_{ij}. The values of k_{ij} so calculated checked rather closely with a set obtained by a graphical method. Our estimated values of k_{ij}, are listed in Table III. To test this set of k_{ij} values and the remainder of the shell correction we plotted in Fig. 5:

TABLE III. Estimated k_{ij} values in mMU.

i,j	2, 2	3, 2	3, 3	4, 3	4, 4	5, 4
k_{ij}	−2.5	2.5	3.0	7.0	3.5	2.5
i,j	5, 5	6, 5	6, 6	7, 6	8, 7	
k_{ij}	5.5	6.5	8.0	3.5	1.5	

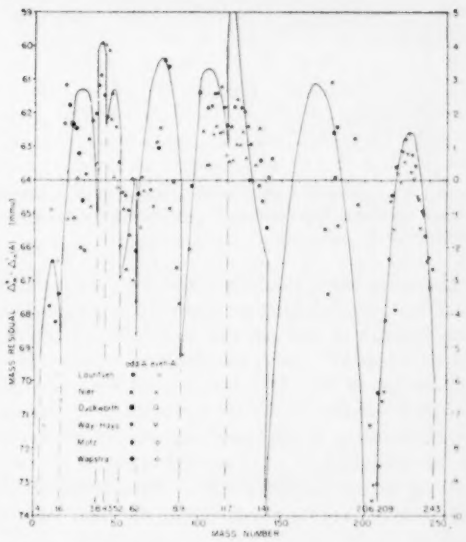

FIG. 5. The mass residuals for beta-stable nuclides *vs* mass number. The solid symbols represent odd-A nuclides and open symbols the even-A nuclides. The symbols used designated the source of experimental data (see references 6–12 in GE). The discontinuous curve represents the mass residuals for the beta-stable points of a surface which incorporates our smooth reference functions and our reference shell stabilizing term. The left vertical scale denotes residuals computed with respect to $\Delta_m{}^r(A) = (A-100)^2/100$, whereas the right vertical scale denotes residuals computed with respect to $\Delta_m{}^r(A) = (A-100)^2/100 - 64$.

$$\Delta_m{}^{ij}(A) - \Delta_m(A) = -\frac{1}{N_u - N_l}\left[N_m(A) - \frac{N_u+N_l}{2}\right]^2 - \frac{1}{Z_u - Z_l} \times \left[Z_u(A) - \frac{Z_u+Z_l}{2}\right]^2 + k_{ij} - \frac{1}{4J^{ij}(A)} \times \left\{\frac{1}{N_u - N_l}\left[N_m(A) - \frac{N_u+N_l}{2}\right]^2 - \frac{1}{Z_u - Z_l}\left[Z_m(A) - \frac{Z_u+Z_l}{2}\right]\right\}^2. \tag{35}$$

The function represented by Eq. (35) is discontinuous at the magic A numbers. These discontinuities are probably not entirely significant, since our shell term is expected to be inaccurate at these shell edges. If in following the atomic model we had joined a nuclide corresponding to a closed shell with a straight line segment to the nuclide with a closed shell plus one neutron or proton in our curves for $-\partial S_{ij}/\partial N$ and $-\partial S_{ij}/\partial Z$, we would have avoided these discontinuities. The residual masses of beta-stable odd-mass nuclides should fall fairly close to this curve except at shell edges.

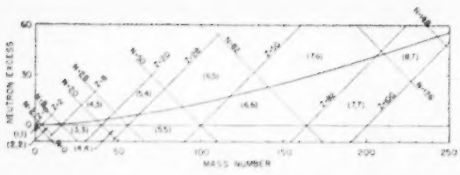

FIG. 6. The line of beta-stability in relationship to zones defined by magic numbers. The numbers in parentheses are the indices of the zone (i, j).

On the other hand, the beta-stable even-mass nuclides, which we included because there are not enough odd-mass nuclides to test our curve, should fall somewhat below ($\sim$1 mMU) the curve representing Eq. (35). An examination of Fig. 5 shows that on the whole these features are borne out by the evidence. The magnitude of the scattering of the points is probably greater than can be attributed to experimental error, to the pairing effect or to the parabolic effect. Thus unquestionably there is room for improvement in the shell stabilizing term.

7. THE SHELL CORRECTION AND Q VALUES

Accepting Eq. (21) as the shell correction, we readily find that for reactions with the target and product nuclides in the same zone

$$Q_s=2\alpha_i(n-n')(N-N_i)+\alpha_i(n-n')^2 +2\alpha_j(z-z')(Z-Z_i)+\alpha_i(z-z')^2. \quad (36)$$

Using the simplified set of constants [Eq. (28)] this becomes

$$Q_s=2(n-n')(N-\bar{N}_i)/(N_u-N_l) +2(n-n')^2/(N_u-N_l) +2(z-z')(Z-\bar{Z}_j)/(Z_u-Z_l) +2(z-z')^2/(Z_u-Z_l), \quad (37)$$

an equation which is quite simple to handle. To test the accuracy of our complete reference surface we have computed Q values of numerous (γ, n) and alpha-decay reactions. Upon comparing these predicted values with the (γ, n) threshold values given by Sher,[12] and the α-decay energies given by Perlman and Seaborg,[13] we found that 67 percent of our predictions were within 1 mMU of the experimental value. This represents a substantial improvement in accuracy with respect to predictions based upon our smooth reference function alone, or the semi-empirical mass functions.

8. CONCLUSION

Our study of the discontinuities of the experimental mass surface has led us to certain conclusions regarding pairing discontinuities and shell discontinuities.

We have examined the frequently accepted assumption that pairing effects may be represented by $+H(A)$, $-H(A)$, and zero for OO, EE, and (OE and EO) nuclides, respectively, where $H(A)$ is $36/A^{\frac{1}{2}}$ or $140/A$. We find this assumption to be untenable for the following reasons: (1) These functions exaggerate the average magnitude of the pairing effect for light nuclides. The function $12/A^{\frac{1}{2}}$ probably furnishes a closer representation of the average magnitude of the pairing effect. (2) The additional energy of unpaired neutrons or unpaired protons with respect to even N even Z nuclides differ in many regions, i.e., frequently $\pi \neq \nu$. (3) In some regions the energies associated with unpaired particles are non-additive. This suggests that an appreciable pairing interaction is present in OO type nuclides.[14] (4) The expressions for the pairing effect involving shell quantum numbers which were derived by Mayer using the shell model are not inconsistent with the available evidence. In view of the many successes of the shell model, it would seem that the final pairing correction will of necessity embody shell quantum numbers and hence will not be representable as a simple function of A, N, or Z.

In our study of the shell discontinuities we have found evidence that the shell effect upon neutron and proton binding energies may be approximately represented by a series of straight line segments between major magic numbers. This representation is also suggested by the general nature of the discontinuities in atomic ionization energies. Because the available data and our method of analysis did not permit a precise assignment of the parameters which characterize these straight line segments, we chose to study the consequences of a uniquely defined set of straight line segments which we found to be a not unreasonable representation of the available evidence. Pursuing this representation we deduced a shell stabilizing correction to nuclear energies which we found gives a rather good account of the departures from the general trends of beta-stability, nuclear masses, and nuclear Q values.

Perhaps the most startling conclusion to which we are led from this approximate representation is the large variation of masses which may be identified with a shell stabilizing term. The fact that in most regions where accurate mass values are available the line of beta-stability cuts the corners of shell zones, has tended to obscure this feature of the experimental mass surface. Only in the heavy region do we meet a situation where we can gauge the true range of the shell correction from the doubly magic corner of the zone to the peak. In Fig. 6 we indicate how our reference line of beta-stability (which is a fairly good one) crosses with respect to zones defined by magic N and magic Z numbers. We may conclude therefore that shell effects do greatly distort the masses of beta-stable nuclides from what they would be in the absence of shell effects. Accordingly theoretical expressions based upon the statistical theories of the nucleus must be adjusted to mass values

[12] Sher, Halpern, and Mann, Phys. Rev. **84**, 387 (1951).
[13] Perlman, Ghiorso, and Seaborg, Phys. Rev. **77**, 26 (1950).
[14] K. Way and M. Wood, Phys. Rev. **86**, 608 (1952) have noted an n-p interaction above Pb^{208} which is probably related to this.

which are substantially different from the actual masses of nuclides.

Unquestionably a better representation can be found for the shell stabilizing term than our present one. The local adjustment of the parameters incorporated in Eq. (21) probably would lead to a substantial improvement. It is also probable that the true shell correction may embody semimagic numbers and curved segments. At this time the experimental data is too sparse and too inaccurate in many regions of the mass surface to offer great encouragement to an effort to refine the shell correction on the basis of purely empirical considerations. Of necessity such a study will be a tedious one, since it will have to be made in conjunction with a more precise representation of the smooth trends of the nuclear mass surface and a more precise representation of the pairing effect than the simple expressions which we have used thus far. It appears therefore that we have reached a point at which we might best look to current nuclear theories to find a better representation of the shell stabilizing term.

We would like to express our appreciation to R. B. Minogue, N. J. Marucci, R. Oppenheim, J. S. Nader, N. Engler, R. Oswald, and Mrs. W. Steiger for their assistance in this study, and to Dr. C. D. Coryell for sending us a manuscript prior to publication.

PHYSICAL REVIEW VOLUME 91, NUMBER 1 JULY 1, 1953

The Parameters for the Slow Neutron Resonance in Rhodium*

V. L. SAILOR
Brookhaven National Laboratory, Upton, New York
(Received March 30, 1953)

Measurements of the 1.26-ev resonance in rhodium have been made with a crystal spectrometer and the following values were obtained for the parameters: $E_0=1.260\pm0.004$ ev, $\sigma_0=(5000\pm200)\times10^{-24}$ cm², $\Gamma=0.156\pm0.005$ ev, $g\Gamma_n=(3.8\pm0.2)\times10^{-4}$ ev, and $\sigma_{fa}=(5.5\pm1.0)\times10^{-24}$ cm². The shape of the resonance agrees to very high accuracy with the one-level Breit-Wigner formula. The procedure is discussed for analyzing experimental data in cases where small corrections are required for instrument resolution and Doppler broadening.

I. INTRODUCTION

THE slow neutron resonance in rhodium at 1.26 ev offers a particularly favorable opportunity for studying the details of an absorption resonance. Several factors contribute to simplify greatly the analysis of this case: Rhodium is monoisotopic; the 1.26-ev resonance is well isolated from other resonances and presumably is not complicated by interference effects; the contribution to the cross section form resonant scattering is very small and may be neglected in the analysis; and the resonant energy lies within the range of very high resolution of modern neutron spectrometers.

Several previous measurements of the rhodium cross section have been made;[1–3] however, in these cases the instrument resolution was inadequate for a detailed analysis. The relatively high resolution which can be obtained with newer spectrometers has justified a remeasurement of the rhodium cross section. The purpose of these new measurements is to obtain accurate values of the Breit-Wigner parameters and to study the details of the shape of the resonance. The measurements reported below were made with the BNL crystal spectrometer, which has been described elsewhere.[4]

II. PROBLEMS IN ANALYZING DATA

The experimentally observed shape of a resonance differs from the "true" shape because of the distortion introduced by finite instrument resolution and by the Doppler broadening resulting from the thermal motion of the atoms in the specimen. The corrections required to account for these effects are appreciable even for cases of very high resolution and small Doppler broadening. The problem of fitting experimental data to a theoretical dispersion curve is greatly complicated by the need for the above corrections. As experimental technique advances and the data becomes more refined, the problem of finding an adequate and practical method of analysis becomes more pressing.

There are several possible approaches to the analysis problem. The "area" method of Havens and Rainwater,[5] which corrects for resolution, has recently been made more quantitative by Melkonian[6] and is now being extended to include the Doppler correction.[7,8] Another less elegant approach which could best be described as the "trial and error" method has been frequently used.[3,5,9] This consists of choosing trial values of the Breit-Wigner parameters and then computing the effect

* Research supported by the U. S. Atomic Energy Commission.
[1] Borst, Ulrich, Osborne, and Hasbrouck, Phys. Rev. **70**, 557 (1946).
[2] W. J. Sturm, Phys. Rev. **71**, 757 (1947).
[3] R. R. Meijer, Phys. Rev. **75**, 773 (1949).
[4] L. B. Borst and V. L. Sailor, Rev. Sci. Instr. **24**, 141 (1953).
[5] W. W. Havens, Jr., and J. Rainwater, Phys. Rev. **70**, 154 (1946).
[6] E. Melkonian, Phys. Rev. **90**, 362 (1953).
[7] G. v. Dardel and R. Persson, Nature **170**, 1117 (1952).
[8] E. Melkonian, Bull. Am. Phys. Soc. **28**, No. 3, 26 (1953).
[9] B. D. McDaniel, Phys. Rev. **70**, 832 (1946).

of resolution and Doppler broadening on the curve. Sets of such computed curves are compared with the observed curve and the best fit selected.

A slight variation of the "trial and error" method has been chosen for analyzing the rhodium data because it is capable of any desired degree of accuracy. The steps in the analysis are thought to be of practical interest to many and therefore have been outlined in the next section. The method in its present form is too laborious for general application, but is of practical value for those cases in which the instrument resolution is very high.

III. METHOD FOR ANALYZING THE DATA

The total neutron cross section of an element containing an isolated resonance having negligible resonant scattering can be expressed in terms of the one-level Breit-Wigner formula,

$$\sigma(E)=\sigma_{fa}+(E_0/E)^{\frac{1}{2}}\sigma_0\Gamma^2[4(E-E_0)^2+\Gamma^2]^{-1}, \quad (1)$$

where σ is the total cross section at energy E, σ_{fa} is the free atom scattering cross section, σ_0 is the cross section at exact resonance E_0, and Γ is the total width of the resonance at half-maximum.

The parameter σ_0 is actually a composite quantity involving the more fundamental parameters as follows:

$$\sigma_0=4\pi\lambda_0^2 g\Gamma_n\Gamma_\gamma/\Gamma^2, \quad (2)$$

where $2\pi\lambda_0$ is the neutron wavelength at resonance; g is the statistical weight factor which for s neutrons is given by $g=\frac{1}{2}[1\pm(2I+1)^{-1}]$, I being the spin of the initial nucleus; Γ_n and Γ_γ are, respectively, the neutron and radiation widths.

The parameters which completely characterize the resonance are therefore E_0, σ_{fa}, g, Γ_n, and Γ_γ. From a total cross-section curve one might hope to obtain E_0, σ_{fa}, σ_0, and Γ. Additional measurements of the resonance scattering would be required to evaluate g, Γ_n, and Γ_γ separately.

(A) Analysis when Corrections are Required

Doppler Broadening

The theory of Doppler broadening has been presented by Bethe and Placzek[10] and elaborated by Lamb.[11] It was shown that the resonance term in Eq. (1) becomes

$$\sigma_c=\frac{\sigma_0}{\pi^{\frac{1}{2}}\Delta}\int_0^\infty\left(\frac{E_0}{E'}\right)^{\frac{1}{2}}\frac{\exp[-(E-E'/\Delta)^2]}{1+4(E'-E_0)^2/\Gamma^2}dE'. \quad (3)$$

For a free gas the Doppler width Δ is given by

$$\Delta=2(mE_0kT/M)^{\frac{1}{2}}, \quad (4)$$

where m is the mass of the neutron, M the mass of the nucleus, k the gas constant, and T the temperature of the sample. Lamb has shown that if the specimen is a solid, Eqs. (3) and (4) are valid only when the width of the resonance is much greater than the Debye temperature of the specimen; i.e., if $\Gamma\gtrsim 4\theta$. If this condition is met it is possible to account for lattice binding merely by substituting in Eq. (4) for the real temperature T an effective temperature T_{eff} as defined by Lamb. For rhodium $T_{\text{eff}}\approx 1.2T$.

In order to deal with Eq. (3), one may expand the $(E_0/E')^{\frac{1}{2}}$ term in a Taylor's series about $E'=E$. It is then possible to show that if $E_0>0.5$ ev, only the first term of the expansion need be considered. Equation (3) can now be written in the form

$$\sigma_c=\sigma_0(E_0/E)^{\frac{1}{2}}\psi(\xi, x), \quad (3a)$$

where

$$\psi(\xi, x)=\frac{\xi}{2\pi^{\frac{1}{2}}}\int_{-\infty}^{\infty}\frac{\exp[-\frac{1}{4}\xi^2(x-y)^2]}{1+y^2}dy, \quad (5)$$

and x, y, and ξ are defined as follows:

$$x\equiv(E-E_0)/\tfrac{1}{2}\Gamma, \quad y\equiv(E'-E_0)/\tfrac{1}{2}\Gamma, \quad \text{and} \quad \xi\equiv\Gamma/\Delta.$$

The function $\psi(\xi, x)$ has been evaluated only for a limited number of values of the arguments ξ and x.[8,12] For values applicable to the rhodium resonance, ψ was computed by numerical integration.

Effect of Instrument Resolution

The total cross section at each energy is obtained by measuring the transmission of the specimen with monochromatic neutrons. The cross section can be computed from the relationship

$$T=e^{-N\sigma}, \quad (6)$$

where N is the thickness of the sample expressed as the number of nuclei per cm^2. If the instrument resolution were infinitely sharp the true transmission T would be obtained from the measurement. However, the instrument resolution will cause the measured transmission T_i to differ from true transmission as follows:

$$T_i(E_i)=\int_0^\infty T(E,\psi)R(E-E_i)dE\Big/\int_0^\infty R(E-E_i)dE, \quad (7)$$

where $R(E-E_i)$ is the resolution function of the instrument. The experimentally determined resolution function of the BNL crystal spectrometer can be closely approximated by an error function modified by an additional $E^{-5/2}$ term which accounts for the reactor spectral distribution, the crystal reflectivity, and the $1/v$ variation of the detector efficiency:[4]

$$R(E-E_i)=AE^{-5/2}\exp[-a(E-E_i)^2], \quad (8)$$

where A is a numerical constant which will cancel in

[10] H. A. Bethe and G. Placzek, Phys. Rev. **51**, 450 (1937); H. A. Bethe, Revs. Modern Phys. **9**, 69 (1937), see p. 140.
[11] W. E. Lamb, Jr., Phys. Rev. **55**, 190 (1939).
[12] M. Born, *Optik* (Verlag Julius Springer, Berlin, 1933), p. 486.

the normalization performed in Eq. (7). The nominal energy setting of the spectrometer is E_i, and $a \equiv 4 \ln 2/\epsilon^2$, where ϵ is the full width at half-maximum of the error function.

Treatment of Data

The object of the analysis is to obtain the values of E_0, σ_0, and Γ which best satisfy the experimental points. First E_0 is obtained graphically and preliminary values σ_0' and Γ' are estimated from the experimental curve. Corresponding to each measured transmission T_{mi} a calculated value $T_{ci}(\sigma_0', \Gamma')$ is obtained from Eq. (7) using the preliminary parameters. The evaluation of Eq. (7) is carried out by numerical integration.

As the next step, corrections to σ_0' and Γ' will be found which give a better fit to the experimental points. T_{ci} is a function of σ_0 and Γ and can be expanded about σ_0' and Γ' in a Taylor's series:

$$T_{ci}(\sigma_0, \Gamma) = T_{ci}(\sigma_0', \Gamma') + \frac{\partial T_{ci}}{\partial \sigma_0}\Delta\sigma_0 + \frac{\partial T_{ci}}{\partial \Gamma}\Delta\Gamma + \cdots. \quad (9)$$

Higher terms in the expansion can be neglected provided the original choices were not too far in error. A set of residual equations can be written using the calculated values and the measured values as follows:

$$T_{ci}(\sigma_0', \Gamma') + \frac{\partial T_{ci}}{\partial \sigma_0}\Delta\sigma_0 + \frac{\partial T_{ci}}{\partial \Gamma}\Delta\Gamma - T_{mi} = r_i, \quad (10)$$

where

$$\frac{\partial T}{\partial \sigma_0} = \frac{-\int_0^\infty (N\sigma/\sigma_0) e^{-N\sigma} R(E-E_i)dE}{\int_0^\infty R(E-E_i)dE},$$

and

$$\frac{\partial T}{\partial \Gamma} \approx \frac{-\int_0^\infty \frac{N\sigma}{\Gamma}\left[\frac{8(E-E_0)^2}{4(E-E_0)^2+\Gamma^2}\right] e^{-N\sigma} R(E-E_i)dE}{\int_0^\infty R(E-E_i)dE}.$$

The latter partial derivative assumes $\psi = \frac{1}{2}\pi^{-1}\xi(1+x^2)^{-1}$, which gives only a small error in the case of rhodium. These terms must also be computed by numerical integration.

The method of least squares is now applied to the Eqs. (10) to find the values of $\Delta\sigma_0$ and $\Delta\Gamma$ which reduce Σr_i^2 to a minimum, the statistical weights of the measured values T_{mi} all being approximately equal. The values of the parameters which give the best fit are, therefore, $\sigma_0 = \sigma_0' + \Delta\sigma_0$ and $\Gamma = \Gamma' + \Delta\Gamma$. At the conclusion a test can be carried out to prove that the higher terms in the Taylor's series, Eq. (9), were actually negligible. If not, it would be necessary to repeat the process.

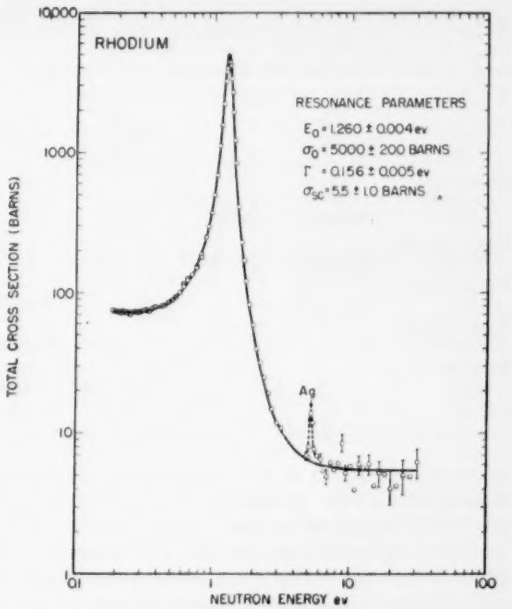

FIG. 1. The total cross section of rhodium as a function of energy. The curve is a plot of the one-level formula using $E_0 = 1.260$ ev, $\sigma_0 = 5000$ barns, $\Gamma = 0.156$ ev, and $\sigma_{fa} = 5.5$ barns. The experimental points do not deviate significantly from the theoretical curve except at the center of the resonance where corrections must be made.

The numerical integration mentioned above can be carried out using Weddle's rule with 12 intervals which for this case gives an accuracy of about 0.1 percent. The limits of integration 0 to ∞ can be replaced with the limits $(E_i - \frac{3}{2}\epsilon)$ to $(E_i + \frac{3}{2}\epsilon)$.

(B) Analysis in the Wings of the Resonance

In the wings of the resonance the variation of σ is negligible over the resolution width, and Eq. (3) reduces to Eq. (1) so that the Doppler correction can be ignored. The data may be fitted directly to Eq. (1) in these regions using the method of least squares to solve for σ_{fa} and $\sigma_0\Gamma^2$. The resonant energy E_0 can be obtained graphically and only an approximate value of Γ need be used in the denominator. Such an analysis is useful for comparison with the results obtained from the complicated curve fitting which is necessary near the center of the resonance.

The best value of σ_{fa} is obtained at higher energies where the effects of coherent scattering and resonant scattering are completely negligible.

IV. EXPERIMENTAL RESULTS

(A) Measurements

The total cross section of rhodium was measured over the energy range from 0.18 to 30 ev with samples of four different thicknesses (see Fig. 1). Only one

TABLE I. Parameters for the rhodium resonance derived from the analysis of several sets of experimental data. The resonant energy $E_0=1.260\pm0.004$ was obtained graphically. The uncorrected measured values are listed as the first entry for comparison.

Region analyzed	σ_0 $\times10^{-24}$ cm²	Γ ev	$\sigma_0\Gamma^2$ $\times10^{-24}$ cm² (ev)²	σ_{fa} $\times10^{-24}$ cm²
Uncorrected measured values	(4460)	(0.180)	(144.5)	
Near center of resonance	5000±200	0.156±0.005	121.7±2	
Wings of resonance			118.1±6	(8.6±4)
Wings of resonance			122.2±8	(13.3±6)
Wings of resonance			131.0±12	(5.3±4)
6–30 ev				5.5±1

resonance was found in this range except for a weak resonance at 5.2 ev attributed to a small impurity of silver. The variety of sample thicknesses is necessary to obtain reliable values over the wide range of magnitude of the cross section. Cross sections were computed only for those points having transmissions lying within the limits from 0.10 to 0.90. When the transmission lies outside these limits the uncertainty in the computed cross section becomes excessive unless an unreasonable amount of time is spent in improving statistics. Enough counts were taken on most points to give 1 percent statistics for the transmission.

The rhodium specimen was of high purity; a spectroscopic analysis[13] disclosed approximately 0.01 percent Ag, 0.01 percent Cu and traces of Pd and Pt. The specimens were in the form of metal foils which had been cut to carefully measured sizes. The thickness of each foil was determined by weighing.

The resolution of the spectrometer at the center of the resonance, 1.26 ev, was 0.026 percent; i.e., the resolution function had a full width at half-maximum of $\epsilon=0.033$ ev. The Doppler width for $T_{\text{eff}}=1.2T=355°\text{K}$ was $\Delta=0.0386$ ev.

(B) Results of the Analysis

The analysis described in Sec. III(A) was carried out using 13 experimental points. The values of the parameters which were obtained are listed in Table I. Included in the table are the uncorrected experimental values of maximum cross section and total width. The experimental values, when compared to the values obtained from the analysis, show the magnitude of the correction. Also listed in Table I are values of σ_{fa} and $\sigma_0\Gamma^2$ which were obtained from three sets of data by analyzing the wings of the resonance as outlined in Sec. III(B).

A curve was constructed by substituting the values $\sigma_0=5000\times10^{-24}$ cm², $\Gamma=0.156$ ev, and $\sigma_{fa}=5.5\times10^{-24}$ cm² into Eq. (1). This curve is shown with the experimental points in Fig. 1. A detailed linear plot of the central portion of the resonance is shown in Fig. 2, where curve A is the true shape of the resonance, curve B shows the effect of resolution and Doppler broadening, and curve C shows a plot of the function $R(E-E_i)$. It should be noted that the Breit-Wigner curve A and the corrected curve B become coincident in the wings of the resonance. The experimental points agree quite well with the calculated curve over the entire range of energy from 0.18 ev to 30 ev. It is apparent from this agreement that the one-level formula accurately fits the rhodium resonance over the entire range of energy for which observations were made. The error caused by neglecting resonant scattering is too small to be distinguished on these graphs.

V. DISCUSSION OF RESULTS

The values in Table I may be used for computing several additional quantities of interest. Assuming $\Gamma\approx\Gamma_\gamma$ and substituting the numerical value of σ_0 in Eq. (2), one obtains $g\Gamma_n=(3.8\pm0.2)\times10^{-4}$ ev. The spin[14] of Rh^{103} is $\frac{1}{2}$ so the two possible choices of g are $\frac{1}{4}$ and $\frac{3}{4}$. If $g=\frac{1}{4}$, $\Gamma_n=(1.52\pm0.07)\times10^{-3}$ ev and $\Gamma_n/\Gamma=(9.7\pm0.8)\times10^{-3}$; while if $g=\frac{3}{4}$, $\Gamma_n=(5.08\pm0.20)\times10^{-4}$ ev and $\Gamma_n/\Gamma=(3.25\pm0.20)\times10^{-3}$. The absorption integral, $\Sigma_a\approx\frac{1}{2}\pi\sigma_0\Gamma/E_0$, is found to be $(980\pm70)\times10^{-24}$ cm². Finally the contribution of the resonance to the thermal absorption cross section σ_{th} may be computed by extra-

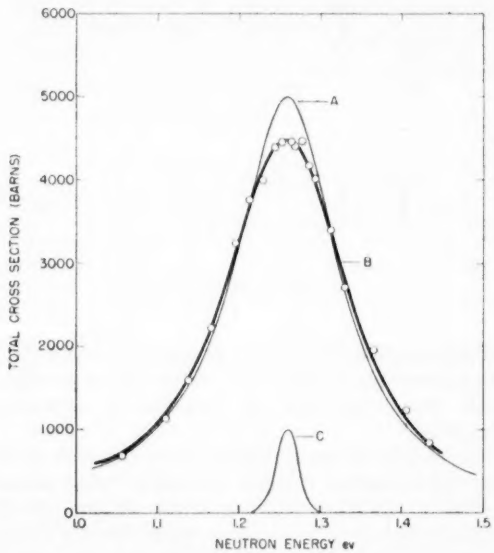

FIG. 2. A linear plot of the central region of the rhodium resonance. Curve A is the Breit-Wigner curve. Curve B is obtained by calculating the effect of instrument resolution and Doppler broadening on curve A. Curve C is a plot of the resolution function with an arbitrary scale as the ordinate.

[13] The author is indebted to Mr. M. Slavin of the Brookhaven National Laboratory for this analysis.

[14] H. Kuhn and G. K. Woodgate, Nature **166**, 906 (1950).

polating Eq. (1) back to an energy of 0.025 ev. This extrapolation gives $\sigma_{th}=(142\pm10)\times10^{-24}$ cm^2.

Table II summarizes the various parameters and compares these with values previously reported. In general the agreement is good but not always within the experimental errors. It should be noted that there is a disagreement with Meijer[3] on the values of σ_0 and Γ, however the product $\sigma_0\Gamma^2$ is in good agreement. The individual values obtained for σ_0 and Γ depend strongly on the resolution correction, but the product $\sigma_0\Gamma^2$ is relatively insensitive to resolution. It appears possible that Meijer underestimated the correction required for instrument resolution.

Scattering measurements by Brockhouse[15] indicate that $\frac{3}{4}$ is probably the proper choice for g; however, the uncertainty is large. Regardless of the choice of g, there is a large discrepancy with the value of the ratio Γ_n/Γ reported by Harris *et al.*[16]

Comparison between the values of σ_{th} listed in Table II indicates that most of the thermal absorption cross section must be attributed to the 1.260-ev resonance. Experimental accuracy is not sufficient to permit a reliable estimate of the residual σ_{th} not due to this resonance.

TABLE II. Various parameters of the rhodium resonance compared to results previously reported. Cross sections are in units of 10^{-24} cm^2 and widths are given in electron volts.

Parameter	Reported in this paper	Previously reported
E_0	1.260 ± 0.004	1.30,[a] (1.21 ± 0.02),[b] 1.28[c]
σ_0	5000 ± 200	2750 ± 200[b]
Γ	0.156 ± 0.005	0.14,[d] (0.21 ± 0.01)[b]
$\sigma_0\Gamma^2$	121.7 ± 2.0	117 ± 8[b]
$g\Gamma_n$	$(3.8\pm0.2)\times10^{-4}$	4×10^{-4}[d]
g	$\frac{3}{4}$	$\frac{3}{4}$[e]
Γ_n	$(5.1\pm0.2)\times10^{-4}$	
Γ_n/Γ	$(3.25\pm0.2)\times10^{-3}$	$(4\pm3)\times10^{-3}$,[e] 4.3×10^{-3}[f]
Σ_a	980 ± 70	529,[f] 790[d]
σ_{fo}	5.5 ± 1.0	5.3,[g] 6 ± 2[b]
σ_{th}	142 ± 10	150 ± 7.5[g]

[a] Reference 1.
[b] Reference 3.
[c] Reference 2.
[d] L. L. Lowry and M. Goldhaber, Phys. Rev. **76**, 189 (1949).
[e] Reference 15.
[f] Reference 16.
[g] H. Pomerance, Phys. Rev. **83**, 641 (1951).

VI. CONCLUSION

Only one resonance has been observed in the rhodium total cross section between 0.18 and 30 ev. It is unlikely that any other resonances of normal width (i.e., $\Gamma\approx0.10$ ev) exist in this interval unless they are unusually weak. The observed resonance may be fitted to a Breit-Wigner one-level formula with excellent agreement over the entire range of observation, provided that small corrections are made near the center of the resonance to account for instrument resolution and Doppler broadening. The curve fitting yielded accurate values of the characteristic parameters with the exception of g which must be determined by other means.

The author is indebted to Mr. J. Chernick, Dr. H. H. Landon, and Mr. H. L. Foote, Jr., for many helpful discussions relating to the analysis problem; and to Dr. E. Melkonian for pointing out the proper method of making the Doppler correction.

[15] B. N. Brockhouse, Can. J. Phys. **31**, 432 (1953).
[16] Harris, Muehlhause, and Thomas, Phys. Rev. **79**, 11 (1950).

Photoprotons from Mo^{100} and Mo^{92}†

W. A. BUTLER* AND G. M. ALMY
Department of Physics, University of Illinois, Urbana, Illinois
(Received March 23, 1953)

The absolute yield and the energy and angular distributions of protons emitted from targets of concentrated isotopes Mo^{92} and Mo^{100}, under betatron x-ray radiation of maximum energy 22.5 Mev, have been determined with nuclear emulsions as detector of protons.

For Mo^{92} the proton is less tightly bound than the neutron by 5.0 Mev; for Mo^{100} the proton is more tightly bound by 2.4 Mev. Comparison of the large yield and the energy distribution of protons from Mo^{92} with those calculated from the statistical model shows good agreement except for an observed excess of high energy protons, which are also anisotropic. They are presumably due to a direct emission process with which neutron emission does not compete in the normal way.

With Mo^{100}, however, the yield, though 20 times smaller, exceeds the yield predicted on the statistical model by 20 to 125 times depending upon the processes and parameters assumed in the calculation. Most of the protons, therefore, must come from a direct process. The observed energy distribution is similar to one computed using the experimental (γ, p) cross section if it is assumed that the residual nucleus is left with a typical exponential energy level density distribution. The angular distribution is strongly anisotropic with a maximum near 45°, for protons of energy greater than 5 Mev.

A NUMBER of experiments on the (γ, p) process in medium weight nuclei have indicated the occurrence of a direct photoproton process in addition to the normal competitive emission of protons and neutrons from an excited statistical model or compound nucleus, calculated according to Weisskopf and Ewing.[1] Hirzel and Wäffler[2] found from activities induced by the 17.6-Mev Li γ-ray that the cross sections of (γ, p) processes relative to (γ, n) were much greater than calculated. In silver[3] and copper,[4,5] on the other hand, the ratio of total yield of protons to neutrons ejected by 20-Mev betatron x-rays is in satisfactory agreement with prediction. For these elements, and in Rh,[6] the evidence for a direct process is that the observed proton energy spectrum rises definitely above the theoretical spectrum at high proton energies and just these protons show a pronounced departure from spherical symmetry in angular distribution. As another example of departure from the expectations based on the statistical model, Wilkinson and Carver[7] have found that the yield of photoprotons from A^{40}, irradiated with Li γ-rays, is several times the predicted yield. The proton energy distribution is, in the main, similar to that expected from a statistical model.

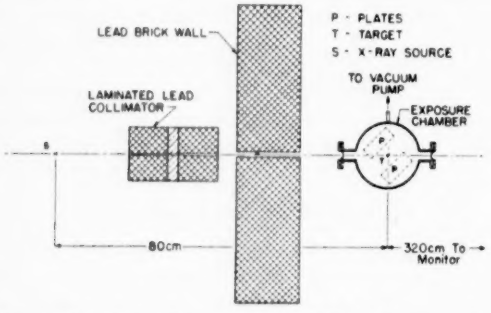

FIG. 1. Experimental arrangement. Collimated x-rays from betatron source S pass through target T and on to monitor. Protons are caught in four plates P arranged in pairs above and below the beam.

Levinger and Bethe[8] and Courant,[9] in their papers on dipole absorption in nuclei, have tentatively proposed a picture of the photonuclear process. It is suggested that in the absorption of the photon only a small part of the nucleus, perhaps only a single proton, is involved. Following absorption a proton may be emitted before a statistical distribution of the excitation energy and normal competition between neutron and proton emission is established. The initial or direct emission of protons is presumably responsible for the excess of high energy anisotropic protons observed in Ag, Cu, and Rh. In cases where the total proton yield, though small, greatly exceeds the yield calculated on the basis of the statistical model the direct process may account for nearly all of the emitted protons.

It therefore becomes of interest to determine the characteristics of the photon-protons in a case where they must be mainly ascribed to the direct process. The work of Duffield, Hsiao, and Sloth[10] has revealed that Mo^{100} is a good nucleus for this purpose. They have shown that the (γ, p) reaction, as well as (γ, n), leads to a radioactive nucleus and that the ratio $\sigma(\gamma, p)/\sigma(\gamma, n)$ is about 100 times that predicted from the statistical model in the range 16 to 19 Mev. They have

† Assisted by the Joint Program of the U. S. Office of Naval Research and the U. S. Atomic Energy Commission.
* Now at Carleton College, Northfield, Minnesota.
[1] V. F. Weisskopf and D. H. Ewing, Phys. Rev. **57**, 472 (1940).
[2] O. Hirzel and H. Wäffler, Helv. Phys. Acta **20**, 373 (1947); see A. Paskin, Phys. Rev. **87**, 197 (1952).
[3] B. C. Diven and G. M. Almy, Phys. Rev. **80**, 407 (1950).
[4] P. R. Byerley, Jr., and W. E. Stephens, Phys. Rev. **83**, 54 (1951).
[5] Mann, Halpern, and Rothman, Phys. Rev. **87**, 146 (1952).
[6] Curtis, Hornbostel, Lee, and Salant, Phys. Rev. **77**, 290 (1951).
[7] D. H. Wilkinson and J. H. Carver, Phys. Rev. **83**, 466 (1951).
[8] J. S. Levinger and H. Bethe, Phys. Rev. **78**, 115 (1950).
[9] E. D. Courant, Phys. Rev. **82**, 703 (1951).
[10] Duffield, Hsiao, and Sloth, Phys. Rev. **79**, 1011 (1950); E. N. Sloth, Master's thesis, University of Illinois, 1950 (unpublished).

also shown that the binding energy of a proton in Mo^{100} is greater than that of a neutron by 2.4 Mev in contrast to Ag, Cu, and Rh where the proton is less tightly bound by a few Mev. It is this difference in the relative thresholds of proton and neutron emission that leads to a much wider predicted variation in numbers of protons, on the basis of the statistical model, than is observed.

The principal purposes of the present investigation are the direct observation of the protons from Mo^{100}, the determination of their absolute yield, their distribution in energy and angle and a comparison of their yield and energy spectrum with theoretical expectations based on various assumptions as to the processes occurring.

As a comparison experiment a parallel study has been made of Mo^{92}. In this case, the proton is 5 Mev less tightly bound than the neutron. It is therefore expected that, as in Ag and Cu, the yield and the energy and angular distributions will be in agreement with statistical model calculations except for deviations at high proton energies. Unpublished data on the (γ, n) cross section of Mo^{92}, essential to the comparison with theory, have been generously provided by Katz.[11]

EXPERIMENTAL PROCEDURES AND RESULTS

The experimental arrangement is shown in Fig. 1. X-rays from the betatron source with a maximum energy of 22.5 Mev for all of the exposures were collimated with lead to a pencil of angular diameter 0.012 radian or a lateral diameter of 1.0 cm at the Mo target T, 80 cm from the x-ray source. The target was mounted in the center of a cylindrical exposure chamber. The x-rays entered and left through 0.002-in. aluminum windows. The plates P were mounted in pairs, one above and one below the beam, sensitive surfaces separated by 1.80 cm. Ilford type C-2, 200 micron emulsions were used throughout. During runs the chamber was evacuated and filled with water vapor to a pressure of about 16 mm Hg. An electromagnet with pole pieces mounted inside the chamber provided a field for deflecting the slower Compton electrons from the plates.

The concentrated isotopes, Mo^{100} and Mo^{92}, were obtained from Oak Ridge as oxides. They were reduced almost quantitatively to the metal by holding them in a hydrogen atmosphere for one hour at 525°C and another hour at 1000°C. The metal granules were pulverized or flattened and attached with thinned zapon to Nylon films which weighed approximately 0.2 mg/cm².

The weights of the Mo isotopes present were checked by intercomparison of the activities of simultaneously irradiated targets of Mo^{92} and Mo^{100} and a sample of natural Mo similarly reduced from the oxide and mounted. The natural abundance of the isotopes was taken from Hibbs.[12] It was determined that the Mo^{92} target, which weighed 23.6 mg, contained 21.6 mg of Mo^{92}. The Mo^{100} target weighed approximately 13 mg and contained 10.9 mg of Mo^{100} and 0.21 mg of Mo^{92}. The Mo^{92} impurity in the Mo^{100} target was determined with care since it yields a substantial background of protons in the Mo^{100} plates.

TABLE I. Exposures selected for study.

X-ray target	Roentgens on target	$\bar{\phi}$*	Area searched in mm²	Number of tracks observed with energies >3 Mev
Mo^{92}	8000	24°	17.29	468
		90°	35.11	1089
		156°	17.60	477
Mo^{100}	8262	29°	170.7	191
		44.5°	171.4	237
		90°	561.7	711
		135.5°	170.7	210
		151°	172.4	190
Background (Nylon films)	6075	29°	172.5	12
		44.5°	173.0	20
		90°	573.7	41
		135.5°	173.2	14
		151°	175.6	18

* ϕ is the average value of ϕ, the angle between the x-ray beam and the protons, for the plate area scanned.

In each target the average density of metal was about 17 mg/cm². The Mo^{100} target was more than covered by the x-ray beam, but only 90 percent of the Mo^{92} target was covered.

The x-ray beam was monitored with a Victoreen thimble mounted in an Al block whose faces were 4 cm from the thimble. The front face was 400 cm from the x-ray source. The response of this monitor had been calculated according to Fowler, Lauritsen, and Lauritsen.[13] Assuming that the x-rays are described by the Schiff forward spectrum, tables were constructed giving the number of quanta per cm² per Mev interval per roentgen, falling on the surface of the Al block.

To check against accidental variations in the primary Victoreen thimble, a second thimble was placed in the block a short distance behind the first. As a second check on the integrated x-ray flux a tantalum disk (0.005×0.83 in.) was placed on the front face of the Al block in each run and the induced activity per gram (8.2-hour) taken as a relative measure of the total flux per unit area, maximum energy held constant. The relative readings of the three monitors agreed within a few percent in the runs from which plates were used.

Since the Mo target and monitor face were 80 cm and 400 cm, respectively, from the x-ray source the flux per cm² on the target was taken as 25 times that on the monitor. To check this, a comparison was made of the activities per g of two simultaneously irradiated tan-

[11] See R. Montalbetti and L. Katz, Phys. Rev. **83**, 892 (1951) for preliminary results.

[12] R. F. Hibbs, Oak Ridge National Laboratory Report AECU-556, 1949 (unpublished).

[13] Fowler, Lauritsen, and Lauritsen, Revs. Modern Phys. **20**, 263 (1948).

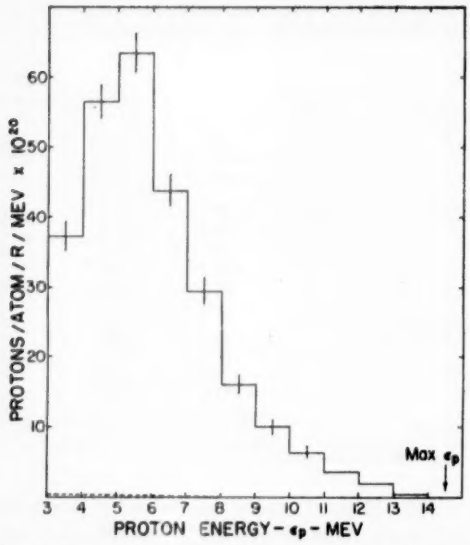

FIG. 2. Energy spectrum of photoprotons from Mo^{92} under 22.5-Mev bremsstrahlung. Dashed line is background. Max $\epsilon_p = 22.5 - B_p = 14.5$ Mev. Vertical lines show statistical uncertainties.

talum samples, each 0.005 in. thick, one shaped like the target and at the target position, the other on the monitor face. In two runs the ratios of specific activities were 25.1 and 25.9.

The nuclear plates were processed and read with standard techniques. The exposures selected for study are listed in Table I, which also gives the angles selected, areas searched, and numbers of proton tracks. Calculation showed that by combining the numbers of tracks on corresponding areas of upper and lower plates errors in the number per unit solid angle due to size, orientation or lack of uniformity of the target or to lack of symmetry of the x-ray beam above and below the midplane of the plate assembly could not exceed a few percent.

Range in emulsion and angle to the beam were determined for each track originating in the emulsion surface (2μ resolution) within predetermined swaths. The energy lost by a proton in the emulsion was determined from curves plotted from data in the literature.[14] To this energy was added the energy loss in the Mo-Nylon target; it was assumed that the proton came from the central plane of the target. The loss in the water vapor was negligible. The uncertainty in this increment is thus equal to its magnitude which at the largest angle varied from 0.7 Mev at a proton energy of 3 Mev to 0.25 Mev at 13 Mev. The few protons which emerged at the bottom or top of the emulsion were each assigned the average energy of all protons of longer range.

[14] Lattes, Fowler, and Cüer, Proc. Phys. Soc. (London) **59**, 883 (1947); Bradner, Smith, Barkas, and Bishop, Phys. Rev. **77**, 462 (1950).

The background exposure plates (Table I) were read in all regions used in the Mo plates. The total background correction was less than 1 percent for Mo^{92} but about 10 percent of the low yield from Mo^{100}. There was, in addition, a larger correction to the Mo^{100} data due to the protons from Mo^{92}, which could be made at each energy and angle since the spectrum of Mo^{92} had been determined in detail.

The contribution of the small amounts of intermediate Mo isotopes to the observed protons from the Mo^{100} target was estimated. For this purpose the abundance analysis supplied by Oak Ridge, the neutron and proton thresholds determined experimentally or from an empirical mass formula[15] and the functions for the relative probability of neutron and proton emission from a statistical model, plotted by Feld *et al.*,[16,17] were used. The result was that the total contribution of statistical theory protons from intermediate isotopes was about 2.5 percent of the total protons observed on the Mo^{100} plates. No correction was made for these protons. Direct process protons should be roughly proportional to isotopic abundance and were also neglected. Background due to (n, p) processes in the target can be neglected.[3]

A numerical integration over all angles for each Mev energy interval of the number of proton per unit

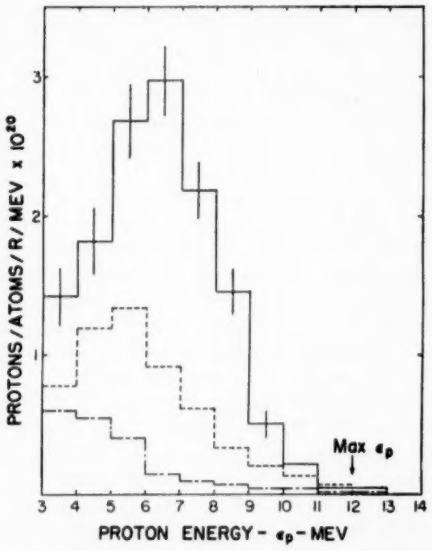

FIG. 3. Energy spectrum of photoprotons from Mo^{100} under 22.5-Mev bremsstrahlung. Backgrounds from run without Mo (lowest histogram) and from Mo^{92} impurity (middle histogram) have been subtracted to give net protons (upper histogram). Max $\epsilon_p = 22.5 - B_p = 12.0$ Mev. Vertical lines show statistical uncertainties.

[15] N. Metropolis and G. Reitwiesner, *Table of Atomic Masses* (1950).

[16] Feld, Feshbach, Goldberger, Goldstein, and Weisskopf, U.S. Atomic Energy Commission Report N-YO-636 (unpublished).

[17] J. M. Blatt and V. Weisskopf, *Theoretical Nuclear Physics* (John Wiley and Sons, Inc., New York, 1952), p. 373.

solid angle gave the total number of protons emitted in each energy interval. The results, with statistical errors, are given in Fig. 2 for Mo^{92} and in Fig. 3 for Mo^{100}. The backgrounds which have been subtracted are also shown.

The angular distributions are for the two isotopes plotted in Figs. 4 and 5. Estimates of multiple and large angle single scattering of protons in the target show that they would not affect the relatively flat distributions for Mo^{92} but may have an appreciable effect for Mo^{100}. The numbers of protons observed at the extreme angles (29° and 151°) are somewhat higher than they would be with a thinner target.

COMPARISON WITH THEORY

On the basis of the statistical model the energy distribution of the photoprotons can be expressed as follows:

$$F(\epsilon_p)=A\epsilon_p\sigma(\epsilon_p)\int_{B_p+\epsilon_p}^{E_{\max}}\frac{N(E)\sigma_\gamma(E)\omega(E_R)dE}{\sum_b\Gamma_b} \quad (1)$$

in which

$F(\epsilon_p)$ = absolute number of protons of energy ϵ_p per Mev interval per roentgen at the target per nucleus in the beam;

$\sigma_p(\epsilon_p)$ = reaction cross section for proton of energy ϵ_p on residual nucleus;

$N(E)$ = number of x-ray quanta per cm^2 per Mev interval per roentgen at the target, at x-ray energy E (Schiff forward spectrum);

$\sigma_\gamma(E)$ = cross section for absorption of quantum of energy E;

$\omega(E_R)$ = energy level density in residual nucleus with excitation energy $E_R=E-B_p-\epsilon_p$; $\omega=C\exp[2(aE_R)]^{\frac{1}{2}}$;

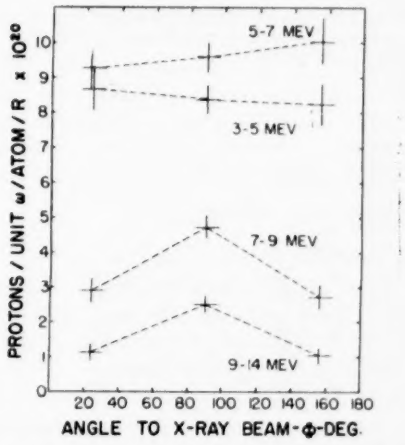

FIG. 4. Angular distribution of photoprotons from Mo^{92}. Horizontal lines are approximate angular intervals.

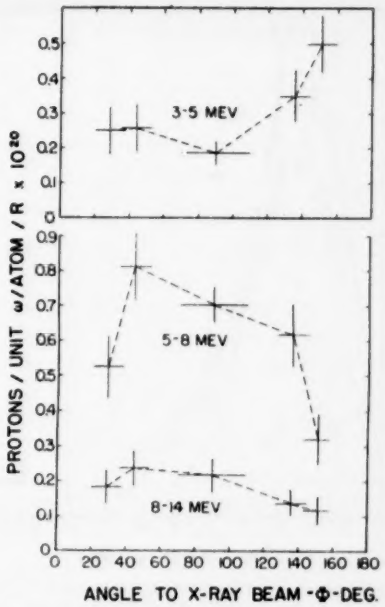

FIG. 5. Angular distribution of photoprotons from Mo^{100}. Horizontal lines are approximate angular intervals.

$\Gamma_b=A\int_0^{\epsilon_{b\max}}\epsilon_b\sigma_b(\epsilon_b)\omega(E_R)d\epsilon_b$, is the probability per unit time of the emission of a particle b. It is a function of E since $E_R=E-B_b-\epsilon_b$ and $\epsilon_{b\max}=E-B_b$;

B_b = binding energy of particle b;

A = a constant, independent of energy. It depends upon the mass of the escaping particle but will be taken the same for neutrons and protons, the only particles for which Γ_b is large enough to be considered here. It therefore cancels out in Eq. (1).

Since $\sigma_\gamma/\sum\Gamma_b=\sigma(\gamma,n)/\Gamma_n=\sigma(\gamma,p)/\Gamma_p$, the first of these equivalents can be replaced by one of the others in Eq. (1). $\sigma(\gamma,n)$ is the cross section usually known from experiment in which case the useful form of Eq. (1) is

$$F(\epsilon_p)=\epsilon_p\sigma_p(\epsilon_p)\int_{B_p+\epsilon_p}^{E_{\max}}\frac{N(E)\sigma(\gamma,n)\omega(E_R)dE}{\Gamma_n'}, \quad (2)$$

where $\Gamma_n'=\Gamma_n/A$. The integrals were evaluated numerically, with energy intervals of 1 Mev.

The neutron energy distribution can be calculated with an expression analogous to Eq. (2). The total number of neutrons or protons can be predicted by numerically integrating $F(\epsilon_n)$ or $F(\epsilon_p)$. The number of neutrons is also given by the integral of $\sigma(\gamma,n)N(E)$ from $E=B_n$ to $E=E_{\max}$.

Mo^{92}

This isotope, for which results similar to those in Cu, Rh, and Ag are to be expected, will be discussed

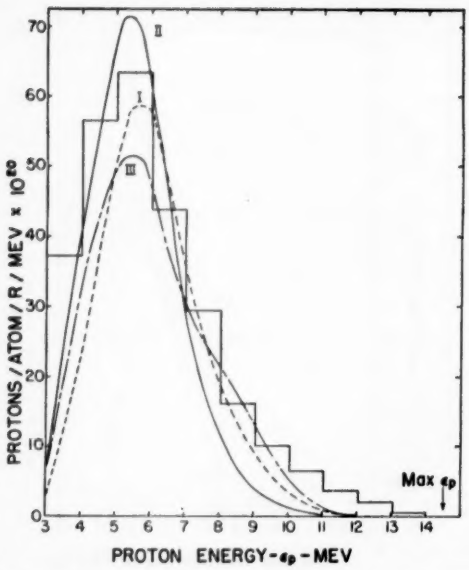

FIG. 6. Comparison of observed and calculated unnormalized proton energy spectra for Mo^{92}. Observed spectrum: histogram. Calculated spectra based on statistical model: $F(\epsilon_p)$ from Eq. (2), with $r_0=1.3\times10^{-13}$ cm, and ω_1 for I, ω_2 for II, ω_2' for III (see text). III fits observed shape best. Observed spectrum shows excess of high energy protons which are anisotropic (Fig. 4) and probably due to a direct emission process.

first. The values and sources of parameters used in the calculation of $F(\epsilon_p)$ by Eq. (2) are as follows.

$\sigma(\gamma, n)$

This is the sum of two curves supplied by Katz,[11] deduced from the yields of positron activity from the two isomers of Mo^{91} excited by betatron x-rays. The half-lives are 15.5 min and 65.5 sec and the yield from the former is about five times the yield from the latter.

B_n and B_p

At Illinois[18] the threshold for the 15.5-min activity was found to be 13.28 ± 0.15 Mev; Katz found 13.2 ± 0.1 Mev. He also found 13.1 ± 0.1 Mev for the 65.5-sec activity and this is taken as the best measure of B_n.

The end point of the positron spectrum of the 15.5-min activity is 3.7 ± 0.1 Mev according to Duffield and Knight;[19] it is 3.32 ± 0.05 Mev according to Katz's more elaborate analysis. Using the latter value and assuming that positron emission of this energy leads to the ground state of Nb^{91}, $B_p-B_n=5.1$ Mev or $B_p=8.0$ Mev. B_p cannot be larger though an elucidation of the decay scheme of Mo^{91} might lead to a lower value. For convenience in calculation B_n has been taken as 13.0 Mev, B_p as 8.0 Mev.

[18] Hanson, Duffield, Knight, Diven, and Palevsky, Phys. Rev. **76**, 578 (1949).
[19] R. B. Duffield and J. D. Knight, Phys. Rev. **76**, 573 (1949).

$\sigma_p(\epsilon_p)$ and $\sigma_n(\epsilon_n)$, r_0

Proton and neutron reaction cross sections were taken from Feld *et al.*,[16] or Blatt and Weisskopf[20] by graphical interpolation. Cross sections have been calculated for two values of the nuclear radius factor r_0, 1.3×10^{-13} cm and 1.5×10^{-13} cm.

$\omega(E_R)$

Proton energy distributions have been calculated with the following choices of $\omega(E_R)$:

1. $\omega_1=C\exp[2(2.85E_R)]^{\frac{1}{2}}$. This choice of the parameter $a=2.85$ corresponds for Mo to a value which proved to be satisfactory for Ag.[3]
2. $\omega_2=C\exp[2(5.3E_R)]^{\frac{1}{2}}$. The value $a=5.3$ was interpolated from values given for various nuclei by Blatt and Weisskopf.[21]
3. $\omega_2'=C\exp[2\times5.3(E_R-3)]^{\frac{1}{2}}$, for $E_R\geq4$ Mev;
   $=C\times10$, for $E_R\leq3$ Mev.

The last form of ω takes cognizance in a rough way of the general observation that the denstiy of levels increases more slowly than exponentially for the first few Mev. It will increase the number of higher energy particles at the expense of those of lower energy.

The range of parameters chosen, a in ω and r_0, are about the extremes of values generally used in the interpretation of nuclear reactions with a statistical nuclear model.

A comparison between the unnormalized experimental proton energy spectrum and those calculated from Eq. (2) is plotted in Fig. 6, for $r_0=1.3\times10^{-13}$ cm and the three choices of ω. The general result is that the absolute numbers of protons in each energy interval can be satisfactorily predicted with reasonable choices of nuclear parameters except that the observed spectrum shows an excess of high energy protons, as was found with Ag and Cu. The modification of $\omega(E_R)$

TABLE II. Total yield of neutrons and protons from Mo^{92}. $E_{max}=22.5$ Mev, $B_n=13.0$ Mev, $B_p=8.0$ Mev.

		Protons atom^{-1} r^{-1} $\times10^{20}$ 3–14 Mev	Neutrons atom^{-1} r^{-1} $\times10^{20}$ 0–9.5 Mev
Observed		269±20	650±200
From $\sigma(\gamma, n)$ (Katz): $\int\sigma(\gamma, n)N(E)dE$			435
Calculated from statistical model, Eq. (2)			
$r_0\times10^{13}$, cm			
ω_1	1.30	200	421
	1.50	328	421
ω_2	1.30	222	434
	1.50	376	434
ω_2'	1.30	204	426
	1.50	337	426

[20] Reference 16, pp. 348, 352.
[21] Reference 17, pp. 371–374.

which assumes it is constant up to $E_R=3$ Mev accounts for some but not all of this discrepancy. It gives a spectrum shaped most nearly like that observed.

There is also an excess of observed protons in the 3–4 Mev interval. It may arise from one or all of three uncertain factors: (1) lack of energy resolution in the steeply rising, low energy range, (2) the absence of neutron competition up to an x-ray energy of 13 Mev, the neutron threshold, (3) a contribution of deuterons, which is energetically possible.

It is seen in Fig. 4 that just the high energy protons exhibit angular anisotropy. Thus, Mo^{92} falls into the group of medium weight nuclei with $B_p<B_n$ in which the photoproton emission is satisfactorily accounted for on the basis of the statistical model, except for the deviations shown by high energy protons.

In Table II, the observed and calculated total numbers of protons and neutrons are given. The calculated numbers of protons for $r_0=1.5\times10^{-13}$, as well as for $r_0=1.3\times10^{-13}$ cm, are listed and the experimental number falls between them. Protons emitted in a direct process are of course not included in the calculated number. The yield of protons is of the same order of magnitude as the yield of neutrons and is the largest (γ, p) yield yet observed in any nucleus. The neutron competiion is held back by the unusually large neutron threshold for Mo^{92}, "magic" in neutrons.

The number of neutrons listed as observed is based on counts of the 15.5-minute activity in the target at the end of two runs in which protons were collected, augmented about 20 percent by an estimate of the number of neutrons corresponding to the 65-sec activity of the isomeric state. The elapsed time of a run was several times the lifetime with several on and off periods; in addition the uncertainty in absolute counting was ±25 percent. Hence the reliability of the number is low and it was considered preferable to use in Eq. (2) Katz's values of $\sigma(\gamma, n)$ without normalization to the observed number of neutrons. If the "observed" number of neutrons were used to normalize Katz's $\sigma(\gamma, n)$, all calculated yields of neutrons and protons would be increased by about 50 percent. The calculation of total neutrons by Eq. (2) gives back satisfactorily the number of neutrons put in, through $\sigma(\gamma, n)$ $N(E)$, which is a comforting check on the method. This comparison appears in the last column of Table II.

Mo^{100}

As stated in the introduction, it has been shown from relative induced activities that $\sigma(\gamma, p)/\sigma(\gamma, n)$ is about 100 times that expected on the basis of the statistical model. In this section the yield and energy distribution of the observed protons will be compared with expectations on various assumptions as to the process producing them.

Information on nuclear parameters was obtained from the following sources.

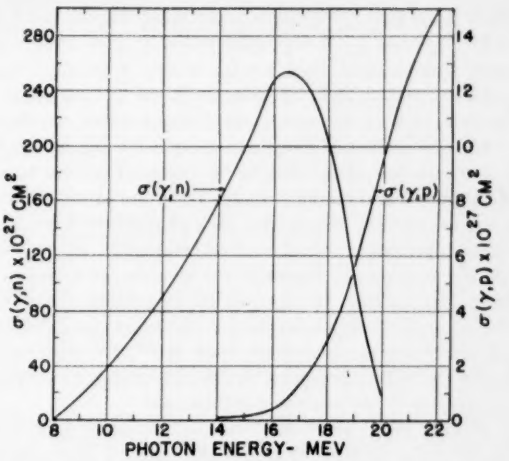

FIG. 7. $\sigma(\gamma, p)$ and $\sigma(\gamma, n)$ for Mo^{100}, obtained on relative scale by Duffield and Sloth. $\sigma(\gamma, p)$ normalized to observed number of protons. $\sigma(\gamma, n)$ normalized by absolute count of (γ, n) induced activity.

$\sigma(\gamma, n)$ and $\sigma(\gamma, p)$

Duffield and Sloth deduced the relative cross sections from the analysis of beta-activity *versus* betatron energy. For the present purpose, their yield curve for the (γ, p) process (leading to Nb^{99}, 2.5 min, $E_{\beta^-}=3.2$ Mev) was normalized to the directly observed yield of protons at 22.5 Mev and $\sigma(\gamma, p)$ was recalculated on an absolute basis. Their relative $\sigma(\gamma, n)$ curve was normalized with an absolute count of the 67-hour β-activity of Mo^{99} in the Mo^{100} target after runs in which protons were collected. The decay scheme of Mo^{99} has been established[22] and the lifetime of the counted activity is much greater than the elapsed time of the intermittent irradiation. Hence the principal uncertainty comes from errors in absolute counting which may amount to ±25 percent. $\sigma(\gamma, n)$ and $\sigma(\gamma, p)$ are shown in Fig. 7.

B_n and B_p

From the threshold of the (γ, n) induced activity Duffield has obtained $B_n=8.1$ Mev (unpublished). From the relation $B_p-B_n=E_{\beta^-}-(n-H)$, B_p was determined to be 10.5 Mev. The values used in calculations were $B_p=10.5$ Mev and $B_n=8.0$ Mev.

$\sigma_p(\epsilon_p)$, $\sigma_n(\epsilon_n)$, r_0, $\omega(E_R)$

Reaction cross sections, nuclear radius, and level density were chosen as described in the section on Mo^{92}. Calculations have been made only with ω_1.

The following calculations have been made for the theoretical proton energy distributions.

(1) *Calculation of $F(\epsilon_p)$ on basis of statistical model.*— The proton spectrum was calculated exactly as for

[22] M. E. Bunker and R. Canada, Phys. Rev. **80**, 961 (1950).

Mo^{92} from Eq. (2) using $\sigma(\gamma, n)$ from Fig. 7, $r_0=1.3\times10^{-13}$ cm and ω_1. It is plotted in Fig. 8, I. As expected from Duffield and Sloth's ratio of $\sigma(\gamma, p)/\sigma(\gamma, n)$, the total calculated yield of protons in the proton energy range 3–14 Mev is about 0.008 of the observed number.

(2) Calculation of $F(\epsilon_p)$ assuming a $(\gamma, 2n)$ process.[23]—The number of protons to be expected on the basis of the statistical model is increased if one assumes that a $(\gamma, 2n)$ process occurs with high probability when the energy of excitation in the initial residual (γ, n) nucleus (Mo^{99}) exceeds the threshold for emission of a neutron from that nucleus. In this case the experimental $\sigma(\gamma, n)$ corresponds to only a fraction of the processes in which an initial neutron is emitted from Mo^{100}, the remainder being $(\gamma, 2n)$. Consequently, the calculated number of competing (γ, p) processes is increased.

B_{2n} for Mo^{100} was taken from an empirical mass formula[15] to be 15 Mev, or B_n for Mo^{99} to be 7 Mev. As an extreme case, leading to the maximum calculated number of protons, it was assumed that whenever the excitation of the residual nucleus Mo^{99} exceeds 7 Mev a second neutron will be emitted. Hence, in Eq. (2), the limits of integration of ϵ_n are set at $\epsilon_n=E-15$ and $\epsilon_{n\max}=E-8$. With these assumptions and taking $r_0=1.30\times10^{-13}$ cm, the total number of protons between 3 and 14 Mev is increased by about threefold, to 0.027 of the observed number (Curve II, Fig. 8). If $r_0=1.5\times10^{-13}$ cm, this fraction is 0.046.

Thus the number of protons observed exceeds by 20 to 125 times the number calculated from the statistical model, depending upon the assumptions as to process and parameters. The photoprotons from Mo^{100} hence must arise mainly from a direct process in which normal competition with neutrons does not occur.

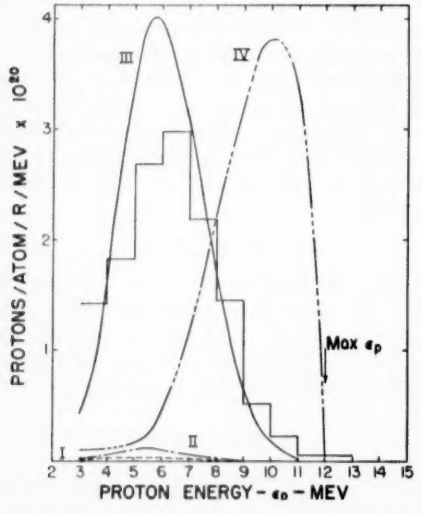

FIG. 8. Comparison of observed and calculated proton energy spectra from Mo^{100}. I (lowest curve) and II are based on the statistical model and account for only a small fraction of observed protons. III and IV make use of the experimental $\sigma(\gamma, p)$; IV assumes residual nucleus after emission of proton is left in ground state; III assumes residual nucleus with typical exponential energy distribution, ω_1.

[23] See L. Eyges, Phys. Rev. 86, 325 (1952).

(3) Calculations of $F(\epsilon_p)$ based on $\sigma(\gamma, p)$.—$\sigma(\gamma, p)$ deduced from experimental data must reflect the actual photoproton processes. If this is mainly a direct emission before statistical distribution in the nucleus occurs, calculations based on the statistical model do not apply.

The direct process has sometimes been thought of as the excitation and ejection of a proton near the nuclear surface with the remainder of the nucleus relatively unexcited. The extreme assumption on this picture is that the residual nucleus is left in the ground state. In this case, $F(\epsilon_p)$ is simply $N(E)\sigma(\gamma, p)$, which is plotted in Fig. 8, IV. This distribution is greatly shifted to high energies from the actual distribution.

The opposite extreme assumption seems to account much better for the observed distribution, namely, that even in a direct emission, the energy states available in the residual nucleus have the usual exponential energy level distribution. In this case the probability of emission of a proton of energy ϵ_p from a single excited state E is given by

$$\epsilon_p\sigma_p(\epsilon_p)\omega(E-B_p-\epsilon_p)\Big/\int_0^{\epsilon_{p\max}}\epsilon_p\sigma_p(\epsilon_p)\omega(E_R)d\epsilon_p,$$

if the usual reaction cross section σ_p is assumed to apply to direct emission. Formally the calculation of $F(\epsilon_p)$ proceeds by Eq. (2) with $\sigma(\gamma, p)/\Gamma_p'$ replacing $\sigma(\gamma, n)/\Gamma_n'$. $F(\epsilon_p)$ so obtained is plotted unnormalized in Fig. 8, III, and is in satisfactory agreement with the observed spectrum. ω_1 and $r_0=1.30\times10^{-13}$ cm were used in the calculation. The agreement would be improved if ω were modified so as to remain constant from $E_R=0$ to $E_R=3$ Mev, as can be seen by comparing II and III in Fig. 6 for Mo^{92}.

The total observed yields of protons and neutrons are listed in Table III, together with the total yields of protons calculated in the ways described above.

The (γ, p) cross section for Mo^{100} has also been calculated on Courant's theory of a direct process[9] in which it is assumed that the photon is absorbed by a single proton in a suitable square-well nuclear potential and that the proton is then emitted through the usual Coulomb barrier without the formation of a compound nucleus. With the experimental proton binding energy and other parameters for Mo^{100} inserted, his expression for $\sigma(\gamma, p)$ leads to values only about 0.025 of that observed at photon energies of 20 to 22 Mev (Fig. 7). Thus, for Mo^{100}, $\sigma(\gamma, p)$ and the proton yield calculated on this basis are much less than observed and about the same as expected from the statistical model.

The angular distributions of photoprotons from Mo^{100} were plotted in Fig. 4. The large group between 5 and 8 Mev, comprising 55 percent of all protons are strongly anisotropic and peaked forward with a maxi-

mum near 45°. The steep drop at low and high angles indicates that the numbers near 0 and 180° are small, especially since multiple scattering in the target which is appreciable will tend to flatten the distribution. The smaller high energy group above 8 Mev shows within statistical errors the same distribution as the 5–8 Mev group.

Thus, nearly all of the protons of energy above 5 Mev show strong anisotropy roughly similar to that reported by Mann, Halpern, and Rothman[5] for the small anisotropic components in copper and cobalt in which most of the protons are accounted for on the statistical theory. The asymmetry about 90° implies interference between the wave functions, corresponding to different angular momenta, which describe the emitted protons.

The lower energy protons, 3–5 Mev, show an entirely different angular distribution. The numbers of protons per unit solid angle are approximately the same at 29°, 45°, and 90° but rise at 135° and 151°. The statistics are not very satisfactory, especially since the background of lower energy protons is comparable to the number from Mo^{100}. On the other hand, neither the background nor the Mo^{92} data taken from plates exposed under similar conditions showed any systematic excess of low energy protons in the backward direction. We have no suggestion as to how to account for the apparently anomalous distribution.

SUMMARY

The yield and energy and angular distributions of photoprotons from Mo^{92} for which $B_p=B_n-5$ Mev can be accounted for on the basis of the statistical model, except for the expected departures at high proton energy. On the other hand, the observed number of protons from Mo^{100}, for which $B_p=B_n+2.5$ Mev, exceeds the number expected on the statistical model by a factor of 20 to 125 depending upon the parameters and processes assumed in the calculation. The excess of protons requires a special assumption such as a direct process in which competition with neutron emission does not occur in the normal way. The proton energy distribution may be adequately described by a calculated distribution based on the observed $\sigma(\gamma, p)$ if it is assumed that the protons have the usual reaction cross section (Coulomb barrier) and that the energy levels available in the transition to the residual nucleus have a typical exponential level density. The observed yield of protons is also more than an order of magnitude greater than predicted on the basis of Courant's model for the direct emission of protons.

In angular distribution the protons from Mo^{100} with energies above 5 Mev are strongly anisotropic and unsymmetrical about 90°, with a maximum near 45° to the x-ray beam.

It is a pleasure to acknowledge the generous assistance of Robert A. Reitz during the runs with the betatron and the processing of the plates.

TABLE III. Total yield of protons and neutrons from Mo^{100}.

	Protons atom^{-1} r^{-1} $\times 10^{30}$ 3–12 Mev	Neutrons atom^{-1} r^{-1} $\times 10^{30}$ 0–14.5 Mev
Observed	13.4±1 (from tracks)	1180±300 (from activity)
$\int\sigma(\gamma, p)N(E)dE$	15.3	
Calculated:		$r_0\times 10^{13}$, cm
(1) Statistical model, Eq. (2)	0.11	1.30
Using experimental $\sigma(\gamma, n)$, ω_1, assuming no $(\gamma, 2n)$ process	0.19	1.50
(2) Similar to (1), but assuming $(\gamma, 2n)$ process occurs	0.36	1.30
	0.62	1.50
(3) Using experimental $\sigma(\gamma, p)$, ω_1 in Eq. (2)	14.8	1.30
	15.0	1.50

Total Neutron Cross Sections of Chlorine and Carbon*

R. M. KIEHN, CLARK GOODMAN, AND K. F. HANSEN
Laboratory for Nuclear Science, Massachusetts Institute of Technology, Cambridge, Massachusetts
(Received March 2, 1953)

Using CCl_4 in good geometry, $Li^7(p,n)$ neutrons and a pressurized hydrogen counter, σ_t(Cl) has been measured by the transmission method from 0.4 to 1 Mev at 30-kev intervals and from 0.15 to 0.75 Mev at 2-kev intervals.

THE total neutron cross section of chlorine has been measured at Columbia by time-of-flight techniques up to about 300-ev neutron energy.[1] Aoki[2] obtained values of 2.66 to 2.84 barns in the energy range from 2.2 to 2.85 Mev. Zinn *et al.*[3] obtained 3.42 barns at 2.85 Mev, and Sherr,[4] using $C^{12}(n,2n)$ as a threshold detector, obtained 1.88 barns at 25 Mev. Snowdon[5] has recently made measurements from about 100 kev to 500 kev with 40-kev resolution.

Using the $Li^7(p,n)$ reaction and the Rockefeller

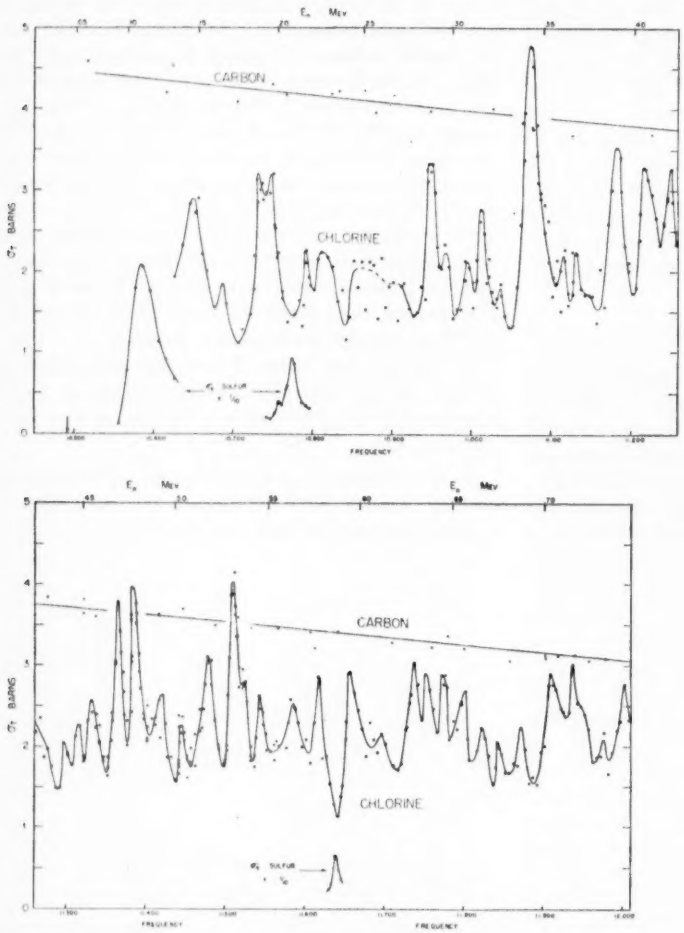

FIG. 1. Total neutron cross section of chlorine and carbon *vs* incident neutron energy in the laboratory coordinate system (upper scale) and *vs* frequency of proton resonance magnet control in megacycles (lower scale). Carbon tetrachloride contained in a thin-walled iron cylinder (7.5×2.6 cm) was used in the chlorine measurements. Correction for carbon content was made from similar measurements for a number of the same frequency settings using a graphite cylinder (2.5×2.5 cm) as a scatterer. The three resonance peaks of sulfur, plotted at $\frac{1}{10}$ scale for σ_t, were used as secondary energy calibrations and as an over-all check on the experimental method.

* This work was supported by the Bureau of Ships and the U. S. Office of Naval Research.
[1] *Neutron Cross Sections*, U. S. Atomic Energy Commission Report 2040 (Office of Technical Services, Department of Commerce, Washington, D. C., 1952).
[2] H. Aoki, Proc. Phys. Math. Soc. Japan **21**, 232 (1939).
[3] Zinn, Seely, and Cohen, Phys. Rev. **56**, 260 (1939).
[4] R. Sherr, Phys. Rev. **68**, 240 (1945).
[5] S. C. Snowdon and W. D. Whitehead, Phys. Rev. **90**, 615 (1953).

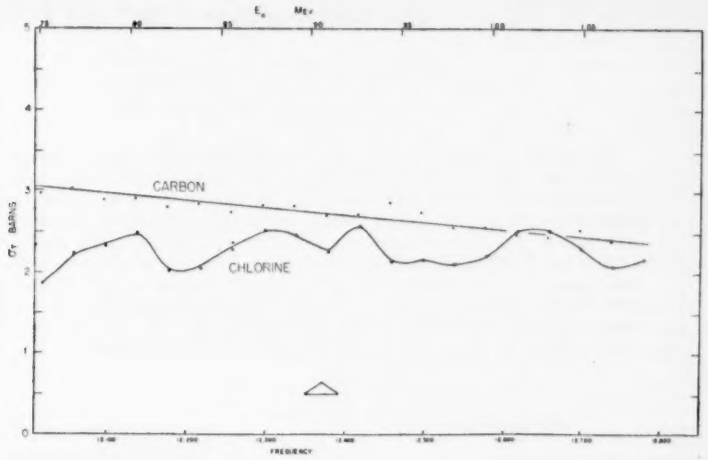

FIG. 1 (*continued*).

generator as a neutron source, and CCl_4 as a scatterer, σ_t(Cl) was measured in good geometry at approximately 2-kev intervals from 150 kev to 750 kev. The targets used were 2 to 4 kev thick at the lower neutron energies. From 750 kev to 1.1 Mev, the resolution was approximately 25 kev.

The detector was a pressurized (70-psi) hydrogen recoil counter,[6] the bias voltage of which was changed continuously to cut out low energy neutron background. Two BF_3 counters, at 15° and 90°, served to monitor the neutron beam, in addition to proton current integration. Corrections were made for the carbon in the CCl_4 by measuring the total cross section of carbon, using graphite as a scatterer. Corrections have also been made for the thin-walled iron tube used as a container.

Assuming isotropic scattering in the center-of-mass system, the scattering-in correction was less than one percent. Figure 1 summarizes the results. Though it is impossible to distinguish between the different isotopes of Cl (24.6 percent Cl^{37}, 75.4 percent Cl^{35}) the average level spacing is ~14 kev, in accord with the high level density expected for odd-odd compound nuclei. It is felt that many of the resonances are not yet resolved, and a few small energy regions need more work. The average cross section observed, $\sigma_t(\mathrm{Cl}) \approx 2.5$ barns, is relatively low compared to neighboring elements.

Energy calibration of the proton resonance controlled magnetic analyzer was made using the $Li^7(p,n)$ threshold at $E_p = 1.882$ Mev.[7] As an operational check, a few of the resonances of sulfur were done simultaneously with the chlorine. The sharp resonances in sulfur[8] not only lend themselves as secondary energy calibrations, but also give a measure of the experimental resolution, see Fig. 1. The sixth resonance in sulfur was also used to test the experimental reproducibility and as a guage of the thickness of the targets as shown in Fig. 2.

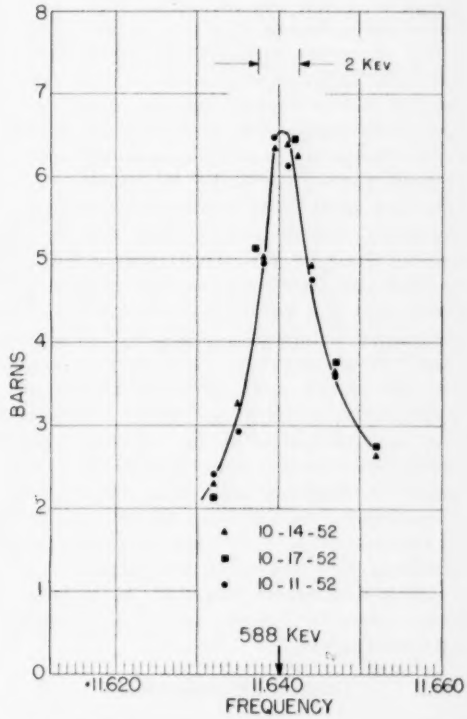

FIG. 2. Repeated measurements on a major resonance of sulfur (observed as 588 kev relative to the $Li^7(p,n)$ threshold which was reported by Peterson *et al.* (reference 8) as 585 kev). During an interval of 2 months, the data fall on the same resonance curve within the statistical uncertainty of the measurements.

The assistance of the other members of the Neutron Physics Group and of Donald C. Thompson is gratefully acknowledged.

[6] F. S. Replogle, Servomechanisms Engineering Memo No. 29, Massachusetts Institute of Technology, March 18, 1952 (unpublished).
[7] Herb, Snowdon, and Sala, Phys. Rev. **75**, 246 (1949).
[8] Peterson, Barschall, and Bockelman, Phys. Rev. **79**, 593 (1950).

The Disintegration of Sr^{91} and Y^{91m}†

D. P. AMES,* M. E. BUNKER, L. M. LANGER,‡ AND B. M. SORENSON
University of California, Los Alamos Scientific Laboratory, Los Alamos, New Mexico
(Received March 9, 1953)

The radiations from the fission product Sr^{91} (9.67-hr) and its daughter isomer Y^{91m} (50.3-min) have been studied using a magnetic lens spectrometer, a high resolution 180° focusing spectrometer, and a scintillation spectrometer. Coincidence measurements were made to check on certain genetic aspects of the decay scheme. Five beta-ray groups are observed with end-point energies and relative intensities of 2.665 Mev, 26.4 percent; 2.03 Mev, 4.1 percent; 1.359 Mev, 29.2 percent; 1.093 Mev, 33.1 percent; and 0.62 Mev, 7.2 percent. The 2.665-Mev group has a shape characteristic of a once forbidden transition involving a spin change of 2 units. Gamma-rays are found with energies of 1.413, 1.025, 0.93, 0.748, 0.645, and 0.5512 Mev. The 50.3-min isomeric level in Y^{91} decays only by gamma-emission to the ground state. The 0.5512-Mev gamma-ray associated with this transition has a $K/(L+M)$ internal conversion ratio of 6.00, which is consistent with an $M4$ assignment. A disintegration scheme is proposed.

INTRODUCTION

STRONTIUM-91 (9.67-hr) is formed in fission as the daughter of the two isomers of Rb^{91}.[1] Previous studies of the radiations from this isotope have been limited to absorption methods. The work of Finkle, Katcoff, and Sugarman[2] indicated that the beta-ray spectrum of Sr^{91} is complex and that there are two gamma-rays of approximate energy 1.3 and 0.61 Mev involved in the decay, the one of lower energy representing an isomeric transition in Y^{91}. The isomer Y^{91m} was found to have a half-life of 51 minutes. Their absorption measurements yielded an end point for the beta-spectrum of about 3.2 Mev. Thus, $\log ft$ for the highest energy group was determined as ~ 8.0, suggesting the possibility that this group might exhibit the unique spectrum shape characteristic of $\Delta I = 2$ (yes) transitions. This possibility was given further support by consideration of the nuclear shell model[3] which suggests $d_{\frac{5}{2}}$ and $p_{\frac{1}{2}}$ for the respective ground states of Sr^{91} and Y^{91}.

A further investigation of the radiations from Sr^{91} employing higher resolution seemed desirable in view of the suggested complexity of the decay and the possibility of establishing the forbidden character of the high energy beta-transition. It was soon discovered that the decay scheme was considerably more complex than had been indicated. However, study of the radiations in detail by various techniques has led to a consistent energy level diagram.

SOURCE PREPARATION

The Sr^{91} sources were produced by irradiating samples of 0.025 to 0.7 g of uranium enriched in U^{235} in a thermal column of the Los Alamos water boiler. The irradiation times ranged from 2 to 6 hours. The neutron flux at the sample position is estimated to be about 6×10^{11} n/cm^2 sec. Some of the uranium samples exhibited radioactivities of several hundred roentgens per hour shortly after irradiation.

Chemical separation of strontium from the fission product mixture was accomplished by using a modification of a procedure devised by Glendenin.[4] Strontium and barium were precipitated initially as nitrates from the gross fission product solution by the addition of fuming nitric acid. Then the rare earth fission products were decontaminated from the strontium and barium activities by the precipitation of iron (III) hydroxide from an ammoniacal solution. The precipitation of barium chromate from a buffered acetic acid solution served to separate the barium activity from the strontium activity. Additional iron (III) hydroxide decontamination steps were performed on the purified strontium fraction in order to remove any lanthanum activity resulting from barium decay prior to the barium separation. For the Sr^{91} work where it was necessary to have the sources as free of Y^{91m} as possible, an iron (III) hydroxide precipitation was made immediately preceding the source preparation. Strontium oxalate sources were used in the scintillation work. For the beta-spectrometer sources, the final strontium oxalate precipitate was dissolved in concentrated nitric acid and strontium nitrate was precipitated by the addition of fuming nitric acid. This precipitate was dissolved in a minimum amount of distilled water, and a portion of the resulting solution was evaporated on a rubber hydrochloride film.

Y^{91m} sources were prepared by allowing Sr^{91}, separated by the above procedure, to decay for a period of from two to three hours. Yttrium was separated initially from its strontium parent by the precipitation of yttrium hydroxide from an ammoniacal solution. Additional strontium decontaminations from the yttrium fraction

† Work performed under the auspices of the U. S. Atomic Energy Commission.
* Now at the University of Kentucky, Lexington, Kentucky.
‡ Indiana University, Bloomington, Indiana.
[1] O. Kofoed-Hansen and K. O. Nielsen, Phys. Rev. **82**, 96 (1951).
[2] Finkle, Katcoff, and Sugarman, *Radiochemical Studies: The Fission Products* (McGraw-Hill Company, Inc., New York, 1951), Paper No. 74, National Nuclear Energy Series, Plutonium Project Record, vol. 9, Div. IV.
[3] M. G. Mayer, Phys. Rev. **78**, 16 (1950).
[4] L. E. Glendenin, *Radiochemical Studies: The Fission Products* (McGraw-Hill Book Company, Inc., New York, 1951), Paper No. 236, National Nuclear Energy Series, Plutonium Project Record, Vol. 9, Div. IV.

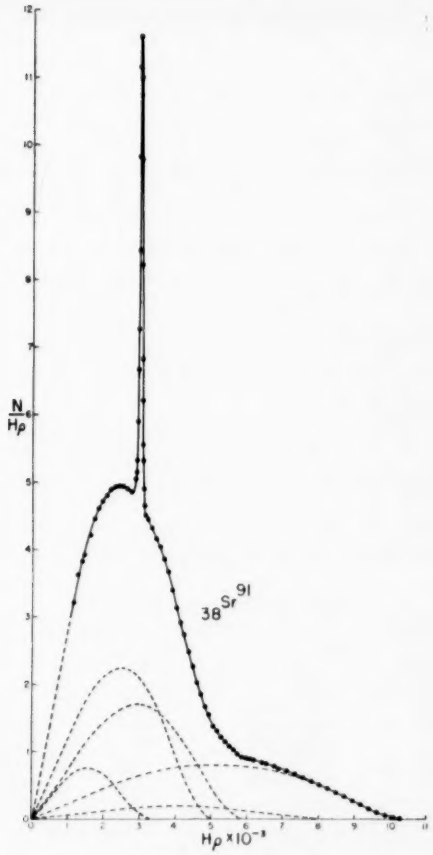

FIG. 1. Beta-spectrum of Sr^{91}. The partial spectra are determined from the Fermi plot analysis.

were performed by precipitating barium nitrate from a solution of the yttrium activity in fuming nitric acid. Then the yttrium activity was separated from the supernatant solution by the addition of concentrated hydrofluoric acid. The resulting yttrium fluoride was dissolved in a concentrated nitric acid—boric acid solution. An additional yttrium hydroxide precipitation was performed to reduce the total solid content of the solution. Following the dissolution of the precipitated hydroxide in dilute hydrochloric acid, yttrium oxalate was precipitated by the addition of a monium oxalate. This precipitate served as the Y^{91m} source material for both the scintillation and beta-spectrometer work.

The strontium separation was normally begun 30 to 40 hours after irradiation. This time lapse was necessary in order to effectively suppress $Sr^{92}-Y^{92}$ contamination. A small amount of long-lived contamination resulting from Sr^{89} and Sr^{90} was unavoidable, however, and had to be taken into account. In order to check the purity of the strontium source material, decay data were taken over a period of several days, using a standard Geiger counter arrangement. When the contribution of the long-lived components was subtracted, a logarithmic decay curve was obtained which was linear and which, on the basis of the data taken during the first 36 hours, yielded a half-life for Sr^{91} of 9.67 ± 0.02 hours. Decay measurements were also made on a source of Y^{91m}, obtained by the above procedure. The logarithmic decay curve remained linear for more than two decades, yielding a half-life of 50.3 ± 0.25 minutes for Y^{91m}.

BETA-SPECTRA

Measurement of the composite beta-spectra of Sr^{89} (54-day), Sr^{90} (25-year), and Sr^{91} was begun as soon as feasible after the chemical separation. At the tiime of this measurement, the Sr^{91} activity amounted to roughly 75 percent of the total activity. A week later the spectrum was remeasured and the separate contributions of Sr^{89} and Sr^{90} were determined by a unique once forbidden Fermi analysis. These spectra were then corrected for decay and appropriately subtracted from the original composite distribution. The difference spectrum thus obtained is assumed to be that of Sr^{91}.

The beta-ray measurements referred to above were made with a large magnetic lens spectrometer.[5] An end-window Geiger tube having a 2.4-mg/cm² mica window and a 0.5-in. diameter aperture was employed as a detector. The spectrometer baffle system was adjusted so that the resolution was approximately 2.4 percent.

The beta-ray source consisted of approximately 0.2 mg of strontium nitrate spread over an area of 0.4 cm² on a backing of rubber hydrochloride 0.54 mg/cm² thick. The edge of the source was connected to ground by a narrow strip of aluminum foil.

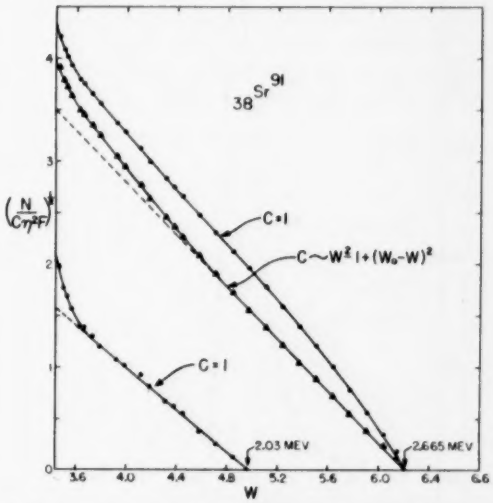

FIG. 2. Conventional and forbidden Fermi plots of the higher energy portion of the Sr^{91} data.

[5] L. M. Langer, Phys. Rev. **77**, 50 (1950).

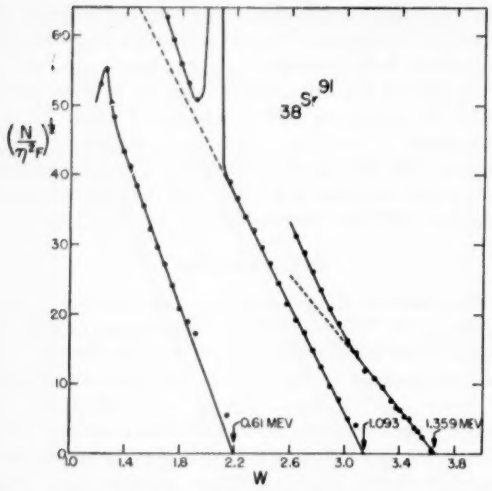

FIG. 3. Fermi plot of lower energy beta-groups of Sr^{91}. The continuous spectrum is obscured in the vicinity of $W=2.0$ by conversion lines of the 0.551-Mev gamma-ray.

The momentum distribution of the electrons from Sr^{91} is shown in Fig. 1. A statistical accuracy of about 1 percent was obtained on all points. The obviously complex spectrum has been resolved into five groups on the basis of a Fermi analysis of the data. Figure 2 shows the high energy portion of the Fermi plot. It is seen that the conventional plot of the highest energy group is concave toward the energy axis which, in conjunction with the calculated value of $\log[(W_0^2-1)ft]=9.65$, suggests that this transition is once forbidden with a spin change of 2 units.[6] In order to establish this assignment with greater certainty, the forbidden factor $a=W^2-1+(W_0-W)^2$, applicable to such transitions, has been appropriately applied to the data and yields the points plotted as triangles in Fig. 2. This "forbidden" plot is seen to be linear from near its end point of 2.665 Mev back to the end point of the next group at 2.03 Mev. The fact that the two points beyond $W=6.0$ lie slightly above the straight line is expected, since no correction was made for the finite resolution of the spectrometer.

The remainder of the Fermi plot analysis is shown in Fig. 3. The four inner groups are assumed to have the allowed shape. Unfortunately, the end point of the 0.61-Mev group is obscured by conversion electrons. However, in spite of the numerous subtractions, the data on this lowest energy group seem to be reasonably good, and the extrapolated end point is not thought to be in error by more than 20 kev. The rise of the Fermi plot below $W=1.4$ is a characteristic behavior of spectra emitted from a source of $\sim$0.5-mg/cm^2 surface density and is therefore not interpreted as indicating another group. The gamma-ray measurements further substantiate this assumption. The end-point energies, intensities, and logft values of the five observed groups are given in Table I.

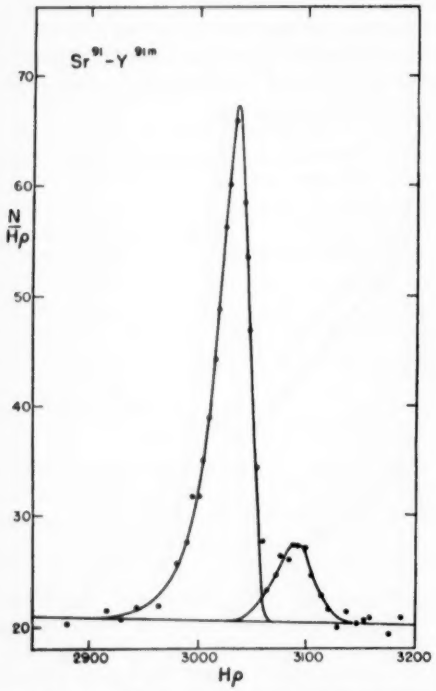

FIG. 4. K and $L+M$ internal conversion lines of the 551.2 kev isomeric transition in Y^{91}.

TABLE I. The beta-ray groups of Sr^{91}.

Group	End-point energy (Mev)	Intensity (%)	logft[a]
β_1	2.665±0.01	26.4	8.07
β_2	2.03 ±0.02	4.1	8.39
β_3	1.359±0.01	29.2	6.82
β_4	1.093±0.01	33.1	6.38
β_5	0.61 ±0.02	7.2	6.10

[a] Determined from the curves given by S. A. Moszkowski, Phys. Rev **82**, 35 (1951).

The strong conversion electron peak which appears in Fig. 1 arises from the decay of 50.3-min Y^{91m}. This peak could not be resolved into its separate K, L, and M components using the magnetic lens spectrometer. However, examination of a Sr^{91} source in a high resolution 180° focusing spectrometer[7] yielded the conversion electron spectrum shown in Fig. 4. The two peaks are, respectively, the K and $L+M$ lines of a 551.2±1.0 kev gamma-ray. The $K/(L+M)$ ratio is 6.00 which empirically classifies the transition as $M4$.[8] This classification is also suggested by the semi-empirical

[6] F. B. Shull and E. Feenberg, Phys. Rev. **75**, 1768 (1949).
[7] L. M. Langer and C. S. Cook, Rev. Sci. Instr. **19**, 257 (1948).
[8] Graves, Langer, and Moffat, Phys. Rev. **88**, 344 (1952).

lifetime-energy formulas given by Goldhaber and Sunyar.[9]

It was thought possible that Y^{91m} might be beta unstable. To check this point, an Y^{91m} beta-ray source was prepared by chemically extracting the yttrium from a Sr^{91} sample. Examination of the electron spectrum revealed only the conversion lines from the 551.2-kev gamma-ray.

GAMMA-SPECTRA

The photo- and Compton electrons ejected from a uranium radiator by the gamma-rays of Sr^{91} were examined with the magnetic lens spectrometer. The resulting spectrum is shown in Fig. 5. The source material was contained in a small brass capsule which had walls thick enough to stop 3-Mev beta-particles and which had attached to its front side a $\frac{3}{8}$-in. diameter, 33 mg/cm² disk of uranium.

A total of seven photoelectron lines were observed,

TABLE II. Photoelectron lines ejected from a uranium radiator by the gamma-rays of Sr^{91}.

Line	Energy (kev)	Converter thickness correction[a]	Binding energy (kev)	Gamma-energy (kev)	Gamma-best value (kev)
K_1	430.6	5.0	115.6[b,c]	551.2	
L_1	524.7	6.0	19.3[d]	550.0	551.2±1.0
K_2	524.7	6.0	115.6	646.3	645 ±5
K_3	625.4	7.2	115.6	748.2	
L_3	720.7	8.3	19.3	748.3	748 ±2
K_5	899.7	9.7	115.6	1025.0	
L_5	992.0	9.8	19.3	1021.1	1025 ±5
K_6	1288.8	9.0	115.6	1413.4	1413 ±5

[a] Hornyak, Lauritsen, and Rasmussen, Phys. Rev. **76**, 731 (1949).
[b] Y. Cauchois, J. phys. et radium **13**, 113 (1952).
[c] Hill, Church, and Mihelich, Rev. Sci. Instr. **23**, 523 (1952).
[d] A weighted average of the three L subshell binding energies given in reference *c*. Each shell was given a weight equal to the number of electrons it contains.

two of which are known to be superpositions of K and L lines. A summary of the energies and assignments of these lines is given in Table II. The K photoelectron line of the 551.2-kev gamma-ray (K_1) was used as a calibration. The peak which occurs at the approximate energy of the L line of this gamma-ray (L_1) was observed to have about twice the expected L_1 intensity, strongly suggesting that this peak is a composite of the L_1 line and a K line of about the same energy and intensity. Therefore, since the composite peak occurs at an energy of about 1 kev less than the calculated energy of the L_1 line, the K line (K_2) must have an energy of about 1 kev less than that of the peak. This is the reason why the energy of the gamma-ray responsible for K_2 is estimated in Table II to be 645 kev instead of 646.3 kev which one calculates from the observed (K_2, L_1) peak.

The Sr^{91} gamma-radiation was also studied with a

[9] M. Goldhaber and A. W. Sunyar, Phys. Rev. **83**, 906 (1951).

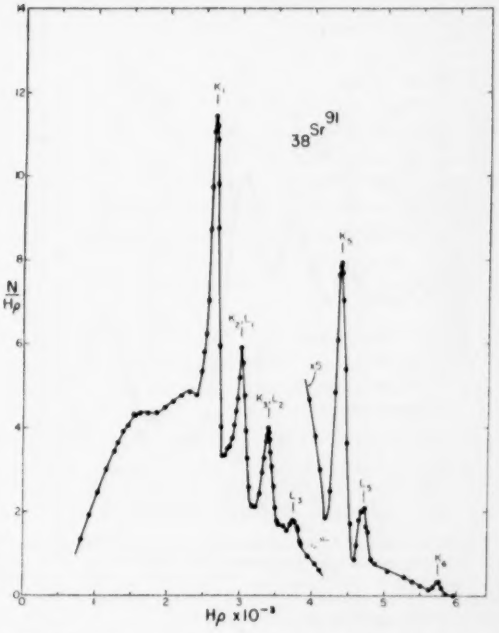

FIG. 5. Compton and photoelectrons ejected from a uranium radiator by the gamma-rays of Sr^{91}.

NaI(Tl) scintillation spectrometer. The phosphor, $1\frac{1}{2}$ in. in diameter and $1\frac{1}{2}$ in. high, was mounted on a Dumont K-1177 photomultiplier tube, and the amplified output pulses were sorted with a 10-channel pulse-height analyzer. A lead collimator 1 in. in diameter, and 4 in. long was placed between the source and detector.

A portion of the measured pulse-height distribution is shown in Fig. 6. Although a careful search was made down to energies as low as 20 kev, no photoelectron (or total energy) peaks of lower energy than 551 kev

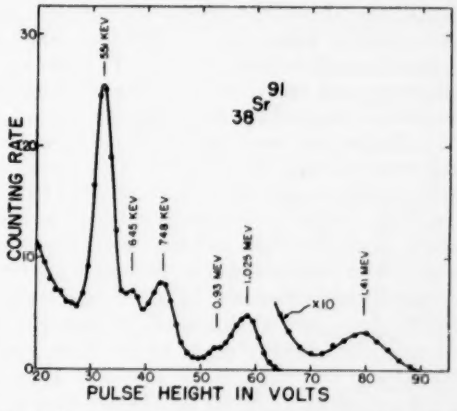

FIG. 6. Gamma-ray spectrum of Sr^{91} taken with a NaI(Tl) scintillation spectrometer. The 50.3-min Y^{91m} activity has been allowed to grow into secular equilibrium with the Sr^{91} activity.

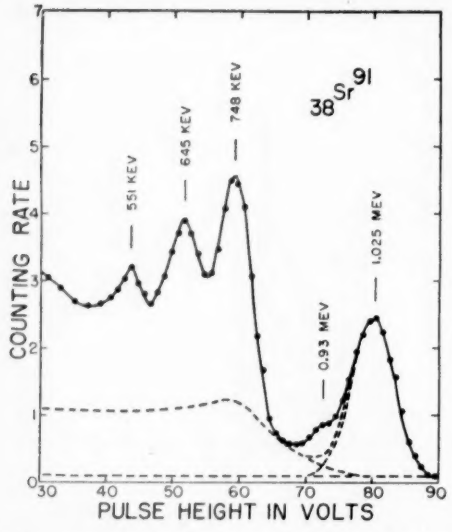

FIG. 7. A portion of the gamma-ray spectrum of Sr^{91} taken with a NaI(Tl) scintillation spectrometer approximately 3½ minutes after chemically removing the Y^{91m} activity. The uppermost dotted line is an estimate of the sum of the spectra of the 1.025- and 1.41-Mev gamma-rays.

could be found. Five of the observed peaks agree in energy with the gamma-ray values listed in Table II. In addition, a weak line is in evidence at about 0.93 Mev which was not resolved in the secondary electron spectrum. Examination of an Y^{91m} source in the scintillation spectrometer proved that of the six observed gamma-rays, only the 551.2-kev transition is associated with the yttrium isomer. Therefore, this gamma-ray must be a ground-state transition.

The scintillation spectrum was used to estimate the relative intensities of the observed gamma-rays. In order to obtain a more reliable estimate of the intensity of the incompletely resolved 645-kev line, a Sr^{91} source was examined with the scintillation spectrometer approximately 3½ minutes after an yttrium separation (which initially eliminates the 551-kev line). The spectrum obtained is shown in Fig. 7. The 551-kev line is sufficiently weak that a good estimate of the intensity of the 645-kev line could be made. The manner in which the scintillation data were analyzed is indicated by the dotted lines in Fig. 7, which show the estimated contribution to the spectrum of the 1.41- and 1.025-Mev gamma-rays. Guided by experimental data on monoenergetic lines of various energies, such curves were constructed for each gamma-ray. Gamma-ray intensity ratios were than calculated by correcting the areas under the photopeaks for crystal efficiency on the basis of an empirical efficiency curve for the 1½-in. crystal. The results of this analysis are shown in Table III. The last column in Table III is discussed later in this report.

A gamma-gamma coincidence study was also made on the Sr^{91} gamma-radiation, using a pair of scintillation spectrometers. The resolving time of the coincidence circuit was about one microsecond. The experimental arrangement was very similar to that used by Bell *et al.*[10] With the so-called "gate" spectrometer set to count all pulses representing 400-kev energy or greater, the coincidence spectrum obtained is that shown in Fig. 8. This spectrum indicates that of the six known gamma-rays, only the 0.645-, 0.93-, and 1.41-Mev transitions are involved in prompt gamma-cascades. This fact was quite useful in the deciphering of the decay scheme.

DISCUSSION

A decay scheme for Sr^{91} can be deduced which is consistent with the various measurements described above. This is shown in Fig. 9. Consideration of energies and intensities alone would lead to this scheme. In addition, its validity is greatly strengthened by the information obtained in the gamma-gamma coincidence experiment. The strong 0.748- and 1.025-Mev gamma-rays do not appear in the coincidence spectrum since they both feed the isomeric level.

TABLE III. Sr^{91} gamma-ray data obtained with a NaI(Tl) scintillation spectrometer.

Gamma-energy (Mev)	Relative peak area	Crystal efficiency (arb. units)	Relative intensity (arb. units)	Normalized intensity[a] (%)
0.551	6.31[b]	0.308	20.5	59
0.645	1.39	0.267	5.2	15
0.748	2.15	0.234	9.2	27
0.93	0.21	0.192	1.1	3
1.025	1.84	0.177	10.4	30
1.41	0.25	0.138	1.8	5

[a] Relative to the total number of disintegrations.
[b] Corrected for internal conversion. The measured peak area was 6.02.

In order to convert the observed relative intensities of the gamma-rays to percentages relative to the total number of disintegrations, it was assumed that the sum of the intensities of the 1.025- and 0.93-Mev gamma-rays equals the intensity of the 1.093-Mev beta-ray group. The resulting normalized intensities are listed in Table III and also appear in Fig. 9. The fact that the intensity of the 0.748-Mev gamma-ray calculates to be slightly lower than expected and that of the 0.645-Mev gamma-ray slightly higher than expected suggests the possibility that there is a weak 0.654-Mev transition between the 1.299- and 0.645-Mev levels which is masked by the 0.645-Mev gamma-ray. However, the data are not good enough to decide this question. In this respect, it is interesting to note that if the spin assignments are correct, the 0.654-Mev gamma-ray would be an $M2$ transition and would not be expected to compete measurably with the 0.748-Mev $M1$ transition.

[10] Bell, Cassidy, and Kelley, Phys. Rev. **82**, 103 (1951).

From the 59 percent intensity of the 551.2-kev isomeric transition and the measured ratio of the area of its K conversion line to the area of the beta-spectrum, it is possible to calculate a value for the K internal conversion coefficient. This coefficient is found to be $(4.6\pm0.2)\times10^{-2}$, which is in excellent agreement with the theoretical value $(4.7)\times10^{-2}$ given by the tables of Rose *et al.*[11] for an $M4$ transition.

In regard to spin assignments, the beta-spectrum from 61-day Y^{91} has been identified as once forbidden $\Delta I=2$(yes),[12] and, since the measured ground state of Zr^{91} is $\frac{5}{2}$ (the shell model assignment is $d_{\frac{5}{2}}$), the ground state of Y^{91} must be $p_{\frac{1}{2}}$. Similarly, since the beta-transition from Sr^{91} to the Y^{91} ground state is also of the $\Delta I=2$(yes) type, the ground state of Sr^{91} must be $d_{\frac{5}{2}}$, which is consistent with shell model predictions. The $M4$ character of the isomeric transition makes the 0.551-Mev level a $g_{9/2}$ state. Thus, the reason there is no

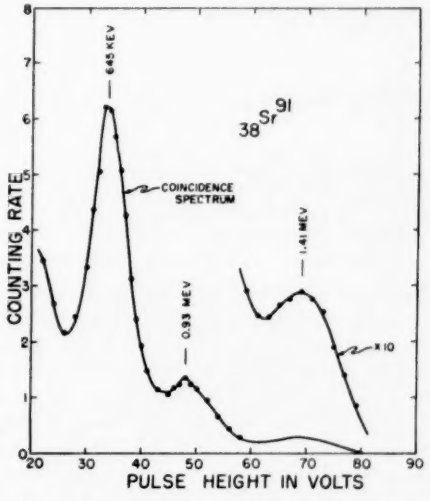

FIG. 8. Gamma-gamma coincidence spectrum of Sr^{91} obtained using coincident scintillation spectrometers. The pulses contributing to this spectrum are those that are in coincidence with pulses representing 400-kev energy or greater.

observed beta-emission to this level is that the transition is twice forbidden.

The rest of the spin assignments are less definite; but, as shown below, they provide a reasonable explanation of the experimental data consistent with beta-ray selection rules and gamma-ray transition probabilities. An attempt was also made to keep the assignments consistent with what might appear to be a reasonable extension of the one-particle shell model to the higher excited states. It is realized, of course, that the one-particle model is not necessarily applicable to highly excited states.

[11] Rose, Goertzel, Spinrad, Harr, and Strong, Phys. Rev. **83**, 79 (1951).

[12] L. M. Langer and H. C. Price, Jr., Phys. Rev. **76**, 186 (1949).

The beta-ray groups designated in Table I as β_2, β_3, and β_4 have logft values which suggest they are either once forbidden or l forbidden. Consequently, $p_{\frac{1}{2}}$, $g_{7/2}$, $f_{\frac{1}{2}}$, and $f_{7/2}$ seem to be the only shell model states available for assignment to the 0.645, 1.299, and 1.576 Mev levels. A $p_{\frac{1}{2}}$ assignment appears to be the best choice for the 0.645-Mev level for the following reasons: (1) there is no intermediate gamma-transition observed between the 0.645-Mev and the 0.551-Mev levels, which limits the choice to $p_{\frac{1}{2}}$ or $f_{\frac{1}{2}}$; (2) the choice of $f_{\frac{1}{2}}$ makes it difficult to explain the observed gamma-ray branching ratios from the upper levels to the 0.551- and 0.645-Mev levels.

The 1.299- and 1.576-Mev levels both decay predominantly to the 0.551-Mev, $g_{9/2}$ level. This fact eliminates $f_{\frac{1}{2}}$ as a possibility for either level, leaving only the choices $g_{7/2}$ and $f_{7/2}$. Now, it appears definite that there is a weak transition (0.93 Mev) between the 1.576-Mev level and the 0.645-Mev level, whereas it is questionable whether or not there is an observable transition to the $p_{\frac{1}{2}}$ level from the 1.299-Mev level. This suggests assignment of $f_{7/2}$ to the 1.576-Mev level and $g_{7/2}$ to the 1.299-Mev level, since it seems likely that a 0.93-Mev, $E2$ transition would compete more strongly with a 1.025-Mev, $E1$ transition than a 0.93-Mev, $M2$ transition would compete with a 1.025-Mev, $M1$ transition.

The data indicate that the 2.058-Mev level decays mainly to the 0.645-Mev, $p_{\frac{1}{2}}$ level. If β_5 is a once forbidden transition, an assignment of $f_{\frac{1}{2}}$ to the 2.058-Mev level seems to be the most likely possibility. This would make the 1.413-Mev gamma-ray an $M1$ (or $M1+E2$) transition. The fact that the higher energy $E2$ transition to the ground state does not compete detectably with the 1.413-Mev gamma-ray is not in contradiction with the empirical data on $M1$ and $E2$ transition probabilities.[9] There is some possibility that β_5 is an allowed transition, in which case the most logical assignment for

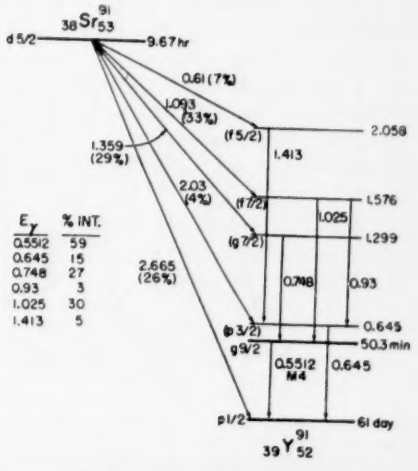

FIG. 9. Proposed disintegration scheme of Sr^{91}.

the 2.058-Mev level would be $d_{\frac{1}{2}}$. This assignment would be as consistent with the gamma-ray data as an $f_{\frac{1}{2}}$ assignment.

The fact that Y^{91m} does not exhibit detectable beta-emission leads to an interesting conclusion regarding the spacing of certain energy levels of Zr^{91}. The first excited state of Zr^{91} would be expected to be a $g_{7/2}$ state, and beta-emission to this level from Y^{91m} would be *allowed*. From the experimental data it is possible to to say that, if Y^{91m} does beta-decay to Zr^{91}, the intensity of the beta-transition must be less than 1.5 percent of that of the isomeric transition. From this fact and the fact that the logft values of allowed transitions have an empirical upper bound of about 6.0, it is possible to calculate an upper limit on the energy of the hypothetical Y^{91m} beta-transition. This value is found to be $\sim$0.75 Mev, which leads to the conclusion that the $g_{7/2}$ excited state of Zr^{91} is more than 1.34 Mev above the ground state. The same lower bound holds for the $g_{9/2}$ excited state. These conclusions are supported by the preliminary data of Shull and McFarland[13] on the Q values of the proton groups from the reaction $Zr^{90}(d,p)Zr^{91}$. The two proton groups they observed were found to have associated Q values of 5.03 and 2.93 Mev, suggesting that the first excited state of Zr^{91} is 2.1 Mev above the ground state.

We wish to extend our thanks to Mr. John W. Starner for his invaluable assistance with the scintillation experiments.

[13] F. B. Shull and C. E. McFarland, Phys. Rev. **87**, 216 (1952).

PHYSICAL REVIEW VOLUME 91, NUMBER 1 JULY 1, 1953

Gallium-64

BERNARD L. COHEN
Oak Ridge National Laboratory, Oak Ridge, Tennessee
(Received March 27, 1953)

A new isotope, 2.5-minute Ga^{64}, was produced by the (p,n) reaction on Zn^{64} and identified by measurement of the excitation function, by bombardment of separated isotopes, and by chemical separation. Its decay scheme includes gammas of 0.97 Mev, 3.8 Mev, and probably 2.2 Mev. The maximum energy of the principle beta is about 5 Mev. The threshold for Zn^{64} (p,n) is 8.1 ± 0.5 Mev.

A PREVIOUSLY unidentified isotope, 2.5-min gallium 64, has been produced by bombarding zinc with high energy protons from the ORNL 86-in. cyclotron. The following tests were made to ascertain its identity.

(1) A rough excitation function for the various activities found from proton bombardment of zinc was measured by a stacked foil technique. The results, shown in Fig. 1, indicate that the 2.5-min activity has all the characteristics of a (p,n) reaction, as can be seen by comparing it with the 68-min (Ga^{68}) and 9.4-hr (Ga^{66}) activities which are known to be produced by (p,n) reactions. The ratio of the cross sections for production of the 2.5-min and 9.4-hr activities in natural zinc was found to be about 2:1 at 13 Mev, which is approximately the isotopic abundance ratio of Zn^{64} to Zn^{66}. After the excitation function was measured, all further investigation was carried out by bombarding under an absorber calculated to reduce the proton energy to 13 Mev.

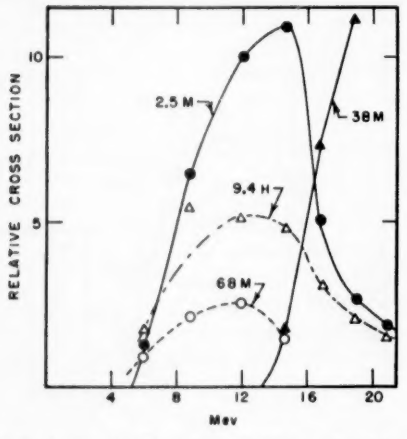

FIG. 1. Excitation functions for activities produced by proton bombardment of zinc. The 9.4-hr, 68-min, and 38-min activities are known to be produced by (p,n) reactions on Zn^{66} and Zn^{68}, and the (p,pn) reaction on Zn^{64}, respectively.

(2) A series of bombardments was made with isotopically enriched Zn^{64}.[1] This essentially eliminated the 68-min and 9.4-hr activities, but yielded very good intensities of the 2.5-min activity. Most of the spectroscopy was done with this isotopically enriched material.

(3) Chemical identification was obtained by ether extraction. The ratio of the 2.5-min to 9.4-hr activities in the ether fraction was found to be about the same as in an unprocessed zinc foil. By counting under a thick absorber to remove the 68-min activity, the decay could be followed above the 9.4-hr background through nine half-lives even after three half-lives had been con-

[1] Separated isotopes were obtained from the Stable Isotopes Division, Oak Ridge National Laboratory, Oak Ridge, Tennessee.

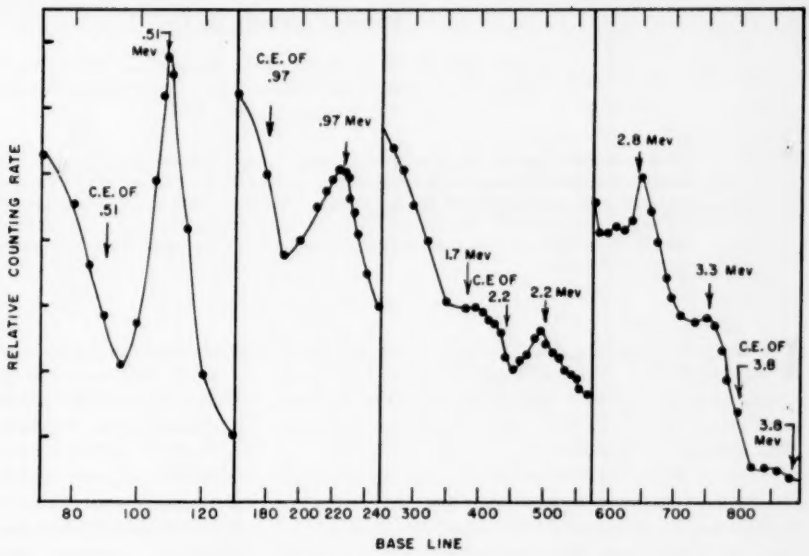

FIG. 2. Pulse-height distribution from Ga^{64} as measured with a NaI scintillation spectrometer. Various sections were obtained with different absorbers between sample and crystal. Note change in base line scale. C.E. is "Compton Edge."

sumed in removal of the target from the cyclotron and in chemical processing.

It should be noted that all isotopes, except Ga^{64}, which can be produced by (p,n) or (p,α) reactions on any of the zinc isotopes are well identified according to recent isotope tables. Both the natural zinc and isotopically enriched Zn^{64} used in the bombardments were spectroscopically analyzed and found to be free of imputities to one part per thousand.

The pulse-height spectrum of the 2.5-min activity, as obtained with a NaI scintillation spectrometer, is shown in Fig. 2. The four parts of the spectrum were obtained with different absorbers between the sample and the crystal since the large intensities necessary to obtain good statistics in the high energy portion produced total counting rates larger than could be handled by the single channel discriminator. Each point in Fig. 2 represents a three point decay curve over at least six half-lives of the 2.5-min activity. While the results of several runs differ somewhat in detail, each maximum, minimum, and edge marked in Fig. 2 was evident in every run. The low energy portion of the spectrum shows only the Compton edge and photoelectric peak of the 0.51-Mev annihilation radiation, which confirms the fact that the 2.5-min activity is a positron emitter. The next portion shows the Compton edge and photoelectric peak for a strong gamma-ray at 0.97 Mev. The highest energy portion shows a fairly definite Compton edge, the two pair peaks (at 2.8 and 3.3 Mev) and a poorly resolved photoelectric peak for what is probably a 3.8-Mev gamma-ray. The medium energy portion gives some indication of a 2.2-Mev gamma, but this interpretation should certainly be considered no more than tentative.

Considerable effort was expended in measuring the beta-ray spectrum by both the collimator and hollow crystal methods[2] with an anthracene scintillation spectrometer. Because of the difficulty in obtaining a thin and intense source, the lack of experience in handling very high energy betas with a complex spectrum, the difficulty in correcting for the gamma-ray background attributable to the short half-life, and the other well known troubles associated with beta-ray scintillation spectroscopy, only mediocre success was realized. The indications are that the most intense beta has a maximum energy in the vicinity of 5 Mev.

A relatively accurate measurement of the threshold for the $Zn^{64}(p,n)$ reaction was made by comparing the excitation function near the threshold with those of Cu^{63} and Zn^{66}, making corrections for the beam energy inhomogeneity. The Zn^{64} threshold was determined as 8.1 ± 0.5 Mev; this corresponds to a Ga^{64} maximum beta-energy of 6.4 Mev, and $\log ft > 6.1$ for the ground-state transition.

The author would like to acknowledge the very considerable help of E. L. Olson in the beta-spectroscopy.

[2] W. H. Jordan, *Annual Review of Nuclear Science* (Annual Reviews, Inc., Stanford, 1952), Vol. 1, p. 207.

Nuclear Levels in Cs^{131}†

J. M. Cork, J. M. LeBlanc, W. H. Nester, and M. K. Brice
Department of Physics, University of Michigan, Ann Arbor, Michigan

(Received March 5, 1953)

Using enriched barium 130, activated in the pile, a spectrometric study has been made of the radiation from the resultant barium 131. Decaying by K capture with a half-life of 11.8 days, thirteen gamma-rays are found to be associated with the disintegration, eight of which have not been previously reported. From the relative intensities of the electron lines and the photoelectron peaks, the multipolarities of six of the transitions are given. A consistent nuclear level scheme of seven terms accounts completely for the observed gamma-transitions.

IN an early report on the radioactivity in barium it was concluded[1] that the isotope of mass 130 whose normal abundance is only 0.10 percent could by neutron capture produce a radioactive isotope of mass 131. This emitter, whose half-life is about 12 days, was believed to decay by K capture and gamma-radiation to a radioactive daughter product, Cs^{131}. This isotope in turn decays by K capture with a half-life of about 9.7 days, to stable xenon. Many subsequent investigations have been made, particularly to evaluate the energies of the associated gamma-rays. These energies as reported by various observers[1–7] are shown collected in Table I. Seven gamma-rays are listed in Table I. It now appears quite certain that the transition at 0.196 Mev does not exist, and it is quite unlikely that there is any radiation with energy above 1 Mev.

TABLE I. Previously reported gamma-energies.

	Gamma-energies in Mev as reported by						
Item	YGK[a]	K[b]	K[c]	Z[d]	C[e]	CM[f]	E[g]
γ_1			0.122		0.16	0.122	0.122
γ_2						0.196	
γ_3	0.22		0.206			0.213	0.214
γ_4		0.26				0.241	0.241
γ_5			0.372		0.42	0.371	0.370
γ_6	0.50	0.50	0.494	0.496		0.497	0.494
γ_7	1.7	1.2			1.2		

[a] See reference 1.
[b] See reference 2.
[c] See reference 3.
[d] See reference 4.
[e] See reference 5.
[f] See reference 6.
[g] See reference 7.

In the present investigation it is shown that there are thirteen gamma-rays in addition to Auger radiation present in the disintegration. A sample of barium was kindly provided by the Oak Ridge National Laboratory in which the mass 130 was enriched from its normal abundance of 0.10 percent up to 27.5 percent. On irradiation in the Argonne heavy-water pile, sources of high specific activity were obtained for studies in photographic magnetic spectrometers. In addition to the electron lines resulting from internal conversion, the photoelectrons ejected from a lead radiator have been observed. A careful survey has been made in the double focusing spectrometer to detect the presence of any positrons in the decay, with negative results. Similarly, by the use of a scintillation spectrometer no evidence could be found to indicate the existence of the 0.82- or the 1.2-Mev gamma-rays as previously reported.[5]

In Table II the energies of the observed electron lines are presented in column 1. All but four lines decay with the same half-life, namely 11.8±0.2 days, and fit best the work functions for cesium. The other four lines have shorter half-lives and are K and L lines from isomeric transitions in Ba^{133} and Ba^{135}. Their K and L lines fit the work functions of barium. The interpretation of the lines and the resultant energy sums are shown in succeeding columns. The low energy Auger lines are broad as might be expected since x-rays of both cesium and xenon are present. The energies of the thirteen gamma-rays, eight of which have not been previously observed, are summarized in Table III. Arbitrary numbers are assigned in column 1, increasing in the order of increasing energy.

Traces were made of the photographic plates with a Leeds and Northrup recording microphotometer. When corrected for solid angle and the variation in emulsion sensitivity with energy, it becomes possible to express the K/L ratios for six of the gamma-rays, as shown in column 3. For three of the remaining gammas a visual estimate of the ratio is recorded. From these observed intensity ratios and a consideration of the results of other investigators, it becomes possible to make reasonably unique conclusions regarding the multipolarities of certain of the transitions. For example, the ratio of the photoelectric intensities of the 373-kev to the 497-kev gammas has been variously reported[3,6,7] as 0.07, 0.12, and 0.25. While these numbers differ widely and are uncertain as a result of the poor resolution of the

† This investigation received the joint support of the U. S. Office of Naval Research and the U. S. Atomic Energy Commission.

[1] Yu, Gideon, and Kurbatov, Phys. Rev. **71**, 382 (1947).
[2] S. Katcoff, Phys. Rev. **72**, 1160 (1947).
[3] E. Kondiah, Arkiv Fysik **2**, 28, 295 (1950).
[4] Zimmerman, Dale, Thomas, and Kurbatov, Phys. Rev. **80**, 908 (1950).
[5] W. Cuffy, Phys. Rev. **82**, 461 (1951).
[6] R. Canada and A. Mitchell, Phys. Rev. **83**, 76 (1951).
[7] Elliott, Cheng, Haskins, and Kurbatov, Phys. Rev. **88**, 263 (1953).

TABLE II. Energy of electrons from Ba^{131} in kev.

Electron energy	Interpretation	Energy sum	Electron energy	Interpretation	Energy sum
24.8	Auger KL_1L_1		180.0	K	216.0
25.6	Auger KL_2L_2		203.5	K	239.5
30.1	Auger KLM		210.0	L_1	215.7
33.9	Auger KMM		213.0	K	249.0
42.7	K	78.7	230.7	K(Ba)	268.1
49.8	L_2	55.2	233.8	L	239.5
53.9	M	55.1	238.5	K(Ba)	275.9
56.3	K	92.3	243.0	L	248.7
73.1	L_2	78.5	262.1	L(Ba)	267.6
77.5	M	78.7	270.0	L(Ba)	275.6
88.1	K	124.1	337.5	K	373.5
97.5	K	133.5	368.5	L	374.0
118.4	L_2	123.8	461.5	K	497.5
122.4	M	123.6	492.0	L	497.5
123.4	N	123.6	549	K	585
127.6	L_1	133.3	584	K	620
132.1	M	133.3			

spectrometers employed, they probably give the correct order of magnitude. The corresponding ratio for the K-conversion peaks of the same gamma-rays in the present investigation is found to be 1:2.1. It should then follow that the inverse ratio of the K-conversion coefficients must lie somewhere between 0.14 and 0.53. By reference to the calculated K coefficients of Rose[8] at these energies it can be seen that of all the possible multipolarities consistent with K/L ratio measurement, as numerator or as denominator, only three combinations fall within the observed limits, namely, M_2/M_3 (0.13), M_3/M_3 (0.37), and E_2/E_2 (0.45). The K/L ratios of 6 ± 0.5 and 7.7 ± 0.5 would indicate that the 373-kev radiation could be $E2$ or $M3$ in character, and the 497-kev radiation could be $E2$, $M3$, $M2$ or $M1$. The lifetime of $M3$ radiation would probably be too long for the 373-kev transition, since coincidences have been observed.[3] It seems reasonable then to express a preference for the $E2$ assignments to both. In a similar way, each of the other designations shown in column 4 has been determined. For the low energy gamma-rays the assignment is aided by the relative intensities of the three L conversion lines.

TABLE III. Energies and nature of the observed gamma-rays.

Arbitrary number	Energy, kev	K/L ratio	Type
1	55.2	$\leqq 1$	$E2$
2	78.7	10 ± 2	$M1$
3	92.3		
4	123.8	3.6 ± 0.3	$(M1+E2)$
5	133.4	5.8 ± 0.5	$(M1+E2)$
6	215.8	9 ± 2	$M1$
7	239.3	$\leqq 6$	
8	248.8	$\geqq 6$	
9	373.5	6 ± 0.5	$E2$
10	488.5		
11	497.5	7.7 ± 0.5	$E2$
12	585		
13	620		
Ba^{133}	275.7		
Ba^{135}	267.9		

[8] Rose, Goertzel, and Perry, Oak Ridge National Laboratory Report No. 1023 (1951) (unpublished).

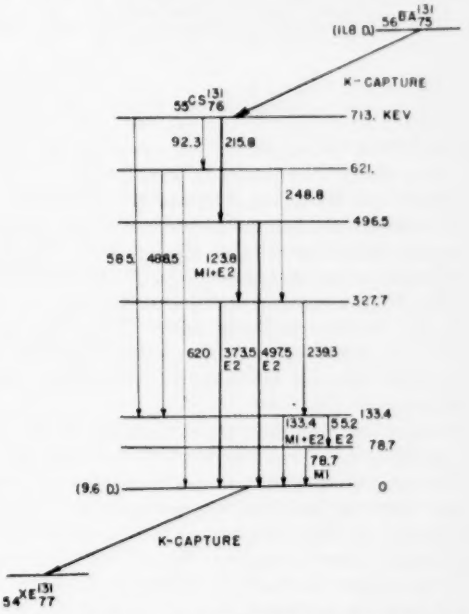

FIG. 1. Nuclear levels in Cs^{131} following K capture in Ba^{131}. (Note: the value 327.7 in the figure should read 372.7.)

The numerical values of the energies of the observed gamma-rays exhibit significant equivalent combinations, thereby suggesting a nuclear level scheme as shown in Fig. 1. All of the thirteen gamma-rays are satisfactorily accommodated as transitions between the seven nuclear levels.

The Decay of Au^{197m}†

J. W. MIHELICH, *Brookhaven National Laboratory, Upton, New York*

AND

A. DE-SHALIT,* *Palmer Physical Laboratory, Princeton University, Princeton, New Jersey*

(Received March 6, 1953)

The conversion electron spectra of Hg^{197m} and Au^{197m} have been re-examined. The 7.4-sec lifetime of Au^{197m} is found to be determined by a previously unresolved $E3$ transition of 130.2 kev energy, whose transition probability is 3×10^{-3} that expected on the Weisskopf estimate. The multipolarity of a "prompt" 77.4-kev transition in Au^{197} is found to be $M1+E2$ (the ratio of magnetic to electric transitions being 1.5). A consistent decay scheme is presented. Some systematics of L sub-shell conversion are discussed.

INTRODUCTION

PREVIOUS investigations[1] of the decay of Hg^{197m} have shown that the 23-hr level in Hg decays via a 164-kev $M4$ transition, followed by a 133-kev $E2$. It was also shown that the 23-hr level has a 3 percent K capture branch to a 7.4-sec level in Au^{197}. This level was thought to be depopulated by a 275-kev transition, possibly $M3$, followed by a 191-kev $M1$ and a 77-kev transition of low multipole order. There were 98.8 percent and 1.2 percent K capture branches from the 65-hr ground state of Hg to the 77- and 268-kev levels of Au, respectively.

However, certain discrepancies remained. First of all, the experimental K conversion coefficient (0.5) for the 275-kev transition was not in accord with the theoretical value[2] for an $M3$ (3.0). In addition, with this scheme, the 268-kev level had to have a spin of $5/2-$, thus making the 1.2 percent electron capture branch from the ground state of Hg^{197} inconsistent, since the levels in Hg are believed to be $i_{13/2}$, $f_{5/2}$, and $p_{1/2}$. It had been shown by Huber *et al.*[1] that the 191- and 77-kev transitions were in coincidence. Also, by a coincidence measurement between the supposed 191-K electron line (detected in a lens spectrometer) and the more energetic conversion electrons (those of the 275-kev γ-ray), the value of the supposed K conversion coefficient was determined to be 1.7. One purpose of this paper is to point out that the lifetime-determining transition is not the one of 275 kev, but a hitherto unresolved γ-ray transition of multipole order $E3$, and that in the experiment quoted above, the coincidence measurement was made between the L conversion electrons of the 130.2-kev $E3$ transition and the 275-kev transition conversion lines. The 191-K and 130-L electron lines differ by only 5 kev. In addition, we have determined the multipolarity of the 77-kev transition by a study of the L conversion ratios, and have redetermined the K conversion coefficient of the 275-kev transition. Energies of the electron lines have been measured with high resolution spectrographs with somewhat greater accuracy than before. A consistent decay scheme is presented. Some systematics of L conversion are discussed.

TABLE I. Conversion electron lines observed for γ-ray transitions in $Hg^{197m}-Au^{197m}$.

Transition energy (kev)	Conversion electrons observed
77.4	L_I, L_{II}, L_{III}, M_I, M_{II}, M_{III}, N
130.2	K, L_{II}, L_{III}, M_{II}
134.0	K, L_I, L_{II}, L_{III}, M_{II}, M_{III}, N
165.3	K, L_I, L_{II}, L_{III}, M_I, M_{III}, N
191.6	K, L_I, M
279.3	K, L_I

EXPERIMENTAL PROCEDURE AND RESULTS

The radioactive sources were prepared in the Princeton cyclotron by the $Au^{197}(p,n)Hg^{197}$ reaction. The radioactive Hg was distilled, in vacuum onto thin Au foils of proper dimensions ($\sim$2 cm$\times$0.3 mm), thus forming a source which was almost weightless. The low energy electron lines show some broadening, due probably to the diffusion of Hg into the Au. The electron lines were photographed in permanent magnet 180° spectrographs. Figure 1 is a reproduction of one of the spectrograms. This film had been deliberately overexposed on the lower energy end. Table I lists the conversion lines observed for each transition. Some of the energies differ slightly from the first published ones.

Recent measurements by Cork *et al.*[3] of the transition energies observed in a source of Hg^{197m} yield the following values: 134.3, 165.4, 191.4, and 77.6 kev. The transition energies observed[4] in a source of Pt^{197} (17.4 hr) are 191.2 and 77.4 kev.

All the L components are resolved in the higher intensity transitions, as are some of the M sub-shell

† Work supported by the U. S. Atomic Energy Commission and Higgins Scientific Trust Fund.

* Now at Massachusetts Institute of Technology, Cambridge, Massachusetts.

[1] Huber, Humbel, Schneider, deShalit, and Zunti, Helv. Phys. Acta XXIV, 127 (1951); M. Goldhaber and R. D. Hill, Revs. Modern Phys. 24, 179 (1952).

[2] Rose, Goertzel, Spinrad, Harr, and Strong, Phys. Rev. 83, 79 (1951).

[3] Cork, Martin, LeBlanc, and Branyan, Phys. Rev. 85, 386 (1952).

[4] Cork, LeBlanc, Stumpf, and Nester, Phys. Rev. 86, 415 (1952).

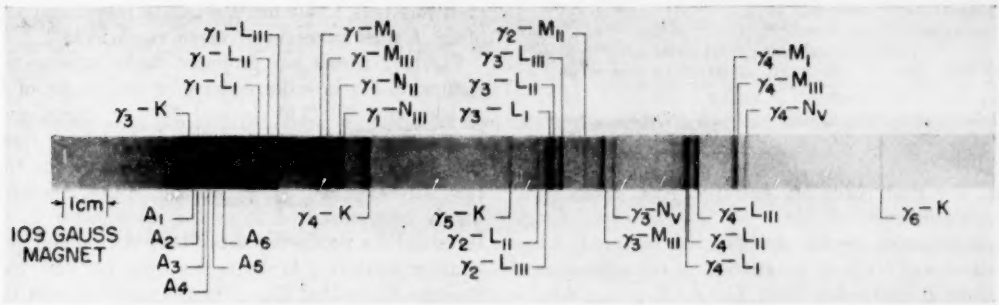

FIG. 1. Conversion electron spectrum of $Hg^{197m}-Au^{197m}$. The transition energies in kev are as follows: $\gamma_1=77.4$ (Au); $\gamma_2=130.2$ (Au); $\gamma_3=134.0$ (Hg); $\gamma_4=165.3$ (Hg); $\gamma_5=191.6$ (Au); $\gamma_6=279.3$ (Au). A_1 to A_6, which are the Auger lines (L_I, $L_I \rightarrow K_I$, ∞ etc.) arising from the internal conversion of K series radiations have been previously reported [J. W. Mihelich, Phys. Rev. **88**, 415 (1952)].

electrons. Of particular interest in this study are the K, L_{II} and L_{III}, and M lines of the 130.2-kev transition, and the three L lines of the 77.4-kev transition. Previous investigations were performed with spectrometers of insufficient resolving power to separate the comparatively weak conversion lines of the 130.2-kev transition from the conversion lines of the 134-kev transition. Evidence presented below indicates that the 130.2-kev transition is of $E3$ multipolarity and determines the lifetime of the 7.4-sec level.

Photometry of the spectrogram showed that the K/L ratio of the 130-kev transition was less than $\frac{1}{3}$ of the K/L ratio for the 134-kev $E2$ transition. The electrons were analyzed in a Siegbahn-type[5] spectrometer at Princeton in order to obtain more accurate intensity data. It was found that the $K:L:M$ ratio was 1:7.5:3.6, in good agreement with the K/L ratio expected for an $E3$ transition.

As mentioned above, in the coincidence experiment of Huber, etc., what was obtained was $\kappa_L^{130}=Ne_L^{130}/(Ne_{total}^{130}+N_\gamma^{130})$ rather than κ_K^{191} as was supposed. Since $\kappa_T^{130}=Ne_{total}/N_T\leqq 0.96$, we find that $\alpha_{total}^{130}\leqq 24$. Using the electron intensity ratios as determined in the counter spectrometer, we find that $\alpha_K^{130}\leqq 2.0$. Extrapolating the values of Rose *et al.*,[2] the theoretical values obtained are: $\beta_K^1=3.4$, $\alpha_K^1=0.14$, $\alpha_K^2=0.5$, and $\alpha_K^3=1.0$. The $L_{II}:L_{III}$ conversion is characteristic of that for electric γ-transitions.[6] The conversion coefficient and K/L ratio make the assignment of $E3$ reasonable.

The following reasoning also makes the assignment of $E3$ reasonable. The 65-hr K capture in Hg^{197} is most probably first forbidden, since it involves the changing of a neutron in one shell into a proton in a neighboring shell. Energy-lifetime considerations then make it likely that the 23-hr K capture transition is also first forbidden. Since the 65-hr and 23-hr levels in Hg^{197} have different parities, the isomeric and ground levels of Au^{197} should have opposite parities. Since the transition following the 7.4-sec isomeric transition in Au is $M1$ ($\Delta I=1$, No), as will be shown later, the isomeric transition must involve a change in parity. The L conversion indicates an electric transition, and only $E3$ is consistent with the 7.4-second half-life.

The $E3$ transition is of considerable interest, since it is the first observed odd-proton $E3$ transition which may occur between single particle levels. Previously observed $E3$'s have occurred between 7/2+ and $p_{1/2}$ levels, the presence of a 7/2+ level indicating a considerable deviation from a single particle model. In the case of Cd^{111}, the $h_{11/2}\rightarrow d_{5/2}$ transition involved an odd neutron.[7,8] This fact was thought to explain the slowness of the transition. In the case of $_{79}Au^{197}$, we should expect an odd proton $h_{11/2}\rightarrow d_{5/2}$ transition. The experimental value of the transition probability is 3×10^{-3} that expected on the Weisskopf estimate.[9] This may be explained by assuming that the "$d_{5/2}$" level is really not a single particle level, but is formed by the coupling of a number of nucleons.

Information was obtained regarding the multipolarity of the 279-kev transition. It is easily seen that

$$\alpha_K(279)=\alpha_L(134)\cdot\frac{N_K(279)}{N_L(134)}\cdot\frac{N_\gamma(134)}{N_\gamma(279)}.$$

$\alpha_L(134)$ and $N_K(279)/N_L(134)$ had previously been determined accurately.[1] Hence a measure of the ratio of the numbers of these two γ-rays will allow a determination of the K conversion coefficient of the 279-kev transition. This ratio was determined with a NaI scintillation spectrometer. The value of $\alpha_K(279)$ is ~ 0.27. The theoretical values are $\beta_K^1=0.5$, $\alpha_K^2=0.08$, and $\alpha_K^3=0.20$.[2] The experimental conversion coeffi-

[5] Thanks are due Dr. E. P. Tomlinson for kindly putting his spectrometer at our disposal.

[6] J. W. Mihelich, Phys. Rev. **87**, 646 (1952).

[7] M. Goldhaber and A. W. Sunyar, Phys. Rev. **83**, 906 (1951).

[8] A. W. Sunyar, Phys. Rev. **83**, 864 (1951); C. L. McGinnis, Phys. Rev. **83**, 651 (1951); and S. Johansson, Phys. Rev. **79**, 896 (1950).

[9] J. M. Blatt and V. Weisskopf, *Theoretical Nuclear Physics* (John Wiley and Sons, Inc., New York, 1952).

TABLE II. Conversion data on 77.4-kev transition in Au^{197}.

Sub-shell	Theoretical internal conversion coefficient $E2$	$M1$	Exp. rel. int.
L_I	~0.15	3.4	1.0
L_{II}	9.5	0.25	0.45
L_{III}	8.5	0.005	0.34

cient, the short lifetime, and the K/L ratio ($\geqq 6$) indicate a magnetic dipole.

Determination of the multipolarity of the 77.4-kev transition was made by an analysis of the intensities of the three L conversion lines. The $L_I:L_{II}:L_{III}$ ratio is 1.0:0.45:0.34. Comparison of these data with the theoretical prediction of Gellman, Griffith, and Stanley[10] will make possible an estimate of the multipolarity. The absence of a measurable lifetime and the L conversion coefficient of 2.5[1] indicates that the multipolarity is $E2$, $M1$, or a mixture of both. In Table II are listed the theoretical values of Gellman *et al.* for the individual L shells. It will be recalled that these calculations are done neglecting screening and are available for only a few values of Z. Considerable uncertainty is introduced by the rather extensive interpolation required. Probably the absolute values are in considerable error, but a comparison of relative values may be fairly good.

One finds that the experimental intensity observed may be explained by a mixture of magnetic γ-rays to electric γ-rays of 7.0, or a ratio of magnetic to electric transitions of 1.5. It may be noted that a comparison of the relative L-shell conversion is a very powerful tool for detecting or measuring proportion of mixtures. In the case of $M1$ and $E2$ mixtures, the $M1$ L_I internal conversion coefficient is ~20 times larger than the value of the L_I internal conversion coefficient for $E2$. On the other hand the L_{II} and L_{III} internal conversion coefficients for $E2$ are many times those for $M1$. Hence a small admixture of either will alter the L conversion to a considerable degree. Accurate determination of such mixtures await more accurate theoretical values of the L shell internal conversion coefficients.

Figure 2 shows our proposed decay scheme. Some comments are in order concerning the choice of level assignments. The 130-kev and 279-kev transitions are in coincidence, as stated above. It had been thought that the 279-kev was followed by the 77.4-kev transition. However, Dr. H. C. Martin of Los Alamos has kindly communicated to us the information that the threshold for producing the 7.4-sec Au isomer by fast neutron scattering in Au is less than 420 kev. Hence, it seems likely that the 279-kev transition goes to the ground state. It is then likely that the upper levels in Au^{197} are $h_{11/2}$, and $d_{5/2}$, as predicted by the shell model. The ground state has been determined as $d_{3/2}$.

In previous experiments,[1] a high coincidence rate between the 279-kev conversion electrons and other conversion electrons was measured. This coincidence was 30 percent greater than would be expected for a simple two step decay (130 and 279 kev). Hence the conclusion was drawn that these two transitions were also in coincidence with the 77.4-kev transition. In the light of the inelastic scattering data, these results have to be reinterpreted. Due to the geometry of the spectrometer, coincidences between the 279-K electron and the 130-L electrons are taken at 180°. It is possible that there is sufficient angular correlation to produce the high coincidence rate at 180°.

The 191-kev γ-ray is probably in a branch separate from the 279-kev γ-ray. The K/L ratio of 6 indicates it is an $M1$. The 191- and 77.4-kev transitions are in coincidence, and the ratio of the intensity of the two transitions is a constant with time, both activities exhibiting the same growth and decay.

No crossover transitions were definitely observed via conversion electrons. One doubtful electron line of 328 kev is present. Such a line could be the K conversion line of a 409-kev $M4$ $h_{11/2} \rightarrow d_{3/2}$ crossover. It is too faint to allow any accurate measurements. An electron line

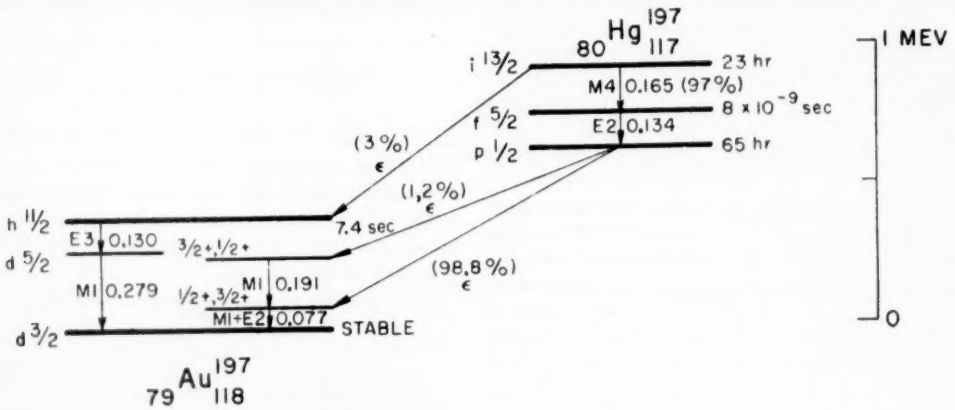

FIG. 2. Proposed decay scheme for $Hg^{197m} - Au^{197m}$.

[10] Gellman, Griffith, and Stanley, Phys. Rev. **85**, 944 (1952).

(intensity roughly that of the 191-M line) of 185.8 kev is observed. It cannot be assigned to any expected transition.

The spins assigned to the 77.4- and 269-kev levels are consistent with the available data. Tentatively, we designate the two levels as $\frac{1}{2}+$ or $\frac{3}{2}+$ and $\frac{3}{2}+$ or $\frac{1}{2}+$, respectively. The $\frac{1}{2}+$ assignment for the spin of the 77.4-kev level is preferred since the 201.9-kev transition from the 279-kev ($d_{5/2}$) level to the 77.4-kev level is not observed.

Some comments may be made regarding the systematics of L shell conversion. This is the first $E3$ isomeric transition for which adequate resolution of the L lines has been obtained. The establishing of the systematics of L conversion for a transition of this multipole order, energy, and Z is invaluable for deciding multipole orders of other transitions. For the $E3$ isomeric transition of 130 kev in Au, the (L_I:L_{II}:L_{III}) ratio is (<0.1:~ 2.5:1). Taking the K-shell internal conversion coefficient as 2.0 and the K/L ratio as 0.133, the empirical values of the absolute L-shell internal conversion coefficients are (L_I: <0.4; L_{II}:10.4; L_{III}:4.2). Rutledge, Cork, and Burson[11] have reported that for certain transitions, designated by them as $E3$, the L conversion is predominantly L_I. These transitions occur in Se($Z=34$). In order to establish that the conversion is in the L_I shell, one has to measure the $K-L$ energy difference well enough to distinguish between $K-L_I=9.99$ kev and $K-L_{II}=10.18$ kev. However, it would not be impossible that for this low Z, $E3$ L conversion occurred in the L_I shell. It has been pointed out[6] that for the $E2$ transition of 247 kev in Cd^{111m}, the L conversion is probably mostly in the L_I shell, as borne out by the calculations of Gellman *et al.*

For the 166-kev $M4$ in Hg, the L ratio is 1: <0.1:1.5. The theoretical estimate of Tralli and Lowen[12] would predict the ratio to be 1: <0.5: ~ 2.2.

The 134-kev $E2$ has an L ratio of 0.04:1.1:1 as compared to the theoretical value (obtained by interpolation of the data of Gellman *et al.*) of 0.1:1.4:1. Owing to the absence of theoretical data and the paucity of experimental data on $E3$ transitions, one cannot yet distinguish between $E2$ and $E3$ transitions on the basis of L ratios alone.

We are indebted to Dr. M. Goldhaber for his continued interest in this problem.

[11] Rutledge, Cork, and Burson, Phys. Rev. **86**, 775 (1952).

[12] N. Tralli and I. S. Lowen, Phys. Rev. **76**, 1541 (1949).

PHYSICAL REVIEW VOLUME 91, NUMBER 1 JULY 1, 1953

Nuclear Magnetic Resonance in Thallium Compounds*

H. S. Gutowsky and B. R. McGarvey†
Noyes Chemical Laboratory, University of Illinois, Urbana, Illinois

(Received March 2, 1953)

A precision, resonance absorption measurement has been made of the ratio of the magnetic moments of Tl^{205} and Tl^{203}. The experimental ratio is $\mu^{205}/\mu^{203}=1.009838\pm0.000001$. This result, when compared with the value observed by Berman for the ratio of hyperfine structure separations in the $^2P_{\frac{1}{2}}$ state, $\Delta\nu^{205}/\Delta\nu^{203}=1.00974\pm0.00003$, establishes the reality of effects attributable to the finite nuclear size.

Shifts of about 0.2 percent have been found in the thallium resonance position in Tl^{+3} compared to Tl^{+1} compounds. The resonance shifts in aqueous solutions varied linearly with the anion concentration. Complex formation and interionic electronic exchange interactions, respectively, account qualitatively for the observed effects.

INTRODUCTION

THESE experiments were initiated to obtain data for comparison with theoretical values for the nuclear magnetic shielding. Thallium is one of the very few elements with two different, simple oxidation states, Tl^{+1} and Tl^{+3}, for which nuclear magnetic resonances might be observed and any differences in position compared with theory.[1,2] However, we have found the nuclear magnetic shielding to depend not only upon the oxidation state of the thallium but also upon the anions present in solution. Moreover, the magnetic shielding changes remarkably in solutions of different concentration. Here, results are given for several compounds and concentrations.

In addition, we have made a precision determination of the ratio of the Tl^{205} and Tl^{203} magnetic moments, because this ratio is important in analyzing hyperfine structure anomalies. Berman[3] reported recently a precise value for the ratio of the hyperfine structure separations of the $^2P_{\frac{1}{2}}$ ground states of Tl^{205} and Tl^{203} by the atomic beam magnetic resonance method. This ratio differs by 9 to 12 parts in 10^5 from values determined for the ratio of the magnetic moments by nuclear magnetic resonance methods.[4–7] But the combined

* Supported in part by the U. S. Office of Naval Research.
† U. S. Atomic Energy Commission Predoctoral Fellow.
[1] W. E. Lamb, Jr., Phys. Rev. **60**, 817 (1941).
[2] W. C. Dickinson, Phys. Rev. **81**, 717 (1951).
[3] A. Berman, Phys. Rev. **86**, 1005 (1952).
[4] W. G. Proctor, Phys. Rev. **75**, 522 (1949).
[5] H. L. Poss, Phys. Rev. **75**, 600 (1949).
[6] R. E. Sheriff and D. Williams, Phys. Rev. **82**, 651 (1951).

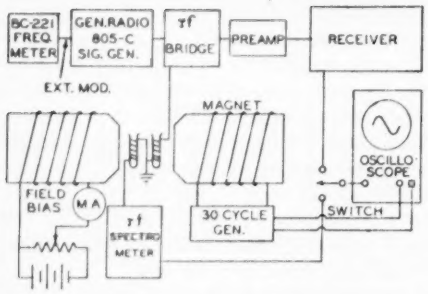

FIG. 1. Block diagram of experimental arrangement used in measuring the magnetic moment ratio.

errors in the ratios was about 8 parts in 10^5, with 5 parts from the nuclear magnetic resonance value, so the reality of the difference was not established with certainty. However, as pointed out by Berman,[3] a difference of about the magnitude observed should arise from the finite size of the nucleus. We undertook a more precise measurement of the magnetic moment ratio in order to obtain a better value for the difference, if any.

EXPERIMENTAL DETAILS

Most of the apparatus and procedures used here have been described.[8,9] A block diagram of the setup for measuring the magnetic moment ratio is given in Fig. 1. It is a double resonance apparatus, one part being a bridge system, the other a spectrometer, with separate coils and samples, and a manual switch for displaying the resonance from either system on a common oscilloscope. The magnetic field of 6365 ± 2 gauss was supplied by a permanent magnet.[8] The rf bridge used is a null-T type.[10] The rf spectrometer is a regenerative oscillator.[9] The two sample coils were mounted side by side, separated by about 5 mm. The coils had a common ground in the support probe on which they were mounted. The samples were contained in thin-walled 10-mm o.d. Pyrex test tubes; care was taken to insure that both samples were identical for a given set of measurements.

The magnetic moment ratio was obtained by measuring directly the frequency difference between the resonance frequencies of the two isotopes in the same field and also measuring the actual resonance frequencies of the two isotopes. The magnetic moment ratio, since both spins are $\frac{1}{2}$, is then given by the equation

$$\mu_{Tl^{205}}/\mu_{Tl^{203}}=\nu_{Tl^{205}}/\nu_{Tl^{203}}=1+\Delta\nu'/\nu_{Tl^{203}},$$

where $\Delta\nu'$ is the *directly measured* difference in the two resonance frequencies. A similar equation is used to compute the ratio from the resonance frequency of Tl^{205}. The increased precision of our measurement of this ratio results largely from the direct measurement of $\Delta\nu'$, which is fairly small, instead of computing the ratio from the two resonance frequencies themselves. The stability and high homogeneity[8] of the field of the permanent magnet were also essential.

$\Delta\nu'$ was measured in the following manner. The General Radio 805C signal generator and rf bridge system were tuned approximately to the resonance of one isotope, and the spectrometer to the other. The rf bridge resonance was centered on the oscilloscope by adjusting the dc field biasing current. The bias field was kept as constant as possible and varied no more than about 0.03 gauss during a series of measurements. The spectrometer resonance was then displayed on the same scope by means of the switching system shown in Fig. 1, and tuned to center. The frequency difference was then the difference between the frequency of the signal generator and the frequency of the spectrometer. The output of a Signal Corps BC-221 frequency meter was connected to the external modulation terminal of the signal generator, producing side bands separated by the frequency of the meter. The frequency meter was adjusted so the first side band of the signal generator zero beated against the frequency of the spectrometer, as indicated by a stationary spectrometer resonance pattern on the scope. Loose coupling of the two systems was provided by the common ground of the two sample coils. The frequency separation, $\Delta\nu'$, was then just the frequency of the frequency meter itself. In a given run ten measurements of $\Delta\nu'$ were made in the manner outlined above; half of the measurements were made with the coil connections interchanged to correct for the very small field difference between the two sample coils. The actual frequency of the signal generator or the spectrometer was measured by loosely coupling the frequency meter with either the rf bridge preamp or the spectrometer and zero beating.

The chemical and concentration shifts in the thallium resonance were measured with a simple rf bridge system similar to that included in Fig. 1. In most cases, including the samples used for the magnetic moment ratio experiment, the resonance line widths were governed by the inhomogeneities in the magnetic field, and the lines could be positioned accurately on the oscilloscope. The shifts were measured by interchanging samples in the rf coil and noting the difference in the field biasing current needed to center the resonance first from one sample and then from the other. This method eliminates the field corrections required in a double probe system, but it has the disadvantage that the signal generator may drift a small amount while samples are interchanged and the bridge rebalanced. The error introduced by frequency drift was minimized by doing the measurements rapidly and by inverting the order of measuring the samples halfway through a

[7] H. E. Walchli, "A Table of Nuclear Moment Data", Preliminary Issue, Oct. 1, 1952, p. 89; we learned of this result after completing our measurements.
[8] H. S. Gutowsky and C. J. Hoffman, J. Chem. Phys. **19**, 1259 (1951).
[9] Gutowsky, Meyer, and McClure, Rev. Sci. Instr. (to be published).
[10] W. N. Tuttle, Proc. Inst. Radio Engrs. **28**, 23 (1940).

series of measurements so a constant drift would tend to cancel out. It is believed that most of the error was in centering the resonance line, especially for the weaker lines, with probable errors of ± 0.02 gauss for most of the measured shifts, and maximum systematic errors in the calibration of the field biasing current of ± 1 percent of the measured shift.[8]

The samples used were either of commercial origin, of cp grade, or were prepared as described in the text.

RESULTS AND DISCUSSION

The Ratio of the Magnetic Moments

This ratio was measured in two different samples. One was a 1.4 molar aqueous solution of thallous acetate and the other a thallic solution prepared by dissolving Tl_2O_3 in *aqua regia*. The magnetic moment ratio was the same in the two oxidation states. The results of the several series of measurements are given in Table I. These measurements give an average of

$$\mu_{Tl^{205}}/\mu_{Tl^{203}} = 1.009838 \pm 0.000001.$$

This value agrees quite well with the earlier less precise values[4-7] which are given also in Table I.

The ratio of the hyperfine structure separations of the $^2P_{\frac{1}{2}}$ ground states of Tl^{205} and Tl^{203} has been reported by Berman[3] as

$$\Delta\nu_{Tl^{205}}/\Delta\nu_{Tl^{203}} = 1.00974 \pm 0.00003.$$

This ratio is smaller than our magnetic moment ratio by an amount

$$\Delta = 9.8 \pm 3 \times 10^{-5}.$$

The uncertainty in this value of Δ is due almost entirely to the uncertainty in the ratio of the hyperfine structure separations, but the errors are small enough certainly to prove the reality of the difference.

In the first-order theory of hyperfine structure, Δ is zero. However, the theory assumes the nucleus to be both a point charge and a point magnetic dipole. These assumptions are valid enough for electrons whose wave functions are negligible in the region of the nucleus; but otherwise, as is true for electrons in the $S_{\frac{1}{2}}$ and $P_{\frac{1}{2}}$ states, some error is introduced. The finite size of a nucleus changes the electrostatic potential within the nucleus from that of a point charge and thus changes the electronic wave function in the immediate vicinity of the nucleus from that in a pure Coulombic field. The resulting change in the hyperfine structure differs for isotopic nuclei because the nuclei differ in size, thereby changing the ratio of the hyperfine splittings. In much the same way the finite distribution of the magnetic moment in a nucleus modifies the electronic wave function in the region of the nucleus from that applying to a point dipole. If the distribution of magnetic moment is different in two isotopic nuclei, their hyperfine splittings are perturbed by different amounts, and the ratio is also changed.

Crawford and Schawlow[11] have considered the effect on the hyperfine structure, of the non-Coulombic potential in the region of the nucleus, while Bohr and Weisskopf[12] have investigated the effect of the finite distribution of the magnetic moment. From these two theories Berman[3] calculated values for Δ of

$$\Delta_1 = 9.3 \times 10^{-5},$$

for a uniform distribution of charge and neglectable nonelectrical forces in the nucleus;

$$\Delta_1 = 10.4 \times 10^{-5},$$

for a surface distribution of charge; and

$$\Delta_2 = 1.4 \times 10^{-5},$$

a *maximum* value for the effect of the finite magnetic moment distribution. These combine to give theoretical values for Δ of 11.8 and 10.7×10^{-5} which are to be compared with the experimental value of $9.8 \pm 3 \times 10^{-5}$. The excellent accord suggests the validity of the theories used in the calculation. But the uncertainties, experimental and in Δ_2, are too great to differentiate between the nuclear models proposed in calculating Δ_1. However, some preference is given to the model in which the nuclear charge is distributed uniformly.

Chemical and Concentration Effects

Our observations of chemical shifts in the thallium resonance were concerned primarily with the concentration dependence in aqueous solutions. Most thallium compounds are sparingly soluble in water, if at all, so the investigation was limited mainly to $TlC_2H_3O_2$, $TlNO_3$, and $Tl(NO_3)_3$. The sample to which the shifts were referred was taken somewhat arbitrarily as a 2.39 molar thallous acetate solution; a saturated solution was not chosen because the solubility was found to be highly temperature dependent. The resonance shifts are reported as $\Delta\sigma$ which is defined by

$$\Delta\sigma = 10^4 \times (H_s - H_r)/H_r,$$

TABLE I. The ratio of the thallium magnetic moments.

Source	Run	Sample	$\mu_{Tl^{205}}/\mu_{Tl^{203}}$		
This research	1	$TlC_2H_3O_2$	1.009	8389	
	2	$TlC_2H_3O_2$	1.009	8380	
	3	Tl_2O_3+*aqua regia*	1.009	8379	
	4	Tl_2O_3+*aqua regia*	1.009	8382	
	5	Tl_2O_3+*aqua regia*	1.009	8363	
	6	Tl_2O_3+*aqua regia*	1.009	8367	
		Average	1.009	838	(1)
Proctor[a]			1.009	7	(2)
Poss[b]			1.009	86	(5)
Sheriff and Williams[c]			1.009	83	(5)
Walchli[d]			1.009	822	(19)

[a] See reference 4.
[b] See reference 5.
[c] See reference 6.
[d] See reference 7.

[11] M. F. Crawford and A. L. Schawlow, Phys. Rev. **76**, 1310 (1949).
[12] A. Bohr and V. F. Weisskopf, Phys. Rev. **77**, 94 (1950).

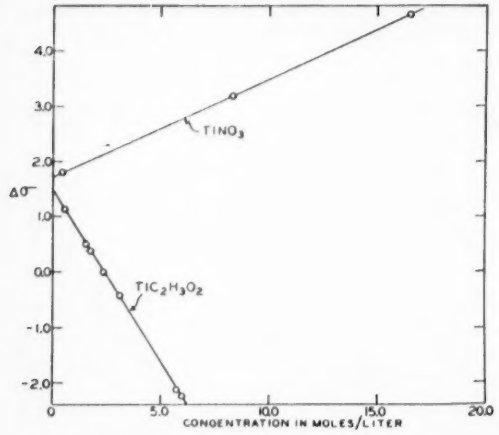

FIG. 2. Chemical shifts in the thallium resonance in aqueous solutions of various composition. The $TlNO_3$ solutions were about 0.5 molar in $TlNO_3$; with nitric acid making up the balance of the nitrate ion concentration, which is plotted. The $TlC_2H_3O_2$ solutions contained no other solute.

where H_s and H_r are the resonance magnetic fields, at a fixed rf frequency, for the unknown sample and the reference, respectively. The reported observations are of Tl^{205} because its absorption is much stronger than that of Tl^{203}. All measurements were made at room temperature which varied between 22° and 28°C.

A set of measurements was made on both isotopes to confirm the isotopic independence of the shifts. The shift was observed between a thallous acetate and a thallic nitrate solution. The shift obtained in a series of five measurements was 8.745 gauss for both Tl^{203} and Tl^{205}. The exact agreement is fortuitous since the probable errors in the measurements for each isotope were ± 0.045 gauss.

$TlC_2H_3O_2$

The chemical shifts found in thallous acetate solutions of various concentrations are given in Fig. 2. The concentrations were determined by a method given in Kolthoff and Sandell.[13] It can be seen that the concentration dependence of the resonance shift is linear over the observed range, from 0.5 to 6.0 molar. The slope of the straight line is -0.62 liter mole^{-1}.

Other observations were made on solutions containing both thallous acetate and sodium acetate. The thallous acetate concentration was kept between 1.8 and 2.0 molar while the concentration of sodium acetate was varied. In Fig. 3 the thallium resonance shifts are plotted against the total concentration of the acetate ion, giving again a linear relation. Moreover, the slope of the line is -0.60 liter mole^{-1} which is the same, within experimental error, as that for the solutions containing only thallous acetate. The sodium resonance was investigated in the mixed solutions, but no measurable shifts in its position were detected.

The shifts, $\Delta\sigma$, were measured for two thallous acetate solutions at a lower field of 4180 gauss, using another permanent magnet.[9] The resonance shifts in gauss, $(H_s - H_r)$, were directly proportional to H_r, that is, $\Delta\sigma$ was independent of the applied magnetic field. This is consistent with the field dependence of the chemical shifts in nuclear magnetic shielding.[14]

$TlNO_3$

Included in Fig. 2 are the resonance shifts observed for thallous nitrate. The lowest concentration, 0.48 molar,[15] was a saturated solution at 27°C. The other two solutions were thallous nitrate dissolved in nitric acid. The resonance shifts are plotted against the total nitrate concentration. The thallous concentration was estimated to be 0.5 molar in the more concentrated nitric acid solution and 0.3 molar in the other.

The shifts appear to depend upon the nitrate concentration and not upon the thallium concentration. Measurements were made at higher temperatures on more concentrated, saturated, aqueous thallous nitrate solutions, and shifts in the same direction and of the same magnitude were found as those of the nitric acid solutions in Fig. 2. These measurements have not been included, however, since the concentrations are uncertain, and the data are only qualitative.

The three points in Fig. 2 lie almost exactly on a straight line, with a slope of 0.18 liter mole^{-1}. It is noteworthy that the thallous acetate and thallous nitrate data extrapolate to almost the same point at zero concentration, but that there is a slight difference which is outside experimental error provided the straight line extrapolation is valid.

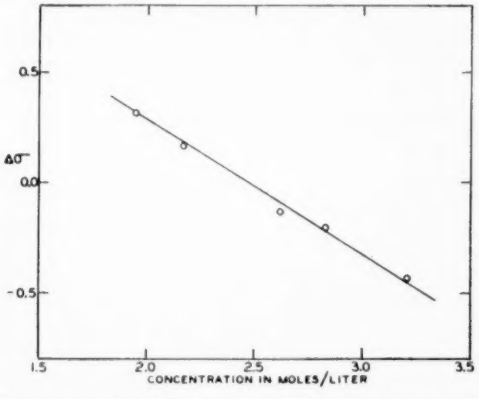

FIG. 3. Chemical shifts in the thallium resonance in mixed $TlC_2H_3O_2$ and $NaC_2H_3O_2$ solutions. The $TlC_2H_3O_2$ concentration was kept constant at about 1.8 molar. The shifts are plotted against the total acetate concentration.

[13] I. M. Kolthoff and E. B. Sandell, *Textbook of Quantitative Inorganic Analysis* (The Macmillan Company, New York, 1949), revised edition, p. 637.

[14] N. F. Ramsey, Phys. Rev. **78**, 699 (1950); **86**, 243 (1952).

[15] This value was interpolated from solubility data given by Lord Berkeley, Trans. Roy. Soc. (London) **A203**, 189 (1904).

$Tl(NO_3)_3$

In water, thallic nitrate hydrolyzes immediately to thallic oxide, but is stable in nitric acid solutions. Consequently, the samples were prepared by dissolving solid thallic nitrate in nitric acid of different concentrations. The quantities were chosen such that the thallic nitrate concentration was about 1.5 molar in the various solutions. The $Tl(NO_3)_3$ was obtained by dissolving Tl_2O_3 in 8*N* nitric acid and evaporating the excess water and nitric acid in a vacuum desiccator. Analysis of the actual samples was difficult so the nitric acid concentration was estimated from the original concentration of the acid and the change in volume when the solid $Tl(NO_3)_3$ was added. Further uncertainty in the nitrate concentrate arises from variations in the amount of solid $Tl(NO_3)_3$ dissolved and in the occlusion of HNO_3 with the solid.

The resonance shift is given in Fig. 4 as a function of the nitric acid concentration. The data appear to give a straight line within the very limited accuracy with which the concentrations are known. The slope of this line is 0.18 liter mole^{-1}, which is the same as the slope of the similar graph for $TlNO_3$.

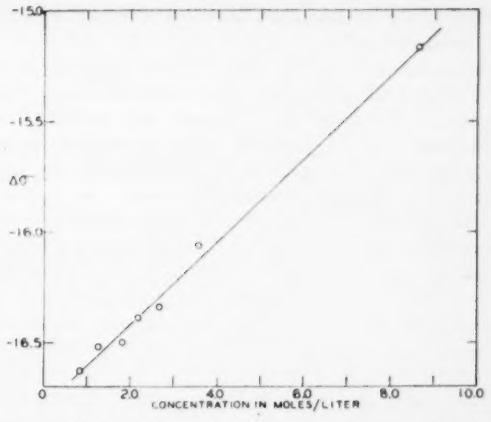

FIG. 4. Chemical shifts in the thallium resonance in mixed $Tl(NO_3)_3$ and HNO_3 solutions. The $Tl(NO_3)_3$ concentration varies about 1.5 molar; the concentrations plotted are approximate values for HNO_3 alone.

Other Thallium Compounds

The thallium resonance in solid $TlC_2H_3O_2$ was observed with a narrow band amplifier. The line was broad, with a separation of 1.5 gauss between the points of inflection. The shift was found to be -2.67.

A dilute solution of $TlCl_3$ was prepared by passing Cl_2 through a suspension of TlCl[16] in water. The resonance shift, $\Delta\sigma$, was measured to be -21.8 in this solution. Measurements on solutions of Tl_2O_3 in various mixtures of HCl and HNO_3 indicated the thallic $\Delta\sigma$ decreases with chloride concentration.

Discussion of the Resonance Shifts

It is a relatively simple matter to compute the nuclear magnetic shielding of the spherically symmetric, free atoms and ions. But the theoretical values[1,2] have not been subjected to experimental verification. It was our original thought that if Tl^{+1} and Tl^{+3} in aqueous solution might be considered as equivalent to the free ions from a nuclear magnetic resonance standpoint, a measurement of their resonance shift could be compared with theory. The experimental shift in the Tl^{+3} with respect to the Tl^{+1} resonance, extrapolated linearly to infinite dilution, is about -19. On the other hand, the resonance shift predicted by Lamb's equation[1] is -0.15. This was computed[17] from the radial charge density of the 6*s* electrons of the thallous ion, determined by Williams[18] using the Hartree self-consistent field method. Since the observed shift is more than a hundred times the theoretical value, it seems clear the ions cannot be considered as monatomic, but that there is a very large chemical effect from hydration of the ions or from complex formation. In fact thallic ion is known to form a large number of complexes, for instance[19,20] $TlCl_2^+$ and $TlCl_4^-$; and a few complexes have been suggested for thallous ion.

The existence of chemical effects is not surprising, therefore, but several of the observed aspects warrant closer scrutiny. The experimental evidence shows the shifts in the thallium resonance to depend only upon the nature and the concentration of the anions in the solutions. Thus, in the mixed solutions containing $TlC_2H_3O_2$ and $NaC_2H_3O_2$ the shifts were the same as in pure $TlC_2H_3O_2$ solutions containing the same amount of acetate, the Na^+ ion in the mixed solutions being without apparent effect. Moreover, the resonance shifts are linear in the anion concentration; and with a given anion, the concentration dependence is the same for *both* Tl^+ and Tl^{+3} in spite of the large shift between the Tl^+ and Tl^{+3} states. At least this is the case for the nitrate solutions within the rather large experimental error.

The position of the proton resonance has been found to be concentration dependent[21] in aqueous solutions of electrolytes which ionize to give hydrogen containing ions, and where rapid chemical exchange averages the chemical shifts over the different hydrogen containing chemical species to give a single narrow resonance. The thallium concentration effects could arise in a similar manner from fast exchange among the thallium ions and one or more complex forms. For $TlC_2H_3O_2$, where the different chemical states of the thallium might be

[16] This method of preparing $TlCl_3$ is similar to that given by A. S. Cushman, Am. Chem. J. **26**, 505 (1901).

[17] We wish to thank Dr. W. C. Dickinson for an earlier estimate of the shift, made from the wave functions for Hg and Hg^{++}, giving the value -0.13.

[18] F. Williams, J. Chem. Phys. **19**, 457 (1951).

[19] G. Harbottle and R. W. Dodson, J. Am. Chem. Soc. **73**, 2442 (1951).

[20] R. Benoit, Soc. Chim. France **5-6**, 518 (1949).

[21] H. S. Gutowsky and A. Saika, J. Chem. Phys. **21** (to be published).

taken as the ion and the undissociated molecule, shifts of the proper order of magnitude can be calculated by taking the shift of the undissociated molecule to be that of the solid $TlC_2H_3O_2$, and using the dissociation constant calculated by Robinson and Davies[22] from conductance data. However, this mechanism cannot give the linear dependence of the shift over the large concentration ranges investigated.

Nonetheless, the existence of the chemical effects demonstrates that the electronic distribution about the thallium nucleus and, consequently, its magnetic shielding, are altered in some manner from the free ion by the anions and water molecules surrounding it. Besides the chemical equilibrium mechanism which appears inadequate, we have considered polarization and electronic exchange effects. The electric fields generated by nearby ions and molecular dipoles strongly polarize the thallium ions. The effect of the polarization on the magnetic shielding of the thallium nucleus was calculated as a second-order perturbation, assuming point charges and dipoles. Although the computed effect on the shielding is large for a given orientation, the net effect is zero when all orientations are equally probable as is the case in the solutions. The only satisfactory model of those we have considered is based on electronic exchange effects, intermediate in nature between the covalent bonding implied in the analysis in terms of chemical equilibria and the purely Coulombic interactions considered in the polarization model.

Ordinarily, in not too concentrated solution, the cation of a strong electrolyte is surrounded by a layer of water molecules of hydration, with the anions remaining outside this layer. However, Fajans[23] has shown by means of refractivity measurements on solutions of strong electrolytes that this shell of water molecules is sometimes penetrated by the anions, and that the amount of penetration increases with concentration. This penetration is essentially a replacement by an anion of one of the water molecules surrounding the cation, forming an "ion pair." This "ion pair" is not quite the same as a "truly undissociated molecule," since the time of association may be less than the time needed by the molecule to execute a single vibration along its bond. Thus, the association can be regarded as little more than a sticky collision. If electronic exchange interactions occur during the association, the diamagnetic shielding of the nuclei would be reduced from the free ion values. This can be seen from Ramsey's[14] theory of nuclear magnetic shielding in molecules; the electronic exchange introduces the second-order paramagnetic term, which is absent for the free ions.

The ideas expressed above lead directly to a qualitative explanation of the experimental results. The shift in the thallium resonance will be proportional to the average number of anions and of water molecules surrounding the thallium ions. The average numbers should be proportional linearly to the total concentration of anions, so the shift should depend linearly on the anion concentration. The direction of the shift depends upon the relative values of the thallium ion-water and of the thallium ion-anion interactions. The direction of the shifts observed for $TlC_2H_3O_2$ correspond to the Tl^+ anion interaction being larger than the Tl^+ H_2O, while the shifts for $TlNO_3$ correspond to the reverse situation. The decreasing order of interaction, acetate, water, and nitrate, is reasonable in terms of the general chemical properties of the species.

The large resonance shift between the thallous and thallic solutions results probably from the formation of a stable coordination complex by Tl^{+3}, such as $Tl(NO_3)^{+2}$ in the nitrate solutions, filling the low-lying $6s$ orbital. Therefore, the concentration dependent shifts in both thallous and thallic solutions involve electronic exchange with the thallium $6p$ orbitals. This could account for about the same concentration dependence being observed in the thallous nitrate and thallic nitrate solutions, providing the reasonable assumption is made that the different manner in which the $6s$ orbital is filled in the two ions does not affect very much the solvent and anion interactions with the $6p$ orbitals.

The question arises as to why effects of the sort reported here have not been observed in other ions. It may be simply that the effects occur, but are too small to be observed in the lighter elements previously investigated. In this connection we should mention that preliminary measurements on cesium chloride solutions have shown some concentration dependence of the Cs^{133} resonance, but the shifts are much smaller than those in thallium. The largeness of the thallium shifts may be attributable partly to the fact that in this case we are not dealing with the rare gas electron configurations possessed by most ions.

Besides their bearing upon the structure of solutions of electrolytes, these results demonstrate it is not always possible to regard ions in solution as equivalent to free ions as far as magnetic resonance is concerned. Therefore, the use of shielding fields calculated for free ions to compute corrected magnetic moments from measurements on ions in solution may not be valid in many cases. In any event, the possibility of concentration dependence should be considered when nuclear magnetic moments are measured using ionic salts in solutions.

The equipment for this work was provided mainly by a grant-in-aid from the Research Corporation. Also, we wish to thank Mr. R. E. McClure for his assistance with some of the preliminary chemical shift measurements and with the comparison of the shifts for Tl^{203} and Tl^{205}.

[22] R. A. Robinson and C. W. Davies, J. Chem. Soc. **1937**, 574 (1937).
[23] K. Fajans, Trans. Faraday Soc. **23**, 357 (1927).

The Calculation of the Half-Widths of One-Body Resonances

JOHN L. JOHNSON AND J. L. MCHALE
Yale University, New Haven, Connecticut*
(Received March 13, 1953)

Half-widths of resonances for protons incident on a number of light nuclei with Z ranging between 4 and 14 are calculated in the one-body approximation. It is found that neglecting the tail of the wave function in the integral representing the probability of the proton being in the incident state can lead to errors of the order of 50 percent. Estimates of level shifts are also made using formulas derived by Breit. These represent approximately the difference between the energy at which the phase shift is 90° and the energies corresponding to maxima of the absolute value of the radial function $\mathfrak{F}$ or else of the absolute value of $\mathfrak{F}/G$, where G is the irregular function. Both $\mathfrak{F}$ and G are normalized to unit amplitude at a large distance.

INTRODUCTION

IN nuclear reaction theories there occurs a quantity usually denoted by Γ which is closely related to the half-value breadth of resonance levels. Differences in formulation and viewpoint lead to different forms of final expressions for the collision cross sections with correspondingly different definitions of the resonance half width Γ. In some discussions[1,2] the quantity Γ is defined in close analogy to the disintegration probability of a nearly stationary state. In other work[3] the connection with the semistable states is given less prominence. In the former type of consideration Γ is essentially proportional to

$$v\Big/\Big[\int|\Psi|^2 d\tau+\text{correction term}\Big],$$

where v is the relative velocity of the particles while the integral is extended over most of the region within which $|\Psi|^2$ is large. A correction term to the integral is introduced in order to reproduce the experimental half-value breadth. If the correction term is to be relatively small, the integration usually has to be extended through appreciable portions of the reaction channels.

In the latter type of development the definition of a level is made in terms of a preassigned nuclear radius and extensions of the region of integration to portions of the outer channels are not natural in these theories, the usual definitions of reduced widths involving integrals confined to the nuclear interior. In the former method the theoretical 2Γ is adjusted to be a first approximation to the experimental half-value resonance breadth. In the latter the adjustment to experiment is carried out by means of "level shift" calculations and changes such as the introduction of Γ' in the work of Thomas.[4]

In the present note the difference caused by including the tail of the wave function through a disintegration channel is partially studied in the special case of the one-body problem. It is realized that by neglecting the many-body character of the process an exaggerated importance may be given to this "tail" effect. On the other hand, the work of Thomas[4] shows that the interaction of an s particle with C^{12} or O^{16} is reasonably well represented by a one-particle model in a limited energy region and the exaggeration involved is therefore not always serious. Admittedly, however, the whole interpretation of C^{13} and N^{13} states still contains some contradictions regarding preference for one- *versus* many-body formulations. Table I contains a comparison of the values of different kinds of Γ computed in different conventions. The first of the three columns starting with the one marked Γ represents a reasonably conscientious approximation to the half-width. The second is calculated by extending the integral to the turning point in the radial motion corresponding to a classical dynamics treatment of the actual problem. The third gives the value computed by terminating the integration at the nuclear radius. The rather large differences between the values in the last two columns show that the level shift and Γ correction terms may be quite serious in the "black box" type of calculation. Special circumstances accounting for relative prominence of the effects in some cases and their relative absence in others will be discussed toward the end of this note. The values in the table have been calculated for hypothetical rather than actual resonances, the well depth and radius having been treated as in the work of Freeman and McHale,[5] who employed the one-body approximation of Ostrofsky, Breit, and Johnson.[6]

It was felt that this procedure provides a better picture of the relationships between quantities as a

* Assisted by the joint program of the U. S. Office of Naval Research and the U. S. Atomic Energy Commission.

[1] G. Breit, Phys. Rev. **40**, 127 (1932); G. Breit and F. L. Yost, Phys. Rev. **48**, 203 (1935); G. Breit and E. P. Wigner, Phys. Rev. **49**, 519 (1936); H. A. Bethe and G. Placzek, Phys. Rev. **51**, 450 (1937); H. A. Bethe, Revs. Modern Phys. **9**, 71 (1937); G. Breit, Phys. Rev. **58**, 1068 (1940); G. Breit, Phys. Rev. **69**, 472 (1946).

[2] G. Breit, Phys. Rev. **58**, 506 (1940).

[3] P. R. Kapur and R. Peierls, Proc. Roy. Soc. (London) **A166**, 277 (1938); E. P. Wigner, Phys. Rev. **70**, 15 (1946); E. P. Wigner, Phys. Rev. **70**, 606 (1946); E. P. Wigner and L. Eisenbud, Phys. Rev. **72**, 29 (1947); T. Teichmann, Phys. Rev. **77**, 506 (1950); J. B. Ehrman, Phys. Rev. **81**, 412 (1951); R. G. Thomas, Phys. Rev. **81**, 148 (1951); **88**, 1109 (1952).

[4] See R. G. Thomas, footnote 3.

[5] B. E. Freeman and J. L. McHale, Phys. Rev. **89**, 223 (1953).

[6] Ostrofsky, Breit, and Johnson, Phys. Rev. **49**, 22 (1936).

function of the atomic number, orbital angular momentum, nuclear radius, and incident energy than could be accomplished by studying experimentally observed reactions, since for the latter the values of the parameters are restricted by practical circumstances. The conventions regarding nuclear radii are explained in the second of the two footnotes to Table I. During the course of the work some improvements in methods of computation have been developed which are also briefly reported on below.

Notation

F_L, $G_L\cdots$ regular and irregular Coulomb functions for angular momentum Lh normalized to be asymptotic to the sine and cosine of the same phase at large r with $F>0$ at small r. When no ambiguity arises the subscript L is omitted in the list of notation and in the text.

r, $v\cdots$ relative distance and velocity.

$k\equiv\mu v/h$.

$F'\equiv dF/d\rho$, $G'\equiv dG/d\rho$, $\rho\equiv kr$.

b, $r_{ctp}=r(ctp)\cdots$ values of r at nuclear boundary and at classical turning point.

$K=$ phase shift.

$\mathfrak{F}=e^{iK}[F\cos K+G\sin K]$ for $r>b$ and the continuation of this function into $r<b$ by means of the differential equation for r times the radial function.

$\Gamma=$ resonance half-width.

$U=$ depth of square well representing one-body potential.

$E_0=$ energy for which $K=90°$.

PROCEDURE AND RESULTS

For one-body resonances which are not too wide one may calculate the half-width[7] by means of the formula[8]

$$E/\Gamma\cong k\int_0^R|\mathfrak{F}|^2dr+[(G^2E/k)(\partial/\partial E)(kG'/G)]_{r=R}, \quad (1)$$

where $R\geq b$ and $E=E_0$. This formula was originally derived from the relation

$$\Gamma\cong-(F^2\delta)/(\partial/\partial E)(1-FG\delta), \quad (2)$$

which was employed by Freeman and McHale.[5] They determined the denominator of Eq. (2) graphically.

A difficulty in the numerical evaluation of the right side of Eq. (1) is the calculation of the derivative $(\partial/\partial E)(kG'/G)$. If kG'/G is obtained from the Coulomb tables,[9] the energy derivative can be obtained by differences with a corresponding loss of accuracy. This can often be improved by performing the calculation at a different radius, using the identity,[10]

$$\left[\frac{G^2E}{k}\frac{\partial}{\partial E}\left(\frac{kG'}{G}\right)\right]_{r=b}-\left[\frac{G^2E}{k}\frac{\partial}{\partial E}\left(\frac{kG'}{G}\right)\right]_{r=R}=k\int_b^R G^2dr. \quad (3)$$

In principle the quantity $[(G^2E/k)(\partial/\partial E)(kG'/G)]_{r=b}$ can be obtained by applying Eq. (3) in the limit $R\to0$.[11] Such a form is awkward for numerical work, especially for $L>0$.

The direct numerical evaluation of $(\partial/\partial E)(kG'/G)$ can be avoided by utilizing the equation[12]

$$(\partial/\partial E)(kG'/G)=(k/\rho)(\rho/FG)^2(\partial/\partial E)(FG/\rho)-(k^2/F^2E)\int_0^R F^2dr, \quad (4)$$

which follows from the Wronskian relation. Equation (4) is often more convenient because $(\partial/\partial E)(FG/\rho)$ is readily obtained by differences of the tabulated function[9] $\Phi\Theta$. Since in many cases F is relatively small the last term in Eq. (4) is often needed only with little relative accuracy and this form appears preferable, therefore, to others involving integrals over G^2, the danger of cancellation of terms of roughly equal absolute values being minimized.

As indicated previously the reactions and parameters L, b, U, and E_0 selected for the calculation of Γ are those used by Freeman and McHale[5] and do not correspond to real resonances. It is assumed in the present work that Γ is sufficiently well given by Eq. (1). Current ways of dealing with reduced widths suggest the desirability of comparison of Γ with an approximation to this quantity in which the last term on the right side of Eq. (1) is omitted and the upper limit of the integral is set at $r=b$. Accordingly, computations were made for the value of

$$\Gamma_b=E/k\int_0^b|\mathfrak{F}|^2dr, \quad E=E_0. \quad (5)$$

Since, on the other hand, the second term on the right side of Eq. (1) is likely to be relatively unimportant if the integration is extended to the classical turning point, an alternative approximation to Γ was also considered in the form

$$\Gamma_{ctp}=E/k\int_0^{r(ctp)}|\mathfrak{F}|^2dr, \quad E=E_0. \quad (6)$$

[7] The expression "half-width" is used here for half of the half-value breadth. The latter is the breadth measured between points of the resonance curve at half of the resonance maximum. The occurrence of the factor $\frac{1}{2}$ in resonance formulas is thus avoided.

[8] The second and third parts of reference 1.

[9] Bloch, Hull, Broyles, Bouricius, Freeman, and Breit, Revs. Modern Phys. **23**, 147 (1951).

[10] This result is implicitly contained in BW, the third reference in footnote 1.

[11] R. G. Thomas (the last reference of footnote 3) obtained a formula for the $L=0$ case which corresponds to the calculation of the limit in Eq. (3), using the connection between the second term on the left of Eq. (3) and the f_0 function in the limit $R\to0$ with $K_0=90°$.

[12] Equations of this type are presented in BW. Compare formula appearing in their reference 17.

TABLE I. One-body half-widths and level shifts in Mev for protons incident on light nuclei.[a]

Isotope	δ[b]	L	U(Mev)	E_0(Mev)	Γ	Γ_{etp}	Γ_b	Π	$-(E'-E_0)$	$-(E''-E_0)$
Be^9	$\mathfrak{B}$	2	19.10	2.34	0.22	0.20	0.44	0.31	0.023	0.0061
B^{11}	$\mathfrak{B}$	2	19.10	0.76	4.9×10^{-3}	4.9×10^{-3}	8.7×10^{-3}	7.1×10^{-3}	3.7×10^{-5}	3.1×10^{-6}
C^{12}	$\mathfrak{A}$	2	28.63	2.54	0.11	0.11	0.22	0.17	0.0058	0.0011
N^{14}	$\mathfrak{A}$	2	28.63	0.63	3.3×10^{-4}	3.4×10^{-4}	5.3×10^{-4}	4.6×10^{-4}	2.0×10^{-7}	9.0×10^{-9}
F^{19}	$\mathfrak{B}$	3	19.10	2.57	0.034	0.033	0.054	0.041	0.00076	0.00014
Ne^{20}	$\mathfrak{B}$	0	0	2.10	1.0	0.69	0.93	1.1	0.52	0.33
Na^{23}	$\mathfrak{B}$	3	19.10	0.81	3.1×10^{-5}	3.0×10^{-5}	4.3×10^{-5}	3.9×10^{-5}	2.2×10^{-9}	1.2×10^{-10}
Mg^{24}	$\mathfrak{B}$	0	0	2.02	0.44	0.36	0.54	0.66	0.13	0.089
Al^{27}	$\mathfrak{A}$	3	28.63	1.83	0.81×10^{-3}	0.81×10^{-3}	1.2×10^{-3}	1.0×10^{-3}	6.6×10^{-7}	5.8×10^{-8}
	$\mathfrak{B}$	1	19.10	1.93	0.15	0.14	0.25	0.24	0.017	0.0084
	$\mathfrak{B}$	0	0	1.97	0.29	0.24	0.35	0.52	0.065	0.046
Si^{28}	$\mathfrak{A}$	3	28.63	1.40	1.0×10^{-4}	0.99×10^{-4}	1.4×10^{-4}	1.3×10^{-4}	1.4×10^{-8}	9.1×10^{-10}
	$\mathfrak{B}$	1	19.10	1.66	0.062	0.059	0.11	0.10	0.0032	0.0013
	$\mathfrak{B}$	0	0	2.03	0.26	0.21	0.33	0.45	0.052	0.035

[a] The reactions considered and the choice of parameters b, L, U, E_0 are the same as those in Table III of the reference in footnote 5.
[b] $\mathfrak{A}=1.6\times10^{-13}(A+1)^{\frac{1}{3}}$ cm; $\mathfrak{B}=2.1\times10^{-13}(A+1)^{\frac{1}{3}}$ cm. A is the mass number of the target nucleus.

In Table I comparisons are made of the half-width Γ with the approximations Γ_b and Γ_{etp} as defined by Eqs. (5) and (6). The results indicate that Γ_{etp} is a much better approximation than Γ_b in all cases except Ne^{20} for which the resonance is so broad that Eq. (1) should not be expected to hold. For the sharp resonances occurring for small E_0 and large L in the N^{14}, F^{19}, Na^{23}, Al^{27}, and Si^{28} cases, the agreement between Γ and Γ_{etp} is particularly good, and the disparity between Γ and Γ_b is a minimum. In such cases the effect of the tail of the wave function on the half-width is adequately accounted for by evaluating the approximation Γ_R at a point slightly beyond the thin shell where G^2 is rapidly decreasing. For low flat barriers Γ_{etp} remains a better approximation than Γ_b but the correction term to the integral is of increased importance. In the Be^9 case for example the difference between Γ and Γ_{etp} is 8.5 percent, while Γ and Γ_b differ by almost a factor of 2. Similar results are obtained for C^{12}, and to a lesser extent for Mg^{24}, as well as the Al^{27} and Si^{28} reactions with $L\leq1$. The quantity[13]

$$\Pi=(2E/\rho^2)(\rho/G^2) \tag{7}$$

is also tabulated since it might be expected that $\Gamma\propto\rho/G^2$ for sharp resonances, the proportionality constant being a function of parameters like L or Z. This is in fact approximately the case. Thus, Γ/Π is roughly 0.8 for $L=3$, 0.7 for $L=2$, and 0.6 for $L=1$.

It is well known that $|\mathfrak{F}|^2$ is not a maximum when the phase shift is 90°. Breit[14] obtained the approximate formula,

$$E'-E_0\cong-\Gamma(F/G)+\Gamma^2(\partial/\partial E)\ln G, \tag{8}$$

for the energy shift of the minimum of $1/|\mathfrak{F}|^2$, and a corresponding relation

$$E''-E_0\cong-\Gamma(F/G) \tag{9}$$

for the minimum of $|G/\mathfrak{F}|^2$. For sharp resonances this is only a small fraction of Γ, the ratio $|(E'-E_0)|/\Gamma$ being about 10^{-4} when Γ is less than one kev and varying from 0.05 to about 0.1 when Γ is in the approximate range 50–200 kev. In Ne^{20}, where $\Gamma\sim1$ Mev, the ratio is about 0.5. Since the ratio $(E'-E_0)/(E''-E_0)$ contains the factor G/F, it is large (about 20) for narrow resonances and varies roughly from 1.5 to 5 for broad resonances.

It is thus seen that in a number of circumstances Eq. (1) and the approximation Γ_{etp} are suitable for the calculation of resonance widths, the level shifts being relatively insignificant. The approximation Γ_b is seen to be far from safe, however, an error of 30 to 50 percent being reasonably representative. In some cases the error is much larger. It is expected nevertheless that for reactions of a typically many-body interaction type the errors will be less significant, the $\int|\Psi|^2d\tau$ owing its origin only in part to the radial integrals considered here.

We are greatly indebted to Professor G. Breit for initiating and guiding the course of this work and for several valuable suggestions in the preparation of this note. In particular we wish to thank him for pointing out the utility of transformations such as Eq. (4). We also wish to thank Miss Cecilie Smolen for assistance with the numerical work.

[13] This particular approximation is obtained from Eq. (1) by neglect of the correction term and the quantity $-\mathfrak{F}_{L-1}\mathfrak{F}_{L+1}/G_L^2$ which arises from the internal integration.
[14] Equations (5.8) and (5.9) of reference 2.

The Interaction of 14-Mev Neutrons with Protons and Deuterons*

J. C. Allred, A. H. Armstrong,† and L. Rosen
University of California, Los Alamos Scientific Laboratory, Los Alamos, New Mexico
(Received January 12, 1953)

Nuclear emulsions in conjunction with a neutron collimator have been used to measure the differential cross section as a function of angle for the elastic scattering of monoenergetic 14-Mev neutrons by protons and by deuterons. Measurements were carried out in the angular regions corresponding to neutrons being scattered at angles between 48° and 154.5° in the center-of-mass system by protons and between 46° and 176° in the same coordinate system by deuterons. The *n-p* scattering data are consistent with isotropic scattering in the center-of-mass system, and are in excellent agreement with the data of Barschall and Taschek. The *n-d* elastic scattering data are strongly anisotropic. The shape of the angular distribution of the neutrons elastically scattered by deuterons may be inferred from the differential cross sections in millibarns for the following laboratory angles: 2°, 435±28; 10°, 342±27; 20°, 78±9.3; 30°, 38±4.2; 40°, 59 ±5.2; 50°, 104±9.0; 60°, 136±12; 65°, 142±14. Strong evidence for the reaction $D(n, 2n)H^1$ has been found and an attempt to determine the energy and angular distribution of the disintegration protons was moderately successful.

I. INTRODUCTION

THE extensive theoretical calculations which have already been carried out on the scattering of fast neutrons by protons and deuterons are a good indication of the importance attached to these two reactions in the eventual understanding of the nature of nuclear forces.

Most theories[1] dealing with the interaction between neutrons and protons predict spherically symmetric scattering below 10-Mev neutron energy and this is indeed well borne out by all recent experiments.[2] For energies above 10 Mev, however, appreciable deviations from symmetry are predicted, depending upon the nature of the forces assumed for the neutron-proton interaction. Although angular distribution measurements[3] at incident neutron energies between 10 and 15 Mev have not all been in good agreement, the most recent such measurements are consistent with spherical symmetry to within approximately 5 percent. In the study of *n-p* scattering there is some advantage to be gained in not using neutron energies much in excess of 14 Mev, since for high neutron energies the analysis is complicated by the presence of nonzero angular momentum states as well as relativistic effects.

Calculations by Buckingham and Massey[4] on the neutron-deuteron collision up to 11.5-Mev neutron energy have recently been extended by Buckingham, Hubbard, and Massey[5] to include neutron energies up to 16 Mev. Here, also, the theoretical predictions concerning the angular distribution of the neutrons elastically scattered by deuterons show a marked dependence on the type of nuclear force assumed. From a comparison of their theoretical results with available experimental data, these authors conclude that the experimental evidence is consistent with the equivalence of *n-n* and *p-p* forces at the energies involved and that the symmetrical exchange type forces are favored over ordinary forces. Gordon and Barfield[6] arrived at somewhat the same conclusions from their phase shift analysis of low energy *n-d* scattering data in which they showed that *d*-waves are significant at 4.5 and 5.5 Mev.

Latter and Latter[7] made phase shift analyses of both *p-d* and *n-d* elastic scattering data for incident neutron and proton energies below 5.5 Mev. From a comparison of Wantuch's[8] *n-d* angular distributions at 4.5 and 5.5 Mev with the *p-d* angular distributions of Rosen and Allred[9] at 10.4-Mev incident deuteron energy, they conclude that these experimental data are consistent with the principle of charge independence of nuclear forces. This conclusion agrees with that previously arrived at by Breit[10] from a consideration of the same data.

The *n-d* problem is complicated by two features which do not arise in the *n-p* interaction below 14 Mev. In the first place, the angular distribution in the center-of-mass system is strongly anisotropic. Therefore, unless measurements can be made over the entire angular region (0° to 180° in the center-of-mass system), which has so far not been done, it is quite

* Work performed under the auspices of the U. S. Atomic Energy Commission.
† Now at Wellesley College, Wellesley, Massachusetts.
[1] W. Pauli, *Meson Theory of Nuclear Forces* (Interscience Publishers, Inc., New York, 1946), p. 55.
[2] L. Rosenfeld, *Nuclear Forces* (Interscience Publishers, Inc., New York, 1948) Vol. 1, p. 123.
[3] Amaldi, Bocciarelli, Ferretti, and Trabacchi, Naturwiss. **30**, 582 (1942); F. C. Champion and C. F. Powell, Proc. Roy. Soc. (London) **A183**, 64 (1944); C. F. Powell and G. P. S. Occhialini, *Fundamental Particles* (The Physical Society, London, 1947), p. 150. G. Wentzel, Revs. Modern Phys. **19**, 10 (1947), footnote 38; J. S. Laughlin and P. G. Kruger, Phys. Rev. **73**, 197 (1948); H. H. Barschall and R. F. Taschek, Phys. Rev. **75**, 1819 (1949); W. G. Cross, Phys. Rev. **87**, 223 (1952).
[4] R. A. Buckingham and H. S. W. Massey, Proc. Roy. Soc. (London) **A179**, 123 (1941); H. S. W. Massey and R. A. Buckingham, Phys. Rev. **71**, 558 (1947).
[5] Buckingham, Hubbard, and Massey, Proc. Roy. Soc. (London) **A211**, 183 (1952).
[6] M. M. Gordon and W. D. Barfield, Phys. Rev. **86**, 679 (1952).
[7] A. L. Latter and R. Latter, Phys. Rev. **86**, 727 (1952).
[8] E. Wantuch, Phys. Rev. **79**, 729 (1950).
[9] L. Rosen and J. C. Allred, Phys. Rev. **82**, 777 (1951).
[10] G. Breit, Phys. Rev. **80**, 1110 (1950).

essential that absolute differential cross sections be measured with high precision. In the second place it is energetically possible for the deuteron to disintegrate upon impact with a neutron having an incident energy above 3.3 Mev. To determine the energy and angular distribution of the emitted protons and the total cross section for deuteron breakup is in itself an interesting and challenging problem which has thus far not been resolved for the energy region under consideration. Furthermore, in order to evaluate the absolute, or even the relative, differential cross section for elastic scattering, it is quite essential that account be taken of the inelastic cross section. This problem is especially troublesome in the angular region where the elastic scattering cross section goes through a minimum.

Angular distribution data for *n-d* elastic scattering have been published for various energies from 1.5 Mev to 14 Mev.[8,11] Most of these data fall into a fairly consistent pattern. However, where two or more investigators have reported detailed results for the same neutron energy, the quantitative agreement is often somewhat less than adequate from the standpoint of theoretical interpretation.[5] This situation may be expected to change with the increasing availability of more intense and more nearly monoenergetic neutron sources.

A universal difficulty in almost all neutron experiments involving the measurement of differential cross sections is the lack of adequate neutron intensity. This limitation follows from the fact that the neutrons must themselves be produced in a nuclear reaction. It is therefore usually the case that one must either sacrifice angular resolution to permit the detector to subtend a relatively large solid angle or "make do" with relatively few angles and poor statistical accuracy. In order partially to circumvent these difficulties we have used nuclear plates in a manner which has the following advantages.

(a) Data in the laboratory angular region 10° to 170° are taken simultaneously during a given run. The relative accuracy of the differential cross sections is thus improved, since inaccuracies involved in the absolute measurement of the neutron flux enter alike for each angle.

(b) Nuclear emulsions enable one to establish the directions in space for the particles recorded and one can divide the plates into small areas whose relation in space to the target is accurately known. It is therefore possible to arrange the detectors so that they subtend rather large angles at the target without undue loss of angular or energy resolution.

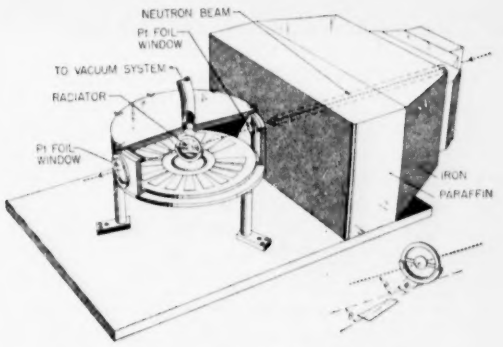

FIG. 1. Perspective drawing of neutron collimator and multiplate camera.

(c) The solid angles subtended at the target by the detector areas analyzed were determined from the orientation of the plates with respect to the target. Determination of these angles was made possible by accurate positioning of the plates and there was no need for defining slits. Thus possible difficulties due to slit edge penetration and scattering were eliminated.

II. EXPERIMENTAL METHOD

The experimental arrangement is shown in Fig. 1. The source of neutrons for this experiment was the $T(d, n)He^4$ reaction. The accelerator used was the Los Alamos Cockcroft-Walton set from which the molecular beam of 250-kev deuterons is magnetically analyzed, collimated through a $\frac{1}{4}$-in. diaphragm and intercepted by a thick zirconium-tritium target. The plane of the target makes an angle of 45° with the deuteron beam direction. The tritium is absorbed in a zirconium film which is deposited on a thin tungsten disk.[12] The axis of the neutron collimator (Fig. 1) formed an angle of very nearly 90° with the deuteron beam, the mean neutron energy in this direction being 14.1±0.1 Mev. The intersection of the Zr-T target area with the deuteron beam formed an ellipse of which the largest projected dimension along the collimator axis was $\frac{3}{8}$ in. The neutrons were monitored by counting a known fraction of the alphas from the above reaction by means of a proportional counter mounted 22 in. from the target in a geometry permitting a view of the entire target area.[13]

The neutron collimator has two components. The 18-in. section nearest the source is made of iron and has a $\frac{3}{4}$-in. diameter circular channel along its axis.

[11] Kruger, Shoupp, and Stallman, Phys. Rev. **52**, 678 (1937); H. H. Barschall and M. H. Kanner, Phys. Rev. **58**, 590 (1940); Coon, Davis, and Barschall, Phys. Rev. **70**, 104 (1946); J. H. Coon and H. H. Barschall, Phys. Rev. **70**, 592 (1946); J. F. Darby and J. B. Swan, Nature **161**, 22 (1948); J. H. Coon and R. F. Taschek, Phys. Rev. **76**, 710 (1949); Hamouda, Halter, and Scherrer, Helv. Phys. Acta **24**, 217 (1951); Martin, Burhop, Alcock, and Boyd, Proc. Phys. Soc. (London) **A63**, 884 (1950); Griffith, Remley, and Kruger, Phys. Rev. **79**, 443 (1950); J. Sanada and S. Yamabe, Phys. Rev. **80**, 750 (1950); W. F. Capelhorn and G. P. Rundle, Proc. Phys. Soc. (London) **A64**, 546 (1951).

[12] Graves, Rodriguez, Goldblatt, and Meyer, Rev. Sci. Instr. **20**, 579 (1949).

[13] We are indebted to J. H. Coon for making available to us the Cockcroft-Walton source and the auxiliary equipment required to produce and monitor precisely the neutrons used in these experiments, and for his generous assistance.

TABLE I. Compilation of target composition and target thickness used and of time integrated neutron flux incident on each target.

A. Single plate camera

Run number	Target	Surface density of target (mg/cm²)	Neutron flux (neutrons/cm²)
ND-1	deutero-paraffin	10.9	5.1×10^{9}
NP-1	ordinary paraffin	10.4	5.0×10^{9}
ND-2	deutero-paraffin	9.8	5.0×10^{9}
NP-2	ordinary paraffin	6.04	5.0×10^{9}
ND-3	deutero-paraffin	3.20	5.0×10^{9}
ND-9	deutero-polyethylene	5.64	4.3×10^{9}
ND-10	deutero-polyethylene	7.8	2.0×10^{9}
NP-10	polyethylene	7.8	3.8×10^{9}

B. Multiplate camera

Run number	Surface density of front target (mg/cm²)	Surface density of back target (mg/cm²)	Neutron flux (neutrons/cm²)
ND-4	4.73 deutero-paraffin	3.14 ordinary paraffin	2.62×10^{9}
ND-5	4.74 ordinary paraffin	2.53 deutero-paraffin	2.62×10^{9}
ND-6	2.53 deutero-paraffin	4.73 deutero-paraffin	4.35×10^{9}
ND-7	4.73 deutero-paraffin	3.14 ordinary paraffin	2.62×10^{9}
ND-8	blank backing	3.16 ordinary paraffin	1.75×10^{9}

Externally this part of the collimator has the approximate shape of a pyramid with apex nearest the neutron source. Such a design combines a minimum amount of scattering material (and weight) with a maximum thickness of iron between the detectors and source. Iron was chosen for the basic shielding material since it has a relatively large cross section for inelastic scattering and since the neutrons which are inelastically scattered are greatly degraded in energy.[14] Immediately adjacent to the base of the pyramidal iron section of the collimator is mounted a 6-in. slab of paraffin. A $1\frac{1}{4}$-in. diameter hole through the paraffin slab is coaxial with the hole through the iron. The primary purpose of the paraffin is further to degrade those neutrons which result from inelastic processes in the iron.

After proceeding down the collimator channel, the neutrons pass into the nuclear plate camera through a 0.003-in. platinum window, thence into the targets at the center of the camera and then out of the camera by way of a second 0.003-in. platinum window. The targets at the center of the camera face in opposite directions, thus permitting simultaneous recording of data from 10° to 170° in the laboratory system. The plane of each target makes an angle of 45° with the axis of the collimator.

Both the deuterium- and hydrogen-containing targets were made by evaporation of paraffin onto 0.007-inch platinum backings.[15] In order to make targets which would be stable in a vacuum, it was found necessary to fractionate the heavy paraffin at 240°C and 0.02 mm Hg, and then to use the higher melting point fraction for the evaporations. The evaporation of the heavy fraction of the deutero-paraffin was carried out at 310°C in a good vacuum ($<10^{-4}$ mm Hg before evaporation started). The procedure was to place an appropriate amount of the deutero-paraffin in the bottom of a glass tube $\frac{1}{2}$ in. in diameter and 5 in. long, above which was mounted the platinum backing with all portions except the center $\frac{1}{2}$ in. masked off. The tube containing the deutero-paraffin was then immersed in an oil bath at 310°C and left there until refluxing action ceased. The weight of deutero-paraffin originally placed in the system to give the desired foil thickness was determined to a first approximation by experiments with ordinary paraffin and then determined empirically by trials with deutero-paraffin. The above simple procedure permitted almost complete recovery of that portion of the deutero-paraffin which was not deposited on the target. Also, the initial amount of heavy paraffin required to make the targets was less than 0.5 g.

The target weights were determined with an accuracy of approximately 1 percent on a Mettler Gram-atic balance. After the experiment the targets were reweighed and there was good agreement with the previous weighings. Table I gives the surface densities of the targets used for each run as well as the time-integrated neutron flux incident on the targets. The target facing in the direction of the neutron beam will be designated the front target while that facing in the opposite direction will be designated the back target.

The hydrogen content of the light (ordinary) paraffin and the deuterium content of the heavy paraffin were determined by chemical analyses.[16] The procedure was to oxidize a given weight of paraffin to carbon dioxide and water and then to determine the weights of these combustion products.

The hydrogen content of the light paraffin was determined to be 14.98 ± 0.02 percent by weight. This corresponds to an average chemical formula which is very close to $C_{22}H_{46}$. Comparison of the combined weights of the C and H^1, as determined from the weights of CO_2 and H_2O, with the original weight of the paraffin indicated a completely negligible amount of high atomic weight impurity.

The analysis of the deutero-paraffin presented some complications due to the presence of an appreciable amount of H^1. The oxidation of this wax thus yields CO_2, D_2O, and H_2O. In order to determine the deuterium content by the above chemical procedure, it is first necessary to determine the H^1 content. This information is, however, immediately available from the range analyses which were carried out at each angle at which cross-section measurements were made. Each of these range analyses contains a group of tracks corresponding in range to protons knocked on by the incident neutrons. From the number of such protons, the n-p cross section and the weight of the target, the H^1 contamination in the heavy wax was determined to be 0.5 to 0.7 percent by weight. By utilizing this

[14] E. R. Graves and L. Rosen, Phys. Rev. **89**, 343 (1953).

[15] The deutero-paraffin was made for us during the war by Texaco. This sample of wax had been prepared by the reduction of carbon monoxide using the Fischer-Tropsch process.

[16] These analyses were carried out for us by A. R. Ronzio of this laboratory.

result along with the results of the chemical analysis one immediately obtains the respective weights of D_2O and H_2O from the oxidation of a given weight of heavy wax, and hence the deuterium content which, for the deutero-wax used, turned out to be 24.8 ± 0.4 percent by weight. From the sum of the weights of CO_2, D_2O, and H_2O and the uncertainties in their values it is again possible to place an upper limit on heavy impurities. If, for example, one assumes a contaminant with atomic weight 16, it is deduced that there must certainly be less than 0.3 atomic percent of such an impurity. If the impurity is heavier the above upper limit is correspondingly less.

The nuclear plates (Ilford *C-2*) were placed around the periphery of the camera in a plane perpendicular to the plane of the targets, so that the longitudinal axes of the plates lay on radii passing through the vertical axis of the target support. The long range of the recoil particles and the large angle these particles made with the emulsion surfaces made it desirable to use 400μ emulsions in the forward 50°; 200μ emulsions proved adequate elsewhere.

The procedure for making a run, after loading the camera, was to evacuate the camera for a period of 1 hour before starting up the Cockcroft-Walton. The vacuum system contained a liquid air trap for the purpose of desiccating the emulsion. Pumping on the camera was maintained for the duration of the run, which usually lasted about 14 hours. When the run was completed, the plates were transferred to a light-tight box for transportation to the darkroom. The loading and unloading of the camera was accomplished under a light-tight tent equipped with a Wratten No. 2 safelight.

All plates were processed by a combination of the temperature development method[17] and the two solution technique.[18] For the 400μ plates the only significant departure from the procedure described by Stiller *et al.*[17] was substitution of two solutions for the amidol developer. For the 200μ plates only the soak and developer solutions were at low temperature. In this modified procedure, the 200μ plates are first soaked in distilled water for 1 hour at 5°C. They are then placed consecutively in solution *A* for 50 minutes and in solution *B* for 50 minutes, both solutions being maintained at 5°C. The formulas for solution *A* and *B* are given in reference 18.

Upon removal from solution *B* the plates are placed, emulsion side up, on toweling at a room temperature of 22°C, and permitted to remain so for 20 minutes. The plates are now placed consecutively in a stop bath of 2 percent acetic acid for 20 minutes, neutral hypo for approximately 5 hours (the hypo being changed every hour), acid hypo for $\frac{1}{2}$ hour and, finally, into wash water for 2 hours. The acetic acid, hypo, and wash water are all maintained at approximately 22°C. The surface silver is rubbed off with chamois or a finger when the plates are removed from the stop bath. The plates are placed, still in Lucite holders which keep them horizontal with emulsion side up, in a room at 22°C and permitted to dry.

The plates were scanned under magnifications from 450 to 900 diameters, using apochromatic oil immersion objectives and compensating eyepieces. Tracks of length less than 100μ were measured with a calibrated eyepiece graticule, whereas tracks of length greater than 100μ were measured by means of a micrometer screw and graduated drum assembly built by Erb and Gray of Los Angeles. The device makes possible the precise and rapid measurement of long tracks. (A 1000μ projection can be measured to an accuracy of ± 3 microns.) The orientation of a given track was determined from its dip into the emulsion and its displacement in the horizontal plane. The latter measurement was made with the eyepiece graticule while the former was made with the fine focus screw. The dip was corrected for shrinkage of the emulsion. Each plate was divided into nine areas, each 1 cm long and 2 to 4 mm wide. Two to eight such areas of 20 to 40 mm^2 were scanned on each plate. The size and position of the plate area analyzed determine the solid angle subtended at the target, while the position of this area and the position of the plate in the camera determine the angle of observation in the laboratory system with respect to the direction of the neutron beam. (The angular resolution varied from 10° at 45° to 5° at 20°.) Tracks whose directions were inconsistent with the radiator-detector geometry were considered to be spurious. Such tracks were due to a variety of factors such as protons from the nuclear emulsion being knocked on by background neutrons, (n, p) reactions in the 0.010-in. gold lining of the camera, (n, p) reactions in the residual gas and water vapor in the camera, and, at small angles, protons produced by neutron interactions outside the camera with sufficient energy and in the proper direction to enter the camera via the window facing the collimator. Such elimination from consideration of tracks on the basis of direction was further justified by background runs made with a blank target. Since the solid angle of acceptance of tracks was only about 10^{-3} of the total solid angle, this criterion for excluding spurious tracks was of considerable help in coping with the background tracks which are, to a greater or lesser extent, always present in neutron experiments.

The problem of determining the differential cross sections for the *n-d* and *n-p* elastic scattering involved the extraction of the peaks of *n-d* and *n-p* recoils due to 14.1-Mev neutrons from the measured range distributions. The above procedure for eliminating most of the background plus the use of nearly monoenergetic

[17] Dilworth, Occhialini, and Vermaesen, Bull. centre phys. nucléaire univ. libre Bruxelles, Belgium No. 13a (Februrary, 1950); Bonetti, Dilworth, and Occhialini, Bull. centre phys. nucléaire univ. libre Bruxelles, Belgium No. 13b (March, 1951); Stiller, Shapiro, and O'Dell, Phys. Rev. **85**, 712 (1951).

[18] M. Blau and J. A. De Felice, Phys. Rev. **74**, 1198 (1948).

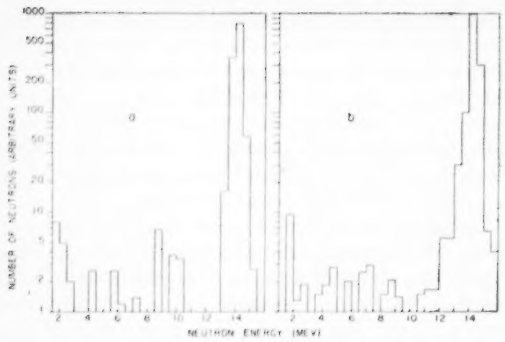

FIG. 2. Neutron spectrum incident on target.

neutrons made this determination quite straightforward and precise.

One objective of these experiments was to determine the cross section for the reaction $D(n, 2n)H^1$. It was therefore necessary to have precise information on the energy distribution of the neutrons striking the deuterium target, since degraded neutrons can produce knock-on deuterons which, at any given angle, will have a range less than that of the deuterons elastically scattered by 14-Mev neutrons and may therefore be confusable with protons from deuteron breakup. After a small background correction has been made on the basis of the blank target run, the energy spectrum of the neutrons incident on the target is determined from the *n-p* scattering experiment by the following procedure.

The distribution in range of the recoil protons, at any given angle, is converted to a proton energy distribution by using the appropriate range-energy curves; the proton energy distribution is in turn converted into a neutron energy distribution by the relation $E_p = E_n \cos^2\psi$, where E_p = observed proton energy, E_n = inferred neutron energy, and ψ is the average angle between the directions of the incident neutron beam and the recoil proton. Finally the relative number of neutrons in each energy interval is divided by the neutron-proton scattering cross section for the mean energy of that interval. The resultant histogram represents the neutron spectrum incident on the target. Two examples are shown in Figs. 2a and 2b. Figure 2a is based on data taken at 13° with respect to the neutron beam direction; Fig. 2b is based on the combined data taken at 15 angles from 15° to 40°. The large apparent spread in energy of the main neutron group in Fig. 2b is the result of a decrease in measuring resolution on account of the following two factors: One, at large angles the stopping power of the target is no longer small compared to the range of the scattered protons; Two, for large values of ψ, relatively small variations in ψ (induced by the angular resolution) are reflected as large variations in $\cos^2\psi$, the factor which determines the neutron energy corresponding to a given proton energy. The blank target background correction is less than 2 percent of the proton group which corresponds to the main neutron group in each figure.

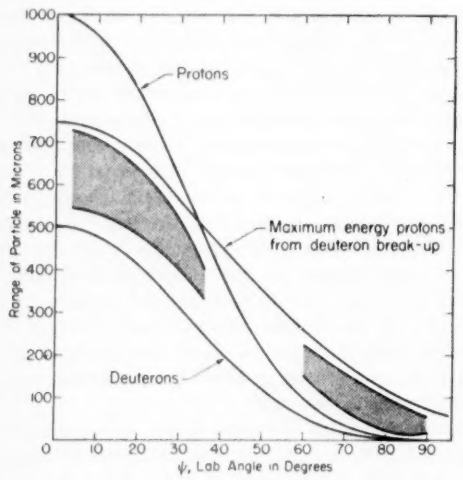

FIG. 3. Range *versus* angle for charged particles arising from the interaction of 14.1-Mev neutrons with deuterons. The shaded area indicates the region in which protons from deuteron disintegrations can be resolved on the basis of their range.

In experiments involving the neutron-deuteron interaction it is essential to distinguish between recoil deuterons, recoil protons from the hydrogen contamination of the deutero-paraffin, and protons from deuteron breakup. Figure 3 shows the variation of range with laboratory angle for the particles from the first two reactions and for the maximum energy protons from the third reaction. This latter is calculated on the assumption that the two neutrons go off in the same direction and with equal velocities. It is apparent that the recoil protons from hydrogen contamination in the heavy paraffin are always separable from the recoil deuterons but not from the highest energy disintegration protons. However, once the degree of contamination is firmly established at angles where adequate separation in range does exist, a correction can be made at other angles on the basis of the hydrogen content of the deutero-paraffin and the differential *n-p* scattering cross section for 14-Mev neutrons. The correction for deuterons knocked on by degraded neutrons is much more difficult to evaluate. Since such low energy deuteron recoils are indistinguishable, in the emulsion, from protons of the same range, it is necessary to make a correction for these tracks. The correction was calculated on the basis of the neutron spectrum incident on the target (Fig. 2b) and the known differential cross sections with respect to energy and angle for *n-d* and *p-d* scattering. The *p-d* scattering data were used in addition to *n-d* scattering data since insufficient *n-d* scattering data are available. For the purpose of these calculations the differential cross section at energy E for *n-d* scattering is assumed equal to the differential cross section for *p-d* scattering at

energy (E+0.7) Mev. (The p-d scattering data were used only at large angles where Coulomb scattering would be unimportant.)

To obtain data at laboratory angles smaller than 10° and to lend additional credence to the cross-section values obtained at angles investigated by means of the arrangement shown in Fig. 1, we have utilized the target-detector geometry shown schematically in Fig. 4 to measure cross-section values for n-d scattering and deuteron breakup at 2°, 13°, 15°, and 24.4°. This geometry does not involve use of a neutron collimator. The agreement, on an absolute scale, of the data from the single plate camera shown in Fig. 4 with that from the multiplate camera is a welcome check.

In addition to making runs with a single plate camera and with different target thicknesses as well as with a blank target in the multiplate camera, the following checks were made to establish the fact that the various range groups of tracks observed actually came from the target.

(a) A plot was made of the number of tracks observed *versus* projected angle in the horizontal plane. A similar plot was made with respect to the angle in the vertical plane. The variation of number of tracks with angle was determined to be consistent with the position of the area of the plate analyzed and the size of target as seen by this area.

(b) Areas at various distances from the target were analyzed to determine whether the number of tracks of each range group was proportional to the solid angle subtended at the target by the plate area analyzed.

In the n-d experiment grain counts were made, at several angles, of tracks in the elastically scattered range group, and between the deuteron peak and the range group caused by knock-on protons from H^1 contamination in the deutero-paraffin. The tracks between the deuteron and proton peaks were thus established to be protons rather than deuterons, a conclusion which, at forward angles, is unavoidable on the basis of energy considerations.

TABLE II. Summary of n-p scattering data.

Ω c. m. angle (degrees)	$\sigma(\Omega)$ (barns/steradian)	Statistical error (percent)
154.5	0.0547	2.6
146.6	0.0540	3.5
131.7	0.0533	3.8
114.7	0.0518	3.5
100.5	0.0513	4.7
84.1	0.0533	4.4
66.9	0.0493	5.0
48.0	0.0507	4.6

III. RESULTS AND DISCUSSION

(A) n-p Scattering

The differential cross section for n-p scattering in the laboratory system is determined by the relation

$$\sigma(\psi)=N_pR^2/n_0NA\sin\phi, \qquad (1)$$

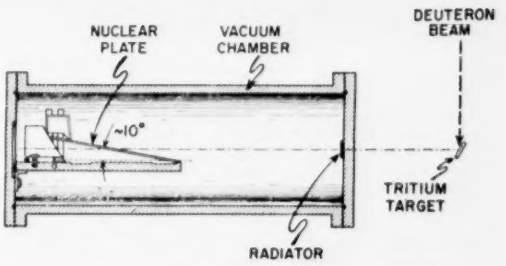

FIG. 4. Schematic drawing of single plate camera.

where

$\sigma(\psi)$ = cross section per unit solid angle in the laboratory coordinate system at angle ψ,
ψ = arc cos(cosθ cosϕ) (see Fig. 1),
A = area of plate scanned,
N_p = number of protons of proper length and direction counted in A,
R = distance from center of target to center of A,
ϕ = angle between plane of emulsion, (i.e., of A) and line from center of A to center of target = angle of dip into unprocessed emulsion,
n_0 = number of hydrogen atoms in the target = weight of target in grams×0.1498×6.025×10^{23}, and
N = number of neutrons per cm² that passed through the target.

In order to convert $\sigma(\psi)$ to the differential cross section in the c.m. system one simply multiplies by the factor giving the ratio of solid angles in the laboratory and c.m. systems. This factor is $1/(4\cos\psi)$. The c.m. angle Ω which corresponds to a laboratory angle ψ is $\Omega=180°-2\psi$.

Figure 5 and Table II give the results, in the center-of-mass system, for the angular distribution of 14.1-Mev neutrons scattered by protons. Although these results are not inconsistent with spherical symmetry, a slight asymmetry is by no means ruled out. The errors

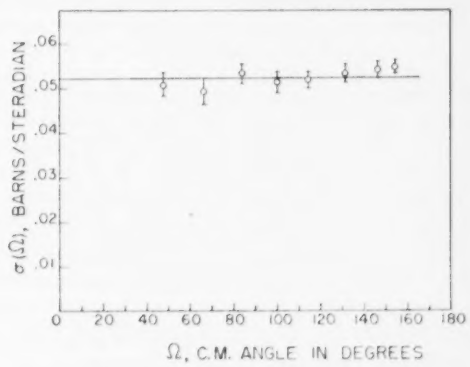

FIG. 5. Angular distribution of 14.1-Mev neutrons scattered by protons.

TABLE III. Summary of *n-d* scattering data.

ψ lab angle (degrees)	$\sigma(\psi)$ (barns/ steradian)	Ω c.m. angle (degrees)	$\sigma(\Omega)$ (barns/ steradian)	Statistical error (percent)	Estimated error arising from confusable protons (percent)
* 2.0	0.440	176.0	0.110	3.4	0
11.0	0.308	158.0	0.0795	5.9	0
12.4	0.228	155.2	0.0585	5.0	0
*13.0	0.230	154.0	0.0590	6.0	0
14.0	0.196	152.0	0.0505	5.8	2
14.5	0.208	151.0	0.0537	5.1	2
*15.0	0.189	150.0	0.0489	8.0	3
17.5	0.125	145.0	0.0328	7.1	5
18.3	0.113	143.4	0.0298	6.2	6
20.8	0.0712	138.4	0.0191	9.2	7
22.9	0.0553	134.2	0.0150	8.3	7
23.6	0.0455	132.8	0.0123	9.7	7
*24.4	0.0410	131.2	0.0113	12.0	10
26.7	0.0390	126.6	0.0110	8.5	7
29.3	0.0401	121.4	0.0115	8.5	7
30.3	0.0398	119.4	0.0115	6.5	7
32.8	0.0399	114.4	0.0122	6.4	7
34.8	0.0433	110.4	0.0132	8.4	6
38.6	0.0530	102.8	0.0171	5.7	4
46.7	0.0970	86.6	0.0355	5.1	4
51.2	0.106	77.6	0.0422	5.5	4
52.4	0.117	75.2	0.0477	5.4	4
55.3	0.119	69.4	0.0520	7.7	4
57.8	0.128	64.4	0.0598	3.9	5
65.5	0.139	49.0	0.0841	6.5	5
67.0	0.134	46.0	0.0859	10.8	5

* Single plate camera data.

indicated in the figure and table are standard deviations due to statistical uncertainties alone. The standard error arising from the evaluation of R, A, ϕ, n_0, and N in Eq. (1) is approximately 5 percent. The most probable value of the ratio of the cross section in the region of 130° to 155° to the cross section in the angular region of 65° to 105° is 1.04 ± 0.05.

Our angular distribution is in quite good agreement with the angular distribution of Barschall and Taschek. The total cross section obtained from our data, by assuming spherical symmetry, is 0.66 ± 0.05 barn. The value obtained by transmission measurements at this energy is 0.689 ± 0.005 barn.[19]

(B) *n-d* Interaction

The method of calculating the differential cross section in the center-of-mass system as a function of angle for *n-d* elastic scattering is identical with that outlined for the *n-p* scattering. n_0 was determined from the weight and composition of the deutero-paraffin.

Figure 6 and Table III give the results of the angular distribution measurements for *n-d* elastic scattering. Figure 6 gives all of the points obtained in the various runs. The large degree of scattering of the points shown is due chiefly to statistical fluctuations. Table III gives the weighted averages of the cross-section values displayed in Fig. 6. In addition to statistical inaccuracies there exist errors attributable to the following:

(a) Uncertainties in the evaluation of the background in the range group of the elastically scattered deuterons. The portion of this background caused by $D(n, 2n)H^1$ was, of course, not present in the *n-p* problem; estimates of these errors are given in column six of Table III.

(b) Geometrical factors (R^2, A, ϕ, Eq. (1)): 3 percent.

(c) Number of deuterium atoms in target [n_0, Eq. (1)]: 3 percent.

(d) Number of neutrons per cm² passing through target [N, Eq. (1)]: 3.5 percent.

The 14-Mev neutron flux at the target was calculated on the basis of the number of neutrons generated in the source, as given by the alpha-particle counter and the distance between source and target. No correction was made for a possible contribution to the flux at the target by elastic scattering in the walls of the collimator channel. Experiments which we have performed to date indicate that this effect is less than 2 percent. However, if such a systematic error did exist it would mean that all the cross-section values obtained from the multiplate camera are too high by the amount of this error.

Our *n-d* elastic scattering results are in reasonably good agreement with the most recent results of Coon and Taschek.[20] There still appears to be a discrepancy in the region of the minimum where the present results are lower than those of Coon and Taschek by an amount which is somewhat outside the combined errors. This difference, however, may be due to the fact that we have corrected our data for the presence of those protons from deuteron breakup which fall into the range group of elastically scattered deuterons. The

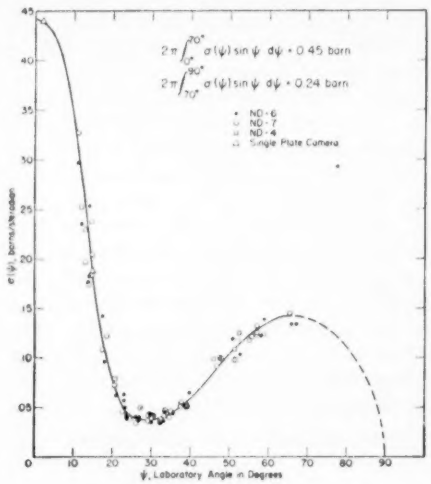

FIG. 6. Angular distribution of deuterons knocked on by 14.1-Mev neutrons.

[19] Poss, Salant, Snow, and Yuan, Phys. Rev. **87**, 11 (1952).

[20] J. H. Coon (private communication).

correction was made on the basis of the shape of the range distribution of the charged particles recorded above and below the elastically scattered deuteron range group at each angle.

It is rather difficult to compare the data of Griffith, Remley, and Kruger[11] with the present data since theirs were taken at a lower energy and their cross-section scale is not absolute. However, if one normalizes the Illinois data to our own at 90°, the agreement is as good as one might expect, especially since their elastic scattering cross sections include a contribution from the cross section for deuteron breakup. This contribution is in the proper direction and probably of sufficient magnitude to account for any discernible disagreement in the region of the minimum.

Figure 7 compares our results with the theoretical predictions of Buckingham, Hubbard, and Massey[5] on the assumption of symmetrical exchange type forces. The disagreement may well be due to the fact that the theoretical calculations assumed no contribution from relative angular momentum states above $l=2$ (d scattering). A detailed analysis of these data has recently been carried out by Christian and Gammel.[21] Their calculated n-d angular distribution at 14.1-Mev neutron energy is in excellent agreement with the present experimental results.

In Figs. 6 and 7, the experimental angular distributions have been extrapolated to zero degrees and the curves integrated. The average total cross section for elastic scattering arrived at in this manner is 0.67 ± 0.10 barn. This value is significantly lower than the total cross section value of 0.802 barn obtained from transmission measurements.[19] The rather large difference appears to be good evidence for the existence of an appreciable cross section for deuteron disintegration at this energy. There is, moreover, additional evidence

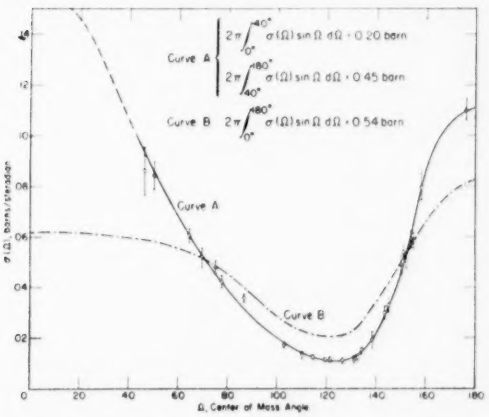

FIG. 7. Comparison of experimental and theoretical angular distributions of 14.1-Mev neutrons scattered by deuterons.

[21] R. S. Christian and J. L. Gammel (following paper), Phys. Rev. **91**, 100 (1953).

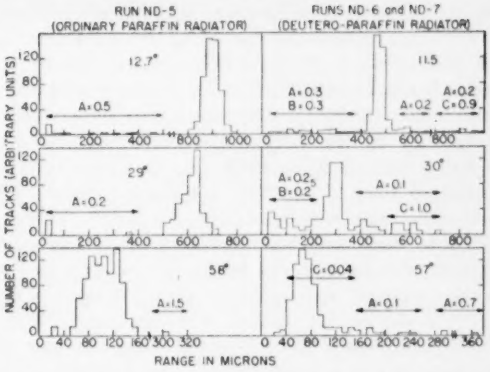

FIG. 8. Distribution in range of charged particles from n-d and n-p interactions at various angles.

for this process based on the observation of the protons which result from such breakup.

Figure 8 shows the distributions in range of all the charged particles from the n-d and n-p interactions at various angles. The values assigned to A in this figure give the fraction of the tracks, in the range interval indicated, which must be subtracted on the basis of the blank target run for the forward angles and *Run ND-7* (Table I) for the backward angles.[22] It is apparent, at least qualitatively, that the histograms of the charged particles from the n-d interaction show more tracks outside of the range groups corresponding to elastic scattering than do the corresponding n-p histograms. In particular, those tracks which fall between the range groups of elasticically scattered deuterons and protons, cannot be due to deuterons elastically scattered by the primary beam of 14.1-Mev neutrons. The tracks which appear below the range group of elastically scattered deuterons can, however, be due to deuterons elastically scattered by degraded neutrons and corrections must accordingly be applied. The values assigned to B in Fig. 8 give the fraction of the plotted tracks, in the range interval indicated, which is deduced to be due to deuterons elastically scattered by degraded neutrons. C designates the range interval within which one expects to find tracks of knock-on protons from the hydrogen in the target. The values assigned to C refer to the fraction of tracks in the designated range interval which one calculates to come from such scatterings on the basis of a 0.05 ratio of H^1 to H^2 atoms. These corrections were made on the basis of what is known about n-d and p-d elastic scattering cross sections as a function of angle and energy. Figure 9 gives the angular distributions used for these corrections. In energy regions where no data are available, a log-log extrapolation of the data illustrated in Fig. 9

[22] At 11° the relatively large number of background tracks of range greater than 500μ were determined to be caused by a small amount of grease on the outside of the front window. At larger angles such tracks were eliminated from consideration on the basis of their direction.

was used. The dotted curve is an example of the results of such an extrapolation for 14.1-Mev *n-d* scattering.

Figure 10 shows, in a semiquantitative manner, the deduced angular distribution for emission of protons from deuteron breakup. The large errors arise from the uncertainty in the background correction. It is to be noted that tracks of range less than 25μ were not considered since it was felt that the measurement of their orientation with respect to the target could not be made with sufficient precision. This limitation, together with energy loss in the target, implies that protons emitted with less than approximately 2-Mev energy would not be counted. A serious source of error in the assignment of differential cross sections for deuteron breakup arises from the possibility that unknown contaminants might give rise to protons from (n, p) reactions which would be indistinguishable, energywise, from deuteron breakup protons. The chief sources of such contaminants are probably the catalysts used in the preparation of the wax. To check further on this point we repeated a number of the single-plate camera runs using deutero-polyethylene as a target rather than deutero-paraffin. For the background run we used ordinary polyethylene prepared by exactly the same process.[23] The preparation of the polyethylene involved different catalysts from those used in the preparation of the heavy wax. The results for both elastic scattering and deuteron disintegration were independent of the target used and this fact, together with the very reasonable variation with angle of the range distribution of the disintegration protons, gives us considerable confidence that contaminants are not causing serious difficulty.

The total cross section for deuteron breakup with the emission of protons of energy above 2 Mev is deduced, from the data given in Fig. 10, to be 53 ± 15 millibarns. This value does not appear to be in violent disagreement with the total cross section for this process as deduced from the data of other investigators. Coon and Taschek,[11] for example, report a maximum value of 50 millibarns for the cross section for the disintegration process over the range from 0° to 80° in the laboratory system.

Ageno, Amaldi, Bocciarelli, and Trabacchi[24] estimated a cross section for this process of 40 to 90 millibarns; while Griffith, Remley, and Kruger[11] also

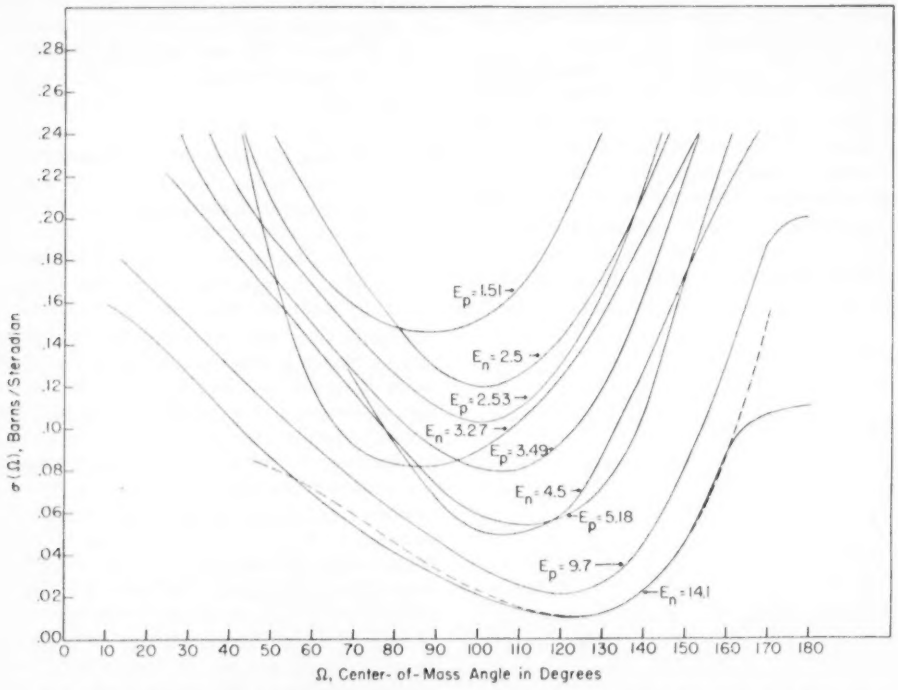

FIG. 9. Experimental angular distributions for *n-d* and *p-d* scattering. The dashed curve is a log-log extrapolation to 14-Mev neutron energy of the following lower energy data: $E_p=1.51$, 2.53, and 3.49 Mev—Sherr, Blair, Kratz, Bailey, and Taschek, Phys. Rev. **72**, 662 (1947); $E_n=2.5$ Mev—R. K. Adair (private communication); $E_n=3.27$ Mev—I. Hamouda and G. de Montmollin, Phys. Rev. **83**, 1277 (1951); $E_n=4.5$ Mev—E. Wantuch, Phys. Rev. **84**, 169 (1951); $E_p=5.18$ Mev—L. Rosen and J. C. Allred, Phys. Rev. **82**, 777 (1951); $E_p=9.7$ Mev—Allred, Armstrong, Bondelid, and Rosen, Phys. Rev. **88**, 433 (1952); $E_n=14.1$ Mev—present data.

[23] The polyethylene was also prepared for us by A. R. Ronzio.
[24] Ageno, Amaldi, Bocciarelli, and Trabacchi, Phys. Rev. **71**, 20 (1947).

observed a significant probability for this reaction at 12- to 13-Mev neutron energy. All the above data, present experiment included, indicate a lower cross section for deuteron breakup, by an order of magnitude, than is theoretically predicted.[25]

It is interesting to speculate concerning the reason that more high energy protons are not emitted in the forward direction. It may be that this mode of disintegration is, to some extent, inhibited by the Pauli exclusion principle, for if the incident neutron transfers most of its energy to the proton in the deuteron, the two remaining neutrons might well be left in an S-state of orbital angular momentum and this is, of course, only possible in the case of antiparallel spins.

The authors are indebted to the entire staff of the nuclear plate laboratory for the very careful plate analysis work upon which this report is based. We wish also to express our appreciation to Rexine Booth, Juanita Gammel, and Leona Stewart for their assistance in the reduction and compilation of the data and to Leona Stewart for her very considerable help in the preparation of the manuscript.

[25] B. H. Bransden and E. H. Burhop, Proc. Phys. Soc. (London) **A63**, 1337 (1950).

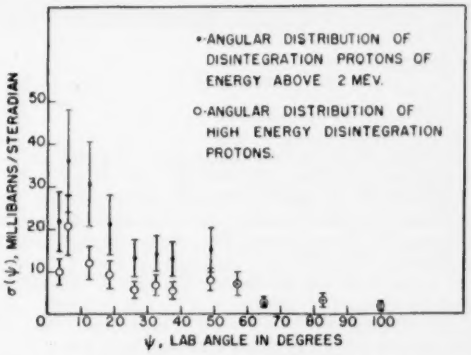

FIG. 10. Angular distribution for emission of protons from deuteron breakup. The dots represent the angular distribution of all disintegration protons of energy greater than 2 Mev; the open circles represent the angular distribution of only those protons whose range is greater than the range of the elastically scattered deuterons at the same angle.

Elastic Scattering of Protons and Neutrons by Deuterons

R. S. CHRISTIAN AND J. L. GAMMEL
University of California, Los Alamos Scientific Laboratory, Los Alamos, New Mexico
(Received February 9, 1953)

Phase shifts for p-d and n-d scattering are calculated in Born approximation for partial waves with $l \geq 1$. These are used as a starting point for a phase shift analysis of the p-d data in the energy range 0–10 Mev. For $l \geq 1$, the phase shifts resulting from the phase shift analysis agree with those calculated in Born approximation. The ^4S and ^2S phase shifts have a reasonable energy dependence; that is, the "$k \cot\delta$" plots are smooth functions of the energy and extrapolate to a set of scattering lengths near one of the known sets of n-d scattering lengths. It is concluded that the correct set of n-d scattering lengths is

$$a_4 = 6.2 \pm 0.2 \times 10^{-13} \text{ cm}, \quad a_2 = 0.8 \pm 0.3 \times 10^{-13} \text{ cm}.$$

Since this is in disagreement with some previous theoretical conjectures, the scattering lengths and S phase shifts in the energy region 0–10 Mev are calculated using a variational method with neglect of polarization (a theoretical estimate of the effect of polarization is made) and the results support the conclusion. N-d angular distributions are calculated and compared with experiments. The agreement of the theoretical results with the experimental ones provides a strong *a fortiori* justification of conclusions drawn from the theory about the importance of the internucleonic potentials in low energy p-d and n-d scattering. The scattering is nearly independent of the odd parity n-p potentials and of the forces between like particles. Furthermore, it is nearly independent of the shape of the ^3S and ^1S-n-p potentials. However, the ^2S scattering length is sensitive to the singlet even parity n-n potential, and is calculated as a function of the depth of this potential. It is insensitive to other n-n potentials.

I. INTRODUCTION

OUR primary purpose is to find out what can be learned about the internucleonic forces from the p-d and n-d scattering data. Of course, a complete solution of the three body problem is not possible, but the program described in the next section leads to a clarification of the importance of the forces between like particles and the odd parity n-p forces in the p-d and n-d scattering. Unfortunately, it will be shown that these forces influence the scattering to only a minor degree, and the scattering is determined by the ^3S and ^1S n-p force. Furthermore, the scattering is insensitive to the shape of the ^3S and ^1S n-p potentials.

An important result is obtained from a phase shift analysis of the p-d data in the energy range 0–10 Mev.[1–4] It is concluded that the correct set of n-d scattering lengths[5] is the set

$$\begin{aligned} a_4 &= 6.2 \pm 0.2 \times 10^{-13} \text{ cm}, \\ a_2 &= 0.8 \pm 0.3 \times 10^{-13} \text{ cm}. \end{aligned} \tag{1}$$

Because this is in disagreement with some previous theoretical conjectures[6–8] even though in agreement with others,[9] we have recalculated the scattering lengths, and the results support the concluion. As a further test of the results of the phase shift analysis, we have calculated the S phase shifts in the energy region 0–10 Mev, and the calculation confirms the results of the phase shift analysis.

II. PROGRAM

The calculations are carried out for a general central nuclear potential with either a Yukawa or Gauss radial dependence. These potentials are adjusted in range and depth to fit the low energy n-p[10,11] and p-p[12] data and, in the case of the Yukawa potential, the high energy n-p data.[13] Tensor forces are not taken into account since the n-p data can be well described by an "equivalent central potential" and possible relatively weak tensor forces in p-p and n-p odd parity states are expected to play a small role in n-d or p-d scattering (Sec. VIII-A.2). Any effects attributable to inelastic scattering have been neglected throughout because the experimentally determined inelastic cross section[14] is much smaller than the elastic cross section at these energies (see also Sec. VIII-A.4).

The first step is to calculate the phase shifts for $l \geq 1$ using Born's approximation with the symmetry of the like particles taken into account (Secs. III, IV). The validity of this approximation is discussed in detail in Sec. VIII-A.1. It may be expected to yield reasonable results for the higher angular momentum states because of the large spatial extent of the deuteron and the presence of the centrifugal barrier. Further justification comes from the smallness of the calculated phase shifts.

The next step is to determine the ^4S and ^2S phase shifts so that calculated and experimental angular

[1] Brown, Freier, Holmgren, Stratton, and Yarnell, Phys. Rev. **88**, 253 (1952).
[2] Sherr, Blair, Kratz, Bailey, and Taschek, Phys. Rev. **72**, 662 (1947).
[3] L. Rosen and J. C. Allred, Phys. Rev. **82**, 777 (1951).
[4] Allred, Armstrong, Bondelid, and Rosen, Phys. Rev. **88**, 433 (1952).
[5] D. G. Hurst and N. Z. Alcock, Can. J. Phys. **29**, 36 (1951); Wollan, Shull, and Koehler, Phys. Rev. **83**, 700 (1951). The latter paper contains references to other experimental work on the n-d scattering lengths.
[6] A. Troesch and M. Verde, Helv. Phys. Acta **24**, 39 (1951).
[7] M. M. Gordon, Phys. Rev. **80**, 111 (1950).
[8] F. G. Prohammer and T. A. Welton, Quarterly Report Oak Ridge National Laboratory, Oak Ridge, Tenn. ORNL-1005 (unpublished).
[9] L. Motz and J. Schwinger, Phys. Rev. **58**, 26 (1940).
[10] J. M. Blatt and J. D. Jackson, Phys. Rev. **76**, 18 (1949).
[11] H. A. Bethe, Phys. Rev. **76**, 38 (1949).
[12] J. D. Jackson and J. M. Blatt, Revs. Modern Phys. **22**, 77 (1950).
[13] R. S. Christian, Repts. Progr. Phys. **15**, 68 (1952).
[14] J. H. Coon and R. F. Taschek, Phys. Rev. **76**, 710 (1949).

distributions for p-d scattering in the energy range 0–10 Mev agree within quoted experimental error (Sec. V-A). Improvement in the fits is obtained by allowing the ^4P phase shift to change from its value calculated in Born approximation. When this is done, it is found that the change in the value of the ^4P phase shift is small and a smooth function of energy.

The ^4S and ^2S phase shifts found in this manner have a reasonable energy dependence. That is, the "$k\cot\delta$" plots extrapolate to zero energy to give a set of scattering lengths near one of the known sets of n-d scattering lengths. We find for the p-d scattering lengths

$$a_4 = 12.5 \pm 1.0 \times 10^{-13} \text{ cm}, \qquad (2)$$
$$a_2 = 1.4 \pm 1.0 \times 10^{-13} \text{ cm}.$$

Because of the connection between n-d and p-d scattering lengths (Sec. V-C), this means that the scattering lengths (l) are the correct n-d scattering lengths, in disagreement with some previous theoretical work.[6–8] A careful recalculation of the scattering lengths is undertaken in order to resolve this difficulty.

The calculation of the n-d scattering lengths is carried out using a variational method neglecting polarization of the deuteron (Sec. VI-A). The variational treatment is similar to that used by Massey and Buckingham[15] and Verde.[6,16] In its details, the work has some similarity to the work of Motz and Schwinger.[9] The neglect of polarization (discussed in Sec. VIII-A.3) is not expected to be serious in the case of the quartet state because the exclusion principle prevents the three particles from being close together simultaneously at low energies. Because the phase shift analysis shows that the doublet state makes only a small contribution to the low energy scattering, errors attributable to neglect of polarization are of little consequence for the angular distribution calculations. The results of the calculation,

$$a_4 = 5.9 \times 10^{-13} \text{ cm}, \quad a_2 = 1.5 \times 10^{-13} \text{ cm}, \qquad (3)$$

check the scattering lengths (1) closely for the quartet state and are even in fair agreement for the doublet state. However, they definitely rule out the other set allowed by the experiments:

$$a_4 = 2.4 \times 10^{-13} \text{ cm}, \quad a_2 = 8.3 \times 10^{-13} \text{ cm}. \qquad (4)$$

The quartet and doublet n-d S phase shifts at energies up to 10 Mev are calculated using a somewhat more crude approximation than that employed for the the scattering length calculation (Sec. VI-B). The energy variation of the "$k\cot\delta$" plots is in fair agreement with that found from the phase shift analysis.

n-d angular distributions are calculated (Sec. VII-A) using the theoretical corrections to the p-d phase shifts necessitated by the absence of the Coulomb forces (Sec. IV-D). These are compared with the experimental data.

In Sec. VII-B the problem of deducing information about the n-n forces from the n-d scattering data is discussed. It is shown that the angular distributions are not sensitive to the n-n forces. The ^2S scattering length is, however, and is calculated as a function of the depth of the singlet even parity n-n potential. It is shown to be insensitive to other n-n potentials. The ^4S scattering length depends only on the triplet odd parity n-n potential, to which it is very insensitive.

III. THE BORN APPROXIMATION

Others have described the formulation of Born's approximation for n-d[17,18] and p-d[19] scattering.

There are eight two body potentials ${}^3V_{np}^+$, ${}^3V_{np}^-$, ${}^1V_{np}^+$, ${}^1V_{np}^-$, ${}^1V_{pp}^+$, ${}^3V_{pp}^-$, ${}^1V_{nn}^+$, ${}^3V_{nn}^-$. The superscript to the left of ${}^3V_{np}^+$, for example, specifies that ${}^3V_{np}^+$ is the potential for a triplet state, while the superscript to the right specifies that it is the potential for a state of even parity. The subscript specifies that ${}^3V_{np}^+$ is the potential between a neutron and a proton. Thus ${}^3V_{np}^+$ is the potential for the deuteron ground state. We suppose that all of these potentials have the same radial dependence, so that, for example, ${}^1V_{np}^+(r) = {}^1V_{np}^+ U(r)$, the V's becoming pure numbers. $U(r)$ is taken to be the potential for the ground state of the deuteron, so that ${}^3V_{np}^+ = 1$. $U(r)$ is understood to be multiplied by $4M/3\hbar^2$ which reduces it dimensionally to the reciprocal of the square of a length. Let

$$J_1(\theta) = \int \exp(-i\mathbf{k}'\cdot\mathbf{q})\phi(|\mathbf{r}|)U(|\mathbf{q}+\tfrac{1}{2}\mathbf{r}|) \times \exp(i\mathbf{k}\cdot\mathbf{q})\phi(|\mathbf{r}|)d\mathbf{r}d\mathbf{q},$$

$$J_2(\theta) = \int \exp(-i\mathbf{k}'\cdot\mathbf{q})\phi(|\mathbf{r}|)U(|\mathbf{q}+\tfrac{1}{2}\mathbf{r}|) \times \exp[-i\mathbf{k}\cdot(\tfrac{1}{2}\mathbf{q}-\tfrac{3}{4}\mathbf{r})]\phi(|\mathbf{q}+\tfrac{1}{2}\mathbf{r}|)d\mathbf{r}d\mathbf{q}, \qquad (5)$$

$$J_3(\theta) = \int \exp(-i\mathbf{k}'\cdot\mathbf{q})\phi(|\mathbf{r}|)U(|\mathbf{q}+\tfrac{1}{2}\mathbf{r}|) \times \exp[-i\mathbf{k}\cdot(\tfrac{1}{2}\mathbf{q}+\tfrac{3}{4}\mathbf{r})]\phi(|\mathbf{q}-\tfrac{1}{2}\mathbf{r}|)d\mathbf{r}d\mathbf{q},$$

where

$$\mathbf{r} = \mathbf{r}_3 - \mathbf{r}_2, \quad \mathbf{q} = -\mathbf{r}_1 + \tfrac{1}{2}(\mathbf{r}_2 + \mathbf{r}_3), \qquad (6)$$

are the center-of-mass coordinates; $\mathbf{k}$, given by

$$k^2 = \frac{8M}{9\hbar^2} E(\text{lab}), \qquad (7)$$

where E is the energy of the incident nucleon in the

[15] R. A. Buckingham and H. S. W. Massey, Proc. Roy. Soc. (London) **A179**, 123 (1941).
[16] M. Verde, Helv. Phys. Acta **22**, 339 (1949).
[17] M. Verde, Helv. Phys. Acta **22**, 339 (1949).
[18] T.-Y. Wu and J. Ashkin, Phys. Rev. **73**, 986 (1948). In the last of their Eqs. (29), the coefficient of λ^2 is 1 instead of $\frac{1}{3}$.
[19] J. L. Gammel, "Elastic scattering of neutrons and protons by deuterons," Cornell thesis, 1950 (unpublished).

laboratory, is the wave number vector of the incident particle, and $\mathbf{k}'$ is the wave number vector of the scattered particle. Because the scattering is elastic, $|\mathbf{k}|=|\mathbf{k}'|$. The angle between $\mathbf{k}$ and $\mathbf{k}'$ is the scattering angle in the center-of-mass system, θ. $\phi(r)$ is the wave function for the ground state of the deuteron.

For n-d scattering, the scattering amplitude is given by

$$4\pi f(\theta)=\alpha J_1(\theta)+\beta J_2(\theta)+\gamma J_3(\theta), \tag{8}$$

where

$$\begin{aligned}\alpha&=\tfrac{1}{2}\,{}^3V_{np}{}^+ +\tfrac{1}{2}\,{}^3V_{np}{}^- +{}^3V_{nn}{}^-,\\ \beta&=-{}^3V_{np}{}^+,\\ \gamma&=\tfrac{1}{2}\,{}^3V_{np}{}^+ -\tfrac{1}{2}\,{}^3V_{np}{}^- -{}^3V_{nn}{}^-,\end{aligned} \tag{9}$$

for $S=\frac{3}{2}$; and

$$\begin{aligned}\alpha&=\tfrac{1}{8}\,{}^3V_{np}{}^+ +\tfrac{1}{8}\,{}^3V_{np}{}^- +\tfrac{3}{8}\,{}^1V_{np}{}^+ +\tfrac{3}{8}\,{}^1V_{np}{}^-\\ &\quad +\tfrac{3}{4}\,{}^1V_{nn}{}^+ +\tfrac{1}{4}\,{}^3V_{nn}{}^-,\\ \beta&=+\tfrac{1}{2}\,{}^3V_{np}{}^+,\\ \gamma&=\tfrac{1}{8}\,{}^3V_{np}{}^+ -\tfrac{1}{8}\,{}^3V_{np}{}^- +\tfrac{3}{8}\,{}^1V_{np}{}^+ -\tfrac{3}{8}\,{}^1V_{np}{}^-\\ &\quad +\tfrac{3}{4}\,{}^1V_{nn}{}^+ -\tfrac{1}{4}\,{}^3V_{nn}{}^-,\end{aligned} \tag{10}$$

for $S=\frac{1}{2}$.

Corrections to Eq. (8) required by the presence of the Coulomb force in p-d scattering are discussed in Sec. IV-D.

The phase shifts are computed from

$$kf(\theta)=\textstyle\sum_l (2l+1)\delta_l P_l(\cos\theta), \tag{11}$$

and these phase shifts are substituted in the rigorous formula for the angular distribution, which for p-d scattering is

$$\begin{aligned}k^2\sigma(\theta)=&\frac{2}{3}\left|\frac{\eta}{1-\cos\theta}\exp\left(i\eta\ln\frac{2}{1-\cos\theta}\right)+\frac{1}{2i}\sum_l (2l+1)\right.\\ &\left.\times[\exp(2i^4\delta_l)-1]\exp(i\phi_l)P_l(\cos\theta)\right|^2\\ &+\frac{1}{3}\left|\frac{\eta}{1-\cos\theta}\exp\left(i\eta\ln\frac{2}{1-\cos\theta}\right)+\frac{1}{2i}\sum_l (2l+1)\right.\\ &\left.\times[\exp(2i^2\delta_l)-1]\exp(i\phi_l)P_l(\cos\theta)\right|^2,\end{aligned} \tag{12}$$

where the superscript on the δ_l's specify the spin state for which they are the phase shifts, and

$$\eta=e^2/\hbar v, \quad \phi=\text{phase}\Gamma(l+1+i\eta). \tag{13}$$

Reasons for using the exact expression (12) rather than $f^2(\theta)$ corrected for S phase shifts are discussed in Sec. VIII-A.5.

Each of the above integrals forming the scattering amplitude can be given a simple physical interpretation[20] in the sense of validity of Born's approximation, since only a single collision takes place. $J_1(\theta)$ represents potential scattering in which the incident particle scatters off one of the two particles in the deuteron. $J_3(\theta)$ represents a type of scattering or direct "knock out" in which the incident particle exchanges directly with one of the particles in the deuteron so that the "struck" particle is ejected from the deuteron and the original incident particle remains to form the deuteron. (This exchange is attributable in part to the exclusion principle and in part to explicit exchange forces.) $J_2(\theta)$ is a manifestation of the exclusion principle and represents pickup by the incident particle of a dissimilar particle in the deuteron to form a new deuteron, the remaining particle becoming the scattered particle. It can, therefore, be expected that $J_1(\theta)$ is peaked in the forward direction. $J_3(\theta)$ should also be peaked in the forward direction since in order to reconstitute a deuteron the incident particle must transfer most of its momentum to the struck particle. [Actually $J_3(\theta)$ is almost spherically symmetrical.] $J_2(\theta)$ is peaked in the backward direction since following the pickup process the "new" deuteron is most probably traveling in the direction of the incident nucleon.

[20] The physical significance of these integrals has been discussed by others. See the papers of reference 29.

IV. COMPUTATION OF PHASE SHIFTS

The integrals $J_1(\theta)$, $J_2(\theta)$, and $J_3(\theta)$ are calculated using Gauss and Yukawa radial forms for $U(r)$ with ranges adjusted to fit the low energy data.

A. Zero Range Approximation

In order to gain some further insight into the nature and magnitude of the terms in Eq. (5), we first consider the "zero range" approximation. Actually, this need not be thought of as strrictly a zero range approximation; it can be thought of as an approximation in which it is assumed that the other terms in the integrands in Eq. (5) vary slowly compared to the potential. This would be the case if the range of $U(r)$ were very small compared to the deuteron radius and the wavelength of the incident particle. With the potential

$$U(r)=U_0\delta(|\mathbf{r}|), \tag{14}$$

where $\delta(|\mathbf{r}|)=1$ for $r<r_0$ and $\delta(|\mathbf{r}|)=0$ for $r>r_0$, and U_0 is a potential depth such that $U_0r_0^2$ is a constant whose value is $2\pi/3$, we find

$$\begin{aligned}J_1(\theta)&=\frac{4\pi}{3}(2r_0)^3U_0\int\exp(-i\mathbf{k}'\cdot\mathbf{q})\phi^2(|2\mathbf{q}|)\\ &\qquad\times\exp(i\mathbf{k}\cdot\mathbf{q})d\mathbf{q},\\ J_2(\theta)&=\frac{4\pi}{3}(2r_0)^3U_0\langle\phi(r_0)\rangle_{\text{Av}}\int\exp(-i\mathbf{k}'\cdot\mathbf{q})\\ &\qquad\times\phi(|2\mathbf{q}|)\exp(-2i\mathbf{k}\cdot\mathbf{q})dq,\\ J_3(\theta)&=\frac{4\pi}{3}(2r_0)^3U_0\int\exp(-i\mathbf{k}'\cdot\mathbf{q})\phi^2(|2\mathbf{q}|)\\ &\qquad\times\exp(i\mathbf{k}\cdot\mathbf{q})d\mathbf{q},\end{aligned} \tag{15}$$

$\langle\phi(r_0)\rangle_{Av}$ is the average value of the deuteron wave function for $r<r_0$. In this approximation we may evidently use the zero range deuteron wave function

$$\phi(r)=(\alpha/2\pi)^{\frac{1}{2}}e^{-\alpha r}/r, \tag{16}$$

inside the integrands as we are only interested in its low Fourier components. The results are

$$J_1(\theta)=\left(\frac{8\pi}{3}\right)^2\frac{\alpha r_0}{k\sin(\theta/2)}\tan^{-1}\left(\frac{k\sin(\theta/2)}{2\alpha}\right),$$

$$J_2(\theta)=\left(\frac{8\pi}{3}\right)^2\left[r_0\langle\phi(r_0)\rangle_{Av}\left(\frac{2\pi}{\alpha}\right)^{\frac{1}{2}}\right]\frac{2\alpha}{4\alpha^2+k^2(5+4\cos\theta)}$$

$$=\left(\frac{8\pi}{3}\right)^2\frac{\pi\alpha}{4\alpha^2+k^2(5+4\cos\theta)},$$

$$J_3(\theta)=J_1(\theta),$$

$\langle\phi(r_0)\rangle_{Av}$ was calculated for square wells, and in evaluating $J_2(\theta)$,

$$\lim_{r_0\to 0}\langle\phi(r_0)\rangle_{Av}=\left(\frac{\alpha}{2\pi}\right)^{\frac{1}{2}}\frac{\pi}{2r_0}$$

is used.

We note that $J_1(\theta)$ is peaked in the forward direction as is $J_3(\theta)$ and $J_2(\theta)$ is peaked in the backward direction in agreement with our physical arguments of the last section.

Also we note that $J_1(\theta)$ and $J_3(\theta)$ are of order $(r_0\alpha)J_2(\theta)$. Detailed analysis shows they also have less angular variation than $J_2(\theta)$, and the contributions of $J_1(\theta)$ and $J_3(\theta)$ to the phase shifts fall off more rapidly with increasing l than the contribution of $J_2(\theta)$.

In calculating $J_1(\theta)$ and $J_2(\theta)$ for other radial forms of the potential, it is convenient to make the transformation

$$\mathbf{q}+\tfrac{1}{2}\mathbf{r}=\mathbf{w}, \quad \mathbf{r}=\mathbf{z}.$$

Then

$$J_1(\theta)=\int\exp(-i(\mathbf{k}-\mathbf{k}')\cdot\tfrac{1}{2}\mathbf{z})\phi^2(|\mathbf{z}|)d\mathbf{z}\times\int\exp(i(\mathbf{k}-\mathbf{k}')\cdot\mathbf{w})U(|\mathbf{w}|)d\mathbf{w},$$

$$J_2(\theta)=\int\exp(-i(\mathbf{k}+\tfrac{1}{2}\mathbf{k}')\cdot\mathbf{z})\phi(|\mathbf{z}|)d\mathbf{z}\times\int\exp(-i(\mathbf{k}'+\tfrac{1}{2}\mathbf{k})\cdot\mathbf{w})\phi(|\mathbf{w}|)U(|\mathbf{w}|)d\mathbf{w}.$$

From these forms we note several things. First, as the energy increases, the angular variation of $J_1(\theta)$ increases more rapidly than the angular variation of $J_2(\theta)$ primarily attributable to the part of $J_1(\theta)$ containing $\phi^2(|\mathbf{z}|)$ in its integrand. Thus at very high energy the elastic scattering becomes potential scattering. Second, $J_1(\theta)$ is sensitive to the shape of the potential. At low energies, it is larger for potentials which have a long tail. Third, the potential may be eliminated from $J_2(\theta)$ by making use of the two-body equations of motion

$$U(w)\phi(w)=(\nabla^2-\alpha^2)\phi(w).$$

Then $J_2(\theta)$ is of the form

$$J_2(\theta)=[(\tfrac{1}{2}\mathbf{k}+\mathbf{k}')^2+\alpha^2]\int\exp(i(\mathbf{k}+\tfrac{1}{2}\mathbf{k}')\cdot\mathbf{z})\phi(z)d\mathbf{z}\times\int\exp(-i(\mathbf{k}'+\tfrac{1}{2}\mathbf{k})\cdot\mathbf{w})\phi(w)d\mathbf{w}. \tag{17}$$

At low energies, $J_2(\theta)$ is practically independent of the shape or range of the potential.

$J_3(\theta)$ cannot be separated into the product of two integrals nor can the potential be eliminated. We have seen that in "zero range" approximation it is $J_1(\theta)$. However, this is an overestimate for finite range. A detailed examination of the expansion of $J_3(\theta)$ in spherical harmonics shows that its contributions to the higher phase shifts are less than those of $J_1(\theta)$ because there is no line up of the potential and a deuteron wave function or two deuteron wave functions, which makes it necessary to perform an average over $P_l(\cos\psi)$, where ψ is the angle between $\mathbf{q}$ and $\frac{1}{2}\mathbf{q}+\frac{3}{4}\mathbf{r}$ which varies from $0°$ to $3\alpha r_0/2$ (about $30°$). The effect is more pronounced the longer the tail of the potential.

B. Gauss Radial Form

We use

$$U(r)=U_0\exp(-(r/\lambda)^2),$$
$$U_0=86.4\text{ Mev}, \quad \lambda=1.332\times10^{-13}\text{ cm}. \tag{18}$$

In this calculation, the unit of length was taken to be 1.332×10^{-13} cm, so that

$$k^2=0.03806E.$$

It is necessary to represent the deuteron wave function by the sum of three Gauss terms:

$$\phi(x)=0.02133\exp(-0.03x^2)+0.08582\exp(-0.16x^2)+0.18115\exp(-0.76x^2), \tag{19}$$

which approximates the actual deuteron wave function for the potential (17) to within 3 percent to three times the deuteron radius. Wu and Ashkin[18] have given formulas for $J_1(\theta)$, $J_2(\theta)$, and $J_3(\theta)$ in this case.

Each of the integrals is of the form

$$(k/4\pi)J(\theta)=k\sum_i a_i\exp(-b_ik^2)\exp(-c_ik^2\cos\theta), \tag{20}$$

where the a's, b's, and c's are given in Table I.

A partial wave analysis of $kJ_1(\theta)$, $kJ_2(\theta)$, and $kJ_3(\theta)$ is made as follows:

$$(k/4\pi)J_i(\theta)=\sum_l(2l+1)\delta_i{}^lP_l(\cos\theta). \tag{21}$$

TABLE I. Constant for Gauss potential.

	J_1			J_2			J_3		
i	a_i	b_i	c_i	a_i	b_i	c_i	a_i	b_i	c_i
1	0.37966	2.5834	−2.5834	1.0197	10.720	8.5760	0.36854	2.3659	−1.8062
2	0.53992	1.1579	−1.1579	3.4332	10.686	8.5489	0.51846	0.95370	−0.39784
3	0.13499	0.65822	−0.65822	3.8774	10.594	8.4752	0.12840	0.45752	0.089197
4	0.49912	0.89061	−0.89061	1.1217	2.2225	1.7780	0.44144	0.65104	−0.13021
5	0.43223	0.63585	−0.63585	1.2668	2.1307	1.7045	0.35617	0.39603	0.10081
6	0.21063	0.58224	−0.58224	0.25829	0.58874	0.47099	0.13153	0.28604	0.12157
7				0.33314	2.2566	1.8053			
8				0.05854	0.64716	0.53405			
9				0.22869	0.68058	0.54528			

$J_1(\theta)$ and $J_3(\theta)$ do not contribute to the phase shifts for $l \geq 3$.

$\delta_1{}^l$, $\delta_2{}^l$, and $\delta_3{}^l$ are presented graphically in Fig. 1.

C. Yukawa Radial Form

We use

$$U(r)=U_0\frac{\exp(-r/\lambda)}{r/\lambda}, \tag{22}$$

$$U_0=68.0 \text{ Mev}, \quad \lambda=1.18\times10^{-13} \text{ cm}.$$

In this calculation, the unit of length was taken to be 10^{-13} cm, so that

$$k^2=0.0214E.$$

For the deuteron wave function we use

$$\phi(r)=\left[\frac{\alpha\beta(\alpha+\beta)}{2\pi(\alpha+\beta)^2}\right]^{\frac{1}{2}}\frac{\exp(-\alpha r)-\exp(-\beta r)}{r}, \tag{23}$$

where[21]

$$\alpha=0.2316, \quad \beta=1.268. \tag{24}$$

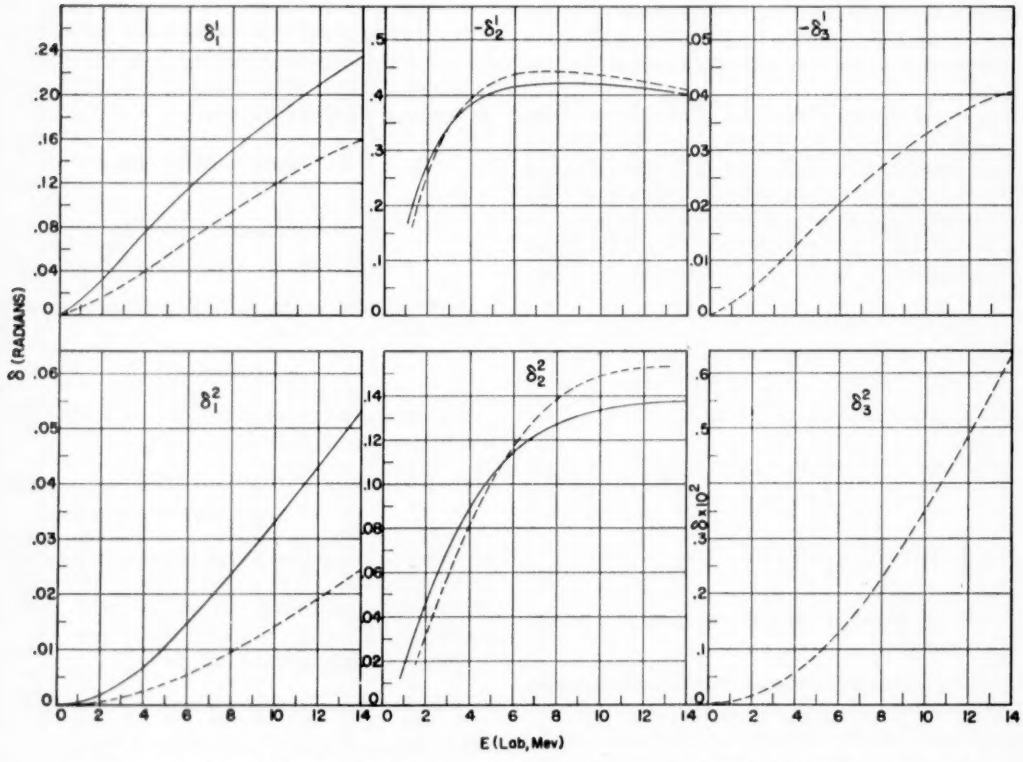

FIG. 1. Plots of $\delta_i{}^l$ for the Gauss (dotted curves) and Yukawa (solid curves) potentials as a function of energy.

[21] G. F. Chew, Phys. Rev. 74, 809 (1948). We have used Chew's value $\beta=5.5\alpha$. More recently, R. L. Gluckstern and H. A. Bethe, Phys. Rev. 81, 761 (1951), have given $\beta=7.0\alpha$. This makes little difference (see their footnote 32).

We find for $J_1(\theta)$:

$$\frac{k}{8\pi}J_1(\theta)=\frac{2k}{K}\left[\tan^{-1}\frac{K}{4\alpha}-2\tan^{-1}\frac{K}{2(\alpha+\beta)}+\tan^{-1}\frac{K}{4\beta}\right]\frac{g}{\nu^2+K^2}, \quad (25)$$

where

$$\nu=\frac{1}{\lambda}, \quad K=2k\sin\frac{\theta}{2}, \quad g=\frac{4M}{3\hbar^2}U_0\lambda\frac{\alpha\beta(\alpha+\beta)}{(\alpha-\beta)^2}=1.056, \quad (26)$$

and for $J_2(\theta)$:

$$\frac{k}{8\pi}J_2(\theta)=\frac{k}{K'}\left[\frac{1}{K'^2+\beta^2}-\frac{1}{K'^2+\alpha^2}\right]\times\left[\tan^{-1}\frac{K'}{\nu+\alpha}-\tan^{-1}\frac{K'}{\nu+\beta}\right]g, \quad (27)$$

where

$$K'=k(\cos\theta+5/4)^{\frac{1}{2}}. \quad (28)$$

A partial wave analysis is also made of these. Again $J_1(\theta)$ does not contribute to the phase shifts for $l\geq 3$. The calculations with a Gauss potential show that $J_3(\theta)$ is nearly spherically symmetrical and does not contribute appreciably to the phase shifts for $l\geq 1$, and exploratory numerical calculations of $J_2(\theta)$ showed that with a Yukawa potential it gives even smaller contributions to the phase shifts for $l\geq 1$. Rather than evaluate $J_3(\theta)$ numerically, we have assumed that it is also spherically symmetrical for a Yukawa potential.

$\delta_1{}^l$ and $\delta_2{}^l$ are presented graphically in Fig. 1.

D. Effect of the Coulomb Force in *p-d* Scattering

The *n-n* potentials are replaced by *p-p* potentials, of course. There are two additional integrals

$$C_1(\theta)=\frac{4M}{3\hbar^2}e^2\int\exp(-i\mathbf{k}'\cdot\mathbf{q})\phi(|\mathbf{r}|)\left(\frac{1}{|\mathbf{q}|}-\frac{1}{|\mathbf{q}+\tfrac{1}{2}\mathbf{r}|}\right)\exp(i\mathbf{k}\cdot\mathbf{q})\phi(|\mathbf{r}|)d\mathbf{r}d\mathbf{q}, \quad (29)$$

$$C_3(\theta)=\frac{4M}{3\hbar^2}e^2\int\exp(-i\mathbf{k}'\cdot\mathbf{q})\phi(|\mathbf{r}|)\left(\frac{1}{|\mathbf{q}|}-\frac{1}{|\mathbf{q}+\tfrac{1}{2}\mathbf{r}|}\right)\times\exp(-i\mathbf{k}\cdot(\tfrac{1}{2}\mathbf{q}+\tfrac{3}{4}\mathbf{r})\phi(|\mathbf{q}-\tfrac{1}{2}\mathbf{r}|)d\mathbf{r}d\mathbf{q}. \quad (30)$$

These allow for the fact that the deuteron's charge is not concentrated at its center, but distributed throughout it. The scattering amplitude is given by

$$4\pi f(\theta)=P[\alpha J_1(\theta)+\beta J_2(\theta)+\gamma J_3(\theta)+C_1(\theta)+\epsilon C_3(\theta)], \quad (31)$$

where

$$\epsilon=+1, \ S=\tfrac{3}{2}, \quad \epsilon=-1, \ S=\tfrac{1}{2}, \quad (32)$$

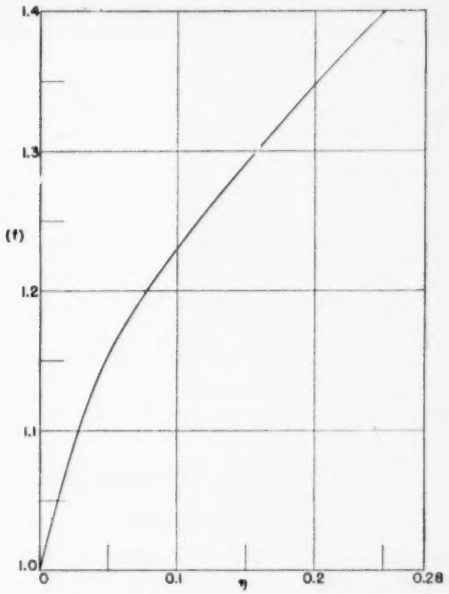

FIG. 2. f, a correction factor to the usual Coulomb penetration factor, defined by Eq. (34) *versus* η.

and P is a penetration factor given by

$$P=fC_0^2, \quad C_0^2=\frac{2\pi\eta}{\exp(2\pi\eta)-1}. \quad (33)$$

C_0^2 is the penetration factor one might use offhand. However, the regular Coulomb function $F(\rho)/\rho$ is greater than $C_0^2 j_l(\rho)$.[22] Therefore, C_0^2 over estimates the effect of the Coulomb force in reducing the *p-d* phase shifts from the *n-d* phase shifts. To correct for this, we have defined the penetration factor P as follows

$$P=\frac{\frac{1}{k^2}\int_0^\infty\exp(-2\alpha q)F_l(kq)F_l(2kq)(dq/q)}{\int_0^\infty\exp(-2\alpha q)j_l(kq)j_l(2kq)qdq}=fC_0^2. \quad (34)$$

We have used the zero range approximation for the integrals with Coulomb functions can be handled. f furns out to be independent of l. It is plotted as a function η in Fig. 2.

Actually, we have used only a mean value of f in calculating the Born approximation *p-d* phase shifts; namely

$$\bar{f}=1.273. \quad (35)$$

The integrals $C_1(\theta)$ and $C_3(\theta)$ are found to contribute nothing to the phase shifts for $l\geq 1$.

[22] Bloch, Hull, Broyles, Bouricius, Freeman, and Breit, Revs. Modern Phys. **23**, 147 (1951).

TABLE II. Born approximation phase shifts for p-d scattering (radians).

				For $l \geq 3$, ${}^2\delta_l = -\frac{1}{2}\,{}^4\delta_l$				
E (lab, Mev)	${}^4\delta_1$	${}^4\delta_2$	${}^4\delta_3$	${}^4\delta_4$	${}^4\delta_5$	${}^4\delta_6$	${}^2\delta_1$	${}^2\delta_2$
9.66	0.549	−0.127	0.0478	−0.0154	0.00618	−0.00246	−0.058	0.103
5.18	0.466	−0.101	0.0336	−0.0094			−0.116	0.064
3.49	0.380	−0.074	0.0204	−0.0049			−0.118	0.043
3.00	0.345	−0.064					−0.113	0.036
2.53	0.307	−0.053	0.0120	−0.0025			−0.110	0.029
2.08	0.264	−0.042					−0.096	0.023
1.61	0.212	−0.029					−0.082	0.016
1.51	0.200	−0.027	0.0043	−0.0006			−0.078	0.014
1.495	0.196	−0.026					−0.077	0.014
1.355		−0.022						0.011
1.23	0.162	−0.019					−0.065	0.010
1.105		−0.0164						0.0082
0.985		−0.0130						0.0065
0.825		−0.0099						0.0049
0.73		−0.0082						0.0041
0.6		−0.0062						0.0031
0.48		−0.0047						0.0023

V. ANALYSIS OF p-d EXPERIMENTS

A. Phase Shift Analysis

According to Eqs. (8), (11), and (21), the phase shifts are given by

$$\delta_l = \alpha\delta_1{}^l + \beta\delta_2{}^l + \gamma\delta_3{}^l, \tag{36}$$

where α, β, and γ are given by (9) for $S=\frac{3}{2}$ and by (10) for $S=\frac{1}{2}$.

In calculating the phase shifts, we have taken ${}^3V_{np}{}^+=1$, ${}^1V_{np}{}^+=0.69$ in agreement with the low energy n-p data. We have taken the odd parity potentials to be zero in agreement with the high energy n-p data. We have assumed that n-n, p-p, and n-p potentials are equal in equivalent states. Because of the small size of $\delta_1{}^l$ and $\delta_3{}^l$ compared with $\delta_2{}^l$ for $l \geq 1$, and because $\delta_2{}^l$ depends only on ${}^3V_{np}{}^+$, it does not matter much (not at all for $l \geq 3$) what we take for the odd parity forces or what we assume about the n-n and p-p potentials, a point returned to in Sec. VII-B. The phase shifts are tabulated in Table II.

Using these phase shifts as a starting point, a phase shift analysis of the p-d data in the energy range 0–10 Mev[1–4] is made using the rigorous expression (12). The method used in making the phase shift analysis is the same as that used by Dodder and Gammel in analyzing the p-He^4 elastic scattering data.[23] The phase shift analyses were performed on IBM card-programmed electronic calculators. The decks were prepared so that if fits could not be obtained with the S phase shifts alone, the P phase shifts could be changed from their values calculated in Born approximation and the data analyzed for them; the same is true of the D phase shifts.

The results of the phase shift analysis are given in Table III. Some improvement is obtained by allowing the ${}^4P$ phase shift to change from its value calculated in Born approximation. The ${}^4P$ phase shift found if this is done is compared with that calculated in Born approximation in Fig. 3. The ${}^2P$ phase shift and phase shifts for $l \geq 2$ agree with those calculated in Born approximation. In analyzing for the S phase shifts or the S and ${}^4P$ phase shifts, the ${}^2P$ phase shifts and phase shifts for $l \geq 2$ used are those calculated with the Yukawa shaped potential. No significance is to be attached to this since those calculated with the Gauss shaped potential would have served as well.

Calculated and experimental angular distributions are compared in Fig. 4. The effect of omitting the contribution of partial waves with $l \geq 3$ is illustrated in several figures, making it clear that the higher phase shifts are certainly necessary in the analysis.

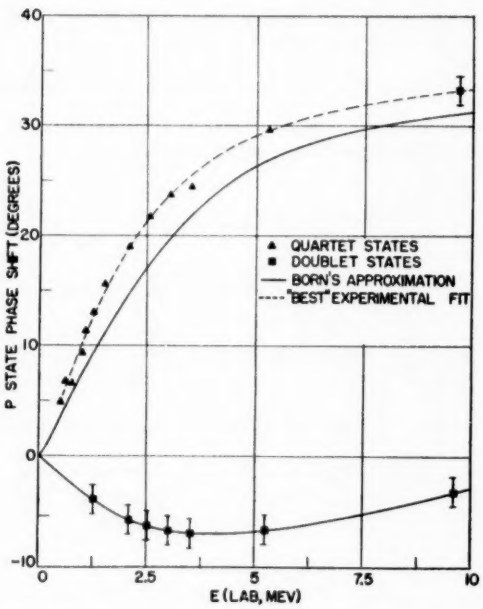

FIG. 3. Comparison of calculated and "experimental" P phase shifts.

[23] D. C. Dodder and J. L. Gammel, Phys. Rev. **88**, 520 (1952).

TABLE III. Results of phase shift analysis.

					^4P on Born approx.		
E	^4S	^2S	^4P	rms	^4S	^2S	rms
9.66	73.34°	79.05°	31.78°	3.2 percent	72.64°	78.65°	4.72 percent
5.18	−78.93°	−39.84°	29.73°	3.56 percent	−78.23°	−40.45°	5.13 percent
3.49	−66.94°	−22.2°	24.5°	6.70 percent			
3.00	−66.27°	−19.3°	23.77°	2.63 percent			
2.53	−61.01°	−17.1°	21.78°	2.0 percent			
2.08	−54.89°	−14.1°	18.93°	1.9 percent			
1.61	−52.48°		14.67°	0.9 percent			
1.51	−46.92°	−10.5°	15.76°	3.2 percent			
1.495	−49.27°		15.60°	1.46 percent			
1.355	−45.38°		14.33°	1.73 percent			
1.23	−44°		13.0°	2.1 percent			
1.105	−42.40°		11.54°	1.9 percent			
0.985	−38.50°		9.50°	1.67 percent			
0.73	−32.09°		6.69°	3.75 percent			
0.6	−27.5°		6.83°	2.58 percent			
0.48	−23.19°		5.08°	1.6 percent			

The question of how well the data determines a given phase shift is an important one. The p-d data at 5.2 and 9.7 Mev were carefully examined to determine how well the ^4S and ^2S phase shifts are determined with the phase shifts for $l \geq 1$ given values calculated in Born approximation. Figures 5(a) and (b) show plots of the sum of the squares of the percent deviations from the experimental points ($\sum$) as a function of the ^2S phase shift for several values of the ^4S phase shift. These make it possible to visualize a surface

$$\sum = \sum ({}^4\delta_0, {}^2\delta_0).$$

It can be seen that at 5.2 Mev. there are two solutions for the ^2S phase shift. The solution with ${}^2\delta_0 = 57°$ can be ruled out after the calculations of Sec. VI-B make it certain that the "$k \cot\delta$" plot for the ^2S state has a certain energy dependence. At 9.7 Mev, these two solutions blend, which makes for a very great uncertainty in the value of the ^2S phase shift. The ^4S phase shifts are reasonably well determined, however. All this has its origin in the fact that the doublet state makes only a small contribution to the elastic scattering. Unfortunately, only the ^2S phase shift is sensitive to the n-n forces in n-d scattering, and it is sensitive only to the singlet even parity n-n potential. As this analysis shows, the ^2S phase shift is hard to determine from the experimental data. In Sec. VII-B, further illustrations of the fact that wide changes in the ^2S phase shift do not affect the angular distribution are presented.

Uncertainties in quantities (phase shifts, "$k \cot \delta$") deduced from experiment are indicated on the graphs. These are based on studies similar to those described in the previous paragraph.

B. p-d Scattering Length and Effective Ranges

Plots of

$$\begin{aligned} &\text{"}k \cot \delta\text{"} = C_0^2 k \cot\delta + h(\eta)/R, \\ &R = \tfrac{3}{4}(\hbar^2/Me^2) = 21.6\times 10^{-13} \text{ cm}, \end{aligned} \tag{37}$$

for the ^4S and ^2S states are shown in Fig. 6. The scattering lengths are the set (2), and the effective range for the ^4S state is

$$\rho_4 = 1.99 \pm 0.07 \times 10^{-13} \text{ cm}. \tag{38}$$

For $S = \frac{1}{2}$, the scattering length is very short so that an effective range theory is not very useful. The large uncertainties in the ^2S phase shifts make it unadvisable to quote a value of ρ_2 deduced from experiment.

C. Connection between p-d and n-d Scattering Lengths

Blatt and Jackson[12] give the following connection between the p-p and n-p scattering lengths

$$\frac{1}{a_p} = \frac{1}{a_N} + \frac{1}{R}\left[\ln\frac{r_0}{R} + 0.330\right]. \tag{39}$$

They use for the wave function in the "internal" region

$$u = \sin(\pi r/2r_0).$$

Our wave functions (Sec. VI-B, Fig. 9) have maxima at about 2.0×10^{-13} cm. Taking this as an estimate of r_0, we find

$$1/a_p - 1/a_N = -0.095.$$

For the ^4S state, with our value of ${}^4a_p = 12.5\times 10^{-13}$ cm, this gives

$${}^4a_N = 5.7\times 10^{-13} \text{ cm}.$$

For the ^2S state, with our value ${}^2a_p = 1.4$, it gives

$${}^2a_N = 1.2\times 10^{-13} \text{ cm}.$$

Of course, the value for the doublet state means almost nothing because we cannot get an accurate value of ${}^2a_p$ from the experiments. Had we used a slightly larger value of r_0, the value for the quartet state would have been in better agreement with (1).

However, the set (4) is definitely ruled out, and the p-d scattering lengths indicate that the correct set of n-d scattering lengths is the set (1).

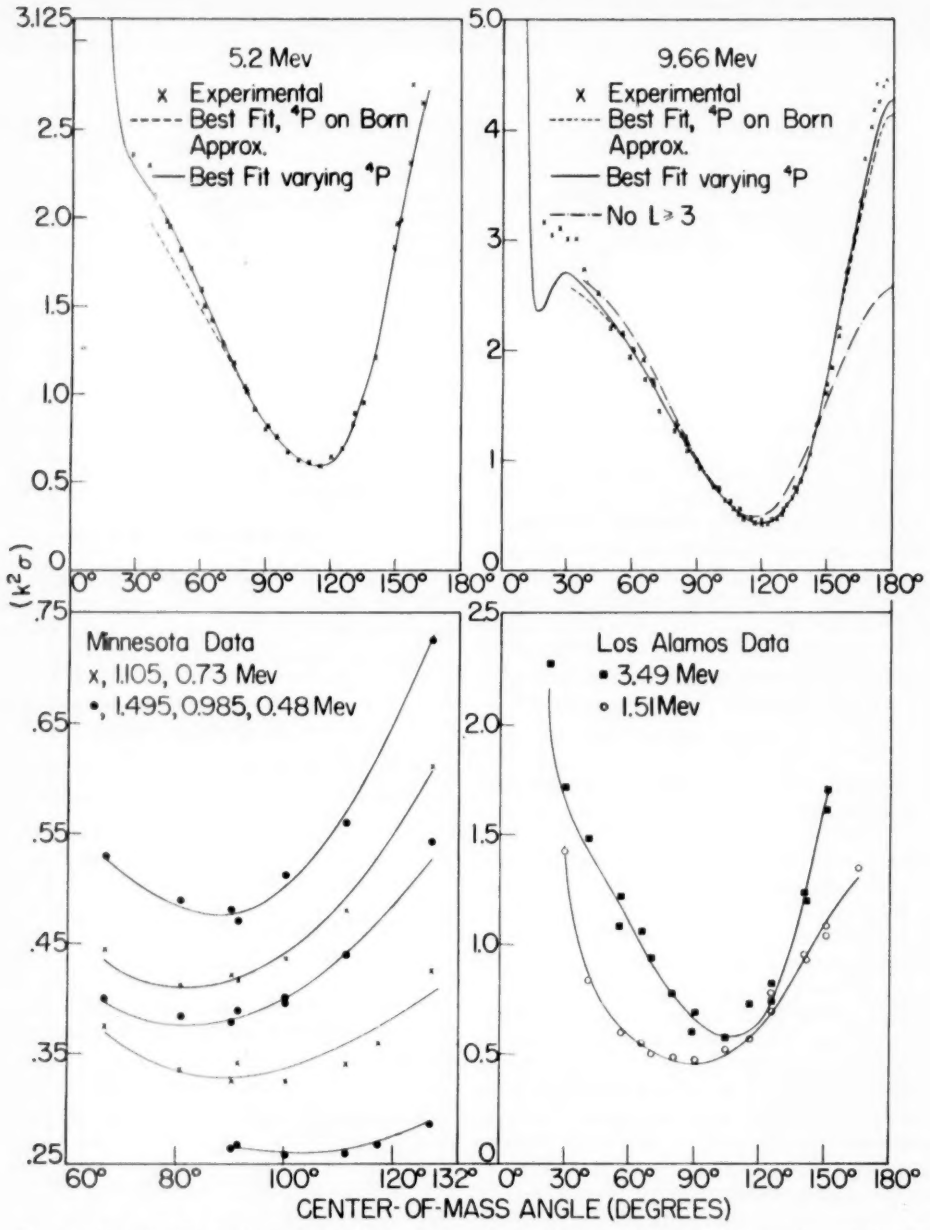

FIG. 4. p-d angular distributions calculated using S phase shifts adjusted to give best fits to experimental data. The The ordinate is the dimensionless quantity $k^2\sigma(\theta)$.

VI. S-STATE CALCULATIONS

A. Scattering Lengths, Effective Ranges

To support the conclusion of the last paragraph, we have calculated the n-d scattering lengths.

For $S=\frac{3}{2}$, assuming for purposes of illustration that the nuclear potentials are spin independent but that the odd parity forces are zero, the equations of motion are

$$T\psi' = -\tfrac{1}{2}U'\psi' - \tfrac{1}{2}(U''\psi' - U'\psi''),$$
$$T\psi'' = -\tfrac{1}{2}U'\psi'' - \tfrac{1}{2}(U'\psi' - U''\psi''). \quad (40)$$

This is written in Verde's notation.[16] This can be written

$$T\begin{pmatrix}\psi'\\ \psi''\end{pmatrix} = (U)\begin{pmatrix}\psi'\\ \psi''\end{pmatrix}, \quad (41)$$

where (U) is a matrix. Verde[16] gave the variational principle

$$\delta\int(\psi',\psi'')[T-(U)]\begin{pmatrix}\psi'\\ \psi''\end{pmatrix}d\tau_1d\tau_2d\tau_3=0. \quad (42)$$

In the no polarization approximation, ψ' and ψ'' are written

$$\begin{aligned}\psi'&=\tfrac{1}{2}\sqrt{3}\{\phi(12)f(3)-\phi(13)f(2)\},\\ \psi''&=-\phi(23)f(1)+\tfrac{1}{2}\phi(12)f(3)+\tfrac{1}{2}\phi(13)f(2),\end{aligned} \quad (43)$$

where ϕ is the wave function of the ground state of the deuteron and f is a function to be determined. The coordinate are labeled such that a pair of numbers indicate a vector extending from the first particle of the pair to the second number while a single number indicates a vector extending from that particle to the center of the other two remaining particles.

Substituting Eq. (43) into Eq. (42), eliminating integrals with $f(1)$ by permuting 1 and 2 (the integrals are invariant with respect to these permutations), varying $f(2)$ and $f(3)$ independently, and equating the coefficients of $\delta f(2)$ and $\delta f(3)$ to zero leads to a differential equation for $f(3)$:

$$\begin{aligned}(\nabla_3^2+k^2)f(3)-\int\phi(12)(\nabla_2^2+k^2)f(2)\phi(13)d\tau_1d\tau_2\\ =\int\phi(12)U(12)\phi(13)f(2)d\tau_1d\tau_2\\ -\tfrac{1}{2}\int\phi(12)U(13)\phi(12)f(3)d\tau_1d\tau_2\\ -\tfrac{1}{2}\int\phi(12)U(23)\phi(13)f(2)d\tau_1d\tau_2.\end{aligned} \quad (44)$$

The second term on the left and the first term on the right may be put in a different form by making use of the fact that $\phi(13)$ is a solution to the deuteron problem. We may then replace Eq. (44) by

$$\begin{aligned}(\nabla_3^2+k^2)\left[f(3)-\int f(2)\phi(13)\phi(12)d\tau_1d\tau_2\right]\\ =\int\phi(12)U(13)\phi(13)f(2)d\tau_1d\tau_2\\ -\tfrac{1}{2}\int\phi(12)U(13)\phi(12)f(3)d\tau_1d\tau_2\\ -\tfrac{1}{2}\int\phi(12)U(23)\phi(13)d\tau_1d\tau_2.\end{aligned} \quad (44')$$

Equations (44) and (44′) lead to identically the same results if ϕ is an exact solution of the deuteron problem. The exact time dependent equations of motion satisfy the reciprocity theorem;[24] that is, the transition probability for a process and its inverse (obtained by reversal of time) are equal. To insure this property for any choice of a trial function in which ϕ is not an exact solution, we must use a fifty-fifty mixture of Eqs. (44) and (44′).

Use of the zero energy Green's function $1/4\pi|\mathbf{r}_3-\mathbf{r}_3'|=1/4\pi R_3$ in (44′) leads to

$$\begin{aligned}f(3')=1+\int f(2)\phi(13')\phi(12)d\tau_1d\tau_2\\ +\int\frac{1}{4\pi R_3}\phi(12)U(13)\phi(13)f(2)d\tau_1d\tau_2d\tau_3\\ -\tfrac{1}{2}\int\frac{1}{4\pi R_3}\phi(12)U(13)\phi(12)f(3)d\tau_1d\tau_2d\tau_3\\ -\tfrac{1}{2}\int\frac{1}{4\pi R_3}\phi(12)U(23)\phi(13)f(2)d\tau_1d\tau_2d\tau_3.\end{aligned} \quad (45)$$

The first integral, which we call the "orthogonality" integral arises from the Pauli principle and vanishes in Born approximation. (Because of this term it appears

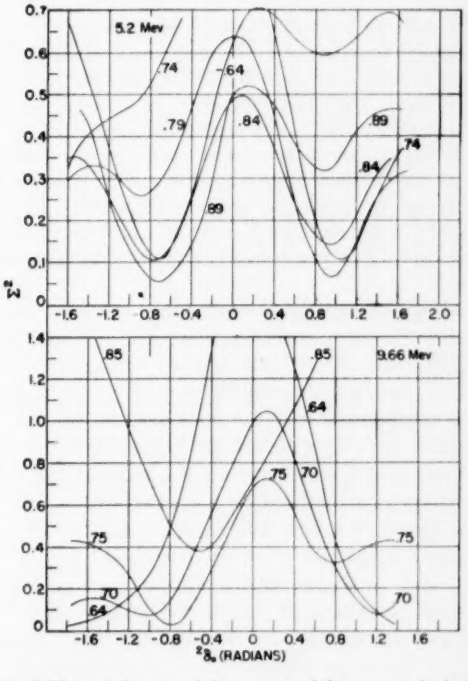

FIG. 5. Plots of the sum of the squares of the percent deviations of calculated points from experimental points *versus* the ^3S phase shift for several values of the ^1S phase shift (the curves are labeled with one-half of the value of the ^1S phase shift). At 5.2 Mev, 13 points are used; at 9.66 Mev, 15 points are used.

[24] B. A. Lippman and J. Schwinger, Phys. Rev. **79**, 469 (1950).

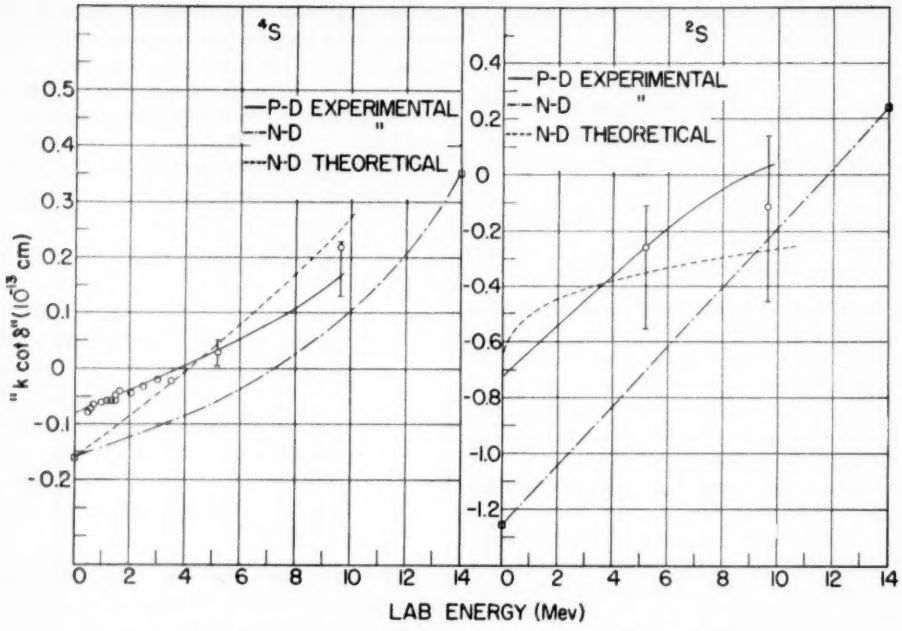

FIG. 6. Plots of "$k\cot\delta$" defined by Eq. (37) for the ^4S and ^2S phase shifts.

as though the interaction would be different from zero even if the force between the incoming particle and the deuteron were zero. However, the interaction between the deuteron and the incoming particle cannot be zero because of the identity of the two like particles unless the interaction of the two particles forming the deuteron is also zero.) When Born's approximation is made and the second, third, and fourth integrals examined asymptotically in the variable 3, they are of the form $J_2(\theta)$, $J_1(\theta)$, and $J_3(\theta)$, respectively, and are labeled accordingly.

Calculations were performed with three forms of J_2; namely, (1) that resulting from Eq. (44), (2) that resulting from a fifty-fifty mixture of Eqs. (44) and (44′), and (3) that resulting from Eq. (44′). In all these calculations, only the form of O in Eq. (44′) or (45) was used. This means that the scattering lengths resulting with the first and second forms of J_2 are not stationary as is the scattering length resulting with the third form. However, if ψ' and ψ'' (Eq. (43)) were exact solutions of the wave equations, $\phi(12)f(3)$, $\phi(13)$-$f(2)$, and $\phi(23)f(1)$ would also be exact (unsymmetrized) solutions of the wave equation, and both forms of O used with any combination of J_2's would lead to the same results. Thus a comparison of the results of the calculations with the forms (1) and (2) of J_2 and the results of the calculation with from (3) of J_2 reflects in some manner the adequacy of the no polarization approximation.

Motz and Schwinger had equations similar to Eq. (45), but their derivation is not based on a variational principle and did not contain the orthogonality integral.

For the rest, the procedure is the same as that of Motz and Schwinger. For this calculation we use the potential (17) and the wave function (19). The dummy variable and angle variables are integrated out leading to an equation of the form

$$qf(q)=q+\int K(q,q')q'f(q')dq', \tag{46}$$

where

$$K(q,q')=-\beta O(q,q')+\alpha J_1(q,q') +\beta J_2(q,q')+\gamma J_3(q,q'). \tag{47}$$

Here the dependence on the two body potentials has been put back in. Contour plots of the kernels $O(q,q')$, $J_1(q,q')$, both forms of $J_2(q,q')$ and $J_3(q,q')$ are shown in Fig. 7. Equation (46) was solved by replacing it by set of linear algebraic equations. Twenty points were used for this. Contributions to the integral from four times the deuteron radius were required and retained. The sets of linear equations were solved on the MANIAC.

The results of the calculation are summarized in Table IV. Graphs of $u(q)=qf(q)$ are shown in Fig. 8.

Effective ranges can be derived from $u(q)$. Verde[25] and Breit[26] have given formulas for the effective ranges.

[25] M. Verde, Atti accad. nazl. Lincei **8**, 228 (1950). (See also reference 6.)
[26] G. Breit, Revs. Modern Phys. **23**, 228 (1951).

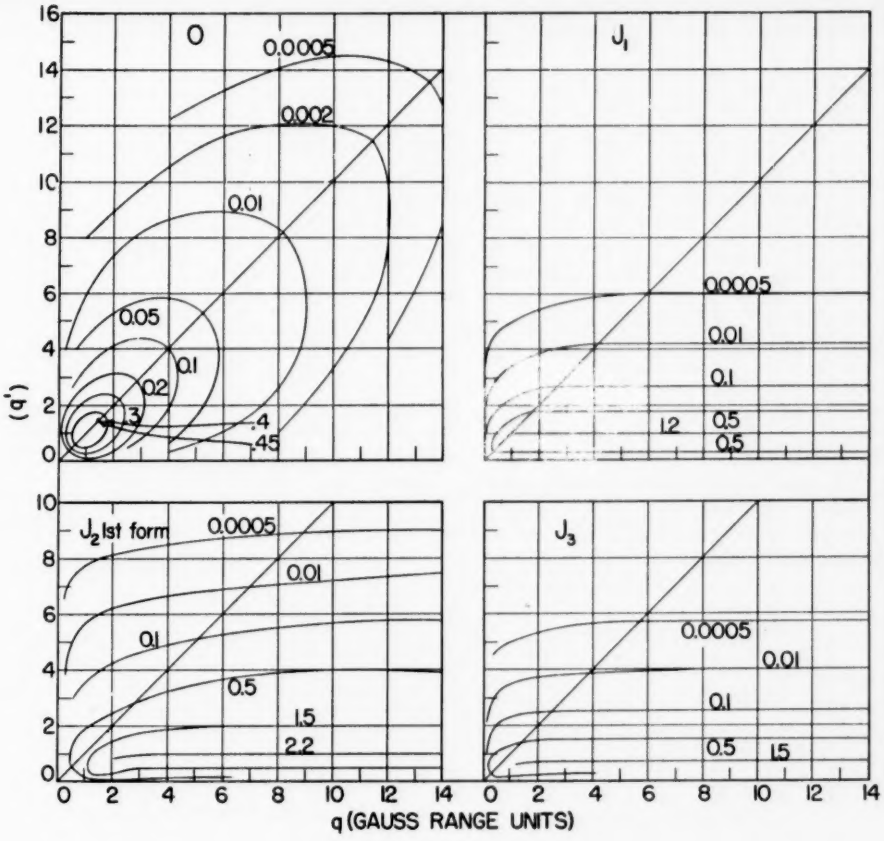

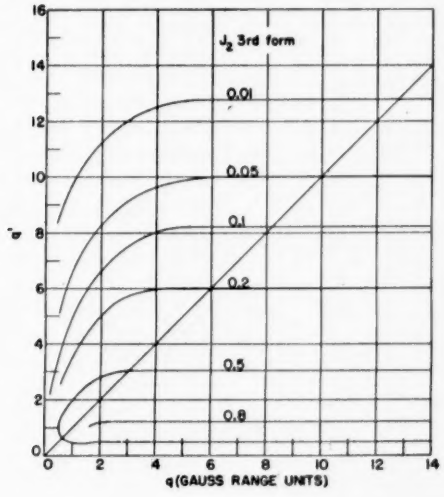

FIG. 7. Contour plots of the zero energy kernels q and q' are plotted in Gauss range units (1.332×10^{-13} cm). The value of the kernel in Eq. (46) is found from Eqs. (9), (10), and (47) with ${}^3V_{np}{}^+=1$.

TABLE IV. Results of scattering length calculations.

Case	${}^3V_{np}{}^+$	${}^1V_{np}{}^+$	${}^3V_{np}{}^-$	${}^1V_{np}{}^-$	${}^1V_{nn}{}^+$	${}^3V_{nn}{}^-$	Form of J_2	a_4 ($\times 10^{-13}$ cm)	a_2 ($\times 10^{-13}$ cm)
1	1	0.69	0	0	0.69	0	(1) As in Eq. (44)	6.398	1.651
							(2) Fifty-fifty mixture	5.871	1.544
							(3) As in Eq. (44′)	5.334	1.520
2	1	0.69	0	0	0.552	0	(1)	6.398	2.507
							(2)	5.871	
							(3)	5.334	
3	1	0.69	0	0	0.345	0	(1)	6.398	4.280
							(2)	5.871	
							(3)	5.334	
4	1	0.69	0	0	0	0	(1)	6.398	11.75
							(2)	5.871	9.774
							(3)	5.334	
5	1	0.69	1	0.69	0.69	1.0	(1)	6.396	
							(2)	5.903	1.412

These reduce in the no polarization approximation to

$$\rho_4=\frac{2r_0^3}{a_4^2}\left\{\int[(-q+a_4)^2-u^2(q)]dq + \int O(q,q')u(q)u(q')dqdq'\right\}, \quad (48)$$

for $S=\frac{3}{2}$, and

$$\rho_2=\frac{2r_0^3}{a_2^2}\left\{\int[(-q+a_2)^2-u^2(q)]dq - \tfrac{1}{2}\int O(q,q')u(q)u(q')dqdq'\right\}, \quad (49)$$

for $S=\frac{1}{2}$. The effective ranges are calculated with the wave functions resulting with the form (1) (see Table IV) for J_2 and the potentials of cases 1 and 3 of Table IV. The results are

$$\rho_4=2.9\times10^{-13}\text{ cm}, \quad \rho_2=45.1\times10^{-13}\text{ cm}. \quad (50)$$

However, we wish to stress that since these are not variationally determined quantities the error in using the no polarization approximation may be considerably larger than in the case of the scattering lengths.

B. *S* Phase Shifts 0–10 Mev

A very approximate calculation of the S-phases in the 0–10 Mev energy range was considered necessary from a theoretical standpoint because of the uncertainty in the experimental determination of the ${}^2S$ phase shifts. Most situations investigated so far in potential scattering have a bound state lying close to zero energy and the "$k\cot\delta$" plot extrapolates reasonably well into the negative energy region using the scattering length and zero energy effective range to give the binding energy approximately (as it does for the ${}^3S$ state in the two body problem). A square well which gives the binding energy of the extra neutron in the triton and the short n-d ${}^2S$ scattering length has a negative effective range. To eliminate this possibility, it was thought that a very elaborate calculation was not necessary since there is little likelihood that an equivalent potential could be found for the three body problem. We consider the finite energy extension of the no polarization approximation Eq. (45)

$$f(q)=\frac{\sin(kq)}{kq}+\left(\frac{4}{3}\right)^3\int\phi\left(\left|\frac{2}{3}\mathbf{q}+\frac{4}{3}\mathbf{q}'\right|\right)\phi\left(\left|\frac{2}{3}\mathbf{q}'+\frac{4}{3}\mathbf{q}\right|\right)f(q')d\mathbf{q}'+\left(\frac{4}{3}\right)^3\int\int\frac{\exp(ik|\mathbf{q}-\mathbf{q}''|)}{4\pi|\mathbf{q}-\mathbf{q}''|}$$
$$\times\phi\left(\left|\frac{2}{3}\mathbf{q}'+\frac{4}{3}\mathbf{q}''\right|\right)\tfrac{1}{2}\left[U\left(\left|\frac{4}{3}\mathbf{q}'+\frac{2}{3}\mathbf{q}''\right|\right)+U\left(\left|\frac{4}{3}\mathbf{q}''+\frac{2}{3}\mathbf{q}'\right|\right)\right]\phi\left(\left|\frac{4}{3}\mathbf{q}'+\frac{2}{3}\mathbf{q}''\right|\right)f(q')d\mathbf{q}'d\mathbf{q}''$$
$$-\frac{1}{2}\int\int\frac{\exp(ik|\mathbf{q}-\mathbf{q}'|)}{4\pi|\mathbf{q}-\mathbf{q}'|}\phi^2(|\mathbf{q}''|)U(|\mathbf{q}'+\tfrac{1}{2}\mathbf{q}''|)f(q')d\mathbf{q}'d\mathbf{q}''$$
$$-\frac{1}{2}\left(\frac{4}{3}\right)^3\int\int\frac{\exp(ik|\mathbf{q}-\mathbf{q}''|)}{4\pi|\mathbf{q}-\mathbf{q}''|}\phi\left(\left|\frac{4}{3}\mathbf{q}'+\frac{2}{3}\mathbf{q}''\right|\right)U\left(\left|\frac{2}{3}\mathbf{q}'-\frac{2}{3}\mathbf{q}''\right|\right)\phi\left(\left|\frac{2}{3}\mathbf{q}'+\frac{4}{3}\mathbf{q}''\right|\right)f(q')d\mathbf{q}'d\mathbf{q}''. \quad (51)$$

Employing the "zero range" approximation allows us to write

$$f(q)=\frac{\sin(kq)}{kq}+\left(\frac{4}{3}\right)^3\int\phi\left(\left|\frac{4}{3}\mathbf{q}+\frac{2}{3}\mathbf{q}'\right|\right)\phi\left(\left|\frac{4}{3}\mathbf{q}'+\frac{2}{3}\mathbf{q}\right|\right)f(q')d\mathbf{q}'$$
$$+\frac{1}{2}\Big\{(2r_0)^3\left(\frac{4\pi}{3}\right)U_0\langle\phi(r_0)\rangle_{Av}\int\frac{\exp(ik|\mathbf{q}+2\mathbf{q}'|)}{4\pi|\mathbf{q}+2\mathbf{q}'|}\phi(2q')f(q')d\mathbf{q}'$$
$$+(r_0)^3\left(\frac{4\pi}{3}\right)U_0\langle\phi(r_0)\rangle_{Av}\int\frac{\exp(ik|\mathbf{q}+\tfrac{1}{2}\mathbf{q}'|)}{4\pi|\mathbf{q}+\tfrac{1}{2}\mathbf{q}'|}\phi(q')f(q')d\mathbf{q}'\Big\}$$
$$-\tfrac{1}{2}(2r_0)^3\left(\frac{4\pi}{3}\right)U_0\int\frac{\exp(ik|\mathbf{q}-\mathbf{q}'|)}{4\pi|\mathbf{q}-\mathbf{q}'|}\phi^2(2q')f(q')d\mathbf{q}'-\tfrac{1}{2}(2r_0)^3\left(\frac{4\pi}{3}\right)U_0\int\frac{\exp(ik|\mathbf{q}-\mathbf{q}'|)}{4\pi|\mathbf{q}-\mathbf{q}'|}\phi^2(2q')f(q')d\mathbf{q}'. \quad (52)$$

Thus in "zero range" approximation the net effect is simply to change the "Green's function factor" from

$$\frac{1}{4\pi|\mathbf{q}-\mathbf{q}'|}\rightarrow\frac{\exp(ik|\mathbf{q}-\mathbf{q}'|)}{4\pi|\mathbf{q}-\mathbf{q}'|}, \quad (53)$$

for $J_1(q, q')$ and $J_3(q, q')$ type terms, and

$$\frac{1}{4\pi|\mathbf{q}+2\mathbf{q}'|}\rightarrow\frac{\exp(ik|\mathbf{q}+2\mathbf{q}'|)}{4\pi|\mathbf{q}+2\mathbf{q}'|}, \quad (54)$$

for the first form of $J_2(q, q')$, and by

$$\frac{1}{4\pi|\mathbf{q}+\frac{1}{2}\mathbf{q}'|}\rightarrow\frac{\exp(ik|\mathbf{q}+\frac{1}{2}\mathbf{q}'|)}{4\pi|\mathbf{q}+\frac{1}{2}\mathbf{q}'|}, \quad (55)$$

for the third form of $J_2(q, q')$. $O(q, q')$ remains unchanged. (It should be noted that only the spherically symmetric term in the expansion of the source function is necessary; however, to simplify the writing we have not indicated this. It is also interesting to note that these "zero range" forms of the "Green's function factor" for $J_2(q, q')$ are physically intelligible and represent a pick up process even when Born's approximation is not valid. The reason that $\frac{1}{2}\mathbf{q}'$ and $2\mathbf{q}'$ occur instead of $\mathbf{q}'$ when integrating the wave function in the neighborhood of the source function is that the neutron that we were originally following was picked up by the proton in the deuteron and afterward the wave function describes the motion of the "freed" neutron which will not originate at the point of collision. In the same manner we see it is justified to say that $J_3(q, q')$ represents a direct knock out" process.) We thus divided our zero energy kernels $K(q, q')$ of the previous section by the zero energy "Green's function factor." We believe this procedure eliminates most of the error arising from the fact that the range of the forces is not very small compared to the deuteron radius. The method should be satisfactory as long as $kr_0<1$. As 9.7 Mev, $kr_0=0.6$.

With these kernels we proceed as before, replacing the integral equations by sets of 20×20 linear systems. The wave functions are shown in Fig. 9, and the "$k\cot\delta$" plots are compared with those deduced from experiment in Fig. 6. The theoretical "effective ranges" determined in this way are in good agreement with those calculated in the preceding section. The results conclusively rule out the possibility mentioned at the beginning of this section. They also rule out the solution for the S phase shifts at 5.2 Mev which has ${}^2\delta_0=57°$ (see Sec. V-A, Fig. 5).

VII. *n-d* SCATTERING

A. *n-d* Angular Distributions

A phase shift analysis of the 14-Mev *n-d* data[27] is made. The results are summarized in Table V. Phase shifts for $l\geq2$ agrees with those calculated in Born approximation. The phase shift analysis makes it

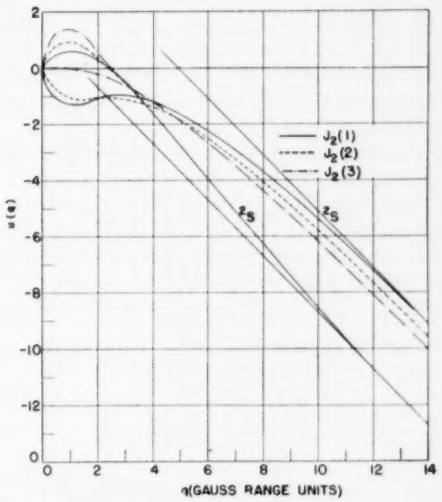

FIG. 8. Graphs of the zero energy radial wave functions $u(q)$ calculated with the "no polarization" approximation. Curves are labeled by $J_2(1)$, $J_2(3)$, and $J_2(2)$ depending upon whether the form of $J_2(q, q')$ has the form it has in Eq. (44), the Motz-Schwinger form, or a fifty-fifty mixture of the two, respectively. (Note: the ²S on the right in the figure should read ⁴S.)

[27] Allred, Armstrong, and Rosen (preceding paper), Phys. Rev. **91**, 90 (1953).

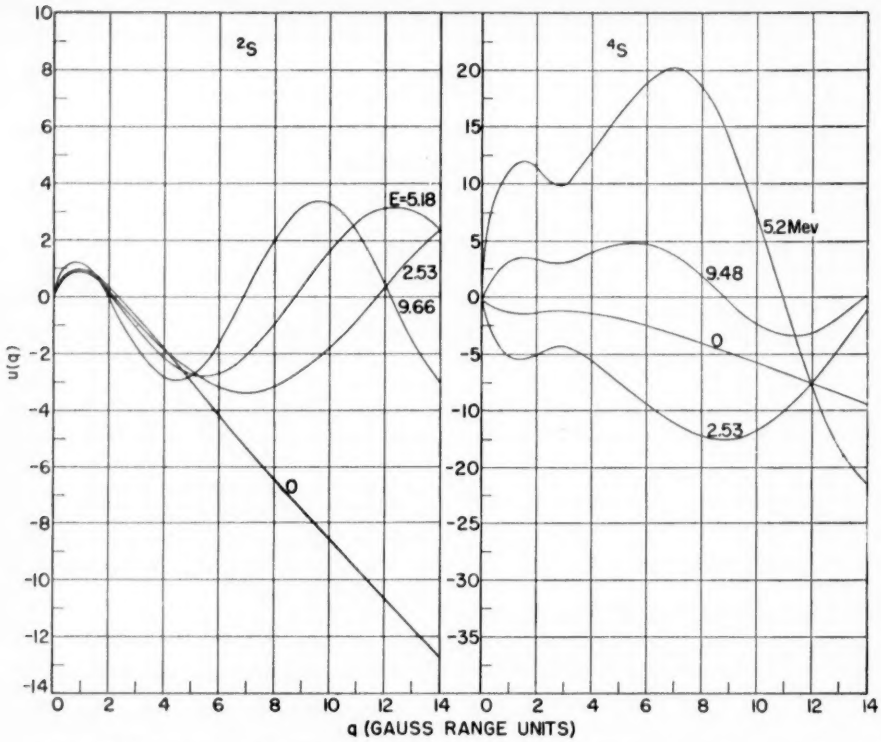

FIG. 9. Graphs of the radial S wave function $u(q)$ calculated with the "no polarization" approximation at several energies. The fifty-fifty mixture form of $J_2(q, q')$ is used in this calculation. The normalization is such that for large q, $u(q) = [\sin(kq) + \tan\delta \cos(kq)]/k$.

possible to pin down the 14-Mev points on the n-d "k cotδ" plots as shown in Fig. 6. The n-d "k cotδ" plots are completed by drawing them to intersect the zero energy axis at the points determined by the known n-d scattering lengths.[1]

This makes it possible to find the S phase shifts for any intermediate energy. Phase shifts for $l \geq 1$ are taken from the Born approximation. Angular distributions computed at 14, 5.5, and 3.27 Mev are shown in Fig. 10 and compared with the experimental data.[28,29] The agreement is good except for the low angle measurements at $E = 3.27$ Mev. This suggests that this data is not reliable because of a hydrogen contamination in the target.

TABLE V. Phase shift analysis of 14-Mev n-d data.

	Phase shift analysis	Born approximation
^4S	57.53°	
^2S	66.23°	
^4P	33.23°	29.91°
^2P	0.0±1.7°	0°
^4D	−3.217°	−3.217°
^2D	3.37°	3.37°
rms	26 points, 9.3 percent 23 points, 6.2 percent	

[28] Hamouda, Halter, and Scherrer, Phys. Rev. **79**, 539 (1950); I. Hamouda and G. de Montmollin, Phys. Rev. **83**, 1277 (1951).
[29] E. Wantuch, Phys. Rev. **86**, 679 (1952).

B. Sensitivity of n-d Scattering to n-n Forces

1. *Angular Distribution*

In Fig. 11, the effects of various potentials on angular distributions are shown. Effects of these potentials on partial waves with $l \geq 1$ could be estimated using Eqs. (9) and (10) because it has been found that the Born approximation is satisfactory for them. (When an increase in the ^4P phase shift was necessary to achieve a fit with experiment, it is assumed that all of the increase occurs in $J_2(\theta)$ in making these estimates; this is justified in Sec. VIII-A.1.) While there is less basis for estimating the effect of the n-n potentials on the S phase shifts it is shown in Fig. 11 that large changes in the ^2S phase shift do not affect the angular distributions. At 15 Mev, appreciable changes do occur near the minimum, but it is just at this point that the experiments are most inaccurate. The ^4S phase shift does not depend on $^1V_{nn}{}^+$ and is weakly dependent on $^3V_{nn}{}^-$ because $^3V_{nn}{}^-$ occurs with different signs in the coefficients of $J_1(\theta)$ and $J_3(\theta)$ (see the following Sec. VII-B.2).

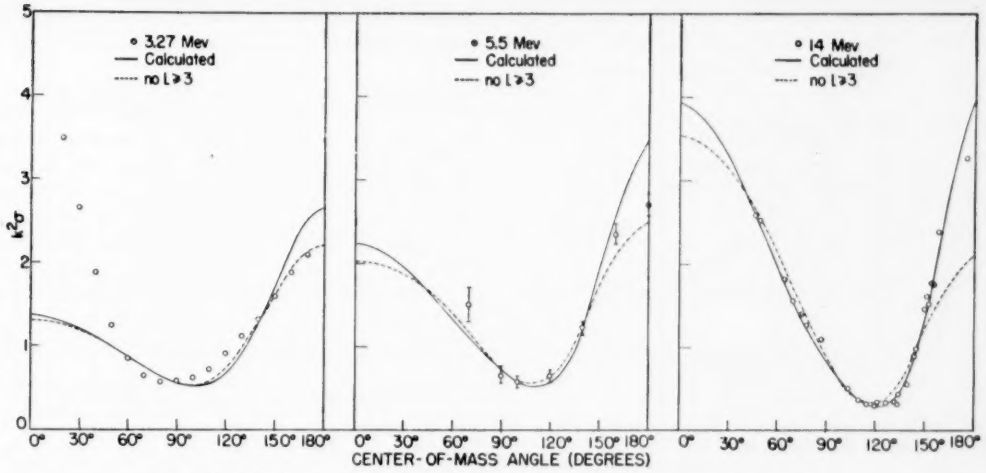

FIG. 10. Calculated and experimental *n-d* angular distribution at several energies.

2. *Scattering Lengths*

Table IV shows that the scattering lengths do not depend on the *n-n* potentials. The exception is the sensitive dependence on ${}^1V_{nn}{}^+$ of the ${}^2S$ scattering length. From the data of Table IV. a graph of the ${}^2S$ scattering length as a function of ${}^1V_{nn}{}^+$ is prepared and shown in Fig. 12.

Why is the *n-d* scattering insensitive to the *n-n* forces? The answer is contained in Eqs. (9) and (10). For states with $l \geq 1$, $J_2(\theta)$ is large compared to $J_1(\theta)$ and $J_3(\theta)$, but the coefficient of $J_2(\theta)$ depends only on ${}^3V_{np}{}^+$. For S states, $J_1(q, q')$ and $J_3(q, q')$ are about equal, so that terms with odd parity potentials cancel, since these occur with opposite signs in the coefficients of $J_1(q, q')$ and $J_3(q, q')$. The ${}^4S$ phase shifts do not depend on the even parity *n-n* potential, and the ${}^2S$ state contributes so little to the scattering that it hardly matters what the ${}^2S$-phase shifts are.

Were our theory stronger, we could deduce a value for ${}^1V_{nn}{}^+$ from Fig. 12. At first glance, Fig. 12 might suggest that ${}^1V_{nn}{}^+$ is small and the second of the scattering lengths (4) is permissible, but it must be re-

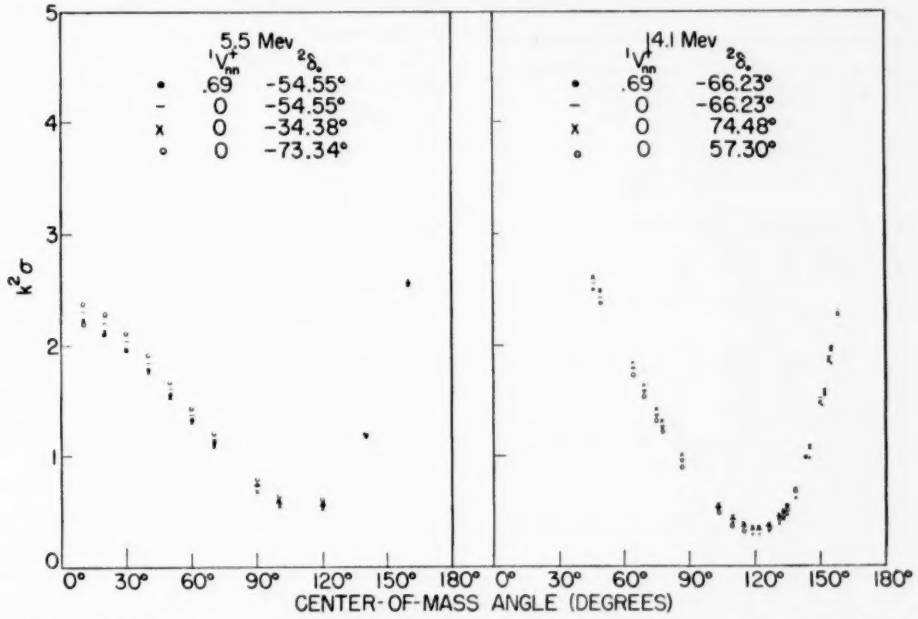

FIG. 11. Effect of the *n-n* potential on the *n-d* distributions. ${}^1V_{nn}{}^+=0.69$ is the value obtained assuming ${}^1V_{nn}{}^+ = {}^1V_{np}{}^+ = {}^1V_{pp}{}^+$. Also the effect of varying the ${}^2S$ phase shift is shown.

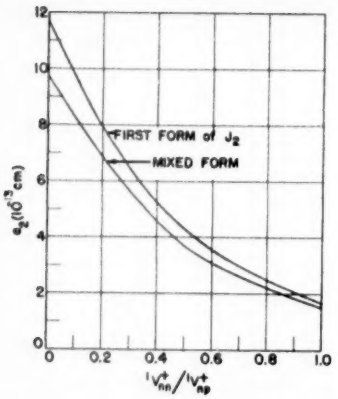

FIG. 12. The ^2S scattering length *versus* the ratio $^1V_{nn}^+/^1V_{np}^+$ for the first and second (mixed) form of $J_2(q, q')$.

membered that the first of the scattering lengths (4) does not follow from any combination of potentials allowed by the low energy two body data. Figure 12 strongly suggests that $^1V_{nn}^+=^1V_{np}^+$. It could not be much larger than $^1V_{np}^+$, otherwise there would exist a bound singlet state of the "di-neutron."

It is clearly indicated that a comparison of the binding energies of H^3 and He^3 should make it possible to set an accurate limit on $^1V_{nn}^+/^1V_{np}^+$.

VIII. THEORETICAL CONSIDERATIONS

A. Validity of Approximations

To discuss the various approximations made let us consider the quartet states using ordinary forces (no charge, spin, or parity dependence of the potentials). We assume the wave function for the *n-d* system may be expanded in the complete set of deuteron function labeled $\phi_\kappa(\mathbf{r})$ for the continuum states, so that

$$\psi(\mathbf{r},\mathbf{q})=\phi(r)f(\mathbf{q})+\int\phi_\kappa(\mathbf{r})f_\kappa(\mathbf{q})d\kappa \equiv\phi(r)f(\mathbf{q})+\chi(\mathbf{r},\mathbf{q}). \quad (56)$$

Substituting the antisymmetrical combination

$$\psi_A(\mathbf{r},\mathbf{q})=\psi(\mathbf{r},\mathbf{q})-\psi(\mathbf{q}+\tfrac{1}{2}\mathbf{r},\tfrac{3}{4}\mathbf{r}-\tfrac{1}{2}\mathbf{q}) =\psi(\mathbf{r},\mathbf{q})-\psi(\mathbf{r},\mathbf{q}), \quad (57)$$

into the variational principle (42) we find the following coupled integral equations for $f(\mathbf{q})$ and $\chi_A(\mathbf{r},\mathbf{q})$

$$\begin{aligned}f(\mathbf{q})=&\exp(i\mathbf{k}\cdot\mathbf{q})+\int\phi(r)[\phi(\mathfrak{r})f(\mathbf{q})+\chi_A(\mathbf{r},\mathbf{q})]d\mathbf{r}\\&+\int\frac{\exp(ik|\mathbf{q}-\mathbf{q}'|)}{4\pi|\mathbf{q}-\mathbf{q}'|}\\&\times\phi(r')[U(|\mathbf{q}'+\tfrac{1}{2}\mathbf{r}'|)+U(|\mathbf{q}'-\tfrac{1}{2}\mathbf{r}'|)]\\&+[\phi(r')f(\mathbf{q}')-\phi(\mathfrak{r}')f(\mathbf{q}')+\chi_A(\mathbf{r}',\mathbf{q}')]d\mathbf{r}'d\mathbf{q}',\end{aligned} \quad (58)$$

$$\chi_A(\mathbf{r},\mathbf{q})=\int K(rr';qq')[U(|\mathbf{q}'+\tfrac{1}{2}\mathbf{r}'|)+U(|\mathbf{q}'-\tfrac{1}{2}\mathbf{r}'|)] \times[\phi(r')f(\mathbf{q}')-\phi(\mathfrak{r}')f(\mathbf{q}')+\chi_A(\mathbf{r}',\mathbf{q}')]d\mathbf{r}'d\mathbf{q}',$$

where

$$\begin{aligned}&K(rr';qq')\\&=\int_{\kappa^2<k^2-\alpha^2}d\kappa\phi_\kappa(\mathbf{r})\frac{\exp(i(k^2-\alpha^2-\kappa^2)^{\frac{1}{2}}|\mathbf{q}-\mathbf{q}'|)}{4\pi|\mathbf{q}-\mathbf{q}'|}\phi_\kappa(\mathbf{r}')\\&+\int_{\kappa^2>k^2-\alpha^2}d\kappa\phi_\kappa(\mathbf{r})\frac{\exp(-(\kappa^2-k^2+\alpha^2)^{\frac{1}{2}}|\mathbf{q}-\mathbf{q}'|)}{4\pi|\mathbf{q}-\mathbf{q}'|}\phi_\kappa(\mathbf{r}'),\end{aligned} \quad (59)$$

and

$$\chi_A(\mathbf{r},\mathbf{q})=\chi(\mathbf{r},\mathbf{q})-\chi(\mathbf{r},\mathfrak{q}). \quad (60)$$

$\chi_A(\mathbf{r},\mathbf{q})$ gives the effect of including excited states of the deuteron in the expansion and therefore contains the effects of polarization (not caused by the exclusion principle) and inelastic scattering.

Let us consider then the effect of neglecting $\chi_A(\mathbf{r},\mathbf{q})$, (the so-called no polarization approximation). We may then make a partial wave analysis of $f(\mathbf{q})$ in the usual way

$$f(\mathbf{q})=\sum(i)^l(2l+1)\exp(i\delta_l)f_l(q)P_l(\mathbf{k},\mathbf{q}), \quad (61)$$

where

$$f_l(q)\rightarrow\sin(kq-\tfrac{1}{2}l\pi+\delta_l)/kq, \quad (62)$$

so that the resulting integral equation for $f_l(q)$ becomes

$$\begin{aligned}f_l(q)=&j_l(kq)+(-1)^l\left(\frac{4}{3}\right)^3\int\phi\left(\left|\frac{2}{3}\mathbf{q}-\frac{4}{3}\mathbf{q}'\right|\right)\phi\left(\left|\frac{4}{3}\mathbf{q}-\frac{2}{3}\mathbf{q}'\right|\right)P_l(\cos\mathbf{q}\mathbf{q}')f_l(q')d\mathbf{q}'\\&+\left(\frac{4}{3}\right)^3\int G_l(kq;kq'')\phi\left(\left|\frac{2}{3}\mathbf{q}'+\frac{4}{3}\mathbf{q}''\right|\right)\frac{1}{2}\left[U\left(\left|\frac{4}{3}\mathbf{q}'+\frac{2}{3}\mathbf{q}''\right|\right)+U\left(\left|\frac{4}{3}\mathbf{q}''+\frac{2}{3}\mathbf{q}'\right|\right)\right]\\&\times\phi\left(\left|\frac{4}{3}\mathbf{q}'+\frac{2}{3}\mathbf{q}''\right|\right)P_l(\cos\mathbf{q}',\mathbf{q}'')f_l(q')d\mathbf{q}'d\mathbf{q}''-\frac{1}{2}\int G_l(kq;kq')\phi^2(q'')U(|\mathbf{q}'+\tfrac{1}{2}\mathbf{q}'')f_l(q')d\mathbf{q}'d\mathbf{q}''\\&\times(-1)^l\frac{1}{2}\left(\frac{4}{3}\right)^3\int G_l(kq;kq'')\phi\left(\left|\frac{4}{3}\mathbf{q}'+\frac{2}{3}\mathbf{q}''\right|\right)U\left(\left|\frac{2}{3}\mathbf{q}'-\frac{2}{3}\mathbf{q}''\right|\right)\phi\left(\left|\frac{2}{3}\mathbf{q}'+\frac{4}{3}\mathbf{q}''\right|\right)\\&\times P_l(\cos\mathbf{q}',\mathbf{q}'')f_l(q')d\mathbf{q}'d\mathbf{q}'',\end{aligned} \quad (63)$$

where

$$G_l(kq; kq') = kj_l(kq_<) j_{-l}(kq_>), \tag{64}$$

where $j_l(kq)$ and $j_{-l}(kq)$ are the regular and irregular spherical Bessel functions of order l, respectively, and $q_<$ means the lesser of q and q'. In the above a fifty-fifty mixture of the possible forms of $J_2(q, q')$ is used. We have adopted the half exchange force and changed the normalization of $f_l(q)$ from that of Eq. (62). In the case of the S state these equations have been solved numerically. For the higher partial waves only the first Born approximation has been computed; that is, wherever $f_l(q)$ occurs inside the integrals it has been replaced by $j_l(kq)$.

1. *Validity of First Born Approximation for $l \geq 1$*

We shall compute the first-order distortion of the wave function and the corresponding second Born approximation to the phase shift. Fortunately, the distortion arising from $J_1(q, q')$ and $J_3(q, q')$ is small and may be neglected compared to that arising from $J_2(q, q')$ and $O(q, q')$. This is most easily seen from the "zero range" approximation in which the integrands in $J_1(q, q')$ (exclusive of the Green's functions) are of the nature of weak long-range potentials (exactly for $J_1(q, q')$) for which it is known that the Born approximation is quite good. The first-order distortion of the incident plane wave caused by terms which give rise to δ^1 and the "orthogonality" integral have been calculated numerically. In the case of the orthogonality term this has been done using the Gauss potential (17) and the deuteron wave function (19). The "zero range" approximation has been used in the calculation of the distortion caused by the $J_2(q, q')$ type term. This is not believed to lead to any appreciable error since the results of the first Born approximation for the zero range, Yukawa, and Gauss potentials were nearly the same (see Fig. 1). The first-order distorted ^4P wave function at 5 Mev is shown in Fig. 13. The corrected ^4P phase shift is 0.38 radian as compared to the first Born approximation value of 0.41 radian. The correction to the ^2P phase shift is $+0.016$ radian. This shows that the use of Born's approximation in the no polarization approximation leads to very little additional error. The distortion of the incident wave is even smaller for D and higher partial waves. Further justification comes from the calculation of Buckingham and Massey[15] who numerically integrated the no polarization equation (cast in a somewhat different form) and found results for the phase shifts agreeing closely with those of the Born approximation.

2. *Neglect of Tensor Forces*

Let us consider next the effect of tensor forces which are known to be necessary in the two body problem. When tensor forces are included, integrals of the type $J_1(\theta)$, $J_2(\theta)$, and $J_3(\theta)$ still occur.[18] Those of the type $J_1(\theta)$ and $J_3(\theta)$ are small compared to those of the type $J_2(\theta)$, so that the most important effects of tensor forces arise from integrals of the type $J_2(\theta)$. Fortunately, however, it is possible to eliminate the two body potentials in the Born approximation for $J_2(\theta)$. The result has been given previously in Eq. (17). In the presence of tensor forces the deuteron function is

$$\phi(r) + \frac{1}{\sqrt{2}} P_2(\boldsymbol{\sigma}, \mathbf{r}) \omega(r), \tag{65}$$

so that

$$\begin{aligned} J_2(\theta) = -\frac{4}{3}(P^2+\alpha^2) \Big\{ & \int \phi(r) j_0(Pr) r^2 dr \\ & + \frac{1}{\sqrt{2}} P_2(\sigma, \mathbf{P}) \int \omega(r) j_2(Pr) r^2 dr \Big\} \\ & \times \Big\{ \int \phi(r) j_0(Qr) r^2 dr \\ & + \frac{1}{\sqrt{2}} P_2(\sigma, \mathbf{Q}) \int \omega(r) j_2(Qr) r^2 dr \Big\}, \end{aligned} \tag{66}$$

where

$$\mathbf{P} = \tfrac{1}{2}\mathbf{k} + \mathbf{k}', \quad \mathbf{Q} = \mathbf{k} + \tfrac{1}{2}\mathbf{k}'.$$

From the above expression it is clear why $J_2(\theta)$ is not dependent upon the tensor character of the two body potential. First the S state part of the deuteron wave function is very little changed even in the presence of a strong tensor force. Secondly, the additional term in Eq. (66) which depends upon the D state part of the deuteron ground-state wave function are small because the D state part of the deuteron wave function is at most 20 percent of the amplitude of the S state part even for extremely strong tensor interactions. Its effect is further diminished because the Fourier-Bessel coefficients of order two rather than zero occur together with $\omega(r)$ in Eq. (66).

This argument is weakened for the S state calculations because $J_1(q, q')$ and $J_3(q, q')$ are not small and

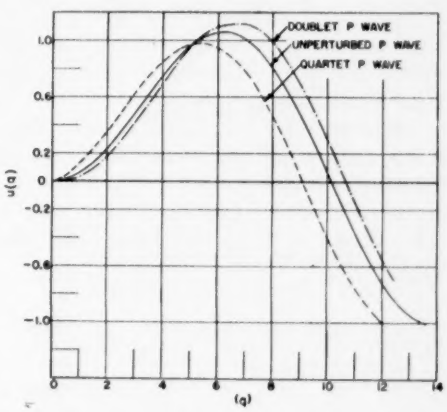

FIG. 13. The first-order distortion of the P-wave radial wave function $u(q)$ at 5 Mev.

the potential cannot be eliminated. However, $J_2(q, q')$ is still the most important kernel in determining the wave function for the quartet state. Since the potential may again be eliminated from this kernel, the effect of the tensor force in causing transitions to the ^2S state and altering the scattering length must be small. The effect on the ^2S state is probably more pronounced, but large errors in the ^2S phase shifts can be tolerated in calculating the angular distributions. However, neglect of tensor forces adds to the doubt about the accuracy of the ^2S scattering length calculation and makes it impossible to draw quantitative conclusions from Fig. 12.

3. *Effect of Polarization*

The effect of polarization has been estimated for zero energy using Eq. (58). The first approximation to $\chi_A(\mathbf{r}, \mathbf{q})$ is calculated from the second equation using the no polarization result. Then this is substituted into the first equation to find a correction to the scattering length. Again use is made of the "zero range" approximation in that all terms in which the combination $\phi(|\mathbf{q}+\frac{1}{2}\mathbf{r}|)U(|\mathbf{q}+\frac{1}{2}\mathbf{r}|)$ or $\phi_k(\mathbf{q}+\frac{1}{2}\mathbf{r})U(|\mathbf{q}+\frac{1}{2}\mathbf{r}|)$ does not occur in the integrands are neglected. All other terms are expected to be smaller by the first or second power of the ratio of the range of forces to the deuteron radius. The correction due to terms of the type retained is

$$\frac{\Delta f(q)}{q}=\frac{1}{16\pi^2}\int\frac{1}{|\mathbf{q}-\mathbf{q}''|}\phi(r)V(|\mathbf{q}''+\tfrac{1}{2}\mathbf{r}|)\phi_k(\mathbf{q}+\tfrac{1}{2}\mathbf{r})\times\frac{\exp(-(k^2+\alpha^2)^{\frac{1}{2}}|\frac{1}{2}\mathbf{q}''-\frac{3}{4}\mathbf{r}+\mathbf{q}'|)}{|\frac{1}{2}\mathbf{q}''-\frac{3}{4}\mathbf{r}+\mathbf{q}'|}\times\phi_k(\mathbf{r})V(|\mathbf{q}'+\tfrac{1}{2}\mathbf{r}'|)\phi(|\mathbf{q}'+\tfrac{1}{2}\mathbf{r}'|)\times\frac{f(|\frac{1}{2}\mathbf{q}'-\frac{3}{4}\mathbf{r}'|)}{|\frac{1}{2}\mathbf{q}'-\frac{3}{4}\mathbf{r}'|}d\mathbf{q}'d\mathbf{q}''d\mathbf{r}d\mathbf{r}'d\mathbf{k}. \quad (67)$$

For large q,

$$1/|\mathbf{q}-\mathbf{q}''|=1/q. \quad (68)$$

Using the "zero range" approximation, the correction to the scattering length is

$$\Delta a=\frac{1}{16\pi^2}\int d\mathbf{q}''d\mathbf{q}'d\mathbf{k}\phi_k(0)V_0{}^2\phi(0)\left[\frac{4\pi}{3}(2r_0)^3\right]^2\times\phi(2q'')\frac{\exp(-(k^2+\alpha^2)^{\frac{1}{2}}|2\mathbf{q}''+\mathbf{q}'|)}{|2\mathbf{q}''+\mathbf{q}'|}\phi_k(2\mathbf{q}')\frac{f(2q')}{2q'}. \quad (69)$$

Let

$$2\mathbf{q}''+\mathbf{q}'=\mathbf{Q}, \quad \mathbf{q}'=\mathbf{q}'. \quad (70)$$

The Jacobian of this transformation is $\frac{1}{8}$. Then

$$\Delta a=\frac{1}{16\pi^2}\frac{1}{8}\int d\mathbf{k}\phi_k(0)V_0{}^2\phi(0)\left[\frac{4\pi}{3}(2r_0)^3\right]^2\int d\mathbf{q}'\times\int d\mathbf{Q}\phi(|\mathbf{Q}-\mathbf{q}'|)\frac{\exp(-(k^2+\alpha^2)^{\frac{1}{2}}|\mathbf{Q}|)}{|\mathbf{Q}|}\times\phi_k(2\mathbf{q}')\frac{f(2q')}{|2\mathbf{q}'|}. \quad (71)$$

Now, with (16) for the deuteron wave function and $\beta=(\alpha^2+k^2)^{\frac{1}{2}}$, the integral over $\mathbf{Q}$ is

$$\left(\frac{\alpha}{2\pi}\right)^{\frac{1}{2}}\int d\mathbf{Q}\frac{\exp(-\alpha|\mathbf{Q}-\mathbf{q}'|)}{|\mathbf{Q}-\mathbf{q}'|}\frac{\exp(-\beta Q)}{Q}$$

$$=\frac{4\pi}{2q'}\left(\frac{\alpha}{2\pi}\right)^{\frac{1}{2}}\left\{\exp(-\alpha q')\int_0^{q'}\sinh\alpha Q\exp(-\beta Q)dQ+\sinh\alpha q'\int_{q'}^{\infty}\exp(-(\alpha+\beta)Q)dQ\right\},$$

$$=\frac{4\pi}{2q'\alpha}\left(\frac{\alpha}{2\pi}\right)^{\frac{1}{2}}\left(\frac{2\alpha}{k^2}\right)\exp(-\alpha q')\times(1-\exp(-(\beta-\alpha))q'),$$

$$\approx\frac{4\pi}{2\alpha}\left(\frac{\alpha}{2\pi}\right)^{\frac{1}{2}}\exp(-\alpha q'), \quad k<\alpha, \quad (72)$$

or

$$\approx\frac{4\pi}{k^2q'}\left(\frac{\alpha}{2\pi}\right)^{\frac{1}{2}}\exp(-\alpha q'), \quad k>\alpha,$$

so that

$$\Delta a=\frac{1}{16\pi^2}\frac{1}{8}\int_0^{\alpha}d\mathbf{k}\phi_k(0)V_0{}^2\phi(0)\left[\frac{4\pi}{3}(2r_0)^3\right]^2\times\frac{4\pi}{2\alpha}\left(\frac{\alpha}{2\pi}\right)^{\frac{1}{2}}\int d\mathbf{q}'\phi_k(2\mathbf{q}')\frac{f(2q')}{2q'}\exp(-\alpha q')+\frac{1}{16\pi^2}\frac{1}{8}\int_{\alpha}^{\infty}d\mathbf{k}\phi_k(0)V_0{}^2\phi(0)\left[\frac{4\pi}{3}(2r_0)^3\right]^2\times\int d\mathbf{q}'\frac{4\pi}{k^2q'}\left(\frac{\alpha}{2\pi}\right)^{\frac{1}{2}}\phi_k(2\mathbf{q}')\frac{f(2q')}{2q'}\exp(-\alpha q'). \quad (73)$$

We take

$$\phi_k(\mathbf{r})=\frac{1}{(2\pi)^{\frac{1}{2}}}\left(\exp(i\mathbf{k}\cdot\mathbf{r})+\frac{\exp(2i\delta_0)-1}{2i}\frac{\exp(ikr)}{kr}\right), \quad (74)$$

so that

$$\lim_{r_0\to 0} r_0\phi_k(r_0)=\frac{1}{(2\pi)^{\frac{1}{2}}}\exp(i\delta_0)\frac{\sin\delta_0}{k}. \quad (75)$$

Then

$$\lim_{r_0\to 0} r_0\phi_k(r_0)=\frac{1}{2\pi\alpha^{\frac{1}{2}}}\lim_{r_0\to 0} r_0\phi(r_0), \quad k<\alpha, \quad (76)$$

since in zero range approximation

$$\sin\delta_0=-k(\alpha^2+k^2)^{-\frac{1}{2}}. \quad (77)$$

For $k<\alpha$, we take

$$\phi_k(2\mathbf{q}')=\frac{1}{2\pi\alpha^{\frac{1}{2}}}\left(\frac{\alpha}{2\pi}\right)^{\frac{1}{2}}\frac{\exp(-2\alpha q')}{2\alpha q'}, \quad (78)$$

that is, we assume that the shape of the wave function for a low excited state of the deuteron is the same as the shape of the ground-state wave function out to the deuteron radius for $k<\alpha$.

The second integral with $k>\alpha$ cuts off for several reasons. It can be seen from Eq. (75) that $\phi_k(0)$ decreases as $1/k$. The zero range approximation is not very reasonable for large k because the continuum wave function oscillates inside the potential once $kr_0>1$ which of course cuts off the integral. In the following we drop out the second integral.

Let

$$B=\frac{4\pi}{3}(2r_0)^3\frac{4}{3}\frac{M}{\hbar^2}U_0\phi(0). \quad (79)$$

Substituting Eq. (78) and Eq. (76) into Eq. (73), the integral over k gives just $(4\pi/3)\alpha^3$. Then if $\alpha q'=x$,

$$\Delta a=\frac{B^2}{384\pi^2}\int_0^\infty dx f\left(\frac{2x}{\alpha}\right)\exp(-3x). \quad (80)$$

In "zero range" approximation, the part of the scattering length arising from terms of the type $J_2(q, q')$ is

$$a=\left(\frac{\alpha}{2\pi}\right)^{\frac{1}{2}}\frac{B}{4}\int_0^\infty dx f\left(\frac{2x}{\alpha}\right)\exp(-2x). \quad (81)$$

The integral which occurs in (81) is less than the integral in (82) because of the exponential factors. However, taking as an estimate of the effect of polarization just the ratio of coefficients

$$\frac{\Delta a}{a}=\frac{4B}{384\pi^2}\left(\frac{2\pi}{\alpha}\right)^{\frac{1}{2}}\approx 0.19. \quad (82)$$

Thus it seems that polarization could change the ^4S scattering length calculations by about 20 percent. The third form of $J_2(q, q')$ gives a ^4S scattering length which is about 15 percent too low. One does not believe the estimate for the ^2S state because the scattering length is so short (were the scattering length calculated in "zero range" approximation zero, the percentage correction would be infinite). Probably the absolute correction is about the same for both states, about 1×10^{-13} cm, so that our ^2S calculations are untrustworthy.

4. *Inelastic Scattering*

Our calculated total elastic cross section at 14.1 Mev is 0.62 barn as compared to an experimental total cross section of 0.79 barn. This makes the inelastic cross section about 0.17 barn. This is larger than the value 0.05 barn quoted by Coon and Taschek.[14]

5. *Use of the Exact Scattering Formula*

We wish to emphasize that it is necessary to use the rigorous scattering formula in the calculation of the angular distributions even though the higher phase shifts are calculated in Born approximation. The imaginary part of the scattering amplitude [Eq. (12)] is not small compared to the real part because the S phase shifts are large. Thus, for example, even if the D phase shifts are small, S-D interference may lead to considerable angular variation in the cross section arising from the imaginary part of the scattering amplitude.

Use of the rigorous Eq. (12) guarantees that the scattering matrix is unitary so that at least one does not get theoretical nonsense.

It is worth noticing that a variational expression for the higher phase shifts can be derived similar to that derived for the S phase shifts, where now the form of $f_l(q)$ is not varied but the trial function is the appropriate plane wave component times a deuteron wave function. Then instead of Eq. (36) we find

$$\tan\delta_l=\alpha\delta_1{}^l+\beta\delta_2{}^l+\gamma\delta_3{}^l,$$

where $\delta_i{}^l$ is given as before by Eq. (21). Because the $\delta_i{}^l$'s are small, Eq. (36) and the equation above give numerically equivalent results. The point is that if we use the rigorous scattering formula, we have a variational calculation of the angular distribution.

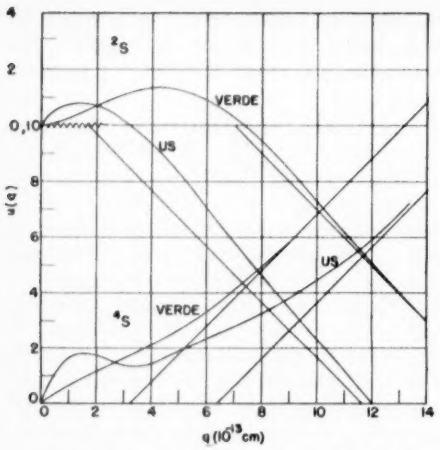

FIG. 14. Comparison of the zero energy radial wave functions determined by Verde (reference 25) and the present authors. (Note the difference in the zero of the ordinate for the quartet and doublet states.)

B. Comparison with and Criticism of Previous Work

It has been thought that since states of higher angular momentum appear at lower energies in *p-d* and *n-d* scattering than in *n-p* or *p-p* scattering the exchange nature of nuclear forces would be determined at lower *p-d* and *n-d* energies. This argument received some support from the calculations of Buckingham and Massey. At that time, (1941), nuclear ranges were generally taken somewhat longer than recent determinations have shown are necessary. Furthermore, nothing was known about the exchange nature of the forces and they assumed large forces in the odd parity states. It is known from *n-p* and *p-p* scattering that actually the odd parity forces are quite weak. Thus their two assumptions combined to give great theoretical promise for the determination of exchange forces in the 5- to 10-Mev region. The calculations presented here with more realistic internucleonic forces suggest that the scattering is determined primarily by the even parity *n-p* potentials. Possibly the only advantage to be gained in *n-d* or *p-d* scattering stems from the increase by a factor 1.33 of the energy in the center of mass system. This advantage is more than offset by the greater theoretical complexity of the problem.

Critchfield[30] has made a phase shift analysis of the data of reference 2. He assumes that the ^4S and ^2S phase shifts are equal and finds some justification for this in the work of Buckingham and Massey. However, it is known that the ^4S and ^2S *n-d* scattering lengths are unequal, so that it is unlikely that the ^4S and ^2S phase shifts are equal. With a different approach to the phase shift analysis, we were able to avoid this assumption. The data at these energies admit of many solutions for the phase shifts and it is necessary to start with some idea of what they should be in fitting the data. We have used the scattering lengths as a guide in finding the *S* state phase shifts and the Born approximation as a guide in finding the phase shifts for partial waves with $l \geq 1$.

Other workers[31] studying the 5-Mev data on *n-d* scattering have used Critchfield's method and tried to draw conclusions from the work of Buckingham and Massey about the exchange character of nuclear forces. Latter and Latter[32] avoided the assumption that the ^4S and ^2S phase shifts are equal. Although the neglect of partial waves with $l \geq 3$ is not justified at 5 Mev (see figures) perhaps the most severe criticism of both these works is that data at only one energy is examined, and it is impossible to correlate the results with the known *n-d* scattering lengths.

Previous calculations of the scattering lengths exist. Gordon[7] replaced the *n-d* interaction by an effective central potential. This could be done if $O(q, q')$, $J_2(q, q')$, and $J_3(q, q')$ had the form of $J_1(q, q')$; that is, if for a given q', they were linear in q to $q=q'$ and constant thereafter. However, they do not have this form.

Prohammer and Welton[8] assumes that the "k cotδ" plot for the doublet state in *n-d* scattering should extrapolate to the binding energy of the triton, just as the *n-p* "k cotδ" for the triplet state extrapolates to the binding energy of the deuteron in *n-p* scattering. However, since we know that the potential Eq. (17) gives the scattering lengths Eq. (3) and the binding energy of the triton at least approximately, we can conclude only that this is not the case for the ^2S state in the three body problem.

The wave functions found by Troesch and Verde[6] are compared with ours in Fig. 14. Our calculation is equivalent to theirs except we have a continuum of variational parameters where they had only a few.

IX. CONCLUSIONS

The excellent fits obtained of both *n-d* and *p-d* angular distributions attest to the reasonableness of our calculations. The close agreement between phase shifts calculated using Born's approximation in states with $l \geq 1$ and a "no polarization" approximation in the *S* states with those found from the phase shift analysis provide strong *a posteriori* justification for the approximations. The neglect of deuteron polarization has been shown on theoretical ground to give little error in the case of the ^4S state, and because of its unimportance in scattering, to give no serious discrepancy for the ^2S state. In higher angular momentum states polarization is of even less importance and it has been shown that

[30] C. L. Critchfield, Phys. Rev. **73**, 1 (1948).

[31] M. M. Gordon and W. D. Barfield, Phys. Rev. **86**, 679 (1952).
[32] A. L. Latter and R. Latter, Phys. Rev. **86**, 727 (1952).

for the P states the distortion of the incident waves may be neglected, allowing one to use the Born approximation. Since the major physical process that determines the phase shifts in the higher angular momentum states at low energies has been shown to be the pick up by one of the particles in the deuteron of the incident particle to form a "new" deuteron, the two body force of primary importance is the triplet even parity n-p force. It has been further shown that only very slight differences occur in the phase shifts depending upon the range, shape, or tensor nature of this force, it being sufficient to bind the deuteron. Thus tensor forces may be replaced by central forces in the higher states. In the S states, the neglect of tensor forces is not so justified; however, even here the pickup process accounts for a major portion of the scattering.

The calculated phase shifts are hardly dependent upon the nature of the odd parity two body interaction for any reasonable choice of the parameters.

The ^2S phase shifts are sensitive to the even parity singlet interactions. However, since this is the state in which the calculations are most susceptible to error due to the "no polarization" approximation in the calculations and the difficulty in determining the phase shifts from experimental data, the limits on the singlet n-n potential in terms of the singlet n-p potential can not be accurately determined. It is extremely improbable though that the singlet n-n potential depth is less than 0.7 that of the singlet n-p potential depth if they both have the same radial dependence. It is quite likely that very accurate limits on the n-n singlet depth could be determined by a comparison of the binding energies of H^3 and He^3.

It is a pleasure to acknowledge the continued encouragement of John Allred, Alice Armstrong, and Louis Rosen of group P-10 of this laboratory. Many members of group T-1 assisted with the hand calculations, especially Max Goldstein and William Anderson. Richard von Holdt developed the method for solving systems of linear equations used in the S state calculations, and Lois Cook coded this method and prepared the S state calculations for the MANIAC.

Matrix Elements of β-Decay in *jj* Coupling

IGAL TALMI
Palmer Physical Laboratory, Princeton University, Princeton, New Jersey
(Received March 23, 1953)

Matrix elements of various allowed β-transitions are calculated in the *jj* coupling scheme. It is found that for Gamow-Teller matrix elements there is no distinction between favored and unfavored transitions, which appears to be in contrast with the experimental facts.

THE success of the shell model in explaining the experimental facts about the low-lying levels of nuclei is often attributed to the *jj* coupling scheme. Yet one could think of a model in which the order of the single nucleon levels is that of, say, the harmonic oscillator potential well but in which the order of the different states is determined by short-range attractive forces in the *LS* coupling scheme; this model would successfully explain the spins and parities of the low-lying nuclear levels. Whereas in the *jj* coupling model the strong spin-orbit interaction accounts for the magic numbers, in an *LS* coupling model some assumption is required which will lead to a break in the energy of the l shell after the filling of the first $2l+2$ (identical) nucleons. Also, spin-orbit interaction does not lead to *jj* coupling unless it is large as compared to the mutual interaction. In the light of these facts it seems interesting to test the *jj* coupling wave functions by using them to calculate matrix elements of allowed β-transitions in light nuclei. Although it might be argued that in these cases *jj* coupling is not fully manifested, it is not unreasonable to assume that it can already serve as a good approximation. The results show that *jj* coupling is not an adequate scheme in the mass range in which image transitions occur.

In the supermultiplet theory, which yields an *LS* coupling scheme, β-transitions are allowed only between states which belong to the same supermultiplet.[1] If small deviations from Wigner's first approximation[2] take place, supermultiplets will mix and transitions which were forbidden will occur; yet their matrix elements will be smaller than those of the transitions which were allowed. This can explain the occurrence of distinct favored and unfavored transitions among those which are allowed according to the spin, parity, and isotopic spin selection-rules. (These allowed transitions are separated into distinct favored and unfavored groups, characterized by widely separated values of the ft values.) In *jj* coupling there are no supermultiplets but only charge multiplets, and one cannot see any selection-rule that will make a distinction between the Gamow-Teller matrix elements of favored and unfavored transitions. The Fermi matrix elements between two states will vanish also in *jj* coupling, unless the two states have the same value of the isotopic spin T and belong to the same charge-multiplet, and will, therefore, contribute to transitions between ground states only in the case of mirror nuclei. It can be said that in *jj* coupling there is a strong mixing of supermultiplets and this destroys the distinction between favored and unfavored transitions, yet it could be hoped that the complexity (in this sense) of the *jj* coupling wave functions would yield big matrix elements for the actually observed favored transitions and small matrix elements for the unfavored.[3] The cases in which matrix elements were calculated before[4] did not justify such a hope, and the calculations presented here show more clearly that matrix elements of transitions which are found experimentally to be favored are not essentially bigger (and even smaller in some cases) than those of transitions with much higher ft values. Also, Feenberg[5] has carried out similar calculations and arrived at the same results. This shows that the *jj* coupling scheme does not give a good approximation to the wave functions at least in the region where the distinction between favored and unfavored transitions is observed. The highest A for which this is found in $A=43$, which is already in the region of what is described as the $f_{7/2}$ shell. For higher A, image transitions are not observed and no definite conclusions can be drawn.

In the following, we shall use the isotopic spin formalism and the method of tensor operators[6] in the calculation of the β-decay matrix elements. The operator which causes the transitions is a double tensor and has the form

$$\mathfrak{M}_q^{(k)} = \sum_i \tau_{\eta i} B_{qi}^{(k)}, \tag{1}$$

where $\tau_\eta = \sqrt{2}(t_{+1}+t_{-1})$ and $B_q^{(k)}$ is a tensor operator of

[1] E. P. Wigner, Phys. Rev. **56**, 519 (1939).
[2] E. P. Wigner, Phys. Rev. **51**, 106 (1937).

[3] One has in mind the case of the spin of the ground state which is the same in the case of short-range forces in *LS* coupling and in *jj* coupling and the example of the magnetic moment of the ground state in the case of n (odd) identical nucleons. This has the Schmidt value either in the ground state j^n, $J=j$ or in the ground state of l^n, ^2l_j. In this case the magnetic moment is an odd tensor operator (being simply a vector) and its value depends on the seniority of the state but is independent of n, and as the case of $v=1$ in both coupling schemes is the case of a single nucleon, the values of the magnetic moments are equal for $v=1$ in *LS* coupling and in *jj* coupling. The Gamow-Teller operator is, however, an even double tensor (as a part of the magnetic moment is in the general case) and therefore not independent of n, so that the property described here should not necessarily hold.
[4] E. P. Wigner, "The *jj* Coupling Shell Model for Nuclei," Wisconsin Lecture Notes, 1952 (unpublished).
[5] E. Feenberg, *Nuclear Shell Structure* (Princeton University Press, Princeton, to be published).
[6] G. Racah, Phys. Rev. **62**, 438 (1942). The notation defined there will be used in this paper.

degree k ($k=0$, $B_0^{(0)}=1$ for Fermi interaction, whereas $k=1$, $B_q^{(1)}=\sigma_q$ for Gamow-Teller interaction). In order to illustrate the method of calculation we derive here the matrix elements for the case of a single nucleon β-decay in this formalism.

The matrix element of (1) between the state characterized by l, j, m, $t=\frac{1}{2}$, $t_z=\frac{1}{2}$ and the state l, j', m', $t'=\frac{1}{2}$, $t_z'=-\frac{1}{2}$ is given by

$$\begin{aligned}(\mathfrak{M}_q^{(k)})_{mm'} &= (ljm\tfrac{1}{2}\tfrac{1}{2}|\tau_\eta B_q^{(k)}|lj'm'\tfrac{1}{2}-\tfrac{1}{2})\\ &= (-1)^{j+m+\frac{1}{2}+\frac{1}{2}}(lj\tfrac{1}{2}\|\sqrt{2}tB^{(k)}\|lj'\tfrac{1}{2})\\ &\quad\times V(jj'k;-mm'q)V(\tfrac{1}{2}\tfrac{1}{2}1;-\tfrac{1}{2}-\tfrac{1}{2}1)\\ &= -(-1)^{j+m}\sqrt{2}(\tfrac{1}{2}\|t\|\tfrac{1}{2})V(\tfrac{1}{2}\tfrac{1}{2}1;-\tfrac{1}{2}-\tfrac{1}{2}1)\\ &\quad\times(lj\|B^{(k)}\|lj')V(jj'k;-mm'q),\end{aligned}\quad(2)$$

as in this case only t_{+1} contributes to the transition. Introducing the values

$$(\tfrac{1}{2}\|t\|\tfrac{1}{2})=(\tfrac{3}{2})^{\frac{1}{2}}\quad\text{and}\quad V(\tfrac{1}{2}\tfrac{1}{2}1;-\tfrac{1}{2}-\tfrac{1}{2}1)=(3)^{-\frac{1}{2}},$$

we obtain

$$\begin{aligned}(\mathfrak{M}_q^{(k)})_{mm'} &= -(-1)^{j+m}(lj\|B^{(k)}\|lj')\\ &\quad\times V(jj'k;-mm'q).\end{aligned}\quad(3)$$

In order to compute the transition probability, we have to sum $|(\mathfrak{M}_q^{(k)})_{mm'}|^2$ over q and m' for a fixed value of m (it should then be independent of m). Instead it is more convenient to sum $|(\mathfrak{M}_q^{(k)})_{mm'}|^2$ over q, m, and m' and divide by $2j+1$. Using the properties of the V's we obtain

$$\begin{aligned}&\frac{1}{2j+1}\sum_q\sum_{mm'}|(\mathfrak{M}_q^{(k)})_{mm'}|^2\\ &=\frac{1}{2j+1}(lj\|B^{(k)}\|lj')^2\sum_q\sum_{mm'}V(jj'k;-mm'q)^2\\ &=\frac{1}{2j+1}(lj\|B^{(k)}\|lj')^2\sum_q\frac{1}{2k+1}\\ &=\frac{1}{2j+1}(lj\|B^{(k)}\|lj')^2.\end{aligned}\quad(4)$$

This is the quantity usually written as $|\int 1|^2$ or $|\int\sigma|^2$. The connection with the usual formulation is given by

$$\begin{aligned}(lj\|1\|lj')^2 &= (2j+1)\delta_{jj'},\\ (l,l+\tfrac{1}{2}\|\sigma\|l,l+\tfrac{1}{2})^2 &= (2j+1)(j+1)/j\\ &= 2(l+1)(2l+3)/(2l+1),\\ (l,l-\tfrac{1}{2}\|\sigma\|l,l-\tfrac{1}{2})^2 &= (2j+1)j/(j+1)\\ &= 2l(2l-1)/(2l+1),\\ (l,l\pm\tfrac{1}{2}\|\sigma\|l,l\mp\tfrac{1}{2})^2 &= 8l(l+1)/(2l+1).\end{aligned}\quad(5)$$

In the treatment of wave functions of many nucleons we shall assume that the total isotopic spin T is a good quantum number. This assumption is certainly justified in the region $A<50$ as in this region the protons and neutrons occupy the same shells and highly favored image transitions occur (charge symmetry is not enough to account for the big matrix elements between mirror nuclei). The easiest way to calculate the matrix elements is to express the totally antisymmetrized wave function of n nucleons by means of the coefficients of fractional parentage (c.f.p.). These are defined by[7]

$$\begin{aligned}\psi(j^n\alpha TT_zJM) &= \sum_{\alpha'T'J'}\psi(j^{n-1}(\alpha'T'J')jTT_zJM)\\ &\quad\times(j^{n-1}(\alpha'T'J')jTJ\}j^n\alpha TJ).\end{aligned}\quad(6)$$

In the case $n=2$ the c.f.p. are given by means of trivial considerations, but in the case $n=3$, which will be treated in the following, the evaluation of the c.f.p. requires some work. Most of the c.f.p. that will be used below are given by Edmonds and Flowers.[8] The matrix elements can be calculated in terms of the c.f.p. by using the analogs of the formulas (in Sec. 5 of reference 7). The l, L, and S appearing in those formulas should be properly replaced by j, J, and T.

We shall compare the matrix element of the transition I from the state j^3, J, $T=\frac{3}{2}$ to the state j^3, J', $T=\frac{1}{2}$, to those of the image transition II from j^3, J, $T=\frac{1}{2}$, $T_z=\frac{1}{2}$ to j^3, J, $T'=\frac{1}{2}$, $T_z'=-\frac{1}{2}$. The matrix elements for the case of transitions within the j shell are given by

$$\begin{aligned}(\mathfrak{M}_q^{(k)})_{MM'} &= (j^n\alpha TT_zJM|\textstyle\sum_i\tau_{\eta i}B_{qi}^{(k)}|j^n\alpha'T'T_z'J'M')\\ &= n\sum_{\alpha_1T_1J_1}(j^n\alpha TJ\{|j^{n-1}(\alpha_1T_1J_1)jTJ)\\ &\quad\times(T_1J_1\tfrac{1}{2}j_nTT_zJM|\tau_{\eta n}B_{qn}^{(k)}|T_1J_1\tfrac{1}{2}j_nT'T_z'J'M')\\ &\quad\times(j^{n-1}(\alpha_1T_1J_1)jT'J'|\}j^n\alpha'T'J'),\end{aligned}\quad(7)$$

where α stands for the additional quantum numbers necessary to define the state. Using (44) of reference 6, we obtain

$$\begin{aligned}(\mathfrak{M}_q^{(k)})_{MM'} &= n\sum_{\alpha_1T_1J_1}(j^n\alpha TJ\{|j^{n-1}(\alpha_1T_1J_1)jTJ)\\ &\quad\times(j^{n-1}(\alpha_1T_1J_1)jT'J'|\}j^n\alpha'T'J')\\ &\quad\times V(TT'1;-T_zT_z',(T_z-T_z'))V(JJ'k;-MM'q)\\ &\quad\times(-1)^{J_1+k-j-J'+T_1+1-\frac{1}{2}-T'}\sqrt{2}(\tfrac{1}{2}\|t\|\tfrac{1}{2})(lj\|B^{(k)}\|lj)\\ &\quad\times[(2T+1)(2T'+1)(2J+1)(2J'+1)]^{\frac{1}{2}}\\ &\quad\times W(\tfrac{1}{2}T\tfrac{1}{2}T';T_1)W(jJjJ';J_1k).\end{aligned}\quad(8)$$

This expression becomes, upon putting $n=3$, $T'=\frac{1}{2}$,

[7] G. Racah, Phys. Rev. **63**, 367 (1943).
[8] A. R. Edmonds and B. H. Flowers, Proc. Roy. Soc. (London) **214**, 515 (1952).

$T_z'=\frac{1}{2}$, and inserting the value $(\frac{1}{2}\|t\|\frac{1}{2})=(\frac{3}{2})^{\frac{1}{2}}$,

$$(\mathfrak{M}_q^{(k)})_{MM'}$$
$$=(-1)^{k-j-J'}3(6)^{\frac{1}{2}}(2T+1)^{\frac{1}{2}}V(T\tfrac{1}{2}\tfrac{1}{2};-T_z,\tfrac{1}{2},T_z-\tfrac{1}{2})$$
$$\times[(2J+1)(2J'+1)]^{\frac{1}{2}}(lj\|B^{(k)}\|lj)V$$
$$\times(JJ'k;-MM'q)\sum_{T_1J_1}(j^3\alpha TJ\{|j^2(T_1J_1)jTJ)$$
$$\times(j^2(T_1J_1)j\tfrac{1}{2}J'|\}j^3\alpha'\tfrac{1}{2}J')$$
$$\times W(\tfrac{1}{2}T\tfrac{1}{2}\tfrac{1}{2};T_1\tfrac{1}{2})W(jJjJ';J_1k). \quad (9)$$

In order to compare the image transition to the other, let us put $J=J'=j$, then we obtain for the two cases

I. $T=\frac{3}{2}$, $T_z=\frac{3}{2}$:

$$(\mathfrak{M}_q^{(k)})_{MM'}=-(-1)^k3(6)^{\frac{1}{2}}(2j+1)(lj\|B^{(k)}\|lj)$$
$$\times V(jjk;-MM'q)\sum_{J_1}(j^3\alpha\tfrac{3}{2}j\{|j^2(1J_1)j\tfrac{3}{2}j)$$
$$\times(j^2(1J_1)j\tfrac{1}{2}j|\}j^3\alpha'\tfrac{1}{2}j)W(jjjj;J_1k)W(\tfrac{1}{2}\tfrac{3}{2}\tfrac{1}{2}\tfrac{1}{2};11) \quad (10)$$

II. $T=\frac{1}{2}$, $T_z=-\frac{1}{2}$:

$$(\mathfrak{M}_q^{(k)})_{MM'}=-(-1)^k6(2j+1)(lj\|B^{(k)}\|lj)$$
$$\times V(jjk;-MM'q)\sum_{T_1J_1}(j^3\alpha\tfrac{1}{2}j\{|j^2(T_1J_1)j\tfrac{1}{2}j)$$
$$\times(j^3(T_1J_1)j\tfrac{1}{2}j|\}j^3\alpha'\tfrac{1}{2}j)W(jjjj;J_1k)W(\tfrac{1}{2}\tfrac{1}{2}\tfrac{1}{2}\tfrac{1}{2};T_11).$$

The α characterizing the state should now be specified. In some of the cases to be considered the total spin J and the total isotopic spin T are sufficient to characterize the state uniquely. In other cases, however, in which more than one state with the same J and T are found in the configuration considered (as can be the case for j^3, $j\gtrsim 5/2$) we shall take for the ground state the one which is the lowest in the case of short-range attractive (spin independent) forces. This is the state with $J=j$ (for $T=\frac{3}{2}$ or $T=\frac{1}{2}$) which belongs to the irreducible representation of the symplectic group in $2j+1$ dimensions characterized by the partition (10). This state may be said to have the lowest seniority. Inserting in (10) the proper c.f.p. of the ground states thus specified and summing the square of $(\mathfrak{M}_q^{(k)})_{MM'}$ over q, M, and M' and dividing by $2j+1$, we obtain the appropriate transition probabilities. These can be naturally written down as the product of (4) of the single nucleon transition $j\to j$ and a certain factor which is found to be, for the two cases considered, as follows: $(2j-1)/3(j+1)$ in case I and $[(j+4)/3(j+1)]^2$ in case II. These expressions have the following values (for $k=1$):

j	1/2	3/2	5/2	7/2
I	...	4/15	8/21	4/9
II	1	121/225	169/441	25/81

We see that for $j>\frac{1}{2}$ these two expressions are of the same order of magnitude; for $j=5/2$ they are almost equal, and for $j\gtrsim 7/2$ the transition I should be more favored than the image transition II. The result shows clearly that jj coupling cannot account for the observed favored transitions, it leads to the conclusion that image transitions should not be more favored than the others. The situation is not essentially changed if we also take into account the Fermi matrix elements, as it is usually assumed that these have an almost equal weight to that of the Gamow-Teller matrix elements; their addition will multiply the $|(\mathfrak{M}_q^{(k)})_{MM'}|^2$ of the image transitions by a factor ~ 2 which is far less than the observed ratios.

The cases to which this formula apply are A^{35} ($\log ft\gtrsim 3.53$) as compared to S^{35} ($\log ft=4.98$) in the $d_{7/2}$ shell, and Ti^{43} ($\log ft\sim 3.40$) as compared to Sc^{43} ($\log ft\gtrsim 4.77$) in the $f_{7/2}$ shell.

Short-range attractive forces (and also attractive tensor forces) predict that the ground state of the configuration j^n, n odd, shall have the spin $J=j$. Therefore, if in an actual case the ground states (of the nuclei involved in the transition) have other spins, we must conclude that other interactions take here place and that the wave functions which transform according to the irreducible representations of $Sp(2j+1)$ (and which diagonalize the energy in the case of short-range forces) are not adequate to the description of the states. Only if we assume that the spin of the ground state of Na^{25} is 5/2 (unlike Na^{23}) does it make sense to apply our previous results for $j=5/2$ to a comparison of its β-decay ($\log ft=5.25$) with the image transition of Al^{25} ($\log ft\sim 3.53$). In the case of $A=23$ the ground state of Na^{23} has a spin $\frac{3}{2}$ and therefore we do not know what are the adequate quantum numbers which characterize this state (there are three independent states of $(d_1)^7$ with $J=\frac{3}{2}$, $T=\frac{1}{2}$).

In the case of $A=19$ one finds that the ground state of F^{19} has $J=\frac{1}{2}$ and that of O^{19} probably has $J=\frac{3}{2}$. These spins of ground states in the $(d_1)^3$ configuration cannot be explained by assuming short-range forces (or tensor forces) alone, and one might think that either other forces are present or that configuration interaction (probably with s_1 orbits) is important in this case. However, if the configuration considered is to a large extent pure $(d_1)^3$ we can still calculate the transition probability of O^{19} to the ground state of F^{19} without saying anything about the interaction, as in this configuration there is only one state with $J=\frac{3}{2}$, $T=\frac{3}{2}$ and only one state with $J=\frac{1}{2}$, $T=\frac{1}{2}$. Using (9), we obtain for the transition probability of O^{19} the factor, used above, equal to 4/7 (experimentally, $\log ft=5.57$) as compared with the case of the image transition of Ne^{19} $[(d_1)^3, J=\frac{1}{2}]$ for which the factor is equal to 121/105 (for this transition $\log ft=3.23$).

If there are only two j nucleons outside closed shells, the matrix element of the β-transition between the odd-odd and the even-even nucleus can be easily written

down. We also give here the factor by which the transition probability of the single j nucleon should be multiplied in order to obtain the probability of the transition considered. The even-even nucleus has $T=1$ and $T_z=1$, say, whereas for the odd-odd nucleus $T_z=0$ and T is either 1 or 0; the transition probability is the same for the two cases. The factor defined above is

$$2(2j+1)(2J+1)W(jJjJ';\,jk)^2, \qquad (11)$$

where J' is of the initial state and J is of the final state. In case one of the J, J' vanishes the other must be equal to 1 (if $k=1$) and the result is, for initial $J'=1$, final $J=0$: $2(2j+1)/3(2j+1)=\frac{2}{3}$, and for initial $J'=0$, final $J=1$: $2(2j+1)3/3(2j+1)=2$. Both of these factors are of order of magnitude of unity and all such transitions should be favored. A similar conclusion is also the result of the supermultiplet theory, and both these theories account for the cases in which the ft value is low (He^6, C^{10}, and F^{18})[9] and both have difficulty in explaining the high ft values of such transitions as of P^{30}, Cl^{34}, and K^{38}.*

The other cases of odd-odd to even-even transitions, where $N\neq Z$ in the odd-odd nucleus, are not favored and should be forbidden according to the supermultiplet theory. It is interesting to calculate the matrix elements in jj coupling in the case that in the odd-odd nucleus there are a j' nucleon and a j hole. The ratio between the transition probability in this case to the probability of the single nucleon transition $j'\rightarrow j$ is given by

$$n\tfrac{1}{2}(2j'+1)(2J+1)W(jJj'J';\,jk)^2, \qquad (12)$$

where n is the number of nucleons in the closed j shell $-2(2j+1)$. J must vanish and J' must be equal to 1 (for $k=1$) in which case the factor (12) becomes simply $(2j'+1)/3$. The only cases to which this result is applicable are B^{12} and N^{12} for which $j=\frac{3}{2}$ and $j'=\frac{1}{2}$ and the correction factor is $\frac{2}{3}$. This is not enough to explain the high ft values of these transitions (log ft $=4.17$ and >4.3, respectively).

The author would like to express his sincere thanks to Professor E. P. Wigner and Professor E. Feenberg for many helpful discussions.

[9] And also Al^{26} for which neither J nor J' are known; in this case the correcting factors for the reasonable possibilities are as follows:

$J'\backslash J$	0	2	4
1	2/3	128/105	
3		162/245	32/49
5			2/7

* *Note added in proof.*—A super-allowed transition between the ground states of Cl^{34} and S^{34} is reported to have been found in the E.T.H., Zurich.

PHYSICAL REVIEW VOLUME 91, NUMBER 1 JULY 1, 1953

Thermal Neutron-Proton Capture

S. P. Harris, C. O. Muehlhause,* D. Rose, H. P. Schroeder, G. E. Thomas, Jr., and S. Wexler
Argonne National Laboratory, Lemont, Illinois

(Received March 19, 1953)

Measurement of the thermal neutron capture cross section of hydrogen has been effected by a comparison with boron using the technique of pile oscillation. The 2200-m/sec value obtained, 0.332 b, has a 2 percent uncertainty resulting primarily from the effect of neutron moderation by hydrogen. However, the result indicates an exchange moment contribution to the cross section of $\sim 6\pm 3$ percent.

INTRODUCTION

THE thermal $n-p$ capture cross section is of theoretical interest[1–5] in studying the nucleon-nucleon interaction; $n-p$ scattering data from thermal energies to ~ 5 Mev in conjunction with the deuteron binding energy allow one to fix the so-called "effective singlet and triplet ranges."[6] It is the near equality of $n-p$ and $p-p$ singlet ranges ($2.4\pm 0.3\times 10^{-13}$ cm and $2.7\pm 0.2\times 10^{-13}$ cm, respectively) that suggests charge independence of nuclear forces. $n-p$ capture, in addition to involving the singlet and triplet range, also involves an exchange moment.[7] This has the effect of increasing the $n-p$ capture cross section by ~ 5 percent. Owing primarily to the large ratio of scattering to absorption (~ 150) the uncertainty in the measured value of the $n-p$ capture cross section[8] is also ~ 5 percent. It is the object of the present work to improve on the accuracy of this measurement in order to better estimate the exchange moment contribution to the $n-p$ capture cross section. An improved technique has become available for this purpose since the recent refueling of the heavy-water reactor at the Argonne National Laboratory.

* Now at Brookhaven National Laboratory, Upton, New York.
[1] H. A. Bethe, Phys. Rev. **76**, 38 (1949).
[2] J. M. Blatt and J. D. Jackson, Phys. Rev. **76**, 18 (1949).
[3] H. A. Bethe and C. Longmire, Phys. Rev. **77**, 647 (1950).
[4] J. D. Jackson and J. M. Blatt, Revs. Modern Phys. **22**, 77 (1950).
[5] E. E. Salpeter, Phys. Rev. **82**, 60 (1951).
[6] Hafner, Hornyak, Falk, Snow, and Coor, Phys. Rev. **89**, 204 (1953).
[7] N. Austern and R. G. Sachs, Phys. Rev. **81**, 710 (1951).
[8] W. J. Whitehouse and G. A. R. Grahm, Can. J. Research **A25**, 261 (1947).

METHOD

(a) Enriched Heavy-Water Reactor

The Argonne National Laboratory's heavy-water reactor has recently had its fuel rods of normal uranium replaced with rods of enriched U^{235} Al alloy. In addition to genertting a larger ratio of thermal to epithermal neutron flux, a former difficulty in interpreting a pile absorption cross section for a moderating substance has been eliminated. A strong moderator, such as hydrogen, when inserted into a normal uranium fueled reactor, exhibits an absorption cross section which is less than its actual value. This is because a fraction of the epithermal neutrons which would have been absorbed in the 7-ev absorption resonance of U^{238} during moderation is able to escape this energy band and enter the thermal region where fission can take place. This phenomenon is termed resonance escape (p), the probability for which is increased by the presence of a good moderator. As an example of the magnitude of this effect, the apparent capture cross section of hydrogen is $\sim$75 percent of its actual value when measured in a pile in which p is $\sim$0.9. In the present enriched reactor, however, $(1-p)$ is $\sim 10^{-5}$. This insures that the above effect is negligible. A smaller moderation effect still exists, however, and this will be discussed in (d) of this section.

(b) Pile Oscillator

The pile oscillator[9] is a mechanical device which periodically inserts and removes from the pile a sample to be measured. The resulting oscillating component of pile flux is observed via the current it produces in a BF_3 ionization chamber. This is taken as a measure of sample absorption. Calibration is effected by similarly oscillating a known quantity of some standard material such as boron.

The pile flux is composed of a thermal-Maxwellian and an epithermal $1/E$ distribution. A pile absorption cross section σ_{pile} measured by comparison with a $1/v$ absorber such as boron is given, therefore, by

$$\sigma_{\text{pile}}=\sigma_a^{(th)}+kC_r\Sigma_a^{(r)}. \tag{1}$$

Here k is the ratio of epithermal to thermal flux; C_r is the relative statistical weight of resonance to thermal neutrons; $\Sigma_a^{(r)}$ is the resonance absorption integral other than that resulting from $1/v$ absorption. Only in the case of two $1/v$ absorbers is a pile-oscillator comparison exact. In any other case it is necessary to make supplementary measurements of the resonance absorption integral.

Since the present work is one of comparing two $1/v$ absorbers, hydrogen and boron, no difference in absorption cross-section behavior exists. However, a marked difference in scattering cross section σ_s and slowing down power ξ does exist, and this will be shown to be equivalent to an effective negative absorption integral for hydrogen.

[9] Harris, Muehlhause, Rasmussen, Schroeder, and Thomas, Phys. Rev. **80**, 342 (1950).

(c) Simple Scattering

By "simple scattering" the authors wish to indicate the effects of elastic scattering other than moderation. A sample which is not oscillated from the exact flux center of the pile generates an in-out scattering effect. That is, a sample which is off center will make a first-order change in the spatial neutron distribution, which in turn will cause a first-order change in the spatial neutron statistical weight. This effect is proportional to the neutron flux gradient at the sample in-position. It can be made equal to zero, therefore, by oscillating the sample from that point in the pile for which the gradient of the flux is zero or the flux itself is a maximum. The flux center is determined by oscillating boron as a function of in-position. The in-position yielding the maximum absorption effect is taken to be the flux center. This is actually the maximum of the product of the flux and its adjoint, both of which peak at the same position.

(d) Moderation

Having determined the proper point in the pile from which to oscillate in order to eliminate errors resulting from simple scattering, it is impossible to avoid the effects of moderation. Moderation makes itself felt by causing epithermal neutrons to age (i.e., slow down) faster than they would otherwise age in the absence of the moderator. An aged neutron counts for more, i.e., has a higher statistical weight in the pile than it had in its previous less aged condition. Viewing the effect of moderation spatially rather than energetically, it may be regarded as one which pulls thermal neutrons closer to the center of the pile where they cause greater reactivity. At any rate moderation increases pile reactivity via the slowing down power ξ, the epithermal scattering integral Σ_s, and the change in statistical weight δC, effected by the moderation collisions.

Let us assume that at most a single scattering takes place. Then the moderation cross section σ_m is given by

$$\sigma_m=k\delta C_1\Sigma_s, \tag{2}$$

where "k" is the quantity defined in (1) and δC_1 is the change in statistical weight C caused by one collision. The pile cross section of a moderator which is also a $1/v$ absorber is given, therefore, by

$$\sigma_{\text{pile}}=\sigma_a^{(th)}+\sigma_m. \tag{3}$$

The statistical weight C is given in terms of the geometry of the reactor and the reactor moderator,

$$C=1-K^2\tau, \tag{4}$$

where K^2 is the so-called buckling constant, and τ is the age to thermal energies in the reactor moderator in question. The Argonne heavy-water reactor is in the

shape of a right cylinder, so that K^2 is given by

$$K^2=\pi^2/H^2+(2.405)^2/R^2, \tag{5}$$

where H is the effective height (including reflector savings) and R is the effective radius (includes reflector savings).[10] For the reactor in question, K^2 has the value 6.96×10^{-4} cm^{-2}, and

$$\tau=\tau_0\log(\epsilon/\epsilon_{th}), \tag{6}$$

where τ_0 has the value 7.15 cm^2.

Therefore

$$\delta C_1=-K^2\tau_0\xi, \tag{7}$$

and

$$\sigma_m=-kK^2\tau_0\xi\Sigma_s. \tag{8}$$

Equation (8) is an approximation and should only be used to indicate that σ_m varies as $\xi\Sigma_s$ for different samples. Experimentally one should observe σ_m for H^2 and He^4 and scale the results to the H^1 case. It is impractical to oscillate liquid He^4, and the results on H^2 presented below are sufficiently inaccurate to make them useless in determining σ_m for H^1. Another approach would be to change K^2, but the small changes permissible are not worth while. Therefore (8) is used to estimate $\sigma_m(H^1)$. The authors consider this estimate to be their primary source of error.

APPARATUS

(a) Mechanical

The mechanical apparatus consists of a motor-driven cam and rocker-coupled arm which is periodically raised and lowered to two fixed positions. The amplitude of the end of the arm to which is attached a hanger rod and sample can is five feet. The total period is twenty seconds, during which time the sample rests in the in-position for 9.3 sec, transits out for 0.7 sec, rests in the out-position for 9.3 sec, and transits in for 0.7 sec.

The moving parts which enter the active portion of the pile are made of low neutron absorbing materials: hanger rod and sample can of Dow metal $FS-1$, bearings of graphite, hanger rod to sample can clamp of zirconium, and sample container bottles of either quartz or Teflon.

(b) Electrical

The detection system consists of a large enriched BF_3 ionization chamber placed in the thermal column of the reactor. The current resulting from neutron absorption is conducted into the bridge circuit shown in Fig. 1. The high sensitivity galvanometer shown is used as a null indicator for adjusting R_1. A system of relays adds R_1 to R_0 during the sample in-time and shorts R_1 during the sample out-time. Except for a second harmonic, balance may be achieved by adjusting R_1. Not shown are other switches controlled by relays which rectify the current through the galvanometer. R_1, therefore, is a measuring of $\Delta i/i$, i.e., the ratio of oscillating to mean current value.

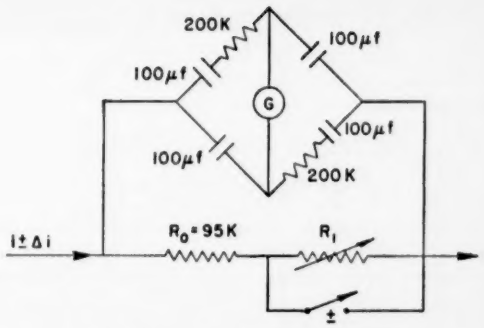

FIG. 1. Bridge circuit for measuring $\Delta i/i$.

SAMPLES

(a) Containers

Good sample containers for general use are constructed of a material which is low in neutron absorption and also noncorrosive. Quartz (SiO_2) and Teflon (CF_2) satisfy these conditions. Most of the measurements presented herein employ sealed quartz bottles in the shape of a right cylinder of inside diameter 1.5 cm and of active length 15 cm.

(b) Boron Standards

Calibration material is taken from the Argonne stock of primary standard boric acid.[11] This boron is known to have a 2200 m/sec absorption cross section of 755 ± 3 b. Since the relative abundance of B^{10} and B^{11} may vary depending upon the source from which it is obtained, it is important to employ a boron standard whose cross section is known from an absolute transmission measurement.

A known amount of boric oxide is prepared by igniting some boric acid. This is added to a known amount of high purity heavy water to make a known-concentration stock solution. The stock solution is then diluted by various amounts with additional heavy water to make the various boron standards to be used in the oscillator. A typical standard has a total macroscopic absorption area of ~0.5 cm^2.

(c) Hydrogen Samples

Hydrogen is obtained in the form of multiply distilled light water from the Biology Division of the Argonne National Laboratory. This material is diluted by various amounts with heavy water to make the different hydrogen samples.

[10] S. Glastone and M. C. Edlund, *The Elements of Nuclear Reactor Theory* (D. Van Nostrand Company, Inc., New York, 1952).

[11] Kimball, Ringo, Robillard, and Wexler (unpublished Argonne National Laboratory data).

(d) Background Samples

Empty quartz bottles and quartz bottles with pure heavy water are also made available for "background" determinations.

TECHNIQUE OF MEASUREMENT

(a) Oscillation Point

The central thimble or axial hole is chosen for oscillation measurements. Three samples are oscillated as a function of depth or in-position in this hole. These are: (1) a boron standard, (2) a heavy-water sample, and (3) an empty quartz bottle. From these the net effect of boron is calculated, and that position is chosen for which the effect of boron is a maximum. The exact location of this position is not critical but may be determined to within half an inch.

(b) Determination of k

k in (1) is determined essentially by measuring the cadmium ratio R_{Cd} (total activation over epithermal activation) of very thin gold (<0.1 mg cm^{-2}). Two one-mil iron foils on which the gold is evaporated are placed in the pile at the oscillation point. One foil is covered with cadmium; the other foil is uncovered. The activity (Au^{198}) ratio is observed.

In addition, it is necessary to know the cadmium ratio of a $1/v$ absorber. This is measured by observing the cadmium ratio of a BF_3 counter in a beam outside the reactor, and in the same beam also observing the cadmium ratio for gold. Since the ratio $[R_{Cd}(Au)-1]/[R_{Cd}(B)-1]$ is invariant, the cadmium ratio for boron in the thimble may be calculated. k is then given by

$$k=\frac{\sigma_a^{(th)}(\mathrm{Au})}{\Sigma_a^{(r)}(\mathrm{Au})}\left\{\frac{1}{R_{Cd}(\mathrm{Au})-1}-\frac{1}{R_{Cd}(\mathrm{B})-1}\right\}. \quad (9)$$

The measured results are $R_{Cd}(Au)=5.63$, $R_{Cd}(B)=133$ $\sigma_a^{(th)}(Au)$ is taken to be 94 b, and $\Sigma_a^{(r)}(Au)$ to be 1180 b. This results in a k value of 0.0166.

(c) Check on K^2

A rough check on the calculated value of K^2 is made by making both axial and transverse static measurements of both the flux and the product of the flux and its adjoint. These data are fitted to the proper Bessel functions, and result in a value of K^2 of 6.8×10^{-4} cm^{-2}. Within the limits of error this value agrees with the one calculated from (5). The latter value is the one employed to calculate σ_m.

TABLE I. The apparent cross section of hydrogen uncorrected for moderation.

Run	Cross section (barns)
1	0.3127
2	0.3125
3	0.3069
4	0.3145
5	0.3106
6	0.3139
7	0.3149
8	0.3061
Average	0.3115±0.003

(d) Sample Measurements

Four different hydrogen samples are available: three as H_2O-D_2O solutions, and one as a $B_2O_3-H_2O-D_2O$ solution. This latter sample is used to observe a possible local two-collision process; that is, to observe whether the presence of a moderating agent (H^1) increases the absorption by boron. Such an effect is expected to be small, and none is observed.

In all, eight complete runs of all hydrogen, boron, and blank samples are available, the measurements having taken place during two oscillator sessions which were over a month apart. This represents about thirty hours' observation time since each sample takes from twenty to thirty minutes to achieve balance. This much time is needed to eliminate pile drift during the measurement (i.e., while balancing the bridge). In effect it is necessary to first make a static balance and then a dynamic balance. The latter is about ten times more sensitive to the sample than the former, which is a major advantage of the oscillation method.

TREATMENT OF RAW DATA

(a) Electrical

Since R_1 of Fig. 1 is in the circuit for one half of the cycle, it is necessary to convert R_1 to R_1' in order to obtain a value proportional to $\Delta i/i$. R_1' is given by

$$R_1'=10^5R_1/(R_0+\tfrac{1}{2}R_1), \quad (10)$$

where $R_0=95\,000\Omega$ and $R_1\sim2000$ to 70000Ω.

(b) Pile Power

Though R_1 is nearly independent of pile power (i), it is not entirely so. Observations are made always within 5 percent of the same mean current value, but when the mean current is purposely altered by 10 percent, a change of 1 percent in R_1 is observed. This is used to correct observations made at slightly different settings from the mean ($\sim$200 watts).

(c) Pile History

Observations are usually begun at the beginning of a week following a two-day shutdown from a high power ($\sim$250 kilowatts). The decaying "source strength" of the reactor causes a drift in the observed sample readings. Over any one day, measurements repeat to about a half-percent, but over the course of a week a drift in all readings of about 2 percent occurs. A "time correction" is made, therefore, by scaling daily sets to a "standard day." In this manner a high relative accuracy

is preserved, and at the same time proper averaging of sets is made possible.

(d) Nonlinearity

Since the samples are not infinitely dilute, a small but observable amount of self-protection exists. Readings (i.e., ohm values) are corrected on the basis of the following formula:

$$R''=\frac{R_1'}{1-R_1'/R_\infty}. \tag{11}$$

Equation (11) is similar to the one used to correct for the dead time in counters. R_∞ is a parameter which should have the significance of being that number of ohms which corresponds to blackbody absorption by the sample. That is, $R_\infty \gg R_1'$, and should be given by

$$R_\infty = A_p(dR_1'/da)_{R_1'=0}, \tag{12}$$

where A_p is the projected area of the sample and $(dR_1'/da)_{R_1'=0}$ is the initial slope in ohms cm^{-2} of the boron calibration curve (ohms *vs* cm^2 absorption).

R_∞ and $(dR'/da)_{R_1'=0}$ are determined by fitting the boron calibration data to (11). The value of R_∞ is then checked by calculating A_p from the bottle shape (18.55 cm^2) and multiplying this by $(dR_1'/da)_{R_1'=0}$. The two figures agree to within 5 percent, R_∞ being $\sim$105 000Ω. Such agreement is good for a correction term which is always <7 percent and usually ~4 percent.

EXPERIMENTAL RESULTS

(a) Deuterium

The application of (8) to deuterium in which the scattering cross section of deuterium is taken as constant and equal to 3.33 b from cadmium cutoff ($\sim$0.5 ev) to mean fission energy (1.5 Mev) yields a value for $\sigma_m(H^2)$ of -3.0 mb.

The observed pile cross section must be corrected for (1) the absorption cross section of deuterium, (2) the absorption of a trace amount of hydrogen ($\sim$0.15 percent), and (3) the effect of displacing nitrogen in the atmosphere for the sample-in position. These corrections make for a considerable error in $\sigma_m(H^2)$, the result being -2 ± 1 mb.

(b) Hydrogen

The apparent cross section of hydrogen uncorrected for moderation is given by the average of the eight mentioned complete runs shown in Table I. The average value is 0.3115 b. The internal error in this number as obtained from the mean deviations is only $\sim$1.0 percent. However, application of Eq. (8) for the evaluation of $\sigma_m(H^1)$ yields the value -0.0205 b. This gives for the 2200-m/sec absorption cross section of hydrogen the value 0.332 b, which is ~6 percent higher than the uncorrected value.

The final boron-to-hydrogen ratio is 2274, which compares favorably with the values of 2270 and 2292 reported elsewhere.[8,12] Considering the uncertainty in estimating σ_m, however, the uncertainty in our figure is at least 2 percent. That is,

$$\sigma_a^{(th)}(H^1)=0.332\pm0.007 \text{ b}.$$

The important theoretical quantity is not the cross section but the product of the cross section, and the corresponding velocity

$$\sigma_a^{(th)}(H^1)v=7.30\times10^{-20} \text{ cm}^3/\text{sec}.$$

Table II. Shape independent ϵ-values for various assumed values of r_{0s}.

$r_{0s}<10^{13}$ cm	$D<10^{13}$ cm	ϵ (%)
2.6	1.080	7.9
2.5	1.055	6.7
2.4	1.030	5.5
2.3	1.005	4.3

EXCHANGE MOMENT

If ϵ is the fractional contribution of the exchange moment to the capture cross section,[5]

$$[\sigma_a^{(th)}(H^1)v](1-\epsilon) = [\sigma_a^{(th)}(H^1)v]_0\frac{[1-\gamma a_s+\gamma^2 a_s D]^2}{(1-\gamma a_s)^2(1-\gamma r_{0T})}. \tag{13}$$

$[\sigma_a^{(th)}(H^1)v]_0$ is the zero-range approximation of $\sigma_a^{(th)}(H^1)v$ and has the value 6.52×10^{-20} cm^3/sec, and $\gamma=2.318\times10^{12}$ cm^{-1} is the so-called "reciprocal radius of the deuteron." $a_s=-23.68\times10^{-13}$ cm is the singlet $n-p$ scattering length; $r_{0T}=1.720\times10^{-13}$ cm is the effective triplet $n-p$ range; and $2.6\times10^{-13}>r_{0s}>2.3\times10^{-13}$ cm is the effective singlet $n-p$ range. Also

$$D\simeq\tfrac{1}{4}(r_{0s}+r_{0T}). \tag{14}$$

Substituting the observed value of $\sigma_a^{(th)}(H^1)v$ into (13) yields

$$D\simeq0.915+2.1\epsilon, \tag{15}$$

where D is now in units of 10^{-13} cm. Combining (14) and (15) for different values of r_{0s} yields Table II, where ϵ is expressed in percent.

Inspection of Table II with consideration for the error in $\sigma_a^{(th)}(H^1)v$ indicates that $\epsilon\sim6\pm3$ percent. If, in fact, ϵ is only ~1 or 2 percent, the intrinsic singlet ranges[2] of the $n-p$ and $p-p$ interaction are outside the experimental limit of being equal. The inclusion of a variety of possible nuclear potentials in the above calculations only slightly increases the spread in ϵ-values. The authors are indebted to Dr. G. Snow for a discussion of this last point.

[12] Hamermesh, Ringo, and Wexler, Phys. Rev. **90**, 603 (1953).

Unusual π-μ Decays in Photographic Emulsions*

W. F. Fry†
Department of Physics, University of Chicago, Chicago, Illinois, and Department of Physics, Iowa State College, Ames, Iowa
(Received March 2, 1953)

A total of 11 841 π-μ decays has been studied in Ilford C-2 and G-5 photographic plates, where both the π- and μ-meson tracks stopped in the emulsion. In 12 cases the range of the μ-meson track from the π-meson decay is less than 480 microns and in 2 cases the range is greater than 720 microns. The ranges of the μ-meson tracks of the 14 unusual π-μ decays are: 120, 185, 258, 260, 290, 416, 430, 441, 444, 470, 470, 476, 828, and 1035 microns. The normal range of the μ-meson from π-meson decays is about 600 microns. A study of the grain density in C-2 plates, gap density in G-5 plates, and the number and energy of the δ-rays along the short μ-meson tracks indicates that the μ-mesons were ejected from the π-decays with a lower velocity than from normal π-μ decays. It is possible to explain the short range of the μ-meson in 4 of the events and the long range of the μ-meson in the 2 events by assuming that the π-meson decayed in flight. The grain density or gap density along the μ- and π-meson tracks in the remaining 8 events is inconsistent with the assumption that the short range of the μ-meson is due to the decay in flight of the π-meson. If a correction is made for the thickness of the emulsion, the probability that a μ-meson from a stopped π-meson decay will have a range less than 480 microns is found to be $3.3\pm1.3\times10^{-4}$. This probability is in general agreement with theoretical predictions based upon the assumption that a soft photon is occasionally emitted from the π-μ decay resulting from the charge acceleration of the μ-meson.

I. INTRODUCTION

ONE of the striking characteristics of the π-meson decays in photographic emulsions that were first observed by Lattes, Occhialini, and Powell[1] was the length of the μ-meson tracks. The lengths of the μ-meson tracks from π-meson decays were found to be nearly constant. This fact suggested the possibility that the π-meson decays into a μ-meson plus one additional particle, presumably a neutrino,[2]

$$\pi \rightarrow \mu + \nu. \quad (1)$$

The range distribution of 1000 μ-mesons from π-meson decays in two Ilford C-2 plates has been obtained.[3] The range distribution is Gaussian within the statistical limits; it has a mean of 597 ± 1 microns and a standard deviation of 29.1 ± 0.7 microns. The results of this study are in general agreement with the earlier results of Barkas.[4]

A π-μ decay was found by Powell[5] where the range of the μ-meson was estimated to be less than 350 microns. The π-meson was ejected from a cosmic-ray star. The short range of the μ-meson was ascribed to the decay of a negative π-meson from a mesonic "Bohr" orbit of an atom. A short μ-track from a positive π-meson decay was found by Smith.[6] It was possible to explain the short range of the μ-meson by assuming that the π-meson decayed in flight.

Recently, several positive π-μ decays have been observed by the author[7] where the short range of the μ-meson cannot be explained by the decay in flight of the π-meson. The analysis of the π-μ decays, where the range of the μ-meson is abnormal, is reported in this paper.

II. PROCEDURE

A study of π-μ decays has been made in both Ilford C-2 and G-5 photographic emulsions. C-2 plates of 200 microns in thickness which had been exposed in the spiral orbit spectrometer to the Berkeley cyclotron, were made available to the author by Dr. R. Sagane. Ilford G-5 plates of 400 microns in thickness were exposed to the University of Chicago cyclotron. The G-5 plates were so arranged that the tracks of the π-mesons are about 1000 microns long. It is desirable to have the π-meson tracks long and nearly in the plane of the emulsion in order that the π-μ junction can be easily identified. Both the C-2 and G-5 plates were searched for π-μ decays with a total magnification of about 250×. Only those decays were studied where the π- and μ-meson tracks stopped in the emulsion. The horizontal projected length of each μ-meson track was estimated by a calibrated scale in the eyepiece of the microscope, with a total magnification of 250×. If the length of the μ-meson track in the plane of the emulsion was found to be less than 520 microns, the true length was determined by successive measurements of small sections of the track with a total magnification of 1000×. The largest uncertainty in the measurement of the length of a track was found to be due to the measurement of the vertical component of the track. Nevertheless the uncertainty in the length of the μ-meson track from a normal π-μ decay is estimated to be no greater than 20 microns for an extreme case in 400-micron thick plates. For a μ-meson track which does not make a

* Supported in part by a joint program of the U. S. Office of Naval Research, the U. S. Atomic Energy Commission, and the Research Corporation.
† Present address, Department of Physics, University of Wisconsin, Madison, Wisconsin. A portion of the work was undertaken while the author was a U. S. Atomic Energy Commission Postdoctoral Fellow (1951–1952) at the University of Chicago.
[1] Lattes, Occhialini, and Powell, Nature **160**, 453 (1947).
[2] C. O'Ceallaigh, Phil. Mag. **41**, 838 (1950).
[3] W. F. Fry and George R. White, Phys. Rev. **90**, 207 (1953).
[4] W. H. Barkas, Am. J. Phys. **20**, 5 (1952).
[5] C. F. Powell in "Cosmic Radiation," *Calston Papers* (Butterworth Scientific Publications, London, 1949).
[6] F. M. Smith, reported in reference 4.
[7] W. F. Fry, Nuovo cimento **8**, 590 (1951); Phys. Rev. **83**, 1268 (1951); Phys. Rev. **86**, 418 (1952).

large angle with the plane of the emulsion, the true range can be estimated to within about 5 microns. Since the distortion of the emulsion usually increases with increasing emulsion thickness, and since the largest error in the measurement of the range is introduced by the vertical sections of the track, it is advantageous to use relatively thin emulsions for this study.

Two types of plates, the relatively insensitive C-2 and electron sensitive G-5 plates, were used for this study because of the many desirable characteristics of each type. In C-2 plates the individual grains along the track can be counted, except for the region near the very end of the track. The relatively large variation in grain density with velocity, for slow mesons in C-2 plates, can frequently be used to an advantage. For example, the change in grain density between the π- and μ-meson tracks usually makes it possible to distinguish visually a π-μ decay fron a scattered μ-meson without counting the number of grains along the two tracks. The velocity of a π- or μ-meson can be estimated from the grain density for meson energies as low as 1.5 to 2 Mev. The estimation of the π-meson velocity was found to be important in connection with the possibility of decay in flight of the π-meson. On the other hand, the ability of G-5 plates to record minimum ionizing particles is of considerable importance in the study of the δ-rays along the μ-meson tracks and the decay electrons from the μ-mesons.

III. RESULTS

A total of 3922 π-μ decays, where both the π- and μ-mesons stopped in the emulsion has been studied in C-2 plates. Similarly, 7919 decays have been studied in G-5 plates. Among these 11 841 π-μ decays, 13 unusual π-μ decays are observed where both meson tracks stop in the emulsion and where the range of the μ-meson track is less then 480 microns or greater than 720 microns. In one additional case a π-μ decay is observed where the μ-meson track leaves the emulsion after 975 microns. The residual range has been estimated to be 60 microns by a comparison of the gap density with the gap density along a μ-meson track of a normal decay which occured within 100 microns of the unusual event. A decay electron track is observed from each of the 7 μ-meson tracks of the unusual π-μ decays which are in G-5 plates. The characteristics of the 14 unusual π-μ decays are given in Table I.

TABLE I. Characteristics of unusual π-μ decays.

Event	Type of emulsion	Range of μ-meson track in microns	Energy of μ-meson in Mev	Measured angle between directions of π- and μ-meson tracks	Energy in Mev of π-meson assuming decay in flight
1[a]	C-2	120	1.6	73	5.0
2[a]	C-2	185	2.1	20	16.6
3[a]	G-5	290	2.7	59	6.6
4[a]	G-5	416	3.3	51	8.3
5[a]	G-5	430	3.35	26	15.4
6[a]	G-5	441	3.4	56	5.1
7[a]	G-5	470	3.5	28	15.4
8[a]	G-5	470	3.5	36	11.9
9	C-2	258	2.5	93	1.7
10	C-2	260	2.5	113	0.7
11	C-2	444	3.4	160	0.03
12	G-5	476	3.5	117	0.09
13[b]	C-2	828	4.8	10	0.05
14	G-5	1035	5.5	55	0.5

[a] Events which do not appear to be decay in flight of the mesons.
[b] Interpreted as a flight of a negative π-meson. See reference 12.

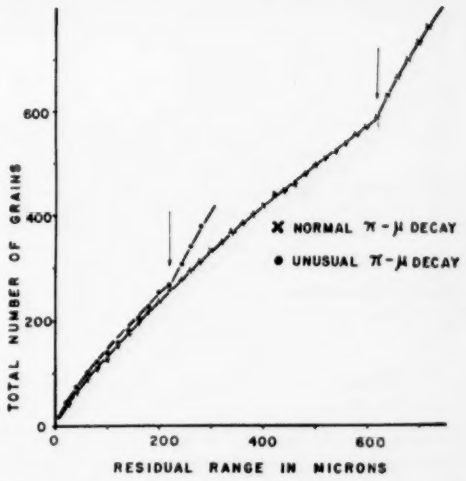

FIG. 1. The integral number of grains, starting at the end of the μ-meson track, as a function of the residual range is shown for the unusual π-μ decay which is listed as event 9, and for a normal π-μ decay. The π-μ junction is indicated by the arrow.

The probability that a μ-meson from a π-decay at rest will have a range less than 480 microns can be estimated from the standard deviation of the previously measured range distribution, assuming that the events are distributed according to the Gaussian distribution. This probability is about 6×10^{-5}. Since the probability is very low that the range will be less than 480 microns resulting only from straggling, all π-μ decays where the length of the μ-meson track is less than 480 microns have been carefully studied.

Tracks of μ-mesons as well as π-mesons are observed to enter the surfaces of the emulsions in both the C-2 and G-5 plates. The μ- mesons were probably due to the decay in flight of π-mesons before they entered the emulsion. Occasionally a slow μ-meson was scattered through a large angle in the emulsion and subsequently stopped in the emulsion after traveling several hundred microns from the scattering point. It is necessary to be able to distinguish this type of event from a π-μ decay. If the range of the μ-meson, from the π-decay or the scattering point, is greater than about 400 microns, the two types of events can be readily disinguished by a visual comparison of the grain densities in C-2 plates or gap densities in G-5 plates along the two tracks at the junction. For events where the length of the μ-meson track is less than about 400 microns, the two

FIG. 2. A portion of the π- and μ-meson tracks of event 9 is shown in the drawing. The event was found in a C-2 plate. The range of the μ-meson is 258 microns. The difference in the grain density along the π- and μ-meson tracks can be seen, indicating that the event is a π-μ decay and not a scattered μ-meson.

types of events can be distinguished by grain counting or gap counting. The total number of grains has been counted along the π- and μ-meson tracks starting from the end of the μ-meson track, for the π-μ decay which is listed as event 9 in Table I. The results are shown in Fig. 1 as well as the results of a similar count in the same plate of a normal π-μ decay. A comparison of the integral number of grains as a function of the residual range of the μ-meson for the unusual decay and for the normal π-μ decay indicates that the μ-meson was ejected with a lower velocity in the unusual decay than in the normal decay. There is no evidence for an abrupt change in the velocity of the μ-meson along the track as has been recently reported by Riezler and Rudloff.[8] A projection drawing of a portion of the π-μ decay which is listed as event 9 is shown in Fig. 2. The difference in the gap densities in a G-5 plate along the end of a π-meson track and the beginning of a μ-meson track is illustrated in Fig. 3(a) and Fig. 3(b) by the projection drawing of the unusual π-μ decay which is listed as event 3 in Table I. The total number of gaps along the π- and μ-meson tracks starting at the end of the μ-meson track has been counted in event 4. The results are shown in Fig. 4. The π-μ junction is clearly evident by the abrupt change in the slope of the curve at the π-μ junction.

In general, it is easier to distinguish visually π-μ decays from scattered μ-meson tracks in C-2 than in G-5 plates. However, the δ-rays which are observed along the tracks of particles in G-5 plates can be used in some cases to distinguish the two types of events. The maximum velocity that a meson can give to an electron in a collision is twice the velocity of the meson. The maximum energy of a δ-ray is then $E_e = 4E_m m_e/M$ where E_m is the kinetic energy of the meson and m_e and M are the mass of the electron and the meson, respectively. If δ-rays are observed along a meson track, a lower limit of the kinetic energy of the meson can be determined from the energy of the δ-rays. A few events have been observed in G-5 plates which would appear upon casual inspection to be π-μ decays but which are shown to be scattered μ-mesons by the presence of one or more δ-rays near the scattering point, along the portion of the track which was assumed to be the

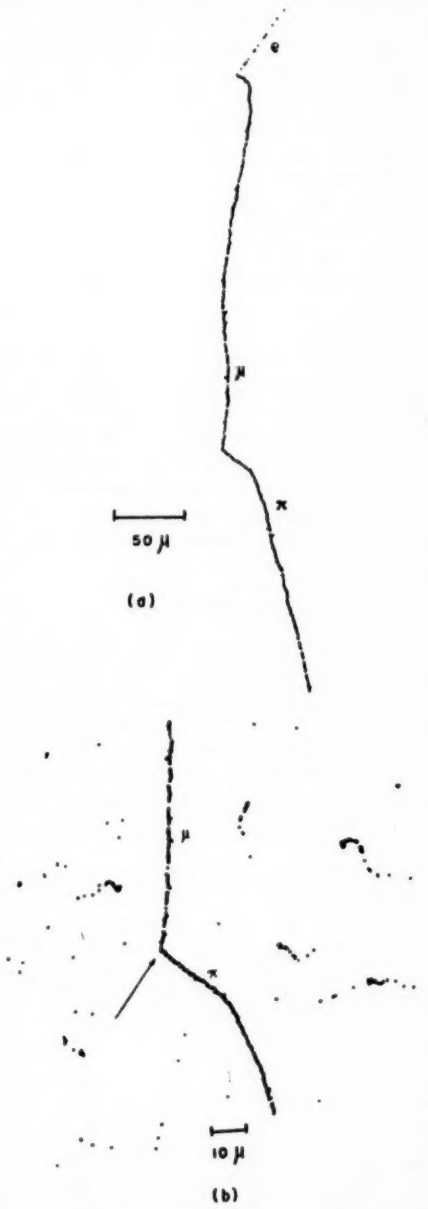

FIG. 3. (a) A projection drawing of a π-μ decay in a G-5 plate, which is listed as event 3, is shown above. The range of the μ-meson is 290 microns. (b) A projection drawing of a π-μ decay in a G-5 plate listed as event 3. Only a portion of the π- and μ-meson tracks is shown. The range of the μ-meson is 290 microns. The difference in the number of gaps along the π- and μ-meson tracks can be seen.

[8] W. Riezler and A. Rudloff, Z. Naturforsch. **7a**, 570 (1952) and private communications.

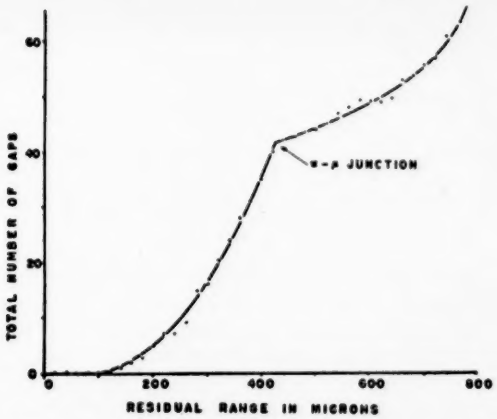

FIG. 4. The total number of gaps up to a range R beginning at the end of the μ-meson track for event 4 is shown in the above curve. The unusual π-μ decay was found in a G-5 plate. The π-μ junction can be clearly disinguished by the abrupt change in the slope of the curve. The range of the μ-meson is 416 microns.

π-meson track. The assumption that these events were not π-μ decays was subsequently verified by gap counting along both tracks near the scattering point.

The total energy of the δ-rays along the μ-meson tracks of the unusual π-μ decays has been obtained. The measurements were undertaken to see if the short range is due to a statistical fluctuation in the total energy given to the high energy δ-rays for the events where the μ-meson range is around 450 microns. The energy of the electrons was estimated by measuring their range and utilizing the range-energy relationship of Zajac and Ross.[9] The total energy of the δ-rays ($E>12$ kev) along the last 450 microns of the μ-meson tracks from normal π-μ decays has been obtained for 25 events. The results are summarized by the histogram in Fig. 5. The total energy of the δ-rays ($E>12$ kev) along the μ-meson tracks of 7 unusual π-μ decays is listed in Table II. The estimation of the total energy of the δ-rays is crude, mainly for two reasons. Some of the "knock-on" electron tracks or δ-rays are masked by the heavy μ-meson track and are not observed. Also the estimation of the energy of an electron from the length of the track is poor for electrons of energy below 20 kev. Nevertheless, if the short range of the μ-mesons is due to an increased number of high energy δ-rays, the excess energy should be observable. About 500 kev will change the mean range of a μ-meson from 450 microns to 600 microns. A comparison of the energy of the δ-rays along the μ-meson tracks from the unusual decays (Table II) with the total energy of the δ-rays along the μ-meson tracks from normal π-μ decays (Fig. 5) strongly indicates that the short range in these events is not due to an abnormally high energy loss to energetic δ-rays.

It may be possible in certain cases to explain the

[9] B. Zajac and M. Ross, Nature **164**, 311 (1949).

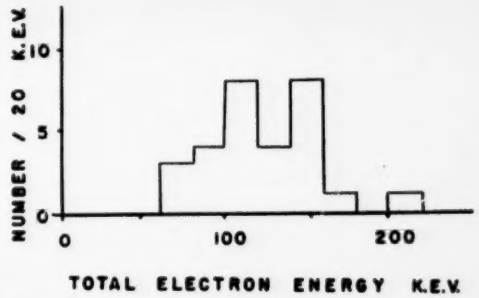

FIG. 5. The distribution of the total energy of the δ-rays ($E>12$ kev) along the last 450 microns of the μ-meson track from normal π-μ decays is shown in the histogram.

abnormal range of the μ-meson from a π-meson decay by assuming that the π-meson decayed while still in motion. This mechanism would be expected to produce abnormally long μ-meson tracks as well as short μ-meson tracks. If the abnormal range of a μ-meson from a π-meson decay is due to the decay in flight of the π-meson there should be a correlation of the angle between the directions of the π- and μ-meson tracks, the energy of the π-meson at the time it decayed and the energy of the μ-meson. Assuming that the abnormal ranges of the μ-mesons that are listed in Table I are due to the decay in flight of the π-mesons, the energy of the π-meson at the time of decay can be calculated for each event. It is assumed that the direction of the π-meson at the time of decay is the same as the direction of the last few microns of the π-meson track. The calculated energy of the π-meson at the time of decay is shown in the last column of Table I. In events 1 through 8 the grain density in C-2 plates and the gap density in G-5 plates along the π-meson track near the π-μ junction is definitely inconsistent with the estimated energy of the π-meson assuming that the π-meson decayed in flight. It is possible that the π-meson was scattered in the backward direction while still in motion. In order to estimate this probability the number of large angle scatterings along π-meson tracks of normal π-μ decays, in the interval from 4 to 8 microns from the junction, has been measured. The range-energy relationship for very low energy mesons is not accurately known, but the energy of a π-meson which as a range of 6 microns is estimated to be 0.3 Mev. The range of a μ-meson

TABLE II. δ-rays along μ-meson tracks.

Event	Range of μ-track in microns	Total energy in kev of δ-rays with $E>12$ kev
4	416	75
5	430	80
6	441	167
7	470	88
8	470	166
11	444	134
12	476	145

would be 250 microns from the decay in the backward direction of a π-meson of 0.3 Mev. The scattering in the 4-micron interval along the π-meson track in each of the 100 normal π-μ decays has been measured. Only in 5 cases was the π-meson scattered through an angle larger than 60 degrees. Thus, the probability that a π-meson of 0.3 Mev will be scattered through an angle greater than 60 degrees, per micron length of track, is about one percent. The probability that a π-meson in a given energy interval will decay in flight can be calculated from an estimate of the time spent in the energy interval and the probability of decay per unit time.[10,11] The upper limit of the π-meson energy that must be considered is determined by the requirement that the π-meson track must appear heavier than the μ-meson track in order that the event will be recognized as a π-μ decay. The lower limit to the energy interval is determined by the condition that the range of the μ-meson must be less than 480 microns. These conditions fix the energy interval from about 2 Mev to 20 kev. The time spent in this energy interval is approximately 4×10^{-12} sec. The meson spends nearly all of this time near the high energy portion of the interval where the probability of large angle scattering is small. The probability that a π-meson will decay in flight in a photographic emulsion in the energy interval from 2 Mev to 20 kev is 1.7×10^{-4}. The probability that a π-meson will be scattered through a large angle in the last micron of track (in the energy interval from 20 kev to 2 Mev) and subsequently decay in flight is less than 1.7×10^{-6}. This probability is considerably lower than the occurrence of short μ-meson tracks from π-meson decays. Therefore the short range of the μ-meson tracks in events 1 through 8 do not appear to be due to the decay in flight of the π-mesons.

In the events 9 through 12 the angle between the π- and μ-meson tracks is such that the possibility cannot be excluded that the short range of the μ-meson is due to the decay in flight of the π-meson. In fact, the long range of the μ-meson tracks in events 13 and 14 is thought to be due to the decay in flight of the π-mesons.[7,12] If the events (9 through 12) which can be explained by decay in flight of the π-meson are excluded and if a correction is made for the thickness of the emulsions, the probability that a μ-meson from a π-meson decay will have a range less than 480 microns is found to be $3.3\pm1.3\times10^{-4}$.‡

An explanation for the unusual π-μ decays has been given independently by several investigators, namely, Nakano *et al.*,[13] Primakoff,[14] Eguchi,[15] Fialho and Tiomno,[16] and Fialho.[17] It has been proposed that a soft photon may accompany the π-μ decay due to the charge acceleration of the μ-meson at the time of decay:

$$\pi\rightarrow\mu+\nu+\gamma. \qquad (2)$$

The theoretical predictions are in general agreement with the experimental results for the ratio of "radiative" to normal decays. The theoretical value for this ratio is 1.3×10^{-4} which is to be compared with the experimental value of $3.3\pm1.3\times10^{-4}$. Fialho[17] has considered the effect of the magnetic moment of the μ-meson on the probability of emission of the γ-ray. Unfortunately, no definite conclusions can be drawn concerning the magnetic moment of the μ-meson from the comparison of the experimental results with the theoretical predictions because of the relatively small number of radiative decays that have been observed.

Short μ-meson tracks from π-meson decays have been observed by Powell,[5] Smith,[6] Bramson *et al.*,[18] George,[19] and Riezler and Rudloff.[8]

The author is greatly indebted to Professor J. K. Knipp and Professor M. Schein for their continued interest and encouragement in the many phases of the problem. The author is greatly indebted to Dr. R. Sagane for making his plates available to the author for a portion of this study. The author is grateful to Professor T. Eguchi for many interesting and stimulating discussions. The author is indebted to Professor H. L. Anderson for permission to use the facilities of the University of Chicago cyclotron. A portion of the plates was scanned by Miss M. McLean.

‡ *Note added in proof.*—This value is slightly higher than previously reported (see reference 7) due to the inclusion of an additional event (event 8 in Table I).

[10] E. A. Martinelli and W. K. H. Panofsky, Phys. Rev. **77**, 465 (1950).
[11] Durbin, Loar, and Havens, Phys. Rev. **88**, 179 (1952).
[12] W. F. Fry, Phys. Rev. **84**, 385 (1951).
[13] Nakano, Nishimura, and Yamaguchi, Prog. Theoret. Phys. **6**, 1028 (1951).
[14] H. Primakoff, Phys. Rev. **84**, 1255 (1951).
[15] T. Eguchi, Phys. Rev. **85**, 943 (1952) and private communications.
[16] G. E. A. Fialho and J. Tiomno, Anais acad. brasil. cienc. **24**, 245 (1952).
[17] G. E. A. Fialho, Notas De Fisica No. 1, 1952 (unpublished).
[18] H. J. Bramson and W. W. Havens, Jr., Phys. Rev. **83**, 861 (1951); Seifert, Bramson, and Havens, Phys. Rev. **86**, 603 (1952); Seifert, Bramson, and Havens, Bull. Am. Phys. Soc. **28**, No. 1, 20 (1953).
[19] E. P. George (private communications).

A Diffusion Cloud-Chamber Study of Pion Interactions in Hydrogen and Helium*

E. C. FOWLER,† W. B. FOWLER, R. P. SHUTT, A. M. THORNDIKE, AND W. L. WHITTEMORE
Brookhaven National Laboratory, Upton, New York

(Received March 27, 1953)

A description is given of the operation of a high pressure diffusion cloud chamber filled with hydrogen or helium and exposed to pion beams of both signs and energies near 60 and 100 Mev. Interactions occurring in the gas filling are investigated. The cross sections found in hydrogen agree with the results of others, including the large difference between the cross sections for positive and negative mesons. In helium the total cross sections are 89 ± 18 and 207 ± 27 mb with beams at 60 and 105 Mev, respectively. These cross sections include elastic and inelastic scattering, charge exchange, and absorption. The charge exchange cross sections, estimated at 20 and 60 mb for the two respective energies, are much larger than observed by others for different nuclei. Assuming that the mesons interact with the individual nucleons in the nucleus, an approximate calculation shows that a fairly consistent picture can be obtained making use of phase shifts determined by Anderson *et al.* for meson scattering on hydrogen.

I. INTRODUCTION

INTERACTIONS of pions in hydrogen and helium gas have been observed in a diffusion cloud chamber operated in various pion beams at the Nevis cyclotron[1] of Columbia University. Both results and experimental techniques are discussed in the present article. Since pions are considered to be nuclear-force mesons, an investigation of their interactions with light nuclei is of particular interest. Detailed theoretical predictions concerning the scattering of pions by nucleons on the basis of weak coupling theory have been presented by Ashkin, Simon, and Marshak,[2] and by Peshkin.[3] The strong coupling theory has been applied by Brueckner, leading to quite different results.[4]

At the time this work was started no data were available on the scattering of pions by hydrogen or helium, although a number of cosmic-ray experiments had indicated that pions have an approximately geometrical cross section for interactions with nuclei.[5–8] While this work was in progress a number of pion-proton cross sections were measured by Sachs, Steinberger, and co-workers[9,10] and energy and angular dependences determined by Anderson *et al.*,[11–14] both employing scintillation counter telescopes. Furthermore, data were obtained by Goldhaber and Lederman[15] using nuclear emulsions. Our data are in general agreement with those results and provide an independent confirmation of their correctness. The comparison is made in Sec. V. We are not aware of any other data on helium. Preliminary reports on some of our results have already been given.[16–18]

II. APPARATUS

A. The Diffusion Cloud Chamber

The development of high-pressure diffusion cloud chambers at Brookhaven arose from the need for a cloud chamber for use with the Brookhaven Cosmotron, which could accept pulses once every five seconds (the repetition rate of the machine). Normal pressure expansion cloud chambers of the required size can accept a beam pulse only about once a minute. If it is desired to study events directly in the gas, operation at high pressure becomes necessary, lengthening the cycling time even more. Continuously sensitive cloud chambers were built first by Langsdorf[19] and later by Cowan[20] and by Needels and Nielsen.[21] With the heavier gases diffusion cloud chambers cannot be operated far above normal pressure. However, with the light gases, of particular interest to us, diffusion cloud chambers operate best at pressures from 10 to 50 atmospheres.[22]

We used a diffusion chamber filled with hydrogen or helium at pressures near 20 atmospheres.[16] Its construc-

* Work performed under the auspices of the U. S. Atomic Energy Commission.

† Now at Yale University, New Haven, Connecticut.

[1] Supported jointly by the U. S. Office of Naval Research and the U. S. Atomic Energy Commission.

[2] Ashkin, Simon, and Marshak, Progr. Theoret. Phys. **5**, 634 (1950).

[3] M. Peshkin, Phys. Rev. **81**, 425 (1951).

[4] K. A. Brueckner, Phys. Rev. **86**, 106 (1952).

[5] Camerini, Fowler, Lock, and Muirhead, Phil. Mag. **41**, 413 (1950).

[6] Butler, Rosser, and Barker, Proc. Phys. Soc. (London) **A63**, 145 (1950).

[7] W. W. Brown and A. S. McKay, Phys. Rev. **77**, 342 (1950).

[8] B. P. Gregory and J. H. Tinlot, Phys. Rev. **81**, 667, 675 (1951).

[9] Chedester, Isaacs, Sachs, and Steinberger, Phys. Rev. **82**, 958 (1951).

[10] Isaacs, Sachs, and Steinberger, Phys. Rev. **85**, 803 (1952).

[11] Anderson, Fermi, Long, Martin, and Nagle, Phys. Rev. **85**, 934 (1952).

[12] Anderson, Fermi, Long, and Nagle, Phys. Rev. **85**, 936 (1952).

[13] Anderson, Fermi, Nagle, and Yodh, Phys. Rev. **86**, 793 (1952).

[14] Anderson, Fermi, Martin, and Nagle, Phys. Rev. **91**, 155 (1953).

[15] G. Goldhaber, Phys. Rev. **87**, 220 (1952); G. Goldhaber and L. Lederman, Phys. Rev. **90**, 343 (A) (1953).

[16] Shutt, Fowler, Miller, Thorndike, and Fowler, Phys. Rev. **84**, 1247 (1951).

[17] Thorndike, Fowler, Fowler, and Shutt, Phys. Rev. **85**, 929 (1952).

[18] Fowler, Fowler, Shutt, Thorndike, and Whittemore, Phys. Rev. **86**, 1053 (1952).

[19] A. Langsdorf, Rev. Sci. Instr. **10**, 91 (1939).

[20] E. W. Cowan, Rev. Sci. Instr. **21**, 991 (1950).

[21] T. S. Needels and C. E. Nielsen, Rev. Sci. Instr. **21**, 976 (1950).

[22] Miller, Fowler, and Shutt, Rev. Sci. Instr. **22**, 280 (1951); J. M. Wyckoff, Phys. Rev. **87**, 185 (1952).

tion is indicated by Fig. 1. The chamber consists of welded steel top and bottom cans separated by a bakelite insulating ring.

The bottom can has a $\frac{1}{4}$-in. stainless steel cylinder wall (1), and a 1.25-in. bottom plate (2), and top flange (3), both made from cold rolled steel. There are two rectangular-shaped ducts at opposite sides of the cylinder to provide for windows. Each duct ends in a window face plate (4) provided with an *O*-ring groove. The bottom plate carries a drain for liquid at the center.

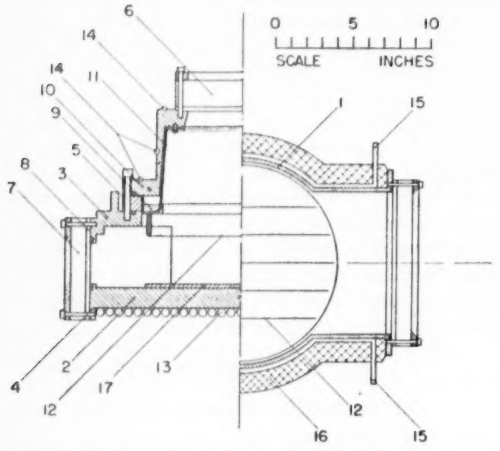

FIG. 1. Diagram of diffusion cloud chamber designed for operation at 20 atmospheres.

The bakelite ring (5), placed between top and bottom cans, is sealed by *O*-rings. The bolts fastening the top to the bottom are thermally insulated from the top by Bakelite washers and fiber sleeves.

The top was made in a hat shape so that the top window (6) could be close to the camera and hence be small in size. In addition, the extra space provides an improved vapor supply.

In principle the construction of each of the three windows is the same. Supported by a 1-in. thick plexiglass slab (7), a $\frac{1}{4}$-in. thick piece of Allite[23] (8) in contact with an *O*-ring seals against the pressure. Special low temperature *O*-rings[24] are used at the side windows. Allite is used because it is not attacked by alcohol. Plastic windows were thought to be superior to glass windows because of the large temperature gradients present in the side windows while under high mechanical stress. Lucite also has a lower thermal conductivity than glass, making it easier to maintain the proper temperature gradients.

The top carries a liquid reservoir in the form of a copper trough (9) in good thermal contact with the top's base plate (10). In order to enhance evaporation from the trough a piece of felt lines the vertical portion of the top (11), and hangs in the trough so that the felt is kept wet by capillary action. A set of five wires (12), 0.025 in. in diameter, spaced $1\frac{7}{8}$ in. apart, is mounted on insulated posts to provide a grid to which an electric sweeping voltage may be applied. The top is pierced by a Kovar-glass lead-through for the sweeping voltage and also by a filling line which terminates just above the copper reservoir trough.

In order to provide temperature control the chamber has cooling coils (13) at the bottom and nichrome heating wires at the top (14) and at the side (15). Furthermore, the chamber is insulated (16) from the surrounding air. These facilities, aided by the bakelite ring, make it reasonably easy to vary the temperature gradient in the side wall while holding the top and bottom temperatures approximately constant.

A circular piece of black glass (17) forms the photographic background. The side walls of the chamber are lined with black velvet, and the inner metallic surfaces of the top are painted with black glyptal where necessary.

B. Auxiliary Equipment

The chamber is cooled by trichloroethylene circulated directly over pieces of dry ice contained in a can. A turbine pump[25] driven by a $\frac{1}{3}$-hp motor pumps 6 gal/min through a screened intake and through the cooling coils of the chamber at a gauge pressure of about 20 lb/in.^{2}. This brings the temperature of the chamber's bottom plate to about -70°C.

The chamber is illuminated by two flash tubes of 4-mm i.d. Vykor tubing, 8 in. long, with tungsten anode and sintered tungsten-bariumoxide cathode,[26] filled with Kr and Xe at pressures of about 20 and 160 mm Hg, respectively. For photographing tracks a 70-μf capacitor at 2000 v is discharged through each tube. The light is focused to a beam about $2\frac{1}{2}$ in. high by parabolic reflectors 8 in. long with focal length $\frac{7}{8}$ in. The reflectors consist of chrome-on-brass ferrotype plates forced into a set of ribs machined to the required parabolic shape. Each parabola is mounted in a sheet metal box through which air is blown to cool the flash tube and reduce condensation on the Lucite windows.[27] Under these conditions flash tubes have a useful life of many thousand flashes. For visual observation of the chamber a 1.0-μf condenser charged to 2000 v is discharged through the flash tube at a rate of about 40 times per second.

Stereoscopic photographs are taken through two f/2.3, 30-mm Baltar wide-angle lenses, mounted just above the top window of the chamber. Apertures of

[23] Procured from the Homalite Corporation, Wilmington, Delaware, and Cast Optics Corporation, Riverside, Connecticut.

[24] Procured from Linear Incorporated, Philadelphia, Pennsylvania.

[25] Procured from Aurora Pump Company, New York, New York.

[26] Procured from P. R. Mallory Company, Indianapolis, Indiana.

[27] Fogging of the windows at the outside is prevented by occasional wiping with "Photo-Flo," procured from Eastman Kodak Company, Rochester, New York.

$f/5.6$ or $f/8$ are normally used. Each lens views the center of the chamber at an angle of about 8°. Interchangeable film magazines fit into the lens mount, holding 100 ft of 35-mm film, normally unperforated Linagraph Ortho. Film is advanced by a motor drive so that the two stereo views are interspaced on the same film.

Timing circuits are necessary to determine the overall repetition rate and the timing of sweeping field, cyclotron beam, light flash, and camera film advance. The sequence of operations is indicated in Fig. 2, and typical time intervals are given. All the necessary timing is achieved by means of delay units consisting of *RC* circuits on the grids of 2D21 tubes driving Struthers-Dunn relays. Each unit controls an operation and starts the next unit. The last one removes the plate voltage, which resets all units. The delays are variable over wide ranges and have proved to be reliable and sufficiently accurate for the purpose.

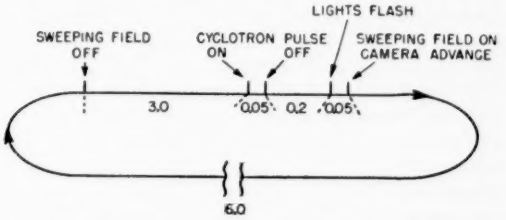

FIG. 2. Schematic cycle of operations with typical time delays indicated. All times are in seconds.

III. OPERATION OF DIFFUSION CHAMBER

A. General Procedure

Light gases can be employed conveniently in diffusion cloud chambers if the pressure is increased appropriately.[22,28] In these experiments either hydrogen at about 300 lb/in.^{2} pressure (above atmospheric) or helium at about 200 lb/in.^{2} were employed. The vapor used has been methyl alcohol in all cases. It has desirable properties of high vapor pressure, low freezing point, and low critical supersaturation for the formation of droplets.

The temperature of the bottom of the chamber is kept at about −70°C. The top of the chamber is kept at about 15°C. Since it is insulated from the bottom by the bakelite ring, its temperature is fairly uniform. Practically all the gradient occurs across the bakelite ring and along the side wall of the bottom part of the chamber. Just below the bakelite ring the temperature is kept at about 0°C. This leaves a gradient of about 7°C per cm in the side wall of the chamber. Under these conditions a sensitive layer 6-7 cm deep may be obtained at the bottom of the chamber. Conditions in the chamber vary considerably, and the largest droplets are found near the top of the sensitive layer. Nevertheless photographs of tracks passing through the sensitive layer rarely show a marked change in density except near the top or bottom.

The depth of the sensitive layer can be increased by making the bottom colder. By reducing the temperature to −90°C an increase of about 2 cm in layer depth was obtained, but the tracks near the bottom were rather thin and slow-forming because of the very low vapor pressure at the bottom. This procedure was not employed during runs with the cyclotron. If the top temperature is raised to increase the vapor supply, a background fog with a cellular structure appears with H_2 or He fillings. This is believed to be caused by local turbulent currents induced by the heat released by the condensation process. If the temperature gradient is reduced, tracks become less dense and the sensitive layer may lift off the bottom of the chamber. The temperature distribution described gave the deepest layer of satisfactory quality. These observations are in agreement with theoretical estimates.[28]

Since the supply of vapor existing in the gas is limited, it may be exhausted by excessive ionization in the chamber, in which case the chamber becomes completely insensitive. A continuous intensity need only be 3 to 10 times (depending on the gas and pressure used) cosmic-ray intensity to do this. If the source of radiation is removed, the chamber recovers in about one minute. In experiments with the cyclotron-produced meson beam a short pulse of fairly high intensity passes through the chamber, which then has a recovery period before the next pulse. Under such conditions intensities many times cosmic-ray intensity are possible as long as the average intensity does not become too great. Under some conditions the chamber may be locally insensitive. A dense background track may take enough vapor from a certain region to make it temporarily insensitive. A beam track passing through this region shortly afterward will then have a "gap" in it due to this insensitivity. Such gaps have, in fact, been frequent, and have made the analysis of the pictures obtained more difficult. These effects are caused both by background particles passing through the sensitive layer of the chamber and by those passing above it. The ions formed above the sensitive layer diffuse down into it and then act as nuclei for the formation of droplets, either in the form of a uniform "rain" or as broad diffuse tracks.

The chamber can be made more radiation-resistant by the application of an electric sweeping field, especially in the case where the radiation occurs mainly in pulses. The sweeping field is turned on for a period after the pulse and serves mainly to sweep out ions formed in the upper part of the chamber before they can diffuse into the sensitive region. The sweeping field does, however, sweep some ions into the sensitive region and causes some distortion of tracks formed in the sensitive region, so that it should be turned off some time before the desired particles pass through the

[28] R. P. Shutt, Rev. Sci. Instr. **22**, 730 (1951).

chamber, as shown in Fig. 2. In most cases the sweeping field potential has been about 1000 v.

B. Operation with the Nevis Cyclotron

The experiments reported here were all carried out using pion beams produced at the Columbia University Nevis cyclotron. The pions were produced in an internal target, partially focussed in the fringing field of the cyclotron, and allowed to emerge through holes in the six-foot thick concrete shield of the cyclotron. The arrangement is shown in Fig. 3. The cyclotron beam was controlled by pulsing the ion source, usually with a cycle time of about six or eight seconds. The number of particles traversing the chamber could be adjusted by changing the pulse length. The cyclotron usually ran with a repetition rate of 40 to 80 per sec and the beam pulse was long enough to include one to four cycles, or occasionally more.

In most cases the diffusion chamber was run concurrently with the Columbia 16-in. expansion chamber.[29] During the recovery period of the expansion chamber the diffusion chamber was automatically cut in, operated for six to eight beam pulses, then cut out when the expansion chamber was ready for a pulse. This procedure was quite successful on the whole, although there was some difficulty in obtaining meson-beam intensities satisfactory for both chambers.

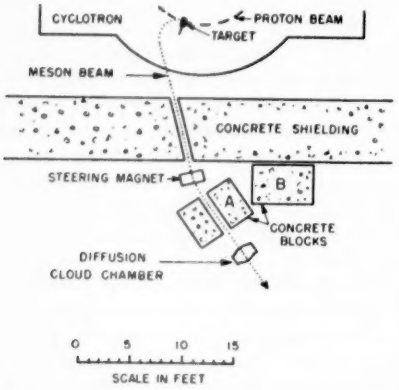

FIG. 3. Position of cloud chamber, steering magnet, and shielding, relative to cyclotron.

The steering magnet deflected the pions out of the direct line of sight through the hole in the shielding. Concrete shielding blocks were necessary to reduce background. In lining up the equipment and during operation a beam monitor consisting of two scintillation counters in coincidence proved very useful. Despite all these precautions high background remained one of the chief problems, consisting of both particles occurring between desired beam pulses and particles occurring at the time of the beam pulse but with random directions.

[29] Byfield, Kessler, and Lederman, Phys. Rev. **86**, 17 (1952).

Under these conditions it has been possible to obtain about 10–20 beam tracks per pulse with fairly good picture quality. Pictures were taken at a rate of about 400 per hour, so that a typical two-shift day resulted in about 5000 pictures, allowing some time lost for setting up, adjustment, and repair of minor casualties.

IV. RESULTS

A. Pictures Obtained

Major portions of eight days of cyclotron operation were required to obtain the pictures upon which we are now reporting. In an attempt to survey the various interactions which might be studied with a diffusion chamber, H_2 and He fillings were employed, each with positive and negative pions of about 60 Mev and negative pions of about 100 Mev. The conditions of the various runs are summarized in Table I, where the pion energies inside the chamber are listed. A total of 33 700 pictures were taken and analyzed. On the average each picture has about 10 pion tracks.

TABLE I. Summary of pictures obtained.

Day	Gas	Beam	No. of pictures
6 April 1951	H_2	60-Mev π^-	5600
1 June 1951	He	53-Mev π^+	3400
28–29 June 1951	H_2	53-Mev π^+	8400
28–29 January 1951	He	68-Mev π^-	5700
3 June 1952	H_2	105-Mev π^-	5400
11 June 1952	He	105-Mev π^-	5200

B. Analysis of Pictures

The analysis of the pictures was carried out in two steps; the films were first scanned and interesting events noted, then each event was analyzed in detail. For scanning modified Stereo-Vivid projectors[30] were used, which enabled either stereo view to be thrown upon the screen. By looking at the image obliquely, so that the beam tracks are foreshortened, any deflection is readily recognized. Under these conditions confusion due to background tracks is much reduced. Once the procedure was established, the majority of the scanning was done by nonscientific personnel, as has often been done in nuclear emulsion work.

For analysis of the scattering events a projector was built in which the camera lenses could be used in the same geometry as employed for taking pictures. The two stereo images were made to coincide on a ground glass screen by properly adjusting its position in space.[31] In this way the true lengths of tracks and angles between them were measured.

During the scanning each beam track was inspected, as in "along-the-track" scanning in emulsions,[32] and

[30] Procured from Three Dimension Company, Chicago, Illinois.
[31] W. Powell, Rev. Sci. Instr. **20**, 402 (1949).
[32] Bernardini, Booth, Lederman, and Tinlot, Phys. Rev. **82**, 105 (1951).

any event was noted which might possibly be a pion interaction. In addition all decays in flight of pions (π) into mesons (μ) with projected angles of 4° or more (in either view) were recorded. (Such π-μ decays appear as sudden deflections of straight tracks without the recoil track characteristic of a scattering event.) About 20 percent of the pictures were scanned twice independently as a check on the consistency of the scanning procedure and on scanning efficiency. The number of π-μ decays checked was great enough that the discrepancies could be used to estimate the probability that a single observer would find a π-μ. This scanning efficiency was determined to be 86 percent, 91 percent, 83 percent, 93 percent, 88 percent, and 87 percent on the various runs (in the order appearing in Table I). For pion-interaction events the probability of detection should be somewhat higher, since they are easier to recognize. It seems certain that not many events were missed.

A considerable number of events were noted during scanning which were not pion interactions. When the events were reprojected and analyzed the following criteria were used to determine whether the event was acceptable: (1) Incoming track must be straight and in the direction of the meson beam. (2) Angles between tracks must be consistent with those expected for a pion interaction, in particular, an elastic scattering must be coplanar, with the right angular relationships. (3) Lengths of recoil tracks must be consistent with those expected. (4) Densities of tracks must be reasonably consistent with those expected. These considerations usually determine whether the event is a pion interaction or not, although there are a few doubtful cases. In particular, scatterings with small scattering angle and very short recoil are always doubtful, and elastic scatterings through less than 20° were not counted.

C. Determination of Pion Path Length

The number of π-μ decays observed is used as an indication of the total path length of the pions that have traversed the cloud chamber. The mean path length for decay of a pion of momentum p, rest mass μ_0, and rest lifetime τ_0, is

$$X = p\tau_0/\mu_0. \tag{1}$$

Taking $\tau_0 = 2.55\times10^{-8}$ sec,[33-35] and $\mu_0 = 277m_e$,[36] this gives (X in cm, pc in Mev)

$$X = 5.44pc. \tag{2}$$

From this length and the average gas density in the sensitive depth the path length in g/cm² per π-μ decay is calculated.

[33] Lederman, Byfield, and Kessler, Phys. Rev. **85**, 719 (1952).
[34] W. L. Kraushaar, Phys. Rev. **86**, 513 (1952).
[35] Durbin, Loar, and Havens, Phys. Rev. **88**, 179 (1952).
[36] Barkas, Smith, and Gardner, Phys. Rev. **82**, 102 (1951).

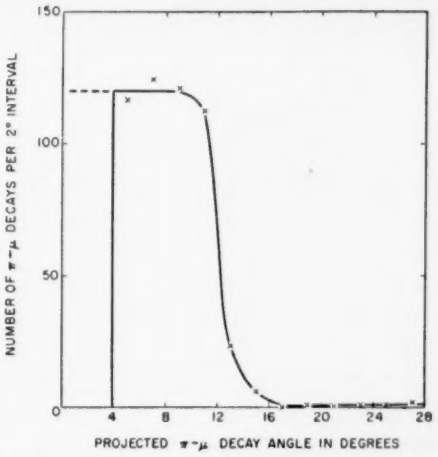

FIG. 4. Typical distribution of projected π-μ angles. The points shown were obtained for the 105-Mev π^- beam which gave the sharpest cutoff.

To obtain the total number of π-μ decays a correction must be made to the number of π-μ's counted to take account of those with projected angles less than 4°. This correction is determined by plotting the distribution of π-μ decay angles, as in Fig. 4. The dotted curve gives the number of π-μ's of small angle that were not counted. (While the distribution of true π-μ angles in space is peaked at the maximum angle, calculation shows that the projected angle distribution should be quite flat for the present pion energies.) The correction factor is therefore the ratio of the total area under the curve to that under the solid part. The cut-off angle of the distribution is also useful since it provides a measure of the pion momentum. A broad distribution of pion momenta would lead to a gradual decline rather than the sharp cut-off seen in Fig. 4.

The π-μ counts and π-path lengths derived from them are given in Table II.

D. Interactions Observed

The numbers of interactions observed are given in Table III. From the numbers of interactions and the π-μ decays the path lengths and cross sections for interactions can be calculated. These results are also given in Table III. Statistical standard errors are

TABLE II. Pion path lengths observed.

Gas	Beam	π-μ count $\theta \geqslant 4°$ in left view	Correction factor	Path length per π-μ g/cm²	Total path length g/cm²
H_2	60-Mev π^-	642	1.32	1.65	1400
H_2	53-Mev π^+	967	1.24	1.49	1780
H_2	105-Mev π^-	504	1.54	2.22	1720
He	68-Mev π^-	298	1.35	2.16	865
He	53-Mev π^+	345	1.25	2.12	915
He	105-Mev π^-	516	1.47	3.09	2340

TABLE III. Summary of interactions.

Filling	Beam	Number of interactions	Interaction path length g/cm²	Cross section in millibarns (10^{-27} cm²)
H_2	60-Mev π^-	3	470	3.5±2
H_2	53-Mev π^+	21	85	22±5
H_2	105-Mev π^-	11	160	11±3
He	68-Mev π^-	11	79	84±26
He	53-Mev π^+	13	70	95±27
He	105-Mev π^-	72	33	207±24

quoted. The cross sections calculated directly from the number of observed interactions have been increased by 5 percent–13 percent to correct for the elastic scatterings through less than 20° which were not counted. The amount of correction depends on the amount of elastic scattering and on the shape of the angular distribution above 20°.

It is not likely that any of the observed interactions listed in Table III involved carbon or oxygen in the alcohol rather than H_2 or He. At our operating pressures there is at most (at the top of the sensitive layer) one molecule of methyl alcohol per 800 molecules of H_2 or 600 atoms of He. In addition interactions of pions with C or O would certainly not be confused with elastic scatterings from H_2 or He and would not be expected to resemble inelastic scatterings or absorptions in the light elements very often. A few pion interactions apparently involving C or O were observed in addition to those given in Table III.

V. DISCUSSION OF HYDROGEN DATA

In the case of hydrogen, negative pions (π^-) can undergo elastic scattering, charge exchange scattering, or radiative capture, while positive pions (π^+) undergo elastic scattering only. The reactions are given in Eq. (3). Only the elastic scatterings were observed in the cloud chamber:

$$\begin{aligned} &\pi^-+p\rightarrow\pi^-+p && \text{(elastic)}\\ &\pi^-+p\rightarrow\pi^0+n && \text{(charge exchange)}\\ &\pi^-+p\rightarrow\gamma+n && \text{(radiative capture)}\\ &\pi^++p\rightarrow\pi^++p && \text{(elastic).} \end{aligned} \tag{3}$$

The other interactions should appear as beam meson tracks disappearing without recoil or scattered particle. Because of the frequent gaps in tracks and insensitive areas in the chamber such disappearances were not generally recognizable, although one definite example was noticed. Consequently, the hydrogen cross section given in Table III for π^+ is the total cross section while those given for π^- are not. Results obtained at Chicago indicate that elastic scattering is only about $\frac{1}{3}$ the total cross section for π^- at 118 Mev.[37] Radiative capture is thought to be small (see Sec. VI).

The cross sections here reported for π^- suggest that also at 60 Mev elastic scattering of π^- is much smaller than the total cross section. The cross section for π^+ is consistent with the Chicago data. A summary of cross sections reported in the literature[9–14,38] is given in Fig. 5.

From the π^+-p scattering events at 53 Mev it was possible to obtain some information concerning the angular distribution. As previously reported[18] the scatterings are concentrated in the forward and backward directions. They are consistent with $\cos^2\theta_0$ or $(1+3\cos^2\theta_0)$ distributions (θ_0 is the angle in the center-of-mass system), but not with an isotropic one, indicating that p-wave scattering is important at these energies. However, because of the large statistical errors, there may also be some s-wave scattering. This would lead to asymmetries in the distributions as observed by the Chicago group at higher energies.[13,14]

VI. DISCUSSION OF HELIUM DATA

A. Experimental Cross Sections

When a pion strikes a helium nucleus, the interactions shown in Eq. (4) can take place. The combination $(2p+2n)$, for instance, signifies

$$\pi^++\text{He}\rightarrow\pi^++\text{He},\quad \pi^-+\text{He}\rightarrow\pi^-+\text{He} \quad \text{(elastic)} \tag{4a}$$

$$\rightarrow\pi^++(2p+2n),\quad \rightarrow\pi^-+(2p+2n) \quad \text{(inelastic)} \tag{4b}$$

$$\rightarrow\pi^0+(3p+n),\quad \rightarrow\pi^0+(p+3n) \quad \text{(charge exchange)} \tag{4c}$$

$$\rightarrow(3p+n)\quad \rightarrow(p+3n) \quad \text{(absorption),} \tag{4d}$$

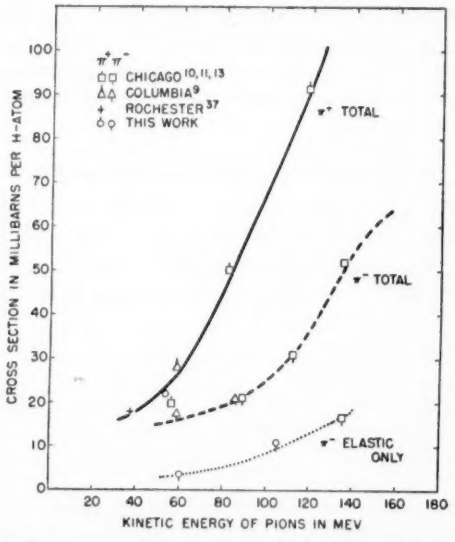

FIG. 5. Summary of cross sections obtained by various experimenters for π-p scattering. The solid curve gives the π^+-p cross section, the dashed curve the total π^--p, and the dotted curve the elastic π^--p cross section only. The highest energy points obtained at Chicago are off scale on this graph.

[37] Fermi, Anderson, Lundby, Nagle, and Yodh, Phys. Rev. **85**, 935 (1952).

[38] Barnes, Clark, Perry, and Angell, Phys. Rev. **87**, 669 (1952).

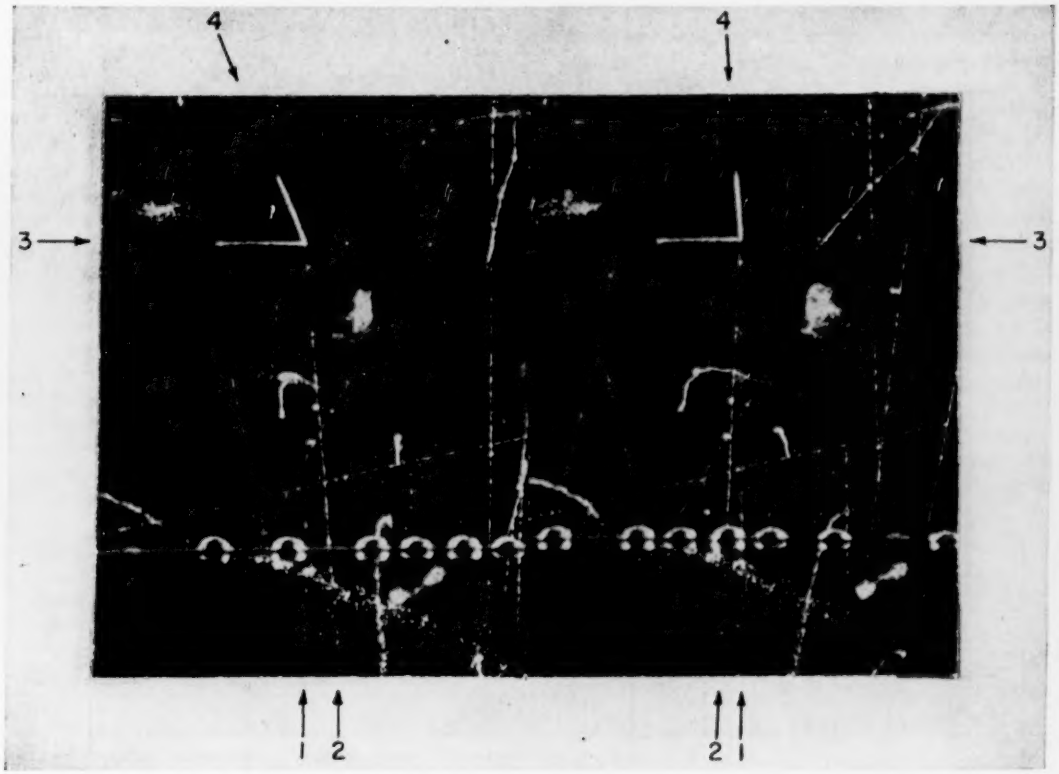

FIG. 6. Photograph of a 105-Mev negative pion scattered inelastically in helium. Tracks 1 and 2 show incident and scattered pions, respectively. Tracks 3 and 4 are two charged recoils, both stopping in the gas.

two protons and two neutrons, some of which may be bound together as He^3, H^3, or H^2.

The pion may be scattered elastically with cross section σ_e [Eq. (4a)], or the interaction may lead to a reaction with cross section σ_r [Eq. (4b, c, d)]. The total cross section is therefore $\sigma_t=\sigma_e+\sigma_r$. Examples of photographs are given in Figs. 6 and 7.

σ_r can be split into several other cross sections. The pion can transfer enough energy to the constituent nucleons of the nucleus to excite the latter. Since helium has no excited states except for a broad level near its binding energy of 28 Mev, this will practically always result in a disintegration of the nucleus [Eq. (4b)]. In addition to the incoming meson track, one therefore should see a track of a considerably slowed-down meson and either one heavily ionized track due to a He^3 nucleus, or two such tracks attributable to H^3+H^1, $2H^2$, or $2H^1$ (Fig. 6). σ_i shall stand for the cross section for these events. The other class of events results in a transfer of the electric charge of the meson to a nucleon [Eqs. (4c) and (4d)], with a cross section σ_c so that $\sigma_r=\sigma_i+\sigma_c$. Here no meson track can be seen after the collision (Fig. 7). If the meson had positive charge, 2 or 3 heavily ionized tracks will emerge, consisting of He^3+H^1, H^2+2H^1, or $3H^1$. If the meson was negative there will be only one heavy track after the collision consisting of H^3, H^2, or H^1.

σ_c can be subdivided further. The transfer of charge may either have occurred by a scattering of the meson with charge exchange, [Eq. (4c)], with cross section σ_γ, or by absorption of the meson [Eq. (4d)], with cross section σ_a. Therefore $\sigma_c=\sigma_a+\sigma_\gamma$. The pion can be absorbed by a single nucleon, resulting in a gamma-ray and a recoil particle, or by several nucleons simultaneously, resulting in several recoil particles of fairly high energy exhibiting a certain amount of correlation between their directions of flight. Without application of a magnetic field for momentum measurements some difficulty is encountered in deciding whether a particular event classified under σ_c belongs to σ_a or σ_γ. For π^+, where three outgoing prongs are visible, a conclusion might be drawn from the spatial correlation of the prongs, their range, and their apparent density of ionization. However, for π^- events, with only one outgoing prong, no such arguments are available.

As stated above, observations were made with π^+ at 53 Mev, and with π^- at 68 and 105 Mev. The observed

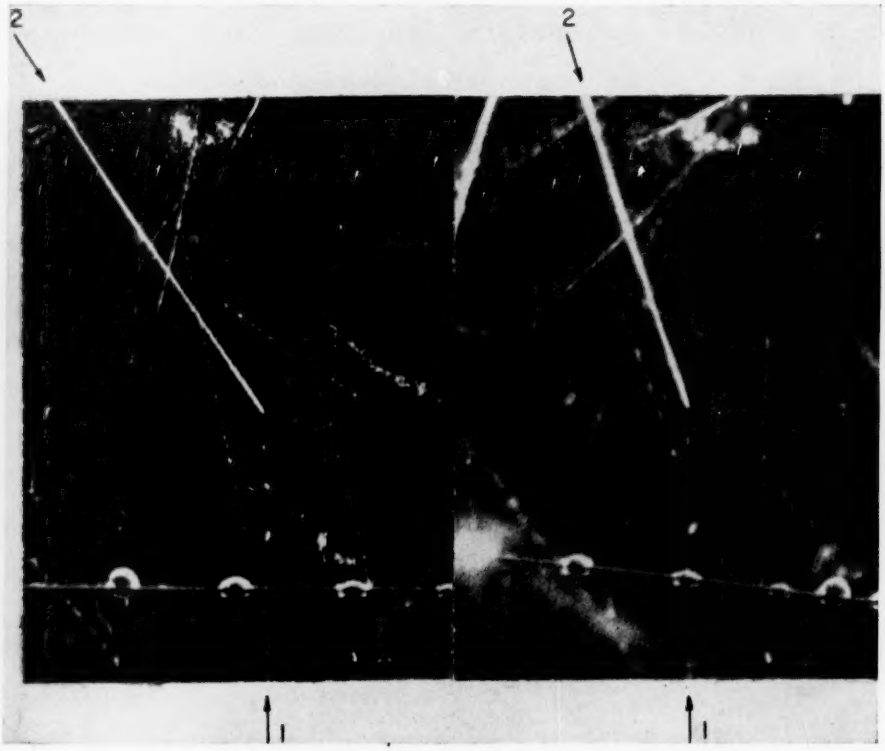

FIG. 7. Photograph of charge exchange or absorption of a 105-Mev negative pion. Track 1 is the incident pion and Track 2 is the only charged recoil.

frequencies of the different types of interactions are compiled in Table IV.

The absorption event noted for π^+ at 53 Mev has been exhibited previously.[17] It shows what are believed to be two fairly fast protons emerging in almost opposite directions, and a third short, heavy track. The four other events noted under "charge transfer" are believed to be caused by charge exchange for the following reasons. Since the maximum energy transfer from a 53-Mev pion to a nucleon is about equal to the total binding energy of 28 Mev of the helium nucleus, one might expect that the most probable event to happen after a charge exchange would be a disintegration of He^4 into He^3+H^1 requiring only 21 Mev. In such a break-up the proton, formed by collision with charge exchange of the incoming π^+ with a neutron, would receive most of the available energy. The He^3 particle, receiving only a small portion of the energy, loses its energy quite fast because of its twofold electric charge and thus exhibits a very short range. Therefore at the present fairly low energy a π^+ charge-exchange event may be expected to consist of a fairly heavy proton prong of medium range and a very short He^3 prong. The four events under discussion show this feature. When a π^+ is absorbed by helium, on the other hand, one should usually see at least 2 energetic charged particles. The statistical argument given below in connection with the prong distribution from π^- interactions also indicates these π^+ interactions to be charge exchange. The possibility of radiative absorption by a single neutron is not yet excluded by these arguments but will be excluded shortly. With this identification of events the charge-exchange cross section for 53-Mev positive pions on helium is $\sigma_\gamma = 29 \pm 15$ millibarns. This cross section has been singled out because it is based on fairly direct evidence. Since the numbers of π^+ and π^- events at 53 and 68 Mev, respectively, are quite similar, taking into account the respective total observed paths through helium (see Tables II and III), we shall lump these data together for further discussion,

TABLE IV. Frequency of different types of interactions observed in helium.

Pion energy (Mev)	Electric charge	Elastic cases	Inelastic cases	Charge transfer	
				Charge exchange cases	Absorption cases
53	pos.	6	2	4	1
68	neg.	4	2	5	
105	neg.	25	18	29	

referring to the average energy of 60 Mev. All cross sections thus calculated are listed in Table V, columns 1–4.

Although for π^- collisions with helium there is no way to distinguish between charge exchange and absorption for a single event without a magnetic field, a statistical argument favors an interpretation of σ_c mainly in terms of charge exchange. A meson can be absorbed by two or more nucleons[39,40] where some of the absorbing nucleons may remain bound together. In the center-of-mass system (cms) the statistical prong distribution is expected to be symmetric with respect to the backward and forward directions. The motion of the cms in the laboratory system distorts this distribution towards the forward direction. The degree of distortion has been calculated, for different angular distributions in the cms, with the result that at both energies considered here the ratio of the number of forward prongs to the number of backward prongs should be at most 1.5:1. Therefore one should observe not many more prongs in the forward direction than in the backward direction. Actually, at 60 Mev 9 prongs go forward and none backward, while at 105 Mev 23 prongs go forward and 6 backward, which is quite different from any distribution expected for non-radiative absorption. Similar calculations for the effect of radiative absorption by a single nucleon show that here a predominantly forward distribution might be expected. However, from results on photoproduction of mesons one can estimate for the inverse reaction a cross section of only about 0.5 mb. We therefore conclude that the observed charge-transfer events cannot be explained by radiative absorption by a single nucleon, few of them are due to absorption by two or more nucleons, and most are due to charge exchange. If, on the other hand, most of the charge-transfer events were to be ascribed to absorption by two or more nucleons some explanation of the observed forward prong distribution would have to be found.

TABLE V. Cross sections found experimentally for helium.

Pion energy (Mev)	1 σ_t(mb)	2 σ_e(mb)	3 σ_i(mb)	4 σ_s(mb)	5 σ_α(mb)	6 σ_γ(mb)
60 (av.)	89±18	37±12	15±8	37±12	15	22
105	207±24	74±14	51±12	82±12	20	62

Since helium in the ground state contains two protons with opposite spins and two neutrons with opposite spins, all charge-exchange events must be inelastic according to the Pauli principle. One would therefore expect that their prong distribution would look similar to the distribution of prongs for inelastic events. This is indeed shown by the diagram in Fig. 8, plotted for the 105-Mev data. Of the 18 inelastic events 8 show a single heavy prong going forward, while 10 show 2 heavy prongs. All 28 prongs are plotted. Of these 19 pass forward and 9 backward, compared with 23 forward and 6 backward for the charge-transfer events. Since the binding energy of the He^3 observed in the 8 single-prong inelastic events is the same as that of H^3 produced by charge exchange, one might expect that $29\times8/18=13$ of the latter correspond to the 8 single-forward-prong inelastic events, leaving 16 events corresponding to the 10 double-prong inelastic events. The latter 10 events contain 9 heavy prongs going backward and 11 going forward. Thus for the remaining 16 charge-exchange events about 14 corresponding particles should pass backward and 18 forward. Due to exchange of charge only one-half of each of these groups can be visible as prongs in the cloud chamber. Therefore, from the prong distribution for inelastic events we infer that $13+9=22$ of the charge-transfer events should have forward prongs and 7 backward ones, in

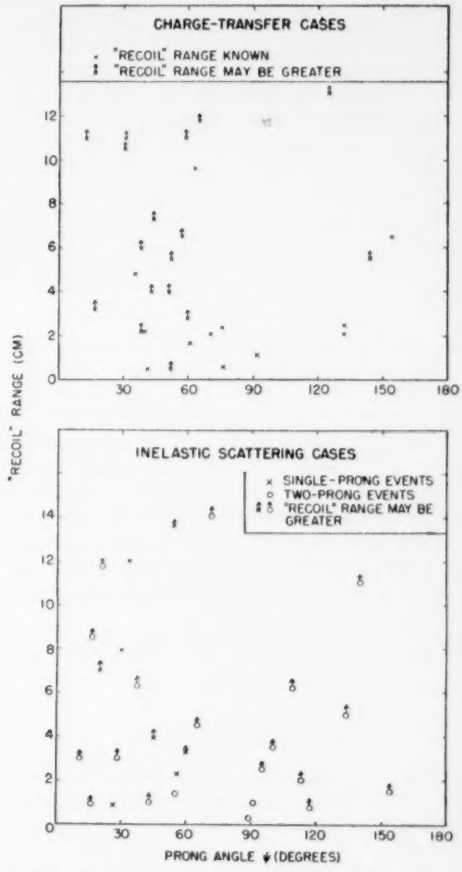

FIG. 8. Scatter diagrams of "recoil" ranges of heavy prongs for charge transfer and inelastic scattering, plotted from 105-Mev π^- helium results. Prong angle ψ is measured with respect to direction of incident pion track.

[39] F. L. Adelman, Phys. Rev. **85**, 249 (1952).
[40] S. Ruddlesden and A. Clark, Nature **164**, 487 (1949).

agreement with the observed distribution. Of course, because of the relatively small number of events studied here this agreement is partially fortuitous, and we cannot rule out that a fair portion of the events in question is caused by absorption. Another argument involving the magnitude of σ_e also favors the interpretation of the observed charge-transfer events given above and will be presented in Sec. VI C. Weighting all of the evidence presented we have arrived at the estimates for σ_γ and σ_a given in Table V, columns 5 and 6.

The apparently large charge-exchange cross section found here is not in agreement with results obtained by other authors for deuterium[41] and for heavier nuclei, from beryllium on up.[29,42,43] None of these authors report charge-exchange cross sections greater than a few millibarns.

The angular distribution of the elastically scattered mesons is given in Table VI. This table shows the data listed in two ways as functions of the cms-angles θ_0. For the ranges $0<\theta_0<60°$, $60°<\theta_0<120°$, and $120°<\theta_0<180°$ average differential cross sections $\Delta\sigma_e/\Delta\omega$ ($\Delta\omega=\omega_2-\omega_1=2\pi(\cos\theta_{01}-\cos\theta_{02})$) are given, while for the ranges $0<\theta_0<90°$ and $90°<\theta_0<180°$ "total" forward and backward cross sections are noted. Despite the large statistical errors, there appear to be two possibly significant features. At 60 Mev the scattering is almost completely backward, and at 105 Mev the scattering appears to be almost isotropic.

In the following sections an attempt will be made to interpret the present results in some more detail and to correlate them to the observed pion-nucleon cross sections.

B. General Considerations Concerning the Pion-Helium System

For the pion energies of 60 and 105 Mev the wavelengths in the cms of helium nucleus and pion are $\lambda_0=1.45\times10^{-13}$ and 1.04×10^{-13} cm, respectively. A radius for the nucleus can be defined by $R_1=A^{\frac{1}{3}}(\hbar/\mu_0 c)$, where A is the number of nucleons in the nucleus. For helium $R_1=2.21\times10^{-13}$ cm. Thus λ_0 and R_1 are almost equal, which implies that for the present case not much meaning can be attributed to a geometrical interpretation of R_1.

It follows quite generally from collision theory that

$$\sigma_e=A_n|1-C|^2, \tag{5}$$

and

$$\sigma_r=A_n(1-|C|^2), \tag{6}$$

where the "nuclear area" A_n is equal to πR_1^2 only if $\lambda_0\ll R_1$, and where C is a complex number with absolute value $\leqq 1$. C is related to the nuclear potential and is therefore of interest. One can write

$$C=|C|e^{2i\alpha}, \tag{7}$$

where α can be called the average phase shift of the scattered wave due to the nuclear potential. Therefore we have

$$\sigma_e=A_n(1-2|C|\cos2\alpha+|C|^2). \tag{8}$$

Although σ_e and σ_r have been measured, $|C|$ and α cannot be determined if A_n is not known. But since we have the condition that $|\cos2\alpha|\leqq1$ a lower limit for A_n can be found. From the data in Table V we obtain $A_n\geqq54\pm17$ mb at 60 Mev and $A_n\geqq147\pm29$ mb at 105 Mev. (πR_1^2 is equal to 154 mb.) Except for these lower limits for the nuclear area nothing can be said about C without further assumptions for A_n. Assuming different values for the nuclear radius R so that πR^2 is greater than the lower limits just determined for A_n we can make use of the "optical model"[44,45] in order to obtain estimated values for λ, the mean free path in nuclear matter, and V, the average potential between the helium nucleus and the pion. (Since $R\approx\lambda_0$ the "optical model" is not strictly valid here.) λ depends on $|C|$ only and V on α alone. Table VII shows the results. In this table λ was found from the graph $\sigma_r/\pi R^2$ *vs* KR in reference 44, with $\lambda=K^{-1}$, and V from the graph $\sigma_e/\pi R^2$ *vs* $\sigma_r/\pi R^2$ in reference 45, remembering that the quantity k_1 in reference 45 is determined by $V=1.97\times10^{-11}\beta k_1(1+\frac{1}{2}k_1\lambda_0)$ (where β is the pion velocity in the cms divided by c).

It is apparent that, while λ is quite sensitive to the assumed value of R, V is not. However, both quantities are much affected by the experimental uncertainties. Our values for V appear to agree with the values of 18 Mev reported for 62-Mev mesons[29] and 15 Mev reported for 48-Mev mesons[46] both found for carbon.

A considerable number of data would have to be available to allow more definite conclusions. By assuming that only s-wave and p-wave scattering is involved ($\lambda_0<R_1\lesssim2\lambda_0$), a conclusion can be drawn on the relative signs of the phase shifts of these waves at 60 Mev. (At 105 Mev the elastic scattering distribution appears to be compatible with a pure s-wave interaction.) Taking into account only s-waves and p-waves

TABLE VI. Elastic scattering angular distribution in helium.

Pion energy (Mev)	$\frac{\Delta\sigma_e}{\Delta\omega}\Big\vert_{0}^{60°}$ (mb/sterad)	$\frac{\Delta\sigma_e}{\Delta\omega}\Big\vert_{60°}^{120°}$ (mb/sterad)	$\frac{\Delta\sigma_e}{\Delta\omega}\Big\vert_{120°}^{180°}$ (mb/sterad)	$\sigma_e\Big\vert_{0}^{90°}$ (mb/sterad)	$\sigma_e\Big\vert_{90°}^{180°}$ (mb/sterad)
60	1±1	0.6±0.6	10±4	7±5	30±11
105	7±3	6±2	4±2	40±10	34±10

[41] Roberts, Spry, and Tinlot, Bull. Am. Phys. Soc. **28**, No. 1, 14 (1953).
[42] R. Wilson and J. P. Perry, Phys. Rev. **84**, 163 (1951).
[43] Kessler, Byfield, Lederman, and Rogers, Bull. Am. Phys. Soc. **28**, No. 1, 14 (1953).
[44] Fernbach, Serber, and Taylor, Phys. Rev. **75**, 1352 (1949).
[45] H. A. Bethe and R. R. Wilson, Phys. Rev. **83**, 690 (1951).
[46] A. M. Shapiro, Phys. Rev. **84**, 1063 (1951).

TABLE VII. Mean free paths in nuclear matter and pion-helium potentials from "optical model."

Pion energy (Mev)	R (10^{-13} cm)	λ (10^{-13} cm)	V (Mev)
60	$=R_1=2.2$	7 ± 2	22 ± 11
	$=2\lambda_0=2.9$	14 ± 4	17 ± 9
105	$=R_1=2.2$	$1.6^{+0.8}_{-0.3}$	17 ± 17
	$=3\lambda_0=3.1$	6 ± 0.8	19 ± 10

the differential scattering distribution is

$$d\sigma_e/d\omega=\tfrac{1}{4}\lambda_0^2[\,|b_0|^2+3(b_0b_1^*+b_0^*b_1)\cos\theta_0 +9|b_1|^2\cos^2\theta_0]. \quad (9)$$

Here $b_L=1-e^{2i\alpha_L-\delta_L}$, where α_L represents the phase shift corresponding to angular momentum number L (=0 or 1) and δ_L represents attenuation factors due to reactions that may take place. b_L^* is complex conjugate to b_L. The sign of the numerical value of the term multiplied by $\cos\theta_0$ determines whether forward or backward scattering predominates. In the present case this term is negative because of the observed strong backward scattering. One can show easily that therefore α_0 and α_1 must have opposite signs, indicating that repulsive as well as attractive potentials are involved in the scattering process.

Applying the isotopic spin formalism, one can give the pion isotopic spin $t=1$ with charge component $t_{13}=+1$ (for a negative meson taken as an example), and give the helium nucleus isotopic spin $T_1{}^N=0$ with $T_{13}{}^N=0$. Therefore the total charge is $T_3=T_{13}{}^N+t_{13}=+1$ and the total isotopic spin of the system is $T=t+T_1{}^N=1$. T and T_3 must remain constant throughout the collision process. After an elastic collision $T_2{}^N=T_1{}^N=0$ and $T_{23}{}^N=T_{13}{}^N=0$. After an inelastic collision resulting in up to 4 separate nucleons in addition to the pion, $T_2{}^N$ could be 0, 1, or 2. For $T_2{}^N=1$ one can have $T_{23}{}^N=1$, $t_{23}=0$ ($T_3=T_{23}{}^N+t_{23}=+1$) or $T_{23}{}^N=0$, $t_{23}=1$, the former reaction representing inelastic events with charge exchange ($t_{13}=1$, $t_{23}=0$), the latter concerning inelastic events without charge exchange. For each of these two possibilities one obtains[47] a probability of $\frac{1}{2}$. If one assumes that after a disruption of the helium nucleus the state $T_2{}^N=1$ prevails, the prediction is that $\sigma_\gamma=\sigma_i$. This is indeed indicated in Table V. For $T_2{}^N=2$ one can have $T_{23}{}^N=2$, $t_{23}=-1$, or $T_{23}{}^N=1$, $t_{23}=0$, or $T_{23}{}^N=0$, $t_{23}=1$. The first possibility would represent a double charge exchange turning a negative pion into a positive pion, the second possibility represents single charge exchange and the third simply inelastic events. The relative probabilities are 6:3:1, respectively. Since probably most of the interaction process is a result of individual collisions with the nucleons in the nucleus it appears that double charge exchange is quite unlikely even if one disregards any selection rules for $|T_2{}^N-T_1{}^N|$, and spin and parity considerations. Therefore probably $T_2{}^N=0$ or 1, in agreement with the experiment.

[47] E. U. Condon and G. H. Shortley, *Theory of Atomic Spectra* (Cambridge University Press, Cambridge, 1951), p. 76.

C. Helium Reactions in Terms of Pion-Nucleon Interactions

The ratio of the total cross section σ_t at 105 Mev to that at 60 Mev is 2.3 as inspection of Table V shows. Within the errors the same is true for the corresponding ratios of the partial cross sections σ_e, σ_i, and σ_c. Similar increases have been found for hydrogen as shown in Fig. 5 and for deuterium,[48] while for carbon and heavier nuclei the energy dependence is less marked.[9,49] One can conclude that the observed energy dependence of the cross sections for the light nuclei reflects the energy dependence of the π-nucleon cross sections as long as the interaction mean free path does not become small compared to the size of the nuclei. An attempt can therefore be made to explain the results for helium in terms of the observations on hydrogen.[9–14] Since the nucleons are bound, selection rules must apply limiting certain transitions, and the probability of a reaction of a given type must be determined in part by the number of final states accessible. In what follows such rules are not everywhere taken into account. However, mention will be made where a calculated result appears likely to be modified by a more complete treatment. $\pi^\pm$ proton nuclear forces are assumed to be identical in magnitude to $\pi^\mp$ neutron forces.

When a pion strikes a nucleon in a nucleus, the collision may be inelastic in the pion-nucleus system if the energy transfer from pion to nucleon is large. Thus for large scattering angles the differential elastic scattering cross section for the nucleus can become considerably smaller than the corresponding cross section for a single nucleon. This has been investigated theoretically by several authors.[50,51] The large-angle events that have been lost from the elastic scattering cross section contribute to the inelastic cross section. This partial cross section will be called σ_ρ. The other contribution to inelastic scattering is the result of pion-nucleon scattering with spin-flip, called here σ_φ so that $\sigma_i=\sigma_\rho+\sigma_\varphi$. In the p-state ($L=1$) the total angular momentum J of the pion-nucleon system is $J=L\pm S=1\pm\frac{1}{2}$, ($S=\frac{1}{2}$=nucleon spin). L, J, and the component of J, $m_j=m_L+m_S$, must remain constant. The possibility ($\Delta m_L=\pm1$, $\Delta m_S=\mp1$) results in a flip of the spin of the struck nucleon. Because of the Pauli principle an event of this kind taking place in helium must be inelastic just as for the case of charge exchange, as mentioned before. We finally can put $\sigma_r=\sigma_\alpha+\sigma_\gamma+\sigma_\rho+\sigma_\varphi$. All of the partial cross sections refer to the nucleus

[48] Anderson, Fermi, Nagle, and Yodh, Phys. Rev. **86**, 413 (1952).
[49] R. L. Martin, Phys. Rev. **87**, 1052 (1952).
[50] D. C. Peaslee, Phys. Rev. **87**, 862 (1952).
[51] M. Kawaguchi and Y. Yamaguchi (private communication).

as a whole. If σ_n stands for σ_α, σ_γ, σ_ρ, or σ_φ, we can call σ_n' the corresponding average cross section for an individual nucleon bound in the nucleus, where σ_n' represents σ_α', σ_γ', σ_ρ', or σ_φ'. Thus the σ_n' are defined as the cross sections for nucleons under the conditions prevailing in the particular nucleus under discussion. If there are equal numbers of neutrons and protons in the nucleus, and if we put σ_{nN}' and σ_{nP}' for neutrons and protons, respectively, then $\sigma_n'=\frac{1}{2}(\sigma_{nN}'+\sigma_{nP}')$. The quantity σ_α', particularly, is defined as one-half the average absorption cross section per nucleon pair in the nucleus. Since the range of the nuclear forces is limited and since the different types of interactions are in competition, we have $\sigma_r<(\sigma_\alpha'+\sigma_\gamma'+\sigma_\rho'+\sigma_\varphi')A$. However, one can write

$$\sigma_\alpha:\sigma_\gamma:\sigma_\rho:\sigma_\varphi=\sigma_\alpha':\sigma_\gamma':\sigma_\rho':\sigma_\varphi', \tag{10}$$

since the individual nucleon cross sections are proportional to the probabilities of occurrence for the different events and since these relative probabilities should not be changed by the fact that in the nucleus the different processes are in competition. It follows that

$$\sigma_n'=\sigma_n f, \tag{11}$$

where f is a constant for a given nucleus at a given pion energy. If some model, such as the "optical model" is assumed for the nucleus, with a given radius R, f can be calculated. As has been discussed, no such specific assumption can be made here since $\lambda_0\approx R$, and we will instead calculate f later from the experimental results. If all of the σ_n' are quite small, $f\approx 1/A$, of course. In the following paragraphs values for σ_γ' and σ_φ' will be calculated from information concerning pion-nucleon scattering, and a reasonable assumption can be made for σ_α', while more uncertainty exists about a calculation of σ_ρ'. From the equations [following from Eqs. (10) and (11)]

$$\sigma_\alpha'+\sigma_\gamma'=\sigma_c f, \tag{12}$$

and

$$\sigma_\rho'+\sigma_\varphi'=\sigma_i f, \tag{13}$$

we can, however, infer σ_ρ' in addition to f, making use of the calculated values of σ_γ', σ_φ', and σ_α', and the experimental values of σ_c and σ_i. (If σ_ρ' could be calculated with some certainty, Eqs. (12) and (13) could be used for a check of consistency.)

We shall proceed to calculate σ_γ'. Since charge exchange can take place only on either the neutrons or the protons in the nucleus, depending on the sign of the pion, the average cross section σ_γ' is one-half the pion-nucleon cross section for charge exchange. The nucleons in the nucleus can be assumed to move with an average kinetic energy $E_1=20$ Mev and a Gaussian momentum distribution[52] proportional to $\exp(-P^2/z)\,dp$, where P is the momentum, z is determined by E_1, and dp is a volume element in phase space. The charge-exchange cross section is given as a function of the relative energy between pion and nucleon by the graph, Fig. 5. Multiplication of the latter by the momentum distribution and numerical integration gives the upper limits for σ_γ' given in Table VIII, column 1. It may be of interest that the values thus calculated for pion energies of 60 and 105 Mev are 20 percent and 35 percent higher, respectively, than the values obtained if there were no nucleon motion.

One can argue that a pion-nucleon collision will result in a disruption of the helium nucleus with high probability if the pion loses more than 21 Mev in the process. (He^3 or H^3 have binding energies of 7 Mev leaving 21 Mev of the 28-Mev total binding energy of He^4 to be supplied.) Thus, only if the pion is scattered by a nucleon through a fairly large angle, is an inelastic collision possible relative to the pion-helium system. Considering the angular distribution for charge-exchange scattering[14] an integration through angles resulting in energy transfers greater than 21 Mev yields what might be considered more appropriate values for σ_γ'. These values are also given in Table VIII, column 1, below the upper limits given before.

TABLE VIII. Calculated values of partial pion-nucleon cross sections. For every number an upper limit is given as well as a value believed to be more appropriate, as discussed in the text.

Pion energy (Mev)	1 σ_γ'(mb)	2 σ_φ'(mb)	3 σ_α'(mb)	4 f	5 σ_ρ'(mb)	6 σ_α(mb)
60	<9.0	<2.7	<8	$<0.46\pm0.16$	4.2 ± 3.8	17 ± 6
	6.0	0.8	>5	$>0.30\pm0.10$	3.7 ± 3.5	17 ± 6
105	<15.2	<13.2	<10	$<0.31\pm0.07$	$2.8^{+4.0}_{-2.8}$	32 ± 8
	11.0	9.0	>7	$>0.22\pm0.05$	3.2 ± 3.2	32 ± 8

The spin-flip scattering cross section σ_φ' has been obtained by a similar calculation except that this type of scattering is not given explicitly but must first be inferred by means of a phase shift calculation. We shall use here the results of the phase shift analysis by Anderson *et al.*[14] Accordingly we have for the upper limit of σ_φ' at a particular energy

$$\sigma_\varphi'=\tfrac{3}{2}\pi\lambda_0^2[|A_\beta|^2+|A_{P\beta}|^2], \tag{14}$$

having integrated over the spin-flip angular distribution which is proportional to $\sin^2\theta_0$. λ_0 is here the wavelength in the pion-nucleon cms. A_β is the spin-flip scattering amplitude for a π^+ scattered by a proton, given by $A_\beta=\frac{1}{3}\sqrt{2}(e_{33}-e_{31})$ (in the notation used in reference 14), while $A_{P\beta}$ is the amplitude for a π^+ scattered by a neutron (or a π^- scattered by a proton), given by $A_{P\beta}=\frac{1}{6}\sqrt{2}(e_{33}-e_{31}+2e_{13}-2e_{11})$. The first index ($n$) on the contributing amplitudes e_{nm} is twice the total isotopic spin, and the second index (m) is twice the total angular momentum of the pion-nucleon system. e_{nm} is given by $1-e^{2i\alpha_{nm}}$. The α_{nm} were obtained mostly by interpola-

[52] E. M. Henley, Phys. Rev. 85, 204 (1952).

tion between results given by Anderson *et al.*,[14] and partially from what few data are available at lower energies.[9–13,18] Integration over all nucleon momenta gives the upper limits for σ_φ' shown in Table VIII, column 2. The other values given here for σ_φ', considered to be more appropriate, were obtained by integration over large θ_0 only, corresponding to large energy transfers, as before for σ_γ'.

The cross section for absorption of a pion by a deuteron is about 8 mb at 60 Mev and about 10 mb at 105 Mev, as an interpolation of results on this reaction shows.[53,54] Byfield *et al.*,[29] have shown that these cross sections must be multiplied by a factor $\lesssim 3.3$ to obtain the cross section per proton in carbon. For helium we shall assume that this factor is between 1.5 and 2 because of the small number of nucleons present. The values for σ_a' (upper and lower limits per nucleon in helium) have been entered in Table VIII, column 3. From the values in Tables V and VIII and Eqs. (12) and (13) the values for σ_ρ' and f given in Table VIII, columns 4 and 5 have been calculated. The indicated errors are determined from the experimental uncertainty of σ_e and σ_i. From f and σ_a' one can calculate σ_a given in Table VIII, column 6. It is seen that these values for σ_a agree more or less with those already estimated from other considerations and given in Table V.

The value of f at 60 Mev should be smaller than that at 105 Mev since the individual nucleon cross sections are smaller at 60 Mev, and $f \to 1/A = 0.25$ for small nucleon cross sections. Taking into account the uncertainties in the assumptions made for the calculations and the large experimental uncertainties, the given values for f are not inconsistent with each other.

At both energies the values for σ_ρ' turn out to be rather small. σ_ρ' should increase with energy because at larger pion energies the energy transfer from a scattered pion to a nucleon becomes comparable to the binding energy of the nucleus for smaller scattering angles, in addition to the general increase of almost all of the pertinent cross sections with energy. Whether σ_ρ' indeed increases with energy cannot be recognized because of the large errors.

A more elaborate calculation applying the Pauli principle to the number of possible final states of the nucleons after an inelastic collision[55] and applying selection rules attributable to spin, isotopic spin, and parity considerations may reduce the computed values of σ_γ' and σ_φ' further. Since f must be >0.25, σ_γ' cannot be reduced very much at 105 Mev, while a greater modification might be possible at 60 Mev. If σ_γ' were almost zero at 105 Mev, σ_a' would have to be $>0.25 \times 82 = 20$ mb instead of the estimated value of 10 mb. This is an additional indication that a large portion of the observed "charge-transfer" events are caused by charge exchange.

[53] Clark, Roberts, and Wilson, Phys. Rev. **83**, 649 (1951).
[54] Durbin, Loar, and Steinberger, Phys. Rev. **83**, 646 (1951).
[55] M. H. Johnson, Phys. Rev. **83**, 510 (1951).

D. Pion-Helium Elastic Scattering in Terms of Pion-Nucleon Scattering

Both the protons and the neutrons in the nucleus contribute to the elastic scattering of piens. The amplitudes due to these two contributions interfere so that the total differential scattering distribution is given by

$$d\sigma_e/d\omega = \tfrac{1}{4}\lambda_0^2[|B_l|^2 + 3(B_l A_{al}^* + B_l^* A_{al}) \times \cos\theta_0 + 9|A_{al}|^2 \cos^2\theta_0]\Omega, \quad (15)$$

where $B_l = B + B_P$ for the s-waves and $A_{al} = A_a + A_{Pa}$ for the p-waves. Furthermore,

$$B = e_3,\ e_3 = 1 - e^{2i\alpha_3},$$
$$B_P = \tfrac{1}{3}(e_3 + 2e_1),\ e_1 = 1 - e^{2i\alpha_1},$$
$$A_a = \tfrac{1}{3}(2e_{33} + e_{31}),$$
$$A_{Pa} = \tfrac{1}{9}(2e_{33} + e_{31} + 4e_{13} + 2e_{11}).$$

Here it is important to note that the signs of the individual phase shifts as determined from pion-proton scattering may or may not have to be reversed for pion-neutron scattering. For instance, the nuclear force between a π^- and a proton may be attractive while the force between a π^+ and a neutron may be equal in magnitude but repulsive. Some meson theories lead to such results.[45] Calculations have been carried out for both possibilities.

The factor Ω in Eq. (15) takes into account the presence of several proton-neutron pairs, the term in brackets applying only to one such pair, as well as the possible reduction of the cross section for large energy transfers[50,51] (large θ_0). No attempt is made to calculate exactly the magnitude and dependence on θ_0 of Ω.

The phase shifts α_{nm} must be selected for the proper energies. A pion of given laboratory energy has considerably more energy with respect to a bound nucleon in the pion-helium cms than it has in a free-nucleon-pion cms. Assuming merely that an elastic collision consists of a pion striking a single nucleon bound rigidly in the helium nucleus, the present pion-helium results at 60 and 105 Mev may have to be compared with the pion-proton results at energies as high as 78 and 137 Mev, respectively. Values for the corresponding pion-proton phase shifts[14] are given in Table IX. Pion-neutron phase shifts are assumed to be equal in magnitude, but possibly with opposite signs, as mentioned above. Putting $\Omega = 1$ the scattering due to a neutron-proton pair (σ_e') in the helium nucleus can be calculated. Table X gives the results. The assumption of neutron phase shifts with signs opposite to those given in Table IX seems to represent well the apparently strong backward scattering observed at 60 Mev.

To calculate the final elastic cross sections the values in Table X must be modified. For Ω we are assuming an empirical value of 1.6 which will result in agreement between calculated and experimentally observed values

TABLE IX. Phase shifts used for calculation of elastic pion-helium scattering.

Pion energy (Mev)	Corresponding free-proton-pion energy (Mev)	α_3	α_1	α_{33}	α_{31}	α_{13}	α_{11}
60	78	−6°	+9°	+15′	+3°	0	0
105	137	−15°	+11°	+40°	+6°	+2°	−5°

for σ_e at 60 Mev. The effect of large energy transfers on the angular distribution is still neglected.

An important modification must be made to take into account the diffraction scattering caused by the inelastic reactions discussed in the previous section. This effect will here be taken into account only approximately. We first express $B_l\Omega^{\frac{1}{2}}$ and $A_{\alpha l}\Omega^{\frac{1}{2}}$ in Eq. (15) by terms equal to $(1-e^{2i\beta_0})$ and $D(1-e^{2i\beta_1})$, respectively. The quantities β_0, β_1, and D must be determined so that $d\sigma_e/d\omega$ is properly reproduced. Next, we substitute for $B_l\Omega^{\frac{1}{2}}$ and $A_{\alpha l}\Omega^{\frac{1}{2}}$ the expressions $(1-e^{2i\beta_0-\delta_0})$ and $D(1-e^{2i\beta_1-\delta_1'})$, respectively. The reaction cross section is given by

$$\sigma_r=\pi\lambda_0^2[(1-e^{-2\delta_0})+3D^2(1-e^{-2\delta_1'})]. \qquad (16)$$

The term $D^2(1-e^{-2\delta_1'})$ can be expressed more simply by a term $(1-e^{-2\delta_1})$. The average attenuation factors δ_0 and δ_1 are related to each other by the relative "distances" traveled by the pion through the nucleus in the s- and p-states, respectively. (For diffraction scattering we again assume that only s- and p-wave scattering occurs. This seems justified since $\lambda_0<R_1\lesssim 2\lambda_0$. For the same reason, however, no definite geometry, as is used here, applies in a strict sense.) From the geometry of a sphere of radius $R_1=2.2\times10^{-13}$ cm one infers that here for averages $\delta_1\approx\frac{1}{2}\delta_0$. Equation (16) can now be solved for δ_0, putting σ_r equal to its observed values. For the different quantities defined we have $\beta_0=-12.4°$ and $-24.5°$, $\beta_1=25.6°$ and $30°$, $D=0.43$ and 1.27, $\delta_0=0.16$ and 1.2, and $\delta_1'=0.19$ and 0.43, for 60 and 105 Mev, respectively. The latter calculations were carried out for n-phase shifts opposite to p-phase shifts only, since Table X shows that only for this case one can expect to obtain large backward/forward ratios. One finds the values in Table XI for the elastic scattering cross section of helium with diffraction scattering taken into account in this way.

Comparison with the data in Tables V and VI shows that at 60 Mev the calculated and experimental values for $\sigma_e|_0^{90°}$ and $\sigma_e|_{90°}^{180°}$ are not inconsistent. The calculated value for σ_e at 105 Mev is 100 percent too large while the backward/forward ratio is about 50 percent too small. Comparison of Tables X and XI shows that the interference with the diffraction scattering makes the scattering intensities considerably more pronounced in the forward direction. This makes it difficult to understand large backward/forward scattering ratios if the latter should be verified by further experiments on helium. Particularly, assumptions for Ω to take into account the reduction of $d\sigma_e/d\omega$ at large θ_0, due to large energy transfers, would further reduce the expected backward scattering. However, σ_e', the inelastic cross section due to large energy transfers which must be related to Ω, is fairly small as shown in Table VIII. This may mean that Ω would not have to decrease very much for large θ_0.

So far interference with Coulomb scattering has been neglected. The importance of this effect for the smaller angles ($<50°$) has been shown for pion-proton scattering[56] and for pion-carbon scattering.[29,50] By adding the approximate Coulomb-scattering amplitude $\pm 2i/[137\beta\sin^2(\frac{1}{2}\theta_0)]$ to the s- and p-wave scattering amplitudes considered in the previous paragraphs, one can estimate that for helium Coulomb scattering is important below $\theta_0'=35°$ at 60 Mev, and below $\theta_0'=25°$ at 105 Mev. Below θ_0' the differential scattering distributions may be increased or decreased considerably, depending on the sign of the scattered pions and on the direction of the nuclear forces. However, the solid angle between our lower limit of observation ($\theta_0=20°$) and θ_0' is so small that few events are expected in this interval. Similar considerations apply to scattering in hydrogen. Thus, for the present work, neglecting Coulomb effects seems justified.

VII. CONCLUSIONS

Assuming that all types of interactions between pions and the helium nucleus are due to interactions between pions and the individual nucleons in the nucleus, an approximate calculation based mostly on the phase shifts found from experimental results on pion-proton scattering shows that a fairly consistent picture can be constructed, resulting generally in rough agreement between calculated and observed cross sections. The estimated experimental absorption cross section agrees with that estimated from the pion-deuteron absorption cross section, leaving most of the observed charge-transfer events to be interpreted as due to charge

TABLE X. Calculated elastic scattering cross sections for a neutron-proton pair.

Pion energy (Mev)	Charge	σ_e' (mb)	$\sigma_e'\|_0^{90°}$ (mb)	$\sigma_e'\|_{90°}^{180°}$ (mb)
60	n-phase shifts same as p-phase shifts	58	27	31
	n-phase shifts opposite to p-phase shifts	24	4	20
105	n-phase shifts same as p-phase shifts	170	81	89
	n-phase shifts opposite to p-phase shifts	120	40	80

[56] L. Van Hove, Phys. Rev. **88**, 1358 (1952).

exchange. Some of the inelastic scattering observed can be accounted for by pion-nucleon scattering with spin flip. The relatively large backward-to-forward elastic scattering ratio shows that not much inelastic scattering can be due to pion-nucleon collisions with energy transfers large enough to disrupt the nucleus. The relatively small elastic scattering cross sections, together with the high backward-to-forward scattering ratios, indicate that protons and neutrons in the nucleus scatter with opposite phase shifts. Throughout the computations only s-wave and p-wave scattering has been considered. Particularly at 105 Mev some scattering corresponding to higher angular momenta ($L=2, 3$) may take place. Also many effects due to the bound state of the nucleons have been neglected. A modification affecting all aspects of pion-helium scattering may be introduced by a consideration of multiple scattering inside the helium nucleus as recently worked out for a two-body system by Brueckner.[57]

The authors wish to acknowledge several inspiring conversations on some of the subjects covered in this article with R. Serber and D. C. Peaslee. We are very grateful to E. T. Booth and J. Rainwater for the opportunity to work at the Nevis cyclotron. The untiring cooperation of the cyclotron operating staff under J. Spiro is greatly appreciated. Furthermore, we are indebted to W. F. Goodell, L. M. Lederman, and A. Pevsner for giving us most valuable advice on details of operation with the cyclotron. We also wish to express our thanks to the members of the Brookhaven National Laboratory, without whose support this work would not have been possible. In particular, the diffusion chamber was constructed mostly in the cloud chamber shop under S. G. Hasselriis. W. A. Tuttle and F. W. Rothery were responsible for most of the construction and operation of the electric control circuits. K. J. Kristoffersen contributed much toward the operation of the diffusion chamber and the management of the expeditions to the cyclotron. M. R. Burns and F. S. Keene scanned most of the pictures.

[57] K. A. Brueckner, Phys. Rev. **89**, 834 (1953).

TABLE XI. Calculated elastic scattering cross sections for helium.

Pion energy (Mev)	σ_e (mb)	$\sigma_e\|_0^{90^\circ}$ (mb)	$\sigma_e\|_{90^\circ}^{180^\circ}$ (mb)
60	37	13	24
105	140	100	40

Nuclear Photostar Production*

ISRAEL REFF
Indiana University, Bloomington, Indiana
(Received February 4, 1953)

Cross sections for photonuclear star production are computed phenomenologically for photomeson production in a nucleus followed by meson absorption in the same nucleus. Results are found for values of the mean free path of mesons in nuclear matter of 4×10^{-13} cm and 8×10^{-13} cm as a function of atomic mass number and photon energy. The process accounts for a large part of observed photostars with three and more prongs for elements as heavy as Br, but for only a small part for elements as light as O.

I. INTRODUCTION

MILLER[1,2] and Kikuchi[3,4] observe stars in emulsions formed by bremsstrahlung of various energies up to 300 Mev. Star prong spectra for all emulsion elements as a function of bremsstrahlung energy were found. The yield of stars with three and more prongs as a function of bremsstrahlung energy is found to rise sharply at meson creation threshold. This suggests that above meson threshold a large proportion of the stars with three and more prongs are produced by a mesonic process.

Kikuchi shows that for bremsstrahlung energies greater than 150 Mev, most of the one-prong and two-prong stars are produced by photons of energy less than 150 Mev. Also, two-prong stars are easily confused experimentally with single tracks suffering large angle scattering.

We will consider the following mechanism of star formation to explain the rapid rise in the yield of photostars with three and more prongs at photon energies above meson threshold: A photon interacts with a single nucleon in the nucleus to produce a meson, real or virtual. This meson in traveling through the nucleus in which it is produced is absorbed by two nucleons[5] of the same nucleus. The two nucleons which absorb the meson are ejected from the nucleus with a large amount of energy, leaving an excited nucleus. The nucleus is further excited if one or both of the nucleons which absorb the meson interact after absorption with the other nucleons in the nucleus. The excited nucleus may emit one or more particles. We call the resulting disintegration products a star. The nucleus is also excited by inelastic scattering of the meson inside the nucleus in which it is produced. Emission of one or more particles by this excited nucleus results in a star.

The optical model describes the interaction of meson and nucleus by a complex potential. The optical model[6,7] predicts for σ_π, the photomeson production cross section from a nucleus of atomic mass number A, the formula

$$\sigma_\pi = A\eta\sigma_f(\lambda/V_A)\sigma_{\rm abs}. \tag{1}$$

Here σ_f is the photomeson production cross section from a free nucleon averaged over charge states of nucleon and meson, V_A the volume of the nucleus, $\sigma_{\rm abs}$ is the absorption cross section for mesons of energy equal to the photon energy, and λ is the mean free path in nuclear matter with respect to absorption for mesons of this energy. η is a factor less than 1 which takes into account the effects of nuclear binding on photomeson production. For $A\gtrsim10$,

$$\sigma_{\rm abs}\cong\pi R^2, \tag{2}$$

where R is the nuclear radius. We take $R=1.47\times10^{-13}A^{\frac{1}{3}}$ cm. Also,

$$\sigma = A\eta\sigma_f, \tag{3}$$

where σ is the cross section for photomeson production in the absence of absorption. For large meson energies ($\gtrsim$60 Mev) we may consider the cross section for photostar production to be

$$\sigma_{\rm star}=\sigma-\sigma_\pi. \tag{4}$$

Combining Eqs. (1)–(4),

$$\sigma_{\rm star}=A\eta\sigma_f(1-3\lambda/4R). \tag{5}$$

Our calculation is not based on the optical model, and it is made for all energies and for $A\geqslant12$.

II. DESCRIPTION OF MECHANISM

As already mentioned, we calculate the cross section for photostar production for the following process: Photomesons are produced by interaction of the electromagnetic field with an individual nucleon considered at rest in the nucleus. The nucleus in the neighborhood of meson production is excited, and the excitation travels through the nucleus. The meson travels through the nucleus faster than the excitation and is absorbed by two nucleons of the nucleus in which it is produced. The nuclear medium in the neighborhood of meson absorption has the structure of the ground state. The

* Supported by the joint program of the U. S. Office of Naval Research and the U. S. Atomic Energy Commission.
[1] R. D. Miller, Phys. Rev. **82**, 260 (1951).
[2] R. D. Miller, thesis, University of California (unpublished).
[3] S. Kikuchi, Phys. Rev. **81**, 1060 (1951).
[4] S. Kikuchi, Phys. Rev. **86**, 41 (1952).
[5] Brueckner, Serber, and Watson, Phys. Rev. **84**, 258 (1951).
[6] N. C. Francis and K. M. Watson, Phys. Rev. **89**, 328 (1953).
[7] K. M. Watson (to be published).

two nucleons which absorb the meson are ejected from the nucleus with a large amount of energy, leaving the nucleus excited. The nucleus is further excited if one or both of the nucleons which absorb the meson interact after absorption with the other nucleons in the nucleus. The nucleus thus excited may emit one or more particles. The disintegration products are said to form a star. Calculations for this process are expressed in terms of λ, the mean free path of mesons in nuclear matter with respect to absorption. Photostars are also produced by emission of particles from the nucleus being excited by inelastic scattering of the photomesons in the nucleus in which the photomesons are produced. The cross section for inelastic scattering of mesons is smaller than the cross section for absorption.[8] We therefore obtain the cross section for photostar production via absorption and inelastic scattering of charged mesons by reinterpreting the λ in our calculations as the mean free path of mesons in nuclear matter with respect to absorption and inelastic scattering.

The nucleus is excited by the process of photoproduction. The low degree of excitation of the nucleus thus produced probably does not result in the formation of stars with three and more prongs. This means of photostar production is therefore not included in our calculation.

The initial time-independent state of the system, ϕ_a, consists of a photon of momentum $\mathbf{K}$ (using units $\hbar=1$, $c=1$) and the nucleus at rest in the ground state. The system is described by the Hamiltonian H,

$$H=H_0+H'+R. \tag{6}$$

H_0 is the Hamiltonian for the nucleus and free mesonic and electromagnetic fields. H' is the interaction energy of the electromagnetic field and the nucleus. R is the Hamiltonian of interaction for absorption[5,9] of a meson by two nucleons in the nucleus.

Following Watson,[7] we take

$$H'=\sum_{l=1}^{A} N_l \frac{\exp(-i\mathbf{q}\cdot\mathbf{z}_l)}{\sqrt{q_0}}, \tag{7}$$

where $\mathbf{q}$ is the momentum of the meson and q_0 its energy. $\mathbf{z}_l$ is the coordinate of the lth nucleon. N_l is a function of spin and isotopic spin operators, photon momentum, energy and polarization. The sum is over the A nucleons in the nucleus.

Using the procedure of Lippman and Schwinger,[10]

$$\psi_a^{(+)}=\phi_a+\frac{1}{E_a+i\epsilon-H_0}(H'+R)\psi_a^{(+)}. \tag{8}$$

E_a is the energy of the state ϕ_a. Let

$$\psi_a^{(+)}=\Omega^{(+)}\phi_a; \tag{9}$$

then

$$\Omega^{(+)}=1+\frac{1}{E_a+i\epsilon-H_0}(H'+R)\Omega^{(+)}, \tag{10}$$

$$T_{ba}=(\phi_b,\,(H'+R)\psi_a^{(+)}), \tag{11}$$

where ϕ_b is the time-independent final state. Thus

$$T=(H'+R)\Omega^{(+)}. \tag{12}$$

Define

$$X=\pi R^{+}\delta(H_0-E_a)R. \tag{13}$$

The solution to the integral equation for $\Omega^{(+)}$ is

$$\Omega^{(+)}=1+\frac{1}{E_a+i\epsilon-H_0+iX}H' + \frac{1}{E_a+i\epsilon-H_0}R\frac{1}{E_a+i\epsilon-H_0+iX}H'. \tag{14}$$

The solution is verified by substitution in Eq. (11), using the operator relation

$$\frac{1}{A}-\frac{1}{B}=\frac{1}{A}(B-A)\frac{1}{B}. \tag{15}$$

The solution is to first order in H' and assumes the approximation

$$R\frac{1}{E_a+i\epsilon-H_0}R\sim -iX. \tag{16}$$

This approximation follows from the relation

$$R\frac{1}{E_a+i\epsilon-H_0}R=RP\frac{1}{E_a-H_0}R-i\pi R\delta(H_0-E_a)R. \tag{17}$$

The two terms on the right-hand side of Eq. (17) represent many-body scattering effects, which are expected to be small compared to one body scattering effects.[7] However, the second term of Eq. (17) represents the "shadow" cast by true absorption. We therefore retain this term. Then

$$T=(H'+R)\Omega^{(+)} =\left(1+R\frac{1}{E_a+i\epsilon-H_0}R\frac{1}{E_a+i\epsilon-H_0+iX}\right)H' + R\frac{1}{E_a+i\epsilon-H_0+iX}H'. \tag{18}$$

From Eq. (18) we find for T_a, the transition operator for photostar production,

$$T_a=R\frac{1}{E_a-H_0+iX}H'. \tag{19}$$

[8] Byfield, Kessler, and Lederman, Phys. Rev. **86**, 17 (1952).
[9] K. M. Watson and K. A. Brueckner, Phys. Rev. **83**, 1 (1951).
[10] B. A. Lippman and J. Schwinger, Phys. Rev. **79**, 469 (1950).

The operator $(T-T_a)$ is then the transition operator for photomeson production with absorption present.

Following references 5 and 7, we take

$$R=\sum_\mu R_\mu, \tag{20}$$

and

$$(\mathbf{r}', \mathbf{x}'|R_\mu|\mathbf{z}, \mathbf{r}, \mathbf{x})=R(\mathbf{r}', \mathbf{z}-\mathbf{x})\delta(\mathbf{x}-\mathbf{x}')\delta(\mathbf{r}). \tag{21}$$

The index μ runs over nucleon pairs in the nucleus. $\mathbf{r}$, $\mathbf{x}$ are the relative coordinate and coordinate of center of mass of the pair of nucleons absorbing the meson before absorption, and $\mathbf{r}'$ and $\mathbf{x}'$ are the coordinates after absorption. $\mathbf{z}$ is the meson coordinate.

The operator X appearing in T_a, Eq. (19), is a damping term which results from the absorption of mesons. It is important for real mesons which travel a relatively long distance in the nucleus, and for which the meson energy approximately equals the photon energy. Therefore this X is evaluated for a large nucleus, for which it is diagonal in both meson and nuclear coordinates, with the result,

$$X=v_\pi/2\lambda. \tag{22}$$

Here v_π is the speed of mesons of energy equal to photon energy, and λ is the mean free path with respect to absorption for mesons of this speed. In deriving this result correlations between nucleon pairs in $R^+\delta(H_0-E_a)R$ have been neglected. That is, we have taken

$$\begin{aligned}R^+\delta(H_0-E_a)R&=\textstyle\sum_{\mu,\mu'} R_\mu{}^+\delta(H_0-E_a)R_{\mu'}\\&=\textstyle\sum_\mu R_\mu{}^+\delta(H_0-E_a)R_\mu.\end{aligned} \tag{23}$$

Then

$$T_{ba}=\left(\phi_b, R\frac{1}{E_a-H_0+iX}H'\phi_a\right). \tag{24}$$

The final state ϕ_b is described by the relative momentum $\mathbf{p}$ and the momentum of the center of mass $\mathbf{G}$ after absorption of the two nucleons which absorb the meson, and by the final state F of the nucleus formed from the original nucleus minus the two nucleons which absorb the meson:

$$T_{ba}=(\phi_b, R\phi_I)\frac{1}{E_a-E_I+iX}(\phi_I, H'\phi_a). \tag{25}$$

The intermediate state ϕ_I consists of the nucleus in the state I and a meson of momentum $\mathbf{q}$ and energy $q_0=(q^2+\mu^2)^{\frac{1}{2}}$. Let $\psi_A(\mathbf{z}_1\cdots\mathbf{z}_A)$ be the initial nuclear wave function, $\mathbf{z}_1\cdots\mathbf{z}_A$ the coordinates of the nucleons in this nucleus. Let $\psi_F(\mathbf{z}_3\cdots\mathbf{z}_A)$ be the final nuclear wave function. Setting $K=|\mathbf{K}|$, $E_a-E_I=K-q_0$, and summing over intermediate states I,

$$\begin{aligned}T_{ba}=-\int\psi_F{}^*(\mathbf{z}_3\cdots\mathbf{z}_A)\frac{\exp(-i\mathbf{G}\cdot\mathbf{x})}{(2\pi)^3}f(\Lambda)N_I\delta(\mathbf{r})\\\times\psi_A(\mathbf{r}, \mathbf{x}, \mathbf{z}_3\cdots\mathbf{z}_A)d^3\mathbf{r}d^3\mathbf{x}d^3\mathbf{z}_3\cdots d^3\mathbf{z}_A.\end{aligned} \tag{26}$$

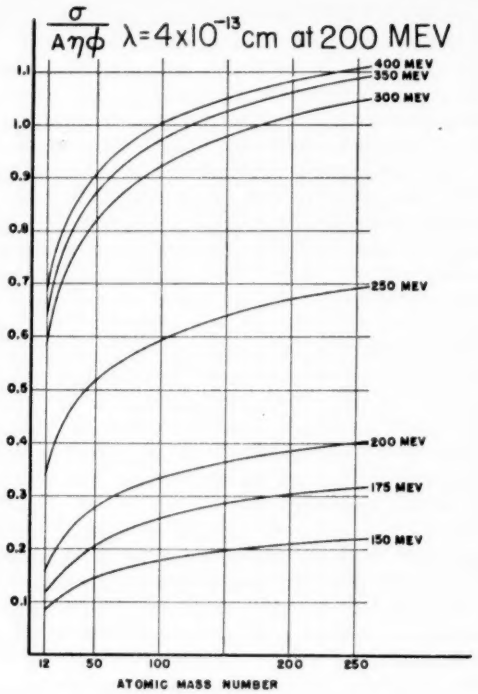

FIG. 1. Photostar production cross sections σ_s divided by $A\eta\phi$ *vs* atomic mass number A for a mean free path of 4×10^{-13} cm, for 200-Mev mesons in nuclear matter. Curves are for fixed photon energy K as indicated.

Here

$$\mathbf{x}=\tfrac{1}{2}(\mathbf{z}_1+\mathbf{z}_2),\quad \mathbf{r}=(\mathbf{z}_1-\mathbf{z}_2).\quad \mathbf{\Lambda}=\mathbf{x}-\mathbf{z}_I,$$

$$\Lambda=|\mathbf{\Lambda}|.\quad f(\Lambda)=\int d^3\mathbf{q}\frac{\exp(i\mathbf{q}\cdot\mathbf{\Lambda})R(\mathbf{p}, \mathbf{q})}{(q_0-K-iX)\sqrt{q_0}}, \tag{27}$$

$$\begin{aligned}R(\mathbf{p}, \mathbf{q})=\frac{1}{(2\pi)^{\frac{1}{2}}}\int d^3\mathbf{r}'d^3\mathbf{z}\exp(-i\mathbf{p}\cdot\mathbf{r}')\\\times\exp[i\mathbf{q}\cdot(\mathbf{z}-\mathbf{x})]R(\mathbf{r}', \mathbf{z}-\mathbf{x}).\end{aligned} \tag{28}$$

The cross section for photostar formation σ_s, by our mechanism, is then

$$\begin{aligned}\sigma_s=A(2\pi)(pM/2)\int d\Omega_p\textstyle\sum_p\int\psi_A{}^*(\mathbf{r}', \mathbf{x}, \mathbf{z}_3\cdots\mathbf{z}_A)\\\times N_I{}^*\delta(\mathbf{r}')f^*(\Lambda)f(\Lambda)N_I\delta(\mathbf{r})\psi_A(\mathbf{r}, \mathbf{x}, \mathbf{z}_3\cdots\mathbf{z}_A)\\\times d^3\mathbf{r}d^3\mathbf{r}'d^3\mathbf{x}d^3\mathbf{z}_3\cdots d^3\mathbf{z}_A.\end{aligned} \tag{29}$$

In deriving Eq. (29), use has been made of Eq. (23). $\sum_p$ means summation over pairs of nucleons. $p=|\mathbf{p}|$ and $d\Omega_p$ is the increment of solid angle corresponding to $\mathbf{p}$.

The experimental data on charged meson production in nucleon-nucleon collisions is in agreement with a

choice of $R(\mathbf{p}, \mathbf{q})$ of the form[9]

$$R(\mathbf{p}, \mathbf{q}) = R_0(\mathbf{p})\mathbf{p}\cdot\mathbf{q}. \tag{30}$$

However, Eq. (30) predicts meson production cross sections in nucleon-nucleon collisions which increase without limit as the meson energy increases. To avoid this situation we insert a cut-off factor q_0 in $R(\mathbf{p}, \mathbf{q})$ of Eq. (30). That is, we take for charged mesons

$$R(\mathbf{p}, \mathbf{q}) = R_0(\mathbf{p})(\mathbf{p}\cdot\mathbf{q})/q_0. \tag{31}$$

Then

$$f(\Lambda) = R_0(\mathbf{p}) \int q^2 dq d\Omega_q \frac{\exp(i\mathbf{q}\cdot\mathbf{\Lambda})\mathbf{p}\cdot\mathbf{q}}{(q_0 - K - iX)q_0^{\frac{1}{2}}}. \tag{32}$$

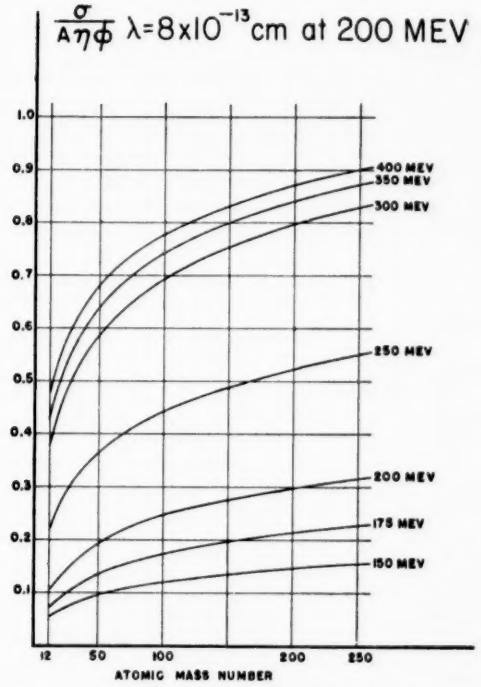

FIG. 2. Photostar production cross sections σ_s divided by $A\eta\phi$ *vs* atomic mass number A for a mean free path of 8×10^{-13} cm, for 200-Mev mesons in nuclear matter. Curves are for fixed photon energy K as indicated.

$d\Omega_q$ is the increment of solid angle corresponding to $\mathbf{q}$. With this $R(\mathbf{p}, \mathbf{q})$, mesons are absorbed in the P state relative to the absorbing nucleons.

With this $R(\mathbf{p}, \mathbf{q})$, σ_s becomes $\sigma_s{}^c$, the photostar cross section for charged mesons. $\sigma_s{}^c$ is evaluated numerically in the range 150 Mev $\leq K <$ 250 Mev, by calculating $f(\Lambda)$ of Eq. (27) after replacing $(q_0 - K - iX)q_0^{\frac{1}{2}}$ by $[(q^2/2\mu) + \mu - K - iX](q^2+\mu^2)/\mu^{\frac{1}{2}}$. In the range 250 Mev $< K \leq$ 400 Mev, the process is repeated after replacing $(q_0 - K - iX)q_0^{\frac{1}{2}}$ by $(q - K - iX)q^2/\mu^{\frac{1}{2}}$. At $K =$ 250 Mev, the average of the two methods of calculation is taken in evaluating $\sigma_s{}^c$.

Computations are made for two values of λ, 4×10^{-13} cm and 8×10^{-13} cm. Byfield, Kessler, and Lederman find $\lambda = 8\times10^{-13}$ cm, using the optical model. Bernardini and Levy[11] find $\lambda = 4.5\times10^{-13}$ cm on a ray tracing model. No experimental data exists on the absorption of neutral mesons in nuclear matter. We include the contribution by neutral mesons to the photostar cross section by making the approximation

$$\sigma_s{}^0/\sigma_s{}^c = \sigma_\gamma{}^0(\mathrm{H})/\sigma_\gamma{}^c(\mathrm{H}). \tag{33}$$

$\sigma_s{}^0$ is the cross section for star formation with neutral mesons. $\sigma_\gamma{}^0(\mathrm{H})$ is the cross section for neutral photomeson production from free protons; $\sigma_\gamma{}^c(\mathrm{H})$ is the same quantity for π^+ mesons. The ratio of $\sigma_\gamma{}^0(\mathrm{H})$ to $\sigma_\gamma{}^c(\mathrm{H})$ was taken from Brueckner and Watson.[12] Let σ_s be the total cross section for photostar production. Then

$$\sigma_s = \sigma_s{}^c + \sigma_s{}^0. \tag{34}$$

Let $\sigma_\gamma{}^c$ be the charged photomeson production cross section in the absence of absorption. Then

$$\sigma_\gamma{}^c = A\eta\phi[1 - (\mu^2/K^2)]^{\frac{1}{2}}, \tag{35}$$

where ϕ is a constant. Using Eqs. (34) and (35), the ratio $\sigma_s/A\eta\phi$ is computed numerically as a function of K, A, and λ. Results of this computation are shown in

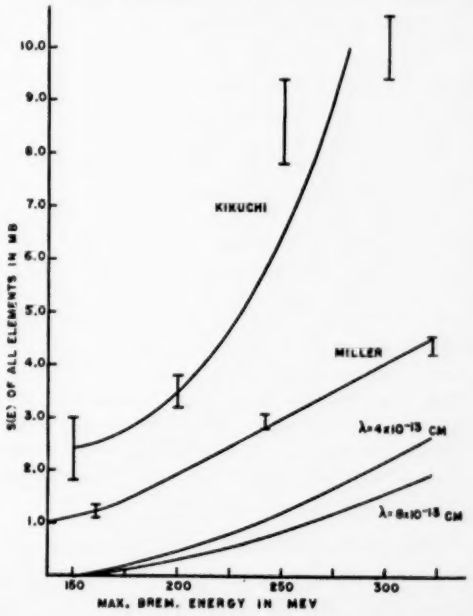

FIG. 3. The function $S(E)$ *vs* bremsstrahlung energy E for $C2$ emulsion. The curves of Kikuchi and Miller are experimental. The curves for λ (the mean free path of 200-Mev mesons in nuclear matter) equal to 4×10^{-13} cm and 8×10^{-13} cm are calculated.

[11] G. Bernardini and F. Levy, Phys. Rev. **84**, 610 (1951).
[12] K. A. Brueckner and K. M. Watson, Phys. Rev. **86**, 923 (1952).

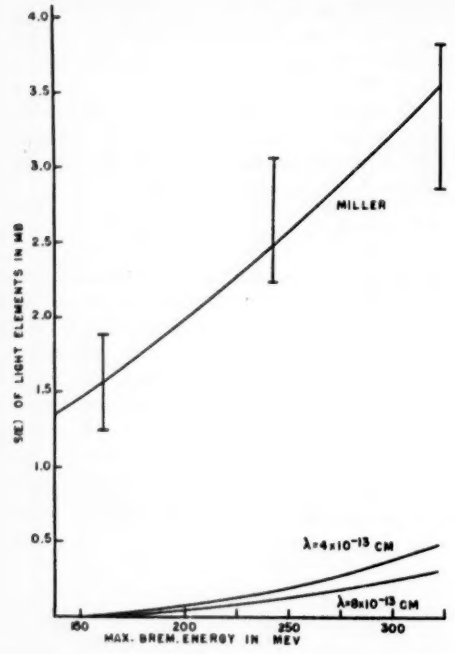

FIG. 4. The function $S(E)$ *vs* bremsstrahlung energy E for the light elements in $C2$ emulsion. Miller's curve is experimental. The curves for λ equal to 4×10^{-13} cm and 8×10^{-13} cm are calculated.

Fig. 1 for $\lambda=4\times10^{-13}$ cm at $q_0=200$ Mev and in Fig. 2 for $\lambda=8\times10^{-13}$ cm at $q_0=200$ Mev.

A threshold for the mechanism is taken as $K=148$ Mev, and σ_s assumed to vary linearly from 148 Mev to 150 Mev. In the above mechanism, mesons are produced in the S state relative to the nucleon from which the meson is produced and absorbed in the P state relative to the absorbing nucleons considered to be in contact during absorption. Hence mesons are absorbed mostly by pairs of nucleons which do not include the nucleon from which the meson is produced. Also, virtual mesons play only a minor role in the mechanism. This is in contradiction with the proposal of Wilson,[13] in which the pair of nucleons which absorb the meson includes the nucleon from which the meson was produced. In Wilson's mechanism, virtual mesons give rise to large photostar yields.

III. COMPARISON WITH EXPERIMENT

As pointed out in the introduction, one- and two-prong stars are produced mainly by photons of energy less than 150 Mev. Also two-prong stars are difficult to distinguish experimentally from large angle scatters of single tracks. Hence the data of Miller[2] and Kikuchi[4] for stars with three and more prongs will be used for comparison with the mechanism of Sec. II.

[13] R. R. Wilson, Phys. Rev. **86**, 125 (1952).

Miller[2] and Kikuchi[4] give experimental cross sections for photostars with three and more prongs, averaged over the emulsion elements of $C2$ emulsion. Multiplying these values by 1.6 we obtain $\sigma(K)$, a photostar cross section averaged over the emulsion elements at energy K Mev. The factor 1.6 is the ratio of total stars to stars with three and more prongs in nuclear absorption of π^+ mesons, taken from Bernardini and Levy.[11] Let E be the energy in Mev of a bremsstrahlung spectrum $N(K)=1/K$, where $N(K)dK$ is the number of photons in the energy range dK Mev. We define

$$S(E)=\int_0^E \sigma(K)N(K)dK. \tag{36}$$

Figure 3 shows the function $S(E)$ for the data of Miller and Kikuchi.

We then compute the function $S(E)$ for the mechanism of Sec. II, taking $\sigma(K)$ to be the cross section for photostar production averaged over the emulsion elements. A value of $\phi=2.284\times10^{-28}$ is used, deduced from the data of Steinberger and Bishop[14] on photomeson production. $\eta=\frac{2}{3}$ is assumed. These values are shown in Fig. 3 for $\lambda=4\times10^{-13}$ cm and $\lambda=8\times10^{-13}$ cm.

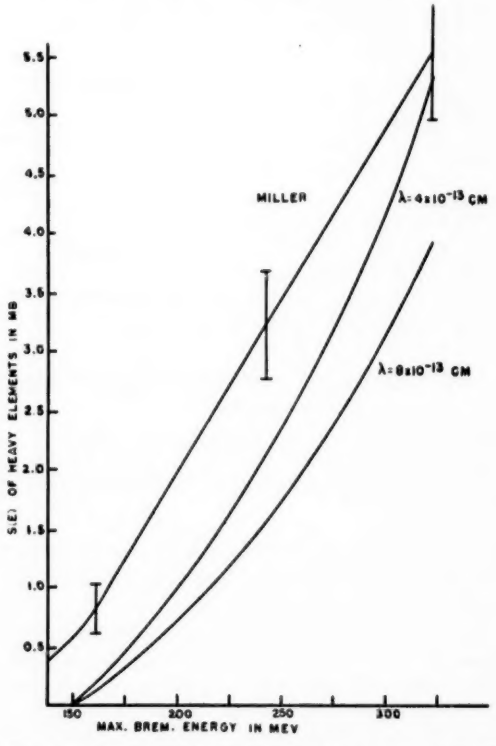

FIG. 5. The function $S(E)$ *vs* bremsstrahlung energy E for the heavy elements in $C2$ emulsion. Miller's curve is experimental. The curves for λ equal to 4×10^{-13} cm and 8×10^{-13} cm are calculated.

[14] J. Steinberger and A. S. Bishop, Phys. Rev. **86**, 171 (1952).

In Fig. 3 we see that both Miller and Kikuchi find appreciable photostar yields at the assumed threshold of 148 Mev. Kikuchi's data rise more rapidly than the predictions of the mechanism of Sec. II. $\lambda=4\times10^{-13}$ cm and $\lambda=8\times10^{-13}$ cm predict approximately the same values of $S(E)$.

Miller has evaluated $S(E)$ for two groups of emulsion elements by potential barrier argument:[2] the light elements C, N, and O, and the heavy elements Br, Ag and I. He ignores S which is present in small amounts. We include S with the light elements using the predictions of Sec. II. The results are shown in Fig. 4 for the light elements, in Fig. 5 for the heavy elements. For both groups of elements, the predictions for $\lambda=4\times10^{-13}$ cm and $\lambda=8\times10^{-13}$ cm do not differ greatly.

The values of $S(E)$ predicted by the mechanism of Sec. II agrees well with the observed $S(E)$ for the heavy element group, but is much smaller than the observed $S(E)$ for the light element group. The observed $S(E)$ may very well result from a superposition of two mechanisms, one of which is that of Sec. II, the other giving photostar cross sections which vary as A. Perhaps the deuteron model of Levinger[15] provides this second mechanism.

IV. CONCLUSION

The mesonic mechanism of Sec. II predicts a large part of the yield of photostars with three and more prongs for elements $A\gtrsim80$, but only a small fraction of the yield for elements $A\lesssim15$.

The results found in Sec. II do not differ greatly from results based on the optical model, using Eq. (1), and using formula (5) from Fernbach, Serber, and Taylor[16] for σ_{abs}. The fact that virtual mesons play only a small role in the mechanism accounts for this agreement.

I am grateful to Professor K. M. Watson for suggesting this problem and for his interest and guidance during its consideration.

[15] J. S. Levinger, Phys. Rev. **84**, 43 (1951).
[16] Fernbach, Serber, and Taylor, Phys. Rev. **75**, 1352 (1949).

PHYSICAL REVIEW VOLUME 91, NUMBER 1 JULY 1, 1953

Angular Distribution of Pions Scattered by Hydrogen*

H. L. Anderson, E. Fermi, R. Martin, and D. E. Nagle
Institute for Nuclear Studies, University of Chicago, Chicago, Illinois
(Received March 6, 1953)

The angular distribution of pions scattered by liquid hydrogen has been studied using the collimated pion beams from the Chicago synchrocyclotron. Differential cross sections have been measured for the laboratory angles 45°, 90°, and 135° for positive pions of energies 78 Mev, 110 Mev, and 135 Mev, and for negative pions of 120 Mev and 144 Mev. For negative pions, separate results were obtained for the elastic scattering and for the charge exchange scattering. The scattering of positive pions and charge exchange scattering of negative pions show a larger intensity in the backward direction. The elastic scattering of negative pions is mostly forward.

The results have been interpreted in terms of phase shift analysis on the assumption that the scattering is mainly due to states of isotopic spins $\frac{3}{2}$ and $\frac{1}{2}$ and angular momenta $s_{\frac{1}{2}}$, $p_{\frac{3}{2}}$ and $p_{\frac{1}{2}}$.

The experimental results are represented quite accurately by the following phase shifts expressed in degrees for the angular momentum states in the order indicated above: at 120 Mev, phase shifts ∓15, ±4, ±30 for isotopic spin $\frac{3}{2}$ and ±9, ∓3, ±2 for isotopic spin $\frac{1}{2}$; at 135 Mev, ∓14, ±5, ±38 for isotopic spin $\frac{3}{2}$ and ±10, ∓5, ±2 for isotopic spin $\frac{1}{2}$.

IN earlier communications[1,2] measurements of the total cross sections of hydrogen for both negative and positive pions at various energies were reported. In order to study in greater detail the features of the interaction between pions and protons, it appeared important to investigate also the nature and the angular distribution of the scattered particles.[3] The experiments are being carried out with the well-collimated pion beams of the Chicago Synchrocyclotron using scintillation counter techniques. This is a report on the progress of this investigation.

I. EXPERIMENTAL ARRANGEMENT

The pions are produced by a 450-Mev proton beam striking a beryllium target inside the cyclotron. Negative pions emitted in the forward direction are bent outward by the cyclotron magnetic field and emerge through a thin aluminum window from the vacuum chamber of the machine. A certain amount of focusing takes place, so that a sizeable fraction of the pions of given energy leave the cyclotron in a fairly parallel beam. The 12-foot thick steel and concrete shield which separates the cyclotron from the experiment room has

* Research supported by a joint program of the U. S. Office of Naval Research and the U. S. Atomic Energy Commission.
[1] Anderson, Fermi, Long, Martin, and Nagle, Phys. Rev. **85**, 934 (1952).
[2] Anderson, Fermi, Long, and Nagle, Phys. Rev. **85**, 936 (1952).
[3] Anderson, Fermi, Nagle, and Yodh, Phys. Rev. **86**, 793 (1952).

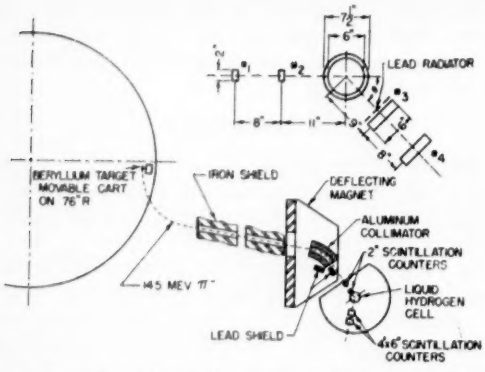

FIG. 1. General experimental arrangement. In the inset the details of the scattering geometry are given.

channels cut through it to accept a number of these beams with different energies.

On the experiment side of the shield a sector magnet deflects the pions through an angle of about 45°. The beam is purified thereby from most of the unwanted radiation (mostly neutrons) which comes through the channel.

Positive pions are obtained by reversing the direction of both the cyclotron and the deflecting magnetic fields. The proton beam in the cyclotron then circulates counterclockwise, and the positive pions which are emitted backward from this direction follow the same trajectories and have the same energy as their negative counterparts. The backward emission is unfavorable and the intensity of the positive pions which is obtained in this way is much smaller than that of the negatives.

The general arrangement is shown in Fig. 1. The pion beam is defined by passing through two 2-in. diameter liquid scintillation counters No. 1 and No. 2, and thereafter enters the hydrogen cell. The scattered particles are detected by a pair of scintillation counters, No. 3 and No. 4, arranged on a table to pivot around the central axis of the hydrogen cell. In some experiments these two counters were 4 in. in diameter; in others they were rectangles of 4 in.×6 in. A quadruple coincidence is recorded when a particle passes through the first two counters and is scattered so as to pass through the second pair. The double coincidences of the first pair are recorded at the same time. The fraction of the incident beam which is scattered is given by the ratio of the quadruple to double coincidences. The hydrogen cell was designed for rapid insertion and removal of the liquid hydrogen in order to distinguish the effect of the hydrogen from the scattering by surrounding materials. The resolving power of the coincidence equipment was fast enough (2×10^{-8} second), and the general background of stray radiation in the room was small enough, that chance coincidences were very few.

II. SCINTILLATION COUNTERS

Liquid scintillation counters were found convenient in this work because they can be made with large areas of sensitivity over which their response is quite uniform. Their speed is quite high (6×10^{-9} second). The use of low density and low Z materials makes the absorption and scattering of pions in them tolerably small. The design of the 2-in. scintillation cell is shown in Fig. 2. The cell is made of clear Lucite $\frac{3}{4}$-in. thick over all with $\frac{1}{16}$-in. thick Lucite windows. The liquid is phenylcyclohexane with 3 grams per liter of terphenyl and 10 mg per liter of diphenylhexatriene according to the prescription of Kallman.[4] The end of the Lucite cell is shaped to fit the photocathode of a 5819 tube and good optical contact is assured by a thin layer of clear silicone grease. The whole cell is wrapped in thin aluminum foil which enhances the light collecting efficiency. Phototube

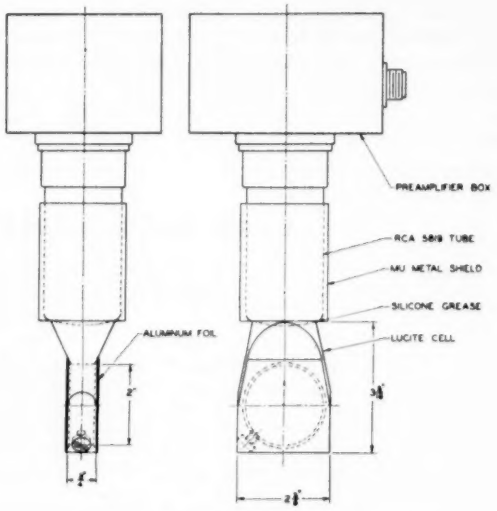

FIG. 2. Two-inch diameter scintillation counters.

and scintillation cell are light-proofed with black Scotch electric tape. An iron shield is necessary to protect the photomultiplier from the stray magnetic field of the cyclotron.

Two different types of counters No. 3 and No. 4 have been used at different times. In the earlier experiments 4-in. diameter scintillation counters were used; later the counters were changed to a newer type with a sensitive region of 4 in.×6 in. The 4-in. diameter counters were 1 in. thick over all with $\frac{1}{16}$-in. thick Lucite windows. The ends of the Lucite cell were shaped to fit the large cylindrical photocathode of an RCA C-7157 photomultiplier. The Lucite cell and the photomultiplier were enclosed in a steel box for magnetic shielding. The box was provided with $\frac{1}{32}$-in. mu-metal windows in front and in back of the sensitive area of the cell.

[4] H. Kallman and M. Furst, Phys. Rev. **81**, 853 (1951).

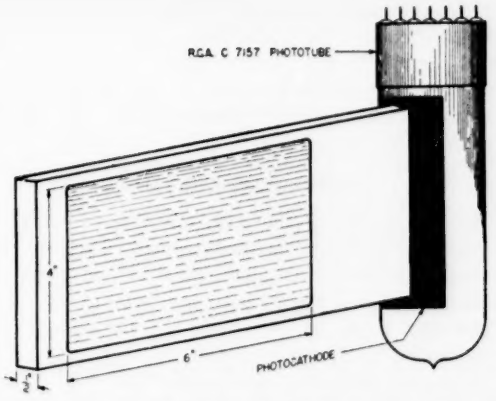

FIG. 3. Rectangular 4-in.×6-in. scintillation counters.

The design of the 4 in.×6 in. scintillation cells is shown in Fig. 3. They are also made of clear Lucite with $\frac{1}{16}$-in. thick Lucite windows. The over-all thickness is $\frac{1}{2}$ in. The ends are shaped to fit the large cylindrical photocathode of the RCA C-7157 photomultiplier. The photomultiplier is protected from the stray magnetic field of the cyclotron by a cylindrical iron enclosure not shown in the figure. The scintillation cell itself was wrapped in thin aluminum foil to improve the light collecting efficiency and to keep out stray light.

The response of both types of scintillators is uniform within 5 percent over their area. This was shown by making traverses with a narrow $\frac{1}{4}$-in. beam of Co^{60} gamma-rays across the diameters parallel and perpendicular to the photocathode and reading the anode current of the photomultiplier directly on a microammeter.

For meson counting the photomultipliers were connected to a preamplifier which incorporated a 200-ohm line, 8 feet long, to clip the pulses into a fairly square shape of 2×10^{-8} second duration. The pulses were fed to the cyclotron control room through some 150 feet of 95-ohm RG7-U cable. The pulses were amplified tenfold by means of 100-ohm distributed amplifiers and fed to the coincidence circuits.

The coincidence circuits were designed using some of the ideas of Garwin.[5] The circuit used is given in Fig. 4. It can be arranged to record either the single pulses from any given scintillator, or the double, triple, quadruple coincidences of any chosen combination, by the manipulation of suitable switches. The outputs of the first two scintillation counters were fed into the first coincidence circuit set to record doubles, and also into the second coincidence circuit set to record quadruples of all four scintillators. The coincidence circuits operate with negative pulses of 2 volts or more provided their duration is greater than 1×10^{-8} second. The photomultipliers were operated to deliver about 0.4 volt from meson pulses. With the amplification by 10, this was ample for reliable operation of the coincidence circuits.

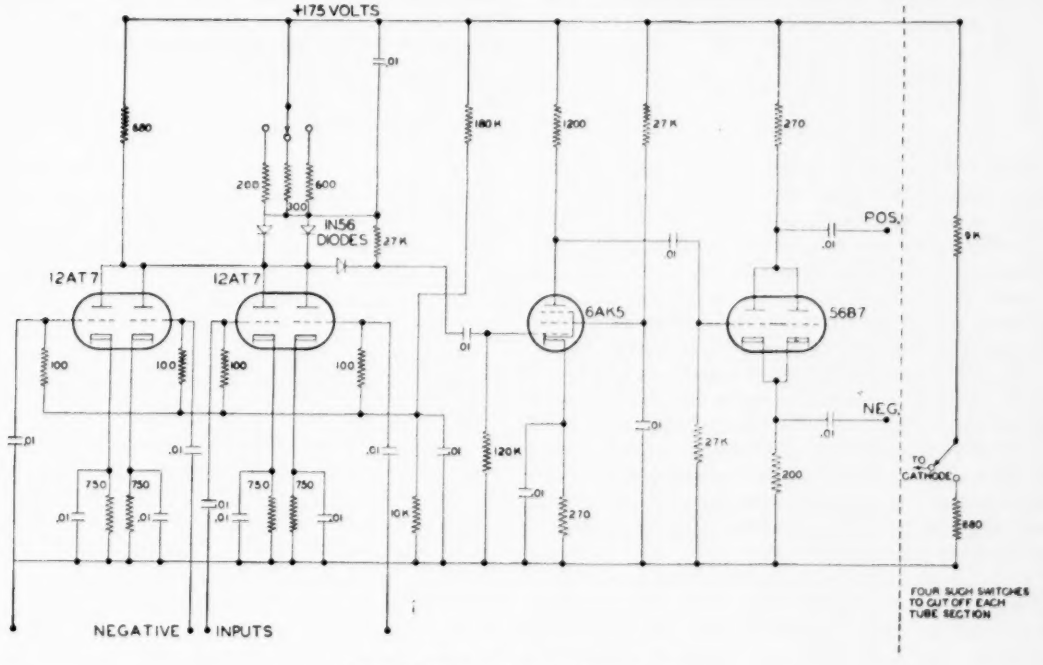

FIG. 4. Diagram of the coincidence circuits.

[5] R. L. Garwin, Rev. Sci. Instr. **21**, 569 (1950).

The meson pulses, as seen with the fast Tektronix Type 517 Oscilloscope, were quite uniform in amplitude.

The counting efficiency of these scintillators should be very close to 100 percent. An over-all check was obtained by comparing the quadruples to doubles rate with counters No. 3 and No. 4 between No. 1 and No. 2 in the line of the pion beam. The ratio obtained was usually quite close to unity.

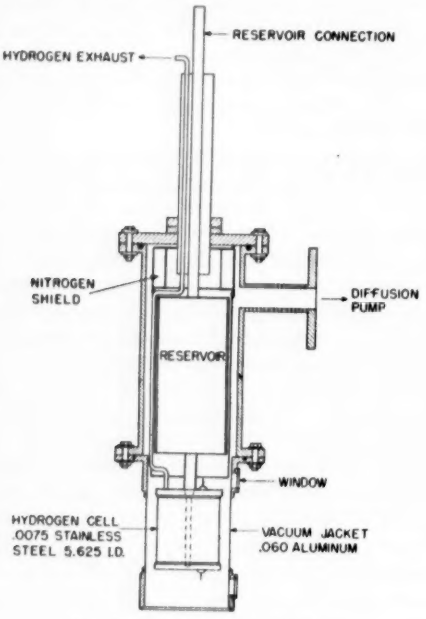

FIG. 5. Liquid hydrogen container.

III. TARGET

The beryllium target in which the mesons are produced has a calibrated thermocouple arrangement which records on a Brown potentiometer the power in watts delivered to the target by the proton beam. Most of this energy is due to ionization loss, some is due to nuclear reactions, but in any case the energy delivered is closely proportional to the path length of protons in the target and hence to the number of mesons produced.

The readings obtained from the thermocouple target do not enter in any essential way in the present experiments. However, by reducing the counting rate to unit energy in watt minutes developed in the target, an over-all check on the operation of the equipment is provided which is useful not only during a given run, but also in judging the reproducibility of the arrangement from one day's run to the next.

In the present experiments the beryllium target was of dimensions 2 in. in the direction of the beam, $\frac{1}{2}$ in. in height and $\frac{1}{4}$ in. in thickness. In most of the runs the intensity ranged from 10 to 25 watts. At the level of operation of 12 watts the double coincidences of counters No. 1 and No. 2 which register the pions entering the equipment were as follows: For positive pions of 78 Mev, 36 000 per minute; for positive pions of 110 Mev, 6000 per minute; for positive pions of 135 Mev, 900 per minute; for negative pions of 120 Mev, 230 000 per minute; and for negative pions of 144 Mev, 65 000 per minute.

IV. HYDROGEN CONTAINER

During the course of this investigation two different liquid hydrogen containers were used. They differed primarily in the materials and the thickness of the two walls of the liquid hydrogen Dewar. One was used in all measurements on positive pions and the other in the measurements of negative pions.

The apparatus for holding the liquid hydrogen is shown in Fig. 5. The mesons passed horizontally through the lower section, where the walls were thinned. In the cell used for the positive pion measurements the outer wall was 0.032-in. stainless steel and the inner wall 0.020-in. brass, and the internal diameter 5.8 in. For the measurements on negative pions, the outer wall was 0.060-in. aluminum and the inner wall 0.0075-in. stainless steel, internal diameter $5\frac{5}{8}$ in. The space between the walls was evacuated to a pressure of about 10^{-6} mm of mercury. The inner cylindrical cell which held the liquid hydrogen had a volume of about 4 liters. A reservoir of 12 liters capacity was directly above the cell and connected to it by a $\frac{3}{8}$-in. diameter tube extending nearly to the bottom of the cell. At the top of the cell there was an exhaust tube which carried off the vapors when liquid filled the cell. Whenever it was required to remove the liquid from the cell, the exhaust tube was closed externally by a valve: whereupon the vapor pressure forced the liquid up into the reservoir. Opening the exhaust valve allowed the liquid to fall back into the

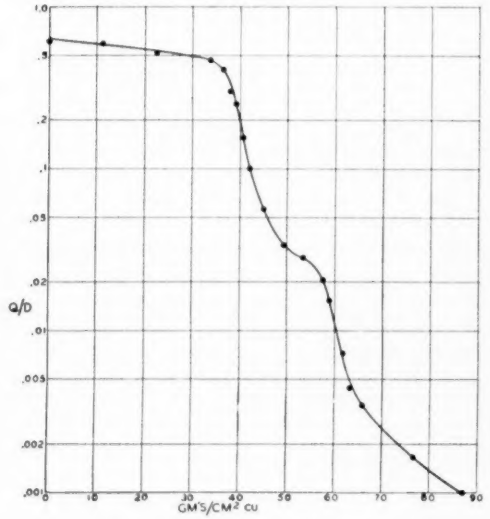

FIG. 6. Range curve of π^+ in copper.

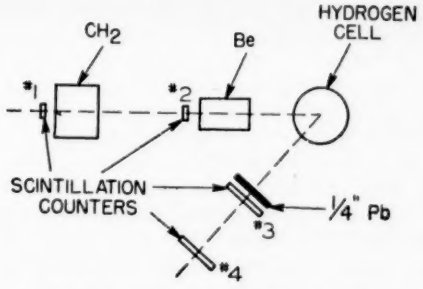

FIG. 7. Arrangement for Panofsky effect.

cell under gravity. By this method successive measurements of the pion scattering could be taken with the cell full or empty of liquid.

Two parallel plate condensers, one above and one below the cell, were used to indicate when the cell was full or empty of liquid, use being made of the sizeable increase in capacity which results when liquid hydrogen fills the space between the condenser plates.

The reservoir was shielded from radiation by a liquid nitrogen jacket so that the evaporation rate was about 0.6 liter per hour. With a 50-liter supply of liquid hydrogen it was possible to continue an experiment for about 24 hours.

V. ENERGY OF THE PRIMARY PIONS

The energy of the primary pions is known approximately from the channel through which they pass. These channels were laid out according to a rather detailed study of the trajectories of the pions of different energy. The channel energy is only nominal, however, because it depends on the target position and on the value of the cyclotron magnetic field, and these are not always precisely reproduced.

For this reason, it is more reliable to measure directly the energy of the pion beam used in each experiment. This has been done sometimes by taking a range curve of the pions and sometimes by observation of the Panofsky effect. A typical range curve is plotted logarithmically in Fig. 6. This was obtained with the positive pion beam from the channel of nominal energy 122 Mev. The four counters were put in line with no hydrogen in the scattering cell, and copper absorbers were inserted between counters No. 2 and No. 3. The absorption curve shows two sharp drops corresponding to the end of the range of the pions and of the muons. The uncorrected mean ranges from the curve are 38.4 and 59.8 g/cm² copper.

In order to compute the energy of the pions in the center of the liquid hydrogen, one must correct these ranges, on account of the different amount of absorbers present in the absorption measurement and in the scattering experiment. The range is finally converted to energy using the range energy tables for protons given by Aron[6] and adopting as a mass ratio 6.65 for the proton to pion. The range curve of Fig. 6 can also be used in order to estimate the contamination of the beam by muons and by electrons. For example, it was estimated that the muon contamination in this case was 7 percent.

In some of the experiments the beam energy was determined by means of the Panofsky effect. One of the geometries used for this type of measurement is shown in Fig. 7. A $\frac{1}{4}$-in. lead sheet was placed in front of counter No. 3 to increase its sensitivity to gamma-radiation. Light atomic weight absorbers, beryllium and

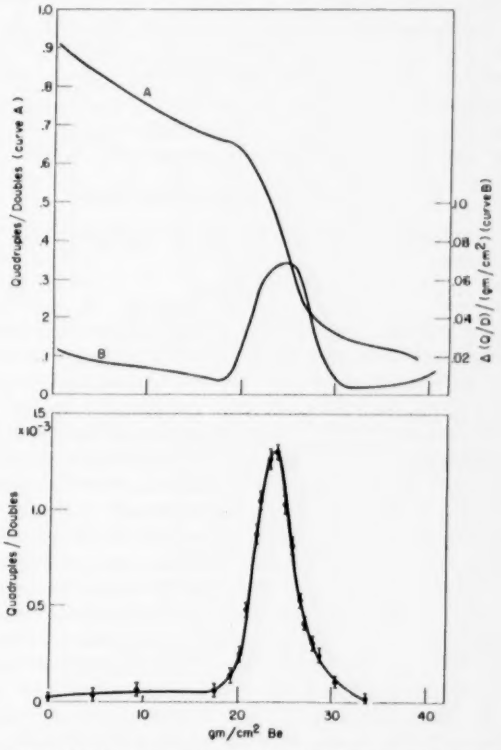

FIG. 8. Abscissas, amount of Be absorber; lower curve, intensity of the Panofsky gamma-radiation; upper curves, absorption curve and its derivative. The additional absorber of 11.24 g/cm² polyethylene between counters No. 1 and No. 2 is not indicated.

polyethylene, were interposed in the beam in front of the liquid hydrogen cell. In Fig. 8 the ratio of quadruple to double coincidences is plotted *versus* the thickness of absorber. The curve shows a sharp maximum at 23.8 g/cm² beryllium. To this one should add the absorber (11.24 g/cm² polyethylene) between counters No. 1 and No. 2. The beryllium equivalent of this is 14.6 g/cm². In conclusion the amount of beryllium necessary to reduce the energy of the pions to the point that they stop in the hydrogen is 38.4 g/cm², corresponding to an energy of 110 Mev.

[6] W. A. Aron, Berkeley Report UCRL 1325, 1951 (unpublished).

TABLE I. Observed value of $10^6 Q/D$ for 110 Mev and 135 Mev positive pions (4-in. diameter counters, corrected to standard geometry).

Angle	With hydrogen	Without hydrogen	Net
	110 Mev		
45°	262.6±15.0	162.3±18.4	100.4±19.8
90°	124.0±10.5	21.0± 6.7	103.0±12.5
135°	243.5±12.7	50.5± 8.1	193.0±15.1
	135 Mev		
45°	454±47	280±47	174±67
90°	199±32	63±28	136±43
135°	403±45	74±30	329±54

In the upper part of Fig. 8 there is plotted the absorption curve obtained in the same geometry of the Panofsky effect, and its derivative. One can see the maximum in the derivative curve matching the Panofsky maximum. A discussion of the quantitative comparison between the two curves will be found in Sec. VIII.

VI. SCATTERING OF POSITIVE PIONS

For positive pions only the elastic scattering, represented by

$$\pi^+ + p \rightarrow \pi^+ + p \qquad (1)$$

was considered possible. After the scattering, a pion and a proton are produced which share the kinetic energy of the primary pion. In our experiment the conditions were always such that the protons could not be detected because they did not have sufficient range to penetrate the detecting counters No. 3 and No. 4. For this reason all observed scattering was attributed to the scattered positive pions. Scattering measurements of positive pions have been performed at three energies of primary pions, 78 Mev, 110 Mev, and 135 Mev (mean energy at center of hydrogen). Measurements were taken for three scattering angles, 45°, 90°, and 135°. At each of these positions, counts were taken both with and without hydrogen in the scattering cell, and the difference of the two results attributed to the hydrogen scattering.

In the measurements at 110 Mev and 135 Mev the 4-in. diameter detecting counters were used in positions 3 and 4. In the 135-Mev measurement the distances of No. 3 and No. 4 from the center of the scattering cell were the "standard" distances 9 in. and 17 in. In some of the measurements at 110 Mev distances of 8.7 in. and 16.7 in. were used, in others the distances were 10.8 in. and 18.8 in. The data for this case are corrected to the "standard" geometry. One measures in both cases the ratio Q/D of quadruple to double coincidences. The results are given in Table I.

In order to compute from these data the corresponding scattering cross section for each angle, the effective solid angle subtended by counters No. 3 and No. 4 is needed. For the scattering angles 45° and 135°, this was 0.0435 steradian. For the 90° geometry, the effective solid angle was 0.0410 steradian, slightly less because some of the particles scattered at the entrance or at the exit of the scattering cell could enter counter No. 4, but not counter No. 3, and would be missed. In computing the cross sections, the fact that only 93 percent of the primary beam were pions was taken into account. The muons, and possibly some few electrons in the beam were assumed not to be scattered appreciably.

The mean path length of pions traversing the hydrogen in these experiments was 14.4 cm. When the cell was filled with liquid hydrogen, the number of atoms/cm³ was 4.2×10^{22}. When the cell was empty, it still contained gaseous hydrogen at liquid hydrogen temperature amounting to 0.07×10^{22} atoms/cm³. The difference, 4.13×10^{22}, multiplied by the effective length of the scattering cell, gives 5.95×10^{23} H atoms/cm².

The efficiency of counters No. 3 and No. 4 for counting a scattered pion that geometrically should be accepted by both counters was not 100 percent because the counter efficiency was not perfect (98 percent), and nuclear absorption in the first counter and in the hydrogen cell further reduced the efficiency to about 93 percent. The cross sections per steradian are given in Table II in the laboratory and in the center-of-mass systems.

TABLE II. Differential cross sections for positive pions.

Energy Mev	Laboratory system: Scattering angle (degrees)	Laboratory system: Differential cross section 10^{-27} cm²/sterad	Center-of-mass system: Scattering angle (degrees)	Center-of-mass system: Differential cross section 10^{-27} cm²/sterad
78	45°	1.96±0.33	53.8°	1.50±0.25
	90°	2.26±0.31	102.0°	2.34±0.32
	135°	3.09±0.34	143.2°	4.29±0.47
110	45°	4.48±0.88	54.9°	3.33±0.65
	90°	4.88±0.59	103.2°	5.09±0.62
	135°	8.62±0.67	143.9°	12.34±0.96
135	45°	7.77±3.00	55.7°	5.66±2.18
	90°	6.42±2.03	104.2°	6.75±2.14
	135°	14.70±2.41	144.5°	21.64±3.55

The probable errors given in Table II are those due to statistics alone. Uncertainties in the beam energy and its pion content as well as in the estimates of the efficiency of detection all contribute to the inaccuracy of the experiment. These additional errors have not been added in this case because the statistical error was believed to be dominant.

The measurement with 78-Mev positive pions was performed at a later date using as detecting counters No. 3 and No. 4 the rectangular 4 in.×6 in. counters. In this case the distances of the two counters No. 3 and No. 4 from the center of the scattering cell were respectively 9 in. and 17 in. The beam intensity at the average operation level of 23 watts yielded approximately 70 000 doubles per minute. The results of the measurement are collected in Table III. The conversion of these data to cross sections is similar to the previous cases. We assumed in this case that 92 percent of the doubles were due to pions. The solid angle was ap-

proximately 0.083 with very minor geometrical and scattering corrections. The cross sections in the laboratory and in the center-of-mass system are given in Table II. It will be noticed that in all these cases $(d\sigma/d\omega)$ is appreciably larger in the backward than in the forward direction. This fact seems to indicate a negative interference between the scattering due to the s and the p waves, as will be discussed later.

The differential cross sections in the laboratory system can be integrated over the solid angle in order to obtain the total cross sections. The results are given in column 2 of Table IV. In column 3 of the same table are reported the cross sections at the same energy obtained by interpolation from the data of the transmission measurements.[2] The agreement is within the experimental error.

TABLE III. Observed values of $10^6Q/D$, 78-Mev positive pions (4-in.×6-in. counters, standard geometry).

Angle	With hydrogen	Without hydrogen	Net
45°	510.9±10.4	425.7±9.8	85.2±14.3
90°	217.5±10.4	121.5±7.8	96.0±13.0
135°	390.9±11.4	256.6±9.3	134.4±14.8

VII. SCATTERING OF NEGATIVE PIONS

The measurement of the scattering of negative pions was carried out for two energies of the primary beam, 120 and 144 Mev (mean energy at the center of the hydrogen). Three processes are believed to be possible:

$$\pi^-+p\rightarrow\pi^-+p, \tag{2}$$

$$\pi^-+p\rightarrow\pi^0+n\rightarrow 2\gamma+n, \tag{3}$$

$$\pi^-+p\rightarrow\gamma+n. \tag{4}$$

TABLE IV. Total cross sections of positive pions.

Energy	Total cross section 10^{-27} cm² From integration	From transmission
78 Mev	31± 3	45±13
110 Mev	77± 6	82± 8
135 Mev	126±20	149±14

Equation (2) represents the elastic scattering of negative pions and protons. Equation (3) represents scattering with charge exchange, in which the proton is converted to a neutron and the negative pion is converted to a neutral pion which almost immediately disintegrates into two photons. Equation (4) is the inverse reaction of the photoeffect in which a photon produces a negative pion by striking a neutron. The cross section of process (4) is estimated by detailed balancing from the inverse process[7] to be only about 0.8×10^{-27} cm². The present measurements confirmed the fact, previously reported,[8] that process (3) is appreciably more intensive than process (2).

The sensitivity of the pair of counters No. 3 and No. 4 to photons produced in the scattering process is normally rather low. However, it can be increased very appreciably by interposing in front of counter No. 3 a lead sheet to convert the gamma-rays into electron-positron pairs which are detected by the counters. For this reason, with π^-, four measurements were taken at each angle, namely, measurements of the ratio Q/D with and without liquid hydrogen in the scattering chamber and with and without a $\frac{1}{4}$-in. thick lead radiator in front of counter No. 3. The net effect due to the hydrogen is computed as the difference with and without hydrogen.

In order to obtain separately the numbers of scattered pions and photons entering the detecting counters No. 3 and No. 4 it is necessary to know the efficiencies for the two types of particles. The counters used in the experiments on negative pions were thinner than those used in the positive pion experiments. There was a smaller loss due to absorption. The over-all efficiency without lead radiator was estimated to be 97 percent. With the lead radiator the efficiency is reduced both by nuclear absorption and by scattering. The latter effect depends on the energy of the pions and therefore also on the scattering angle. Moreover, the geometry at 90° is somewhat different than at 45° and 135°. An estimate of these effects gives the efficiencies listed in Table V.

In the same table the efficiencies for photon detection with and without lead are listed. The procedure for calculating these efficiencies is described in Sec. VIII.

The energies of the primary negative pions used in these two measurements were determined from the amount of absorber needed to produce a maximum in the Panofsky radiation. In one set of measurements the absorber was 44.3 g/cm² of aluminum corresponding to a pion energy of 120 Mev. In the other measurements it was 57.3 g/cm² of aluminum corresponding to 144 Mev. In both cases the detecting counters No. 3 and No. 4 had a sensitive area of 4×6 sq in., and were placed re-

TABLE V. Efficiencies of the detecting counters.

Energy Mev	Angle	Lead	Efficiency for pions (percent)	Efficiency for photons (percent)
120	45°	out	97	4
120	45°	in	91	67
120	90°	out	97	4
120	90°	in	88	61
120	135°	out	97	4
120	135°	in	88	59
135	45°	out	97	4
135	45°	in	92	70
135	90°	out	97	4
135	90°	in	89	63
135	135°	out	97	4
135	135°	in	88	60

[7] Bishop, Steinberger, and Cook, Phys. Rev. **80**, 291 (1950); Feld, Frisch, Lebow, Osborne, and Clark, Phys. Rev. **85**, 680 (1952).

[8] Fermi, Anderson, Lundby, Nagle, and Yodh, Phys. Rev. **85**, 935 (1952).

spectively, at 9 in. and 17 in. from the center of the scattering cell.

Each individual measurement consists of a determination of the ratio Q/D of the quadruple coincidences to the double coincidences. The results of the measurements with their statistical errors are collected in Table VI.

For each primary energy and for each scattering angle, one needs the numbers II and Γ of pions and photons per million primaries whose line of propagation enters the solid angle subtended by counter No. 4. These two numbers are obtained by solving two linear equations. For example, for 120-Mev pions and 90° scattering angle, we have from Table VI counts per million with and without lead 103.4±4.0 and 25.6±3.2. Using the efficiencies listed in Table V, one obtains the two equations

$$0.61\Gamma+0.88\Pi=103.4\pm4.0,$$

$$0.04\Gamma+0.97\Pi=25.6\pm3.2.$$

These equations have the solution

$$\Gamma=139.8\pm8.7, \quad \Pi=20.6\pm3.6.$$

In order to convert these numbers to differential cross sections they must be divided by the following factors: 930 000 (this is the number of pions per million primaries, the remainder of 7 percent being due to muons and electrons which are assumed to have no appreciable nuclear scattering), 0.083 (this is the solid angle subtended by counter No. 4), 5.9×10^{23} (this is the average number of hydrogen atoms per cm² traversed by the primary beam). Dividing the values of II and Γ by the product of these factors, one obtains the following cross sections per steradian at 90°, for 120-Mev negative pions:

$$d\sigma_-/d\omega=(0.45\pm0.08)\times10^{-27}\ \text{cm}^2/\text{sterad},$$

and

$$d\sigma_\gamma/d\omega=(3.08\pm0.20)\times10^{-27}\ \text{cm}^2/\text{sterad}.$$

The errors indicated in these two cross sections comprise only the statistical error. Other sources of error are, in order of importance, the uncertainty in the efficiencies listed in Table V in the actual pion content and energy of the beam, and geometrical errors. We have estimated that the over-all effect of these errors may amount to 10 percent, and this error has been combined with the statistical error in the final results.

In Table VII are collected the values of the differential cross sections in the laboratory and in the center-of-mass frames of reference.

As an over-all check the total cross sections obtained by integration from the data of Table VII may be compared with the results of total cross-section measurements by transmission.[1] The results of the integration are collected in Table VIII, columns 2 and 3. The contribution of the $\pi^-\rightarrow\gamma$ process to the total cross section is about one-half the cross section listed in column three because each neutral pion produced in the exchange scattering process yields two photons. A very small correction has been included on account of the contribution of the inverse photoeffect. The total cross section obtained from the contributions of columns 2 and 3 is given in column 4. The total cross section given in column 5 is obtained instead by interpolation of the results of the transmission measurements. The two sets of results agree within the experimental errors.

TABLE VI. Observed values of $(Q/D)\times10^6$ for negative pions.

Angle	Lead	With hydrogen	Without hydrogen	Net
		120 Mev		
45°	out	235.6±3.3	167.2±2.8	68.4±4.5
90°	out	82.0±2.3	56.4±2.1	25.6±3.2
135°	out	112.7±2.8	75.1±3.1	37.6±4.2
45°	in	290.6±4.3	150.4±3.4	140.2±5.6
90°	in	161.4±3.2	58.0±2.4	103.4±4.0
135°	in	223.9±3.9	75.8±3.1	148.1±5.0
		144 Mev		
45°	out	237.6±4.9	126.0±4.0	111.6±6.4
90°	out	93.3±3.4	55.0±3.0	38.3±4.6
135°	out	135.3±3.9	88.5±4.2	46.8±5.8
45°	in	355.9±6.0	115.1±1.8	240.8±7.1
90°	in	202.2±5.0	52.3±3.0	149.9±5.9
135°	in	264.1±5.2	75.3±4.3	188.8±6.8

TABLE VII. Differential cross sections for negative pions.

Energy (Mev)	Process	Laboratory system: Scattering angle (degrees)	Laboratory system: Diff. cross section (10^{-27} cm²/sterad)	Center-of-mass system: Scattering angle (degrees)	Center-of-mass system: Diff. cross section (10^{-27} cm²/sterad)
120	$\pi^-\rightarrow\pi^-$	45	1.44±0.18	55.2	1.06±0.14
		90	0.45±0.09	103.6	0.47±0.10
		35	0.67±0.12	144.3	0.97±0.18
120	$\pi^-\rightarrow\gamma$	45	2.64±0.36	53.0	2.07±0.30
		90	3.08±0.37	100.5	3.19±0.39
		135	4.53±0.51	142.0	5.98±0.69
144	$\pi^-\rightarrow\pi^-$	45	2.35±0.29	56.0	1.70±0.21
		90	0.69±0.14	104.6	0.73±0.15
		135	0.83±0.17	144.6	1.23±0.25
144	$\pi^-\rightarrow\gamma$	45	4.48±0.55	54.0	3.43±0.42
		90	4.25±0.51	101.6	4.43±0.53
		135	5.71±0.66	142.6	7.78±0.90

VIII. SENSITIVITY OF THE DETECTING COUNTERS FOR PHOTONS

The sensitivity of the detecting counters No. 3 and No. 4 for the photons produced in the decay of neutral pions is very small without lead radiator and is of the order of magnitude of 50 percent with the lead radiator in place. Without the lead radiator a photon may be detected when it materializes while traversing the hydrogen, the wall of the hydrogen cell, or counter No. 3, provided in this latter case that the materialization does not take place too close to the exit of the photon out of the sensitive region of the counter because the

pulse will then be too small to be recorded. Finally, according to Dalitz,[9] a photon has a probability of 0.63 percent of being converted into a pair by internal conversion at the moment of its formation. In order to compute these various effects, the cross section for pair formation was obtained by interpolation between the data of Lawson[10] at 88 Mev and the data of DeWire, Ashkin, and Beach[11] at 280 Mev. Some small contribution to the detection of gamma-rays comes from Compton electrons. A Compton electron, however, has a high probability to give a coincidence of counters No. 3 and No. 4 only when its energy is an appreciable fraction of the energy of the photon. For this reason only one-half of the Compton cross section was added to the pair formation cross section, in order to obtain an effective cross section for materialization. The cross sections finally adopted are given in Table IX.

TABLE VIII. Integrated cross sections of negative pions (10^{-27} cm^2).

Energy	$\pi^-\to\pi^-$	$\pi^-\to\gamma$	Total	Total from transmission
120 Mev	11.3±1.6	43.4±5.4	33.4±3.2	38±9
144 Mev	17.0±2.4	61.2±7.5	48.1±4.5	55±6

TABLE IX. Cross sections for materialization σ pair$+\frac{1}{2}\sigma$ Compton (cm^2/g).

Element	90 Mev	135 Mev
H	0.0097	0.0097
C	0.0135	0.0143
Al	0.0240	0.0256
Fe	0.0422	0.0453
Cu	0.0454	0.0487
Pb	0.0909	0.0983

The probability of observing a photon without the lead radiator computed for the average energy photon emerging in the various directions and for the actual thickness of material traversed was in all cases about 4 percent, and this value has been adopted in Table V. With the lead radiator in place (7.36 g/cm^2), the probability of pair formation is greatly increased. For example, for 90-Mev photons, it is 51 percent.

The probability of pair formation, however, gives only a rough indication of the efficiency. There are primarily two reasons for this, namely, absorption of the electrons and effect of the multiple scattering. The first effect leads to a reduction, the second to an increase in efficiency. In order to understand the reason for the increase, we observe that if a single particle and not a pair were produced in the materialization, the effect of the multiple scattering would be cancelled in first approximation because some particles would be scattered in and some would be scattered out. In the case of a pair, however, it is sufficient that one electron only of the pair be detected; therefore a photon is lost if both electrons are scattered out but is detected if both electrons or even only one of them is scattered in. An attempt was made to calculate these effects by assuming that all the pairs originate in the middle of the lead radiator. It was assumed further that the energy of the photon is divided evenly between the electron and the positron. The calculation was carried out for photons of 90 and 135 Mev. From the results of Wilson[12] it was estimated that the probability of a pair electron traversing the lead with sufficient energy to be recorded is 0.76 for photons of 90 Mev and 0.85 for photons of 135 Mev.

TABLE X. Efficiency for photons.

Angle of scattering	90 Mev	135 Mev
45° or 135°	0.567	0.691
90°	0.558	0.681

TABLE XI. Mean energy of the photons (Mev).

Primary pions \ Angle	45°	90°	135°
120 Mev	126	109	97
144 Mev	137	117	102

Consider now a photon whose line of propagation crosses the plane of counter No. 4 at a certain position. If a pair is formed, the probability q of observing the positron of the pair will be obtained by multiplying the probability that the positron of the pair escapes the lead with sufficient energy to be counted times the probability that after multiple scattering the positron falls inside counter No. 4. There is, similarly, an equal probability q of observing the electron of the pair. The probability of observing the photon that has materialized is the probability of observing either the electron or the positron or both. This probability is given by $q(2-q)$. Multiplying this probability by the probability of materialization of the photon, one obtains the probability of observing the photon. Integrating this probability over the area, one obtains an effective area of counter No. 4. We define the efficiency as the ratio of the effective to the true area of the counter. The geometry is slightly different at 90° and at 45° and 135°. The computed efficiencies are given in Table X. It is seen that the efficiency has an appreciable energy dependence. The mean energy of the photons produced by neutral pion decay in the scattering experiment depends on the energy of the primaries and the scattering angle as is given in Table XI. The efficiencies were then

[9] R. H. Dalitz, Proc. Roy. Soc. (London) **A64**, 667 (1951).
[10] J. L. Lawson, Phys. Rev. **75**, 433 (1949).
[11] DeWire, Ashkin, and Beach, Phys. Rev. **83**, 505 (1951).
[12] R. R. Wilson, Phys. Rev. **84**, 100 (1951).

computed by linear interpolation from the data of Table X and are given in Table V.

An attempt was made to obtain an experimental confirmation of the results of the efficiency calculation described in this section. This is done by an absolute measurement of the sensitivity of the detecting counters No. 3 and No. 4 to the gamma-rays emitted in the Panofsky effect. In Fig. 8 the ratio of quadruple to double coincidences is plotted *versus* the thicknesses of absorber for the geometry represented in Fig. 7. By integration of the curve of Fig. 8 one finds that the total area of the Panofsky bulge after subtracting background is

$$P=6430 \text{ counts per million} \times \text{g/cm}^2 \text{ Be}.$$

In the same figure is plotted also the derivative of the absorption curve. The derivative curve shows a bulge matching in position the Panofsky bulge. Its integrated area after subtracting background is found to be

$$A=4.41\times10^5 \text{ counts per million}.$$

The thickness of hydrogen traversed by the pions is in the average 0.987 g/cm². Using for short range pions the equivalence factor in stopping power of hydrogen to beryllium of 2.58 one finds that this amount of hydrogen is equivalent to 2.546 g/cm² Be. Denoting this factor by H, we obtain now the effective solid angle ω of the detecting counters from the following relationship:

$$P=fHA\omega/4\pi,$$

where f is the average number of photons emitted when a negative pion comes to rest within the liquid hydrogen. According to Panofsky[13] one has $f=1.485\pm0.054$. We obtain in this way $\omega=0.0485\pm0.005$. The error includes an estimate of the uncertainties in the various quanties that enter in the determination of ω. The efficiency is the ratio of the effective solid angle ω to the geometrical solid angle which is 0.083. We obtain, therefore, an efficiency of 0.58 ± 0.06. The average energy of the pions to which this result refers is about 90 Mev. In Table X the efficiency was found, in excellent agreement, to be 0.57.

IX. ANALYSIS OF THE SCATTERING DATA

The data of Secs. 6 and 7 may be analyzed by assuming that the scattering is due mainly to the contributions of s and p waves. The angular distribution of the scattered particles in the center-of-mass system will then have the form

$$d\sigma/d\omega=a+b\cos\chi+c\cos^2\chi, \tag{5}$$

where χ is the scattering angle in the center-of-mass system. The coefficients a, b, and c for the elastic scattering of 78, 110, and 135 Mev π^+ and for the elastic scattering of 120 and 144 Mev π^- are readily computed from the data of Tables II and VII.

[13] Panofsky, Aamodt, and Hadley, Phys. Rev. **81**, 565 (1951).

The calculation of these coefficients for the charge exchange scattering is complicated by the fact that the direct measurement gives the cross section for the production of gamma-rays, and the angular distribution of these differs somewhat from that of the neutral pions which decay into them.

The problem can be solved by imagining the angular distribution of the neutral pions in the center-of-mass system to be analyzed into spherical harmonics. Each spherical harmonic component in the original distribution of the neutral pions gives rise, in the gamma-ray distribution, to a component proportional to the same spherical harmonic multiplied by a constant coefficient. The value of this coefficient depends upon the order of the spherical harmonic in question. It is equal to 2 for spherical harmonics of the order zero; to

$$k_1=\frac{2\gamma}{\eta}-\frac{1}{\eta^2}\ln\frac{\gamma+\eta}{\gamma-\eta} \tag{6}$$

TABLE XII. Coefficients of $d\sigma/d\omega=a+b\cos\chi+c\cos^2\chi$ for various processes (10^{-27} cm²/sterad).

Energy Mev	λ (10^{-13} cm)	Process	a	b	c
53	1.777	$+\rightarrow+$	0.46±0.39	−0.08±0.84	3.60±1.46
78	1.439	$+\rightarrow+$	1.9 ±0.3	−1.7 ±0.4	1.6 ±0.9
110	1.186	$+\rightarrow+$	3.6 ±0.7	−4.8 ±0.8	7.5 ±1.9
135	1.057	$+\rightarrow+$	3.9 ±2.3	−7.1 ±2.8	18.0 ±6.8
120	1.129	$-\rightarrow-$	0.49±0.11	0.34±0.16	1.16±0.34
144	1.018	$-\rightarrow-$	0.82±0.16	0.73±0.24	1.52±0.50
120	1.129	$-\rightarrow\gamma$	2.68±0.40	−2.39±0.46	2.29±1.20
144	1.018	$-\rightarrow\gamma$	3.80±0.55	−2.49±0.62	3.17±1.62
120	1.129	$-\rightarrow0$	0.6 ±0.4	−1.9 ±0.5	3.2 ±1.7
144	1.018	$-\rightarrow0$	1.05±0.5	−1.9 ±0.5	3.9 ±2.0

for spherical harmonics of order one; and to

$$k_2=2+\frac{6}{\eta^2}-\frac{3\gamma}{\eta^3}\ln\frac{\gamma+\eta}{\gamma-\eta} \tag{7}$$

for spherical harmonics of order two. In the above equations η and γ are the momentum and the total energy of the neutral pion in the center-of-mass system, in units of μ_0c and μ_0c^2, respectively.

Writing (5) for neutral pions as the sum of spherical harmonics

$$a+\tfrac{1}{3}c+b\cos\chi+c(\cos^2\chi-\tfrac{1}{3}), \tag{8}$$

and applying the above coefficients, the angular distribution for the π^0 gamma-rays in the center-of-mass system is found to be

$$d\sigma_\gamma/d\omega=2a+\tfrac{1}{3}(2-k_2)c+k_1b\cos\chi+k_2c\cos^2\chi. \tag{9}$$

It is seen that the gamma-rays originating from the π^0 decay also have an angular distribution of the type (5) and one can readily compute the coefficients for the angular distribution of the neutral pions from the measured coefficients for the angular distribution of the photons.

Table XII summarizes the values of the coefficients a, b, and c for all the reactions studied. The first column gives the energy of the primary beam in Mev, the second column gives the deBroglie wavelength divided by 2π, in the center-of-mass system. The third column indicates the type of reaction; 0, +, and − are used to indicate neutral, positive, and negative pions, γ for the photons. The next three columns are the coefficients a, b, and c for the reaction in question. The data at 53 Mev are computed from cross-sections measured at Brookhaven with a diffusion cloud chamber.[14]

Striking features of the table are the rather large values of the coefficients b and c which indicate strong deviations from spherical symmetry. The negative values of b for $\pi^+\to\pi^+$ and $\pi^-\to\pi^0$ corresponds to the predominance of the backward scattering of these processes. The coefficient b has a positive value for $\pi^-\to\pi^-$ because, in this case, by contrast, the scattering is more pronounced in the forward direction.

X. PHASE SHIFT ANALYSIS

The data may be analyzed on the assumption that in the scattering of pions by nucleons the isotopic spin is conserved, or more precisely, that the isotopic spin behaves as a quantized angular momentum vector in isotopic spin space.[15] In the scattering of positive pions by protons only the isotopic spin $\frac{3}{2}$ will be involved because both the proton and the pion have their isotopic spin vectors "up." In the scattering of negative pions by protons, on the other hand, the orientation of the vectors is mixed and both isotopic spins, $\frac{3}{2}$ and $\frac{1}{2}$, will be involved.

From this basic assumption, it follows that the scattering features at any given energy will be determined by the phase shifts of the different states of given isotopic spin, orbital and total angular momentum. If it is assumed, as was done in the previous section, that only s- and p-states are important, there will be six phase shifts at each energy. They correspond to the possible values $\frac{3}{2}$ and $\frac{1}{2}$ of the isotopic spin, and, for each isotopic spin value, to the s-wave shifts and to the phase shifts of the two p-waves of angular momenta $\frac{3}{2}$ and $\frac{1}{2}$.

A complete set of measurements at any given energy consists of nine data: the values of the differential cross sections for each of the three processes $\pi^+\to\pi^+$, $\pi^-\to\pi^0$, and $\pi^-\to\pi^-$, at each of three angles. Alternately the experiments supply nine constants, a, b, and c for each of the three reactions observed. If the assumptions are correct, these nine data will be expressible in terms of the six phase shifts, a situation which permits a check of the soundness of the procedure.

To obtain a complete set of data at each of two energies we have interpolated the π^+ data obtained at 110 Mev and 135 Mev to give values at 120 Mev to go with the π^- data at this energy. We interpolated the π^- data between 120 Mev and 144 Mev to give values at 135 Mev to go with the π^+ data at this energy. The measurements at 78 Mev, on the other hand, are incomplete because only the π^+ reaction was investigated. However, in this case, only the three phase shifts for isotopic spin $\frac{3}{2}$ are involved. The data allow these phase shifts to be calculated but nothing remains for an internal check.

The phase shifts of the s waves of isotopic spin $\frac{3}{2}$ and $\frac{1}{2}$ will be indicated by α_3 and α_1. The phase shifts of the p waves will be indicated by α_{33}, α_{31}, α_{13}, α_{11}, where the first index is twice the isotopic spin of the state in question and the second index is twice the angular momentum. The quantities a, b, and c for the reaction $\pi^+\to\pi^+$ will be indicated by a_+, b_+, c_+. Similarly they will be indicated by a_-, b_-, c_-, for the reaction of elastic scattering of the negative pions, and by a_0, b_0, c_0 for the exchange scattering of the negative pions. In order to express the nine quantities a, b, c in terms of the six angles α, it is convenient to introduce the following notation:

$$e_3=e^{2i\alpha_3}-1,\ \cdots,\ e_{11}=e^{2i\alpha_{11}}-1. \tag{10}$$

By applying the standard procedures of the phase shift analysis of the collision theory, the amplitudes of the scattered waves may be expressed in terms of these quantities. There are nine such amplitudes in all. Three corresponding to the scattering of positive pions; amplitude of the scattered s wave and amplitudes of the scattered p waves with and without spin flip. These are indicated by B, A_β, and A_α. The scattering of the negative pions contributes six amplitudes because in each case scattering without and with exchange of charge must be considered. The corresponding amplitudes are indicated by B_p, $A_{p\beta}$, and $A_{p\alpha}$ for the non-exchange process, and B_n, $A_{n\beta}$, and $A_{n\alpha}$ for the exchange process. These nine scattering amplitudes are given in terms of the quantities e of (10) by the relations

$$\begin{aligned}
&B=e_3;\quad A_\beta=\tfrac{1}{3}\sqrt{2}(e_{33}-e_{31});\quad A_\alpha=\tfrac{1}{3}(2e_{33}+e_{31});\\
&B_p=\tfrac{1}{3}(e_3+2e_1);\quad A_{p\beta}=(\sqrt{2}/9)(e_{33}-e_{31}+2e_{13}-2e_{11});\\
&\qquad\qquad A_{p\alpha}=(1/9)(2e_{33}+e_{31}+4e_{13}+2e_{11});\\
&B_n=\tfrac{1}{3}\sqrt{2}(e_3-e_1);\quad A_{n\beta}=(2/9)(e_{33}-e_{31}-e_{13}+e_{11});\\
&\qquad\qquad A_{n\alpha}=(\sqrt{2}/9)(2e_{33}+e_{31}-2e_{13}-e_{11}).
\end{aligned} \tag{11}$$

The coefficients a_+, b_+, c_+ for the scattering of positive pions are given by

$$\begin{aligned}
&\frac{a_+}{\lambda^2}=\frac{1}{4}|B|^2+\frac{9}{8}|A_\beta|^2;\quad \frac{b_+}{\lambda^2}=\frac{3}{4}(BA_\alpha^*+B^*A_\alpha);\\
&\qquad\qquad \frac{c_+}{\lambda^2}=\frac{9}{4}|A_\alpha|^2-\frac{9}{8}|A_\beta|^2.
\end{aligned} \tag{12}$$

In these formulas a star means complex conjugation. The quantities a_-, b_-, c_- and a_0, b_0, c_0 are given by

[14] Fowler, Fowler, Shutt, Thorndyke, and Whittemore, Phys. Rev. **86**, 1053 (1952).

[15] N. Kemmer, Proc. Cambridge Phil. Soc. **34**, 354 (1938); W. Heitler, Proc. Roy. Irish Acad. **51**, 33 (1946).

TABLE XIII. Cross sections computed from phase shifts at 120 Mev (10^{-27} cm²/sterad).

Process	Measured cross sections	Computed First solution	Computed Yang solution
$-\rightarrow-$	1.06±0.14	1.06	1.06
	0.47±0.10	0.48	0.47
	0.97±0.18	1.02	1.02
$+\rightarrow+$	4.26±1.16	4.15	4.12
	5.75±1.16	5.13	5.14
	16.00±1.82	15.15	15.09
$-\rightarrow\gamma$	2.07±0.30	2.06	2.07
	3.19±0.39	3.38	3.40
	5.98±0.69	6.01	6.00

Phase shifts

First solution: $\alpha_3=-15.2°$; $\alpha_1=9.0°$; $\alpha_{33}=29.6°$; $\alpha_{31}=3.9°$; $\alpha_{13}=1.8°$; $\alpha_{11}=-2.8°$.

Yang solution: $\alpha_3=-15.4°$; $\alpha_1=9.1°$; $\alpha_{33}=12.9°$; $\alpha_{31}=38.6°$; $\alpha_{13}=-1.4°$; $\alpha_{11}=3.8°$.

similar formulas in which B, A_β, and A_α are replaced, respectively, by B_p, $A_{p\beta}$, $A_{p\alpha}$ and B_n, $A_{n\beta}$, $A_{n\alpha}$. It is possible, of course, to eliminate the intermediary quantities e, B, A from (10), (11), and (12), and to express directly the nine quantities a, b, c in terms of the six angles α. The formulas, however, are more complicated and not as well suited to numerical calculations.

If the accuracy of our measurement of the nine cross sections at a given energy were high enough, it would be possible to use six of them for determining the six angles α. Then, if the basic assumptions were right, the remaining three cross sections would be given correctly in terms of the same angles. Since, however, the experimental errors are rather large, this procedure is not very effective and it is more fruitful to try to use all the available experimental information in determining for each energy the best set of angles α by a least squares method. Some attempts to obtain by this method a set of "best" phase shifts were made by numerical computation on a preliminary set of cross-section values already published.[3]

The problem of determining the best set of phase shifts at each energy is managed much more efficiently with a modern electronic computer.[16] We are indebted to Dr. N. Metropolis for carrying out these computations for us using the Los Alamos Maniac computer. Given a set of nine measured cross sections, with the experimental errors, the machine finds the best set of six phase shifts according to the least squares criterion. Such a solution minimizes a least square sum $M=\Sigma_1^9(\Delta_i/\epsilon_i)^2$, where ϵ_i is the experimental error in the ith cross section, and Δ_i is the deviation of the calculated from the observed cross section.

This procedure does not permit a determination of the sign of the phase shifts. One recognizes easily that if

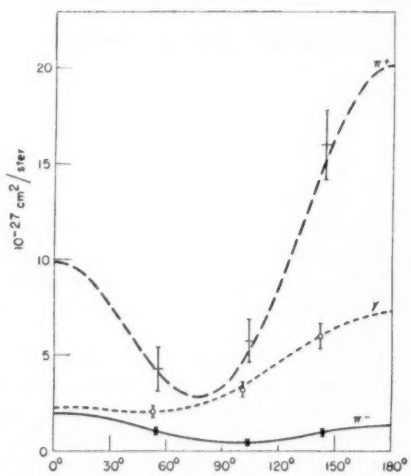

FIG. 9. Computed and observed cross sections at 120 Mev.

the sign of all the phase shifts is changed the cross sections are not affected. It would be possible in principle to determine the signs by a study of the interference of the nuclear scattering with the Coulomb scattering. Thus far, however, measurements of the scattering at angles sufficiently close to the forward direction to observe this interference have not been carried out. Aside from this indeterminacy of the sign, one might raise the question whether the determination of phase shifts is unique. It appears that there are two fairly equivalent sets of angles that yield a rather low value of the least square sum. One of them corresponds to angles fairly close to those already published[3] and will be called "first solution." Yang has pointed out[17] that there is a second solution, that, although not equivalent to the

TABLE XIV. Cross sections computed from phase shifts at 135 Mev (10^{-27} cm²/sterad).

Process	Measured cross sections	Computed First solution	Computed Yang solution
$-\rightarrow-$	1.46±0.19	1.45	1.45
	0.63±0.13	0.63	0.63
	1.13±0.23	1.20	1.21
$+\rightarrow+$	5.66±2.18	6.35	6.20
	6.75±2.14	5.95	5.90
	21.64±3.55	18.13	17.95
$-\rightarrow\gamma$	2.92±0.38	2.85	2.85
	3.96±0.47	4.07	4.11
	7.10±0.82	7.40	7.36

Phase shifts

First solution: $\alpha_3=-14.0°$; $\alpha_1=10.3°$; $\alpha_{33}=37.9°$; $\alpha_{31}=5.4°$; $\alpha_{13}=2.0°$; $\alpha_{11}=-4.6°$.

Yang solution: $\alpha_3=-14.2°$; $\alpha_1=10.4°$; $\alpha_{33}=17.2°$; $\alpha_{31}=49.3°$; $\alpha_{13}=-2.9°$; $\alpha_{11}=5.6°$.

[16] E. Fermi and N. Metropolis, Los Alamos unclassified report LA-1492, 1952 (unpublished).

[17] C. N. Yang, private communication.

first, is in many cases almost eqully good. An extensive numerical analysis of the problem[16] has indicated that the first solution and the Yang solution are very probably the only two for which the least square sum is small. There is apparently another set of angles that yields a relative minimum of M. This, however, is so high as to make it of no practical value.

In Tables XIII and XIV are collected the cross sections for 120 Mev and for 135 Mev, together with the cross sections computed from the best sets of phase shifts. Results corresponding to the first solution and to the Yang solution are given. The agreement with the experimental results is extremely close for both solutions. Only a very considerable improvement in the experimental accuracy would permit to distinguish between the two.

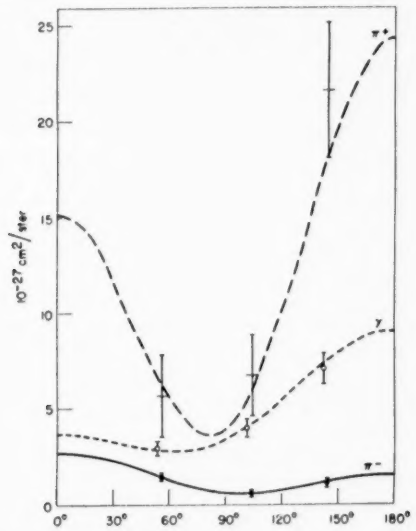

FIG. 10. Computed and observed cross sections at 135 Mev.

In Figs. 9 and 10 are plotted the cross sections in the center-of-mass system *versus* the scattering angle χ. The curves are computed from the scattering angles of the first solution. Also the experimental points are put on the same graph for reference.

TABLE XV. Phase shift angles.

		Phase shifts in degrees					
Mev	η	3	1	33	31	13	11
53	0.78	0		9	2		
78	0.97	−6		13	−3		
120	1.24	−15	9	30	4	2	−3
135	1.32	−14	10	38	5	2	−5

As pointed out above, the sign of all the phase shifts could be changed without affecting the cross sections. The sign chosen corresponds to the assumption that the interaction of the state with both isotopic spin and angular momentum equal to $\frac{3}{2}$ is attractive. Some arguments in favor of this assumption have been advanced by Peaslee[18] on the basis of an analysis of the scattering of negative pions by carbon.

At 78 Mev only the scattering of positive pions has been measured and consequently only three of the phase shifts could be determined. They are $\alpha_3=-6°$, $\alpha_{33}=13°$, $\alpha_{31}=-3°$. Also a similar analysis can be made on the data for scattering of 53-Mev positive pions by hydrogen published by the Brookhaven group.[14] The result is $\alpha_3=0°$, $\alpha_{33}=9°$, $\alpha_{31}=2°$. In Table XV are collected the various values of the phase shifts (first solution only). The second column gives the pion momentum in the center-of-mass system in units of μc. Due to experimental errors the phase shifts given above have an uncertainty of perhaps 5°. Experience gathered in successive calculations of the phase shifts has indicated, however, that some of them appear to be not very sensitive to changes in the cross sections, whereas others have a higher sensitivity and are for this reason less reliable. This appears to be particularly true of the phase shifts α_{13} and α_{11}.

XI. CONCLUSIONS

1. The fact that 9 cross sections measured at each energy can be represented in terms of 6 phase shifts is a demonstration of the fruitfulness of regarding the isotopic spin as a good quantum number. Such a demonstration would be even more meaningful if the experimental errors were smaller.

2. According to quantum mechanics one might expect that the phase shifts at sufficiently low energy should be

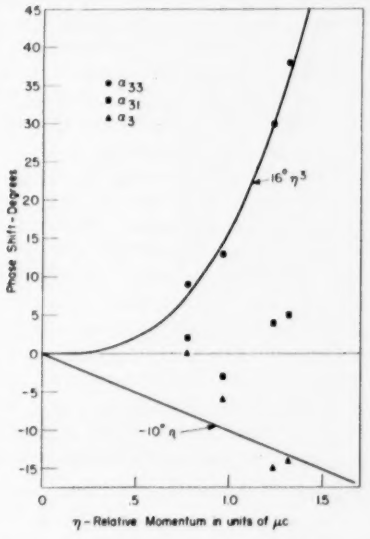

FIG. 11. Phase shifts plotted *versus* relative momentum.

[18] Quoted by H. Bethe at the Rochester Conference, December, 1952. See also G. F. Chew, Phys. Rev. **89**, 591 (1953).

proportional to the relative momentum η of the 2 colliding particles for s-terms and to η^3 for p-terms. In Fig. 11 some of the data of Table XV are plotted. The values of η are on the abscissas and the phase shifts of isotopic spin $\frac{3}{2}$ are plotted on the ordinates. One might expect that the phase shift α_3 should lie on a straight line through the origin. Actually the points do not at all show this property and this may or may not be due to the rather large experimental error. If one attempts to draw the "best" straight line through these points the coefficient of η would be approximately $-10°$. On the other hand, the points suggest an appreciably stronger dependence of α_3 on the energy. This in fact would be quite compatible with the possibility that α_3 may actually change sign at about 60 Mev, a possibility whose implications have been discussed by Marshak.[19] The ratio α_3/η at low energy gives the scattering length in units $\hbar/\mu c$. A coefficient of $-10°$ would correspond to a scattering length $a_3=-0.24\times10^{-13}$. However, this value for the reasons explained is quite tentative and even its sign could be wrong. Similarly from the data of Table XV we may make an equally tentative guess that the scattering length of the s-state of isotopic spin $\frac{1}{2}$ may be 0.18×10^{-13} cm.

The phase shifts α_{32} fit fairly well a proportionality to η^3 with a coefficient of about 16°. Very little can be said of the energy dependence of the other phase shifts α_{31}, α_{13}, and α_{11} which are so small that even their sign relative to that of the other phase shifts is uncertain with our present experimental accuracy.

3. We have already commented on the difficulties of deciding experimentally with our present accuracy between the phase shifts corresponding to the first solution and to the Yang solution of the problem. The previous conclusions are obtained on the assumption that the first solution is correct and would have to be modified appreciably if the Yang solution ultimately would turn out to be the right one. Similarly the over-all sign of the phase shifts is uncertain, and the opposite sign to the one chosen here may well be correct.

4. One might attempt to interpret phenomenologically the scattering as if it were due to a force acting between the nucleon and pion. Inspection of the variety of phase shifts obtained indicates immediately that this force should be quite different for different states. Assuming again the first solution to be correct, one would further conclude that the force is very large for the state of isotopic spin $\frac{3}{2}$ and angular momentum $\frac{3}{2}$. One can recognize that the same potential produces a much larger phase shift in the s terms than it does in the p-terms. For example, phase shifts of the order of magnitude observed could be attributed to a potential of radius $\hbar/\mu c$ and of a magnitude of about 40 Mev for the s terms, while the depth of this potential hole should be of the order of several hundred Mev in order to produce a phase shift α_{33} of the observed magnitude. It is very questionable whether it is rewarding to adopt this potential model without a thorough study of its relativistic behavior.

5. From partial evidence on the scattering of pions by hydrogen previously reported,[8] a tentative conclusion had been reached that the states of isotopic spin $\frac{3}{2}$ are dominant. If this were exactly correct one would expect the cross sections for scattering of positive pions and for scattering of negative pions with and without charge exchange to be in the ratio 9:2:1 in all directions. That this is not so, is evident from a direct inspection of the cross sections which shows that the angular distribution for the scattering of positive pions and that of negative pions with charge exchange is mostly backward, whereas the elastic scattering of negative pions is mostly forward. Apparently this difference in angular distribution is due primarily to the phase shift α_1 of isotopic spin $\frac{1}{2}$ which is the largest phase shift with isotopic spin different from $\frac{3}{2}$.

On the assumption that the first solution is correct, the largest phase shift is α_{33} corresponding to a state for which the existence of a resonance has been suspected.[20] Our data do not extend far enough in energy to support the resonance hypothesis. If the hypothesis were correct, one would expect that at some higher energy the phase shift α_{33} should rise appreciably more rapidly than with the η^3 law and rather rapidly cross over from values less to values larger than 90°. It is possible, however, that α_{33} may go through a maximum and start decreasing before reaching 90°.

6. The present experimental data are utterly inadequate to allow any conclusions to be drawn about the d terms, which have been neglected in our analysis. If the interaction of the d levels were of the order of magnitude μc^2, the phase shifts would be a fraction of a degree. This makes our neglect of the d-terms justifiable but not necessarily correct.

This work could not have been carried out without the active cooperation and advice of Professor Earl A. Long. We thank him and Dr. Lothar Meyer for generous supplies of liquid hydrogen. Mr. Gaurang B. Yodh and Mr. Maurice Glicksman took an active part in the work of preparing the experimental equipment and carrying out the measurements; we are indebted to them for their time and skill. Mr. Leo Slattery contributed to the development of the electronic equipment. We are particularly grateful to Mr. Lester Kornblith for the efficient operation of the cyclotron.

[19] R. E. Marshak, Phys. Rev. 88, 1208 (1952).

[20] K. A. Brueckner, Phys. Rev. 86, 106 (1952).

Consequences of Charge Independence for Nuclear Reactions Involving Photons *

MURRAY GELL-MANN AND VALENTINE L. TELEGDI
Institute for Nuclear Studies and Department of Physics, University of Chicago, Chicago, Illinois
(Received January 22, 1953)

Some effects of the charge independence of nuclear forces on the emission and absorption of photons by light nuclei are investigated. It is found that the selection rules governing the change of isotopic spin T in such transitions are of practical importance in nuclei with $T_z=0$, particularly the rule that $E1$ transitions without change of isotopic spin are forbidden. Two examples of forbidden $E1$-emission (in N^{14} and O^{16}) are discussed, and detailed experimental reinvestigation is suggested in connection with each of them.

The main consequence for photonuclear reactions of the aforementioned selection rule is that for each $T_z=0$ nucleus there is a threshold for (allowed) $E1$ absorption, corresponding to the first level with $J=1^-$, $T=1$. For (γ, α)- and (γ, d)-reactions, where no isotopic spin can be carried off by the particle, $E1$ absorption can become effective only when there is enough energy to leave the *residual* nucleus in a $T=1$ state. The roles of $E2$ and $M1$ absorption, with and without change of isotopic spin, are discussed, and appropriate sum rules are derived. The rules governing (γ, α) processes are applied particularly to reactions in C^{12} and O^{16}, where considerable experimental evidence is available and appears to support the theoretical conclusions.

I. INTRODUCTION

CONSIDERABLE evidence[1] has accumulated during recent years in favor of the hypothesis of charge independence of nuclear forces. In light nuclei (say $Z\leq 10$) the effects on nuclear wave functions of the Coulomb force between protons and of the neutron-proton mass difference are expected to be small,[2] and consequently the total isotopic spin T must be considered a good quantum number[3] in purely nuclear processes; some restrictions imposed on nuclear reactions by the conservation of isotopic spin have been discussed by Adair.[4]

When the emission or absorption of photons takes place, isotopic spin need not be conserved, since the electromagnetic interaction of nucleons is charge-dependent. However, as has been pointed out by Radicati[5] and others, there are definite selection rules governing the change of isotopic spin accompanying such processes. It is our purpose to show how these selection rules may be used in the interpretation of certain experimental observations on photonuclear reactions and γ-decay in light elements and to suggest further experiments for which the hypothesis of charge independence has interesting consequences. Kroll and Foldy[6] have shown that the selection rules follow equally well from the much weaker assumption of the *charge symmetry* of nuclear forces. However, we shall adopt the point of view of charge independence since we shall be concerned frequently with the existence of charge triplets, which are sets of $T=1$ states in neighboring isobars with equal (adjusted) energies. Such triplets are difficult to account for in the absence of charge *independence*.

In the discussion that follows we shall always assume that the specific nuclear forces are indeed charge independent, and we shall attribute to Coulomb and mass difference effects any failure of T to be a good quantum number for the nucleus.

II. SELECTION RULES

Many of the results in this section have been given by Radicati[5] and are reproduced here only for completeness.

In order to derive the isotopic spin selection rules for electromagnetic transitions, let us consider the perturbation Hamiltonian H corresponding to the emission or absorption of a photon of wave number k by a system of A nucleons, neglecting certain magnetic exchange and interaction moments:

$$H=\sum_{i=1}^{A}\left\{\frac{e}{c}\frac{d}{dt}\left[\frac{1}{2}(1+\tau_{iz})\mathbf{r}_i\right]\cdot\mathbf{A}(\mathbf{r}_i)\right.$$
$$\left.+\left[\frac{\mu_P}{2}(1+\tau_{iz})+\frac{\mu_N}{2}(1-\tau_{iz})\right]\boldsymbol{\sigma}_i\cdot\boldsymbol{\nabla}\times\mathbf{A}(\mathbf{r}_i)\right\}. \quad (1)$$

Here τ_{iz}, the component along the charge axis of the isotopic spin operator for the ith nucleon, has the eigenvalue $+1$ for a proton state and -1 for a neutron state. $\mathbf{r}_i$ is the position vector of the ith nucleon measured from the center of mass of the nucleus. (d/dt) applied to an operator means its time rate of change, or $i\hbar$ times its commutator with the nuclear Hamiltonian. $\mathbf{A}(\mathbf{r}_i)$ is the vector potential of the electromagnetic field, given

* Work assisted in part by contract with the U. S. Office of Naval Research.

[1] F. Ajzenberg and T. Lauritsen, Revs. Modern Phys. **24**, 321 (1952). All data concerning nuclear levels discussed by us are taken from this article, to which the reader is referred whenever no special references are given.

[2] L. A. Radicati, Proc. Phys. Soc. (London) **A66**, 139 (1953).

[3] The notation I has been used for isotopic spin in some recent papers on charge independence in phenomena involving nucleons and pions. However, for purely nuclear processes it is perhaps wise to retain the older symbol "T" since in discussions of hyperfine structure I is often used to mean the total angular momentum of the nucleus.

[4] R. K. Adair, Phys. Rev. **87**, 1041 (1952).

[5] L. A. Radicati, Phys. Rev. **87**, 521 (1952).

[6] N. M. Kroll and L. L. Foldy, Phys. Rev. **88**, 1177 (1952).

by

$$\mathbf{A}(\mathbf{r}_i)=(2\pi ch/kV)^{\frac{1}{2}}\mathbf{e}\exp[\pm ik\mathbf{n}\cdot\mathbf{r}_i]$$
$$=A_0\mathbf{e}\exp(\pm ik\mathbf{n}\cdot\mathbf{r}_i) \quad (2)$$

in an obvious notation; the + sign applies to emission and the − sign to absorption.

For our purposes, it is convenient to separate H into two parts:

$$H_0\equiv\sum_{i=1}^{A}\left\{\frac{e}{2c}\mathbf{v}_i\cdot\mathbf{A}(\mathbf{r}_i)+\frac{(\mu_P+\mu_N)}{2}\boldsymbol{\sigma}_i\cdot\boldsymbol{\nabla}\times\mathbf{A}(\mathbf{r}_i)\right\}, \quad (3)$$

$$H_1\equiv\sum_{i=1}^{A}\left\{\frac{e}{2c}\frac{d}{dt}(\mathbf{r}_i\tau_{iz})\cdot\mathbf{A}(\mathbf{r}_i)+\tau_{iz}\frac{(\mu_P-\mu_N)}{2}\boldsymbol{\sigma}_i\cdot\boldsymbol{\nabla}\times\mathbf{A}(\mathbf{r}_i)\right\}. \quad (4)$$

Here $\mathbf{v}_i$ is the velocity operator for the ith particle. It is clear that H_0 is a scalar with respect to rotations in isotopic spin space, and hence transitions induced by H_0 obey the selection rule

$$\Delta T=0. \quad (5a)$$

On the other hand H_1 is the z-component of a vector in isotopic spin space and hence gives the selection rules

$$\begin{aligned}&\Delta T=0,\ \pm1 \text{ when } T_z\neq0;\\ &\Delta T=\pm1 \text{ when } T_z=0.\end{aligned} \quad (5b)$$

Here T_z is equal, of course, to $(-1/2)$ times the neutron excess in the nucleus.

The most significant fact contained in (5a, b) is that in nuclei with equal numbers of neutrons and protons ($T_z=0$) electromagnetic transitions without change of isotopic spin must arise from H_0 alone. We will refer to such processes as H_0 transitions.

A multipole expansion of H_0 reveals certain important properties. We shall exhibit the parts of H_0 corresponding to the first few multipoles as power series in the kr_i, keeping only the first term or two.

The electric dipole ($E1$) part of H_0 is

$$H_0(E1)=A_0\mathbf{e}\cdot\left\{\sum_{i=1}^{A}\left[\frac{e}{2c}\mathbf{v}_i-\frac{e}{20c}k^2(r_i^2\mathbf{v}_i+\mathbf{v}_i\mathbf{r}_i^2)+\frac{e}{40c}k^2(\mathbf{r}_i\mathbf{r}_i\cdot\mathbf{v}_i+\mathbf{v}_i\cdot\mathbf{r}_i\mathbf{r}_i)+\frac{k^2}{4}(\mu_P+\mu_N)\mathbf{r}_i\times\boldsymbol{\sigma}_i+\cdots\right]\right\}. \quad (6)$$

The term of lowest order *vanishes* since $\sum_{i=1}^{A}\mathbf{r}_i=0$ identically, and hence there is practically no $E1$ contribution to H_0 for photons having a wavelength large compared to the nuclear radius.

The electric quadrupole ($E2$) part of H_0 is

$$H_0(E2)=\pm ie\frac{k}{2c}A_0\mathbf{e}\cdot\{\sum_{i=1}^{A}[\tfrac{1}{3}(\mathbf{v}_i\mathbf{r}_i\cdot\mathbf{n}+\mathbf{r}_i\mathbf{v}_i\cdot\mathbf{n})+\cdots]\}. \quad (7)$$

We shall estimate in the next section the contribution of (7) to the absorption of photons.

In connection with magnetic dipole ($M1$) radiation, it is necessary to mention the magnetic exchange and interaction moments that have been omitted in (1). However the exchange and interaction moments that are usually assumed to be of importance in nuclei[7] and that are omitted in (1) are either of the form

$$\sum_{i,j}(\boldsymbol{\tau}_i\times\boldsymbol{\tau}_j)_zO_{ij}, \quad (8a)$$

or else of the form

$$\sum_{i,j}(\boldsymbol{\tau}_i-\boldsymbol{\tau}_j)_zO_{ij}, \quad (8b)$$

where O_{ij} is a two-particle operator on space and spin coordinates. Both expressions (8a, b) are z-components of vectors in isotopic spin space and thus will provide corrections to H_1 and not to H_0. We are thus permitted to consider just the operator

$$H_0(M1)=\pm iA_0\mathbf{n}\times\mathbf{e}\cdot\left\{\sum_{i=1}^{A}\left[\frac{ek}{4c}\mathbf{r}_i\times\mathbf{v}_i+\frac{k}{2}(\mu_P+\mu_N)\boldsymbol{\sigma}_i+\cdots\right]\right\}. \quad (9)$$

Corresponding expressions may, of course, be written for higher multipoles as well.

III. SUM RULES

It is well known that sum rules can be obtained for the absorption of radiation of a given multipolarity by nuclei. In light nuclei with $T_z=0$, it is useful to derive separate sum rules for the H_0 transitions alone, using (7) and (8). If $\sigma_0(E2, W)$ is the cross section for H_0 absorption of $E2$ radiation at energy W, then

$$\int\sigma_0(E2,W)\frac{dW}{W^2}=\frac{\pi^2}{137}\frac{A}{12}\frac{\langle r^2\rangle_{00}}{Mc^2}. \quad (10)$$

where M is the mass of a nucleon and $\langle r^2\rangle_{00}$ is the mean squared displacement of a nucleon from the center of mass in the ground state of the nucleus. For $M1$ radiation, we have the sum rule

$$\int\sigma_0(M1,W)\frac{dW}{W}=\frac{\pi^2}{137}\left(\frac{\hbar}{Mc}\right)^2\frac{1}{4}\cdot\frac{\langle(\mathbf{L}+(\mu_P+\mu_N)2\mathbf{S}/\mu_0)^2\rangle_{00}}{\hbar^2}. \quad (11)$$

where μ_0 is the nuclear Bohr magneton. Equations (10) and (11) are derived on the assumption that the nuclear forces are not explicitly velocity-dependent.

[7] R. G. Sachs and N. Austern, Phys. Rev. **81**, 705 (1951); R. K. Osborne and L. L. Foldy, Phys. Rev. **79**, 795 (1950).

However, unlike most nuclear sum rules, they require no correction on account of exchange forces or correlation. Moreover, the $E2$ sum rule is correct even in the presence of interaction potentials that depend linearly on particle momentum, such as the spin-orbit interaction.

IV. EMISSION OF γ-RAYS

The γ-ray spectra of nuclei with $T_z=0$ should be affected in at least two ways by the forbiddenness of H_0 ($E1$) transitions:

(a) $E1$ radiation will be very weak between two $T=1$ states, while the $E1$ transition between the two analogous levels in each of the neighboring isobars may be of normal strength. For example, a level at 6.1 Mev in C^{14} has been found in the reaction $C^{13}(d,p)C^{14}$;[1] the level decays by γ-ray emission to the ground state ($J=0^+$), and there is some evidence that the γ-ray is $E1$.[8] Let us assume for the purpose of illustration that such is the case. Now in N^{14} the level at 2.31 Mev is analogous to the ground state of C^{14}. At around 8 Mev, then, there must be a state with $J=1^-$ analogous to the one at 6.1 Mev in C^{14}; perhaps it is the level at 8.05 Mev observed in $C^{13}(p,\gamma)N^{14}$. At any rate, the γ-transition from that state to the one at 2.31 Mev, though fully allowed by conservation of angular momentum and parity, is forbidden by the isotopic spin selection rules, while the corresponding transitions in the isobars C^{14} and O^{14} are allowed. Of course the transition in N^{14} is not *totally* forbidden; there are two mechanisms by which it can occur—the intervention of the higher term in the expansion (6) of $H_0(E1)$ and the impurity with respect to isotopic spin of the initial and final nuclear states.

The former mechanism should lead to a width for decay to the 2.31 Mev state of the order of $(kR)^4$ times a normal $E1$ width, where R is the nuclear radius—that is, about 0.01 percent. The isotopic spin impurity is certainly more effective; Radicati[2] estimates it as 1 percent in amplitude for the ground state, but for a highly excited $T=1$ state it should be much greater. Still, an impurity of 10 percent in amplitude would yield a width about 1 percent of normal. It would be interesting to make a quantitative experimental comparison of the widths for the forbidden transition and for the allowed $E1$ transition to the ground state.

(b) $E1$ radiation will be very weak between two $T=0$ states. For example, let us consider the level at 7.1 Mev in O^{16}, found in $F^{19}(p,\alpha)O^{16*}$ [9] and $N^{16}(\beta^-)O^{16*}$.[10,11] Its spin and parity, $J=1^-$, have been determined by α-γ angular correlations.[12] Its isotopic spin is 0 since the lowest $T=1$ state of O^{16} is analogous to the ground state of N^{16} and lies at about 13.0 Mev. Since the ground state of O^{16} has $J=0^+$ and $T=0$, the γ-ray transition from the 7.1-Mev level to ground must be $E1$ and consequently forbidden by (5b). However, we must consider the effect of the two mechanisms of transition mentioned in (a). The first one alone would provide a transition rate of an order of magnitude corresponding to $M2$. But any competing mode of de-excitation should proceed even more slowly, according to simple order-of-magnitude estimates. The possibilities are:

(i) γ-decay to the 6.0-Mev level ($J=0^+$) suffers from the same disability as the ground-state decay and there is much less energy available;

(ii) γ-decay to the 6.9-Mev level ($J=2^+$) would proceed by the $E1$ correction term (as above) and by genuine $M2$ and is unfavored by the tiny energy difference;

(iii) γ-decay to the 6.1 Mev level ($J=3^-$) by $E2$ is favored by a factor of $(c/v)^2\simeq 100$ by comparison with the ground state transition but the ratio of energy differences enters to the fifth power, so that the ground state should be preferred by a factor of $7^5/100\simeq 200$;

(iv) internal pair emission to the ground state through the intervention of the scalar potential is unfavored by a factor of at least $e^2/\hbar c\simeq 1/100$.

The experimental evidence, however, seems to indicate that some process *does* compete favorably with the ground-state transition. The 7.1-Mev γ-ray is observed in both the (p,α)-reaction and the β-decay; in the latter case certain information has been obtained about the intensity of the line. It has been reported[10,11] that the β-decay of N^{16} leads with equal probability (40 percent in each case) to the levels at 7.1 Mev and 6.1 Mev, while Millar *et al.*[13] have found 12 times as many 6.1-Mev γ-rays as 7.1-Mev γ-rays following the β-emission.

If both experimental results are accepted as correct, we must conclude that the matrix element for the $E1$ correction term is much smaller than simple dimensional arguments indicate, and furthermore that the admixture of $T=1$ in the wave functions of both the initial and final states is either astonishingly small (≃0.1 percent in amplitude) or else anomalously ineffective in inducing $E1$ transitions. In short, the selection rule (5b) seems to be *oversatisfied*. This curious circumstance calls, in our opinion, for a re-investigation of the β-decay branching ratio and a search for the 1-Mev γ-ray (7.1→6.1).†

[8] R. G. Thomas and T. Lauritsen, Phys. Rev. **88**, 969 (1952).
[9] A. P. French and J. Seed (unpublished).
[10] Bleuler, Scherrer, Walter, and Zünti, Helv. Phys. Acta **20**, 96 (1947).
[11] H. S. Sommers, Jr., and R. Sherr, Phys. Rev. **69**, 21 (1946).
[12] Kraus, French, Fowler, and Lauritsen, Phys. Rev. **89**, 299 (1953).
[13] Millar, Bartholomew, and Kinsey, Phys. Rev. **81**, 150 (1951).

† *Note added in proof.*—Jones and Wilkinson [Phys. Rev. **90**, 722 (1953)] report that the 7.1-Mev γ-ray is at least 120 times more intense than the 1-Mev γ-ray, in agreement with (iii). However, their claim that this result sets a lower limit on the isotopic spin impurity of the 7.1-Mev state appears to us unjustified. They have neglected the effect of the $E1$ correction term, which alone should yield an intensity ratio comparable to that observed.

Boehm, Peaslee, and Perez-Mendez [Phys. Rev. (to be published)] have recently found that the 1-Mev γ-ray following the β-decay of N^{16} is less than one-twentieth as frequent as the

V. ABSORPTION OF γ-RAYS

In nuclear reactions induced by photons, the observation of forbidden electromagnetic transitions may be expected to play no important role. We must rather be concerned with the kinds of particle emission that can follow γ-ray absorption; for W less than about 50 Mev, moreover, we may restrict ourselves to $E1$, $E2$, and $M1$ transitions. The effects of isotopic spin conservation are most striking in even-even nuclei with $T_z=0$; for such nuclei, the lowest $T=1$ state is at a high excitation energy W_1 and the ground state always has $J=0^+$. The following rules can then be deduced from (5b) and the usual conservation laws *in the approximation in which charge independence is rigorously true*:

(1) For $W<W_1$, all absorption proceeds either by $M1$ through a compound state with $J=1^+$, $T=0$, or by $E2$ through a compound state with $J=2^+$, $T=0$.

(2) For $W>W_1$, absorption into $T=1$ states is possible by $M1$, $E2$, or $E1$; but such H_1 absorption can result in emission of deuterons or α-particles only if there is sufficient energy to leave the residual nucleus in a $T=1$ state.

(3) At any energy, a (γ,α)- or (γ,d)-reaction that leaves the residual nucleus in a $T=0$ state must proceed as in (1).

(4) In particular, a (γ,α)-reaction to the ground state of the residual nucleus may proceed only by $E2$ absorption through a state with $T=0$, $J=2^+$.

(5) (γ,n) and (γ,p) cross sections must, for each residual state, be identical with each other as functions of energy and angle except to the extent that there is interference between H_0 absorption and H_1 absorption.

The existence of Coulomb forces and of the neutron-proton mass difference introduces important deviations from some of these rules:

(1′) Following H_1 absorption, there is in general some probability of α- and d-emission to a $T=0$ state on account of isotopic spin impurity in the initial and final states and, to a lesser extent, in the α-particle. While re-emission of γ-rays may not, in general, compete strongly enough to suppress such a process, strong neutron or proton emission should be expected to do so. Consequently there may be a region of energy, between W_1 and the effective threshold for n- or p-emission, in which α-particles are produced with an appreciable probability in violation of rules (2), (3), or (4).

(2′) For each state in the residual mirror nuclei, the thresholds and barrier penetrabilities for n and p are in reality different; only after correction for this effect should (5) be valid. It is not likely that isotopic spin impurity is of any importance here.

The charge-dependent perturbations contribute also to the fate of a residual $T=1$ state produced in accordance with rule (2). Again, if γ-ray emission is the only process that competes effectively, further α-decay to a $T=0$ state may occur. It should be noted that such an α-α cascade through a level with $T=1$ will prevail not only over a corresponding cascade through a $T=0$ level but also over the direct emission of two α's. For these "forbidden" modes of decay of the initial $T=1$ state we expect the smallness of isotopic spin impurity not to be compensated by phase-space factors. In the allowed mode of decay of the initial $T=1$ state the residual nucleus may find itself unable to do anything but violate the conservation law.

Let us apply the preceding considerations to C^{12}. The lowest $T=1$ level, analogous to the ground states of B^{12} and N^{12}, should lie at about 15.2 Mev and have $J=1^+$. Probably it is a level found at 15.09 Mev in $B^{11}(d,n)C^{12*}$. The analog of the first excited state of B^{12} at 0.95 Mev is probably the level at 16.07 Mev with $J=2^+$. That the latter level does indeed have $T=1$ is borne out by the fact that it emits α's to the lowest two states of Be^8 while its total width is only about 5 kev, including the width for proton emission. (Since a typical width for allowed α-emission at this energy should be of the order of 1 Mev, it is apparently an isotopic spin impurity of less than 10 percent in amplitude that is responsible for the (p,α)-process.) We have thus located the thresholds for H_1 absorption of $M1$ and $E2$ radiation, respectively. At some higher energy W_1 ($E1$), there is presumably a level with $T=1$ and $J=1^-$, which is the lowest one accessible to $E1$ radiation. Above this energy the $E1$-absorption should increase rapidly and soon predominate over other multipolarities. It should manifest itself principally in (γ,p)- and (γ,n)-processes as long as the energy is insufficient to meet condition (2). In this energy range, $E1$-induced (γ,α)-reactions may proceed only through isotopic spin impurity. The threshold for the *allowed* reaction leading to the lowest $T=1$ level of Be^8 is about 26 Mev, a value obtained by adding the binding energy of an α-particle in C^{12} and the Coulomb barrier to 16.8 Mev, the energy at which the level in Be^8 is expected to lie. (It is the analog of the ground states of Li^8 and B^8 and should have $J=2^+$.) Thus above 26 Mev there is a fully allowed (γ,α)-reaction induced by $E1$ and it should overshadow all other (γ,α) process. The (γ,d)-reaction should exhibit much less striking behavior. The threshold is at about 25 Mev while that for reactions leading to $T=1$ states of B^{10}, allowed for $E1$, is at about 28 Mev.

The experimental evidence on the photodisintegration of carbon, which in fact prompted this investigation, appears to agree with the conclusions presented here. The data on (γ,n)-[14] and (γ,p)-reactions[15] are too conflicting to be compared with rule (5). However, they indicate a steep rise in the absorption cross section in the neighborhood of 20 Mev, which must correspond to the onset of $E1$ absorption. The

6.1-Mev γ-ray. Their result, together with that of Millar *et al.*, seems to indicate that the β-decay branching ratio is indeed not 1:1, but heavily favors the 6.1-Mev state.

[14] Haslam, Johns, and Horsley, Phys. Rev. **82**, 270 (1951).
[15] J. Halpern and K. Mann, Phys. Rev. **83**, 370 (1951).

(γ,α) cross section[16,17] not resolved into "fine structure" [16] due to absorption into discrete levels, exhibits two principal peaks around 18 and 29 Mev, respectively, each of half-width about 4 Mev and height about 0.3 mb. Let us divide the entire energy range into three regions. The first peak lies in region "A" between threshold and 20 Mev in which we expect all absorption to proceed through $H_0(E2)$ and $H_0(M1)$. In fact Telegdi[18] has found that at 17.6 Mev $E2$ and $M1$ contribute about equally and that $E1$ does not participate noticeably. On the basis of Eq. (11) one sees that appreciable $H_0(M1)$ absorption indicates that the ground state of C^{12} is by no means a pure $^1S_0$ state, as the independent particle model in L-S coupling would predict. In region A, the (γ,α)-reaction leads predominantly to the 3 Mev state ($J=2^+$, $T=0$) of Be^8. While, in accordance with rule (4), $M1$-induced transitions cannot leave Be^8 in its ground state, it is not clear why the $E2$-induced transitions show a marked preference for the 3 Mev state at energies high enough for the s-wave and d-wave barrier penetrabilities to be roughly equal.

Energy region "B," between 20 and 26 Mev, includes the giant $E1$ resonance displayed by the (γ,n)- and (γ,p)-reactions. It is clear, however, from the theoretical discussion above, that the (γ,α)-process should not exhibit such behavior. Rather, we expect in B only forbidden α-emission induced by $H_1(E1)$ and allowed α-emission induced by $H_0(M1)$ and $H_0(E2)$. In B the experimental cross section is indeed smaller than in A and C. The sum rules (10) and (11) for the allowed transitions appear to be exhausted by (γ,p) and (γ,α)-processes in A, and the forbidden (γ,α) transitions in B compete very unfavorably with (γ,n) and (γ,p) reactions. Forbidden transitions due to $H_1(M1)$ and $H_1(E2)$ are certainly negligibly rare.

The second (γ,α) peak lies in region "C" above 26 Mev, in which we expect allowed $E1$ processes to predominate. That this is the case is borne out by the experimental fact that in C^{12} more than 95 percent of the transitions leave Be^8 in an excited state[19,20] at 17.0 ± 0.2 Mev with $J=2^+$.[20] There seems to be no reason to doubt that this is the lowest $T=1$ state of Be^8. Since the total γ-ray absorption in C, as indicated by the (γ,n) and (γ,p) cross sections, is only about 4 percent of the value at the giant resonance peak in B, it is understandable that the allowed $E1$-induced (γ,α)-reactions in C do not produce a very great increase in the (γ,α)-cross section over region B. The higher density of final states for the (γ,n)-process accounts for its predominating by a factor of 10 over (γ,α) even in C.

It should be mentioned that one preliminary experimental result conflicts with the point of view we have expressed. Goward and Wilkins[21] report that the angular distribution (with respect to the incident γ-ray) of α's to the ground state of Be^8 displays strong forward-backward asymmetry in the energy regions 13–15.5 Mev and 17–19 Mev, indicating interference between $E1$ and $E2$. While in the lower interval we can offer no explanation whatever for such an effect, it is conceivable that we could interpret the effect in the upper interval by supposing that the threshold for $E1$ absorption is at 17 Mev rather than around 20 Mev. However, the experimental result[18] obtained at 17.6 Mev appears to be in disagreement with the hypothesis of a large $E1$ contribution, unless we assume that $E1$ absorption is followed with strong preference by transitions to the ground state of Be^8. It should perhaps be emphasized that a unique identification of events as ground-state transitions is extremely difficult, while misassignments may lead to spurious angular distributions.

The situation in O^{16} is roughly analogous to that in C^{12}, though the experimental evidence is less detailed. The lowest $T=1$ state, analogous to the ground states of N^{16} and F^{16}, must lie at about 13 Mev and have $J=2^-$. It may be either of two levels with $J=2^-$ at 12.51 Mev and 12.95 Mev found in $N^{15}(p,\alpha)C^{12*}$. The location of the $E1$ absorption threshold, which defines the boundary between energy regions "A" and "B," cannot be deduced from the known level structure above 13 Mev and it is difficult to obtain information about it from the energy dependence of $\sigma(\gamma,n)$. This cross section rises sharply from threshold at 16 Mev to a plateau of 0.5 mb extending from 17 to 20 Mev and then rises again to the giant resonance peak value of 11 mb at 24 Mev.[22] The plateau has been attributed[22] to $E2$ and $M1$ absorption following a suggestion of Blatt and Weisskopf.[23] In the same energy region we have the results of Millar and Cameron[24] and Nabholz *et al.*[25] on the reaction $O^{16}(\gamma,\alpha)C^{12}$ and a single measurement[26] (0.7 mb at 17.6 Mev) of $\sigma(\gamma,p)$. Now it does not appear possible that all of the absorption below 20 Mev can be due to $H_0(E2)$ and $H_0(M1)$, in view of the sum rules (10) and (11). Both the L-S and j-j independent particle models would make (11) vanish for O^{16}, and it seems unlikely that corrections due to interaction moments would yield $M1$ absorption of normal strength. The sum rule (10) for $H_0(E2)$ alone is overexhausted by the observed cross sections below 20 Mev. It is possible that absorption due to $H_1(E2)$ and $H_1(M1)$ may account for the discrepancy, or it may be that $E1$ absorption is responsible for an appreciable part of the plateau, as

[16] F. K. Goward and J. J. Wilkins, Atomic Energy Research Establishment Memo G/M 127, March, 1952 (unpublished) and private communication (December, 1952).
[17] V. L. Telegdi, Phys. Rev. **87**, 196 (1952); and to be published.
[18] V. L. Telegdi, Phys. Rev. **84**, 600 (1951).
[19] J. J. Wilkins and F. K. Goward, Proc. Phys. Soc. (London) **A64**, 1056 (1951).
[20] V. L. Telegdi (to be published).
[21] F. K. Goward and J. J. Wilkins (private communication, December 1952).
[22] Johns, Horsley, Haslam, and Quinton, Phys. Rev. **84**, 856 (1951).
[23] J. Blatt and V. F. Weisskopf, *Theoretical Nuclear Physics* (John Wiley and Sons, Inc., New York, 1952), p. 656.
[24] Quoted by M. A. Preston, Phys. Rev. **80**, 307 (1950).
[25] Nabholz, Stoll, and Wäffler, Phys. Rev. **86**, 1043 (1952).
[26] H. Wäffler and S. Younis, Helv. Phys. Acta **22**, 614 (1949).

suggested for different reasons by Peaslee.[27] In any case, the (γ,α) reaction to the ground state should be due almost entirely to $H_0(E2)$ and seems to exhaust about half of the sum rule (10).

In the region of the giant $E1$ absorption resonance, Goward and Wilkins[28] have observed several peaks in the cross section for $O^{16}(\gamma,\alpha)C^{12*}\rightarrow 3\alpha$, of heights roughly equal to that of the ground state peak of Millar and Cameron;[24] as in C^{12}, the absence of a spectacular rise in the (γ,α) cross section is in agreement with our theory.

The threshold for the allowed $E1$-induced (γ,α)-process is $7+15+3=25$ Mev. Peaks in the cross section observed by Goward and Wilkins[28] above this energy (up to 30 Mev) are of roughly the same magnitude as in region "B," though the absorption cross section has presumably fallen considerably; again the theory appears to be borne out. It is, of course, extremely important to check whether an overwhelming proportion of the events in region "C" really proceeds via $T=1$ levels in C^{12}. It may be significant that Livesey and Smith[29] have reported a change in mechanism around 25 Mev.

At sufficiently high energies (>35 Mev), the most allowed transition should lead through $T=1$ states in O^{16}, C^{12}, and Be^8; the violation of isotopic spin conservation would be postponed as long as possible. It would be interesting to know whether such cascades do occur.

Experimental effects of the isotopic spin selection rules for γ-ray absorption should, on the whole, be less striking in odd-odd nuclei with $T_z=0$ than in the even-even ones. Perhaps the most noteworthy prediction that can be made is one concerning the competition between (γ,d)- and (γ,np)-reactions in the region of $E1$ absorption. Below the energy at which the residual even-even nucleus can be left in a $T=1$ state, the (γ,d) process is forbidden, while a corresponding reaction in which a neutron and a proton are emitted *together* in a $T=1$ state (particularly in the virtual $^1S_0$ state near zero energy) is fully allowed. Goward and Wilkins[21] appear to have observed an excess of (γ,np) over (γ,d) reactions. It would be useful to search for the allowed (γ,d) process as well; for example, above 25 Mev the reaction $B^{10}(\gamma,d)Be^{8*}$ should lead predominantly to the state at 17 Mev or higher $T=1$ states.‡

For a more detailed discussion of (γ,α)- and (γ,d)-reactions in light nuclei, the reader is referred to a forthcoming review article by one of us (V.L.T.) to appear in the *Reviews of Modern Physics*.

[27] D. C. Peaslee, Phys. Rev. **88**, 812 (1952).
[28] F. K. Goward and J. J. Wilkins, Proc. Phys. Soc. (London) **A65**, 671 (1952).
[29] D. L. Livesey and C. L. Smith, Proc. Phys. Soc. (London) **A65**, 758 (1952).

‡ *Note added in proof.*—Hsiao and Telegdi [Phys. Rev. **90**, 494 (1953)] have recently presented strong evidence that the reaction $O^{16}(\gamma,\alpha)C^{12*}\rightarrow 3\alpha$ does lead to $T=1$ states of C^{12} in energy region C. They have also reported cascades of the type predicted in the text. Our discussion of these cascades ought to be completed by the remark that their probability is greatly reduced through the fact that the emission of the second α suffers competition from nucleon emission.

The same authors, in unpublished work, have found that the reaction $N^{14}(\gamma,d)C^{12}\rightarrow 3\alpha$ proceeds predominantly through a 16-Mev level in C^{12}, presumably with $T=1$, as predicted.

PHYSICAL REVIEW VOLUME 91, NUMBER 1 JULY 1, 1953

A WKB-Type Approximation to the Schrödinger Equation

S. C. Miller, Jr., and R. H. Good, Jr.
Department of Physics, University of California, Berkeley, California

(Received February 9, 1953)

A method of approximating solutions of the one-dimensional Schrödinger equation is presented in this paper. The method closely resembles the usual WKB approximation. Whereas in the ordinary WKB method the exponential function is used as the basis of the approximation, in this paper the solutions of an arbitrary Schrödinger equation are used. The general advantage is that by proper choice of the arbitrary equation an improved approximation can be obtained. The method is illustrated by treating the potential well and potential barrier problems when there are two turning points. The approximations to the wave functions are continuous even across the turning points. The barrier transmission problem is treated uniformly for energies above and below the peak of the barrier.

I. INTRODUCTION

THE WKB method, as well as showing the correspondence between classical and quantum mechanics, provides useful approximations to the solutions of the one-dimensional Schrödinger equation. A limitation on its usefulness as an approximation is that it becomes infinite at the classical turning points of the motion. Langer[1] introduced an approximation based on Bessel functions which remains finite at any one turning point and, far from the turning point, becomes identical with the WKB approximation. However, at a second turning point his result is infinite and, to obtain approximate solutions which are everywhere finite, one must join it to a similar approximation finite at the second turning point.

The ordinary WKB method is based on the exponential function and Langer's approximation on Bessel

[1] R. E. Langer, Phys. Rev. **51**, 669 (1937).

functions. In this paper it is shown that a general WKB-type approximation can be constructed based on the solutions of an arbitrary Schrödinger equation. A good approximation is obtained if the arbitrary equation is chosen to resemble the Schrödinger equation to be solved. In this respect the approximation is similar to perturbation theory. As a particular example of the general approximation, if the arbitrary equation is that of a free particle, one obtains the ordinary WKB approximation. As another special case, Langer's approximation can be interpreted as arising from the Schrödinger equation in which the kinetic energy is a power of the coordinate. Also, by properly choosing the equation, one may find approximate solutions which are finite at several turning points. The only example considered below is that of two turning points; many problems fall into this class.

An advantage of the method used here is that a problem does not need to be broken up into regions with connection formulas between them but instead a single approximate solution can be obtained which is continuous over the whole region. Because of this continuity one can use the approximate wave functions to discuss matrix elements. Ordinarily this is not done because of the infinities at the turning points. In general one must use numerical integration to calculate the matrix elements from the approximate wave functions. However, the numerical integration can be avoided in some special cases discussed in Sec. III. Another advantage of the method is that the problem of transmission through a potential barrier can be discussed uniformly for particle energies above and below the peak of the barrier. The usual WKB approximation gives complete transmission when the energy is above the peak.

The general treatment, for an unspecified basic function, is given in Sec. II. The application to a potential well problem with two turning points is given in Sec. III, basing the approximation on the solutions of the Schrödinger equation for a harmonic oscillator. In Sec. IV the complementary problem of transmission through a potential barrier is discussed.

II. GENERAL TREATMENT

The general problem is to find approximate solutions of the one-dimensional Schrödinger equation,

$$d^2\psi(x)/dx^2+[p^2(x)/\hbar^2]\psi(x)=0, \tag{1}$$

where

$$p^2(x)=W-V(x). \tag{2}$$

Here W is $2m$ times the total energy of a particle of mass m moving in a potential $V(x)/2m$. The approximate solutions are to be based on preselected functions $\phi(S)$ which satisfy

$$d^2\phi(S)/dS^2+[P^2(S)/\hbar^2]\phi(S)=0 \tag{3}$$

for some function $P(S)$. Ordinarily one will be guided to an appropriate choice of $\phi(S)$ by choosing $P(S)$ qualitatively similar to $p(x)$. In the ordinary WKB method[2] one finds approximations to the solutions of Eq. (1) by first changing the dependent variable from $\psi(x)$ to $S(x)$ through the substitution

$$\psi(x)=\exp[i\hbar^{-1}S(x)]. \tag{4}$$

The problem then reduces to finding a solution of

$$-S'^2+i\hbar S''+p^2=0, \tag{5}$$

and one thinks of solving this by a series expansion on $\hbar$, which is assumed to be small:

$$S(x)=S_0(x)+S_1(x)\hbar+S_2(x)\hbar^2+\cdots. \tag{6}$$

Ordinarily only the first two terms are calculated, with the result that

$$\psi\cong p^{-\frac{1}{2}}\exp\left[\pm i\hbar^{-1}\int p(x)dx\right], \tag{7}$$

where the usual connection formulas between regions on opposite sides of the turning points (points at which $p=0$) are to be used.

In parallel with the ordinary WKB method, the first step in attacking the general problem is to change the dependent variable to $S(x)$ by the substitution

$$\psi(x)=T(x)\phi[S(x)], \tag{8}$$

where the function $T(x)$ will be specified below. It is needed in order to obtain an equation in S, independent of ϕ. On substituting Eq. (8) into Eq. (1), one finds immediately that

$$\psi''+(p^2/\hbar^2)\psi=(\hbar^2T''/T-S'^2P^2+p^2)\hbar^{-2}T\phi +(2T'/T+S''/S')TS'd\phi/dS, \tag{9}$$

where Eq. (3) has been used to eliminate ϕ''. Here one sees that if

$$T=S'^{-\frac{1}{2}}, \tag{10}$$

then the problem reduces to finding a solution of

$$\hbar^2T''/T-S'^2P^2+p^2=0. \tag{11}$$

The value of T from Eq. (10) makes this a differential equation in $S(x)$ alone. The next step is to find a series solution for small $\hbar$. Since only $\hbar^2$ appears in Eq. (11) one may write

$$S(x)=S_0(x)+S_2(x)\hbar^2+S_4(x)\hbar^4+\cdots. \tag{12}$$

If, as usual, the approximation is carried to two orders in $\hbar$, only S_0 will be retained in this series, and evidently from Eq. (11)

$$S_0'^2P^2=p^2. \tag{13}$$

If the positive square root is used, the approximate solutions are

$$\psi_{\text{app}}=S'^{-\frac{1}{2}}\phi(S), \tag{14}$$

[2] See, for example, Leonard I. Schiff, *Quantum Mechanics* (McGraw-Hill Book Company, Inc., New York, 1949), first edition, p. 178; Edwin C. Kemble, *The Fundamental Principles of Quantum Mechanics* (McGraw-Hill Book Company, Inc., New York, 1937), first edition, p. 90.

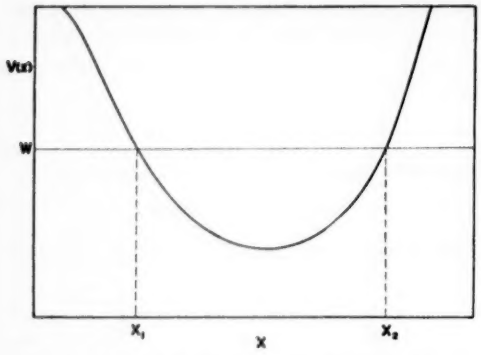

FIG. 1. Type of potential well considered.

where

$$\int_{s_0}^{S} P(\sigma)d\sigma=\int_{x_0}^{x} p(\xi)d\xi. \tag{15}$$

The two independent solutions $\phi(S)$ of Eq. (3) give the approximations to two independent solutions of Eq. (1). In many problems the integration constants s_0, x_0 may be chosen to make the approximate wave function continuous across the turning points, as will be illustrated in Secs. III and IV. With the choice $P^2(S)=1$, the approximation reduces immediately to the ordinary WKB approximation. By taking x_0 to be a turning point of $p^2(x)$, $P^2(S)=S^\nu$, and $s_0=0$, one obtains Langer's approximation for the case when $p^2(x)$ has a zero of the νth order at the turning point.

Whenever the function $S(x)$ is real, as in Secs. III and IV, the approximate wave function will exactly satisfy the conservation of probability equation,

$$\frac{\hbar}{2im}\frac{d}{dx}\left(\psi_{\rm app}^{*}\frac{d}{dx}\psi_{\rm app}-\psi_{\rm app}\frac{d}{dx}\psi_{\rm app}^{*}\right)$$
$$=\frac{\hbar}{2im}S'\frac{d}{dS}\left(\phi^{*}\frac{d}{dS}\phi-\phi\frac{d}{dS}\phi^{*}\right)=0. \tag{16}$$

This is a consequence of the choice of T in Eq. (10) and the fact that ϕ itself satisfies a Schrödinger equation. One may verify that

$$\psi_{\rm app}''+(p^2/\hbar^2)\psi_{\rm app}=\left[\tfrac{3}{4}(S''/S')^2-\tfrac{1}{2}S'''/S'\right]\psi_{\rm app}. \tag{17}$$

The accuracy of the approximation depends on the size of the term on the right.

III. APPLICATION TO POTENTIAL WELL PROBLEMS

In this section the approximation will be applied to the problem of a particle in a potential well with just two turning points x_1 and x_2. Only the simple case when the zeros of p^2 at x_1 and x_2 are of first order will be considered. The potential will then be qualitatively as shown in Fig. 1. The solutions of the harmonic oscillator problem,[3]

$$d^2\phi/dS^2+(E-S^2)\phi=0 \tag{18}$$

(here E is a parameter which will be chosen later), are convenient to use as the basis of the approximation in this problem because their properties are very well known and because $P^2(S)$ has the same type and number of zeros as $p^2(x)$.

Using the notation of Whittaker and Watson to describe the solutions of Eq. (18),[4] one finds the following approximate solutions of Eq. (1):

$$\psi\cong S'^{-\frac{1}{2}}D_{\frac{1}{2}(E-1)}(\sqrt{2}S), \tag{19}$$

$$\psi\cong S'^{-\frac{1}{2}}D_{\frac{1}{2}(E-1)}(-\sqrt{2}S), \tag{20}$$

where

$$\int_{-\sqrt{E}}^{S}(E-\sigma^2)^{\frac{1}{2}}d\sigma=\int_{x_1}^{x}p(\xi)d\xi. \tag{21}$$

These are independent if $(E-1)/2$ is not an integer. The integration constants in Eq. (21) have been chosen for the following reason. Since $S'=p(x)/P(S)$, if the function $S(x)$ is chosen so that the zero of $P(S)$ at $-\sqrt{E}$ corresponds to the zero of $p(x)$ at x_1, then $S(x)$ will be continuous at this point. This means that the approximate wave function itself will be continuous across the turning point x_1. Continuity across the second turning point x_2 is obtained similarly if one chooses the parameter E so that

$$\int_{x_1}^{x_2}p(\xi)d\xi=\int_{-\sqrt{E}}^{\sqrt{E}}(E-\sigma^2)^{\frac{1}{2}}d\sigma=\tfrac{1}{2}E\pi. \tag{22}$$

This makes S real when x is real and completely specifies two independent continuous approximate solutions of Eq. (1). In some problems it is of interest to have asymptotic expansions of the approximate wave functions for large x. From Eq. (21) it is seen that

$$\lim_{x\to\pm\infty}S(x)=\pm\infty$$

so that the asymptotic behaviors of the approximate wave functions depend on the asymptotic forms of the function $D_{(E-1)/2}$. Using these asymptotic forms as given in Eqs. (39) and (45) in the Appendix and expanding Eq. (21) for $S\to\pm\infty$, one finds that

$$\left[(2\pi)^{-\frac{1}{2}}(2e/E)^{\frac{1}{2}E}\Gamma(\tfrac{1}{2}E+\tfrac{1}{2})\right]$$
$$\times 2\cos(\tfrac{1}{2}E\pi)|p|^{-\frac{1}{2}}\exp\left(\int_{x}^{x_1}|p(\xi)|d\xi\right)$$
$$+\sin(\tfrac{1}{2}E\pi)|p|^{-\frac{1}{2}}\exp\left(-\int_{x}^{x_1}|p(\xi)|d\xi\right)$$
$$\underset{x\to-\infty}{\longleftarrow}2^{\frac{1}{2}}(2e/E)^{\frac{1}{2}E}(S')^{-\frac{1}{2}}D_{\frac{1}{2}(E-1)}(\sqrt{2}S)$$
$$\underset{x\to+\infty}{\longrightarrow}|p|^{-\frac{1}{2}}\exp\left(-\int_{x_2}^{x}|p(\xi)|d\xi\right), \tag{23}$$

[3] In this and subsequent equations units have been chosen so that $\hbar=1$.

[4] E. T. Whittaker and G. N. Watson, *Modern Analysis* (The Macmillan Company, New York, 1947), p. 347.

$$|p|^{-\frac{1}{2}}\exp\left(-\int_x^{x_1}|p(\xi)|d\xi\right)$$

$$\xleftarrow[x\to-\infty]{} 2^{\frac{1}{2}}(2e/E)^{\frac{1}{2}E}(S')^{-\frac{1}{2}}D_{\frac{1}{2}(E-1)}(-\sqrt{2}S)$$

$$\xrightarrow[x\to+\infty]{}\left[(2\pi)^{-\frac{1}{2}}(2e/E)^{\frac{1}{2}E}\Gamma(\tfrac{1}{2}E+\tfrac{1}{2})\right]$$

$$\times 2\cos(\tfrac{1}{2}E\pi)|p|^{-\frac{1}{2}}\exp\left(\int_{x_2}^{x}|p(\xi)|d\xi\right)$$

$$+\sin(\tfrac{1}{2}E\pi)|p|^{-\frac{1}{2}}\exp\left(-\int_{x_2}^{x}|p(\xi)|d\xi\right). \quad (24)$$

When W is large, it is clear from Eq. (22) that the parameter E is large. In that case the factor in the square brackets in Eqs. (23) and (24) approaches one, as is seen by using the Stirling approximation for the Γ-function. The connection between the two exponential regions is then identical with the one obtained by the ordinary WKB method using the usual connection formulas across the turning points without regard to direction.

For the bound states one must use the solutions of Eq. (18) which are finite at infinite S. These solutions are

$$D_n(\sqrt{2}S)=2^{-\frac{1}{2}n}H_n(S)\exp(-\tfrac{1}{2}S^2), \quad (25)$$

where $n=(E-1)/2$ is a positive integer or zero and the H_n are the Hermite polynomials. The approximations to the bound state wave functions are then

$$\psi_n\cong A_n S'^{-\frac{1}{2}}\exp(-\tfrac{1}{2}S^2)H_n(S), \quad (26)$$

where S is still given by Eq. (21) and the A_n are normalizing constants. The eigenvalue condition, from Eq. (22), is

$$\int_{x_1}^{x_2}p(\xi)d\xi=(n+\tfrac{1}{2})\pi, \quad n=0, 1, 2, \cdots, \quad (27)$$

which is identical with the usual WKB eigencondition. If a different $P(S)$ had been used, a different condition might have been obtained. The potential[5]

$$V(x)=-1.922e^x(1+e^x)^{-1}-11.20e^x(1+e^x)^{-2} \quad (28)$$

has been chosen for an example. The reason for choosing this type of potential is that the exact solutions for the bound states can be expressed in terms of elementary functions. The constants have been chosen to allow only two energy levels and to make the wave functions unsymmetrical. The exact and approximate wave functions have been plotted in Fig. 2.

Since the approximate wave functions are continuous, they can be used to obtain approximations to matrix elements. In many problems diagonal matrix elements can be found by making a further approximation which avoids calculating the wave functions and making a numerical integration. Consider, for example,

$$\int_{-\infty}^{\infty}|\psi_n|^2x^m dx$$

$$\cong A_n^2\int_{-\infty}^{\infty}(S')^{-1}\exp(-S^2)H_n^2(S)x^m dx$$

$$=A_n^2\int_{-\infty}^{\infty}(S')^{-2}\exp(-S^2)H_n^2x^m dS, \quad (29)$$

where m is some integer. This quantity might be evaluated by expressing x and S'^{-1} as power series in S and performing the integration. As an approximation one may use, instead of power series, $(2K+1)$-degree poly-

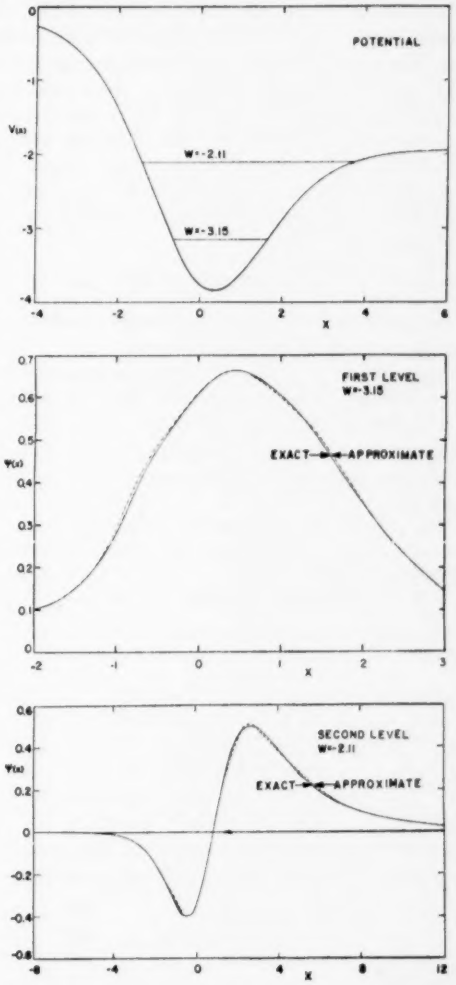

FIG. 2. The potential, $V(x)=-1.922e^x(1+e^x)^{-1}-11.20e^x\times(1+e^x)^{-2}$, and the wave functions of the two bound states. Each wave function separately has been normalized so that the integral-square is 1.

[5] This potential is of the type which was introduced by Carl Eckart, Phys. Rev. **35**, 1303 (1930).

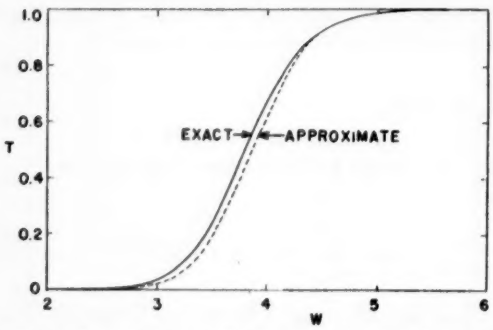

FIG. 3. Transmission coefficient for the potential, $V(x) = 1.922e^x(1+e^x)^{-1}+11.20e^x(1+e^x)^{-2}$. (This is the negative of the potential shown in Fig. 2.)

nomials chosen to give the correct values of $x(S)$ and its derivatives up to the Kth order at both turning points. The values at other points could be used but the turning points are especially suitable since their locations are known immediately once the energy has been found and also since ordinarily the wave function will be large only in the region between these points. The needed derivatives at a first-order turning point can be found by using Eq. (15) to make a series expansion of the type

$$x(S)=x_0+[(dp^2/dx)_{x_0}/(dP^2/dS)_{s_0}]^{-1}(S-s_0)+\cdots. \quad (30)$$

One can easily express $(S')^{-1}$ in terms of S by differentiating the polynomial $x(S)$ with respect to S.

As a special case of Eq. (29) this procedure may be used to normalize the approximate wave functions of bound states so that their integral squares are one. For example, for the two levels of the Eckart potential used above, one finds for the normalizing constants A_0 and A_1:

	A_0 (first level)	A_1 (second level)
Numerical integration	1.627	1.686
First degree polynomial approximation ($K=0$)	1.600	1.483
Third degree polynomial approximation ($K=1$)	1.629	1.700

As a further example $\langle x^2\rangle_{A_0}$, the expected value of x^2, has been calculated for the two bound states of the above Eckart potential. Third-degree polynomials were used, both for normalizing and for evaluating the integral. For comparison the same quantity has been calculated using the exact wave functions and also using the approximate wave functions with numerical integration throughout. The results are as follows:

	First level	Second level
$\langle x^2\rangle_{A_0}$ (approximate wave function, polynomials)	1.237	9.52
$\langle x^2\rangle_{A_0}$ (exact wave function, numerical integration)	1.223	10.19
$\langle x^2\rangle_{A_0}$ (approximate wave function, numerical integration)	1.224	10.51

The polynomial method in general may be criticized because there is no way of estimating the error in the approximation of a matrix element and because it cannot be applied to off-diagonal matrix elements, since different functions $S(x)$ arise for different energies.

IV. APPLICATION TO POTENTIAL BARRIER PROBLEMS

The penetration of a particle through a potential barrier will be discussed in this section. The discussion will be restricted to those potentials for which, when the energy is below the peak of the barrier, $p^2(x)$ has two first order zeros x_1 and x_2, where $x_1<x_2$. As a further restriction on the type of potential discussed, it will be assumed that the two real turning points for energies below the peak of the barrier go unambiguously into two complex turning points for energies above the peak of the barrier. Since $p^2(x)$ is a real function, these two turning points will be complex conjugate; the one with the positive imaginary part will be called x_1 and the other x_2. As basic functions for the approximation the solutions of the equation

$$d^2\phi/dS^2+(E+S^2)\phi=0 \quad (31)$$

will be used. The zeros of $(E+S^2)$ will be labeled in parallel with those of $p(x)$ so that when E is negative $s_1=-\sqrt{(-E)}$, $s_2=+\sqrt{(-E)}$ and when E is positive $s_1=+i\sqrt{E}$, $s_2=-i\sqrt{E}$.

Following the general treatment, and in parallel with the potential well problem, one finds the following approximate solutions:

$$\psi\cong S'^{-\frac{1}{2}}D_{\frac{1}{2}(+iE-1)}(\sqrt{2}Se^{-i\pi/4}), \quad (32)$$

$$\psi\cong S'^{-\frac{1}{2}}D_{\frac{1}{2}(-iE-1)}(\sqrt{2}Se^{+i\pi/4}), \quad (33)$$

where

$$\int_{s_1}^{S}(E+\sigma^2)^{\frac{1}{2}}d\sigma=\int_{x_1}^{x}p(\xi)d\xi, \quad (34)$$

and the parameter E is chosen to satisfy

$$\int_{x_1}^{x_2}p(\xi)d\xi=\int_{s_1}^{s_2}(E+\sigma^2)^{\frac{1}{2}}d\sigma=-\tfrac{1}{2}iE\pi. \quad (35)$$

In performing the σ-integration here and in finding the results below, the branch of the square root used is the one for which, when $E>0$ and S is real, $\arg(E+S^2)^{\frac{1}{2}}$ is 0, and for which, when $E\leqq 0$ and S is real, $\arg(E+S^2)^{\frac{1}{2}}$ is 0 if $S<s_1$, $\pi/2$ if $s_1<S<s_2$, and 0 if $s_2<S$. The similar branch of $p(x)$ must be used in the ξ-integration. From Eq. (35) one sees that E is real and positive when W is above the peak of the barrier $V(x)$ and that E is real and negative when W is below the peak. Using Eqs. (34) and (35), one may verify that S is real when x is real. In order to find the transmission coefficient the asymptotic forms of the approximate solutions for

large x are needed. From Eq. (34) it is seen that

$$\lim_{x\to\pm\infty} S(x)\to\pm\infty.$$

Performing the σ-integration in Eq. (34), expanding for $S\to\pm\infty$, and using the asymptotic forms of $D_n(z)$ as given in Eq. (40) and Eq. (41) in the Appendix, one finds that

$$\begin{aligned}&[(2/\pi)^{\frac{1}{2}}(|E|/2e)^{-\frac{1}{2}iE}\Gamma(\tfrac{1}{2}iE+\tfrac{1}{2})\\&\times\cosh(\tfrac{1}{2}E\pi)]e^{\frac{1}{2}E\pi}p^{-\frac{1}{2}}\exp\left(-i\,\mathrm{Re}\int_x^{x_1}p(\xi)d\xi\right)\\&+e^{-\frac{1}{2}i\pi}p^{-\frac{1}{2}}\exp\left(i\,\mathrm{Re}\int_x^{x_1}p(\xi)d\xi\right)\\&\xleftarrow[x\to-\infty]{}(2e^{-\frac{1}{2}i\pi})^{\frac{1}{2}}(|E|e^{\frac{1}{2}i\pi}/2e)^{-\frac{1}{2}iE}S'^{-\frac{1}{2}}D_{\frac{1}{2}(iE-1)}(\sqrt{2}e^{-\frac{1}{2}i\pi}S)\\&\xrightarrow[x\to+\infty]{}e^{\frac{1}{2}E\pi}p^{-\frac{1}{2}}\exp\left(i\,\mathrm{Re}\int_{x_2}^{x}p(\xi)d\xi\right),\end{aligned}\tag{36}$$

where Re indicates that the real part of the integral is to be used. The corresponding relation for

$$D_{\frac{1}{2}(-iE-1)}(\sqrt{2}e^{\frac{1}{2}i\pi}S)$$

is the complex conjugate of this one. The transmission coefficient T, defined as the ratio of the transmitted to the incident current, is then

$$T\cong(1+e^{-E\pi})^{-1}.\tag{37}$$

An example of the application of this result is given in Fig. 3. A connection similar to the one given in Eq. (36) was found by Guth and Mullin[6] using a method indicated by Kramers and Ittman.[7] Using the relation between the gamma and the trigonometric functions one finds that the absolute value of the quantity in the square brackets in Eq. (36) is $[2\cosh(\frac{1}{2}E\pi)]^{\frac{1}{2}}$. Also, using the Stirling approximation, one finds that for large E the quantity in the square brackets is $e^{\frac{1}{2}|E|\pi}$. For energies below the peak of the barrier one may discuss the same transmission problem with the ordinary WKB method, using the connection formulas without regard to direction. When the energy is so far below the peak of the barrier that $e^{E\pi}$ can be neglected compared to one, the resulting connection across the entire barrier is identical with Eq. (36) when the square bracket can be replaced by $e^{\frac{1}{2}|E|\pi}$.

APPENDIX

The asymptotic representations of $D_n(z)$ are needed in Sec. III when n is real and $\arg z=0$ or π and in Sec. IV when the real part of n is $-\frac{1}{2}$ and $\arg z=-\pi/4$ or $3\pi/4$. In general the asymptotic representation is of the form

$$\begin{aligned}D_n(z)\sim&\alpha\exp(-\tfrac{1}{4}z^2)z^n[1+O(z^{-2})]\\&+\beta\exp(\tfrac{1}{4}z^2)z^{-n-1}[1+O(z^{-2})],\end{aligned}\tag{38}$$

where α and β are independent of $|z|$ but vary with $\arg z$. The predominant terms in this representation are conveniently given by Whittaker and Watson.[8] From their results one may infer immediately that the complete representation is

$$D_n(z)\sim\exp(-\tfrac{1}{4}z^2)z^n,\quad\text{when}\quad\arg z=0,\tag{39}$$

because if β were not zero the term which β multiplies, containing $\exp(\frac{1}{4}z^2)$, would be predominant. Here and below the terms of order z^{-2} compared to one have been omitted. Similarly, when the real part of n is $-\frac{1}{2}$ and $\arg z=-\pi/4$ or $3\pi/4$, the terms multiplying α and β are each of order $|z|^{-\frac{1}{2}}$, so again the predominant terms give the complete representations:

$$D_n(z)\sim\exp(-\tfrac{1}{4}z^2)z^n,\quad\text{when}\quad\arg z=-\pi/4,\tag{40}$$

$$\begin{aligned}D_n(z)\sim&\exp(-\tfrac{1}{4}z^2)z^n-(2\pi)^{\frac{1}{2}}[\Gamma(-n)]^{-1}\\&\times\exp(n\pi i)\exp(\tfrac{1}{4}z^2)z^{-n-1},\quad\text{when}\quad\arg z=3\pi/4.\end{aligned}\tag{41}$$

These are the representations used in Sec. IV.

When $\arg z=\pi$, the β term is the predominant one and therefore $\beta=-(2\pi)^{\frac{1}{2}}e^{n\pi i}[\Gamma(-n)]^{-1}$. One may infer the value of α when n is real and $\arg z=\pi$ by an indirect argument using the fact that

$$\begin{aligned}D_n(z)=&(2\pi)^{-\frac{1}{2}}\Gamma(n+1)[e^{\frac{1}{2}n\pi i}D_{-n-1}(iz)\\&+e^{-\frac{1}{2}n\pi i}D_{-n-1}(-iz)],\end{aligned}\tag{42}$$

as is shown by Whittaker and Watson for all n and z. One may assume that, for z real and positive,

$$\begin{aligned}D_{-n-1}(e^{\frac{1}{2}i\pi}z)\sim&\exp(\tfrac{1}{4}z^2)(e^{\frac{1}{2}i\pi}z)^{-n-1}\\&+b\exp(-\tfrac{1}{4}z^2)(e^{im\pi}e^{\frac{1}{2}i\pi}z)^n,\end{aligned}\tag{43}$$

where b and m are real numbers to be determined. The first term on the right is simply Whittaker and Watson's predominant term and in the second term β has been written as $be^{imn\pi}$. It is seen that m must be an integer or zero since $D_{-n-1}(z)$ is a real function of z. Substituting Eq. (39), Eq. (43), and the complex conjugate of Eq. (43), into Eq. (42), one obtains

$$b=(2\pi)^{\frac{1}{2}}/2\Gamma(n+1)\cos((m+1)n\pi).\tag{44}$$

Here it is seen that m must be -1 if b is to remain finite for all n. Using these values for b and m and replacing z by $-z$ in Eq. (42), one may conclude that

$$\begin{aligned}D_n(z)\sim&\cos(n\pi)e^{-n\pi i}\exp(-\tfrac{1}{4}z^2)z^n\\&-(2\pi)^{\frac{1}{2}}[\Gamma(-n)]^{-1}e^{n\pi i}\exp(\tfrac{1}{4}z^2)z^{-n-1},\\&\text{when}\quad\arg z=\pi.\end{aligned}\tag{45}$$

This representation and the one given in Eq. (39) are used in Sec. III.

[6] Eugene Guth and Charles J. Mullin, Phys. Rev. **59**, 579 (1941).

[7] H. A. Kramers and G. P. Ittman, Z. Physik **58**, 225 (1929).

[8] Reference 4, pp. 347–348.

Generalized Statistical Mechanics and the Onsager Relations*

PETER G. BERGMANN AND ALICE C. THOMSON
Department of Physics, Syracuse University, Syracuse, New York
(Received March 20, 1953)

The Onsager relations assert certain symmetry relations for the cross coefficients that connect rates of flux in stationary nonequilibrium processes with the driving "thermodynamic forces." These relations are usually derived by an argument borrowed from fluctuation theory, with the assumption that the rate at which a fluctuation in an equilibrium ensemble regresses equals the rate at which the ensemble average of the same quantity will change in a nonequilibrium ensemble. In this paper, we have by-passed fluctuation theory and have derived similar symmetry relations for the corresponding cross coefficients in ensembles consisting of thermally isolated systems differing but slightly from an equilibrium canonical ensemble. For the case of large deviations from equilibrium, we have found expressions for the same cross coefficients which possess no symmetry properties but which are exactly the usual correlation coefficients of fluctuation theory. Because our present work is concerned with thermally isolated systems, we cannot yet describe in a satisfactory manner stationary nonequilibrium processes. For the representation of such processes, one would need an ensemble of systems in which the interaction with the surroundings is described in terms of additional random variables.

I. INTRODUCTION

THE first major contribution to a general thermodynamics of irreversible processes was the Onsager theory of interfering linear processes. In this work the cross-coefficients describing the interference were shown to be related by a set of reciprocal relations. These relations have been demonstrated by a statistical mechanical argument using properties of the equilibrium microcanonical ensemble.[1,2] In this proof the techniques used are restricted to processes taking place near equilibrium.

Recently considerable progress has been made toward widening the scope of statistical mechanical methods for treating irreversible processes.[3–5] These investigators also use the equilibrium ensemble as a starting point. They obtain nonequilibrium results by considering suitable nonequilibrium subsets of the equilibrium ensemble. That is, specific fixed values of the interesting time-dependent macroscopic variables of the system at a particular time characterize a certain subset of members of the equilibrium ensemble, and the properties of this subset are investigated. Though this approach is not restricted to near-equilibrium processes, to date results have been obtained only under such conditions.

A second method which is based on the same viewpoint is provided the use of nonequilibrium ensembles, constructed specifically as such. We have felt that this approach might provide a better starting point for the study of more general nonequilibrium situations. One such ensemble, a sort of "generalized microcanonical ensemble," has been used for a long time in connection with the Gibbs form of the H-theorem.[6] We are interested in the potentialities of a second type which we have called "generalized canonical ensembles." These ensembles seem in many cases to be a more adequate statistical collection than the generalized microcanonical ensembles, and are easier to work with.

Generalized canonical ensembles were introduced by one of us (Peter G. Bergmann)[7] in a previous paper. We shall discuss the general properties of these ensembles in greater detail, and then as an example show their use in the near-equilibrium case in deriving the Onsager relations.

II. CONSTRUCTION OF THE ENSEMBLE. ENTROPY

Thermodynamic measurements on a system in nonequilibrium consist of the determination of the values of interesting local variables in the system. For example, one might measure local temperatures and pressures in a gas. The choice of variables is dependent on the type of system and the amount of its deviation from equilibrium. For instance, temperature would be meaningless in a case where the temperature gradient (i.e., the gradient of mean energy per degree of freedom) is large over a mean free path. Furthermore, care must be exercised in nonequilibrium cases that the measured quantity actually is properly interpreted in terms of the variables of the system. For example, different types of thermometers thrust into an anisotropic beam like the sun's rays will measure different "temperatures" because of their different absorption properties.

If any suitable set of variables and measurements is chosen (it might, for instance, include fluxes, or even quantities moving with the flow), then a statistical treatment in principle can be used to obtain a thermodynamic description of the process. "Suitability" here

* This research was supported in part by the United States Air Force, monitored by the Office of Scientific Research.
[1] L. Onsager, Phys. Rev. **37**, 405 (1931); **38**, 2265 (1931).
[2] H. B. G. Casimir, Revs. Modern Phys. **17**, 343 (1945).
[3] Callen, Barasch, and Jackson, Phys. Rev. **88**, 1382 (1952), and references included therein.
[4] R. F. Greene aud H. B. Callen, Phys. Rev. **88**, 1387 (1952), and references included therein.
[5] M. S. Greene, J. Chem. Phys. **20**, 1281 (1952).
[6] R. C. Tolman, *Principles of Statistical Mechanics* (Oxford University Press, London, 1938).
[7] P. G. Bergmann, Phys. Rev. **84**, 1026 (1951), referred to as I in the following.

is taken to mean that the variables selected for observation do not fluctuate significantly during the time required to complete one observation; this, of course, is dependent on the refinement of the apparatus as well as on the extent of non-steadiness of the system with respect to those variables. And it is also necessary that those variables which represent local contributions to a variable characteristic of the whole system, like the energy, have an approximate additive property; that is, that the sum of the local contributions should approximately equal the system variable, with interaction corrections negligible. For example, the total energy should approximately equal the sum of the local energies measured. But this condition generally admits a wide class of variables. In the energy example, the interaction across the boundary between regions where measurements are made is required to contribute little to the total energy, and this is frequently true even though the atomic interactions are strong, merely because of the large number of atoms in each measured region. These requirements are in some sense equivalent to saying that meaningful measurements are indeed possible. An example of the possible use of variables moving with the flow is the use of a Brownian particle as a measuring instrument in a fluid in nonequilibrium.

One further requirement is that the set of variables selected be "complete" enough that the ensemble averages described below are defined. Thus we must avoid a specification which would lead to finite ensemble densities (i.e., densities bounded away from 0) over unbounded regions of γ-space. For instance, we cannot specify temperature measurements at each end of a rod with no measurement bounding the mean total energy of the rod.

Once a set of measurements has been made, the statistical method involves the choice of a suitable collection or ensemble of identical systems in microscopic states which either exactly, or in the ensemble average, correspond to the macroscopic state implied by the measured values. Then the prediction of the future for the actual system is made through the study of the behavior in time of averages over the ensemble.

The ensemble density which was called a "generalized microcanonical ensemble" above is constructed as follows: the μ-space of the system is conceived to be divided up into cells of size corresponding to the definition of the measured local variables. Each molecule-space in the γ-space is similarly divided. The information obtained in the measurement is now interpreted, on account of the macroscopic character of the variables, as giving an occupation number to each cell in μ-space. Then, using the principle of equal a priori probabilities, we construct an ensemble which has initially constant values over corresponding cells in γ-space.

This procedure is not always appropriate. For one thing, certain important thermodynamic measurements are made on intensive parameters, for example, local temperatures, rather than directly on dynamical variables like local energies, and it is easier to treat these parameters meaningfully with a canonical-like ensemble. Such ensembles are really defined by the values of the parameters, whereas it is more difficult to relate such quantities to the generalized microcanonical ensembles. In addition, the physical regions in which measurements are made are not usually isolated but are rather to be considered in loose contact with their neighbors, in the sense of the requirement mentioned above of "additivity" of the selected dynamical variables. This contact suggests the usefulness of canonical-like ensembles which admit members differing slightly in the values of the interesting dynamical variables.

If the interesting variables are designated as $a_i(p_1 \cdots p_n, q_1 \cdots q_n)$, (we shall assume in the following that they are not explicitly time-dependent, although this restriction is not necessary), then the generalized canonical ensemble density is

$$\mu(p, q, t) = (Z^0)^{-1} \exp(-\textstyle\sum_i \beta_i^0 a_i^0),$$
$$Z^0 = \int_{\gamma\text{-space}} \exp(-\textstyle\sum_i \beta_i a_i^0) dX, \tag{1}$$

where dX is the volume element in γ-space; p, q is a symbol for the set of coordinates and momenta $p_1 \cdots p_n$, $q_1 \cdots q_n$; β_i^0 are constants; a_i^0 is that constant of the motion which at the time of measurement equals the value of the variable a_i, that is,

$$\partial a_i^0/\partial t + (a_i^0, H) = 0, \quad a_i^0(p, q, t) = a_i(p_0, q_0), \tag{2}$$

where p_0, q_0 are the values of p, q at t_0. Now in some cases it may turn out that the measured quantities are the variables a_i, in which case the β_i^0 are determined by the conditions:

$$\langle a_i \rangle_{Av}(t_0) = \int a_i \mu(t_0) dX = A_i(t_0), \tag{3}$$

where $A_i(t_0)$ is the measured value of a_i at t_0. In other cases the β_i^0 are the measured quantities. For example, if the a_i are local energies, the β_i^0 are proportional to the reciprocals of the initial local temperatures. In this case the conditions (3) determine the average values of the a_i at time t_0.

The density μ satisfies Liouville's equation. In fact it is merely a way of writing that solution of Liouville's equation which has the canonical form and the correct average properties at t_0.

In (I) a quantity called the "system entropy" was introduced which takes on its minimum value at the time of observation and has other properties suitable to entropy. This quantity is defined as follows:

$$S^* = k(\ln\mu_0 + \ln Z + \textstyle\sum_i \beta_i \langle a_i \rangle_{Av}), \tag{4}$$

where k is Boltzmann's constant, μ_0 is a constant, and

β_i and Z are defined by the requirements

$$Z^{-1}\int a_i \exp(-\textstyle\sum_j \beta_j a_j)dX=\langle a_i\rangle_{Av},$$
$$Z=\int \exp(-\textstyle\sum_j \beta_j a_j)dX. \tag{5}$$

That is, β_j and Z are time-dependent quantities which are used to define a fictitious canonical ensemble which yields at all times the same averages of the a_i as the actual ensemble density μ.

The quantity S^* is a generalization of the ensemble definition of Boltzmann's quantity $(-kH)$ for generalized microcanonical ensembles.[6] S^* reduces to $(-kH)$ if we consider the a_i as designations of cells in phase space. Thus if γ-space is divided into small but not infinitesimal cells as described above, then we define

$$a_i=X_i^{-1}\delta_i(q,p)=\begin{matrix}1 \text{ inside the } i\text{th cell},\\ 0 \text{ outside the } i\text{th cell},\end{matrix} \tag{6}$$

where X_i is the volume of the ith cell. H is defined as

$$H=\textstyle\sum_i \mu_i \ln\mu_i X_i, \tag{7}$$

where μ_i is the average value of μ over the ith cell. Then

$$\langle a_i\rangle_{Av}=X_i^{-1}\int \delta_i\mu(q,p)dX=\mu_i.$$

From the definition of Z and β_k,

$$Z\langle a_i\rangle_{Av}=\int a_i \exp(-\textstyle\sum_k \beta_k a_k)dX,$$
$$=X_i^{-1}\int_{i\text{th cell}} \exp(-\textstyle\sum_k \beta_k a_k)dX=\exp(-\beta_i/X_i).$$

Then

$$S^*=k(\ln Z-\textstyle\sum_i \ln(Z\mu_i)\mu_i X_i+\ln\mu_0)$$
$$=-kH+k\ln\mu_0. \tag{8}$$

In (I) it is shown that S^* has an absolute minimum at the time t_0, both with respect to past times and future times. We conjecture that the usual behavior of this function is an initial increase continuing for very large times with perhaps small undulations, then at vast intervals large fluctuations and eventually a decrease to, but not below, the original value. This behavior is, of course, the same as that usually conjectured for the ensemble definition of $(-H)$, and any entropy defined for a closed system so that it does not eventually decrease would be a violation of the Poincaré Theorem on quasi periodicity of dynamical systems. Note that the property of S^* of having a minimum at t_0 which may later be reached but never surpassed, a property previously proved for $(-H)$,[6] is quite different from the behavior of the Boltzmann μ-space definition of $(-H)$, which we shall designate $(-H')$. This latter quantity can, indeed, fluctuate below its value at t_0. The behavior of S^* and the ensemble quantity $(-H)$ is, of course, an ensemble property which is dependent on the collective behavior of all the systems, and under certain rare dynamical conditions, individual systems in the ensemble may indeed eventually have values of $(-H')$ deviating below their initially observed values. The point is that even the "average" system eventually decreases in entropy, but it does not decrease below the initial value at t_0. We identify the ensemble property of S^* with the "thermodynamic" behavior of entropy for the physical system under observation.

Taking the time derivative of S^* in (4) we get

$$\frac{dS^*}{dt}=-k\textstyle\sum_i \dot\beta_i\langle a_i\rangle_{Av}+k\sum_i \beta_i\langle a_i\rangle_{Av}+k\sum_i \beta_i\frac{d}{dt}\langle a_i\rangle_{Av}.$$

By integrating by parts we can put this equation in the following form:

$$dS^*/dt=k\textstyle\sum_i \beta_i\langle\dot a_i\rangle_{Av}. \tag{9}$$

This equation suggests the role of the $k\beta_i$ as "generalized reciprocal temperatures" and the $\langle\dot a_i\rangle_{Av}$ as "generalized heat flows."

III. NEAR EQUILIBRIUM. ONSAGER RELATIONS

We shall assume that one of the variables a_i, say a_0, is chosen as the Hamiltonian H. The corresponding β_0^0 (the reciprocal of kT), is the "thermodynamic force" associated with the mean total energy of the system. Then the density μ can be written as

$$\mu=(Z^0)^{-1}\exp(-\beta_0^0 H-\sum_{i=1}\beta_i^0 a_i^0),$$

and the equilibrium ensemble is characterized by zero values of all the β_i^0, $i\neq 0$. If, for example, we have chosen the a_i for $i>0$ as local energies (i.e., energies of parts of the system), then the $k\beta_i^0$ for $i>0$ will be not the initial values of the local reciprocal temperatures but the differences between reciprocal local temperatures and the reciprocal over-all temperature.

The quantities $\langle a_i\rangle_{Av}$ can be expressed as functions of the set of β_j^0 and t. The derivatives $\partial\langle a_i\rangle_{Av}/\partial\beta_j^0$ are as follows:

$$\frac{\partial\langle a_i\rangle_{Av}}{\partial\beta_j^0}=-\langle a_i a_j^0\rangle_{Av}+\langle a_i\rangle_{Av}\langle a_j^0\rangle_{Av}. \tag{10}$$

If the initial measurements $\langle a_j^0\rangle_{Av}$ are close to equilibrium values and, accordingly, the $\beta_j^0(j\neq 0)$ small, then we can express $\langle a_i\rangle_{Av}$ by the first terms in a Taylor series expansion in the $\beta_j^0(j\neq 0)$. That is,

$$\langle a_i\rangle_{Av}(\beta_1^0\cdots\beta_n^0,t)$$
$$=\langle a_i\rangle_{Av}(0\cdots 0,t)+\textstyle\sum_j \frac{\partial\langle a_i\rangle_{Av}}{\partial\beta_j^0}(0\cdots 0,t)\beta_j^0+\cdots$$
$$=\langle a_i\rangle_{Av}(0\cdots 0,t)+\textstyle\sum_j A_{ij}\beta_j^0, \tag{11}$$

where

$$A_{ij}(t)=-\langle a_i a_j^0\rangle_{\mathcal{N}}(0\cdots 0,t)+\langle a_i\rangle_{\mathcal{N}}(0\cdots 0,t)\langle a_j^0\rangle_{\mathcal{N}}(0\cdots 0,t). \quad (12)$$

The first term in $\langle a_i\rangle_{\mathcal{N}}(\beta_1^0\cdots\beta_n^0,t)$ is constant in time, being an average over the equilibrium ensemble of a quantity which is not explicitly time-dependent. We shall now show that the quantities A_{ij} have certain symmetry properties. We distinguish between those variables a_i which are even functions of the momenta of the system, and those which are odd functions of the momenta. We assume in the following that the Hamiltonian H of the system is an even function of the momenta. Consider a point $\mathbf{x}$ in phase space which moves from an initial value $\mathbf{x}^0$ according to the equations of motion. We can symbolize this as $\mathbf{x}=M(\mathbf{x}^0,t)$ where $M(\mathbf{x}^0,t)$ is the mapping of $\mathbf{x}^0$ in phase space. Any constant of the motion, in particular an ensemble density μ, will satisfy

$$\mu(\mathbf{x},t)=\mu(\mathbf{x}^0,0)=\mu(M^{-1}(\mathbf{x},t),0).$$

If we designate by a prime the transformation reversing the signs of the p_k, then the even or odd character of the a_i is given by

$$a_i(\mathbf{x})=\epsilon_i a_i(\mathbf{x}'), \qquad \begin{cases}\epsilon_i=1 & \text{for even functions,}\\ \epsilon_i=-1 & \text{for odd functions.}\end{cases} \quad (13)$$

The assumptions on the Hamiltonian lead to the property

$$M(\mathbf{x}^{0\prime},t)=[M^{-1}(\mathbf{x}^0,t)]'. \quad (14)$$

This equation is a consequence of the time reversibility of the equations of motion.

Now we want to show that

$$A_{ik}=A_{ki}\epsilon_k\epsilon_i. \quad (15)$$

We shall show this property for the first term in expression (12); the second term is treated in exactly the same way:

$$\begin{aligned}&\langle a_i a_k^0\rangle_{\mathcal{N}}(0\cdots 0,t)\\ &=(Z^0)^{-1}\int \exp(-\beta_0^0 H)a_k(\mathbf{x}^0)a_i(M(\mathbf{x}^0,t))dX^0,\\ &=(Z^0)^{-1}\int \exp(-\beta_0^0 H)a_k(M^{-1}(\mathbf{x},t))a_i(\mathbf{x})dX,\\ &=(Z^0)^{-1}\int \exp(-\beta_0^0 H)a_k([M(\mathbf{x}',t)]')a_i(\mathbf{x})dX,\\ &=(Z^0)^{-1}\int \exp(-\beta_0^0 H')\epsilon_k a_k(M(\mathbf{x}',t))\epsilon_i a_i(\mathbf{x}')dX',\\ &=\langle a_k a_i^0\rangle_{\mathcal{N}}(0\cdots 0,t)\epsilon_k\epsilon_i. \end{aligned} \quad (16)$$

Equations (15) are true for all time for the near-equilibrium case, but do not hold for the general case. If we carry out a similar transformation of the first term in the general expression (10) for $\partial\langle a_i\rangle_{\mathcal{N}}/\partial\beta_j^0$, we get

$$\begin{aligned}\langle a_i a_k^0\rangle_{\mathcal{N}}&=(Z^0)^{-1}\int \exp(-\beta_0^0 H-\textstyle\sum_j \beta_j^0\epsilon_j a_j[M(\mathbf{x}',t)])\\ &\quad\times\epsilon_k a_k(M(\mathbf{x}',t))\epsilon_i a_i(\mathbf{x}')dX',\\ \langle a_k a_i^0\rangle_{\mathcal{N}}&=(Z^0)^{-1}\int \exp(-\beta_0^0 H-\textstyle\sum_j \beta_j^0 a_j(\mathbf{x}))\\ &\quad\times a_k(M(\mathbf{x},t))a_i(\mathbf{x})dX.\end{aligned} \quad (17)$$

Now we want to relate the quantities A_{ik} to the Onsager coefficients. First note that Eq. (9) identifies the β_k as the Onsager forces.[2] We form the difference quotients

$$G_i=\tau^{-1}[\langle a_i\rangle_{\mathcal{N}}(\beta_1^0\cdots\beta_n^0,t_0+\tau)-\langle a_i\rangle_{\mathcal{N}}(\beta_1^0\cdots\beta_n^0,t_0)] \quad (18)$$

over a time interval τ which is, on the one hand, not infinitesimal, and, on the other hand, so small that the deviation from equilibrium has not materially changed. The condition for the latter is that the generalized reciprocal temperatures β_i remain unchanged over the interval τ:

$$\dot{\beta}_i\approx 0, \quad \beta_i\approx\beta_i^0. \quad (19)$$

Then we investigate the dependence of G_i on β_k:

$$\begin{aligned}L_{ik}=\frac{\partial G_i}{\partial\beta_k}&=\tau^{-1}\left[\frac{\partial\langle a_i\rangle_{\mathcal{N}}}{\partial\beta_k}(t_0+\tau)-\frac{\partial\langle a_i\rangle}{\partial\beta_k}(t_0)\right],\\ &=\tau^{-1}[A_{ik}(t_0+\tau)-A_{ik}(t_0)].\end{aligned} \quad (20)$$

Hence L_{ik} has the same symmetry properties as A_{ik}:

$$L_{ik}=\epsilon_i\epsilon_k L_{ki}. \quad (21)$$

These latter equations are the Onsager relations.[2] The quantities L_{ik} are identified with the thermodynamic coefficients in linear irreversible laws.

The requirement of a lower limit on the time interval τ is necessary because the quantity $\partial\langle\dot{a}_i\rangle_{\mathcal{N}}/\partial\beta_k=-\langle\dot{a}_i a_k^0\rangle_{\mathcal{N}}+\langle\dot{a}_i\rangle_{\mathcal{N}}\langle a_k^0\rangle_{\mathcal{N}}$ is zero at time t_0 if a_i and a_k are either both even or both odd functions of the momenta. In some sense the ensemble fails to demonstrate the dissipative process instantaneously.

The upper limit reflects the fact that the Onsager relations apply to a system in which one portion "drives" another in an approximately steady state, i.e., a state in which the parameters like temperature and chemical potentials are constant in time but vary throughout the system. We may, for example, conceive of a system composed of three parts: two large regions which act as "reservoirs" under different thermodynamic conditions and a small connecting region through which steady-state fluxes take place. In this case the $\dot{\beta}_i$ referring to the small sub-system are zero

by virtue of the steady fluxes, and the $\dot{\beta}_i$ referring to the reservoirs are zero because of the large size of the reservoirs. The a_i of the reservoirs will steadily change. In this situation the interesting relationships are between those a_i characterizing the sub-system and the driving "temperatures" of the reservoirs. Thus we require the time τ over which the difference quotients are calculated to be at least small enough that essentially steady conditions exist over it.

This treatment in terms of difference quotients is analogous to earlier derivations.[2] It is perhaps just as realistic, however, to identify the thermodynamic coefficients with genuine time-derivatives $\partial\langle\dot{a}_i\rangle_{\mathrm{av}}/\partial\beta_k$ evaluated not at t_0 but at a time $t_0+\tau$, where τ satisfies the above restrictions; these quantities, of course, have the same symmetry properties as the difference quotients. This second viewpoint makes clearer the manner in which the nonequilibrium ensemble gives a continued description of the thermodynamic process.

It is sometimes desirable to express the Onsager coefficients as functions of an external magnetic field. We have previously assumed a closed system, but it is nevertheless easy to treat this slightly more general case. We need only remember that if the sources of the field were included within the system, the field would change its direction under reflections of the time axis, and the Hamiltonian would be invariant under the reflection. Hence if we consider the field as external, we must reverse it whenever it would be reversed if its sources were considered internal. The modified Onsager relations are then

$$L_{ik}(\mathbf{H})=L_{ki}(-\mathbf{H})\epsilon_i\epsilon_k. \tag{21}$$

IV. DISCUSSION

In thermodynamics we are in the habit of distinguishing between the "thermodynamic system" and its "surroundings," including possible "reservoirs." In many arguments, foremost among them those leading to the establishment of the Second Law, it is useful to shift one's point of view, to regard a certain accumulation of matter alternately as part of the "system" or as a driving reservoir. It is to be expected that a similar elasticity of approach would serve well in statistical mechanics. In the foregoing discussion, however, we have dealt exclusively with the development of systems that from a time t_0 onward are thermally isolated; hence we have been forced to include possible reservoirs as parts of the composite system. This approach can never lead to a rigorously stationary process, because any reservoir of finite size in a nonequilibrium process will undergo secular changes. If the theory is to be capable of describing stationary nonequilibrium processes, we must introduce idealized reservoirs of infinite size; that step implies that the reservoir must be treated as distinct from the thermodynamic system proper.

On the other hand, the interaction of the reservoir with the system is stochastic, both because of the stochastic nature of the system ensemble and because of the molecular structure of the reservoir or reservoirs. We are planning to address ourselves to this problem and hope to arrive eventually at a realistic statistical-mechanical description of the stationary process. Such a description should yield the Onsager relations in a thoroughly satisfactory manner, without restrictions on the choice of the time constant τ in Eqs. (18) and (20).

Exchange Scattering in a Three-Body Problem*

HARRY E. MOSES
Mathematics Research Group, New York University, New York, New York
(Received February 13, 1953)

It is proved that in the three-body scattering problem, the prototype of which is the scattering of an electron by a hydrogen atom, the coefficient corresponding to exchange scattering behaves like a radially outgoing wave. The essential conjecture used by Mott and Massey in their treatment of the problem is thus verified.

1. INTRODUCTION

We shall consider the problem of the scattering of an electron by a hydrogen atom the nucleus of which is considered to be infinitely heavy. We shall take the case where the electrons are considered identifiable. Furthermore, since we do not wish to discuss convergence difficulties arising from the fact that Coulomb forces die out slowly, we shall replace the Coulomb interactions by shorter-range interactions.

Mott and Massey[1] treat this problem. They obtain an equation for the eigenfunction of the total Hamiltonian by expanding this eigenfunction, insofar as it is a function of the coordinate of the electron of the hydrogen atom, in terms of the eigenfunctions of the hydrogen Hamiltonian, and impose suitable conditions on the coefficients of this expansion. In their treatment of exchange scattering they use this same eigenfunction of the total Hamiltonian, re-expand it, this time insofar as it is a function of the coordinate of the scattered electron, in terms of the eigenfunctions of the hydrogen Hamiltonian. Mott and Massey then assume certain conditions on the coefficient of the second expansion. It is our purpose to show in which sense their assumption is correct. We now proceed to discuss the assumption explicitly.

Let us denote by the subscript 1 the electron which is scattered and by the subscript 2 the electron of the hydrogen atom. Then the Hamiltonian for the problem is the following:

$$H(\mathbf{x}_1, \mathbf{x}_2)=T(\mathbf{x}_1)+H_{\mathrm{H}}(\mathbf{x}_2)+V(\mathbf{x}_1, \mathbf{x}_2)+V(\mathbf{x}_1). \quad (1)$$

The operator $T(\mathbf{x})$ is the kinetic-energy Hamiltonian for a particle of mass m:

$$T(\mathbf{x})=-(1/2m)\nabla^2. \quad (2)$$

The operator $H_{\mathrm{H}}(\mathbf{x})$ is the hydrogenic Hamiltonian which we take as

$$H_{\mathrm{H}}(\mathbf{x})=T(\mathbf{x})+V(\mathbf{x}). \quad (3)$$

$V(\mathbf{x})$ is the interaction of an electron with the nucleus, and $V(\mathbf{x}_1, \mathbf{x}_2)$ is the interaction of the two electrons with each other. These interactions take the place of the usual Coulomb interactions.

In the above expressions we have taken $\hbar=1$ and have designated the three coordinates collectively of the first electron by the vector $\mathbf{x}_1$ and those of the second electron by $\mathbf{x}_2$.

We are interested in eigenfunctions of the total Hamiltonian $H(\mathbf{x}_1, \mathbf{x}_2)$ which describe a situation which corresponds to the condition that before collision the atom have the energy E_a and that the energy of the incident electron be $E-E_a$. We shall denote this eigenstate by $\psi(\mathbf{x}_1, \mathbf{x}_2|E, E_a)$. The total energy initially is thus E. Since the energy of the system is a constant, the total energy of the system at any time is E also, so that $\psi(\mathbf{x}_1, \mathbf{x}_2|E, E_a)$ is an eigenfunction of the total Hamiltonian $H(\mathbf{x}_1, \mathbf{x}_2)$ corresponding to the eigenvalue E; i.e.,

$$H(\mathbf{x}_1, \mathbf{x}_2)\psi(\mathbf{x}_1, \mathbf{x}_2|E, E_a)=E\psi(\mathbf{x}_1\mathbf{x}_2|E, E_a). \quad (4)$$

To specify the boundary conditions on $\psi(\mathbf{x}_1, \mathbf{x}_2|E, E_a)$ corresponding to the initial condition, we introduce the eigenfunctions of $T(\mathbf{x})$ and $H_{\mathrm{H}}(\mathbf{x})$.

Let us designate the eigenfunctions of $T(\mathbf{x})$ associated with the energy E by $\chi(\mathbf{x}|E)$; then

$$T(\mathbf{x})\chi(\mathbf{x}|E)=E\chi(\mathbf{x}|E), \quad (5)$$

where E is in a continuum whose values range from 0 to $+\infty$. Furthermore, let us denote the eigenfunctions of $H_{\mathrm{H}}(\mathbf{x})$ associated with the energy E by $\phi(\mathbf{x}|E)$. Thus

$$H_{\mathrm{H}}(\mathbf{x})\phi(\mathbf{x}|E)=E\phi(\mathbf{x}|E). \quad (6)$$

The argument E of $\phi(\mathbf{x}|E)$ has discrete values for $E<0$ and lies in the continuum for $0<E<+\infty$. We shall call the lowest of the discrete eigenvalues E_g (g indicates "ground" state).

Mott and Massey expand $\psi(\mathbf{x}_1, \mathbf{x}_2|E, E_a)$ in terms of the eigenfunctions $\phi(\mathbf{x}_2|E)$, as follows:

$$\psi(\mathbf{x}_1, \mathbf{x}_2|E, E_a)=\int_{E_g}^{\infty} F(\mathbf{x}_1|E, E_a|E')\phi(\mathbf{x}_2|E')dE', \quad (7)$$

where the integration is to be understood as a summation over values of E' belonging to the discrete spectrum of H_{H}.

The functions $F(\mathbf{x}_1|E, E_a|E')$ have the significance

* This work was performed at Washington Square College of Arts and Science, New York University, and was supported in part by contract with the U. S. Air Force through sponsorship of the Geophysics Research Directorate of the Air Force Cambridge Research Center, Air Research and Development Command.

[1] N. F. Mott and H. S. W. Massey, *The Theory of Atomic Collisions* (Clarendon Press, Oxford, 1949), Chap. VIII, Secs. 2–4.

that $|F(\mathbf{x}_1|E, E_a|E')|^2$ is the probability density of finding electron 1 at $\mathbf{x}_1$ when electron 2 is in the state $\phi(\mathbf{x}_2|E')$ and when the entire system has the energy E. Mott and Massey prescribe that the asymptotic form of $F(\mathbf{x}|E, E_a|E')$ shall be as follows when $|\mathbf{x}_1|\to\infty$:

$$F(\mathbf{x}_1|E, E_a|E')\to\delta(E'-E_a)\chi(\mathbf{x}_1|E-E_a) + \frac{e^{i|\mathbf{p}'||\mathbf{x}_1|}}{|\mathbf{x}_1|}f(\theta), \quad (8)$$

where $\delta(E'-E_a)$ is to be taken as a Kronecker δ if both E' and E_a are in the discrete spectrum of H_{H}, as a Dirac δ if both are in the continuous spectrum of H_{H}, and as zero otherwise. Also

$$|\mathbf{p}'|=[2m(E-E')]^{\frac{1}{2}}. \quad (9)$$

This boundary condition corresponds to the condition which we want, namely that before collision the atom be in the state of energy E_a and the incident particle have the kinetic energy $E-E_a$. After collision there is to be a flux of outgoing electrons.

Mott and Massey's conjecture is that if we use the expansion

$$\psi(\mathbf{x}_1, \mathbf{x}_2|E, E_a)=\int G(\mathbf{x}_2|E, E_a|E')\phi(\mathbf{x}_1|E')dE', \quad (10)$$

instead of expansion (7), then $G(\mathbf{x}_2|E, E_a|E')$ will behave like

$$\frac{e^{i|\mathbf{p}'||\mathbf{x}_2|}}{|\mathbf{x}_2|}g(\theta)$$

for $|\mathbf{x}_2|\to\infty$. That is, having prescribed $\psi(\mathbf{x}_1, \mathbf{x}_2|E, E_a)$ by imposing boundary condition (8) with respect to $\mathbf{x}_1$, we assume that the outgoing wave condition on $\mathbf{x}_2$ can be proved.

The significance of $G(\mathbf{x}_2|E, E_a|E')$ is that $|G(\mathbf{x}_2|\times E, E_a|E')|^2$ is the probability density that the second electron is at $\mathbf{x}_2$ when the first electron has been captured by the hydrogen atom and is in the state $\phi(\mathbf{x}_1|E')$. Since initially the first electron was free and the second electron was part of the hydrogen atom, whereas after collision $|G(\mathbf{x}_2|E, E_a|E')|^2$ for $|\mathbf{x}_1|\to\infty$ gives the probability that the first is part of the hydrogen atom and the second is free, $|G(\mathbf{x}_2|E, E_a|E')|^2$ is called the "exchange probability."

In the following section we proceed to show in what sense Mott and Massey's conjecture is valid.

2. MORE EXPLICIT DISCUSSION OF THE EIGENFUNCTIONS

In order to prove the conjecture we must be more explicit as to the nature of the eigenfunctions involved. In particular, we shall have to take into account the auxiliary variables, which together with the Hamiltonian form a complete set of commuting variables. First let us consider the eigenfunctions of the kinetic energy operator $T(\mathbf{x})$. Usually the three momentum components are taken as the complete set of commuting variables. For our purpose, however, we shall take as the complete set of commuting variables the energy and the polar angles of the momentum θ, ω. In terms of these variables we write the eigenfunctions of $T(\mathbf{x})$ corresponding to the energy eigenvalue E as

$$\chi(\mathbf{x}|E, \theta, \omega)=(2\pi)^{-\frac{3}{2}}(2m^3E)^{\frac{1}{4}}(\sin\theta)^{\frac{1}{2}}e^{i(\mathbf{px})}. \quad (11)$$

Here $(\mathbf{px})$ is the inner product of the momentum vector $\mathbf{p}$ and the coordinate vector $\mathbf{x}$. In the right hand side of (11) we replace p_x, p_y, p_z by $(2mE)^{\frac{1}{2}}\sin\theta\cos\omega$, $(2mE)^{\frac{1}{2}}\sin\theta\sin\omega$, and $(2mE)^{\frac{1}{2}}\cos\theta$, respectively. The eigenfunctions as chosen above satisfy the normalization conditions:

$$\int\bar{\chi}(\mathbf{x}|E, \theta, \omega)\chi(\mathbf{x}|E', \theta', \omega')d\mathbf{x} =\delta(E-E')\delta(\theta-\theta')\delta(\omega-\omega'), \quad (12)$$

$$\int_0^\infty\int_0^\pi\int_0^{2\pi}\bar{\chi}(\mathbf{x}|E, \theta, \omega)\chi(\mathbf{x}'|E, \theta, \omega)d\omega d\theta dE =\delta(\mathbf{x}-\mathbf{x}').$$

For simplicity we shall denote the angular variables θ, ω collectively by the variable α, so that the orthonormality conditions (12) become

$$\int\bar{\chi}(\mathbf{x}|E, \alpha)\chi(\mathbf{x}|E', \alpha')d\mathbf{x}=\delta(E-E')\delta(\alpha-\alpha'), \quad (12a)$$

$$\int_0^\infty\int\bar{\chi}(\mathbf{x}|E, \alpha)\chi(\mathbf{x}'|E, \alpha)d\alpha dE=\delta(\mathbf{x}-\mathbf{x}'),$$

where we write

$$\chi(\mathbf{x}|E, \alpha)\equiv\chi(\mathbf{x}|E, \theta, \omega). \quad (13)$$

The bar means the complex conjugate.

Let us now consider the eigenfunctions of $H_{\mathrm{H}}(\mathbf{x})=T(\mathbf{x})+V(\mathbf{x})$ and for the moment restrict ourselves to the continuous spectrum. If we assume that $V(\mathbf{x})$ dies sufficiently rapidly, we may write the eigenfunctions of $H_{\mathrm{H}}(\mathbf{x})$ belonging to the continuous spectrum as the sum of an "incident wave" which is an eigenfunction of $T(\mathbf{x})$ and a "scattered wave." We shall prescribe the boundary condition that the scattered wave shall be a radially outgoing wave. This condition is the one which will enable us to prove the conjecture. Mott and Massey are not explicit as to the nature of the eigenfunctions of H_{H} in the continuous spectrum. The ones we choose are the natural ones to use. In the expansions (7) and (10) for F and G we shall have to use eigenfunctions of H_{H} with these boundary conditions.

Now as auxiliary variables we shall take the polar angles which describe the incident wave. The eigenfunctions of H_{H} belonging to the eigenvalue E for

$E>0$ satisfy the following integral equation:

$$\phi(\mathbf{x}|E,\theta,\omega)=\chi(\mathbf{x}|E,\theta,\omega)-\frac{m}{2\pi}\int\frac{e^{i|\mathbf{p}'||\mathbf{x}-\mathbf{x}'|}}{|\mathbf{x}-\mathbf{x}'|}V(\mathbf{x}')\phi(\mathbf{x}'|E,\theta,\omega)d\mathbf{x}', \quad (14)$$

where $|\mathbf{p}'|=(2mE)^{\frac{1}{2}}$. If, as before, we denote collectively the polar variables θ,ω by α we have

$$\phi(\mathbf{x}|E,\alpha)=\chi(\mathbf{x}|E,\alpha)-\frac{m}{2\pi}\int\frac{e^{i|\mathbf{p}'||\mathbf{x}-\mathbf{x}'|}}{|\mathbf{x}-\mathbf{x}'|}V(\mathbf{x}')\phi(\mathbf{x}'|E,\alpha)d\mathbf{x}', \quad (14a)$$

where $|\mathbf{p}'|=(2mE)^{\frac{1}{2}}$.

For the discrete spectrum, i.e., for $E<0$, we may choose any convenient set of auxiliary variables: for example, we might choose the total angular momentum if $V(\mathbf{x})$ is spherically symmetric. Denoting these auxiliary variables by α, as above, but keeping in mind that α may be quantum numbers of an entirely different character than the α used for $E>0$, we have as the integral equation for $E<0$

$$\phi(\mathbf{x}|E,\alpha)=-\frac{m}{2\pi}\int\frac{e^{i|\mathbf{p}'||\mathbf{x}-\mathbf{x}'|}}{|\mathbf{x}-\mathbf{x}'|}V(\mathbf{x}')\phi(\mathbf{x}'|E,\alpha)d\mathbf{x}', \quad (15)$$

where $|\mathbf{p}'|=(2mE)^{\frac{1}{2}}$. Note that since E is negative, $|\mathbf{p}'|$ is imaginary, and hence that $\phi(\mathbf{x}|E,\alpha)$ decays exponentially for $|\mathbf{x}|\to\infty$, as required. We can combine (14a) and (15) as follows:

$$\phi(\mathbf{x}|E,\alpha)=\eta(E)\chi(\mathbf{x}|E,\alpha)-\frac{m}{2\pi}\int\frac{e^{i|\mathbf{p}'||\mathbf{x}-\mathbf{x}'|}}{|\mathbf{x}-\mathbf{x}'|}V(\mathbf{x}')\phi(\mathbf{x}'|E,\alpha)d\mathbf{x}', \quad (16)$$

where $|\mathbf{p}'|=(2mE)^{\frac{1}{2}}$, and where $\eta(E)$ is a step function given by

$$\eta(E)=1, \quad E>0; \qquad \eta(E)=0, \quad E<0. \quad (17)$$

These functions satisfy the orthonormality relations:

$$\int\tilde{\phi}(\mathbf{x}|E,\alpha)\phi(\mathbf{x}|E',\alpha')d\mathbf{x}=\delta(E-E')\delta(\alpha,\alpha'),$$
$$\int\int\tilde{\phi}(\mathbf{x}|E,\alpha)\phi(\mathbf{x}'|E,\alpha)d\alpha dE=\delta(\mathbf{x}-\mathbf{x}'), \quad (18)$$

where one has to use care in interpreting $\delta(\alpha,\alpha')$ or equivalently the integration over α, since α may change character for $E>0$ or $E<0$. The function $\delta(E-E')$ is to be interpreted as a Kronecker δ if the arguments belong to the discrete spectrum.

The following, our notational convention is: Generally we shall denote eigenvalues of energy operators by capital Roman letters and eigenvalues corresponding to the auxiliary variables by small Greek letters. The range and nature of the eigenvalues are to be read off from the way in which they appear in the various eigenfunctions. We shall not hesitate to relabel the eigenvalues where necessary to prevent confusion, especially in integrations where they appear as dummy variables.

Now let us consider the eigenfunctions of the total Hamiltonian H which we previously denoted by $\psi(\mathbf{x}_1,\mathbf{x}_2|E,E_a)$. We must now also indicate the dependence of the eigenfunction on the direction of the incident electron, which we shall call α_a, and on the initial auxiliary quantum number of the hydrogenic atom, which we call β_a. We shall now denote this eigenfunction by $\psi(\mathbf{x}_1,\mathbf{x}_2|E,E_a,\alpha_a,\beta_a)$. We write the expansion (7) as

$$\psi(\mathbf{x}_1,\mathbf{x}_2|E,E_a,\alpha_a,\beta_a)=\int_{E_0}^{\infty}\int F(\mathbf{x}_1|E,E_a,\alpha_a,\beta_a|E',\beta')\times\varphi(\mathbf{x}_2|E',\beta')d\beta'dE'. \quad (19)$$

In Eq. (19) and everywhere below, integrations over variables which belong to the discrete spectrum are to be replaced by summations. We impose the condition that for $|\mathbf{x}_1|\to\infty$, $F(\mathbf{x}_1|E,E_a,\alpha_a,\beta_a|E',\beta')$ shall be the sum of an incident wave,

$$\delta(E'-E_a)\delta(\beta-\beta_a)\chi(\mathbf{x}_1|E-E_a,\alpha_a),$$

and a radially outgoing wave. Substituting (19) into (4) and using the orthonormality conditions on $\phi(\mathbf{x}|E,\beta)$ one obtains the following integral equation for F which satisfies the boundary conditions:

$$F(\mathbf{x}_1|E,E_a,\alpha_a,\beta_a|E',\beta')=\delta(E'-E_a)\delta(\beta'-\beta_a)\times\chi(\mathbf{x}_1|E-E_a,\alpha_a)-\frac{m}{2\pi}\int\int\frac{e^{i|\mathbf{p}'||\mathbf{x}_1-\mathbf{x}_1'|}}{|\mathbf{x}_1-\mathbf{x}_1'|}\times[V(\mathbf{x}_1')+V(\mathbf{x}_1',\mathbf{x}_2')]\tilde{\phi}(\mathbf{x}_2'|E',\beta')\times\psi(\mathbf{x}_1,\mathbf{x}_2|E,E_a,\alpha_a,\beta_a)d\mathbf{x}_1'd\mathbf{x}_2', \quad (20)$$

with $|\mathbf{p}'|=[2m(E-E')]^{\frac{1}{2}}$, which, when substituted into (19), gives us the integral equation for ψ:

$$\psi(\mathbf{x}_1,\mathbf{x}_2|E,E_a,\alpha_a,\beta_a)=\chi(\mathbf{x}_1|E-E_a,\alpha_a)\phi(\mathbf{x}_2|E_a,\beta_a)-\frac{m}{2\pi}\int_{E_0}^{\infty}\int\int\int\frac{e^{i|\mathbf{p}'||\mathbf{x}_1-\mathbf{x}_1'|}}{|\mathbf{x}_1-\mathbf{x}_1'|}\times\phi(\mathbf{x}_2|E',\beta')\tilde{\phi}(\mathbf{x}_2'|E',\beta')[V(\mathbf{x}_1')+V(\mathbf{x}_1',\mathbf{x}_2')]\times\psi(\mathbf{x}_1',\mathbf{x}_2'|E,E_a,\alpha_a,\beta_a)d\mathbf{x}_1'd\mathbf{x}_2'd\beta'dE', \quad (21)$$

with $|\mathbf{p}'|=[2m(E-E')]^{\frac{1}{2}}$.

We shall discuss eigenfunctions of two more Hamiltonians which will be useful. The Hamiltonian H_0 is

defined by

$$H_0(\mathbf{x}_1, \mathbf{x}_2) = T(\mathbf{x}_1) + H_H(\mathbf{x}_2). \tag{22}$$

The incident term of the integral equation (21) is an eigenfunction of H_0 corresponding to the eigenvalue E. We note that

$$H(\mathbf{x}_1, \mathbf{x}_2) = H_0(\mathbf{x}_1, \mathbf{x}_2) + V(\mathbf{x}_1) + V(\mathbf{x}_1, \mathbf{x}_2), \tag{23}$$

hence (21) gives the eigenfunction of H in terms of a Green's function of $(E-H_0)$, where $V(\mathbf{x}_1)+V(\mathbf{x}_1, \mathbf{x}_2)$ is considered a perturbation. We shall denote the eigenfunction of $H_0(\mathbf{x}_1, \mathbf{x}_2)$ corresponding to the eigenvalue E, by $\lambda(\mathbf{x}_1, \mathbf{x}_2 | E, E', \alpha, \beta)$, where

$$\lambda(\mathbf{x}_1, \mathbf{x}_2 | E, E', \alpha, \beta) = \chi(\mathbf{x}_1 | E-E', \alpha)\phi(\mathbf{x}_2 | E', \beta). \tag{24}$$

The eigenfunction $\lambda(\mathbf{x}_1, \mathbf{x}_2 | E, E', \alpha, \beta)$ is an eigenfunction corresponding to the situation where the first electron is in the free state $\chi(\mathbf{x}_1 | E-E', \alpha)$ and the second is in the hydrogenic state $\phi(\mathbf{x}_2 | E', \beta)$. From the orthonormality conditions on ϕ and χ we have

$$\begin{aligned}
&\int\int \bar{\lambda}(\mathbf{x}_1, \mathbf{x}_2 | E, E', \alpha, \beta)\lambda(\mathbf{x}_1, \mathbf{x}_2 | \bar{E}, \bar{E}', \bar{\alpha}, \bar{\beta}) d\mathbf{x}_1 d\mathbf{x}_2 \\
&\qquad = \delta(E-\bar{E})\delta(E'-\bar{E}')\delta(\alpha-\bar{\alpha})\delta(\beta-\bar{\beta}), \\
&\int_{E_g}^{\infty}\int_{E'}^{\infty}\int\int \bar{\lambda}(\mathbf{x}_1, \mathbf{x}_2 | E, E', \alpha, \beta) \\
&\qquad \times \lambda(\mathbf{x}_1', \mathbf{x}_2' | E, E', \alpha, \beta) d\alpha d\beta dE dE' \\
&\qquad = \delta(\mathbf{x}_1-\mathbf{x}_1')\delta(\mathbf{x}_2-\mathbf{x}_2').
\end{aligned} \tag{25}$$

Integrations with respect to E have the limits from E' to $+\infty$. Integrations with respect to E' range from E_g to ∞. Thus the order of integration is important: one must integrate over E first. The last Hamiltonian which we shall introduce is $H_1(\mathbf{x}_1, \mathbf{x}_2)$, which is just $H_0(\mathbf{x}_1, \mathbf{x}_2)$ with the first and second particles interchanged:

$$H_1(\mathbf{x}_1, \mathbf{x}_2) = H_0(\mathbf{x}_2, \mathbf{x}_1). \tag{26}$$

The eigenfunctions of H_1 corresponding to the eigenvalue E are given by

$$\begin{aligned}
\mu(\mathbf{x}_1, \mathbf{x}_2 | E, E', \alpha, \beta) &= \lambda(\mathbf{x}_2, \mathbf{x}_1 | E, E', \alpha, \beta) \\
&= \chi(\mathbf{x}_2 | E-E', \alpha)\phi(\mathbf{x}_1 | E', \beta).
\end{aligned} \tag{27}$$

The eigenfunction $\mu(\mathbf{x}_1, \mathbf{x}_2 | E, E', \alpha, \beta)$ is the state vector corresponding to the first electron's being in the hydrogenic state $\phi(\mathbf{x}_1 | E', \beta)$ and the second electron's being the state $\chi(\mathbf{x}_2 | E-E', \alpha)$. The orthonormality relations for μ are analogous to those for λ.

3. METHOD OF PROOF

The function $G(\mathbf{x}_2 | E, E_a | E')$, which we now call $G(\mathbf{x}_2 | E, E_a, \alpha_a, \beta_a | E', \beta')$, is defined by the alternative expansion (10), which we now write as

$$\begin{aligned}
&\psi(\mathbf{x}_1, \mathbf{x}_2 | E, E_a, \alpha_a, \beta_a) \\
&\qquad = \int_{E_g}^{\infty}\int G(\mathbf{x}_2 | E, E_a, \alpha_a, \beta_a | E', \beta') \\
&\qquad\qquad \times \phi(\mathbf{x}_1 | E', \beta') d\beta' dE'.
\end{aligned} \tag{28}$$

Using the orthogonality relations (18) for ϕ we have

$$\begin{aligned}
&G(\mathbf{x}_2 | E, E_a, \alpha_a, \beta_a | E', \beta') \\
&\qquad = \int \psi(\mathbf{x}_1, \mathbf{x}_2 | E, E_a, \alpha_a, \beta_a)\bar{\phi}(\mathbf{x}_1 | E', \beta') d\mathbf{x}.
\end{aligned} \tag{29}$$

To show that G is an outgoing spherical wave in $\mathbf{x}_2$ we shall use the integral equations (21) for ψ. However, to isolate the outgoing part, it is convenient to work in the H_1 representation since the outgoing part will be recognizable in this representation as a δ_+ function.

Let us denote ψ in the H_1 representation by $r(F, G, \gamma, \epsilon | E, E_a, \alpha_a, \beta_a)$, which is given by

$$\begin{aligned}
r(F, G, \gamma, \epsilon | E, E_a, \alpha_a, \beta_a) &= \int\int \psi(\mathbf{x}_1, \mathbf{x}_2 | E, E_a, \alpha_a, \beta_a) \\
&\qquad \times \bar{\mu}(\mathbf{x}_1, \mathbf{x}_2 | F, G, \gamma, \epsilon) d\mathbf{x}_1 d\mathbf{x}_2,
\end{aligned} \tag{30}$$

μ being the eigenfunction of H_1. Using the orthogonality relations (18), (12) for ϕ and χ and the expression (27) for μ, we see that (29) is equivalent to

$$\begin{aligned}
&G(\mathbf{x}_2 | E, E_a, \alpha_a, \beta_a | E', \beta') \\
&\qquad = \int_{E'}^{\infty}\int r(F, E', \gamma, \beta' | E, E_a, \alpha_a, \beta_a) \\
&\qquad\qquad \times \chi(\mathbf{x}_2 | F-E', \gamma) d\gamma dF.
\end{aligned} \tag{31}$$

We shall calculate r in terms of ψ as given in the H_0-representation. Denoting ψ in the H_0 by $u(F, G, \gamma, \epsilon | E, E_a, \alpha_a, \beta_a)$, where

$$\begin{aligned}
&u(F, G, \gamma, \epsilon | E, E_a, \alpha_a, \beta_a) \\
&\qquad = \int\int \psi(\mathbf{x}_1, \mathbf{x}_2 | E, E_a, \alpha_a, \beta_a) \\
&\qquad\qquad \times \bar{\lambda}(\mathbf{x}_1, \mathbf{x}_2 | F, G, \gamma, \epsilon) d\mathbf{x}_1 d\mathbf{x}_2,
\end{aligned} \tag{32}$$

we have, on using (30), (27) and (25) together with orthogonality relations for ϕ and χ:

$$\begin{aligned}
&r(F, G, \gamma, \epsilon | E, E_a, \alpha_a, \beta_a) \\
&\qquad = \int_{E_g}^{\infty}\int_{G'}^{\infty}\int\int u(F', G', \gamma', \epsilon' | E, E_a, \alpha_a, \beta_a) \\
&\qquad \times v(F-G, \gamma | G', \epsilon')\bar{v}(F'-G', \gamma' | G, \epsilon) \\
&\qquad\qquad \times d\gamma' d\epsilon' dF' dG',
\end{aligned} \tag{33}$$

where

$$v(E,\alpha|F,\beta)=\int\tilde{\chi}(\mathbf{x}|E,\alpha)\phi(\mathbf{x}|F,\beta)d\mathbf{x};\quad(34)$$

$v(E,\alpha|F,\beta)$ is thus the eigenfunction ϕ of H_{H} as given in the representation of the kinetic energy operator T. We shall use the integral equations for u and v to obtain the outgoing parts and finally use (33) and (31) to get the expression for G.

4. THE EQUATIONS FOR u AND v

We shall first show that $u(F,G,\gamma,\epsilon|E,E_a,\alpha_a,\beta_a)$ satisfies the relation

$$\begin{aligned}u(F,G,\gamma,\epsilon|E,E_a,\alpha_a,\beta_a)&=\delta(F-E)\delta(G-E_a)\delta(\gamma-\alpha_a)\delta(\epsilon-\beta_a)\\&\quad+\gamma_-(E-F)T(F,G,\gamma,\epsilon|E,E_a,\alpha_a,\beta_a),\end{aligned}\quad(35)$$

where

$$\begin{aligned}T(F,G,\gamma,\epsilon|E,E_a,\alpha_a,\beta_a)&=\int\int\tilde{\chi}(\mathbf{x}_1|F-G,\gamma)\tilde{\phi}(\mathbf{x}_2|G,\epsilon)[V(\mathbf{x}_1)+V(\mathbf{x}_1,\mathbf{x}_2)]\\&\quad\times\psi(\mathbf{x}_1,\mathbf{x}_2|E,E_a,\alpha_a,\beta_a)d\mathbf{x}_1d\mathbf{x}_2,\end{aligned}\quad(36)$$

and where $\gamma_-(\zeta)$ is essentially the δ_+ function; it is defined by

$$\gamma_-(\zeta)=\lim_{\xi\to+0}\frac{1}{\zeta+i\xi}=-i\pi\delta(\zeta)+\mathrm{P}\frac{1}{\zeta},\quad(37)$$

where P indicates that in integrations over ζ, the principal part of the integral is to be used. It might be noted that in accordance with the general formalism of scattering operators, $T(E,G,\gamma,\epsilon|E,E_a,\alpha_a,\beta_a)$ is the amplitude of the scattered spherical wave obtained when one sets $|\mathbf{x}_1|\to\infty$ in the integral equation for ψ [Eq. (21)]. This scattered wave corresponds to the case where after scattering the hydrogen atom is in the state described by the quantum numbers G, γ, and the incident electron has the direction ϵ.

Incidentally, one can write (35) as an equation for u, namely

$$\begin{aligned}u(F,G,\gamma,\epsilon|E,E_a,\alpha_a,\beta|)&=\delta(F-E)\delta(G-E_a)\delta(\gamma-\alpha_a)\delta(\epsilon-\beta_a)\\&\quad+\gamma_-(E-F)[V(x_1)+V(\mathbf{x}_1,\mathbf{x}_2)]^{H_0}\\&\quad\times u(F,G,\gamma,\epsilon|E,E_a,\alpha_a,\beta_a),\end{aligned}\quad(35a)$$

where $[V(\mathbf{x}_1)+V(\mathbf{x}_1,\mathbf{x}_2)]^{H_0}$ is the operator $V(\mathbf{x}_1)+V(\mathbf{x}_1,\mathbf{x}_2)$ as given in the H_0 representation; it operates on the variables F,G,γ,ϵ of

$$u(F,G,\gamma,\epsilon|E,E_a,\alpha_a,\beta_a),$$

on the right-hand side of (35a). Equation (35a) can be made the basis of a discussion of the scattering problem in terms of the scattering operator (see, e.g., Moses[2]).

[2] H. E. Moses (to be published).

The proof of (35) involves the following well-known identity:

$$\begin{aligned}&\int_0^\infty\int_0^\pi\int_0^{2\pi}\tilde{\chi}(\mathbf{x}|E,\theta,\omega)\gamma_-(F-E)\chi(\mathbf{x}'|E,\theta,\omega)d\omega d\theta dE\\&\quad=\int_0^\infty\int_0^\pi\int_0^{2\pi}\tilde{\chi}(\mathbf{x}'|E,\theta,\omega)\gamma_-(F-E)\\&\quad\times\chi(x|E,\theta,\omega)d\omega d\theta dE=-\frac{m}{2\pi}\frac{e^{i|\mathbf{p}||\mathbf{x}-\mathbf{x}'|}}{|\mathbf{x}-\mathbf{x}'|},\end{aligned}\quad(38)$$

where $|\mathbf{p}|=(2mF)^{\frac{1}{2}}$.

The verification of (35) is obtained by replacing ψ in Eq. (32) by the right-hand side of (21). Using the identity (38), we replace

$$-\frac{m}{2\pi}\frac{e^{i|\mathbf{p}'||\mathbf{x}_1-\mathbf{x}_1'|}}{|\mathbf{x}_1-\mathbf{x}_1'|},\quad\text{with}\quad|\mathbf{p}'|=[2m(E-E')]^{\frac{1}{2}},$$

by

$$\begin{aligned}&\int_0^\infty\int\tilde{\chi}(\mathbf{x}_1'|F',\alpha')\gamma_-(E-E'-F')\chi(\mathbf{x}_1|F',\alpha')d\alpha'dF'\\&\quad=\int_{E'}^\infty\int\tilde{\chi}(\mathbf{x}_1'|F'-E',\alpha')\gamma_-(E-F')\\&\quad\times\chi(\mathbf{x}_1|F'-E',\alpha')d\alpha'dF'.\end{aligned}$$

We then have

$$\begin{aligned}u(F,G,\gamma,\epsilon|E,E_a,\alpha_a,\beta_a)&=\int\int\lambda(\mathbf{x}_1,\mathbf{x}_2|E,E_a,\alpha_a,\beta_a)\\&\quad\times\tilde{\lambda}(\mathbf{x}_1,\mathbf{x}_2|F,G,\gamma,\epsilon)d\mathbf{x}_1d\mathbf{x}_2+\int d\mathbf{x}_1'\int d\mathbf{x}_2'\int_{E_g}^\infty dE'\\&\quad\times\int_{E'}^\infty dF'\int d\beta'\int d\alpha'\tilde{\chi}(\mathbf{x}_1'|F'-E',\alpha')\tilde{\phi}(\mathbf{x}_2'|E',\beta')\\&\quad\times\gamma_-(E-F')[V(\mathbf{x}_1')+V(\mathbf{x}_1',\mathbf{x}_2')]\\&\quad\times\psi(\mathbf{x}_1',\mathbf{x}_2'|E,E_a,\alpha_a,\beta_a)\\&\quad\times\left[\int d\mathbf{x}_1\chi(\mathbf{x}_1|F'-E',\alpha')\tilde{\chi}(\mathbf{x}_1|F-G,\gamma)\right]\\&\quad\times\left[\int d\mathbf{x}_2\phi(\mathbf{x}_2|E',\beta')\tilde{\phi}(\mathbf{x}_2|G,\epsilon)\right],\end{aligned}$$

which, on using the orthonormality conditions on ϕ, χ, λ, gives (35).

Similarly we find for v:

$$\begin{aligned}v(E,\alpha|F,\beta)&=\eta(F)\delta(E-F)\delta(\alpha-\beta)\\&\quad+\gamma_-(F-E)T_1(E,\alpha|F,\beta),\end{aligned}\quad(39)$$

where

$$T_1(E,\alpha|F,\beta)=\int\tilde{\chi}(\mathbf{x}|E,\alpha)V(\mathbf{x})\phi(\mathbf{x}|F,\beta)d\mathbf{x}.\quad(40)$$

5. THE EVALUATION OF $r(F, G, \gamma, \epsilon | E, E_a, \alpha_a, \beta_a)$

We shall obtain r in several steps; in each step it will be our objective to isolate a γ_- function, since this function in the $\mathbf{x}$ representation is the radially outgoing wave. We shall first indicate several useful identities for γ_-. First, from (37) we have

$$\bar{\gamma}_-(\zeta) = -\gamma_-(-\zeta). \tag{41}$$

It can also be shown that

$$\gamma_-(\zeta_1)\gamma_-(\zeta_2) = \gamma_-(\zeta_1)\gamma_-(\zeta_1+\zeta_2) + \gamma_-(\zeta_2)\gamma_-(\zeta_1+\zeta_2). \tag{42}$$

On using (41) we see that (42) can be written as

$$\bar{\gamma}_-(\zeta_1)\gamma_-(\zeta_2) = \bar{\gamma}_-(\zeta_1)\gamma_-(\zeta_2-\zeta_1) + \gamma_-(\zeta_2)\bar{\gamma}_-(\zeta_1-\zeta_2). \tag{43}$$

In expression (33) we note that the product $v(F-G, \gamma|G', \epsilon')\bar{v}(F'-G', \gamma'|G, \epsilon)$ appears. We shall use the identity (43) and Eq. (39) for v to isolate a γ_- function.

From (39) we obtain immediately

$$\begin{aligned} v(E, \alpha|F, \beta)\bar{v}(E', \alpha'|F', \beta') &= \eta(F)\eta(F') \\ &\times\delta(E-F)\delta(E'-F')\delta(\alpha-\beta)\delta(\alpha'-\beta') \\ &+\eta(F)\delta(E-F)\delta(\alpha-\beta)\bar{\gamma}_-(F'-E')\bar{T}_1(E', \alpha'|F', \beta') \\ &+\eta(F')\delta(E'-F')\delta(\alpha'-\beta')\gamma_-(F-E)T_1(E, \alpha|F, \beta) \\ &+\bar{\gamma}_-(F'-E')\gamma_-(F-E)T_1(E, \alpha|F, \beta) \\ &\times\bar{T}_1(E', \alpha'|F', \beta'). \end{aligned} \tag{44}$$

We shall simplify the last term of (44). Using (43), we have

$$\bar{\gamma}_-(F'-E')\gamma_-(F-E) = \bar{\gamma}_-(F'-E')\gamma_-(F-E-F'+E') + \gamma_-(F-E)\bar{\gamma}_-(F'-E'-F+E). \tag{45}$$

Hence the last term of (44) is

$$\begin{aligned} &\bar{\gamma}_-(F'-E')\bar{T}_1(E', \alpha'|F', \beta')\gamma_-(F-E-F'+E') \\ &\times T_1(E, \alpha|F, \beta) + \gamma_-(F-E)T_1(E, \alpha|F, \beta) \\ &\times\bar{\gamma}_-(F'-E'-F+E)\bar{T}_1(E', \alpha'|F', \beta') \\ &= \bar{v}(E', \alpha'|F', \beta')\gamma_-(F-E-F'+E')T_1(E, \alpha|F, \beta) \\ &-\eta(F')\delta(E'-F')\delta(\alpha'-\beta')\gamma_-(F-E-F'+E') \\ &\times T_1(E, \alpha|F, \beta) + v(E, \alpha|F, \beta)\bar{\gamma}_-(F'-E'-F+E) \\ &\times\bar{T}_1(E', \alpha'|F', \beta') - \eta(F)\delta(E-F)\delta(\alpha-\beta) \\ &\times\bar{\gamma}_-(F'-E'-F+E)\bar{T}_1(E', \alpha'|F', \beta'), \end{aligned} \tag{46}$$

where we have used (39) to obtain $\gamma_- T_1$ in terms of v. Now the second and fourth terms on the right-hand side of (46) are just the negatives of the third and fourth terms on the right-hand side of Eq. (44). Hence, substituting the last term of (44) as given by (46), we have

$$\begin{aligned} v(E, \alpha|F, \beta)\bar{v}(E', \alpha'|F', \beta') &= \eta(F)\eta(F') \\ &\times\delta(E-F)\delta(E'-F')\delta(\alpha-\beta)\delta(\alpha'-\beta') \\ &+\gamma_-(F-E-F'+E')[\bar{v}(E', \alpha'|F', \beta')T_1(E, \alpha|F, \beta) \\ &-v(E, \alpha|F, \beta)\bar{T}_1(E', \alpha'|F', \beta')], \end{aligned} \tag{47}$$

from which we obtain finally

$$\begin{aligned} v(F-G, \gamma|G', \epsilon')\bar{v}(F'-G', \gamma'|G, \epsilon) &= \eta(G')\eta(G) \\ &\times\delta(F-F')\delta(F-G-G')\delta(\gamma-\epsilon')\delta(\gamma'-\epsilon) \\ &+\gamma_-(F'-F)[\bar{v}(F'-G', \gamma'|G, \epsilon)T_1(F-G, \gamma|G', \epsilon') \\ &-v(F-G, \gamma|G', \epsilon')\bar{T}_1(F'-G', \gamma'|G, \epsilon)]. \end{aligned} \tag{48}$$

In (48) we have achieved our aim of isolating a γ_- function.

To evaluate

$$\begin{aligned} &r(F, G, \gamma, \epsilon|E, E_a, \alpha_a, \beta_a) \\ &= \int_{E_g}^{\infty}\int_{G'}^{\infty}\int\int u(F', G', \gamma', \epsilon'|E, E_a, \alpha_a, \beta_a) \\ &\times v(F-G, \gamma|G', \epsilon')\bar{v}(F'-G', \gamma'|G, \epsilon)d\gamma' d\epsilon' dF' dG', \end{aligned}$$

we use expression (48) for the product of $v\,\bar{v}$, and for u we use equation (35). We obtain four terms as we did when we evaluated the product $v\,\bar{v}$. It turns out that by using (42) for the products of the γ_-'s of the fourth term one can eliminate two of the terms in a manner analogous to the derivation of (47). We have, finally,

$$\begin{aligned} r(F, G, \gamma, \epsilon|E, E_a, \alpha_a, \beta_a) &= \eta(G)\eta(E_a)\delta(F-E) \\ &\times\delta(F-G-E_a)\delta(\epsilon-\alpha_a)\delta(\gamma-\beta_a) + \gamma_-(E-F) \\ &\times\Big\{\int_{E_g}^{\infty}\int_{G'}^{\infty}\int\int v(F-G, \gamma|G', \epsilon')\bar{v}(F'-G', \gamma'|G, \epsilon) \\ &\times T(F', G', \gamma', \epsilon'|E, E_a, \alpha_a, \beta_a)d\gamma' d\epsilon' dF' dG' \\ &+\int_{E_g}^{\infty}\int_{G'}^{\infty}\int\int \bar{v}(F'-G', \gamma'|G, \epsilon)T_1(F-G, \gamma|G', \epsilon') \\ &\times u(F', G', \gamma', \epsilon'|E, E_a, \alpha_a, \beta_a)d\gamma' d\epsilon' dF' dG' \\ &-\int_{E_g}^{\infty}\int_{G'}^{\infty}\int\int v(F-G, \gamma|G', \epsilon')\bar{T}_1(F'-G', \gamma'|G, \epsilon) \\ &\times u(F', G', \gamma', \epsilon'|E, E_a, \alpha_a, \beta_a)d\gamma' d\epsilon' dF' dG'\Big\}. \end{aligned} \tag{49}$$

Now, using the definition (34), (40), (32), (36) for v, T_1 and u, T, respectively, and the orthonormality properties for χ and ϕ, one obtains

$$\begin{aligned} &\int_{E_g}^{\infty}\int_{G'}^{\infty}\int\int v(F-G, \gamma|G', \epsilon')\bar{v}(F'-G', \gamma'|G, \epsilon) \\ &\times T(F', G', \gamma', \epsilon'|E, E_a, \alpha_a, \beta_a)d\gamma' d\epsilon' dF' dG' \\ &= \int\int\bar{\chi}(\mathbf{x}_2|F-G, \gamma)\bar{\phi}(\mathbf{x}_1|G, \epsilon)[V(\mathbf{x}_1) \\ &+V(\mathbf{x}_1, \mathbf{x}_2)]\psi(\mathbf{x}_1, \mathbf{x}_2|E, E_a, \alpha_a, \beta_a)d\mathbf{x}_1 d\mathbf{x}_2, \end{aligned} \tag{50}$$

$$\int_{E_g}^{\infty}\int_{G'}^{\infty}\int\int \bar{v}(F'-G',\gamma'|G,\epsilon)T_1(F-G,\gamma|G',\epsilon')$$
$$\times u(F',G',\gamma',\epsilon'|E,E_a,\alpha_a,\beta_a)d\gamma' d\epsilon' dF' dG'$$
$$=\int\int \bar{\chi}(\mathbf{x}_2|F-G,\gamma)\bar{\phi}(\mathbf{x}_1|G,\epsilon)V(\mathbf{x}_2)$$
$$\times\psi(\mathbf{x}_1,\mathbf{x}_2|E,E_a,\alpha_a,\beta_a)d\mathbf{x}_1 d\mathbf{x}_2, \quad (51)$$

and

$$\int_{E_g}^{\infty}\int_{G'}^{\infty}\int\int v(F-G,\gamma|G',\epsilon')\bar{T}_1(F'-G',\gamma'|G,\epsilon)$$
$$\times u(F',G',\gamma',\epsilon'|E,E_a,\alpha_a,\beta_a)d\gamma' d\epsilon' dF' dG'$$
$$=\int\int \bar{\chi}(\mathbf{x}_2|F-G,\gamma)\bar{\phi}(\mathbf{x}_1|G,\epsilon)V(\mathbf{x}_1)$$
$$\times\psi(\mathbf{x}_1,\mathbf{x}_2|E,E_a,\alpha_a,\beta_a)d\mathbf{x}_1 d\mathbf{x}_2. \quad (52)$$

Hence we have finally

$$r(F,G,\gamma,\epsilon|E,E_a,\alpha_a,\beta_a)=\eta(G)\eta(E_a)$$
$$\times\delta(F-E)\delta(F-G-E_a)\delta(\epsilon-\alpha_a)\delta(\gamma-\beta_a)$$
$$+\gamma_-(E-F)\int\int \bar{\chi}(\mathbf{x}_2|F-G,\gamma)\bar{\phi}(\mathbf{x}_1|G,\epsilon)[V(\mathbf{x}_1,\mathbf{x}_2)$$
$$+V(\mathbf{x}_2)]\psi(\mathbf{x}_1,\mathbf{x}_2|E,E_a,\alpha_a,\beta_a)d\mathbf{x}_1 d\mathbf{x}_2. \quad (53)$$

Equation (53) can be written as an equation for

$$r(F,G,\gamma,\epsilon|E,E_a,\alpha_a,\beta_a),$$

as follows:

$$r(F,G,\gamma,\epsilon|E,E_a,\alpha_a,\beta_a)=\eta(G)\eta(E_a)\delta(F-E)$$
$$\times\delta(F-G-E_a)\delta(\epsilon-\alpha_a)\delta(\gamma-\beta_a)$$
$$+\gamma_-(E-F)[V(\mathbf{x}_1,\mathbf{x}_2)+V(\mathbf{x}_2)]^{H_1}$$
$$\times r(F,G,\gamma,\epsilon|E,E_a,\alpha_a,\beta_a), \quad (53a)$$

where $[V(\mathbf{x}_1,\mathbf{x}_2)+V(\mathbf{x}_2)]^{H_1}$ is the operator $V(\mathbf{x}_1,\mathbf{x}_2)+V(\mathbf{x}_2)$ as given in the H_1 representation; it operates on the F, G, γ, ϵ variables of r on the right-hand side of (53a). Equations (21), (35a), and (53a) are the integral equations for the same eigenfunction of H in the $\mathbf{x}$, H_0, and H_1 representations, respectively.

6. THE EVALUATION OF $G(\mathbf{x}_2|E,E_a,\alpha_a,\beta_a|E',\beta')$

Using Eq. (31) which gives G in terms of r, we have

$$G(\mathbf{x}_2|E,E_a,\alpha_a,\beta_a|E',\beta')=\eta(E')\eta(E_a)$$
$$\times\chi(\mathbf{x}_2|E-E',\beta_a)\delta(E-E'-E_a)\delta(\alpha_a-\beta')$$
$$+\int\int\Big[\int_{E'}^{\infty}\int\chi(\mathbf{x}_2|F-E',\gamma)\gamma_-(E-F)$$
$$\times\bar{\chi}(\mathbf{x}_2'|F-E',\gamma)d\gamma dF\Big]\bar{\phi}(\mathbf{x}_1'|E',\beta')[V(\mathbf{x}_1',\mathbf{x}_2)$$
$$+V(\mathbf{x}_2')]\psi(\mathbf{x}_1',\mathbf{x}_2'|E,E_a,\alpha_a,\beta_a)d\mathbf{x}_1' d\mathbf{x}_2'.$$

Now we use (38) to obtain

$$\int_{E'}^{\infty}\int\chi(\mathbf{x}_2|F-E',\gamma)\gamma_-(E-F)\bar{\chi}(\mathbf{x}_2'|F-E',\gamma)d\gamma dF$$
$$=\int_0^{\infty}\int\chi(\mathbf{x}_2|F,\gamma)\gamma_-(E-E'-F)\bar{\chi}(\mathbf{x}_2'|F,\gamma)d\gamma dF$$
$$=-\frac{m}{2\pi}\frac{e^{i|\mathbf{p}'||\mathbf{x}_2-\mathbf{x}_2'|}}{|\mathbf{x}_2-\mathbf{x}_2'|}, \quad (54)$$

where $|\mathbf{p}'|=[2m(E-E')]^{\frac{1}{2}}$. Finally, our generalization of Mott and Massey's conjecture is

$$G(\mathbf{x}_2|E,E_a,\alpha_a,\beta_a|E',\beta')=\eta(E')\eta(E_a)$$
$$\times\chi(\mathbf{x}_2|E_a,\beta_a)\delta(E-E'-E_a)\delta(\alpha_a-\beta')$$
$$-\frac{m}{2\pi}\int\int\frac{e^{i|\mathbf{p}'||\mathbf{x}_2-\mathbf{x}_2'|}}{|\mathbf{x}_2-\mathbf{x}_2'|}\bar{\phi}(\mathbf{x}_1'|E',\beta')[V(\mathbf{x}_1',\mathbf{x}_2')$$
$$+V(\mathbf{x}_2')]\psi(\mathbf{x}_1',\mathbf{x}_2'|E,E_a,\alpha_a,\beta_a)d\mathbf{x}_1' d\mathbf{x}_2'. \quad (55)$$

where $|\mathbf{p}'|=[2m(E-E')]^{\frac{1}{2}}$.

It is clear that the second term represents outgoing spherical waves. In Mott and Massey's conjecture the first term is ignored. If the initial state of the hydrogen atom is such that the electron is bound, then $E_a<0$ and hence the first term vanishes for all E', β'. Even if initially the hydrogen atom is in an ionized state, the first term vanishes for $E'<0$, i.e., for exchange scattering where the incident electron is captured.

Borowitz and Friedman[3] point out that the integral of the second term diverges for $E'>0$. This is not surprising because G is a symbolic function in the sense of L. Schwartz. That is, G contains a part resembling δ-function. This is clear from the fact that the first term contains a δ-function. This statement can also be shown to be true on more fundamental grounds which we shall not discuss here.

Borowitz and Friedman extract the symbolic part of this integral and are left with a convergent part. We prefer to consider a wave packet of incident electrons and hydrogenic atoms as being given initially. The initial state would then be

$$\int_{E_g}^{\infty}\int_{E_a}^{\infty}\int\int\lambda(\mathbf{x}_1,\mathbf{x}_2|E,E_a,\alpha_a,\beta_a)$$
$$\times f(E,E_a,\alpha_a,\beta_a)d\alpha_a d\beta_a dE dE_a,$$

while at any finite time the state is given by

$$\int_{E_g}^{\infty}\int_{E_a}^{\infty}\int\int\psi(\mathbf{x}_1,\mathbf{x}_2|E,E_a,\alpha_a,\beta_a)$$
$$\times f(E,E_a,\alpha_a,\beta_a)d\alpha_a d\beta_a dE dE_a,$$

where we take $f(E,E_a,\alpha_a,\beta_a)$ to be a quadrically in-

[3] S. Borowitz and B. Friedman, Phys. Rev. **89**, 441 (1953).

tegrable function of its arguments. Then

$$\int_{E_0}^{\infty}\int_{E_a}^{\infty}\int\int G(\mathbf{x}_2|E, E_a, \alpha_a, \beta_a|E', \beta') \times f(E, E_a, \alpha_a, \beta_a)d\alpha_a d\beta_a dE dE_a,$$

is a well-defined function of $\mathbf{x}_2$ and is the probability amplitude for exchange scattering.

Some generalizations of the above expressions are possible, for although we have assumed that $V(\mathbf{x})$, $V(\mathbf{x}_1, \mathbf{x}_2)$ are simply functions of their arguments, our results can be generalized to take into account the possibility that $V(\mathbf{x})$, $V(\mathbf{x}_1, \mathbf{x}_2)$ are operators. The generalization can be obtained immediately, but we refrain from giving it here explicitly.

It should be pointed out that the Mott and Massey's $F_n(\mathbf{r})$, $G_n(\mathbf{r})$, $\psi(\mathbf{r}_1, \mathbf{r}_2)$ are not quite our functions F, G, and ψ. They are related as follows:

$$F_n(\mathbf{r}) = (2\pi)^{\frac{1}{2}}[2m^3(E-E_a)]^{-\frac{1}{4}} \times \sin^{-\frac{1}{2}}\theta_a F(\mathbf{x}|E, E_a, \alpha_a, \beta_a|E', \beta'),$$

$$\psi(\mathbf{r}_1, \mathbf{r}_2) = (2\pi)^{\frac{1}{2}}[2m^3(E-E_a)]^{-\frac{1}{4}} \times \sin^{-\frac{1}{2}}\theta_a \psi(\mathbf{x}_1, \mathbf{x}_2|E, E_a, \alpha_a, \beta_a)$$

$$G_n(\mathbf{r}) = (2\pi)^{\frac{1}{2}}[2m^3(E-E_a)]^{-\frac{1}{4}} \times \sin^{-\frac{1}{2}}\theta_a G(\mathbf{x}|E, E_a, \alpha_a, \beta_a|E', \beta'),$$

where the quantum number n corresponds to the pair of quantum numbers E', β', and α_a represents the pair of polar angles θ_a, ω_a of the incident electron. Also, the vector $\mathbf{r}$ is just our vector, $\mathbf{x}$.

One could also expand $\Psi(\mathbf{x}_1, \mathbf{x}_2|E, E_a, \alpha_a, \beta_a)$ as follows:

$$\Psi(\mathbf{x}_1, \mathbf{x}_2|E, E_a, \alpha_a, \beta_a) = \int\int D(\mathbf{x}_1|E, E_a, \alpha_a, \beta_a|E', \beta') \times \chi(\mathbf{x}_2|E', \beta')d\beta' dE'. \quad (56)$$

Here $D(\mathbf{x}_1|E, E_a, \alpha_a, \beta_a|E', \beta')$ represents the probability amplitude that the incident electron has the position $\mathbf{x}_1$ when the second electron has the definite energy E' and direction β', i.e., where the second electron has a definite momentum. It can be shown by an analysis similar to that used for exchange scattering that

$$D(\mathbf{x}_1|E, E_a, \alpha_a, \beta_a|E', \beta') = \eta(E_a)\chi(\mathbf{x}_1|E-E_a, \alpha_a)\delta(E'-E_a)\delta(\beta', \beta_a) - \frac{m}{2\pi}\int\int \frac{e^{i|\mathbf{p}'||\mathbf{x}_1-\mathbf{x}_1'|}}{|\mathbf{x}_1-\mathbf{x}_1'|}\tilde{\chi}(\mathbf{x}_2'|E', \beta') \times \Psi(\mathbf{x}_1', \mathbf{x}_2'|E, E_a, \alpha_a, \beta_a)d\mathbf{x}_1' d\mathbf{x}_2'. \quad (57)$$

with $|\mathbf{p}'| = [2m(E-E')]^{\frac{1}{2}}$. Hence, except for an incident term, $D(\mathbf{x}_1|E, E_a, \alpha_a, \beta_a|E', \beta')$ is an outgoing spherical wave in $|\mathbf{x}_1|$. The amplitude of this spherical wave as $|\mathbf{x}_1| \to \infty$ can be used to calculate cross sections describing the scattering of the first particle when the second electron has a definite momentum.

Letters to the Editor

PUBLICATION of brief reports of important discoveries in physics may be secured by addressing them to this department. The closing date for this department is five weeks prior to the date of issue. No proof will be sent to the authors. The Board of Editors does not hold itself responsible for the opinions expressed by the correspondents. Communications should not exceed 600 words in length and should be submitted in duplicate.

Diffusion of Lithium into Germanium and Silicon

C. S. FULLER AND J. A. DITZENBERGER
Bell Telephone Laboratories, Murray Hill, New Jersey
(Received May 7, 1953)

THE diffusion of lithium into p type single crystals of germanium and silicon[1] has been measured at temperatures between 450 and 1000°C by the pn junction method previously described.[2] The experiments were carried out by heating metallic lithium[3] on the surfaces of specimens of germanium and silicon (0.125 cm thick) in a helium atmosphere. Hemispherical n type regions of low resistivity were observed to form, showing that lithium not only diffuses rapidly at the temperatures employed but also acts as a strong donor in germanium[4] and silicon.

The diffusivity D and the surface concentration C_0 of Li in Ge and Si were calculated by means of Eqs. (1) and (2) given in reference 1. Corrections were introduced for the change in mobility with impurity concentration.[5] The assumption was also made that each Li atom contributes one conduction electron.

The equations $D=13\times10^{-4}\exp(-10\,700/RT)$ and $D=94\times10^{-4}\exp(-18\,100/RT)$ were found to describe the dependence of diffusivity of Li in Ge and Si, respectively, for the temperature range studied, where D is given in cm²/sec and $R=1.98$ calories. The maximum errors in the activation energies are estimated as ±1000 calories for Ge and ±3000 calories for Si. These results

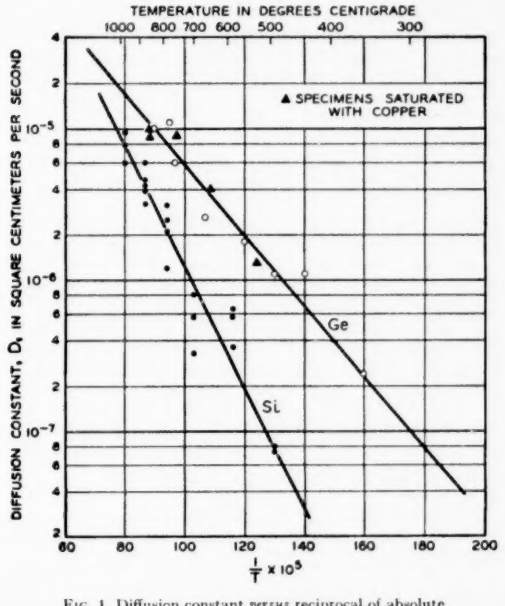
TEMPERATURE IN DEGREES CENTIGRADE
1000 800 700 600 500 400 300
▲ SPECIMENS SATURATED WITH COPPER
Ge
Si
DIFFUSION CONSTANT, D, IN SQUARE CENTIMETERS PER SECOND
60 80 100 120 140 160 180 200
1/T x 10⁵

FIG. 1. Diffusion constant *versus* reciprocal of absolute temperature for Li in Ge and Si.

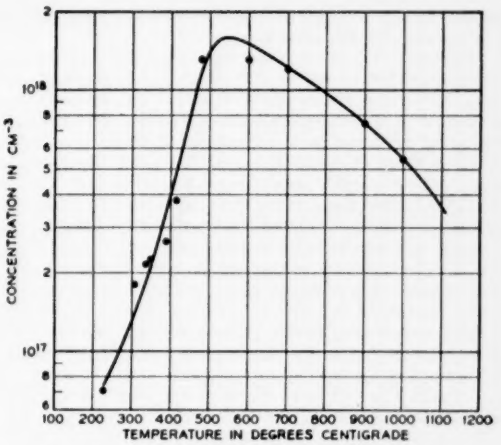

FIG. 2. Solubility of Li in Si as a function of temperature.

are shown in Fig. 1, where D is plotted against reciprocal of mean effective absolute temperature.[6]

Inasmuch as copper is also known to diffuse rapidly into germanium and silicon[7] several specimens of germanium (see Fig. 1) were diffused in the presence of copper. No appreciable effect on the results was evident.

Calculated values of C_0 range from 6.1×10^{16} to 1.4×10^{18} cm^{-3} for Li in Ge and from 2.0×10^{17} to 8.0×10^{18} for Li in Si, but they are subject to large error. Determinations of the solubility of Li in Si have been made by measuring the change in resistivity upon saturation at a series of temperatures. These results are shown in Fig. 2. Similar measurements for Ge have not as yet been possible because of a rapid precipitation of Li at room temperature.

Resistivity and Hall measurements[8] on Li doped Ge single crystals indicate a distribution coefficient between liquid and solid Ge for Li of greater than 0.01 and a donor level 0.01 ev below the conduction band. Precise determinations of distribution coefficient are difficult because of the precipitation previously mentioned.

[1] The authors are indebted to E. Buehler and G. K. Teal for supplying these crystals.
[2] C. S. Fuller, Phys. Rev. **86**, 136 (1952).
[3] Spectrographic analysis made at Bell Laboratories showed only Ca, K, and Na present to greater than 0.005 percent.
[4] It has been called to the authors' attention that W. C. Dunlap, Jr., and R. N. Hall at the General Electric Research Laboratory have independently reported lithium to act as a donor element in germanium.
[5] Haynes, Pearson, Debye, and Prince, unpublished data [Bull. Am. Phys. Soc. **28**, No. 2, 10 (1953)]; Esther M. Conwell, Proc. Inst. Radio Engrs. **40**, 1327 (1952).
[6] J. L. Ham, Trans. Am. Soc. Metals **31**, 849 (1943).
[7] C. S. Fuller and J. D. Struthers, Phys. Rev. **87**, 526 (1952).
[8] J. A. Burton and F. J. Morin, unpublished results.

The Mobility of Slow Electrons in Polar Crystals

FRANCIS E. LOW AND DAVID PINES
Department of Physics, University of Illinois, Urbana, Illinois
(Received May 13, 1953)

WE have calculated the mobility of slow electrons in polar crystals using the same basic approximation as in our calculation (with T. D. Lee) of the effective mass.[1] The mobility has previously been calculated by Fröhlich and Mott[2] using perturbation theory. The dimensionless constant α which measures the strength of the electron lattice interaction is, however, between 1 and 6 for typical polar crystals, whereas the validity of perturbation theory requires $\alpha<1$. The calculation of LLP for the effective mass was found to have considerable validity (~20

percent) for α as large as 6, so that we were encouraged to apply a similar method to this problem.

We describe the polaron (the electron plus its associated phonon cloud) by the same wave function as LLP, and calculate $1/\tau$, the probability per unit time that the polaron be scattered through an angle ϑ by the thermal phonons. We proceed by finding an equivalent Hamiltonian for transitions between bare polaron states, to which we apply the general scattering theory of Lippmann and Schwinger[3] using the approximation that over and above the bound phonons, the state vector contain at most one additional phonon. The transition probability (and thus the mobility) can then be found in closed form in terms of the roots of a fairly complicated transcendental equation. The calculation is enormously simplified provided $(P^2/2m^*)\ll\hbar\omega$, where P and m^* are the polaron momentum and mass, and ω is the frequency of the optical mode phonons. (This is the case for temperatures such that $kT\ll\hbar\omega$.) In this temperature range $1/\tau$ is essentially independent of the polaron momentum. It should be emphasized that results which apply in this range *cannot* be extrapolated to higher temperatures.

We state our results. The mobility u is given by

$$u=\frac{1}{2\alpha\omega}\frac{e}{m}\left(\frac{m}{m^*}\right)^2 f(\alpha)\exp(\hbar\omega/kT),$$

where m is the effective crystal mass of the electron (owing to its interaction with the periodic field of the lattice), $\alpha=(e^2/2\hbar c)\times(2mc^2/\hbar\omega)^{\frac{1}{2}}(1/n^2-1/\epsilon)$, m^* is the polaron effective mass [$m^*=m(1+\alpha/6)$ according to LLP], and $f(\alpha)$ is a slowly varying function of α which may be taken as 5/4 for $3<\alpha<6$. n^2 and ϵ are the high-frequency and low-frequency dielectric constants of the crystal. The perturbation theory limit of m^* is m, and that of $f(\alpha)$ is 1, so that in the limit of weak coupling our result reduces to the correct perturbation-theoretic value.[4]

Details will be described in a forthcoming paper. One of us (D.P.) would like to acknowledge the partial support of the Office of Ordnance Research, U. S. Army, during this work.

[1] Lee, Low, and Pines, Phys. Rev. **90**, 297 (1953), hereafter referred to as LLP.
[2] H. Fröhlich and N. F. Mott, Proc. Roy. Soc. (London) **A171**, 496 (1939). Some corrections to the original theory were made by Fröhlich, Pelzer, and Zienau, Phil. Mag. **41**, 221 (1950).
[3] B. A. Lippmann and J. Schwinger, Phys. Rev. **79**, 469 (1950).
[4] It should be noted that this perturbation-theory limiting value is smaller by a factor of 3 than that quoted by Fröhlich *et al.*, reference 2. Conyers Herring (private communication) was the first to point out that such a correction factor needs to be applied to the previously published perturbation-theoretic calculations.

Radiations of Neutron-Deficient Barium and Cesium Nuclides*

RICHARD W. FINK† AND EDWIN O. WIIG
Department of Chemistry, University of Rochester, Rochester, New York
(Received May 5, 1953)

IN the study of spallation reactions of cesium with high-energy protons, radiations of nuclides Ba^{128}, Ba^{129}, and Cs^{128} were investigated. Previously it has been reported[1] that 2.4±0.1-day Ba^{128} generates a 3.2-minute cesium daughter, accompanied by emission of 3-Mev positrons from the equilibrium mixture. Existence of 2.0-hour Ba^{129} with emission of positrons of unknown energy has also been reported,[2,3] with assignment by mass spectrograph.[2] Recently Lindner and Osborne[4] have reported that Ba^{128} decays purely by orbital-electron capture leading to a 3.8-minute Cs^{128} daughter which decays with emission of 3-Mev positrons. Wapstra *et al.*[5] have studied Cs^{128} and report gamma-rays of 455±5 kev in about 20 percent of the decays, and 980±30 kev present to about 2 percent of the intensity of the 455-kev line.

We have measured the maximum positron energy of 2.0-hour Ba^{129} produced by irradiating CsCl with 60-Mev protons followed by chemical separation similar to that reported previously.[1] At this bombardment energy, the yield of Ba^{128} is extremely small while that of Ba^{129} is at a maximum. This eliminates masking due to the energetic positrons from Ba^{128}. A low-resolution beta-ray spectrometer indicated a maximum positron energy for Ba^{129} of 1.6±0.2 Mev, consistent with a total predicted positron decay energy of 1.8±0.3 Mev computed from the beta-decay systematics of Coryell.[6] These positrons decayed with a half-life of about 2 hours, so that their assignment to Ba^{129} is unequivocal. Conversion electrons of 0.13 Mev also were present in the decay of Ba^{129}. Conversion electrons of 0.24 Mev presumably were due to the presence of Ba^{133m}.

The equilibrium mixture Ba^{128}–Cs^{128} was studied by the method of coincidence absorption using two anthracene scintillation detectors with associated equipment having a measured resolving time of 0.23 microsecond. Coincidence absorption curves in aluminum indicate that there exists a lower-energy positron group which has a maximum energy of 1.1±0.7 Mev based on the range in aluminum and which is in coincidence with one or more gamma-rays. Since no positron-gamma-ray coincidences were observed from the 3-Mev group, the latter must proceed directly to the ground state of Xe^{128}. Computation from Coryell's systematics indicates a total Cs^{128}–Xe^{128} disintegration energy of 3.5±0.5 Mev, consistent with the maximum energy of 3.1±0.2 Mev observed. Lead absorption curves showed no gamma-rays of energy greater than 0.9 Mev. Conversion electrons of 0.2 Mev were observed on the spectrometer. The number of positrons exceeds the number of electrons by a factor of 3 or 4.

That Ba^{128} decays primarily if not entirely by electron capture has been shown by repurification experiments in which a fresh barium sample exhibited a growth due to positrons from daughter Cs^{128}. This growth curve had a t_{max} of about 30 minutes in agreement with that expected on the basis of a 2.4-day parent growing into a 3.2-minute daughter. A calculation from Coryell's systematics indicates that Ba^{128} should have insufficient decay energy for positron emission. Decay of the positron peak from a young sample of Cs^{128}, isolated carrier-free by leaching solid $BaCl_2\cdot H_2O$ with concentrated HCl-ethyl ether (5:1) mixture, was followed on the spectrometer. A half-life of 3.5±0.6 minutes was found.

To study the gamma-emission from Ba^{128}–Cs^{128} equilibrium mixture, a fresh barium sample mounted as $BaCrO_4$ from a bombardment of CsCl with 240-Mev protons on the Rochester 130-inch cyclotron was taken to Brookhaven National Laboratory,[7] where measurements were made by Mr. Alois Schardt using a gray-wedge scintillation spectrometer fitted with a NaI(Tl) crystal. Those gamma-ray lines assigned to the decay of Ba^{128}–Cs^{128} mixture are, in kev: 30 (K x-ray), 135±5 (strong), 285±10, 455±5, and 965±20 (weak). Weak lines at about 220 and 380 kev are attributed to the presence of a certain amount of Ba^{131}. The line at 135 kev is about three times as intense as that at 455 kev. The gray-wedge equipment was calibrated using a Na^{22} source.

Further work is required to establish the exact decay scheme of the Ba^{128}–Cs^{128} chain. No detailed work was done on gamma-gamma coincidences other than a survey with the gray-wedge instrument which demonstrated the existence of gamma-gamma coincidences, indicating a decay involving a gamma-ray cascade.

We wish to thank Professor Sidney W. Barnes, Mr. Kurt Enslein, and Mr. William Coombs of the Cyclotron Laboratory for assistance in bombardments and design of certain equipment used in this study.

* This work was performed under contract with the U. S. Atomic Energy Commission. Part of the data is taken from the Doctoral Thesis of R. W. Fink submitted in partial fullfilment of the requirements for the Ph.D. degree, January 20, 1953.
† U. S. Atomic Energy Commission Predoctoral Fellow in Physical Science, 1951–53.
[1] R. W. Fink and E. O. Wiig, J. Am. Chem. Soc. **73**, 2365 (1951).
[2] R. W. Fink and D. H. Templeton, J. Am. Chem. Soc. **72**, 2818 (1950).
[3] C. C. Thomas, Jr., and E. O. Wiig, J. Am. Chem. Soc. **72**, 2818 (1950).
[4] M. Lindner and R. N. Osborne, Phys. Rev. **88**, 1422 (1952).
[5] Wapstra, Verster, and Boelhouwer, Physica **19**, 138 (1953).
[6] C. D. Coryell, *Annual Reviews of Nuclear Science* (Annual Reviews, Inc., Stanford, 1953), Vol. II, p. 305.
[7] The hospitality of Brookhaven Laboratory was extended by Dr. G. Friedlander of the Department of Chemistry.

Two-Particle Potential from the Bethe-Salpeter Equation

WILHELM MACKE
Instituto de Física Teórica, Sao Paulo, Brazil
(Received April 24, 1953)

A NONRELATIVISTIC derivation of the two-particle potential between two fermions, due to interaction with a boson field, was outlined by Tamm[1] and Dancoff[2] and generalized by Lévy,[3] including higher-order terms in the interaction potential. Following Lévy's treatment, the interaction terms of higher order can be represented by nonrelativistic graphs, distinguishing in addition the sequence of transitions and intermediate states. In this treatment, it does not seem to be understandable why the strongly diverging vacuum graphs are not considered, although according to the derivation they should appear, because the influence of them on the energy denominators is such that they are not separable. Further it is impossible to recognize the other divergent parts of the graphs as terms of mass and charge renormalization. This is impossible because the relativistic invariance has been destroyed in the very beginning of the derivation of the one-time formalism. In these cases Lévy goes back to the Bethe-Salpeter formalism,[4] showing an approximate correspondence of the two formalisms in two special examples and presuming it for the whole.

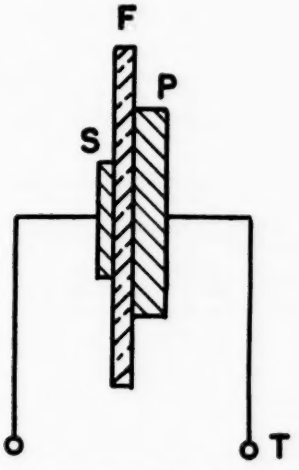

FIG. 1. Example of a Lévy graph with $n=2$ and $m=0$. The energy denominators are

$$\Delta E_1 = E^{(1)}(\mathbf{p}+\mathbf{k}_1)+E^{(1)}(\mathbf{p}+\mathbf{k}_1+\mathbf{k}_2)+\omega(\mathbf{k}_2),$$
$$\Delta E_2 = E^{(1)}(\mathbf{p})+E^{(1)}(\mathbf{p}+\mathbf{k}_1)+E^{(1)}(\mathbf{p}+\mathbf{k}_1+\mathbf{k}_2)+E^{(2)}(-\mathbf{p}-\mathbf{k}_2)-W,$$
$$\Delta E_3 = E^{(1)}(\mathbf{p}+\mathbf{k}_1+\mathbf{k}_2)+E^{(2)}(-\mathbf{p}-\mathbf{k}_2)+\omega(\mathbf{k}_2)-W.$$

To clear up this situation, a rigorous treatment of the two-particle potential was carried through, starting with the relativistic Bethe-Salpeter equation[4] and passing on from this to the one-time formalism. We give the results briefly here, whereas explicit calculations and results will be outlined in detail in an another place.[5] The results correspond to those of Lévy in those special cases he took into consideration. For the difference coordinates in momentum space the wave equation

$$[W-(m_1^2+\mathbf{p}^2)^{\frac{1}{2}}-(m_2^2+\mathbf{p}^2)^{\frac{1}{2}}]a(\mathbf{p})=-Va(\mathbf{p}') \qquad (1)$$

holds, where W is the total energy of the system, $-V$ is the operator of the interaction potential, and $a(\mathbf{p})$ is a four-component wave function, containing the spins of both particles. V is represented by the totality of all Feynman graphs with two fermion lines running from the left to the right (see Fig. 1), but without vacuum graphs. The right ends should not contain self-energy parts but run into the wave function $a(\mathbf{p}')$ of (1). The different graphs should be distinguished by the number of meson lines (n), the number of closed loops (m), and the different topologies τ which are possible with given n and m. Further, we have to distinguish the order of the $2n$ points where the meson lines end. In this way, every Feynman graph ($nm\tau$) consists of $(2n)!$ ordered graphs, built up by all permutations (π) of the points without alteration of the topology. Our interaction operator consists of the sum over all these graphs,

$$V=\Sigma V_{nm\tau\pi}, \qquad (2)$$

where for every term $V_{nm\tau\pi}$ there is an analytic representation of the general form

$$V_{nm\tau\pi}=(-1)^l\lambda^n\int\frac{d\mathbf{k}_1\cdots d\mathbf{k}_{n-m}d\mathbf{q}_1\cdots d\mathbf{q}_m}{2\omega_1\cdot 2\omega_2\cdots 2\omega_n}\cdot\frac{\Gamma_1\cdots\Gamma_{2n}}{\Delta E_1\cdots\Delta E_{2n-1}}. \qquad (3)$$

The meaning of the terms of this formula is

$$\lambda=g^2(2\pi)^{-3},\quad \omega_\nu=(\mu^2+\mathbf{k}_\nu^2)^{\frac{1}{2}},\quad \Delta E=E_{ex}-W, \qquad (4)$$

where g is the coupling constant of the meson field, and μ is the mesonic mass. Every point of the graph means a transition to another virtual state; E_{ex} is the energy of the virtual state and depends on the lines lying between the two points. If two fermion lines of such a virtual state are both in the initial state or in the final state, the energy of both is W (see Fig. 1). All other fermion lines give $E(\mathbf{p})=(m_{1,2}^2+\mathbf{p}^2)^{\frac{1}{2}}$, and the meson lines $\omega(k)=(\mu^2+\mathbf{k}^2)^{\frac{1}{2}}$. Graphs that contain a virtual state with only two fermion lines are to be cut out. The connection between the variables $\mathbf{p}_\nu$ and $\mathbf{k}_\nu$ is given by the graph in the usual way. The Γ's have the same meaning as in Lévy's paper.[3] The lines running backwards are related to negative energy states, the lines with normal direction are related to positive energy states. l in (3) is the number of lines running backwards.

If a graph contains no closed loop ($m=0$), the integrations go over all meson variables $d\mathbf{k}_\nu$. If it contains one closed loop ($m=1$), one variable $\mathbf{k}_\nu$ of the adjacent meson lines can be eliminated, because $\Sigma\mathbf{k}_\nu=0$ holds for those lines. But here the integration goes over the momenta $d\mathbf{q}$ of the particle in the closed loop. All other prescriptions remain unchanged. If the interaction takes place between different particles, every closed loop appears twice, once for m_1 and once for m_2.

By these results an exact description of the interaction operator V is given, being valid for all graphs and orders in the coupling constant. It gives the Tamm-Dancoff equation with the following exceptions: first, it does not contain the vacuum graphs, and second, the excitation energies E_{ex} differ in the case in which the two fermion lines are in the initial or final state. Further, this derivation gives us a direct possibility to carry through the renormalization of the remaining divergent parts; a paper on this matter is in preparation.

[1] J. Tamm, J. phys. (U.S.S.R.) **9**, 449 (1945).
[2] S. M. Dancoff, Phys. Rev. **78**, 382 (1950).
[3] M. Lévy, Phys. Rev. **88**, 72 (1952).
[4] E. E. Salpeter and H. A. Bethe, Phys. Rev. **84**, 1232 (1951).
[5] W. Macke, Z. Naturforsch. (to be published).

Hyperfine Structure of the Metastable Triplet State Helium-3†

GABRIEL WEINREICH* AND GERARD M. GROSOF,
Columbia University, New York, New York
AND
VERNON W. HUGHES, *University of Pennsylvania, Philadelphia, Pennsylvania*
(Received May 18, 1953)

AN experimental determination has been made of the hyperfine structure of the $^3S_1$ metastable state of helium-3. The atomic beam magnetic resonance method was used in a manner similar to that used in experiments on the magnetic moment of the same state in helium-4.[1]

A total of 3 cc NTP of He^3 was available. This was circulated continuously through the system by a mercury diffusion pump. Air leakage into the system was removed by the clean-up action of the aluminum electrodes in the discharge tube. Hydrogen generated within the system in small amounts was oxidized by CuO at a temperature around 500°C. Liquid air traps removed all condensibles.

The rf transition field was supplied by a rectangular cavity with two slits through which the beam entered and left. The cavity was driven in the TE_{101} mode by a Sperry 2K-44 klystron on a conventional regulated power supply, and further stabilized against frequency changes by an Automatic frequency control circuit. The cavity had a Q of about 1000. Major tuning was accomplished by moving a strip of Teflon inside the cavity to regions of weaker or stronger rf electric field. Since the width of the cavity response was considerably more than the width of observed lines, tuning the cavity in the course of a run was not necessary.

A copper loop located near one of the cavity slits served the dual purpose of a cavity monitor and a source of low-frequency magnetic fields when low-frequency resonances were observed.

Transitions $(F, m_F)=(\frac{3}{2}, -\frac{1}{2})\rightarrow(\frac{1}{2}, \frac{1}{2})$ and $(\frac{3}{2}, -\frac{3}{2})\rightarrow(\frac{1}{2}, -\frac{1}{2})$ were observed at fields of about 2/3 gauss. The ultimate accuracy of the measurement was limited by the inhomogeneity of the magnetic field. Line widths due to this were about 0.3 to 1 Mc/sec, depending on the field-dependence of the particular transition.

Our final result for the hyperfine splitting of the state is 6739.71 $\pm$0.05 Mc/sec. This is in agreement with a previous optical measurement[2] of 6630$\pm$150 Mc/sec.

The theoretical value of the hyperfine structure has not yet been computed to an accuracy comparable to the accuracy of the present experimental value. The principal contribution to the hfs due to a point dipole nucleus has been computed using a variationally determined electronic wave function which yields a value for the ionization potential of $^3S_1$ helium accurate to within 5 percent. The hfs splitting thus calculated is 6660 Mc/sec with an estimated accuracy of 5 percent.[3] There will be a relativistic correction of order α^2 which is similar in origin to the Breit correction to the hfs of one-electron atoms.[3] The principal radiative correction will be attributable to the anomalous magnetic moment of the electrons; in addition there will be radiative corrections of order α^2 due to polarization and fluctuation energy effects.[4] The effect of nuclear structure on the hfs is estimated in the accompanying letter to be $\sim$1.3 parts in 10^4.[5]

A more complete report is in preparation.

† Research supported in part by the U. S. Office of Naval Research.
* U. S. Atomic Energy Commission Predoctoral Fellow, 1952; now at Bell Telephone Laboratories, Murray Hill, New Jersey.
[1] V. Hughes and G. Tucker, Phys. Rev. **82**, 322 (1951); Tucker, Hughes, Rhoderick, and Weinreich, Phys. Rev. **86**, 618 (1952).
[2] Fred, Tomkins, Brody, and Hamermesh, Phys. Rev. **82**, 406 (1951). The accuracy figure for the theoretical calculation was kindly supplied as a private communication from M. Hamermesh.
[3] G. Breit, Phys. Rev. **35**, 1447 (1930).
[4] N. M. Kroll and F. Pollock, Phys. Rev. **86**, 876 (1952); R. Karplus and A. Klein, Phys. Rev. **85**, 972 (1952).
[5] A. M. Sessler and H. M. Foley reported a similar estimate at the 1953 Washington meeting of the American Physical Society [Bull. Am. Phys. Soc. **28**, No. 3, 20 (1953)].

Effect of Nuclear Structure on the Hyperfine Structure of He^3

VERNON HUGHES, *University of Pennsylvania, Philadelphia, Pennsylvania*
AND
GABRIEL WEINREICH,* *Columbia University, New York, New York*
(Received May 18, 1953)

THE hyperfine structure of the He^3 atom in its metastable $^3S_1$ state has been measured by the atomic beam magnetic resonance method with an accuracy which is adequate to reveal effects due to the internal structure of the He^3 nucleus.[1] An estimate of the influence of the nuclear structure will be given under the same assumptions as were made by Bohr for the hfs of deuterium.[2] When the electron is close to the nucleus it moves rapidly compared to the nucleon velocities and will therefore be bound to the two apparently stationary protons rather than to the center-of-mass of the He^3 nucleus. This approximation will be valid for distances of the electron from the nucleus which are less than

$$\rho\sim(\hbar/mc)mc^2/\bar{W}_N,$$

in which $\bar{W}_N$ is some mean nuclear excitation energy.[3] The quantity ρ will be larger than the nuclear radius and much smaller that the atomic radius. The contribution to the hfs from inside ρ must be calculated using a wave function with the electrons centered on the two protons; the contribution from outside ρ will be relatively insensitive to where the electrons are centered. When an electron is in the nucleus, the neutron magnetic moment will appear as a moment density distributed around the protons and hence its effect on the hfs will be reduced compared to that of a point magnetic dipole. This reduction is the principal effect of nuclear structure on the hfs. To our approximation the protons will have their spins antiparallel and hence will not contribute to the hfs.

The neutron-electron hfs interaction operator is given by

$$H_n=-e\boldsymbol{\alpha}^{(1)}\cdot\mathbf{A}^{(1)}-e\boldsymbol{\alpha}^{(2)}\cdot\mathbf{A}^{(2)},$$

in which $\boldsymbol{\alpha}^{(1)}$ and $\boldsymbol{\alpha}^{(2)}$ are Dirac matrices operating on electrons 1 and 2,

$$\mathbf{A}^{(1,2)}=-\boldsymbol{\mu}_n\times\nabla_{r_{1,2}}\frac{1}{|\mathbf{r}_{1,2}-\mathbf{R}|}.$$

$\boldsymbol{\mu}_n$ is the magnetic moment of the neutron, $\mathbf{r}_1$ and $\mathbf{r}_2$ are the position vectors of the electrons relative to the mid-point of the line joining the two protons, $\mathbf{R}$ is the position vector of the neutron relative to this same point. The neutron-electron hfs energy will be

$$\langle H_n\rangle=\int\phi^*(r_1, r_2)\chi^*(R)H_n\chi(R)\phi(r_1, r_2)d\tau_1 d\tau_2 d\tau_R,$$

in which $\phi(r_1, r_2)$ is the $^3S_1$ electronic wave function and χ is the nuclear wave function.

The nuclear wave function[4] used was $\chi=N\exp[-\frac{1}{2}\lambda(r_{np_1}+r_{np_2}+r_{p_1p_2})]$, in which λ is an adjustable parameter, r_{np_1} is the distance between the neutron and proton 1, and so on. The normalization factor N is given by $N=(4/7)^{\frac{1}{2}}\lambda^3$. The electronic wave function is actually a 16-component spinor, but the spinor parts of the wave function will play the same role as in the usual hfs calculation; and for the purpose of computing the fractional change in the hfs due to the nuclear structure, it is sufficient to take only a Schrödinger wave function. The spatial electronic wave function used was an antisymmetrized product of $Z=2$ hydrogenic wave functions for the configuration $1s2s$. The result of this calculation can be generalized easily to apply to an admixture of s configurations; however, in view of the other approximations being made and of the low accuracy to which the usual point dipole hfs has been calculated thus far for helium,[5] this extension was not made. A possibly useful wave function which involves the configurations $1sns$ ($n=2, 3, 4, 5, 6$) and which gives a calculated binding energy for $^3S_1$ helium which is within 0.2 percent of the experimental value is being reported.[6]

The integral to be evaluated for the $1s$ contribution to the hfs is of the form[3]

$$\int d\tau_1 u_1^*(1s)u_1(1s)\frac{1}{r_1^3}\left[\int_{R<r_1}\chi^*(R)\chi(R)d\tau_R\right].$$

The integral over the nuclear coordinates was done using Hylleraas variables, $s=r_{np_1}+r_{np_2}$, $t=r_{np_1}-r_{np_2}$, and $r_{p_1p_2}$, in terms of which $R=\frac{1}{2}(s^2+t^2-r_{p_1p_2}^2)^{\frac{1}{2}}$. This integration was only approximate, with an estimated error of $\pm$10 percent. The unwieldy results of the nuclear integration could then be integrated over the electron coordinates and the result expressed as the sum of two terms. One term gives the usual hfs due to a point dipole neutron, and the other involves the nuclear structure parameter

λ. The ratio of these two terms is

$$f=-5.7/\lambda a_0,$$

in which $a_0=0.529\times10^{-8}$ cm. The corresponding ratio for the ns contribution is the same.

The fractional decrease in the hfs of He^3 caused by the nuclear structure will be $(\mu_p/\mu_{He^3})f$. If the parameter λ is chosen so that the binding energy difference of 0.764 Mev between H^3 and He^3 is attributed to the electrostatic energy between the two protons in He^3, it is found that $\lambda=0.74\times10^{13}$ cm^{-1}. If the parameters of an exponential potential well are chosen to fit the two nucleon data and λ is chosen to give the highest binding energy for H^3, it is found that $\lambda=0.93\times10^{13}$ cm^{-1}. This value of λ yields a binding energy of 9.79 Mev for H^3 compared with the experimental value of 8.492 Mev.[4] Hence the uncertainty of the nuclear wave function limits the accuracy of this calculation.[7] For $\lambda=0.74\times10^{13}$ cm^{-1}, the fractional decrease in the He^3 hfs will be -1.3×10^{-4}, with an uncertainty of ±10 percent arising from the approximate integration.

This calculation has neglected nuclear motion effects,[3] admixture of D state in the nuclear wave function,[7] and exchange magnetic moments.[8]

It is a pleasure to thank Dr. Arnold Feingold and Mr. Andrew Sessler for helpful discussions.

[*] Now at Bell Telephone Laboratories, Murray Hill, New Jersey.
[1] G. Weinreich and V. Hughes, Phys. Rev. **90**, 377 (1953). See also the preceding letter [Phys. Rev. **91**, 195 (1953)].
[2] A. Bohr, Phys. Rev. **73**, 1109 (1948).
[3] F. Low, Phys. Rev. **77**, 361 (1950).
[4] J. Blatt and V. Weisskopf, *Theoretical Nuclear Physics* (John Wiley and Sons, Inc., New York, 1952).
[5] Fred, Tomkins, Brody, and Hamermesh, Phys. Rev. **82**, 406 (1951).
[6] W. Perl and V. Hughes, Phys. Rev. (to be published).
[7] R. L. Pease and H. Feshbach, Phys. Rev. **88**, 945 (1952).
[8] E. N. Adams, II, Phys. Rev. **81**, 1 (1951).

Angular Correlation in Allowed β-Transitions

M. E. Rose
Oak Ridge National Laboratory, Oak Ridge, Tennessee
(Received May 14, 1953)

THE purpose of the following is to examine the problem of deducing information concerning the β-interaction from β-recoil angular correlation experiments. We restrict our attention to allowed transitions. Then, in terms of well-established notation, the probability for emission of the β with energy W per dW and with angle ϑ between the β and neutrino, per $\sin\vartheta d\vartheta$, is

$$P(W)=\frac{g^2}{4\pi^3}pW(W_0-W)^2F(Z,W)|M|^2\left(1+\frac{ap}{W}\mu+\frac{b}{W}\right), \quad (1)$$

where $\mu=\cos\vartheta$, $|M|^2$ is the usual square matrix element weighted with the squares of the relative interaction coupling constants, and the constants b and a are defined elsewhere.[1]

Of course, the correlation in Θ, the angle between the β-particle and recoil nucleus, is the pertinent consideration. For β-particles of fixed energy this is

$$Q'(\Theta)=KP_0(W)J(\Theta,W)[1+af(\Theta,W)+b/W], \quad (2)$$

where $P_0=pW(W_0-W)^2F(Z,W)$ and K is a constant proportional to $g^2|M|^2$. In Eq. (2), $J(\Theta,W)$ is the Jacobian of the $\vartheta\to\Theta$ transformation and $f(\Theta,W)$ is $\mu p/W$ written in terms of the indicated variables.[2]

$$J(\Theta,W)=(1-\lambda^2\sin^2\Theta)^{-\frac{1}{2}}[-\epsilon\lambda\cos\Theta+(1-\lambda^2\sin^2\Theta)^{\frac{1}{2}}]^2, \quad (2a)$$

$$f(\Theta,W)=-(p/W)[\lambda\sin^2\Theta+\epsilon\cos\Theta(1-\lambda^2\sin^2\Theta)^{\frac{1}{2}}]. \quad (2b)$$

Here $\lambda=p/q$ and $\epsilon=1$ for $\lambda<1$ while for $\lambda>1$, $\epsilon=\pm1$ according as $\vartheta\lesseqgtr\vartheta_0=\arccos(-1/\lambda)$; in the subsequent integration over W the contributions of both $\epsilon=\pm1$ must be added in the range $p>q$, $W>(W_0^2+1)/2W_0$.

If one envisages an experiment in which only a very narrow band of β-energy is accepted, so that Eq. (2) applies, one cannot determine all the constants separately. Only Ka and $K(1+b/W)$ enter. If one considers pure Gamow-Teller transitions ($\Delta J=1$, He^6 for example) or pure Fermi transitions (say O^{14}), this implies that the ratio of coupling constants (C_A/C_T in the G-T case) is a double-valued function of a, and it would appear necessary to fix b within narrow limits to resolve the ambiguity.[3] However, this ambiguity is not at all present under the conditions of the experiment as it would presumably be carried out. Accepting a wide band of β-energies, one measures

$$Q(\Theta)=\int Q'(\Theta)dW. \quad (3)$$

This is of the form

$$Q(\Theta)=c_1A_1(\Theta)+c_2A_2(\Theta)+c_3A_3(\Theta),$$

where $c_1=K$, $c_2=Kb$, $c_3=Ka$, and the three functions A_i are *linearly independent* and well-defined. They would be obtained by numerical integration over the accepted band of W, except that in no case will energies greater than W_m contribute,

$$W_m=\sec^2\Theta[W_0-\sin\Theta(W_0^2-\cos^2\Theta)^{\frac{1}{2}}]. \quad (4)$$

The constants c_i are fixed from the data, by least squares for example, and then $a=c_3/c_1$. However, for pure G-T transitions a least-squares analysis should take into account the fact that the constants are not independent, but $c_1^2=c_2^2+9c_3^2$.

If one accepts the result of no Fierz interference[4] ($b=0$), the correlation experiment for a $\Delta J=0$ transition (other than $0\to0$) should give $-1<a<\frac{1}{3}$ for pure S and $\frac{1}{3}<a<1$ for pure V composition of the Fermi component. In addition, the value of a gives $C_F^2|\int1|^2/C_T^2|\int\boldsymbol{\sigma}|^2$. If one does not assume $C_SC_V=0$, then the c_i are independent for $\Delta J=0$ transitions and a determination of $|C_F\int1/C_T\int\boldsymbol{\sigma}|$ (for both $C_F=C_S$ and C_V) is possible in principle.

[1] S. R. de Groot and H. A. Tolhoek, Physica **16**, 456 (1950). Of course, the pseudoscalar term appearing in this reference makes no contribution here.
[2] These results appear in Reynolds, Biedenharn, and Beard, Oak Ridge National Laboratory Report ORNL-1444 (unpublished). Misprints occurring therein have here been corrected. As these authors point out, the singularity of the Jacobian is due to neglect of the finite mass of the recoil nucleus but, upon subsequent integration over W, this neglect introduces negligible error.
[3] O. Kofoed-Hansen and A. Winther, Phys. Rev. **89**, 526 (1953).
[4] J. Davidson and D. C. Peaslee (private communication). In this case $C_A=0$; see B. M. Rustad and S. L. Ruby, Phys. Rev. **89**, 880 (1953).

The Absolute Scintillation Efficiency of Anthracene

J. B. Birks and M. E. Szendrei
Physics Department, Rhodes University, Grahamstown, South Africa
(Received May 18, 1953)

MEASUREMENTS have been made of the absolute scintillation efficiency of single anthracene crystals at room temperature. The experimental method included the following observations:

(a) The transmission coefficient of a spectrophotelometer, of constant band width $d\lambda$, as a function of the wavelength λ.

(b) The relative spectral response of an EMI 6262 photomultiplier, using a standard lamp of known color temperature and the calibrated spectrophotelometer.

(c) Reduction of the intensity of the light from the standard lamp by a measured factor, using a diffuse reflector, the inverse square law, and calibrated filters.

(d) The absolute spectral sensitivity of the photomultiplier, using the reduced light source of known intensity and spectral distribution.

(e) The relative intensity distribution of the fluorescence transmission spectrum of single anthracene crystals, using the calibrated spectrophotelometer and photomultiplier.

(f) The flux and energy of a collimated beam of α-particles from a Po^{210} source, using standard scintillation counting techniques.

(g) The absolute light emission from an anthracene crystal excited by this α-particle flux, using the calibrated photomultiplier.

It was found that the fluorescence transmission spectrum and scintillation efficiency were independent of crystal thickness d, for $d>1.5$ mm, and the final results were obtained from the mean of measurements on 4 clear, polished anthracene crystals, exceeding this thickness. The absolute scintillation efficiency C_{1F} (total energy of fluorescence emission/total energy of incident radiation) was measured for several α-particle energies, from 0.042 percent at 1.18 Mev to 0.223 percent at 3.85 Mev, corresponding to 0.324 percent at 5.30 Mev. The mean wavelength of the fluorescence emission was 469 mμ, corresponding to a mean photon energy $E_F=2.65$ ev.

Hopkins[1] has observed that the scintillation efficiency of anthracene for excitation by 5.3-Mev electrons is 11.6 (± 0.2) times that for excitation by α-particles of the same energy. Hence we obtain $C_{1F}=3.76$ (± 0.07) percent for thick anthracene crystals at room temperature, excited by fast electrons. This corresponds to an energy expenditure $E_{1F}=70.5$ (± 3.8) ev/fluorescence photon.

This value may be compared with that derived from the "photon cascade" theory.[2] On this theory, the scintillation process consists of m molecular fluorescence emissions, of decay time $(t_f)_0$, and quantum efficiency q_0. The mean value of m is given by

$$m=(t_1)_T/(t_f)_0, \tag{1}$$

where $(t_1)_T$ is the technical scintillation decay time of a thick crystal. The scintillation quantum efficiency is

$$q_1=(q_0)^m, \tag{2}$$

the scintillation energy efficiency is

$$C_{1F}=E_F q_1/E_Z, \tag{3}$$

and the energy expenditure/emitted photon is

$$E_{1F}=E_Z/q_1. \tag{4}$$

E_Z is the energy expenditure/primary photon, which on the theory is equated to the energy expenditure/ion-pair, i.e., $\sim$30 ev/primary photon.

For anthracene at room temperature, values of $(t_f)_0=3.5$ mμsec, $(t_1)_T=27$ mμ sec, and $q_0=0.9$ have been observed experimentally,[3] giving $m=7.73$ and $q_1=0.443$ from (1) and (2). Hence we obtain $E_{1F}=68$ ev/photon, in agreement with the direct experimental value.

A detailed account of this work will be published later. We wish to acknowledge the support received from the South African Council for Scientific and Industrial Research.

[1] J. I. Hopkins, Rev. Sci. Instr. **22**, 29 (1951).
[2] J. B. Birks, *Scintillation Counters* (Pergamon Press, London; McGraw-Hill Book Company, New York, 1953).
[3] J. B. Birks and W. A. Little, Proc. Phys. Soc. (London) (to be published).

Three-Body Scattering Problems

A. DALGARNO
Department of Applied Mathematics, Queen's University, Belfast, Ireland
(Received May 4, 1953)

IN a recent paper, Borowitz and Friedman[1] obtain an expression for the exchange scattered amplitude in the Born approximation which differs from that given by Mott and Massey.[2] They question the procedure of expanding the entire solution in terms of a complete set of eigenfunctions of a Hamiltonian apparently because the coefficients of such an expansion must contain δ-functions, and they give a detailed proof of this latter assertion. They state further that in the case of, for example, the ionization of atoms by electron impact, Mott and Massey's result diverges.

Firstly we point out that if we make the same assumptions as Borowitz and Friedman, it is obvious that such an expansion will contain δ-functions. Using their notation, it is consistent with their assumptions to choose $V(r)=0$, and since

$$\sin k_0 r=\int dk\delta(k-k_0)\sin kr$$

the statement is immediately proved. However, their assumptions are not comparable to those of Mott and Massey who use essentially

$$r\phi_k(r)\sim\sin(kr+k^{-1}\log 2kr+\eta),$$

and not

$$r\phi_k(r)\sim\sin(kr'+\eta).$$

Since it is not clear in what way the presence of singularities such as δ-functions in the expansion coefficients constitutes an objection to the treatment, the point will not be pursued further.

It is of more importance to note that the result of Mott and Massey, correctly interpreted, does *not* diverge and is in fact on the same basis as that of Borowitz and Friedman, the difference between the two being, of course, the familiar post-prior discrepancy. This discrepancy may be shown to equal

$$\int e^{-i\mathbf{k}_n\cdot\mathbf{r}_2}\phi_0(\mathbf{r}_2)d\mathbf{r}_2\Big[\lim_{r_1\to\infty}\int_{-1}^{+1}\int_0^{2\pi}\{e^{i\mathbf{k}_0\cdot\mathbf{r}_1}\,\mathrm{grad}(\phi_n^*(\mathbf{r}_1))-\phi_n^*(\mathbf{r}_1)\,\mathrm{grad}(e^{i\mathbf{k}_0\cdot\mathbf{r}_1})\}r_1^2 d\mu d\Phi\Big], \tag{1}$$

and if n is discrete it thus vanishes as has been pointed out by Bates, Fundaminsky, and Massey.[3] To prove that this result is, as would be expected, generally true it need only be noted that if n is in the continuum, (1) must be replaced by

$$\frac{1}{\Delta k_n}\int_{k_n}^{k_n+\Delta k_n}dk_n\{\text{expression (1)}\},$$

where Δk_n is arbitrarily small but not identically zero (see Gordon[4]); and clearly this expression vanishes as

$$\sin(r\Delta k_n)/r\Delta k_n.$$

Finally it may be worth while to point out that the formula obtained by Borowitz and Friedman is the same as would be found by following the Mott and Massey procedure for direct scattering and using a properly symmetrized wave function throughout.

I wish to thank Professor D. R. Bates for many helpful comments.

[1] S. Borowitz and B. Friedman, Phys. Rev. **89**, 441 (1953).
[2] N. F. Mott and H. S. W. Massey, *Theory of Atomic Collisions* (Clarendon Press, Oxford, 1949), second edition, Chap. VIII.
[3] Bates, Fundaminsky, and Massey, Trans. Roy. Soc. (London) **A243**, 93 (1950).
[4] W. Gordon, Z. Physik **48**, 180 (1928).

Polarization of the Three-Photon Annihilation Radiation*

L. LEIPUNER, R. SIEGEL, and S. DEBENEDETTI
Carnegie Institute of Technology, Pittsburgh, Pennsylvania
(Received May 14, 1953)

WE have used a triple coincidence counter method to investigate the polarization of the gamma-rays resulting from the three-photon annihilation of positrons and electrons.[1] Of the many polarization effects that one might expect, we have chosen to investigate the simplest from the experimental point of view, i.e., the polarization of any one of the gamma-rays relative to the plane of emission of the three photons. The measurement was conducted for the symmetrical case (equal angles between the photons).

A thin sample of Na^{22} (1.4×10^6 dis/sec) was located in the center of a bell-shaped Al container (2.5 cm in diameter, 0.44 g/cm² thick) filled with a dense atmosphere of SF_6. Positrons from this source formed positronium[2] and provided a sufficiently intense source of three-quantum annihilation events. Three NaI(Tl) scintillation counters were used to detect the gamma-rays, and were placed as indicated in Fig. 1. Counters *A* and *B* detected

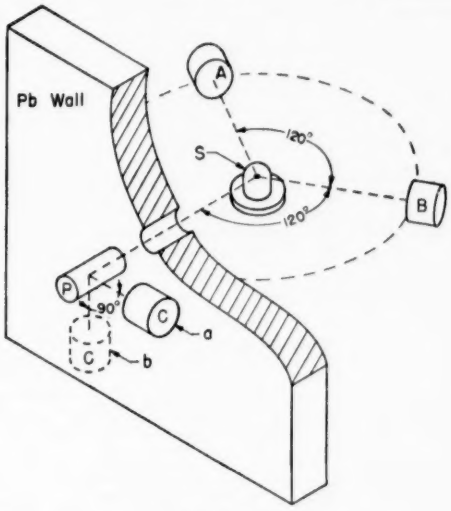

FIG. 1. Apparatus.

two of the three annihilation rays directly, while counter *C* detected the third ray only after it had been scattered by the polystyrene cylinder *P*. Triple coincidences were counted with counter *C* alternatively in positions *a* and *b* (Fig. 1). In such positions counter *C* detected rays scattered respectively parallel or perpendicular to the plane *ABP*. The background of triple coincidences was measured by lifting counter *A* at 45° away from the plane *BPS*, as described in the account of our previous work.[1] The geometric equivalence of positions *a* and *b* was checked by counting single scattered rays; the counting rates never differed by more than 10 percent in the two positions.

The experimental results, after subtraction of background are shown in Table I.

TABLE I. Experimental results.

Series	Position *a* (parallel) counts/hr	Position *b* (perpendicular) counts/hr	Ratio par./perp.
I	7.0±1.2	3.6±1.0	1.92±0.55
II	9.4±1.3	5.4±1.2	1.73±0.37
III	10.3±1.3	5.2±1.0	2.00±0.43
IV	8.3±1.3	4.7±1.1	1.78±0.44
Average			1.87±0.23

The theory[3] predicts a polarization ratio 3/1 in favor of rays plane-polarized with the electric vector perpendicular to the plane of the three photons. A rough Monte-Carlo computation,[3] taking into account the geometry of the experiment and the anisotropy of Compton scattering for polarized photons, leads to the prediction of a ratio (parallel/perpendicular) 1.80±0.15 for the result of the experiment, performed as described above. This is in agreement with the experimental value.

* Supported by a research grant from the National Science Foundation.
[1] S. DeBenedetti and R. Siegel, Phys. Rev. **85**, 371 (1952).
[2] M. Deutsch, Phys. Rev. **82**, 455 (1951).
[3] R. Drisko (private communication).

Effect of the Electric Quadrupole Interaction on the $\gamma-\gamma$ Directional Correlation in Cd^{111}. II

H. ALBERS-SCHÖNBERG, E. HEER, T. B. NOVEY,* AND R. RÜETSCHI
Swiss Federal Institute of Technology, Zürich, Switzerland
(Received May 6, 1953)

IN a previous letter[1] we described experiments with metallic indium single crystals containing In^{111}, which indicate that the interaction which influences the angular correlation in this type of source is electric in origin. Furthermore, the magnetic decoupling experiments showed that the magnetic interaction cannot be responsible for the observed attenuations in polycrystalline sources, which were previously measured.[2] It is therefore reasonable to assume that these attenuations are also due to the coupling between the electric quadrupole moment of the nucleus and the inhomogeneous electric crystalline field.

In this letter we describe some new measurements confirming this hypothesis and we discuss the hypothesis in connection with older experiments.

Angular correlation measurements in sources in which no inhomogeneous electric fields exist at the radioactive nucleus should show the undisturbed correlation according to our quadrupole hypothesis. Experiments on three types of such sources have been carried out:

Type a: Cubic crystals. (The active atoms must be in lattice positions and the crystals must be sufficiently large and perfect. Nevertheless, cubic crystals do not exclude interaction with higher electric moments and therefore offer the possibility to be measured.)

Type b: Solutions. (Care must be taken to avoid hydrolysis and/or precipitation.)

Type c: Melts.

Experiments with sources of the first type were performed in the earlier work of the Zürich group.[2] The active atoms were embedded in different metals by the double stream evaporation method. Cubic crystallizing metals (Ag, Cu) showed close to the maximum anisotropy, $A=[W(180°)-W(90°)]/W(90°)=-0.20$, under certain conditions (sufficiently large and pure crystallites and sufficient thickness of the source), whereas crystals with lower symmetry than cubic (In, Te, Cd, Se) always gave considerably less than the maximum value of the anisotropy.

Experiments with sources of the second type have been reported.[3,4] Aqueous solutions of $InCl_3$, InI_3, $In_2(SO_4)_3$, $In(NO_3)_3$, and others gave $A=-0.20$, whereas crystalline sources of the same compounds showed nearly isotropic correlations. The disappearance of the attenuation of the angular correlation when a crystalline source is dissolved in water gives the most striking evidence for the quadrupole hypothesis.

We have recently measured sources of the third type. Indium metal containing In^{111} was carefully reduced with hydrogen and sealed into an evacuated thin-walled Pyrex glass capsule. As no special crystallization methods were used, the sources were poly-

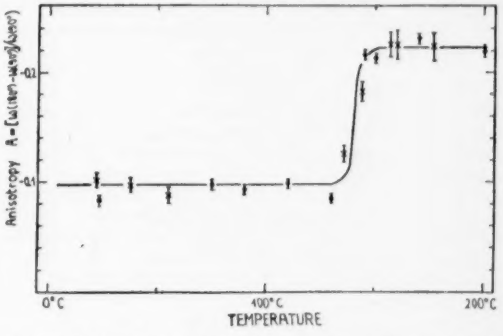

FIG. 1. Elimination of the quadrupole interaction by melting a polycrystal. line metallic indium source. Anisotropy *vs* temperature. ● run 1, ✕ run 2.

crystalline. The anisotropy remained constant while the source was heated up to the melting point, where the anisotropy rose rapidly up to 22 percent and remained constant to higher temperatures. Figure 1 shows a typical run. The curve was measured twice with the same source.

These three types of experiments show that when no appreciable inhomogeneous electric fields are present, one obtains the undisturbed angular correlation. We therefore conclude, that in the case of Cd^{111} the experimental results for the various types of sources (excluding sources with neighboring paramagnetic ions) can be largely and perhaps entirely explained by the quadrupole interaction hypothesis.

The anisotropy measured with the "powder" sources of metallic indium, $A=-0.095\pm0.005$, will be used together with the results of the single crystal—and some other experiments (delayed coincidence, combined magnetic-electric field measurements) to determine the quadrupole coupling and the quadrupole moment by comparison with the theory developed by Alder.[5] This comparison will be treated in a following letter.

We thank Professor P. Scherrer for his continued interest in this work, K. Alder for the very helpful discussions of theory, and O. Braun for assistance during the experiments.

* National Science Foundation Postdoctoral Fellow, on leave from Argonne National Laboratory.

[1] Albers-Schönberg, Hänni, Heer, Novey, and Scherrer, Phys. Rev. **90**, 322 (1953).
[2] Aeppli, Bishop, Frauenfelder, Walter, and Zünti, Phys. Rev. **82**, 550 (1951).
[3] R. M. Steffen, Phys. Rev. **89**, 903 (1953).
[4] J. C. Kluyver and M. Deutsch, Phys. Rev. **87**, 203 (1952).
[5] K. Alder (private communication).

$\gamma-\gamma$ Angular Correlation Measurements*

SANTIMAY CHATTERJEE AND AJIT KUMAR SAHA
Institute of Nuclear Physics, Calcutta, India
(Received March 24, 1953)

IN performing angular correlation measurements of nuclear radiations emitted in cascade, it is necessary to remember certain points which we shall discuss here mathematically.

(a) Time of measurements: Since the angular anisotropy expected is usually very small, it is necessary to keep small $\Delta W(\theta)$, the error in the measurement of $W(\theta)=G(\theta)/G(\pi/2)$; $G(\theta)$ and $G(\pi/2)$ being the genuine coincidence rates for angles θ and $\pi/2$ between the cascaded radiations. We have

$$\frac{\Delta W(\theta)}{W(\theta)}=\left[f^2(\theta)+f^2(\pi/2)+\frac{\bar{R}}{T^2(R)}\left(\frac{1}{G^2(\theta)}+\frac{1}{G^2(\pi/2)}\right)\right]^{\frac{1}{2}}$$

where $f(\theta)$ is defined by $f(\theta)^2=\bar{c}(\theta)/T^2(\theta)G^2(\theta)$, $\bar{c}(\theta)$ being the total number of coincidences recorded in time $T(\theta)$, and $\bar{R}$ is the total number of random coincidences recorded in time $T(R)$. With the error in counting random coincidences made very small and with $f(\theta)=f(\pi/2)$ we have $\Delta W(\theta)/W(\theta)\approx(2)^{\frac{1}{2}}f(\theta)$. We can show that the necessary time of observation $T(\theta)$ is connected to $f(\theta)$ by the relation

$$T(\theta)=\frac{1+\lambda}{f^2(\theta)}\cdot\frac{2\tau}{\epsilon_1\epsilon_2\omega_1\omega_2},$$

where τ is the resolving time of the coincidence circuit, ϵ_1 and ϵ_2 are the fractional efficiencies of the counters, ω_1 and ω_2 are the solid angles subtended by them (and expressed as fractions of 4π steradians), and λ is the ratio of the genuine to random coincidence rates ($=1/2N\tau$, N being the number of disintegrations per second). With this expression for $T(\theta)$ it is possible to plan the experiment for best results. For a typical set-up with scintillation counters where $\epsilon_1=\epsilon_2=0.10$ and with $\omega_1=\omega_2=2.5\times10^{-3}$ of 4π steradians, $\lambda=1.00$, $f=0.01$, the values of T for different values of τ are as follows:

τ(sec)	10^{-6}	10^{-7}	10^{-8}	10^{-9}	10^{-10}
T(hr)	178	17.8	1.78	0.18	0.02

(b) Angular resolution: In actual experiments, counters have definite angular spreads whose effects consist, we find, in modifying the coefficients occurring in the expansion of $G(\theta)$ in powers of $\cos^2\theta$. If the horizontal angular resolutions of the counters are $2\alpha_1$ and $2\alpha_2$ and the vertical angular resolutions are $2\beta_1$ and $2\beta_2$, and if the angles θ_0, ψ, ϕ, ξ, η are defined as in Fig. 1, then using $\cos\theta=\cos(\theta_0+\psi+\phi)+\sin\xi\sin\eta$ and the following expression for total number of genuine coincidence per sec for a separation of θ_0 between the centers of the counters:

$$G(\theta_0)=N\epsilon_1\epsilon_2\int_{-\alpha_1}^{\alpha_1}d\phi\int_{-\alpha_2}^{\alpha_2}d\psi\int_{-\beta_1}^{\beta_1}d\xi\int_{-\beta_2}^{\beta_2}d\eta\cdot g(\theta),$$

where $g(\theta)$ is the correlation function giving the probability of coincidence for an angle θ between the cascaded radiations [$g(\theta)=a_0+a_1\cos^2\theta+a_2\cos^4\theta$], we have

$$G(\theta_0)=N\epsilon_1\epsilon_2\omega_1\omega_2[(a_0+a_0')+(a_1+a_1')\cos^2\theta_0+(a_2+a_2')\cos^4\theta_0].$$

Here a_0', a_1', and a_2' are the correction terms and with $\alpha_1=\alpha_2$, $\beta_1=\beta_2=\beta(<15°)$, and neglecting terms of order of magnitude $<10^{-4}$,

$$a_0'=\frac{a_1}{2}\left[1-\frac{\sin^2(2\alpha)}{4\alpha^2}\right]+a_2\left[-\frac{1}{2}\cdot\frac{\sin^2(2\alpha)}{4\alpha^2}(\sin^2\alpha-\sin^4\alpha)+\frac{3}{8}-\frac{3}{8}\cdot\frac{\sin^2(2\alpha)}{4\alpha^2}\right],$$

$$a_1'=a_1\left\{\frac{\sin^2(2\alpha)}{4\alpha^2}-1\right\}+a_2\left\{\frac{\sin^2(2\alpha)}{4\alpha^2}-\frac{\sin^2(4\alpha)}{16\alpha^2}\right\},$$

$$a_2'=a_2\left\{\frac{\sin^2(4\alpha)}{16\alpha^2}-1\right\}.$$

The corrections introduced by 2β, the vertical angular spread of the counters, are generally very small up to quite an appreciable value of 2β ($\sim15°$). The values in Table I, however, are calculated with the help of more complete expressions for a_0', a_1' and a_2'. We have assumed that $g(\theta)$ stops at $\cos^4\theta$, but there is no difficulty in extending the method to higher powers of $\cos\theta$. Finally, we have

$$W(\theta)=\frac{G(\theta_0)}{G(\pi/2)}=1+\frac{a_1+a_1'}{a_0+a_0'}\cos^2\theta_0+\frac{a_2+a_2'}{a_0+a_0'}\cos^4\theta_0.$$

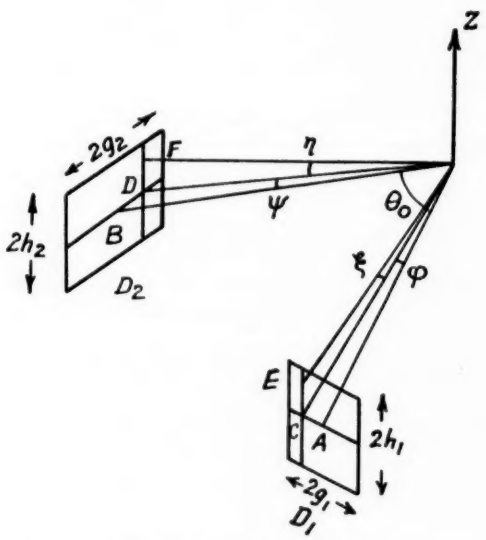

FIG. 1. Geometrical arrangement of the source and the crystal faces, showing the effect of finite angular resolution.

TABLE I. Values of $W(\pi)$ for some typical angular spreads.

Angular spread	2α	0	11°	28.5°	45°
	2β	0	5.5°	28.5°	45°
$W(\pi)$		1.1666	1.1642	1.1525	1.1335

For typical angular spreads the values of $W(\pi)$ are shown in Table I for a transition

$$2^2 \quad 2^2$$
$$0 \rightarrow 2 \rightarrow 4.$$

[a_0, a_1, and a_2 are obtained from Lloyd's tables.[1]]

There are other ways of treating the corrections for angular spreads.[2]

(c) Considerations of the effects produced by scattering when the phosphors are not shielded: As pointed out by Brady and Deutsch[3] there will be a part of the genuine coincidences recorded which are produced not by the cascaded radiation, but by one of them producing a Compton electron in one phosphor and the scattered gamma-quanta being recorded in the second counter. It is possible to find a mathematical expression for the ratio $\delta(\theta_0)$ between the coincidences produced in this way and the number of genuine coincidences,

$$\delta(\theta_0)=\frac{2nzl}{\epsilon}d\sigma(x)\cdot\frac{1}{4\sin^2(\theta/2)},$$

where n = number of molecules/cm^3 of the phosphor, z = number of electrons per mole of the phosphor, l = its length, ϵ = its fractional efficiency, and $d\sigma(x)$ = the Klein-Nishina differential-scattering cross section for the angle $x=\frac{1}{2}(\theta+\pi)$. We see that $\delta(\theta_0)$ varies inversely as ϵ and is independent of the distance between the source and the counter. The effect on the correlation ratio $W(\theta_0)$ is to reduce this quantity appreciably. Therefore, unless we stop this scattering process by proper shielding, the conclusions drawn from the results can be quite misleading.

Our thanks are due Professor M. N. Saha for his kind interest in the progress of the work. A more detailed paper will be submitted for publication in the *Zeitschrift fiir Physik*.

* This work was supported by the Atomic Energy Commission, India.

[1] S. P. Lloyd, Phys. Rev. **83**, 716 (1951).
[2] E. L. Church and J. J. Kraushaar, Phys. Rev. **88**, 419 (1952).
[3] E. L. Brady and M. Deutsch, Phys. Rev. **78**, 558 (1950).

Spin-Orbit Coupling in Pseudoscalar Meson Theory

LAWRENCE DRESNER
Palmer Physical Laboratory, Princeton University, Princeton, New Jersey
(Received May 18, 1953)

RECENTLY the pseudoscalar meson theory of nuclear forces has been subjected to a careful analysis by Lévy[1] and Klein.[2] Both authors have pointed out that the properties of the pseudoscalar matrix γ_5 make it possible to obtain adiabatic nuclear potentials which contain spin-orbit terms. These terms first appear when the matrix elements of γ_5 are expanded in powers of v/c to order $(v/c)^2$. They appear as corrections to the potentials obtained by using the extreme nonrelativistic limit of the matrix elements of γ_5. These latter potentials do not contain spin-orbit coupling terms.[3] Both Lévy[4] and Klein[2] have calculated the lowest-order spin-orbit corrections to the two-nucleon "two-pair" potential [Fig. 1(a)]. It is the purpose of this note to report the results of extending these calculations to include some other important potentials [Figs. 1(b) to (g)]. These potentials include the main contributions to the two- and three-nucleon potentials [Figs. 1(a), (b) and (e), (f), respectively]; some less important two- and three-nucleon potentials [Figs. 1 (c) and (d), respectively]; and the leading four-nucleon potential [Fig. 1(g)]. Only one of these potentials will be spin-dependent [Fig. 1(d)]. Spin-dependent potentials also arise in the second order from the diagram corresponding to exchange of a single meson between two nucleons. However, this diagram does not give rise to spin-orbit potentials.

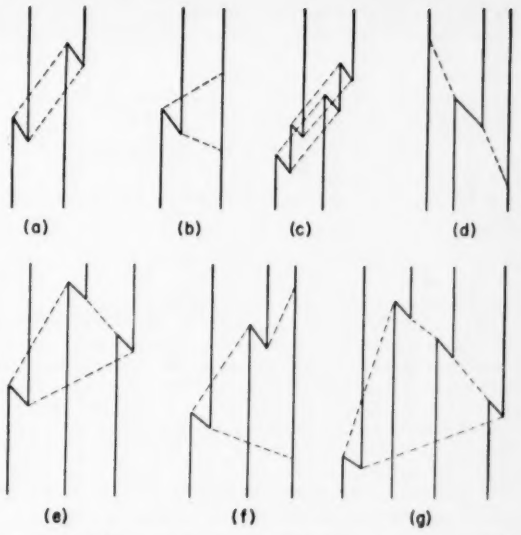

FIG. 1. Each diagram represents a virtual meson exchange process which contributes to the nuclear potential. The temporal ordering of the vertices in these diagrams is important.

Spin-dependent potentials occur again in the leading term of the sixth-order two-nucleon potential. We have ignored this potential because it does not form part of the main contribution to the two-nucleon potential, and because it is considerably simpler to estimate the contributions of the higher-order two-nucleon potentials to the spin-orbit interaction by finding the corrections to diagram (c). It should be pointed out that the two-nucleon, eighth-order potential contains contributions from diagram (a) which arise from expanding the energy denominators in the interaction kernel of diagram (a).

The results of the calculation can be summarized as follows:

Each diagram in the accompanying figure is the prototype of a class of diagrams related either by (1) a change in the way the meson lines are connected, without any change in the nucleon lines, except that self-energy diagrams are specifically neglected, as are diagrams in which a meson line is connected to a nucleon line at a point corresponding to a time during which a virtual nucleon pair is present; or (2) a permutation of the nucleon coordinates; or (3) any combination of (1) and (2). Although the processes (1) and (2) may cause identical diagrams to occur in more than one way, no diagram is enumerated more than once. Two diagrams are identical if they can be superimposed without changing the temporal ordering of the vertices of either. All the diagrams in one of these classes give rise, in the extreme adiabatic limit, to contributions to the potential which all contain a common factor $(G^2/4\pi)^n(\mu/2M)^m$, and which when summed give a potential function V which is symmetric in the coordinates of all the nucleons.

The lowest-order spin-orbit corrections to these potentials can be obtained according to the following rules:

In any one of the diagrams, except (d), consider a vertex on the world line of nucleon i. Suppose that the meson line which originates there ends on nucleon line j. Associated with this vertex is the expression[5]

$$(2M)^{-2}\boldsymbol{\sigma}_i\cdot(\nabla_{ij}V)\times\mathbf{p}_i,$$

where $\boldsymbol{\sigma}_i$ is the spin of nucleon i, $\mathbf{p}_i$ is its momentum, and $\nabla_{ij}=\nabla_i-\nabla_j$ and acts only on V. If we add all the expressions associated with all the vertices in a particular diagram, the resulting sum contains the spin-orbit corrections to the diagram considered.

With diagram (d) the case is somewhat different. The potential arising from diagram (d) in the extreme adiabatic limit is the sum

of three terms, all of which can be obtained from any one by cyclic permutation. If we restrict our attention to one of these terms V_{12}, we see that it depends only on the spins of the two nucleons 1, 2 whose world lines contain no pairs. The spin-orbit corrections involve only the spin of the third nucleon. The spin-orbit corrections of lowest order are contained in the expression

$$(2M)^{-2}[\boldsymbol{\sigma}_2\cdot(\nabla_{21}V_{12})\times\mathbf{p}_1+\boldsymbol{\sigma}_2\cdot(\nabla_{32}V_{12})\times\mathbf{p}_3]$$

and its cyclic permutations.

In the case of all diagrams, except (d) and (f), V is a function only of $|\mathbf{r}_i-\mathbf{r}_j|$. Then

$$\boldsymbol{\sigma}_i\cdot(\nabla_{ij}V)\times\mathbf{p}_i=\frac{1}{r_{ij}}\frac{dV}{dr_{ij}}\boldsymbol{\sigma}_i\cdot\mathbf{L}_i,$$

which shows the spin-orbit coupling explicitly.

The level splittings between states of $j=l-\frac{1}{2}$ and states of $j=l+\frac{1}{2}$ of a single nucleon outside a closed shell can be estimated,[6] and are of the order of 1 Mev or smaller, and of both signs.[7] This is an order of magnitude too small to fulfill the requirements of the shell model. Moreover, there seem to be no indications that consideration of many-nucleon forces involving more than three nucleons, or consideration of two- and three-nucleon forces of high order in the coupling constant, will supply the spin-orbit interaction postulated by the shell model. It should be pointed out that divergent diagrams have been consistently neglected in this investigation. Also, many spin-dependent terms which are not of the form of spin-orbit potentials have been discarded. These factors may possibly affect the level splitting significantly. For example, effects of the tensor force, corresponding to certain reducible diagrams and arising from second and higher orders in ordinary perturbation theory, may be responsible for the splitting.[8] The approximate equality of the splittings due to diagrams (a), (b), (d), (e), (f), and (g) raises the question of convergence[9] and casts doubt on the validity of the whole procedure.

It is a pleasure for the author to acknowledge his gratitude to Dr. F. Rohrlich for suggesting this problem, and for many interesting and stimulating discussions. His thanks are also due Dr. A. Klein for a copy of his unpublished manuscript, and for an interesting correspondence.

[1] M. M. Lévy, Phys. Rev. **88**, 72, 725 (1952).
[2] A. Klein, Phys. Rev. (to be published).
[3] This author has independently calculated the uncorrected three-nucleon potentials arising from diagrams (d), (e), and (f) by the Tamm-Dancoff method. The results agree with those of Klein, reference 2.
[4] M. M. Lévy (private communication).
[5] We use units of $\hbar=c=1$.
[6] For the purpose of numerical estimates we choose $G^2/4\pi=10$.
[7] The level splitting vanishes for diagram (d) on account of its spin dependence.
[8] A. Feingold, Ph.D. thesis, Princeton University (unpublished).
[9] A. Klein, Bull. Am. Phys. Soc. **28**, No. 3, 36 (1953).

Radioactive Charging through a Dielectric Medium*

E. G. Linder and P. Rappaport
Laboratories Division, Radio Corporation of America, Princeton, New Jersey
(Received April 7, 1953)

A STUDY has been made of a process of electrostatic charging in which charged particles pass from a radioactive emitter through a dielectric to a collector. Particular attention has been given to the role played by the dielectric. The process of charging through a vacuum has been discussed in previous publications.[1-3]

If a layer of dielectric F (in Fig. 1) is sandwiched between an electrode S, emitting beta-rays, and an electrode P, acting as a collector, radiation from S will pass through F and charge P negatively, leaving S positive. A voltage will be developed across terminals T. Such a device may be represented by an equivalent circuit consisting of a constant current source of output i_0, representing the radioactive material, in parallel with the capacitance C of the device, and in parallel with its internal resistance and any other resistance which might be connected across terminals

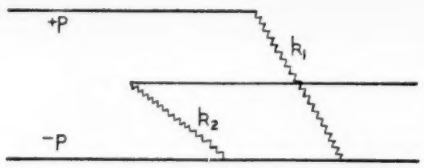

FIG. 1. Schematic diagram showing radioactive source S, dielectric separator F, and collector P.

T. The initial rate of charge is i_0/C. The final equilibrium voltage is Ri_0. These relations have been verified experimentally. Sr90-Y90 sources of effectively 2 millicuries and 54 millicuries were used. The dielectric was polystyrene.

Current-voltage characteristics, made with a 10^{-11} ampere charging current indicated that a maximum voltage of about 3700 could be reached. The internal resistance was found to correspond to a specific resistance for polystyrene of 7×10^{15} ohm-cm. Unbombarded values are given in the literature ranging from 10^{18} to 10^{22}. This decrease is attributed to bombardment-induced conductivity of the polystyrene. With a 2.5×10^{-10} ampere charging current the maximum voltage was determined to be about 6600, and the corresponding specific resistance 0.5×10^{15} ohm-cm, a decrease by a factor of 14 from the former value.

Measurements of the effect of varying the dielectric thickness showed an optimum thickness which yielded maximum charging rate. Charge soakage effects were observed, the charge rate and voltage developed being affected by previous radioactive charging. Backscattering of electrons was found to reduce the charging current. From this reduction backscattering coefficients were calculated as follows: 0.49 for lead, 0.31 for tin, 0.25 for silver, 0.17 for copper, 0.09 for aluminum, and 0.04 for carbon. These are in satisfactory agreement with values found by Trump and Van de Graaff.[4] A discussion of the experiments and their results will be published in detail at a later date.

The apparatus and techniques used in this study seem to offer a new and simple method of studying such effects as bombardment-induced conductivity, secondary emission, charge soakage, radiation absorption, and other effects of radiation on solids.

The work described here was suggested by the possibility of making a radioactive voltage or current source. Such a source could possess the advantages of long life, stability, and simplicity of construction. It is believed that it might find considerable application in the electronics field.

Appreciation is expressed to Dr. M. J. Cohen of these Laboratories and to Professor M. G. White of Princeton University for many valuable discussions.

* This work was supported in large part by the Components and Systems Laboratory, Wright Air Development Center, Air Research and Development Command, United States Air Force.
[1] E. G. Linder, Phys. Rev. **71**, 129 (1947).
[2] E. G. Linder and S. M. Christian, Phys. Rev. **83**, 233 (1951).
[3] E. G. Linder and S. M. Christian, J. Appl. Phys. (to be published).
[4] J. G. Trump and R. J. Van de Graaff, Phys. Rev. **75**, 44 (1949); also J. G. Trump, Massachusetts Institute of Technology Progress Report, January, 1951, pp. 14–15 (unpublished).

Origin of the "Strong-Focusing" Principle*

E. D. Courant, M. S. Livingston,† H. S. Snyder, and J. P. Blewett
Brookhaven National Laboratory, Upton, New York
(Received April 27, 1953)

AFTER our proposal for strong-focusing accelerators[1,2] had been published, our attention was called to an unpublished manuscript by N. Christophilos, entitled "Focussing System for Ions and Electrons and Application in Magnetic Resonance Particle Accelerators." In this paper Christophilos proposes an accelerator which incorporates strong focusing, using a sinusoidal variation of the field gradient with azimuth rather than the stepwise variation considered by us. He points out, as did we, that

by this method the size of the magnet for the accelerator can be reduced very considerably as compared to constant-gradient focusing. He also discusses the change in the mechanism of phase stability mentioned in our paper and the possibility of using this focusing method in linear systems.

Since Christophilos' manuscript is known to have been prepared in early 1950, it is obvious that his proposal antedates ours by over two years. We are, therefore, happy to acknowledge his priority.

* Work performed under the auspices of the U. S. Atomic Energy Commission.

† Massachusetts Institute of Technology, Cambridge, Massachusetts.

[1] Courant, Livingston, and Snyder, Phys. Rev. **88**, 1190 (1952).

[2] J. P. Blewett, Phys. Rev. **88**, 1197 (1952).

PHYSICAL REVIEW VOLUME 91, NUMBER 1 JULY 1, 1953

Proceedings of the American Physical Society

Minutes of the 1953 March Meeting Held at Durham and Chapel Hill, North Carolina, March 26–27–28, 1953

(Corresponding to Bulletin of the American Physical Society, Volume 28, No. 2)

THE 1953 March meeting of the American Physical Society was held on Thursday, Friday, and Saturday, March 26, 27, and 28, in North Carolina: on Thursday and Friday in the buildings of Duke University at Durham, on Saturday in those of the University of North Carolina at Chapel Hill. Nine hundred people registered, making this the largest March meeting in the history of the Society as well as one of the most pleasant. The Division of High-Polymer Physics and the Division of Solid-State Physics made this the annual meeting of each, and arranged for it a considerable number of symposia and of invited papers separate from the symposia. The Southeastern Section of the Society made this its 1953 Meeting, providing a symposium and gathering a large number of ten-minute papers: it should be also mentioned that the ten-minute papers in high-polymer physics were collected by the Division of that name. The Division of Chemical Physics organized a symposium. The predominance of nonnuclear physics was attenuated by ten-minute papers in nuclear physics contributed spontaneously and by invited papers solicited in the main from Southeastern laboratories.

The weather was ideal during the meeting, but those who flew from the Northeast on the preceding night found it otherwise. One is accustomed to laborious and efficient Local Committees, but the aides of the North Carolina Committee set an all-time record in self-sacrifice: three ladies sat up all of the Wednesday night in the lobby of the Washington-Duke Hotel at Durham to make sure that those who arrived in the small hours by belated planes should find accommodations waiting for them! The size of the attendance made it necessary to open dormitories of Duke University to our members. Buses were provided to take our members and guests between Durham and Chapel Hill on all of the days of the meeting, and even between the hotels and the University in Durham. The members of the Local Committee were Eugene Greuling (Chairman), H. W. Lewis and W. Fairbank of Duke University, and W. A. Bowers and J. W. Straley of the University of North Carolina. The names of all of those who helped them would probably cover an entire page.

The banquet of the Society was held on Friday evening in the Duke Union, with an attendance of nearly five hundred. The after-dinner program was offered in the Page Auditorium and consisted of speeches by Vice-President P. M. Gross of Duke University and our colleagues T. J. Killian, R. J. Seeger, and W. Shockley. The demonstrations which were a part of Mr. Shockley's talk continued until past eleven, setting probably an all-time record for the duration of an after-dinner programme of the Society. Nobody left beforehand.

The Council met briefly on Thursday morning. It elected to Fellowship twenty-four candidates and to Membership one hundred and seventy-four candidates: their names follow.

Elected To Fellowship: G. C. Baldwin, H. P. Broida, J. K. Bragg, F. P. Bundy, E. F. Cox, F. L. Friedman, P. F. Gast, M. L. Herlin, J. P. Howe, Henry Hurwitz, R. S. Jessup, W. L. Kraushaar, E. Maxwell, H. M. Parker, J. R. Pellam, W. R. Perret, H. F. Schiefer, R. B. Scott, M. W. P. Strandberg, David Turnbull, R. T. Weidmer, F. E. Williams, R. E. Wilson, and B. H. Zimm.

Elected to Membership: Robert S. Allgaier, Nissim Almeleh, Kinsey A. Anderson, Yasusi Ataka, Richard E. Azuma, David D. Babb, Michel Bader, *Alan H. Barrett, Bernhard E. Bartels, Joseph J. Becker, Richard L. Becker, Robert R. Berlot, Anne L. Blevins, Maurice E. Blevins, *Richard J. Blume, William L. Briscoe, Allen Brodsky, Sybrand Broersma, Glenn L. Brown, Paul P. Budenstein, Paolo Budini, William R. Busing, Guy H. Cain, Jr., Helen D. Callaway, *Frans A. Cerulus, William E. Claxton, Russell L. Collins, Joseph F. Colwell, Charles J. Cook, Robert P. Cox, Thomas D. Crumley, Basil Curnutte, Jr., Emlyn B. Davies, Charles F. Davis, Jr., Joseph E. Davis, Joseph M. Denney, James P. Dietz, Paul L. Donoho, William T. Doyle, Richard E. Durand, *Thomas G. Eck, John O. Erkman, *Marshall P. Ernstene, Leonard R.

Etter, Otto W. Fabian, *Donald W. Feldman, Gaelen L. Felt, *Eldon E. Ferguson, Jerome W. Finnigan, Paul G. Fischer, *Herbert Flicker, William M. Frank, Oliver StC. Franklin, Si C. Fung, James S. Geiger, Harold A. Gersch, Charles S. Godfrey, Paul N. Goodwin, William T. Gray, Robert J. Graydon, *Carsten M. Haaland, Willy Haeberli, James C. Haire, Jr., Stuart M. Hauser, Daniel T. Hedden, Michael Hoch, Michael W. Holm, John G. Holt, William E. Horn, Samuel S. Humphrey, Chiaki Ihara, *Jasper A. Jackson, Jr., David D. Jacobus, Clare P. Johnson, Jr., Orland E. Johnson, Paul O. Johnson, Jr., Robert D. Johnson, *John W. Jones, William H. Jones, Robert E. Kansas, Jerome I. Kaplan, Sheldon B. Kaufman, Deveneux L. Kavanagh, Hazimu Kawamura, *Gerald L. Keech, Donald D. Kerlee, Taro Kihara, John C. Kinzel, Daniel Klein, Jules Z. Klose, Robert G. Kouyoumjian, J. Laurence Kulp, Jeanne Laberrigue-Frolow, John J. Lambe, *Leon F. Landovitz, Issai Lefkowitz, *Jack Leitner, Abraham R. Liboff, Clifford C. Little, Robert J. Lockhart, Hans R. Loeliger, Joseph W. Londeree, Jr., Edwin H. Lougher, Wesley Love, Cecil R. Lubitz, Robert H. Lynch, Robert E. Maringer, *William C. Martin, Jr., Raymond D. McCurdy, Marcus T. McEllistrem, Robert E. McMillan, Norman J. Michaud, Stanley L. Miller, Robert L. Morgan, Samuel V. Nablo, *Daniel A. Naymik, George C. Neilson, Charles H. Ness, Gene D. Nutter, Florian R. Nykiel, Peter L. Ostapkovich, Sol Pearlstein, *James F. Perkins, *Charles C. Peterson, Charles L. Peyrou, John Puzzini, Arthur R. Quinton, William P. Raney, Ebbe Rasmussen, Jeanne D. Richmond, Arthur J. Roach, Carol Robinson, *Kenneth C. Rogers, William D. Rowe, Peter S. Rudman, Richard M. Sanders, Aurelius Sandor, Francis W. Schuller, Edward J. Seppi, Irving Siegel, Richard C. Sill, William F. Sjoborg, Jr., Alan W. Smith, Andrew N. Smith, Jack Sokoloff, Alfred W. Solbrig, Jr., Frank T. Solmitz, Roger H. Soulmagnon, George P. Stefun, Walter R. Steiger, Derald A. Stuart, Robert A. Sulit, James C. Swihart, Raymond E. Szupillo, Mathew P. Thekaekara, *Tibor Tompa, *Carroll C. Trail, Jack R. Turkeltaub, Walter R. Van Antwerp, Joseph T. Vanderslice, Robert L. Varwig, *James Ira Vette, Richard L. Wakefield, Sylvan Wallach, Alford L. Ward, Irving Weinberg, Leo H. Weinberg, William M. Whitney, Everett E. Wicker, Max Wolfsberg, Robert M. Wood, Herbert H. Yoshikawa, Benjamin Zeidman, and *Robert J. Zollweg.

KARL K. DARROW, *Secretary*
American Physical Society
Columbia University
New York 27, New York

*—Student

Errata Pertaining to Papers G5, P10, and P11

G5, Instead of "Irwin Graham, David Pomeroy, W. C. McGarvey, and John G. Randall," the byline should read "Irven C. Graham, David Pomeroy, W. C. McGarvey, and John G. Randall, *Army Medical Research Laboratory, Fort Knox.*"

P10, by Richard L. Petritz. The displayed equation should read

$$G_P(\Delta I_{sc}^2) = \frac{4kT(|z|^2+1)}{R_P}\left\{\frac{e^{-qV_0/kT}+(z+z^*)}{(z+z^*)(z+z^*+1)}\right.$$

In line 8 delete the sentence beginning "For $\omega T_P < |$ the expression . . . ."

P11, by Frances L. Lummis and Richard L. Petritz. In line 13 instead of "(see abstract No. P11)" read "(see abstract No. P10)." In line 18 instead of "whole adequately" read "while adequately."

PROGRAMME

THURSDAY MORNING AT 10:00

Chemistry 116

(CHARLES S. SMITH presiding)

Division of Solid-State Physics

Symposium on Plasticity and Dislocations

A1. The Phenomena of Plastic Flow. R. SMOLUCHOWSKI, *Carnegie Institute of Technology.* (45 min.)
A2. Recent Advances in Dislocation Theory. W. T. READ, *Bell Telephone Laboratories.* (45 min.)
A3. Applications of Dislocation Theory to Plastic Deformation. J. C. FISHER, *General Electric Research Laboratory.* (45 min.)

THURSDAY MORNING AT 10:00

Engineering 125

(J. E. GOLDMAN presiding)

Ferromagnetism; Magnetic Resonance

B1. A Quantum Statistical Mechanics of Ferromagnetism.* RYOICHI KIKUCHI, *M.I.T.*—Heisenberg's model was treated extending the author's treatment of the Ising model. The entropy is approximated as a function of parameters appearing in the density matrix, and the free energy is minimized. The first approximation becomes identical with Yvon's treatment.[1] The second approximations make only three-dimensional lattices ferromagnetic. The high temperature expansion of the partition function gives the first few coefficients of Opechowski's rigorous expansion. Anti-Curie point such as occurred in Weiss' theory does not appear, but the treatment has difficulties near the absolute zero. The above model was extended following Slater's idea[2] so that the overlap integrals can be taken into account. Only one orbital of s type was assumed to be available at each lattice point. Orthogonalized atomic orbitals are used and ionized states are included. The first approximation was formulated and was checked for the simple cubic lattice, in which no ferromagnetic state occurs, confirming Slater's argument.

* Supported by the U. S. Office of Naval Research.
[1] J. Yvon, J. phys. et radium **13**, 488 (1952).
[2] J. C. Slater, Quarterly Progress Report, M.I.T., January 15, 1953, p. 1; H. Statz, *ibid.*, p. 23; see abstract of Slater, Statz, and Koster, Bull. Am. Phys. Soc. **28**, No. 2, B2 (1953).

B2. A Two-Electron Example of Ferromagnetism.* J. C. SLATER, H. STATZ, AND G. F. KOSTER†, *M.I.T.*—We examine the problem of two holes in an otherwise filled band, or two electrons in an empty band, by the method of configuration interaction, using Wannier functions, asking which state lies lower, the triplet or singlet. If the triplet lies lower, it would indicate that the spins set themselves parallel, favoring ferromagnetism. We find that if the band is nondegenerate, the singlet will always lie lower, so that ferromagnetism requires a degenerate band, such as the five-fold degenerate d band. With a degenerate band ferromagnetism results, provided the band is not too broad. The cause of the ferromagnetism is an intra-atomic exchange effect, causing the two electrons or holes to prefer to align themselves with parallel spin when they happen to lie on the same atom. The model leads to a treatment of correlation, showing that with increasing interatomic distance the likelihood of finding the two electrons or holes on the same atom decreases, vanishing at infinite internuclear distance. The ferromagnetic interaction depends on the product of the intra-atomic exchange integral, which persists to infinite distance, multiplied by the probability of finding the electrons or holes on the same atom, which vanishes in the limit.

* Supported in part by the U. S. Office of Naval Research, in part by the Army, Navy, and Air Force.
† Staff member, Lincoln Laboratory, M.I.T.

B3. Electronic Interactions in Ferromagnetic Metals. SOL E. HARRISON, *Remington Rand, Inc.*, AND HERBERT B. CALLEN, *University of Pennsylvania.*—The coupling between d-shells in ferromagnetic metals occurs by direct $d-d$ interaction and also indirectly through the intermediate agency of conduction electrons. Whatever the nature of the direct coupling, the indirect coupling favors ferromagnetic alignment of the d-shells.[1,2] We here propose a model for this indirect interaction with particular reference to nickel. Eight electrons per atom are assumed to be in low-lying d-shells. Above these shells is a broad band of mixed $s-d$ character, containing two conduction electrons per atom and composed of two overlapping sub-bands of opposed spin. The fractional admixture of d-state in each sub-band is governed by the orientation of the low-lying d-shells. The larger admixture, and consequent low energy, occurs for the sub-band with spin opposed to the net magnetization of the low-lying d-shells. Thus the coupling between low-lying d and conduction electrons is antiferromagnetic. The net spin of the conduction electrons is -1.4 magnetons per atom at $T=0$. The predictions of this model with respect to the temperature and magnetization dependence of the resistivity are in good agreement with experimental observations.

[1] C. Zener, Phys. Rev. **81**, 440 (1951).
[2] J. C. Slater, Quarterly Progress Report, M.I.T., January 15, 1953.

B4. Measurement of the Particle Size of Ultrafine Ferromagnetic Powders.* A. D. FRANKLIN, R. B. CAMPBELL, AND J. A. WEINMAN, *Franklin Institute Laboratories.*—The particle size distributions for several ferromagnetic powders with particles in the diameter range from 200 to 800A have been

measured using three techniques. The complete distributions were obtained with the electron microscope. From these distributions the appropriate average sizes, corresponding to the broadening of x-ray diffraction lines and the surface area per gram as measured by nitrogen adsorption, were calculated and compared to the experimental data obtained by these latter techniques. Good agreement was found between the electron microscope and x-ray data, while the nitrogen adsorption method gave somewhat higher values. The over-all agreement obtained supports the validity of the electron microscope distributions.

* This work was supported by the U. S. Office of Naval Research.

B5. The Approach to Saturation in Diluted Ferromagnetic Powders.* A. E. BERKOWITZ AND A. D. FRANKLIN, *Franklin Institute Laboratories.*—As a part of the study of the magnetization processes occurring in ferromagnetic particles dispersed in nonmagnetic media, the approach to saturation of a series of increasingly dilute samples has been measured. The samples were pressed from mixtures of 2 micron carbonyl iron[1] and 50A silicic acid powders, bonded with a suitable resin. At high concentrations of the iron powder, the approach to saturation data agrees with Neel's[2] theory for soft magnetic materials. As the concentration decreases, increasingly large deviations occur. At the extremely dilute end, the main features of the magnetization curve can be accounted for in terms of simple domain theory for weakly interacting particles.

* This work was supported by the U. S. Office of Naval Research.
[1] The carbonyl iron powder used was an experimental material, kindly furnished by the General Aniline and Film Corporation.
[2] L. Neel, J. phys. et radium **9**, 185 (1948).

B6. On Dipolar Anisotropy in Cubic Ferromagnetic Crystals. FREDERIC KEFFER, *University of Pittsburgh.*—The dipolar anisotropy in a cubic ferromagnetic crystal may be obtained from the spin-wave approximation of Holstein and Primakoff.[1] This anisotropy comes from the total spin-wave energy, including zero-point energy, when summed over all values of spin-wave number k. No contribution to this anisotropy comes from $k=0$ spin-waves. Hence, in a ferromagnetic resonance experiment, if only $k=0$ spin-waves were excited, the resonant energy required would be independent of the dipolar anisotropy, in contradiction to the macroscopic theory of Kittel.[2] Terms dropped in the Holstein-Primakoff approximation cause a mixing of spin-waves such that other than $k=0$ waves are excited in resonance experiments. This mixing contributes to spin-spin relaxation[3] and modifies the resonant energy as if a macroscopic dipolar anisotropy field were present.

[1] T. Holstein and H. Primakoff, Phys. Rev. **58**, 1098 (1940).
[2] C. Kittel, Phys. Rev. **73**, 155 (1948).
[3] F. Keffer, Phys. Rev. **88**, 686 (1952).

B7. Thermomagnetic Investigations of Nickel Ferrite-Aluminates.* L. R. MAXWELL, S. J. PICKART, AND R. W. HALL, *U. S. Naval Ordnance Laboratory.*—Trivalent aluminum has been substituted for trivalent iron in nickel ferrite $NiO\cdot Fe_2O_3$ to give the system $NiO\cdot Fe_{(2-x)}Al_xO_3$, where x goes from 0 to 2. The material, annealed and prepared in a powdered form, is a homogeneous spinel with the size of the unit cell (a_0) decreasing linearly from 8.315A to 8.030A as x goes from 0 to 2. The saturation magnetization (σ_s) decreases linearly with increasing x to a minimum at about $x=0.7$; for further increase in x, σ_s increases to a maximum at about $x=1.0$, beyond which it decreases again to zero at $x=2$. Substitution of Al^{+++} for Fe^{+++} at first reduces the resultant moment of the magnetic ions on the B sites (Néel's notation) so that the net moment $(\sigma_s)_B-(\sigma_s)_A$ decreases and tends toward zero. Upon further increase in x the net moment apparently changes sign and increases because of the predominance of $(\sigma_s)_A$ over $(\sigma_s)_B$. Gorter and Herbschleb[1] have also recently found essentially the same effect for the same type of material. The Curie temperature decreases from 560°C to *ca* 50°C as x goes from 0 to 1.5.

* Supported in part by the U. S. Office of Naval Research.
[1] E. W. Gorter (private communication, January, 1953).

B8. Magnetic Resonance Absorption in Nickel Ferrite-Aluminates.* T. R. MCGUIRE, *U. S. Naval Ordnance Laboratory.*—Magnetic resonance measurements were made on small spherical specimens of the nickel ferrite-aluminate compounds at a frequency of 9340 Mc over a temperature range −196°C to +250°C. At −196°C, using the resonance condition[1] $\hbar\omega=g\beta H$, the following g values have been calculated: $x=0$, $g=2.3$; $x=0.25$, $g=2.7$; $x=0.5$, $g=6.9$; $x=0.63$, $g=3.8$; $x=0.75$, $g=1.5$; $x=1.50$, $g=1.5$; where x is the number of Al atoms per molecule $NiOFe_{2-x}Al_xO_3$. The values are seen to shift from $g>2$ to $g<2$ at x approximately 0.7. It is at this same composition that the dominant magnetic moment shifts from the B to the A sites. For samples $x=0.5$ through $x=1$ the g values decrease with increasing temperature. At composition $x=1.75$ and −196°C two resonant peaks were observed, one with $g=1.4$ and a new peak with $g=4.0$. Nickel aluminate ($x=2$) showed no resonance absorption. In most cases the peak heights of the resonance absorption fall off sharply above the Curie temperatures while at low temperatures broadening of the resonance curves was found.

* Supported in part by the U. S. Office of Naval Research.
[1] C. Kittel, Phys. Rev. **73**, 155 (1948).

B9. g Values of the Nickel Ferrite-Aluminates.* ROALD K. WANGSNESS, *U. S. Naval Ordnance Laboratory.*—The resonance frequencies of a system containing two magnetic sublattices having different gyromagnetic ratios γ_1 and γ_2 have been calculated. The resonance condition applicable to a ferrimagnetic sphere is $\omega=\gamma H+\frac{1}{2}\lambda(\gamma_2M_1+\gamma_1M_2)\pm\{\delta H[\delta H-\lambda\times(\gamma_2M_1-\gamma_1M_2)]+\frac{1}{4}\lambda^2(\gamma_2M_1+\gamma_1M_2)^2\}^{\frac{1}{2}}$, where $\gamma=\frac{1}{2}(\gamma_1+\gamma_2)$, $\delta=\frac{1}{2}(\gamma_1-\gamma_2)$, λ is the molecular field coefficient ($\gg$demagnetizing factor), M_1, M_2 are the magnetizations of the sublattices, and $\gamma_i\hbar=g_i\beta$. In first approximation, the resonance frequency is $\omega=\gamma_{eff}H$,[1] where

$$\gamma_{eff}=(M_1+M_2)[(M_1/\gamma_1)+(M_2/\gamma_2)]^{-1}.$$

There is semiquantitative agreement between g values reported in the previous abstract and the calculated values of g_{eff} with respect to their dependence upon the composition of the nickel ferrite-aluminates.

* Supported in part by the U. S. Office of Naval Research.
[1] See N. Tsuya, Prog. Theoret. Phys. **7**, 263 (1952).

B10. Nuclear Resonance Line Shapes at High RF Fields.* W. D. KNIGHT, *University of California, Berkeley.*—The nuclear magnetic resonance absorption and dispersion have been studied in metallic copper for rf fields ranging in magnitude from about 10^{-4} to one oersted. At low values of the rf field the line width is primarily dipolar,[1] except for a small spin-lattice relaxation broadening,[2] and the shape is approximately Gaussian. As the value of the rf field is increased toward one oersted, which is about twice the value necessary to make the saturation parameter equal to unity, the line width between maximum slope of the absorption curve increases from 6.5 to 7.5 oersteds. The dispersion curve broadens in a similar fashion. From the saturation of the absorption and a measurement of the rf field, a spin-lattice relaxation time of approximately one millisecond is calculated. This agrees reasonably with an extrapolation of Bloembergen's result to room temperature, and also with the result obtained from Korringa's formula and the measured line shift.[2] The shapes of the curves during saturation will be discussed. We wish to thank Dr. Carson D. Jeffries for making his nuclear induction spec-

trometer with rf field calibration available for use in these studies.

* Supported in part by the U. S. Office of Naval Research.
[1] H. S. Gutowsky and B. R. McGarvey, J. Chem. Phys. **20**, 1472 (1952).
[2] N. Bloembergen, Physica **15**, 588 (1949); J. Korringa, Physica **16**, 601 (1950).

B11. Saturation of the Paramagnetic Resonance from Color Centers in Alkali Halides.* A. M. PORTIS AND A. F. KIP, *University of California, Berkeley.*—Saturation of the paramagnetic resonance signal in dilute samples of additively colored KCl and KBr has been observed in the 9000 Mc/s region. We find that over a range of 20 db in microwave field, χ' is essentially constant but χ'' is inversely proportional to the magnitude of the microwave field. To within the accuracy of our measurements we observe no change in the width of the absorption or dispersion. We are unable to account for this saturation behavior on the basis of a simple two-level model for the resonance absorption where the width of the levels is ascribed to dipole-dipole interaction. However, if we assume that the over-all resonance line is a superposition of much narrower lines dispersed by an interaction external to the spin system, such as hyperfine interaction, we can account for the observed saturation behavior. A saturation in which only the absorption is affected would seem to be in conflict with the Kramers-Kronig relations. However, as will be shown, the Kramers-Kronig relations in their usual form are valid only in the absence of saturation.

* Supported in part by the U. S. Office of Naval Research.

THURSDAY MORNING AT 10:00

Page Auditorium

(R. G. BRECKENRIDGE presiding)

Semiconductors, I.

C1. Radiationless Trapping of Charge Carriers in Solids. GREGORY H. WANNIER, *Bell Telephone Laboratories.*—It is well known that transitions arising from coupling with the sound field are generally more probable for electrons and holes in solids than radiative transitions. Thus, electrons are trapped in a region of negative potential energy probably by phonon emission. If this is true, then we may tentatively define the trapping probability as the probability of emitting a phonon of such a type as to bring the electron into a negative energy state. This definition yields a trapping cross section which varies violently with electron energy. If the electron moves with twice the velocity of sound, the cross section is essentially infinite, while, for thermal electrons, the cross section is 10^{-16} cm^2 or less. In view of this we may calculate an upper limit for the trapping rate by assuming that all slow electrons are trapped and that the process is limited by the rate at which thermal electrons are slowed down to the speed of sound. For Si this rate comes out to be 10^9 sec^{-1} at room temperature and varying as $T^{-\frac{1}{2}}$. For Ge it is smaller; this may be one of the reasons why it is harder to observe trapping in germanium than in silicon.

C2. Carrier Contribution to the Dielectric Constant of Germanium. T. S. BENEDICT AND W. SHOCKLEY, *Bell Telephone Laboratories.*—The dielectric constant of germanium ($\rho = 5-40$ ohm cm) was measured as a function of temperature using 1.24-cm microwaves.[1] The results were compared with the following formula (M.K.S.):

$$\kappa = \kappa_0 - \frac{Ne^2\tau^2}{\epsilon_0 m^*[1+(\omega\tau)^2]}$$

which is obtained essentially by the method used in the Drude-Zener theory[2] assuming an effective mass m^* and unique relaxation time τ for the carriers. Since the dc conductivity and mobility[3] are known m^* and τ may be deduced. Preliminary results show that $m^* \simeq 0.6m_0$ for n type and 1.1 m_0 for p type germanium. The relaxation time is then given by $6.6\times10^{-9}T^{-1.6}$ for n type and $6.6\times10^{-7}T^{-2.3}$ for p type germanium in the temperature range 160°K to 298°K.

[1] Dielectric measurements have recently been made on germanium at room temperature using 10-cm microwaves. [J. M. Goldey and S. C. Brown, Bull. Am. Phys. Soc. **28**, No. 1, A7 (1953)].
[2] See for example F. Seitz, *Modern Theory of Solids* (McGraw-Hill Book Company, Inc., New York, 1940), Sec. 147.
[3] Drift mobilities of holes and electrons in germanium have recently been measured by M. B. Prince. These values were used in the interpretation of the results.

C3. Diffusion Currents in the Hall Effect in Semiconductors. ROLF LANDAUER AND JOHN SWANSON, *I.B.M.*—The usual Hall effect equation for semiconductors, $eRc = (p-nb^2)/(p+nb)^2$, holds if the concentration of carriers is undisturbed. In a magnetic field, however, holes and electrons are swept to the same side of the conductor. A gradient of carrier concentrations is thereby established, giving rise to diffusion currents across the sample. The magnitude of the diffusion currents depends on the recombination velocity at the surface and on the lifetime of excess carriers in the interior. When recombination is rapid, departures from equilibrium concentrations are small, and the ordinary formula applies. When recombination is absent, the correct equation becomes $eRc = (p-bn)/(n+p)(nb+p)$. Fowler[1] has derived the latter formula, and Welker[2] has treated another special case. It is desirable, however, to have more general formulas, since discrepancies in the Hall effect for samples having identical carrier concentrations may then be correlated with the lifetimes for these samples. Accordingly, the dependence of the Hall voltage on lifetime has been calculated for several geometries.

[1] R. H. Fowler, *Statistical Mechanics* (Cambridge University Press, Cambridge, England, 1936).
[2] H. Welker, Z. Naturforsch. **6a**, 184 (1951).

C4. Current Carrier Mobility Ratio in Semiconductors. L. P. HUNTER, *I.B.M.*—The ratio of the electronic mobility to the hole mobility in germanium has been reported by many workers. The value 1.5 is reported by those deducing the ratio from Hall effect measurements, while those using drift techniques find the value 2.0.[1] In both cases the ratio reported is usually obtained by measurements on two different samples of different conductivity types. The method suggested here deduces the mobility ratio from resistivity measurements made on a single sample. An accurate plot of resistivity as a function of temperature is made. The extrinsic and intrinsic branches of this curve are extrapolated to their intersection. If r is defined as the ratio of the resistivity of this intersection point to the measured resistivity at the same temperature, the quantity $[(1/r-1)-r]$ gives the mobility ratio for P type samples, and its reciprocal for N type samples. Values obtained by Dr. Huibregtse of this laboratory using this method agree well with the value 2.0 obtained by drift measurements near room temperature.

[1] W. Shockley, *Electrons and Holes in Semiconductors* (D. Van Nostrand Company, Inc., New York, 1950), p. 337.

C5. Current Carrier Lifetimes Deduced from Hall Coefficient and Resistivity Measurements. E. J. HUIBREGTSE AND L. P. HUNTER, *I.B.M.*—As a result of the theory of R. Landauer and J. Swanson,[1] a family of curves, having carrier lifetime as parameter, may be calculated to relate certain Hall coefficient and resistivity measurements to the current carrier mobility ratio. A convenient function to use for this purpose is the ratio of the intrinsic Hall mobility to the extrinsic Hall mobility extrapolated to a common temperature. With such a set of parametric curves the lifetime is determined if the two coordinates (Hall mobility ratio and carrier mobility ratio) are known. On a single sample both resistivity and Hall coefficient may be measured simultaneously as functions of temperature. The Hall mobility ratio may be calculated directly, and the mobility ratio may be determined from the resistivity curve as outlined by L. P. Hunter.[2] In this way, current carrier lifetimes may be measured without recourse to carrier injection techniques.

[1] R. Landauer and J. Swanson, Bull. Am. Phys. Soc. **28**, No. 2, C3 (1953).
[2] L. P. Hunter, Bull. Am. Phys. Soc. **28**, No. 2, C4 (1953).

C6. Temperature Variation of Drift Mobilities of Minority Carriers in Semiconductors. M. B. PRINCE, *Bell Telephone Laboratories.*—Experimental data of drift mobilities of electrons in p type germanium and silicon are brought into agreement with theoretical predictions by distinguishing between group velocity and particle velocity of a pulse of minority carriers. Corrected high temperature measurements of electron drift mobility are consistent with the theoretical prediction $\mu = AT^{-\frac{1}{2}}$. The experimentally determined values of A are

$$2.0\times10^{7}\ \text{cm}^2\ \text{deg}^{\frac{1}{2}}/\text{volt-sec for germanium}$$

and

$$0.62\times10^{7}\ \text{cm}^2\ \text{deg}^{\frac{1}{2}}/\text{volt-sec for silicon.}$$

Corrected high temperature measurements of hole drift mobility are consistent with the equation $\mu = BT^{-2.3}$. The experimentally determined values of B are

$$9.1\times10^{8}\ \text{cm}^2\ \text{deg}^{2.3}/\text{volt-sec for germanium}$$

and

$$2.5\times10^{8}\ \text{cm}^2\ \text{deg}^{2.3}/\text{volt-sec for silicon.}$$

At present there is no explanation for the anomalous value of 2.3 in the experimental equation for the hole drift mobility.

C7. Mobilities of Carriers in Crystalline Boron. WM. C. SHAW, D. E. HUDSON, AND G. C. DANIELSON, *Iowa State College.*—Microscopic single crystals of boron have been studied using procedures previously described.[1] Conductivity, Hall, and thermoelectric measurements were made on two low resistivity n type specimens and one high resistivity p type specimen. A statistical treatment allowed determination of small Hall voltages superimposed on noise fluctuations. An n type crystal having a resistivity of (61 ± 12) ohm-cm at 25°C had a Hall coefficient of about -400 cm³/coulomb indicating an electron mobility near 7 cm²/volt sec. The Hall coefficient of this crystal changed sign at higher temperatures. Another crystal, which exhibited at 25°C properties characteristic of an intrinsic semiconductor, had a resistivity of $(1.7\pm0.3)\times10^{6}$ ohm-cm at 25°C. Its Hall coefficient was approximately $+3\times10^{+6}$ cm³/coulomb. These data indicate that the mobility of holes slightly exceeds that of electrons. One low resistivity crystal had a thermoelectric power of about -300 microvolts/degree near room temperature; the thermoelectric power changed sign at about 265°C and finally reached the order of 500 microvolts/degree near 600°C. This change of sign indicates that the hole mobility exceeds the electron mobility, in agreement with the results of the Hall measurements.

[1] Shaw, Hudson, and Danielson, Phys. Rev. **89**, 900 (A) (1953).

C8. Hall Effect and Conductivity of Germanium Containing Arsenic or Gallium as Impurities. PETER P. DEBYE,* *Bell Telephone Laboratories.*—Samples of highly purified germanium to which varying amounts of arsenic or gallium had been added were measured by a dc method from 11 to 300 degrees absolute. Room temperature conductivities ranged from 200 to 0.024 (ohm cm)$^{-1}$ for samples containing arsenic and from 110 to 0.033 (ohm cm)$^{-1}$ for those containing gallium. For low concentrations, donor as well as acceptor impurities showed ionization energies of approximately 0.01 electron volts. The Hall mobility at 300 degrees absolute in high resistivity samples was found to be 4400 cm²/volt sec for electrons and 3500 cm²/volt sec for holes.

* Now at Raytheon Manufacturing Company, Waltham, Massachusetts.

C9. Electrical Properties of n type Germanium.* ESTHER M. CONWELL,† *Sylvania Electric Products Inc.*—Experimental results for carrier concentration and Hall mobility obtained by P. P. Debye for a set of n type germanium samples have been compared with theory. Plots of Hall mobility *vs* resistivity at constant temperature were used to check the theoretical formulas for ionized and neutral impurity scattering and, in particular, to obtain approximate values for the effective mass at various temperatures. An over-all value in the neighborhood of one-quarter the free electron mass is indicated, but this may vary considerably with temperature in this range. The effect of electron-electron collisions on the mobility was considered and in a qualitative way included in the analysis. Curves of $\log_e$ of carrier concentration *vs* the reciprocal of absolute temperature were fitted to obtain values of the activation energy and concentration of acceptors in these samples. The latter are compared with the values computed from the 11.5°K values of the mobility.

* Work done partly at Bell Telephone Laboratories
† On leave from Brooklyn College.

C10. Acceptor States of Gold in Germanium. W. C. DUNLAP, JR., *General Electric Research Laboratory.*—A number of single-crystal ingots of germanium, doped with high purity gold from three separate sources, have been prepared. It was found in most cases that addition of gold increased the resistivity of n type material, and in several cases the gold-doped portions were p type. Hall effect measurements were made between 77°K and 400°K. Many of the samples were intrinsic at temperatures as low as 0°C, whereas adjacent wafers from the "undoped" portion were usually in the range 1–20 ohm cm at room temperature. At 77°K most samples had resistivities of the order of 10^{6} ohm cm. The carriers, for n type samples, had activation energies about 0.18 ev; for p type samples, about 0.15 ev. It is suggested that gold produces acceptor states at various levels in the forbidden region, the highest being 0.18 ev from the conduction band, the lowest about the same distance from the filled band. The properties of the germanium, including type, resistivity, and observed activation energy, are determined by the relative concentrations of the gold-levels and ordinary impurity states.

C11. Broadening of Impurity Levels in Silicon. M. LAX, *Syracuse University,* AND E. BURSTEIN, *Naval Research Laboratory.*—Electrons or holes trapped at an impurity center in a homopolar material move in hydrogen-like orbits that are disturbed by lattice vibrations. Using the Franck-Condon principle, the broadening of the absorption spectrum can be calculated if the energy of the trapped electron is known as a function of the nuclear coordinates.[1] An estimate of the electron energy dependence on lattice coordinates can be made by treating the electron-lattice interaction as a small perturbing energy. The unperturbed electronic state is expressed as a linear superposition of orthogonalized atomic orbitals. By

reformulating the latter in terms of Block orbitals, the first-order perturbation expression for the energy can be re-expressed in terms of the usual matrix elements that occur in the theory of electrical conductivity. The *form* of these matrix elements is known approximately from the Bardeen-Shockley deformation potential method. The normalizing multiplicative constant is determined by the experimental high temperature mobility. Thus a prediction of the broadening of the absorption spectrum as a function of temperature is made from first principles. A comparison between theory and experiment will be given.

[1] M. Lax, J. Chem. Phys. **20**, 1752 (1952).

THURSDAY MORNING AT 10:00

Biology 113

(W. M. NIELSEN presiding)

Invited Papers

D1. One-to-Two-Millimeter Wave Spectroscopy. W. M. GORDY, *Duke University.* (30 min.)

D2. Some Recent Developments in Microwave Spectroscopy. C. H. TOWNES, *Columbia University.* (30 min.)

D3. On the Theory of Liquid Helium. FRITZ LONDON, *Duke University.* (30 min.)

D4. Thermodynamics of Stationary Helium Films. O. K. RICE, *University of North Carolina.* (30 min.)

D5. Negative Ions in the Gaseous Phase. H. E. CARR, *Alabama Polytechnic Institute.* (30 min.)

THURSDAY MORNING AT 10:00

Physics 114

(C. K. BECK presiding)

Nuclear Physics and Cosmic Rays

Contributed Papers

DA1. The Hyperfine Structure and Nuclear Moment Ratios of the Stable Bromine Isotopes.* J. G. KING AND V. JACCARINO, *M.I.T.*—The hyperfine structure of the $^2P_{\frac{1}{2}}$ state of atomic Br^{79} and Br^{81} has been investigated by the atomic-beam magnetic-resonance method. The ratio of the magnetic dipole interaction constants a^{81}/a^{79} is 1.07794 ± 0.00001, and the ratio of the electric quadrupole interaction constants b^{79}/b^{81} is 1.19707 ± 0.00003. Applying the results of recent theoretical calculations by Sternheimer,[1] Koster,[2] and Feld, the following values of nuclear quadrupole moments were computed:

$$Q^{79} = 0.335 \times 10^{-24}\ \text{cm}^2 \quad Q^{81} = 0.280 \times 10^{-24}\ \text{cm}^2.$$

* This work was supported in part by the Signal Corps, the Air Materiel Command, and the U. S. Office of Naval Research.
[1] R. Sternheimer, Phys. Rev. **86**, 316 (1952).
[2] G. F. Koster, Phys. Rev. **86**, 148 (1952).

DA2. Alpha-Particle Straggling in Thin Foils.* P. T. PORTER AND J. I. HOPKINS, *Vanderbilt University.*—Alpha-particles of 5.3 Mev from Po were used to bombard various thicknesses of aluminum, copper, and gold foil. The energy spectra of the emergent alpha-particles were then determined with a scintillation spectrometer using anthracene as the detection crystal. Differential curves of counting rate *versus* energy give the well-known Gaussian distribution; however, a very pronounced tail is found toward the lower energies. The presence of the tail is explained by the fact that a large fraction of the particle's energy can be lost in a single collision. The extent to which the shape and size of this tail is dependent upon the most probable energy of the emergent particles is investigated according to the method developed by Lewis.[1] How the energy distributions differ from a Gaussian for the different absorbers and absorber thicknesses will be discussed.

* Work supported by U. S. Atomic Energy Commission.
[1] H. W. Lewis, Phys. Rev. **85**, 20 (1952).

DA3. Neutron Resonances in Bi, Tl, and Pb. J. H. GIBBONS AND HENRY W. NEWSON, *Duke University.*—Li(p, n) neutrons emerging at an angle of 120° to the proton beam have been used to measure the total cross sections of the heaviest stable nuclides. The resolving power is about 1 kev at 10 kev and somewhat poorer at lower and higher energies. The previously reported resonance in Bi at 2.5 kev has been confirmed, and six more typical scattering resonances have been found at 13, 16, 34, 46, 60, and 68 kev. These numbers are subject to revision after recalibration of the magnetic analyzer. The transmission curve shows evidence for many more poorly and partially resolved resonances. The average level separation appears to be considerably less than 10 kev. Our resolving power has been insufficient so far to find a well-resolved resonance in Tl, but nonstatistical fluctuations in the transmission curve indicate weak resonances spaced about 1 kev apart. The results on Pb are similar to those on Tl. These elements will be investigated with higher resolving power.

DA4. A Ranger Study of the Po-Be Neutron Spectrum.* HERBERT GURSKY, BARBARA WINNEMORE, AND D. A. COWAN, *Vanderbilt University.*—The Ranger,[1] a variable absorption, proportional counter arrangement for the counting of heavy particles of selected species and energies, has been applied to study the neutron spectrum of a homogeneously mixed Po-Be source. For the measurement the source, which had an initial

intensity of 3.28×10^7 neutrons per second, was suspended four inches from a paraffin radiator and the spectrum measured over an energy range from 2.6 to 8.6 Mev. Individual points in the spectrum have been determined with a statistical accuracy of about one percent. The detector, an aluminum foil of 7.15 mg/cm² thickness, gave a resolution of about 0.5 Mev. The spectrum presents broad maxima at 3.2 and 5.5 Mev and a sharp peak at 4.6 Mev with an average neutron energy of 4.68 Mev. These results are consistent with data published by Whitmore and Baker.[2]

* Work supported by the U. S. Atomic Energy Commission.
[1] David L. Hill, U. S. Atomic Energy Commission Report AECD, 1945.
[2] B. G. Whitmore and W. B. Baker, Phys. Rev. **78**, 799 (1950).

DA5. The Average Energy of the Beta-Rays of P^{32} and Ag^{111}. J. M. BRABANT,* L. W. COCHRAN, AND R. S. CASWELL,* *University of Kentucky.*—Utilizing an extrapolation ionization chamber and 4π methane-flow proportional counter technique, the average energy per disintegration $\bar{E}$ of the beta-rays of P^{32} and Ag^{111} has been measured. The extrapolation chamber is used to determine the energy liberated per gram per second E_t of the beta-radioactive medium, and the 4π counter is used to determine the disintegration rate per gram n of the medium. Then $\bar{E}$ is found from the relation, $\bar{E}=E_t/n$. The P^{32} determinations indicate $\bar{E}=0.694\pm0.025$ Mev per disintegration, a value in good agreement with previous results. The value, $\bar{E}=0.376\pm0.014$ Mev per disintegration, obtained for Ag^{111} includes a correction for the gamma-radiation present. A numerical and graphical evaluation of the theoretically expected value for the branched spectra of Ag^{111} gives $\bar{E}=0.382$ Mev per disintegration, a value in close agreement with the observed value. Both experimental determinations include a correction for bremsstrahlung.

* Now at the National Bureau of Standards, Washington, D. C.

DA6. Beta-Ray Spectra of C^{14} and Ni^{63}.† J. P. MIZE AND D. J. ZAFFARANO, *Iowa State College.*—The beta-ray spectra of C^{14} and Ni^{63} have been investigated with a 4π geometry proportional counter spectrometer[1] using internal solid radioactive sources. A C^{14} source of high specific activity was prepared in the form of α-hydroxyglutaric acid, $C_5{}^*H_8O_6$, uniformly labeled. A Ni^{63} source of considerably lower specific activity was prepared from Ni^*Cl_2. The estimated average surface densities of these two water soluble sources were: C^{14}, 11 μg/cm² and Ni^{63}, 50 μg/cm². The end point of C^{14} was in good agreement with previous measurements.[2] but the Fermi plot of the data was concave toward the energy axis below 50 kev. The end point of Ni^{63} was in good agreement with a previous measurement;[3] however, the Fermi plot was concave toward the energy axis below 30 kev. The negatron distributions of these nuclides will be presented and compared with the spectra of S^{35} and Pm^{147} as measured with our spectrometer, which yielded linear Fermi plots to 10 and 15 kev, respectively.

† This work was performed in the Ames Laboratory of the U. S. Atomic Energy Commission.
[1] J. P. Mize and D. J. Zaffarano, Phys. Rev. **89**, 902(A) (1953).
[2] S. D. Warshaw, Phys. Rev. **80**, 111 (1950).
[3] H. M. Wilson and S. C. Curran, Phil. Mag. **40**, 63 (1949).

DA7. Angular Distribution of 12 Mev Gamma-Rays from the Proton Bombardment of Boron.* G. L. JENKINS, L. W. COCHRAN, H. H. GIVIN, J. L. RYAN, T. M. HAHN, AND B. D. KERN, *University of Kentucky.*—The angular distribution of the 12 Mev gamma-rays from proton bombardment of thick boron targets has been obtained in the energy region between 200 kev and 800 kev. Results indicate an angular distribution with respect to the proton beam of the form $Y(\theta)=1+A\cos\theta+B\cos^2\theta$. $A=0$ at 180 kev, and $A=0.10\pm0.02$ in the energy region between 300 kev and 800 kev. $B=0.25\pm0.03$ at 180 kev and 300 kev, and $B=0.05\pm0.02$ in the energy region between 400 kev and 800 kev. The $\cos\theta$ term implies interference between levels of opposite parity.

* Supported by Office of Ordnance Research, Army Ordnance Corps.

DA8. Fission Cross Section of Uranium-234. R. W. LAMPHERE, *Oak Ridge National Laboratory.*—The neutron-induced fission cross section of U-234 has been measured from threshold to 4-Mev neutron energy, using the $T(p, n)$ reaction with a tritium gas target, and the Oak Ridge 5-Mev Van de Graaff. The curve rises from threshold at 350 kev to 1.33 barns at 4 Mev. There is a minimum at 1.08 Mev and another at 2.30 Mev. The shape of the curve is believed to be good to 3 percent; but the ordinate scale factor is in doubt to 14 percent because of uncertainty in the weight of material on the foils. Enough counts were taken in the region of the two minima to establish their reality to a probability of a billion to one relative to a "best fit" curve with no extremes.

DA9. Phenomenological Interpretation of π^+ Meson Production by Protons on Carbon. M. M. BLOCK, *Duke University*, S. PASSMAN, *Hughes Research and Development Laboratories*, AND W. W. HAVENS, JR., *Columbia University.*—A phenomenological calculation of π^+ meson production by protons on carbon, at various laboratory angles and proton bombarding energies, has been carried out under the following assumptions: (1) meson production occurs in nucleon-nucleon collisions; (2) the π^+ meson is produced with the maximum possible kinetic energy in the center-of-mass system; (3) the internal momentum distribution of the nucleons before collision is Gaussian, corresponding to an average energy of 19.3 Mev; (4) the excitation for π^+ production in a nucleon-nucleon collision in a heavy nucleus is the same excitation function as for the reaction $p+p\rightarrow\pi^++d$. The excitation function employed for meson production in an elementary collision was taken from experiment[1] and is essentially given by a T^2 law, where T is the maximum meson energy in the center-of-mass system. The results will be applied to recent experimental results.[1,2]

[1] Passman, Block, and Havens, Phys. Rev. **88**, 1247 (1952).
[2] W. F. Dudziak, Bull. Am. Phys. Soc. **28**, No. 1, D4 (1953).

DA10. Star Clustering in Nuclear Emulsions. FRANK B. BROWN, JR., AND A. V. MASKET.—A study has been made of the distribution of nuclear stars in photographic emulsions which were exposed for 6½ hours at 84 000 feet. The number of close pairs of stars has been found to exceed greatly the number which would be predicted on the basis of a random distribution. All possible spurious effects which might cause this anomaly to appear have been eliminated or taken into consideration. The effect is shown to depend upon the larger stars of six or more prongs. A tentative explanation of the above effect is given, which involves the passage through the emulsion of narrow showers of high energy particles. These particles create large stars in the emulsions in a non-random array, and it is this array, superimposed on a background of randomly placed stars, which produces a statistical surplus of close pairs. Corroborative evidence for this mechanism is (a) the relative surplus of larger stars found on the plates, (b) the collimation of incident particles for star "clusters" which are assumed to be shower produced, and (c) the greater number of tracks which are observed in the vicinity of such a "cluster," compared with the number found in an isolated region.

Invited Paper

DA11. Ionization Energy Losses of Mu-Mesons in Gases. E. D. PALMATIER, *University of North Carolina.* (30 min.)

THURSDAY MORNING AT 10:00

Social Science 117

(L. A. WOOD presiding)

Division of High-Polymer Physics

Invited Paper

DB1. The Reinforcement of Silicone Rubber. A. M. BUECHE, *General Electric Research Laboratory.* (20 min.)

Contributed Papers

DB2. Sedimentation Rates in Dilute and Moderately Concentrated Polymer Solutions. M. WALES (introduced by S. G. Weissberg).—This work is the initial step in an effort to correlate sedimentation rates of chain polymers on a general basis as a function of concentration, solvent, and molecular weight. It is hoped that the conclusions so obtained can be used to deduce information about chain configuration in concentrated solutions. Darcy constants[1] of polystyrene solutions up to 10 percent by weight have been obtained as a function of concentration for polystyrene fractions in butanone and toluene. Empirical equations, which represent the sedimentation behavior over the whole range studied have been devised. The constant K_s, which describes the dependence of sedimentation constant on concentration in dilute solutions, has been found to be 1.7 times the intrinsic viscosity. This relationship is valid with good precision for polystyrene in chloroform, butanone, and toluene, for polyisobutylene in cyclohexane, and for polymethylmethacrylate in acetone. These systems comprise all the data examined, from the literature, and from this work. This proportionality was first noticed experimentally for polystyrene in a number of solvents by Newman and Eirich.[2] It is apparently more generally valid than was originally supposed.

[1] R. Signer and H. Egli, Rec. Trav. Chim. **64**, 45 (1950).
[2] S. Newman and F. Eirich, J. Colloid Sci. **5**, 541 (1950).

DB3. Nucleoprotein Monolayers. ADOLPH B. AMSTER* AND QUENTIN VAN WINKLE, *The Ohio State University.*—A sensitive Wilhelmy apparatus for the study of nucleoprotein monolayers has been constructed. Film pressures may be read to 0.12 dyne/cm and estimated to 0.003 dyne/cm. It was found that rabbit appendix nucleoprotein spread as a gaseous film upon aqueous substrates of *p*H 5 to 9 and ionic strength 0.14 and 1.00. The extent of spreading and the number-average molecular weight were found to be a function of the mass of material spread. From these results it was found that the cross section per molecule was 4.4×10^4 sq A. The molecular weight varied from 2.66×10^6 at an initial spreading concentration of 4.27 mg/meter^2 to 0.24×10^6 at an initial spreading concentration of 0.458 mg/meter.[3] Certain apparent anomalies in the low pressure region are explained. An hypothesis is offered to explain the variations of molecular weight with spreading concentration, coupled with the invariant cross section. The nucleoprotein dissociates and unfolds in a manner dependent upon the surface concentration. This process appears to be irreversible and unchanging.

* Present address: National Bureau of Standards.

DB4. The Dependence of the Photoelastic Properties of GR-S on the Degree of Cross Linking.* G. R. TAYLOR AND S. R. DARIN, *Mellon Institute* (introduced by R. S. Marvin).—The birefringence *vs* stress relationship for decamethylene dis-methylazodicarboxylate vulcanizates of GR-S has been determined as a function of the degree of cross linking. The experimental results show a systematic deviation from Brewster's law (stress proportional to birefringence) at stresses greater than 30 kg/cm^2, the deviations becoming more pronounced as the degree of cross linking is decreased. While most of the measurements were taken during stress relaxation, in the cases where it was possible to obtain approximately equilibrium conditions, it was found that the stress-birefringence ratio was essentially independent of the state of relaxation of the material, i.e., relaxation occurs along the equilibrium stress-birefringence curve. In the light of these results, the applicability of W. Kuhn's[1] expression for birefringence/stress is discussed, and reasons for its failure in light vulcanizates are suggested.

* This work was supported by the Office of Synthetic Rubber, Reconstruction Finance Corporation.
[1] W. Kuhn and F. Grün, J. Polymer Sci. **1**, 183 (1946).

DB5. Stress Crazing Thresholds of Methyl Methacrylate Polymers. T. F. PROTZMAN, J. J. GOUZA, AND W. F. BARTOE, *Rohm & Haas Company.*—Time-deformation studies have been made on stressed cantilever beams of polymethyl methacrylate. The first incidence of crazing on each beam was observed. From the deformation a measure of the strain in the outer fibers of the cantilever beam is calculated at the time of incidence of crazing. It is found that the crazing threshold strain is a linear function of the applied stress. This contrasts with the results obtained by Maxwell and Rahm,[1] who found that polystyrene crazes at a fixed strain. The results of those measurements are interpreted qualitatively on a basis of polymer rheology.

[1] B. Maxwell and L. F. Rahm, Princeton University, Plastics Laboratory Technical Report 11B, September 21, 1948.

DB6. Values of Diffusion Coefficients for Some Chain Polymers Computed from Anomalous Osmotic Pressure Data. T. A. BARR, JR., *University of Georgia.*—In order to explain the anomalous osmotic pressures reported by Matthews[1] and the author,[2] it was necessary to establish a model osmometer into which the solvent flowed under a pressure difference equal to the difference between the theoretical osmotic pressure and observed osmotic pressure, and out of which the solute diffused by virtue of the concentration gradient across the osmometer membrane. Under the condition that the volume of solution be held constant in the model osmometer, an equation has been established which relates the theoretical osmotic pressure, the observed osmotic pressure, and the diffusion coefficient for the solute. The evaluation of a series of diffusion coefficients for a "family" of chain polymers has been made, and a comparison given between these values and those obtained by other observers for the free diffusion of various chain polymers, and for computed values of the diffusion coefficients for prolate spheroids.

[1] D. E. Matthews, "A study of the semipermeability of silver membranes" (unpublished Ph.D. dissertation, Department of Physics, Vanderbilt University, 1951).
[2] T. A. Barr, "Anomalous osmotic pressures of polymer solutions as measured in a metal membrane osmometer" (paper presented at the APS Southeastern Section Meeting, 1952).

THURSDAY AFTERNOON AT 2:00

Engineering 125

(C. G. SHULL presiding)

Magnetism and Ferroelectricity

E1. Magnetic Properties of Pyrrhotite. ROBERT R. HEIKES, *Westinghouse Research Laboratories.*—An explanation of the unusual magnetic properties of Fe-S has recently been given by L. Néel.[1] He proposes that the off-stoichiometric compounds (sulfur rich) are really ferrimagnetic. An alternate explanation will be offered in which the dominant interaction is assumed to be the double exchange of Zener.[2] The present model is also able to account for the unusual properties of Cr-S, a compound with the same structure as Fe-S, whereas the picture presented by Néel apparently fails.

[1] L. Néel, Washington Magnetism Conference (1952).
[2] C. Zener, Phys. Rev. **82**, 403 (1951).

E2. Field and Temperature Dependence of the De Haas-Van Alphen Effect in Zinc Alloy Single Crystals.* F. J. DONAHOE, *University of Pennsylvania.*†—The differential magnetic susceptibilities of zinc alloy single crystals have been measured by a torsion method in uniform magnetic fields in the range 2000–9500 oersteds at temperatures between 1.5 and 20.4°K. The results have been compared with a function of the form given by the theory of the diamagnetism of free electrons[1–4] using the electron mass m^*, Fermi level ζ, and the mean free time τ between electron collisions as adjustable parameters:

$$\chi(\mu_0{}^*H) = -\frac{\mu_0{}^2kT\zeta}{2\pi\rho\hbar^3}\left(\frac{2m}{\mu_0{}^*H}\right)^{\frac{1}{2}}\sum_{r=1}^{\infty}\frac{(-1)^r\cos\left(r\pi\frac{m^*}{m}\right)\sin\left(\frac{r\pi\zeta}{\mu_0{}^*H}-\frac{\pi}{4}\right)}{r^{\frac{1}{2}}\sinh\left(\frac{r\pi^2kT}{\mu_0{}^*H}\right)\exp\left(\frac{r\pi\hbar}{\tau\mu_0{}^*H}\right)}.$$

The approximate form of the first term of the series expansion is a poor fit. Harmonic terms are important at high fields. Satisfactory agreement is found for the temperature dependence. Discrepancies in the field dependence suggest that the exponent of the factor $1/H$ which multiplies the series is 5/2 rather than 3/2 as predicted by the free electron theory.

[1] D. Shoenberg, Proc. Roy. Soc. (London) **A170**, 341 (1939).
[2] E. H. Sondheimer and A. H. Wilson, Proc. Roy. Soc. (London) **A208**, 173 (1951).
[3] R. B. Dingle, Proc. Roy. Soc. (London) **A211**, 500 (1952).
[4] M. C. Steele, Phys. Rev. **88**, 451 (1952).
* Supported by the U. S. Atomic Energy Commission.
† Now at The Franklin Institute Laboratories.

E3. The de Haas-van Alphen Effect in Sn-Sb Alloys.* GEORGE T. CROFT† AND FOSTER C. NIX, *University of Pennsylvania.*—The de Haas-van Alphen effect has been observed in tin and in tin antimony alloys at field strengths less than 10 (kg). Particular care was taken to control the composition and thermal equilibrium state of the alloys. The electronic parameters, β and ζ, associated with the long period oscillations are not affected, within the limits of experimental error (±10 percent), by the addition of Sb into the Sn lattice. The collision broadening parameter, X, increases linearly with atomic percent of solute atoms. X for pure Sn (≃0.1°K) is a factor of 10 less than values quoted by Shoenberg.[1] This is attributed to the careful handling and heat treatment given the samples. A marked angular dependence of X was noted in two of the alloy samples. The results indicate that X increases with the angle between the tetragonal axis and the field. There is evidence that the dependence of the amplitude on H is actually given by a higher power of H^{-1} than $\frac{3}{2}$. These data were obtained using a new technique, which enables one to measure continuously the torque on a sample as a function of the field.

* Supported by the U. S. Atomic Energy Commission.
† Now at the Edison Laboratory, Thomas A. Edison, Inc., West Orange, New Jersey.
[1] D. Shoenberg, Proc. Roy. Soc. (London) **A245**, 1–57 (1952).

E4. Eigenfunctions of S^2 by a Spin-Operator Method.* G. W. PRATT, JR.,† *M.I.T.*—A new spin-operator has been found which when operating on a single determinant of space-spin orbitals generates a state of definite multiplicity. This spin operator O commutes with S^2 and the Hamiltonian H of a many particle system. The operator O is Hermitian and $O^2=O$. By application of this operator in the proper manner, one can write down all of the linearly independent and orthogonal singlet states for an N electron problem. This spin-operator method of generating states of a definite multiplicity from a single determinant can be used to effectively reduce the labor involved in a configuration interaction treatment of an N electron system. The method is being applied to the configuration interaction treatment of the $Mn^{++}-O^{=}-Mn^{++}$ system which has previously been considered by Anderson in regard to superexchange and its relation to the theory of antiferromagnetism.

* Supported jointly by the Army, Navy, and Air Force.
† Staff member, Lincoln Laboratory, M.I.T.

E5. Phase Transitions in Antiferrolelectric $PbHfO_3$.* GEN SHIRANE† AND RAY PEPINSKY, *The Pennsylvania State College.*—Phase transitions in ceramic $PbHfO_3$ have been studied by dielectric and structural measurements. The dielectric constant *vs* temperature curve shows two anomalies, at 160°C and 210°C. Between −170°C and 300°C the $P-E$ relation is almost linear, showing no ferroelectric hysteresis loops. At room temperature $PbHfO_3$ has a tetragonal lattice of perovskite type with $a=4.136$A and $c/a=0.991$, and a powder photograph shows some superstructure lines which have essentially the same character as those of $PbZrO_3$. This shows that $PbHfO_3$ is an antiferroelectric of the $PbZrO_3$ type below 160°C. The crystal structure between 160°C and 210°C has turned out to be also a tetragonal lattice as is the lowest phase, but the axial ratio c/a is much nearer to unity, 0.997, and the observed superstructure lines are different from those of the lowest phase. This indicates that the intermediate phase is another antiferroelectric phase which has a different type of dipole arrangement from that of the lowest phase. At 210°C, it becomes paraelectric, accompanied by a structural change to a cubic lattice.

* Development supported by Wright Air Development Center and U. S. Office of Naval Research Acoustics Branch.
† On leave from Tokyo Institute of Technology, Tokyo, Japan.

E6. A Phase Transition in CsH_2AsO_4.* B. C. FRAZER, *Brookhaven National Laboratory,* AND RAY PEPINSKY, *Pennsylvania State College.*—Ferroelectricity has been reported for all of the tetragonal dihydrogen phosphates and arsenates of K, Rb, and Cs except for CsH_2AsO_4. A Curie point of 143°K has been found for this crystal by dielectric constant measurements on a capacity bridge. Typical ferroelectric hysteresis loops were observed below the transition temperature. This study was undertaken primarily for the purpose of completing the series so that ferroelectric properties of its members could be viewed from the standpoint of their crystal chemistry. One

finds that the larger the alkali cations are, relative to the size of the XO_4 groups, the higher the Curie points. While complete data are lacking, the dielectric constants seem to vary also in a more or less predictable way: the larger the alkali cations relative to the XO_4 groups, the smaller the dielectric constants. These observations bear an interesting relation to the x-ray analysis of the KH_2PO_4 transition, in which the largest ionic displacement occurred in the case of K. As with their dielectric properties, the ammonium salts are exceptions: increasing the relative size of the NH_4^+ ion, by replacing As by P, decreases the transition temperature. This may prove to be of some significance in relation to the presumed antiferroelectricity of these salts

* Research carried out under the auspices of the U. S. Atomic Energy Commission.

E7. Threshold Field and Free Energy for the Antiferroelectric-Ferroelectric Phase Transition in Lead Zirconate. A. DEBRETTEVILLE, JR., *Squier Signal Laboratory.*—Sawaguchi and Kittaka[1] obtained the threshold field of $PbZrO_3$—that necessary to change the antiferroelectric to the ferroelectric phase, below the Curie temperature. The free energy difference between the two phases is obtained by integrating the area between the dielectric displacement (ordinate) and the field strength (abscissa) or the hysteresis loop in the ferroelectric phase. An expression for free energy has been obtained as a function of voltage, by eliminating the temperature parameter. This experimental relationship is compared with the author's theoretical expression—one that involves the product of twice the constant spontaneous polarization[2] (6 microcoulombs/cm^2 in the ferroelectric phase), the threshold voltage, and the molar volume (42 cm^3); the free energy so calculated is small—of the order of 3 calories/mole at 25 kv/cm. The agreement between experimental and theoretical values is good. Equations are also given for calculating the threshold field strength and free energy difference as functions of temperature. The equation for threshold field strength resembles the Clapeyron-Clausius equation, with field strength analogous to pressure and spontaneous polarization analogous to volume.

[1] E. Sawguchi and T. Kittaka, J. Phys. Soc. Japan **7**, 336–337 (1952).
[2] Shirane, Sawguchi, and Takagi, Phys. Rev. **84**, 476–481 (1951).

THURSDAY AFTERNOON AT 2:00

Page Auditorium

(JOHN BARDEEN presiding)

Division of Solid-State Physics

Symposium on Semiconductors

F1. Transistor Experiments on Binary Lead Compounds. H. K. HENISCH, *University of Reading.* (30 min.)

F2. Electrons and Holes in Electric and Magnetic Fields. WILLIAM SHOCKLEY, *Bell Telephone Laboratories.* (30 min.)

F3. Infrared Absorption in Elementary Semiconductors, H. Y. FAN, *Purdue University.* (30 min.)

F4. Infrared Absorption and Photoconductivity in Tellurium. P. H. MILLER, *University of Pennsylvania.* (30 min.)

F5. Optical and Photoconductive Investigations of Impurity Levels in Germanium and Silicon. E. BURSTEIN, *Naval Research Laboratory.* (30 min.)

THURSDAY AFTERNOON AT 2:00

Chemistry 116

(OTTO STUHLMANN presiding)

General Physics

G1. Effect of a Centrifugal Force Field on the Response of a Vibrating Mass-Spring System. W. A. WILDHACK AND R. O. SMITH, *National Bureau of Standards.*—The earth's gravitational field furnishes a convenient sinusoidal forcing function for a vibrating system (e.g., an accelerometer) rotating in a vertical plane. The centrifugal field decreases the restoring force on the vibrating mass. Resonance occurs at lower frequencies and with greater amplitudes than in the case of excitation by linear vibration. The response ratio (vibration amplitude/static displacement caused by gravity) is greater than unity for all damping ratios up to unity. The resonant frequency for zero damping occurs at 0.707 times the natural undamped frequency. From measurements of the maximum response ratio, and of the frequency at which this ratio decreases to unity, one may determine both the damping ratio and the undamped natural frequency of any system whose damping ratio is less than unity. The response to the centrifugal field is infinite at a rate of rotation equal to the natural undamped frequency, although the response to the sinusoidal field decreases asymptotically towards zero at higher rotational frequencies.

G2. The Motion of Ions in Perpendicular HF Electric Fields. M. S. MCCAY AND J. H. COULLIETTE, *University of Chattanooga.*—Ion motion studies, usually limited to the cases of (a) magnetic, (b) electric, and (c) electric and magnetic

fields at arbitrary angles, have been extended to the case of (d) oscillating electric fields at right angles. With the ion injection axis perpendicular to the crossed electric fields, which are operated under circular-sweep phase conditions, excellent isotopic separation is indicated, with defocusing interaction between adjacent beams reduced to a minimum by the rotary-sweep motion.

G3. A Study with a NaI Scintillation Spectrometer of Methods of Estimating I^{131} Contained in the Human Thyroid. ROBERT J. KERR, SHERWOOD K. HAYNES, AND GEORGE R. MENEELY, *Thayer Veterans Administration Hospital and Vanderbilt University.*—External gamma-counting of I^{131} in the human thyroid, widely used in medical diagnosis, is subject to errors due to scattered radiation. A NaI(Tl) scintillation spectrometer was used to investigate the spectrum of I^{131} in the thyroids of two patients to evaluate methods of correcting these errors. Spectra were also taken of a point source, a 100 ml volumetric "duplicate" source and a phantom made by immersing this flask in a two-liter beaker of water. These measurements were also made through a ¼-in. Pb filter. Differences in each of these spectra were observed and will be presented. Computed integral spectra show that either a bare duplicate or a bare phantom may yield errors of ±7 percent for the best discriminator setting (~250 kev) and much larger errors for lower discriminator settings. A ¼-in. Pb filter gave consistent values for the two patients independent of discriminator setting, although in each case the estimated content was 6 to 10 percent low. These inconsistencies would be exaggerated by Geiger counters which are most sensitive at low energies. Therefore, of the methods tested, accurate measurements can only be made with a properly designed phantom and a Pb filter.

G4. Spectrographic Analysis of Human Tissue. ISABEL H. TIPTON, W. D. FOLAND, FRANKLIN C. BOBB, AND W. C. MCCORKLE, *The University of Tennessee.*—Over 200 specimens of normal human tissue from 42 individuals from Boston, Massachusetts; Columbus, Ohio; Memphis, Tennessee; and Birmingham, Alabama have been analyzed semiquantitatively for 23 elements. The tissue spectra were compared visually with the spectra of 10 standards of synthetic tissue ash composed of a matrix of potassium di-hydrogen phosphate, sodium chloride, magnesium oxide, calcium carbonate, and iron oxide with twenty-three elements added in concentrations of 1000, 400, 200, 100, 40, 20, 10, 4, 2, and 1 ppm. Certain elements such as manganese and copper were found in nearly the same concentration in all samples of a certain tissue whereas others, such as boron, chromium, and nickel occurred in widely varying concentrations. The most startling discovery was the appearance of more than 1000 ppm of cadmium in every kidney specimen.

G5. Biophysical Study of Burns. IRWIN GRAHAM, DAVID POMEROY, W. C. MCGARVEY, AND JOHN G. RANDALL.—Rats were irradiated so as to produce local burns of varying severity. The gross appearance of the different stages leading to lesions with the subsequent healing process was correlated with histological analysis. The physical irradiation conditions were varied so as to investigate the influence of wavelength and spectral energy composition changes on the topical reactions. These experiments extended earlier work performed in this lab.[1] In conformity with the pioneering ideas of Selye[2] for a unified theory of medicine, burn studies were made also on adrenalectomized and hypophysectomized rats. Results indicated that vesicles form with greatest difficulty in the case of the adrenalectomized rats and that the healing time is also least for those rats. Rats which have had their pituitary glands removed develop vesicles with the same readiness as intact rats, but the degree of edema appears to be less, and the resorption is easier. Duplication of the course of the burns was obtained with varying success by administration of specially selected substances.

[1] K. Schocken et al., October, 1952 (unpublished).
[2] Hans Sleye, *Stress, a Treatise Based on the Concept of the General-Adaptation-Syndrome and the Diseases of Adaptation* (Acta Inc., Medical Publishers, Montreal, Canada. 1950).

G6. A Report on the Measurement of the Thickness of Thin Films by Employing Electron Microscope Shadowcasting Technique. GEORGE W. CRAWFORD, *Clemson Agricultural College* (introduced by L. D. Huff).—In studying the properties of thin films (thicknesses less than 500A) using the electron microscope, it became necessary to find a method of accurately determining the thickness of very thin films. Such a method was found by applying electron microscope shadowcasting technique to the problem. When the film is first prepared by evaporation, care is taken to obtain an edge whose top is level with the rest of the film and which has a vertical cliff. This edge is then shadowcast and a picture of the edge of the cliff and its shadow is taken using the electron microscope. The length of the shadow on the negative is then measured using a traveling microscope and knowing both the angle at which the shadow was cast and the magnification factor for that negative, the thickness of the film is calculated.

G7. Polarization in Liquids of Intermediate Conductivity.* JOHN A. RIDER, *Louisiana State University* (introduced by Lloyd W. Morris).—This investigation was undertaken in order to test the application of the Jaffé theory of conductance in polarizable media[1] to liquids having a range of conductance which has received little attention from the standpoint of polarization. This is the range between electrolytic solutions of conductance $K < 10^{-6}$ ohm^{-1} cm^{-1} and dielectric liquids of conductance $K > 10^{-17}$ ohm-cm^{-1}.[2,3] Measurements have been made on hexane, isopropyl ether, and dibromobenzene in varying degrees of purity.

* Work supported in part by U. S. Office of Naval Research.
[1] G. Jaffé, Ann. phys. 16, 217, 249 (1933).
[2] G. Jaffé and J. A. Rider, J. Chem. Phys 20, 1077-1087 (1952). This paper contains a complete listing of earlier electrolytic work.
[3] G. Jaffé and C. LeMay, J. Chem. Phys. (to be published). This paper will contain a listing of earlier dielectric work.

G8. A General Method for Predicting the Molar Activity Coefficients of Electrolytes from Conductivity Data.* HENRY P. MARSHALL AND ERNEST GRUNWALD, *Florida State University.*—We have obtained an expression for the molar activity coefficients of uni-univalent electrolytes which applies whenever the electrolyte exists partly as free ions and partly as short-range ion pairs. The derivation is based on the approach of Bjerrum and postulates the existence of a quasi-equilibrium between the free ions and the ion pairs. The interionic free energy of the free ions is calculated by applying the methods of Debye and Hückel to our model. The quasi-equilibrium constant for the ion pair dissociation is obtained from conductivity data by a method similar to that of Fuoss and Kraus but consistent with our model. The equations are tested by means of the data for hydrochloric acid in solvents ranging in dielectric constant from 40 to 10. In this range, the quasi-dissociation constant of the ion pairs is the only constant contained in our equations which is characteristic of the electrolyte. The conductivity data therefore uniquely prescribe the molar activity coefficients, and our predicted values agree well within 2 percent with those determined from emf measurements up to electrolyte concentrations of the order of 0.01M.

* This work was done in collaboration with the Office of Ordnance Research.

G9. Electric Conduction at Metal-Semiconductor and Metal-Solution Interfaces. HUNG-CHI CHANG, *Louisiana State University* (introduced by Lloyd W. Morris).—The

generalized Jaffé theory of polarization for electrolytic solutions, dielectric liquids and semiconductors[1] is further extended so as to include an intermediate layer of high insulation between the metal and the polarization layer. This thin layer may be either the Helmholtz monolayer, or one formed electrochemically. Its thickness is treated as current dependent and is therefore a function of the applied potential, frequency, and concentration. The calculation of the equivalent parallel resistance and capacitance has been carried to the second order of approximation. The introduction of this intermediate layer affords an explanation of the increase in capacitance observed at low frequencies, as well as the long time required for the chanrging current to reach steady state in dielectric liquids. These phenomena have been explained by the Jaffé theory on the basis of slow ions. The present theory provides an alternative interpretation of these phenomena. In addition the inductive character of the action at the interface observed under some conditions of bias can be predicted qualitatively.

[1] Hung-Chi Chang and George Jaffé, J. Chem. Phys. **20**, 1071 (1952).

G10. A Continuous Flow Cell for the Investigation of Polarization at Metal-Solution Interface. L. W. MORRIS AND HUNG-CHI CHANG, *Louisiana State University.*—It is well known that the reproducibility of measurements on electrolytic polarization is rather poor, since the polarization effects depend strongly on surface conditions which are difficult to control, especially when chemical reactions occur at the electrode surface. A continuous flow cell has been developed, which consists of a pair of demountable electrodes with a fixed separation of 0.318 cm and an effective area of 7.92 cm². The solution moves steadily past the electrodes isolated from contact with the unfiltered atmosphere. To give an instance of the reproducibility obtained for one specimen of water, at frequency of 1000 cps, the resistance was measured as 24 720 ohms and the capacitance as 0.172 mfd. At a time 28.5 hours later the measurements yielded 24 710 ohms and 0.171 mfd. This continuous flow cell has been used for studying electrolytic rectification with aluminum as electrodes and ammonium borate as electrolytes. The series capacitance and resistance of this cell were measured over a range of frequencies from 18 cps to 18 kcps. Measurements were made at 0.0001, 0.001, and 0.01 *M* concentrations and after forming at voltages of 22.5, 45, 90, 135, and 180 v. The results are discussed according to the generalized Jaffé theory described in Paper No. G9.

G11. The Solubility of Solids in Gases. A. H. EWALD (introduced by W. G. Schneider).—In a system consisting of a pure solid in equilibrium with a nonreacting compressed gas, the mole-concentration x_2 of the solid component in the gas phase can be expressed by[1]

$$\ln \frac{x_2}{x_2^0} = \frac{V_{\text{solid}} P}{RT} - \frac{2B_{12}}{V_m} - \frac{3}{2}\frac{C_{112}}{V_m^2} - \frac{4}{3}\frac{D_{1112}}{V_m^3},$$

where x_2^0 is the concentration corresponding to the normal vapor pressure of the solid. The first term represents the Poynting pressure effect while the remaining terms represent the interactions of single solute molecules with gas molecules. The mixed virial coefficient B_{12} may be calculated from the properties of the pure components by the principle of corresponding states, while this method leads to only a first approximation for the higher coefficients. Values calculated by the equation are in fair agreement with experiments. Solubilities measured at moderate pressures may be used to determine B_{12}. A radioactive tracer method has been used to measure the solubility of *p*-chloroiodobenzene in compressed ethylene.[2]

[1] Ewald, Jepson, and Rowlinson, "Equilibrium properties of non-electrolytes and non-electrolyte solutions," Faraday Soc. Disc. (to be published).
[2] A. H. Ewald, Ph.D. thesis, Manchester, 1952 (to be published).

THURSDAY AFTERNOON AT 2:00

Biology 113

(FRITZ LONDON presiding)

Cryogenics

GA1. Atomic Heat of Germanium below 4°K. P. H. KEESOM AND N. PEARLMAN, *Purdue University.*—The Debye θ of pure Ge has been reported as 278°K, from measurements below 4°K of the atomic heat of crushed Ge in a Cu calorimeter.[1] We found, however, 369°K for Ge in the form of ingots.[2] We have now also measured the atomic heat of pure crushed Ge. Above 3°K the results agree with the previous ingot measurements. Below this temperature, there is a small additional heat capacity which decreases when the amount of He exchange gas in the calorimeter is reduced. This can be accounted for by desorption of exchange gas from the small Ge particles (0.1–3 mm). We conclude from measurements on seven ingots of various sizes and shapes and the crushed sample that below 3°K (the upper limit of the true T^3 region) θ is (364±3)°K, in agreement with Parkinson's estimate from atomic heat data[3] and the value, 375°K, which we calculate from elastic constants.[4]

[1] I. Estermann and S. A. Friedberg, Phys. Rev. **85**, 715 (1952).
[2] P. H. Keesom and N. Pearlman, Phys. Rev. **85**, 730 (1952).
[3] R. W. Hill and D. H. Parkinson, Phil. Mag. **43**, 309 (1952).
[4] Bond, Mason, McSkimin, Olsen, and Teal, Phys. Rev. **78**, 176 (1950).

GA2. Low Temperature "Breakdown" Effect in Germanium. N. SCLAR, E. BURSTEIN, W. J. TURNER, AND J. W. DAVISSON, *Naval Research Laboratory.*—Current-voltage measurements on germanium at liquid helium temperatures using dc and microsecond pulses have revealed the existence of a reversible, nondestructive, "breakdown" effect for low applied voltages. The "breakdown," which manifests itself as a sharp increase in current of several orders of magnitude over a small range in voltage, takes place in both "*n*" and "*p*" type germanium. Exposure of the specimen to room temperature background radiation increases the current in the pre-breakdown region but does not effect the current at higher voltages. The effects of room temperature radiation, which are due to the photoionization of neutral impurities, imply that the charge carrier density in the breakdown region is markedly greater than in the pre-breakdown region. It is suggested that the "breakdown" effect is the result of charge carrier multiplication by impact ionization of neutral impurities in which the free charge carriers gain the necessary energy from the applied field. The relatively low voltage required for "breakdown" is accordingly attributed to the high mobility of the charge carriers in germanium at low temperatures.

GA3. Method for Measuring Magnetic Moments of Superconductors. TED G. BERLINCOURT AND M. C. STEELE, *Naval Research Laboratory.*—A torsion balance has been used to measure the couple acting on a small tin cylinder placed in a

homogeneous magnetic field with its axis making an angle of approximately 30° with the field. The method, which is also applicable for very nearly transverse or longitudinal fields, differs from that used by Alekseyevsky[1] in that very small deflections are utilized so that the specimen orientation is not appreciably altered even at maximum moment. The observed magnetization curves are strictly linear in the superconducting region. In some cases a discontinuity was observed as the specimen entered the intermediate state, which is qualitatively in accord with current theories of the intermediate state.[2,3] The method should be applicable to magnetic moment measurements on superconductors in the adiabatic demagnetization temperature range.

[1] N. E. Alekseyevsky, J. Phys. (U.S.S.R.) **4**, 401 (1941).
[2] L. D. Landau, J. Phys. (U.S.S.R.) **7**, 99 (1943).
[3] C. G. Kuper, Phil. Mag. **42**, 961 (1951).

GA4. Adiabatic Magnetization of a Superconducting Sphere. R. L. DOLECEK, *Naval Research Laboratory.*—Temperature changes accompanying suppression of the superconductivity of a lead sphere by adiabatic magnetization have been investigated. Measurements were taken of the cooling produced by adiabatic magnetization and the heating produced by adiabatic demagnetization. The magnetic fields were applied and removed as step functions of time and allowance was made for the resulting eddy current heating. Observations were made in the temperature range 2.2°K to 5.0°K for fields in the range. $1.18>h>0.77$ where h is the ratio of applied field to critical magnetic field. This range of magnetic fields corresponds to $0.3<x\leq 1.0$ where x is the fraction of the lead sphere that becomes normal when the sphere is subjected to a magnetic field sufficient to produce the intermediate state, *viz.*, $\frac{2}{3}<h<1.0$. Temperature changes observed on magnetization and demagnetization are in quantitative agreement with values predicted from calorimetric data and thus confirm the gross aspects of current interpretation of the entropy of a superconductor in the intermediate state.

GA5. Search for the Hall Effect in a Superconductor. H. W. LEWIS, *Bell Telephone Laboratories.*—Since the first experiments of Kamerlingh Onnes and Hof, in 1914, it has been widely believed that there is no Hall effect in the superconducting state. However, these first experiments were performed on samples that must have been, in fact, in the intermediate state (which was not, of course, known at the time) so that the experimental question must be considered still open. A search has been made, by a new method, on a specimen of superconducting vanadium, and the preliminary result is negative, with an upper limit of about twenty to thirty percent of the normal expected Hall coefficient. The theoretical implications will be discussed.

GA6. Theory of Pressure Effects on Superconducting Transition Temperatures. PAUL M. MARCUS, *Carnegie Institute of Technology.*—Measurements[1] of effects of hydrostatic pressure, p, on superconducting transition temperatures, T_c, show in general a decrease of T_c. The magnitude of the effect is understandable by a treatment like that given the isotope shift by the lattice vibration interaction theory[2] and constitutes another test of that theory. In both cases the single electron interaction energy, Δ, is assumed proportional to the mean-square lattice vibration amplitude, $(q^2)_{Av}$, in the zero-point oscillation. For isotopes $(q^2)_{Av}$ decreases as lattice mass increases; here it decreases because the force constant increases as the lattice is compressed. Change of force constant or, equivalently, of frequency with lattice size is estimated from Gruneisen's constant γ. Since Δ is proportional to kT_c, as follows easily from a model of the second-order transition, such as the two fluid model, we obtain $(d\ln T_c/dp) = -V\alpha/C_V$ with volume expansivity α, molar volume V, molar heat capacity C_V. This gives for indium, the best case, $dT_c/dp = -2.1\times10^{-11}$ °K dyne^{-1} cm^2 *vs* measured value -4.7×10^{-11}.

[1] Kan, Sudovstov, and Lasarew, J. Exptl. Theoret Phys. U.S.S.R. **18**, 825 (1948).
[2] J. Bardeen, Phys. Rev. **80**, 567 (1950).

GA7. The Superconducting Transition in Aluminum.* D. E. MAPOTHER AND J. F. COCHRAN, *University of Illinois.*—The superconducting transition in aluminum has been studied down to about 0.75°K using a cryostat in which the cooling is produced by pumping over liquid helium. Measurements are made at constant temperature in a dc magnetic field whose value is changed in a stepwise manner by increments of the order of a few tenths of an oersted. The resulting changes in the flux through the sample are detected by a ballistic induction method. Measurements have been made on a single crystal sample of aluminum (purity 99.997 percent) which was cast in an accurate ellipsoidal shape. The transitions observed are quite sharp being of the order of 0.5 oersted when going from the superconducting to the normal state. The transition from the normal to the superconducting state occurs with complete abruptness since the supercooling characteristic of aluminum[1] is very pronounced. The ratio of the field for the supercooled transition to the critical field is about 0.60 at the lowest temperatures measured and decreases with increasing temperature. The Meissner effect for this sample appears to be better than 97 percent complete.

* Supported in part by the U. S. Office of Ordnance Research and the U. S. Office of Naval Research.
[1] D. Shoenberg, Proc. Cambridge Phil. Soc. **36**, 84 (1940).

GA8. Helium II: Bose-Einstein Condensation and Two-Fluid Model. P. R. ZILSEL, *University of Connecticut.**—Imposing a total momentum on a Boltzmann or Fermi-Dirac gas shifts the equilibrium distribution as a whole in momentum space, but does not change its character. However, for some forms of the energy spectrum in the case of a degenerate Bose gas, the condensed state does not participate in the imposed motion, and a relative velocity $\mathbf{v}$ results between the condensed state and the center of mass of the excited states. The total momentum is $\mathbf{P}=M_n\mathbf{v}$ (M_n = effective mass of the excited part). For the energy E' in the rest system of the condensate one then has $dE'=TdS-PdV+\mathbf{v}\cdot d(M_n\mathbf{v})$, which leads to the same two-fluid equations of motion derived previously from a variational principle.[1] The "rigidity" of the condensate in momentum space plays the same role as the rigidity of the superconducting electrons on imposition of a magnetic field in the London theory. The state of relative motion between the condensate and the excited particles is macroscopically metastable.

* Assisted by a Research Corporation grant.
[1] P. R. Zilsel, Phys. Rev. **79**, 309 (1950).

GA9. An Apparatus for Magnetic Measurements at Low Temperatures. R. A. ERICKSON, *University of Tennessee,* AND L. D. ROBERTS, *Oak Ridge National Laboratory.*—A cryostat and Hawtshorn type mutual inductance bridge have been built for the measurement of the magnetic properties of antiferromagnetic and paramagnetic compounds continuously over the temperature region from 80°K down to the temperatures obtained by magnetic cooling (~0.01°K). This apparatus is an improvement on previous designs in that a somewhat higher usable sensitivity (2×10^{-9} henry) has been obtained over a larger frequency range of approximately 0–10 kc. These improvements result from winding all coils in such a way as to reduce internal capacities; in connecting the variable mutual coils through reversing switches so that the calibration of the variable mutual inductance can be quickly and easily checked; and through the use of a twin T feed back amplifier in the CRO detection circuit which gives a Q of ~100 and a sensitivity of 10^{-8} volt. Data on manganous ammonium sulfate will be presented.

Post-Deadline Papers, if Any

THURSDAY AFTERNOON AT 2:00

Physics 114

(R. S. MARVIN presiding)

Division of High-Polymer Physics

Mechanical and Electrical Properties

GB1. Rheology of Polyisobutylene III. Approximation Methods in Linear Viscoelasticity Theory: Wiechert Function Calculations.* HERBERT LEADERMAN, *National Bureau of Standards.*—In connection with previously reported retarded elastic behavior of low molecular weight polyisobutylene,[1] a study has been made of the validity of approximation methods in the calculation of the retardation time function $L(\ln\tau/\tau_0)$ and of dynamic response from creep data obtained from a Wiechert "model" retardation time function with $b=0.4$. First and second approximations for $L(\ln\tau/\tau_0)$ are calculated by the methods of Alfrey and Schwarzl.[2] Second approximations are also obtained by differentiating $J'(\omega\tau_0)$ calculated by Marvin's difference function[3] and by a new successive approximation method. Alfrey's and Schwarzl's approximations were obtained also by fitting retarded elasticity data (from the "model" function) to a Kohlrausch type function. Marvin's difference function method appears to be the best way of computing $J'(\omega\tau_0)$ from creep data. $J''(\omega\tau_0)$ has been computed from $J'(\omega\tau_0)$ (a) by an approximate method using a difference function and (b) exactly by a Kronig-Kramers integral.

* Supported by the U. S. Office of Naval Research and Office of the Quartermaster General.
[1] H. Leaderman and R. G. Smith, Phys. Rev. **81**, 303 (1951).
[2] F. Schwarzl and A. J. Staverman, Physica **18**, 791 (1952).
[3] R. S. Marvin, Phys. Rev. **86**, 644 (1952).

GB2. Dynamic Mechanical Properties of Polyisobutylene. EDWIN R. FITZGERALD,* LESTER D. GRANDINE, JR.,† AND JOHN D. FERRY, *University of Wisconsin.*—Values of complex shear compliance (and rigidity) have been obtained for a sample of polyisobutylene of viscosity-average molecular weight 1.35×10^6, distributed by the National Bureau of Standards, at 22 temperatures from −45 to 100°C and at about 20 frequencies from 30 to 5000 cps. Measurements were made by means of the transducer method of Fitzgerald and Ferry with a precision of ±2 percent and are estimated to be accurate to within ±3 percent as evidenced by agreement obtained between 7 different samples of widely varying dimensions. Values of the real part of the complex shear compliance, J', vary from 3.1×10^{-7} cm²/dyne at 99.9°C to 1.0×10^{-10} cm²/dyne at −44.6°C. The frequency dependence of the loss tangent J''/J' indicates the presence of a low, broad maximum of 1.7 at −10 to −5°C and a second, smaller maximum or plateau at lower temperatures. This second maximum is also evident in a plot of J''/J' at a fixed frequency against temperature. The wide temperature and frequency ranges of the measurements have provided an essentially complete experimental description of the dispersion region in polyisobutylene corresponding to the transition from a rubber-like elasticity to that of a hard glass.

* Present address: Pennsylvania State College.
† Present address: E. I. du Pont de Nemours and Company.

GB3. The Relaxation Distribution Function of Polyisobutylene in the Transition from Rubberlike to Glasslike Behavior and its Dependence on Temperature. JOHN D. FERRY, LESTER D. GRANDINE, JR.,* AND EDWIN R. FITZGERALD,† *University of Wisconsin.*—The steady flow viscosity of a sample of polyisobutylene of viscosity-average molecular weight 1.35×10^6 (distributed by the the National Bureau of Standards) has been measured from 15° to 97°C; its logarithm is a linear function of $1/T^2$. The complex compliance of this material, $J'-iJ''$, as reported previously from −45° to 100° and from 30 to 5000 cps, has been analyzed by the method of reduced variables modified[1] to account for the glasslike compliance; it yields single composite curves for J' and J''. The values of a_T, the temperature reduction factor, are slightly but significantly larger than those derived directly from the viscosity; the latter, however, agree with those derived from stress relaxation measurements of Tobolsky and McLoughlin.[2] The reduced loss tangent, J_p''/J_p', as a function of reduced frequency is broader than in other polymers and shows the secondary plateau apparent in the original data. The distribution functions of relaxation and retardation times are similar in shape to those of other polymers in the transition from rubberlike to glasslike behavior.

* Present address: E. I. du Pont de Nemours and Company.
† Present address: Pennsylvania State College.
[1] Fitzgerald and Ferry, J. Colloid Sci. (to be published).
[2] Tobolsky and McLoughlin, J. Polymer Sci. **8**, 543 (1952).

GB4. Dynamic Properties of Unvulcanized GR-S.* L. J. ZAPAS, S. L. SHUFLER, AND T. W. DEWITT, *Mellon Institute* (introduced by R. S. Marvin).—Dynamic moduli and loss factors have been measured on a sample of unvulcanized GR-S at temperatures between −68°C and +63°C. The frequencies employed ranged from about 5×10^{-4} cps to 3 cps. This range of frequencies and temperatures was sufficient to include nearly the whole of the glassy transition region where the shear modulus drops abruptly from about 1×10^{10} dynes/cm² to about 1×10^7 dynes/cm² where there is a suggestion of a plateau. At higher temperatures, the modulus drops off gradually and continuously, presumably to zero. The lowest measured value was about 3×10^6 dynes/cm². When plotted in terms of reduced variables, the data cover a considerable section of the useful mechanical frequency spectrum for this sample of GR-S. The data are compared with stress relaxation measurements reported in the literature.

* This work was supported by the Office of Synthetic Rubber, Reconstruction Finance Corporation.

GB5. Dynamic Properties of Concentrated Polymer Solutions.* F. J. PADDEN, H. MARKOVITZ, AND T. W. DEWITT, *Mellon Institute.*—The dynamic rigidities and viscosities of a variety of solutions of polyisobutylene in decalin have been determined in the neighborhood of room temperature and at frequencies between 10 and 100 cycles per second. Zero shear viscosities of these solutions have been measured by both falling ball and capillary methods. Concentration and molecular weight of the solute were the main variables and ranged from a 5 percent solution of a sample of molecular weight 2.5×10^6 to a 40 percent solution of a sample of molecular weight 1.5×10^5. When reduced variables that take into account concentration and temperature are used, superposition of data from samples of different molecular weights is not achieved. A scale shift that is equivalent to treating molecular weight semiquantitatively as an inverse concentration achieves reasonable superposition and suggests that the important variable is the number of chains per unit volume The

results are compared with some previously obtained on low molecular weight oils and on whole polymer.

* This work was supported by the Office of Synthetic Rubber, Reconstruction Finance Corporation.

GB6. Calculation of Extrusion Behavior of Viscoelastic Materials from the Relaxation Distribution Function. THOR L. SMITH, *Hercules Powder Company* (introduced by R. S. Marvin).—A viscoelastic material when extruded rapidly through a short capillary or spinneret may exhibit an effective viscosity which is smaller by a factor of several hundred than the viscosity as usually measured at low shear rates. An equation is derived which expresses the effective viscosity as a function of the time the material spends in the spinneret (transit time) and the distribution function of Maxwellian relaxation times. In the derivation it is assumed that the mechanical properties of the material may be represented by a generalized Maxwell model. Effective viscosities observed when a 25 percent cellulose acetate solution is extruded through a spinneret with radius 0.006 cm and effective length 0.0186 cm are given. The relaxation distribution function for the solution is calculated from the published dynamic viscosity data of Philippoff. From the distribution function and values of the transit time, effective viscosities are calculated and found to agree with the experimental values to within factors of 1.2 to 3.1. This agreement is considered satisfactory in view of the fact that all nonlinear effects (non-Newtonian and non-Hookean) are neglected in the calculations and the effective viscosities are smaller than the usual flow viscosity by factors of 150 to 10.

GB7. Dielectric Relaxation in a Styrene-Acrylonitrile Copolymer during and after its Polymerization.* P. EHRLICH AND N. J. DELOLLIS, *National Bureau of Standards* (introduced by P. J. Franklin).—Dielectric relaxation in a plasticized copolymer of styrene and acrylonitrile during its polymerization and in the fully polymerized resin is studied by means of measurements of dielectric constant and loss tangent at frequencies from 10^2 to 10^5 cps. Drastic changes in dielectric constant and loss occur during the polymerization. These are interpreted as resulting from the relaxation of the nitrile groups at a rate which depends strongly on the extent of the polymerization. There is a striking parallelism between the electrical properties of the fully polymerized copolymer as observed at elevated temperatures and those of the partly polymerized reaction system at an early stage of the reaction and at a lower temperature: values of the loss factor are similar at equal average relaxation times and in each case there is a similar broadening of the relaxation distribution function as cross links are introduced. Values of the heats and entropies of activation are consistent with the picture of dipole relaxation.

* Supported by Chief of Ordnance.

GB8. Dielectric Dispersion of Polar Polymers at Microwave Frequencies. T. M. SHAW AND J. J. WINDLE, *Western Regional Research Laboratory.*—The dielectric properties of wool and mohair have been investigated at frequencies of 3000 Mc and 10 000 Mc by means of a cavity resonator method. The resonator previously described[1] was provided with a slot parallel to the direction of current flow in the cavity, which allows the use of taut fiber specimens. Fibers are mounted on a frame which, when inserted in the slot in the cavity, positions the fibers precisely on the cavity axis. It was found that the dielectric constant, ϵ, at 25°C, of oven-dry wool is the same, within experimental error, as that of oven-dry mohair. For wool $\epsilon = 3.70 \pm 0.04$ at 3000 Mc and 3.54 ± 0.04 at 10 000 Mc. These values are significantly smaller than the value $\epsilon = 4.2 \pm 2$ percent reported by Errera and Sack[2] for lower frequencies and are large compared to the square of the index of refraction for visible light, $n^2 \sim 2.4$. In a survey of the dielectric properties of other hydrogen-bonded polymers, large differences between the dielectric constant for frequencies in the microwave range and n^2 were also found.

[1] T. M. Shaw and J. J. Windle, J. Appl. Phys. **21**, 956 (1950).
[2] J. Errera and H. S. Sack, Ind. Eng. Chem. **35**, 712 (1943).

Invited Paper

GB9. Relaxation Distribution Functions of Polymers and Their Concentrated Solutions and Gels. J. D. FERRY, *University of Wisconsin.* (30 min.)

FRIDAY MORNING AT 10:00

Page Auditorium

(HARVEY BROOKS presiding)

Division of Solid-State Physics

Color Centers

Invited Paper

H1. Current Status of the F-Center Problem in Alkali Halides. F. SEITZ, *University of Illinois.* (50 min.)

H2. *Z*-Centers in Alkali Halides.* D. R. WESTERVELT, *North American Aviation, Inc.*—The secondary absorption band resulting from heat treatment of crystals containing *F*-centers differs in several respects from the well-known bands produced by *F*-light bleaching. This band, which has been isolated in additively colored crystals by Scott and Smith,[1] and in electron bombarded crystals by the writer,[2] is produced also in crystals heavily darkened by x-rays; hence it is not peculiar to any coloring method. The earliest systematic study of the effects of thermal annealing on heavily colored crystals appears to be due to Przibram[3] and his coworkers, and it is suggested that their appropriate term *Zwischenzentren* be adopted to designate the absorption centers resulting from heat treatment. The room temperature

absorption peak of the Z-band lies at 580, 765, and 825 mμ in NaCl, KCl, and KBr, respectively. It is independent, in additively colored crystals, of the metal added. The location, height, and width of the Z-band are relatively, but not completely, insensitive to temperature, in contrast to these properties of the F, M, R, N, and K-bands, which are strongly affected. The growth rate of the R-bands during F-light irradiation is independent of the presence of Z-centers.

* This report is based on studies conducted for the U. S. Atomic Energy Commission under contract AT-11-1-GEN-8.
[1] A. B. Scott and W. A. Smith, Phys. Rev. **83**, 982 (1951).
[2] D. R. Westervelt, Phys. Rev. **86**, 643 (1952), Bull. Am. Phys. Soc. **27**, 9 (1952).
[3] K. Przibram, Z. Physik **130**, 269 (1951), summarizes much of this work.

H3. Bleaching Properties of F-Centers in KBr at 5°K.* J. J. Markham, R. T. Platt, Jr., and I. L. Mador, *The Johns Hopkins University*.—The bleaching properties of F-centers in KBr have been investigated experimentally at 5°K and 78°K. A Beckman spectrophotometer was used for measuring the absorption spectra and for bleaching the crystals. The stability of F-centers towards bleaching at 5°K and at 78°K is dependent on the mode of formation. Those produced by additive coloration are stable; those produced at room temperature by x-rays bleach slightly; those produced at 78°K by x-radiation show some bleaching; while those produced at 5°K by x-radiation show a large initial instability. The properties of F-centers made by a pointed cathode by excitons or by electron bombardment have not been explored. Some tentative theoretical conclusions will be made.

* This research was supported by the U. S. Navy Bureau of Ordnance.

H4. The Band Width of F-Centers in KBr.* I. L. Mador, J. J. Markham, and R. I. Platt, Jr., *The Johns Hopkins University*.—The absorption spectra of color centers in alkali halides may be characterized by the wavelength of maximum absorption and the half-width (difference between the wavelengths where the absorption is half the maximum value.) Previous measurements[1,2] indicate that the half-width may not be a unique property of a crystal, but may vary from sample to sample. The comparison of data from various experimenters is not valid because of uncertainty in spectral slit widths employed. A series of measurements have been made on F-centers in KBr at 5°K and at 78°K. The centers were formed by x-radiation at various temperatures and by additive coloration with excess potassium. The data on half-widths and wavelength maxima will be presented.

* This research was supported by the U. S. Navy Bureau of Ordnance.
[1] A. Smakula, Z. Physik **59**, 603 (1930).
[2] W. H. Duerig and J. J. Markham, Phys. Rev. **88**, 1043 (1952).

H5. Production of F'-, M-, and R-Centers in NaCl at Room Temperature.* R. T. Platt, Jr., I. L. Mador, and J. J. Markham, *The Johns Hopkins University*.—One may produce a variety of absorption centers to the long wavelength side of the F-band. The ones most carefully studied are the F'-, R_1-, R_2-, and M-bands. In NaCl at room temperature, the R-bands overlap and resemble the F'-band; indeed, it is not possible to tell if the "erregt" state, so extensively studied by the workers in Gottingen, is due to R- or F'-centers. An experimental study of these bands has been made. It indicates that during x-radiation the F-, F'-, and M-band form. Since the lifetime of the F'-band at 300°K is several minutes it dissociates during the course of the usual absorption measurement. To obtain reliable growth rate of the F-band during x-radiation the contribution of the F'-band must be taken into account. The R-bands are formed primarily by optical bleaching of the F-band. The experiments show that the "erregt" state at room temperature is due to the presence of the R-bands, not the F'-band. The coagulation of vacancies will be considered.

* This research was supported by the U. S. Navy Bureau of Ordnance.

H6. Electronic Structure of F-Centers. C. Kittel, *University of California, Berkeley*.—Observations by Hutchison and Kip on the width of the microwave spin resonance absorption line associated with F-centers in KCl colored with excess K may be accounted for with the molecular orbital model of an F-center previously shown[1] to account for the g-value of the resonance. The observed line is Gaussian with width 57 oersteds, practically independent of concentration and quenching procedure. The theory of dipolar broadening[2] in randomly populated crystals leads to a Lorentzian line of width about 0.01 oersted. Interactions with nuclear spins on the usual central field model of an F-center gives ~1 oersted. The LCAO model[1] gives a width which may be calculated from the hyperfine interaction of the 4s state in the K atom. Taking the electron as shared among the six K^+ ions bounding the anion vacancy, there are 4096 hyperfine components distributed among 19 lines. The envelope is approximately Gaussian; the calculated width is ~50 oersteds and independent of concentration. The agreement with experiment therefore appears to be satisfactory.

[1] A. H. Kahn and C. Kittel, Phys. Rev. **89**, 315 (1953).
[2] C. Kittel and E. Abrahams, Phys. Rev. (to be published).

H7. A Calculation of Electron Energy Levels in F-Centers.* William A. Smith and Allen B. Scott, *Oregon State College* (introduced by Harvey Brooks).—The methods of Simpson[1] have been extended to the calculation of the energies of the 1s and 2p levels for electrons in F-centers of NaCl, KCl, KBr, KI, and of KCl at −194°. The use of a different value of the dielectric constant for NaCl and a more precise evaluation of the parameters λ and β resulted in somewhat better agreement between the observed and calculated energies of maximum absorption than in cases previously reported. The calculations fail to predict a shift of absorption maximum with temperature for KCl, but the observed shift is only 0.08 ev between 20° and −194° and the calculated results generally disagree with observed values by this amount or more. The thermal activation energies necessary to raise electrons from the 2p level to the conduction band were calculated for the four crystals, and ranged from 0.01 ev for KCl to 0.29 for KI. The behavior of F-centers in the four crystals during illumination may be qualitatively correlated with these values.

* This work was supported by the U. S. Office of Naval Research.
[1] J. H. Simpson, Proc. Roy. Soc. (London) **A197**, 269 (1949).

H8. Photoconductivity and V-Centers.* K. Teegarden and R. J. Maurer, *University of Illinois*.—Irradiation of alkali halide crystals with x-rays at −185°C produces a series of absorption bands (V-bands) in the ultraviolet region of the spectrum.[1,2] The V_1 band which occurs at 3600A in KCl and at 4100A in KBr is thermally unstable at higher temperatures. The thermal bleaching of this band is accompanied by the appearance of free charge within the crystal.[3] The V_1 band is also bleached by absorption of radiation at liquid N_2 temperature.[4] Absorption of radiation by the V_1 band is observed to yield negligible photoconductive current at −185°C. Photoconductivity is observed in KBr upon irradiation in the wavelength region between 2500A and 3200A where the V_2, V_4, and V_7 bands occur. KCl shows similar behavior.

* Partially supported by a National Science Foundation Grant.
[1] Casler, Pringsheim, and Yuster, J. Chem. Phys. **18**, 887 (1950).
[2] H. Dorendorf, Z. Physik **129**, 317 (1951).
[3] Dutton, Heller, and Maurer, Phys. Rev. **84**, 363 (1951).
[4] Casler, Pringsheim, and Yuster, J. Chem. Phys. **18**, 1564 (1950).

H9. The Storage of Energy in Silver Activated Potassium Chloride.* C. E. Mandeville and H. O. Albrecht, *Bartol Research Foundation*.—The fluorescence, phosphorescence, and energy storage properties of KCl-Ag have been investigated by noting the behavior of the ultraviolet emission band under alpha-particle bombardment and x-ray irradiation. Particular emphasis is given the study of the release of stored energy by

irradiation with long wave light. The release of the "stored ultraviolet" by photostimulation can be observed only while the stimulating light is on (stimulated fluorescence). There is very little stimulated phosphorescence from KCl-Ag. The storage characteristics of KCl-Ag have been compared with those of NaCl-Ag. The stimulated fluorescence of NaCl-Ag is shown to be much greater than its stimulated phosphorescence, in terms of photons per second. The dosimetric aspects of the data will be discussed.

* Assisted by the joint program of the U. S. Office Naval Research and the U. S. Atomic Energy Commission.

H10. Reversible Bleaching of an Absorption Band of Diamond. PETER PRINGSHEIM, *Argonne National Laboratory.*—When diamonds which show the absorption band in the near ultraviolet, a characteristic of blue fluorescing samples, are exposed to neutron bombardment, a continuous absorption slowly rising toward shorter wavelength is superimposed upon the band. Heating such a diamond to temperatures between 300° and 600°C decreases the continuous absorption and the structure of the band becomes appreciably sharper. Subsequent exposure to light greatly reduces the height of individual peaks in the band, while the continuous absorption at shorter wavelengths is increased. Renewed heating restores the sharp structure of the band and the cycle can be repeated at will. Heating the crystal to 750°C brings the crystal very nearly back into the state before neutron bombardment in which the reversible bleaching cannot be observed. A possible mechanism for this phenomenon will be discussed.

FRIDAY MORNING AT 10:00

Engineering 125

(R. SMOLUCHOWSKI presiding)

Metals

I1. Electron Density in Sodium Tungsten Bronze. W. R. GARDNER AND G. C. DANIELSON, *Iowa State College.*—The electrical resistivity and Hall coefficient measurements of Huibregtse, Barker, and Danielson[1] have been extended to include single crystals of Na_xWO_3 having x values from $x=0.58$ to $x=0.90$. The sodium concentration was determined by comparing the lattice constant with a known lattice constant *versus* concentration curve. A minimum in the resistivity as a function of x was found at $x=0.75$, where $\rho=2.2\times10^{-5}$ ohm-cm, in fair agreement with the results of Brown and Banks.[2,3] The Hall coefficient was found to vary inversely with sodium concentration from $R_H=5.85\times10^{-4}$ cm³/coulomb at $x=0.584$ to $R_H=3.92\times10^{-4}$ cm³/coulomb at $x=0.897$. These results indicate that each sodium atom contributes one conduction electron at any sodium concentration over the entire concentration range. Hence, the anomalous maximum in conductivity at $x=0.75$ must be attributed solely to an anomalous maximum in mobility of the electrons.

[1] Huibregtse, Barker, and Danielson, Phys. Rev. **84**, 142 (1951).
[2] B. W. Brown and E. Banks, Phys. Rev. **84**, 609 (1951).
[3] H. J. Juretschke, Phys. Rev. **85**, 124 (1952).

I2. Thermoelectric Power and Electrical Resistivity of Dilute Solid Solution of Silicon in Copper.* C. A. DOMENICALI AND B. A. BOYD, *Franklin Institute Laboratories.*—We have measured the thermoelectric force against pure copper and the electrical resistivity of Cu-Si alloy wires from −190°C to +600°C, the silicon content varying from 0.1 to 3.9 wt. percent. The relative thermoelectric power against pure copper was always negative and when plotted against Si content has a temperature-dependent minimum of the order of several microvolts/C° at about 1 percent Si at all temperatures within the measured range. The electrical resistivity increases almost linearly with silicon content at all temperatures in the measured range. Matthiessen's rule is fairly well satisfied, the quantity of $d\rho/dt$ increasing from 0.67×10^{-8} ohm cm/C° for pure copper to approximately 1.2×10^{-8} ohm cm/C° for 3.9 percent Si. Chemical analysis of the first set of alloys measured indicated the presence of rather large impurities. A second set was therefore prepared by a completely different technique. The results obtained with the second set agree quite well with those of the first set, considering the smallness of the thermoelectric effects in these alloys; and both agree with the room temperature resistivities found by Norbury in 1926.

* This work was supported by the Signal Corps.

I3. The Debye Temperature of Cu_3Au.* DWAIN B. BOWEN, *North American Aviation, Inc.*—The resistivity of disordered $AuCu_3$ alloy has been measured from 4.2°K to room temperature. From these measurements the Debye temperature has been computed using Gruneisen's formula. There is considerable variation with temperature, but a representative value is 175°. The difference in Debye temperature between this disordered sample, and one partially ordered (heated at 370°C for 50 hours) has been measured by a technique previously described.[1] The Debye temperature has increased on ordering (as might be expected from measurements of elastic constants[2]) by about 10°. Similar measurements will be made on more completely ordered samples. The influence of these Debye temperature changes on the ordering process will be discussed.

* This report is based on studies conducted for the U. S. Atomic Energy Commission under contract AT-11-1-GEN-8.
[1] D. B. Bowen and G. W. Rodeback, Bull. Am. Phys. Soc. **27**, No. 6, G6 (1952).
[2] S. Siegel, Phys. Rev. **57**, 537 (1940).

I4. Hall Effect in Ordered and Disordered Ni_3Mn.* SIMON FONER AND EMERSON M. PUGH, *Carnegie Institute of Technology.*—The two ferromagnetic Hall coefficients,[1] R_0 and α, have been measured in Ni_3Mn for several states of order using fields up to 30 kilogauss. Both R_0 and α are negative in the completely ordered sample ($4\pi M_s\sim9$ kilogauss) and positive in the most disordered sample ($4\pi M_s\sim0.4$ kilogauss). The significance of these data in relation to the band structure, d-band conduction, and electronic specific heat[2] will be discussed.

* Supported by the Office of Naval Research.
[1] Albert I. Schindler and Emerson M. Pugh, Phys. Rev. **89**, 295 (1953).
[2] J. E. Goldman, Magnetism Conference, University of Maryland, September, 1952 [Revs. Modern Phys. **25**, 108 (1935)].

I5. A Dilatometric Study of the Order-Disorder Transformation in Cu-Au Alloys.* W. W. SANVILLE, FOSTER C. NIX, AND FRANK E. JAUMOT, JR., *University of Pennsylvania.*—The order-disorder transformation in Cu-Au alloys in the

composition range from 10 to 32.2 atomic percent Au has been studied by dilatometric means. The interferometric dilatometer and the experimental technique used were similar to those used by Nix and MacNair.[1,2] All samples containing greater than 17.5 atomic percent Au exhibit an anomalous peak in the curve of the coefficient of thermal expansion as a function of temperature. A plot of the critical ordering temperature, T_c, as a function of composition defines an ordered region about 25 atomic percent gold which is in agreement with that defined by resistivity. The coefficient of thermal expansion is rigorously constant above the ordering temperature (to 500°C). The data indicate that the volume expansion is sensitive to small changes in the degree of long-range order, since in all cases the region of anomalous expansion begins at temperatures from 200° to 250°C.

* This work was supported by the Office of Air Research, U. S. A. F.
[1] F. C. Nix and D. MacNair, Rev. Sci. Instr. **12**, 66 (1941).
[2] F. C. Nix and D. MacNair, Phys. Rev. **60**, 320 (1941).

I6. Short-Range-Order in a Cu-Au Alloy.* CHARLES H. SUTCLIFFE AND FRANK E. JAUMOT, JR., *University of Pennsylvania.*—Short-range-order parameters have been measured using x-ray diffraction techniques, at three temperatures above the critical temperature of ordering, for a Cu-Au alloy containing 23 atomic percent gold. The experimental technique used was similar to that employed by Cowley.[1] The diffuse scattered intensity was measured at approximately 900 points within $\frac{1}{32}$ of a unit cell, and corrected for the intensity due to factors other than short-range order. A three-dimensional Fourier analysis was made on the short-range order intensities. The Fourier coefficients are then interpreted as short-range order parameters.[1] The data indicate that an alloy containing less than 25 atomic percent Au exhibits a greater tendency to short-range order than does an alloy at the stoichiometric composition. The tendency to what Cowley has referred to as a "liquid-like" distribution about an origin atom in a Cu_3Au alloy, although present, is considerably less in the 23 percent Au sample.

* This work was supported by the Office of Air Research, U.S.A.F.
[1] J. M. Cowley, J. Appl. Phys. **21**, 24 (1950).

I7. Ordering in the Alloy System Mg-Cd. C. A. WERT, *University of Illinois.**—A part of the anelastic spectrum of the alloy system Mg-Cd has been investigated. One of the relaxations seen in some of the alloys is believed to be that of "pair-relaxation." This relaxation is particularly interesting in the alloy MgCd, since its magnitude depends on the state of order in the alloy. The damping is small in a well-ordered specimen and relatively high in a disordered specimen. This behavior is consistent with Zener's model for this relaxation. The kinetics of ordering have been studied using the magnitude of the relaxation as a measure of the degree of order. Furthermore, the equilibrium amount of order at some temperatures has been determined, again with the damping as a measure. This technique has not yet been successfully applied to other ordering systems, although some attempts have been made. Indeed, in the system Au-Cu the pair-relaxation itself has not yet been positively identified. It is not yet clear whether this is caused by improper experimental technique or whether the relaxation is actually absent in this alloy system.

* Work sponsored in part by the U. S. Office of Ordnance Research.

I8. The Kinetics of the Disorder-Order Transformation in Cu_3Au. NORMAN W. LORD, *Columbia University.**—The isothermal order-dependent change in Young's modulus of a single crystal of Cu_3Au is measured as a function of time at various temperatures in the range 279.3° to 384.3°C. These temperatures were reached by quenching rapidly from an equilibrium state 28.2°C above the critical temperature (386.0°C). The time variations of Young's modulus indicate two distinct stages of the disorder-order transformation. The initial stage starts immediately and is completed a few minutes after quenching, while the later stage requires a few minutes before starting and then proceeds very slowly toward an equilibrium state. "Relative relaxation times" are associated with each of them. In conformance with the work of Sykes and Evans and others, the initial stage is described as the formation of contiguous antiphase ordered domains by means of normal atomic interdiffusion. The later stage consists of the coalescence of these domains, and requires at least two different geometrically constrained diffusion processes.

* Present address: Raytheon Manufacturing Company, Waltham, Massachusetts.

I9. The Decay of Vacancies Frozen into an Alloy by Quenching. A. S. NOWICK AND A. E. ROSWELL, *Yale University.*—Measurement of the relaxation time for stress-induced ordering has been used in the study of atomic mobility in substitutional solid solutions both under equilibrium conditions[1] and in the presence of an excess of vacancies frozen in by quenching.[2] These investigations are continued for a silver-zinc solid solution containing 33 atomic percent Zn. Quenching wire of this alloy from 400°C into water traps a vacancy concentration of about 0.01 atom percent. Since relative values of the rate of relaxation, at a given temperature, measure the relative concentration of vacancies present in the alloy, vacancy decay curves are readily obtained. Each plot of the logarithm of the relative vacancy concentration against time (as obtained at 50°, 60°, 70°, and 80°C) is very closely represented by a broken straight line, with a much lower decay rate below the knee or break in the curve. These results indicate that at least two types of imperfections, capable of producing diffusion, are frozen in by quenching.

[1] A. S. Nowick, Phys. Rev. **88**, 925 (1952).
[2] A. S. Nowick and R. J. Sladek, Acta Metallurgica 1 (1953) (to be published).

I10. Change of Optical Constants of Fresh Thin Copper and Silver Films on Exposure to Air. H. Y. LOH AND PETER CHEO,* *Virginia Polytechnic Institute.*—Three optical constants, reflectivity, transmissivity, and absorptivity, of copper and silver films of various thicknesses have been measured in vacuum as soon as the film was made by evaporation on a glass substrate. It was observed that they remained constant in vacuum if undesirable vapor was kept out of the vacuum chamber. But they showed a rapid change immediately on exposure to air at atmospheric pressure. The rate of change decreased in a few minutes, and the later change as observed by Kuhn and Wilson[1] was a very slow one. Copper showed a rapid decrease in reflectivity at the time of exposure. Its transmissivity showed an increase but the change was more gradual than the change of reflectivity. For silver, both reflectivity and transmissivity decreased a relatively small amount as compared with copper. Under low pressure (10^{-4} mm or less) a slight amount of grease vapor was found to cause a tremendous change of the optical constants.

* Now at the State University of Iowa.
[1] H. Kuhn and B. A. Wilson, Proc. Phys. Soc. (London) **B63**, 745 (1950).

I11. The Effect of the Sputtering Rate on the Resistivity and "Aging" of Sputtered Silver Films.* Richard B. BELSER, *Georgia Institute of Technology.*—Data have been collected which shows a definite relation between sputtering rates and initial resistivities of sputtered silver films of 500–1500 angstroms thickness. In a residual argon atmosphere a sputtering current of ten ma gave an initial resistivity of 3.8 times the resistivity of bulk silver, and, for 60 ma, only 1.9 P_b. By heating these films in an infrared oven the values of resistivity were reduced to 1.8 and 1.5 P_b, respectively. This latter value compares favorably with that of silver films deposited by vacuum evaporation and similarly aged. By plotting the ratio

P/P_0 of the films *versus* sputtering current, before and after aging, two curves are obtained which approach each other asymptotically in the region studied. There is evidence, at 10 ma sputtering currents, that resistivity is reduced in accordance with the time the deposition is continued. It appears that heating during deposition, effected by rate or time of sputtering, reduces the initial resistivity of the films. Further drops in resistivity, observed during external heating thereafter, are dependent on the heating occurring during deposition. An explanation is hereby offered for many results described as anomalous in the literature.

* Supported by U. S. Army Signal Corps.

FRIDAY MORNING AT 10:00

Chemistry 116

(W. M. GORDY presiding)

Microwave Spectroscopy

J1. Microwave Spectrum of Trimethyl Chlorosilicane.* RICHARD C. MOCKLER† AND WALTER GORDY, *Duke University.*—Trimethyl chlorosilicane has been found to have a microwave rotational spectrum characteristic of a symmetric top, with $B_0=2197.31$ Mc for $(CH_3)_3Si^{28}Cl^{35}$ and $B_0=2147.88$ Mc for $(CH_3)_3Si^{28}Cl^{37}$. If tetrahedral angles are assumed with d_{CH} as in methane, the results yield $d_{SiC}=1.871$A and $d_{SiCl}=2.029$A. The rotational lines are split into several components by torsional oscillations or restricted internal rotations of the CH_3 groups.

* Supported by Air Research and Development Command.
† Texas Company Fellow. Present address: Department of Physics, Columbia University.

J2. Microwave Spectrum and Structure of Trichlorogermane.* PUTCHA VENKATESWARLU, RICHARD C. MOCKLER,† AND WALTER GORDY, *Duke University.*—Several rotational lines of different isotopic combinations of $HGeCl_3$ have been observed. The B values so far obtained are 2165.78 Mc for $HGe^{74}Cl_3^{35}$; 2169.18 Mc for $HGe^{72}Cl_3^{35}$; and 2172.69 Mc for $HGe^{70}Cl_3^{35}$. Tentative values for the structural parameters are $d_{GeCl}=2.115$A and $\angle ClGeCl=108°18'$ with d_{GeH} assumed to be 1.52A.

* Supported by Air Research and Development Command.
† Texas Company Fellow. Present address: Department of Physics, Columbia University.

J3. On the Frequencies of the Microwave Absorption Lines of Oxygen.* MASATAKA MIZUSHIMA, *Duke University.*—It is known[1] that the frequencies of the microwave absorption lines of oxygen do not fit well Schlapp's formula.[2] Examining his theory we found two points to be improved. First we must consider the dependence of λ on N, where λ is the coupling constant of electronic spin and molecular axis and N is the quantum number of end-to-end rotation of molecule. This dependence makes $\nu_+(N-1)+\nu_-(N+1)$ dependent on N, which fit with experimental results, while in Schlapp's original theory it is independent of N. Another point is that Schlapp made a mistake in taking the effect of magnetic interaction between spin and end-to-end rotation of molecule into account. It was found that the improved formula agrees well with the recent experimental data obtained at Duke University. The adopted value of the constants are: $B=1.4372605$ cm^{-1}, $\lambda_0=1.984627$ cm^{-1}, $\lambda_1=0.000050$ cm^{-1}, $\mu=-0.008432$ cm^{-1}, where λ_1 gives the slight dependence of λ on N.

* The work supported by Air Research and Development Command.
[1] Burkhalter, Anderson, Smith, and Gordy, Phys. Rev. **79**, 651 (1950).
[2] R. Schlapp, Phys. Rev. **51**, 342 (1937).

J4. Temperature Dependence of the Line Breadths of Oxygen.* ROBERT M. HILL AND WALTER GORDY, *Duke University.*—Line breadths of several of the millimeter wave lines of O_2 have been measured at $T=300°$, 195°, and 90°. The results indicate an average temperature dependence of $1/T$ for the line breadth.

* This work supported by Air Research and Development Command.

J5. Microwave Spectrum and Molecular Properties of Ozone.* R. TRAMBARULO,† S. N. GHOSH,‡ C. A. BURRUS, JR.,§ AND W. GORDY, *Duke University.*—Four low J rotational transitions of ozone have been measured between 42 and 118 kmc. These measurements show ozone to be an isosceles triangle with the apex angle of 116°49′±30′ and with the two equal internuclear distances 1.278±0.003A. The electric dipole moment found from the Stark effect is 0.53 ±0.02 Debye. Zeeman studies show the molecular g factor to have a strong dependence upon rotational state.

* The work supported by Air Research and Development Command.
† Present address: Department of Physics, The Pennsylvania State College.
‡ On leave from the University of Calcutta.
§ Texas Company Fellow.

J6. Zeeman Effect in the Microwave Spectra of Methyl Fluoride and Methyl Acetylene.* J. T. COX, P. B. PEYTON, JR., AND WALTER GORDY, *Duke University.*—Zeeman splitting or rotational lines of methyl fluoride and methyl acetylene have been measured. The results show that the molecular magnetic field in CH_3CCD is generated primarily by rotation about the symmetry axis ($g_K=0.31$, $g_N\approx 0$), but that in CH_3F a measurable field is also generated by the end-over-end rotation ($g_N=0.08$).

* The work supported by the Air Research and Development Command.

J7. The Microwave Spectrum of the Unstable Molecule Carbon Monosulfide. GEORGE R. BIRD* AND RICHARD C. MOCKLER,† *Columbia University.*—The $J=0\rightarrow 1$ transitions of $C^{12}-S^{32}$ and $C^{12}-S^{34}$ were observed at 48 990.55±0.08 Mc and 48 207.038±0.020 Mc, respectively. The C−S was produced in an electrical discharge and continuously flowed through a conventional stark cell. Using values for α_e, and D_e, calculated from ultraviolet data[1] the following results were obtained:

$$C^{12}-S^{32},\ B_e=24\ 588.86\pm 1\text{ Mc},\ r_e=1.5347\text{A}$$
$$C^{12}-S^{34},\ B_e=24\ 194.90\pm 1\text{ Mc},\ r_e=1.5347\text{A}.$$

Mass ratio $S^{34}/S^{32}=1.06242$.The valve of Be for $C^{12}S^{32}$ determined from ultraviolet spectra is in good agreement with the foregoing value.

* National Research Council Post-Doctoral Fellow.
† Carbide and Carbon Company Post-Doctoral Fellow.
[1] G. Herzberg, *Spectra of Diatomic Molecules* (D. Van Nostrand Company, Inc., New York, 1950), second edition.

J8. On the Quadrupole Moments of Mn^{55}, Re^{185}, and Re^{187}.* A. JAVAN, G. SILVEY, AND C. H. TOWNES, *Columbia University,* AND A. V. GROSSE, *Temple University.*—The quadrupole

coupling constant of Mn^{55} has been measured[1] in MnO_3F, but the Mn^{55} quadrupole moment cannot easily be obtained from this coupling constant because of uncertainties in the structure of the Mn bonds in this molecule. The quadrupole coupling constants of Re^{185} and Re^{187} have now been measured in the structurally similar molecule ReO_3Cl. Since the quadrupole moments of the Re isotopes have been measured from atomic spectra, their values can be used to deduce an approximate value for the quadrupole moment of Mn^{55} if it is assumed that the bond structures of MnO_3F and ReO_3Cl are similar. The result is $Q(Mn^{55}) = 0.5 \times 10^{-24}$ cm². This value should be correct in sign and in approximate magnitude. The measurements also confirm spins of $\frac{5}{2}$ for Re^{185} and Re^{187} and give a ratio of the quadrupole moments $Q(Re^{185})/Q(Re^{187}) = 1.06 \pm 0.05$. The quadrupole coupling constant for Re^{185} in ReO_3Cl is 272 ± 6 Mc and for Cl^{35} it is -40 ± 8 Mc.

* Work supported by the U. S. Atomic Energy Commission.
[1] A. Javan and A. V. Grosse, Phys. Rev. **87**, 227 (1952).

FRIDAY MORNING AT 10:00

Biology 113

(PAUL SHEARIN presiding)

Apparatus of Nuclear Physics

JA1. A Van de Graaff Electrostatic Generator.* D. C. SWANSON, *University of Florida*.—A Van de Graaff electrostatic generator, pressure type, has been constructed at the University of Florida. Maximum proton energies of about 1 Mev are expected. The generator has been operated up to about 0.8 Mev at 1 microampere proton beam. A horizontal tripod suspended from the fixed end of the tank supports the sphere, accelerating tube, and charging system. The tank may be rolled back for easy access to the generator for adjustments. The generator is to be used with other equipment now being developed for the study of elastic and inelastic scattering of protons and deuterons.

* This work is being supported in part by the U. S. Atomic Energy Commission.

JA2. 10 Megacycle Radiofrequency Ion Source.* E. W. MCDONALD† AND D. C. RALPH, *Louisiana State University*.—Several modifications of Thonemann[1] type rf ion sources have been employed on a 100-kv Cockcroft and Walton accelerator. The tube base design of Moak *et al.*[2] has been followed. The effects of magnetic field and discharge tube geometry on operating frequency, pressure and power input will be discussed. The discharge tube now in use is 5 cm in diameter and operates at a pressure of about 8 microns. The plate input power to the 10-mc oscillator is 300 to 400 watts. Ion beams of 1.5 ma containing 85 percent monatomic ions are obtained, using either hydrogen or deuterium.

* Supported in part by a grant from the Research Corporation.
† Now at Louisiana College, Pineville, Louisiana.
[1] P. C. Thonemann, Nature **158**, 61 (1946).
[2] Moak, Reese, and Good, Phys. Rev. **83**, 232(A) (1951).

JA3. A High Current 120-Kev Positive Ion Accelerator.* D. L. LAFFERTY, J. A. BIGGERSTAFF, B. D. KERN, AND T. M. HAHN, *University of Kentucky*.—A high current 120-kev positive ion accelerator for fast neutron inelastic scattering studies has been constructed. High voltage is supplied by a Cockcroft-Walton type circuit. The horizontal accelerating tube consists of glass sections and 12 re-entrant aluminum electrodes, sealed together with Vinyl cement, and is 24 inches in length. The 2-inch glass sections for the accelerating tube were cut from 7-inch diameter, ¾-inch wall thickness, Pyrex pipe. The ion source is of the radio-frequency type described by Moak *et al.*[1] A well-focused beam of currents up to 500 microamperes and consisting of 90 percent monatomic hydrogen has been obtained.

* Supported by the Office of Ordnance Research, Army Ordnance Corps.
[1] Moak, Reese, and Good, Nucleonics **9**, 3, 18 (1951).

JA4. Performance of a 125-kv Accelerator and Spectrometer. J. BERGSTEIN, *Oak Ridge National Laboratory*, AND R. D. BIRKHOFF, *Oak Ridge National Laboratory and University of Tennessee*.—Particles are accelerated through voltages up to 125 kv by a conventional ion gun and Cockcroft-Walton tube assembly. A second identical tube is used to decelerate the particles through exactly the same potential by connecting the Faraday cage collector electrically to the cathode of the gun. Any energy lost in an absorber placed in the beam is replaced by running the cage at a slightly different potential from the cathode. Differentiation of the current-voltage curve obtained by varying this potential gives the energy distribution of the electron beam. In use with no absorber and 43 kv applied, a distribution 0.2 volt wide at half maximum has been obtained giving a resolution of about 5 parts per million. Experiments contemplated include an investigation of the excitation and ionization produced in matter by the passage of electrons and positive ions, the measurement of W, the average energy required to create an ion pair in various gases for electrons and ions, and electron capture and loss phenomena for positive ions.

JA5. The Oak Ridge 44-Inch Cyclotron. ROYCE J. JONES, *Oak Ridge National Laboratory* (introduced by R. S. Livingston).—A description of the ORNL 44-inch experimental cyclotron will be presented. This proton accelerator is being used in the study of the transmission of ions in a fixed-frequency cyclotron. A discussion of beam composition and beam attenuation will be presented. The use of focusing grids at the entering edges of the dees increases the ion beam current at small radii, but has little effect at the maximum radius. With proper shaping of the accelerating electrode a focusing effect can be introduced in the ion source region which results in a 50 percent increase in beam current at the maximum radius. A proton current of three milliamperes at 1.5 Mev has been obtained with the ion source described previously.* A deflected beam of 380 microamperes has been measured.

* Livingston, Jones, and Wright, Phys. Rev. **78**, 329 (1950).

JA6. Electromagnetic Shims for Focusing in a Fixed-Frequency Cyclotron. FARNO L. GREEN, *Oak Ridge National Laboratory* (introduced by R. S. Livingston).—The conventional type of iron shims, used for focusing, in the ORNL 44-inch experimental cyclotron (Abstract JA5) has been replaced by electromagnetic shims for studies of magnetic focusing of the beam. Various magnetic field configurations and gradients are easily examined with a great saving of time

and labor. The statement[1,2] that magnetic focusing is of little effect at small radii but is very effective at large radii was verified experimentally. It was shown that for 1.5-Mev protons a linear magnetic field drop-off of two percent along the median plane, radially outward to maximum beam radius, gives optimum beam focusing as indicated by maximum beam intensity. This type of focusing shims has proved to be practical during many months of cyclotron operation.

[1] M. E. Rose, Phys. Rev. **53**, 392 (1938).
[2] Robert R. Wilson, Phys. Rev. **53**, 408 (1938).

JA7. Cyclotron Efficiency and Power Distribution Measurements. A. L. BOCH AND E. D. HUDSON, *Oak Ridge National Laboratory* (introduced by R. S. Livingston).—The high beam power obtained with the ORNL 86-inch cyclotron prompted an experimental study of the power distribution and the efficiency of the machine. As measured calorimetrically, the power transmitted to the internal target by 22-Mev protons has exceeded 60 kw. Power to the target is limited by thermal properties of the target and the available power in the rf system; under off-resonance conditions, over 40 milliamperes of ions can be made to circulate in the dees at an average energy of approximately 2 Mev. The dc isolation of the dees has made it possible to determine the ion losses to the dees for both on- and off-resonance conditions; a power distribution method is used in obtaining the average energy of the ions. For proton currents exceeding 1500 microamperes the target power is over 10 percent of the power input to the oscillator, the ion transport efficiency approaches 15 percent, and the target power is over 50 percent of the total ion loading of the rf system.

JA8. Radioisotope Production in the ORNL 86-Inch Cyclotron. J. A. MARTIN, *Oak Ridge National Laboratory* (introduced by R. S. Livingston).—A proton current in excess of one milliampere at an energy of 22 Mev is available on internal targets in the ORNL 86-inch cyclotron. Currents of this magnitude and at this energy make possible the relatively large-scale production of a number of radioisotopes which cannot be produced in nuclear reactors. The (p, n), $(p, 2n)$, and (p, pn) reactions give comparatively high yields. The yields for several radioisotopes are given. For example, Be^7 is produced by the (p, n) reaction on Li^7 at a yield of 160 millicuries per milliampere-hour; lithium-coated targets have been developed which allow proton currents as high as 600 microamperes to be utilized. Ga^{67} is obtained from both the (p, n) reaction on Zn^{67} and the $(p, 2n)$ reaction on Zn^{68}; from a zinc target, in which the abundance of these two isotopes is 4.1 percent and 18.6 percent, respectively, a yield of 600 millicuries per milliampere-hour is obtained.

JA9. A Measurement of the Neutron Energy Distribution in the ORNL Graphite Reactor. JAMES B. TRICE (introduced by J. H. Crawford, Jr.).—Analyses of many radiation damage experiments require that the energy distribution of the bombarding neutrons be known. This can be accomplished in some cases by using *nuclear threshold detectors* to measure the energy distribution above one Mev and *nuclear resonance detectors* for lower (or epithermal) energies. Such a scheme has been used to examine the neutrons at a certain location in the ORNL graphite reactor. For the high energy component of the spectrum, the nuclear threshold detectors, together with their respective threshold energies are $Cl^{35}(n, \alpha)P^{32}$ at 0.5 Mev, $P^{31}(n, p)Si^{31}$ at 2.4 Mev, $Al^{27}(n, p)Mg^{24}$ at 4.6 Mev, and $Al^{27}(n, \alpha)Na^{24}$ at 8.1 Mev. For the lower energy component of the spectrum an inverse dependence on energy ($\sim 1/E$) was found using Mn^{55} and Na^{23}, which have (n, γ) cross section resonances at 261 ev and 1710 ev, respectively. The neutron spectrum was thus found to consist of principally two components; a strong so-called "fission" group of neutrons in the energy interval 1 to 10 Mev and a group of lower energy (epithermal) neutrons with an energy distribution inversely proportional to energy.

JA10. A Terphenyl-Boron Liquid Neutron Detector.* W. H. CAMPBELL AND J. I. HOPKINS, *Vanderbilt University*.—The scintillation properties of various concentrations of *p*-terphenyl dissolved in *p*-toluene were studied for maximum pulse size response to conversion electrons with a view of possible use in conjunction with ethyl borate as an efficient neutron detector. A suitable cell with a plastic window above a 5819 photomultiplier tube was used with a single-channel pulse-height analyzer to obtain count-rate *versus* pulse-height data. The response of the scintillation solutions to a Po-Be neutron flux was investigated before and after ethyl borate was added. The best response to date has been obtained by adding an 8 g/l solution of *p*-terphenyl in *p*-toluene to an equal volume of ethyl borate. The results thus far for this neutron detector indicate that the count-rate *versus* pulse height can be represented by an equation of the form

$$(n/t) = C_1[1 - C_2 e^{-C_3(PH)}].$$

* Work supported by the U. S. Atomic Energy Commission.

JA11. A Differential Pulse-Height Discriminator.* R. C. SHRECKENGOST, D. C. SWANSON, AND J. W. FLOWERS, *University of Florida*.—A relatively simple differential pulse-height discriminator designed to operate with pulses in the order of one microsecond in length and to one hundred volts in amplitude has been developed for use in scintillation spectroscopy. The discriminator employs differentially biased blocking oscillators with window widths to ten volts. The minimum amplitude bias and window widths can be easily adjusted to 0.1 percent of their respective ranges.

* This work was supported in part by the U. S. Atomic Energy Commission.

JA12. The Characteristics of an Allen Type Electron Multiplier. C. F. BARNETT, *Oak Ridge National Laboratory*.—In experiments being conducted at Oak Ridge National Laboratory it is necessary to have a particle detecting instrument sensitive to positive ions of various masses ($1 \leq A \leq 40$) and energies in the 3–200 kev range which can be used either as a single particle counter or a current measuring device for input currents up to 10^{-12} ampere. The characteristics of an Allen type electron multiplier have been studied to determine the feasibility of its use for this purpose. Results will be presented giving the gain of the multiplier as a function of input current, pressure, and multiplier voltage. Also, the gain as a function of mass and energy will be discussed, as well as the stability of the gain with time. With the first dynode at a potential of negative 5 kv the gain increases practically linearly for H_3^+ ions with energy in the range 3–10 kev. At an energy of 5 kev the secondary emission produced at the first dynode by molecular ion (e.g., N_2^+) is larger than that produced by atomic ions of comparable masses (e.g., Ne^+). It has been concluded that the stability and gain of the electron multiplier is sufficient to justify its use as a quantitative ion detector.

JA13. Gradation Development Method for Nuclear Emulsions. H. G. DECARVALHO, V. DAVIS, AND W. TESH, *North Carolina State College*.—A method is described for the technique of critical development of emulsions in which it is desired to identify ionizing particles. A test strip is first developed with a solution of graded concentration. From this strip the optimum concentration of developer is determined. The optimum concentration is then used with graded time to complete the development. Using plates loaded with boron and lithium and exposed to neutron flux, one is able to discriminate between alpha-triton and alpha-lithium tracks and to measure their lengths readily.

FRIDAY MORNING AT 10:00

Physics 114

(TURNER ALFREY, JR., presiding)

Division of High-Polymer Physics

Symposium on Crystallization in Polymers

K1. Opening Remarks. TURNER ALFREY, JR., *Dow Chemical Company.* (20 min.)
K2. Equilibrium Theory of Crystallization. P. J. FLORY, *Cornell University* (30 min.)
K3. Kinetics of Crystallization. LEO MANDELKERN, *National Bureau of Standards.* (30 min.)
K4. Recent Work on the Structures of Crystalline Polymers. C. W. BUNN, *Imperial Chemical Industries.* (30 min.)

FRIDAY AFTERNOON AT 2:00

Physics 114

(TURNER ALFREY, JR., presiding)

Division of High-Polymer Physics

Symposium continued from Session K

L1. X-Ray and Infrared Studies on the Extent of Crystallization. J. B. NICHOLS, *Du Pont Experimental Station.* (30 min.)
L2. Relations Between Crystallization and Second-Order Transition. R. F. BOYER, *Dow Chemical Company.* (30 min.)
L3. Molecular Structure and the Crystallizability of Polymers. C. W. BUNN, *Imperial Chemical Industries.* (30 min.)

(R. F. BOYER presiding)

Contributed Papers

L4. Orientation in Polymeric Films by Infrared and X-Ray Techniques. W. H. COBBS, JR., S. B. COLE, AND R. L. BURTON, *E. I. du Pont de Nemours & Company* (introduced by W. E. Mochel).—Methods have been evolved for quantitative estimation of degree of orientation of polymeric films by a Weissenberg x-ray technique and by absorption of polarized infrared light. Both axial orientation and uniplanar orientation may be determined in each method. The results from the x-ray method apply only to the crystalline part of the polymer, whereas those from infrared include in addition to a crystalline part a contribution from the amorphous regions. Results from both methods are in general agreement; in certain cases differences can be interpreted in terms of the relative importance of the crystalline and amorphous portions in oriented polymeric materials.

L5. Crystallization in Butadiene-Styrene Copolymers.* LAWRENCE A. WOOD, *National Bureau of Standards.*—Butadiene-styrene copolymers contain the following units: *trans*-1,4-polybutadiene, *cis*-1,4-polybutadiene, 1,2-polybutadiene, and polystyrene. Of these the first is the only type which has been shown by x-ray evidence to form crystals. An examination is made of the consequence of the hypothesis that crystallization in these copolymers in a given time at the optimum temperature requires a certain minimum content of *trans*-1,4 units, independent of the relative amounts of the other three types. Lines of constant *trans*-1,4 content are plotted on a graph with the content of polystyrene units as abscissa and the proportion of *trans*-1,4 units with respect to total polybutadiene content as ordinate. A similar family of curves can be plotted with the temperature of polymerization as ordinate. According to the hypothesis one of the curves will mark the boundary between the region of possible crystallization and the region in which crystallization will not be noted in the given time. Dilatometric and calorimetric studies of the crystallization within about 3 hours at −45°C yield experimental points which conform quite well to the curve for a *trans*-1,4 content of about 58 percent. The fact that the points fall on a single curve appears to give substantial support to the hypothesis.

* Supported in part by the U. S. Office of Naval Research and the Office of the Quartermaster General.

L6. The Melting Transition of Natural Rubber.* DONALD E. ROBERTS AND LEO MANDELKERN, *National Bureau of Standards.*—The statistical thermodynamic theory[1] of semicrystalline polymers has led to the concept of an equilibrium melting temperature, T_m, the temperature at which crystallinity disappears completely. This temperature is characteristic of a given polymer and independent of previous thermal history. The well-known results for natural rubber[2] where the melting temperature is strongly dependent on the crystallization temperature are not in accord with these conclusions, and has been reinvestigated. The melting temperatures of two molecular weight fractions and a third sample of purified rubber hydrocarbon were determined, as a function of crystallization temperature, using dilatometric techniques. After crystallization at −18°C, 0°C, and +8°C, on subsequent slow heating,

the melting temperatures all occurred in the range 22° to 23°C, irrespective of the crystallization temperature. A slow heating rate is important in order to allow imperfect crystallites to reform into a more stable arrangement; if a fast heating rate is employed, results similar to those previously reported[2] are obtained. However, after crystallizing at +14°C and heating slowly, the melting temperatures occur in the range 27° to 28°C. Thus, the effect of the crystallization temperature on the melting temperature is considerably smaller in magnitude than previously thought.

* Assisted by the U. S. Office of Naval Research and Office of the Quartermaster General.

[1] P. J. Flory, J. Chem. Phys. **17**, 223 (1949).
[2] L. A. Wood and N. Bekkedahl, J. Appl. Phys. **17**, 362 (1946); J. Research Natl. Bur. Standards **36**, 489 (1946).

L7. An Infrared Study of the Crystallization of Polyethylene. ALEXANDER BROWN AND F. P. REDING, *Carbide and Carbon Chemicals Company.*—The melting points and the temperatures for the onset of crystallization of a series of polyethylene resins covering a variety of molecular weights and degrees of chain branching have been determined by observing the 13.7-micron crystallinity band of the infrared spectrum. An increase in the amount of chain branching decreases the melting point considerably whereas a decrease in the molecular weight, at least in the range studied, lowers the melting point only slightly. On the other hand an increase in chain branching decreases, but a decrease in molecular weight apparently increases, the temperature at which crystallization starts at any given rate of cooling. The rate of crystallization of polyethylene as a function of temperature, chain branching, and molecular weight will also be discussed. In the temperature range studied the rate increases markedly with a decrease in temperature and a decrease in the amount of chain branching.

FRIDAY AFTERNOON AT 2:00

Chemistry 116

(W. G. POLLARD presiding)

Invited Papers in Nuclear Physics

M1. The Raleigh Research Reactor. C. K. BECK, *North Carolina State College.* (30 min.)

M2. Progress in Reactor Physics and Reactor Technology. A. M. WEINBERG, *Oak Ridge National Laboratory.* (30 min.)

M3. Polarized Photons. F. L. HEREFORD, *University of Virginia.* (30 min.)

M4. Production of Polarized Particles in Nuclear Reactions. ALBERT SIMON, *Oak Ridge National Laboratory.* (30 min.)

M5. Nuclear Reactions with He^3 Nuclei. W. M. GOOD, *Oak Ridge National Laboratory.* (30 min.)

FRIDAY AFTERNOON AT 2:00

Page Auditorium

(W. M. GORDY presiding)

Southeastern Section of the American Physical Society

Programme on the Teaching of Physics

Invited Paper

N1. Responsibilities and Training of Physics Teachers. T. H. OSGOOD, *Michigan State College.* (30 min.)

Contributed Papers

N2. The Teaching of Biophysics. DAVID POMEROY, *Army Medical Research Laboratory, Fort Knox.*—In a discussion on the present status of biophysics[1] the problem was considered largely from a thermodynamic standpoint. It must be conceded, however, that there is a large, growing need to adopt mathematical and physical methods also to problems of biological effects of radiations. The subject may be classified under 3 headings. 1. *Radioactivity.*—Natural and artificial radioactivity; the elementary particles; measurement of half-lives; activity in curies; uses of radioisotopes in biology and medicine. 2. *Passage of radiation through matter.*—Ionization; range-energy relations; stopping power; photoelectric effect; Compton effect; pair production; neutron capture; the intermediate nucleus; nuclear disintegrations; methods for detection and counting of elementary particles; statistics of counting. 3. *Action of radiation on living cells.*—Dosimetry as defined in different types of roentgens; modes of biological and chemical effects; target theory; inactivation of viruses, rickettsia and bacteria; mutations; carcinogenesis and treatment of cancer.

[1] Science **113**, 617 (1951)

N3. Sharp Shadows as "Images." E. SCOTT BARR, *University of Alabama.*—A local eye specialist, Dr. Harvey B. Searcy, found that it is possible to show a patient a cataract or certain other defects of his eye very simply. The patient takes a converging lens of about 6 diopters and looks through it at a distant point source of light. The patient then sees his

cataract clearly imposed upon the bright field. The explanation lies in the fact that this procedure results in making the posterior focal point of the lens coincide with the anterior focal point of the eye. Consequently, the light is essentially parallel after entering the eye, and sharp shadows of any obstructing areas are projected on the retina. The retinal response is such that these shadows are interpreted as images (inverted, of course). The confusion of sharp shadows with images may also arise in optical bench experiments when a bright point source (such as the Western Union arc) is used to illuminate a wire screen as an object. This may lead to the surprising effect that covering the top half of the lens results in the loss of the top half of the "image."

N4. An Experiment with Transistors for the Elementary Electronics Laboratory Course. F. H. MITCHELL, *University of Alabama.*—A simplified experiment using point-contact transistors is described. After the collector volt-ampere family of curves is obtained, a single-stage grounded-base amplifier is designed and built. Its band width and degree of distortion are measured, and the current gain calculated. Next, a sine-wave feedback oscillator of a type selected by the students is constructed, and its stability and range of adjustable audio frequencies is measured. Finally, an assignment is given to construct an amplifier or an oscillator of good quality using a minimum of components, weight, and space. The results obtained by the several groups of students in this miniaturization are compared, and a winner is chosen by vote of the entire class. A considerable rivalry is like to accompany this assignment.

N5. A Classical Neutron Model. ARTHUR E. RUARK, *University of Alabama.*—Students sometimes inquire whether there is a convenient neutron model, a companion to the Lorentz surface-charged electron. The electrical potential $V_0 \exp(-r^2/a^2)$ leads to such a model. It corresponds to a charge-density $(V_0/4\pi a^2)(6-4r^2/a^2)\exp(-r^2/a^2)$. The total charge is zero. The electrostatic energy is $Mc^2=(9\pi/512)^{\frac{1}{2}}aV_0^2$. This model usually incites lively arguments.

N6. Electrolysis of Water: An Experiment in Atomic Physics. CARL C. SARTAIN, *University of Alabama.*—If one measures the current I and the time t required to liberate a mass M of oxygen collected at pressure p and volume v and at absolute temperature T, he can determine seven important physical constants. They are the Faraday F, the mass m of an oxygen atom, the mass of one atomic mass unit, Avogadro's number N_0, Boltzmann's constant k, the universal gas constant R, and the volume V of one mole of gas at standard conditions. One needs to have measured the charge on the electron (oil drop method) or be willing to accept the value of that charge.

N7. Is it Possible to Teach Physics to Humanities Students? N. GOLDOWSKI, *Black Mountain College.*—During the years following the end of the war, physics gradually became a compulsory rather than an elective subject, not only for science students but also for those in liberal arts. The necessity of acquainting humanities students with physics was voiced by many, including this writer. The reason for teaching physics can be expressed by the saying: "man has to know the world he lives in." The understanding of the world seems to be based on the laws and concepts of physics. Teaching physics to mathematically virgin students became a problem, for which several solutions were offered. Essentially, most of them lead to teaching *about* physics, in order to avoid mathematics, the language of physics. It now appears questionable whether teaching about physics provides a knowledge of physics or an understanding of the underlying concepts. It is proposed to teach physics with emphasis on concepts but without translating the language of physics—mathematics—into everyday language, so as to give the student "first hand" experience in science.

N8. Graduate Training for High School Physics Teachers and Cooperation between College and High School Physics Departments. DONALD C. MARTIN, *Marshall College.*—A report of a study made, especially in the Southern states, to determine what is being done by colleges in the way of providing graduate programs in physics for high school teachers, and also what colleges are doing in the matter of cooperating with high school physics departments such as loaning equipment, faculty members presenting demonstration lectures at high school assembly programs, giving assistance to science clubs, and discussing opportunities of a career in physics with high school seniors.

N9. Incentive Grading for the Basic Laboratory Reports. RAY M. MORRISON, *Combustion Engineering Corporation,* AND M. S. MCCAY, *University of Chattanooga.*—The success of incentive wage systems in industrial operations suggests potential benefits from a similar plan in the basic physics laboratory. Blind dependence upon vague, negative grading practices, such as "an average, complete report rates B," can hardly be expected to develop student interest, initiative, accuracy, and thoroughness. On the other hand, nondiscriminating assignment of high grades to all reports encourages carelessness and lack of respect for the course work. In view of the demand on modern colleges for finished products with superior qualities in laboratory (1) experimentation, (2) communication, and (3) initiative it would seem to be scientific to give more attention to quality control of the student product during the production process. Specifically, this study is concerned with the developing and testing of a check list of essential laboratory report features, which serves both as a positive system for determining report grades, and as a constructive guide to incentive-minded students.

FRIDAY AFTERNOON AT 2:00

Engineering 125

(A. H. NIELSEN presiding)

Mostly about Crystals

O1. Vibration Spectrum of a Simple Cubic Lattice.* GORDON F. NEWELL, *University of Maryland.*—Analytic expressions are derived for the frequency distribution function $g(f)$ of a simple cubic monatomic lattice. Only nearest and next-nearest neighbor interactions are considered and the latter are assumed to be weak compared with the former.

The procedure is based upon considering the next-nearest neighbor interactions as a perturbation and the results are correct to the first power of a parameter τ which is essentially a measure of strength of the next-nearest neighbor forces as compared with the nearest neighbor forces. It has been known for some time that the problem with nearest neighbor interactions only degenerates into the equivalent of three one-dimensional problems giving a nonzero $g(f)$ for $f=0$ and an infinite value at the maximum frequency. If, however, one includes even a small interaction between next-nearest neighbors, the behavior of $g(f)$ near both ends of the spectrum changes considerably, in fact it vanishes at both ends. In between these points $g(f)$ is continuous but has four analytic singularities with vertical tangents of the type predicted by van Hove for a quite general type of crystal.

* Partially supported by the U. S. Office of Naval Research.

O2. Dislocations and Edge States in the Diamond Crystal Structure. W. SHOCKLEY, *Bell Telephone Laboratories.*—Dislocations in the diamond structure are somewhat more complicated than those usually considered: An edge, or Taylor's dislocation, with slip vector on a (111)-plane may have its extra half-plane of atoms terminate with broken bonds parallel either to [111]-direction or at tetrahedral directions thereto. In the former case, separation into partial dislocations is impossible whereas in the latter it may occur at the expense of next-next neighbor distrubances only. At the edge of the extra half-plane there may be a one-dimensional band of "edge-states" analogous to two-dimensional surface state bands. As for surface states[1] there are conditions in which these edge states may be partially filled thus causing each dislocation to become a one-dimensional degenerate-electron-gas conductor. Depending upon "work function," such dislocation arrays could form *n*- or *p*-type grain boundaries and make boundaries behave like surface states rather than extrinsic regions.[2] They might also contribute to the anomalously large nonlinear conductivities observed at very low temperatures.[3]

[1] W. Shockley, Phys. Rev. **56**, 317 (1939).
[2] G. L. Pearson, Phys. Rev. **76**, 459 (1949) and Taylor, Odell, and Fan, *ibid.* **88**, 867 (1952).
[3] C. S. Hung and J. R. Gleissman, Phys. Rev. **79**, 726–728 (1950); R. C. Fletcher (personal communication).

O3. Electrical Breakdown Path Orientation in Alkali Halide Crystals. J. W. DAVISSON, *Naval Research Laboratory.*—The general idea of a fast electron scattering mechanism involving Brillouin zone boundaries, conceived by A. von Hippel, has been used by E. L. Offenbacher and H. B. Callen[1] in a quantitative calculation of electrical breakdown path orientation. This calculation predicts a sequence of breakdown directions in alkali halide crystals with increasing temperature consisting of (random:100:111:110 and 100:100). The theoretical treatment does not include the *xxy* star paths which have now been observed in KF and NaCl as well as in the lithium halides.[2] The data suggest that the star patterns appear when the probability for breakdown in 110 and 111 is equal, or nearly so. Experimental observations give the sequences (random:100:*xxy**:110) for K and Rb halides, (random:100*:111:*xxy**:110) for Na halides, and (*xxy**:110:*xxy*:111:110) for the Li halides. The starred orientations above are unstable.

[1] E. L. Offenbacher and H. B. Callen, Phys. Rev. **83**, 227 (1951).
[2] J. W. Davisson, Phys. Rev. **70**, 685 (1946) and **73**, 1194 (1948).

O4. Electron Motion in Polar Crystals. E. P. GROSS, *M.I.T.*—The energy levels of the system consisting of an electron interacting with the longitudinal optical modes of frequency ω in a polar crystal are studied in detail by the method of Fock configuration space.[1] For the lowest levels and for small coupling strengths the energy and effective mass agree with the linear dependence on coupling predicted by the intermediate coupling theory.[2] Deviations in the direction of higher effective masses are found with increasing interaction strengths. For states of energy $\approx\hbar\omega/2$ above the ground state the effective mass is greater than it is for the lowest levels. The depression of the energy continuum of the levels which for zero coupling lies at an energy $\hbar\omega$ is computed as a function of interaction strength.

[1] E. P. Gross, Phys. Rev. **88**, 153 (1952).
[2] T. D. Lee and D. Pines, Phys. Rev. **88**, 960 (1952).

O5. Electronic Energy States of Impurities in Nonmetallic Crystals. KURT LEHOVEC, *Sprague Electric Company.*—The potential around an impurity in a crystal can be divided into two parts: (1) Within a sphere with the radius of the impurity the potential approaches the core potential of the free impurity (except of an additive constant), (2) outside of this sphere the potential is the periodic lattice potential with a superimposed Coulomb-like field determined by the effective charge of the impurity and the lattice polarization. Accordingly two types of wave functions for an electron attached to the impurity can be distinguished: (1) ψ_1 functions resembling orbitals of the impurity in free space and located nearly entirely within the sphere mentioned above; (2) ψ_2 functions resembling hydrogen-like orbitals, extending far beyond the sphere. A crude criterion on the existence of ψ_1 functions is based on (a) energy levels of the free impurity and lattice energy, or (b) on the radius of the free impurity and the space available in the lattice. ψ_1 functions do not exist in covalent crystals [e.g., Ge(Sb)], but may exist in ionic crystals [e.g., KCl(Tl)]. ψ_2 functions exist always. A ψ_1 function, if existing, represents the ground state, whereas ψ_2 functions represent excited states. The significance of the (ψ_1, ψ_2) state for a two-electron problem (ZnS with interstitial Cu) will be discussed.

O6. Density Changes in Glass During Heat Treatment. H. N. RITLAND, *Corning Glass Works.*—The structure of glass is known from x-ray diffraction studies to have a random character similar to that possessed by liquids. In common with liquids, glass has an equilibrium structure that is a function of temperature. At temperatures near the annealing point, about an hour is required for equilibrium to be reached; the time increases rapidly as the temperature is lowered. This loosely defined range of temperature in which physical properties can be observed to vary with time is called the transformation range; room temperature properties of glass are dependent on previous thermal history in the transformation range. The effect of heat treatment on the room temperature density and refractive index of a boro-silicate crown glass has been studied. Data will be presented on the variation of density with length of treatment at a constant temperature in the transformation range and on the approach of the density to its asymptotic value during cooling through this range at a constant rate. These will be discussed in connection with the concept of fictive temperature, in which the state of the glass is characterized by the temperature in the transformation range at which that state would be in equilibrium.

O7. Crystallite Size and Diamagnetic Susceptibility of Carbons.* H. T. PINNICK, *University of Buffalo.*—Single graphite crystals have an anomalously large susceptibility in the *c*-direction (principal axis), while the susceptibility in the aromatic plane is much smaller and of the same order of magnitude as for all hydrocarbons (including the condensed aromatic molecules). In order to get information about the nature of the changes occurring when condensed aromatic molecules grow and transform into graphite crystals, carbons with intermediate range of crystallite sizes were investigated. Purified carbon rods were heat-treated to different temperatures to get a wide variation in crystallite sizes. Furthermore, a number of carbon blacks with particle sizes from 50A to

3000A were all heat-treated to 3000°C; since the particle surfaces limit the growth of crystallites a range of well defined sizes was obtained. The crystallite dimensions were determined from the broadening of x-ray diffraction lines and the susceptibilities measured at room temperature using Gouy balance. When the gram susceptibilities are plotted as a function of the crystallite diameter d ("a" direction), the experimental points lie scattered around a single curve, in which almost all of the increase from $\chi = -0.5\times10^{-6}$ to about -6×10^{-6} occurs in the interval for d from 50A to 150A. The deviations from the average curve are probably caused by differences in origin and history of the individual samples.

* Supported in part by the U. S. Office of Naval Research.

O8. Computations of Three-Dimensional Structure Factors on S-FAC.* R. PEPINSKY AND P. F. EILAND, *The Pennsylvania State College.*—S-FAC was constructed to compute structure factors corresponding to a two-dimensional array of twenty atoms in the asymmetric unit of a crystal cell. Five types of atoms (i.e., different f curves) can be accommodated at one time. The $(x_1^{(n)}, x_2^{(n)})$ coordinates are established as desired by means of two potentiometers for each atom, the atomic centers appearing on the X-RAC 'scope as movable marker pips; and the $F_{H_1H_2}$ values appear as meter readings. Coordinates can be altered at will to permit instantaneous examination of agreement between observed and calculated structure-factor amplitudes. A computation rate of ten $F_{H_1H_2}$ values per minute is readily attained. Three-dimensional factors can be readily computed, while maintaining the mobility of trial atomic positions, by ganging an additional set of twenty potentiometers to produce dc outputs corresponding to $\cos 2\pi H_3x_3^{(n)}$ and $\sin 2\pi H_3x_3^{(n)}$ values. These modulate the f_n values to permit immediate computation of the function

$$F_{H_1H_2H_3} = \sum_{n=1}^{N} f_n\left(\frac{\sin\theta}{\lambda}\right)[\cos 2\pi(H_1x_1^{(n)}+H_2x_2^{(n)})\cos 2\pi H_3x_3^{(n)} - \sin 2\pi(H_1x_1^{(n)}+H_2x_2^{(n)})\sin 2\pi H_3x_3^{(n)} + \sin 2\pi(H_1x_1^{(n)}+H_2x_2^{(n)})\cos 2\pi H_3x_3^{(n)} + \cos 2\pi(H_1x_1^{(n)}+H_2x_2^{(n)})\sin 2\pi H_3x_3^{(n)}].$$

One layer-line (H_3 value) at a time is computed, the $H_3x_3^{(n)}$ values being fed to the new set of potentiometers.

* Development supported by the U. S. Office of Naval Research.

O9. An Iteration-Variation Calculation of the Electronic Structure of Diamond.* M. DANK AND H. B. CALLEN, *University of Pennsylvania.*—The integral iteration method[1] for obtaining the solutions of the Hartree-Fock equations has been improved by the incorporation of variational stages alternating with the iterations. The resulting rapidly convergent technique has been applied, for the purpose of testing its feasibility, to the calculation of the width of the valence band and of the gap width between the top of the filled band and the lowest s-state in the conduction band of diamond. With only three iterations, these computed energies are respectively 27.9 ev and 17.8 ev. The experimental value for the former is approximately 18 ev, whereas the most reliable available value for the latter[2] is 14 ev. The method of successive iteration and variation (SIAV) appears on this basis to be more convenient than the Wigner-Seitz method.

* Research supported by the U. S. Office of Naval Research.
[1] M. Dank and H. B. Callen, Phys. Rev. **86**, 622(A) (1952).
[2] F. Herman, Phys. Rev. **88**, 1210(L) (1952).

O10. Luminescent Effects in Chemically Pure ZnO.* T. TODD REBOUL, *University of Pennsylvania.*—Pills of ZnO, sintered from spectroscopically pure powder, have been examined at various temperatures for luminescent properties when excited by x-rays. The 395 millimicron luminescent peak has a decay $<10^{-8}$ second at all temperatures between 100°K and 300°K; the 510 millimicron peak which is about 10 times more intense than the 395 peak at 100°K has a decay which changes from about 4×10^{-4} second at 125°K to a microsecond at room temperature. Thermoluminescence experiments show that only the 510 millimicron peak is emitted during the heating process and that its temperature of peak emission is not dependent on excitation but does depend upon heating rate going from 137°K at 1.6°K per minute to 154°K at 18°K per minute. From this heating rate-peak temperature data, the activation energy of the traps responsible for the thermoluminescence is found to be 0.24 ev. It was not possible by examining the slope of the log decay time *versus* reciprocal temperature curve to find a value for activation energy consistent with the value found by the thermoluminescence experiments.

* Supported by the U. S. Office of Naval Research.

O11. Adsorbed Oxygen in Zinc Oxide Photoconductivity.* DONALD A. MELNICK AND LEO J. NEURINGER, *University of Pennsylvania.*—It is believed that adsorbed oxygen influences the photoconductivity of sintered zinc oxide. The oxygen atoms capture conduction electrons in the "necks" which connect the sintered grains. These necks, which account for most of the sample's resistance, have a surface to volume ratio sufficiently high to make this electron capture significant. Studies have been made of the process of rise and decay for times up to 10^6 seconds, with a resolution of $\frac{1}{4}$ second. (Over 95 percent of the change occurs in times greater than $\frac{1}{4}$ second.) The plot of photoconductivity *vs* log time shows continuing changes over this entire period of time, and shows only gradual changes in slope. It is therefore impossible to resolve the process into a small number of discrete time constants, but rather it is suggested that there is only one process, which is presumably associated with the adsorption and desorption of oxygen. The rate of decay increases considerably with the pressure of the ambient air. It has been determined experimentally that the effective agent in air is oxygen.

* This work supported by the U. S. Office of Naval Research.

FRIDAY AFTERNOON AT 2:00

Biology 113

(W. SHOCKLEY presiding)

Semiconductors, II

P1. Deuteron Irradiation of Germanium Near Liquid Nitrogen Temperature.* J. H. FORSTER, H. Y. FAN, AND K. LARK-HOROVITZ, *Purdue University.*—Bombardment by 9.3-Mev deuterons (at about 100°K) converted an n-type germanium sample (1.62 mho-cm^{-1}) to p type (1.2×10^{-5} mho-cm^{-1}) and decreased the conductivities of two p-type samples (93.8 and 10.5 mho-cm^{-1}) to 7.75×10^{-6} and 9.7×10^{-7} mho-cm^{-1}, respectively. At the beginning of bombardment the decrease

of holes per deuteron is 2.6 and 0.42 in the p-type samples. Mobilities measured at 90°K (about 10 cm²/volt-sec) are lower than values observed in any chemically doped p-type samples. When bombarded samples are raised to different temperatures T, the resistivity ρ and the Hall coefficient R change with time at a rate depending on T. For $T<141$°K, R and ρ increase, whereas $T>149$°K they decrease. After some time at each T, ρ, and R, curves can be taken reproducibly between T and 77°K. Most curves show two slopes in semi log plot against $1/T$. It follows that defects produced by bombardment undergo changes at relatively low temperatures. The temperature changes after bombardment and the $\sigma(\Phi)$ curves during bombardment are difficult to explain by changes in the concentration of introduced localized levels, without changing their distribution. A possible explanation is clustering of defects.

* Supported by Signal Corps contract.

P2. Germanium Films II.* W. M. Becker and K. Lark-Horovitz, *Purdue University.*—Germanium films were deposited on heated quartz plates by the thermal dissociation of GeH_4. X-ray measurements indicate the normal diamond lattice, with particle sizes >2000A, far larger than the particle sizes found in evaporated films. Film thicknesses ranged from <0.1 microns to 1.5 microns. Hall constant and resistivity were measured as a function of temperature. Log ρ and $\log|R|$ *versus* $10^3/T$ curves differ from similar plots for bulk germanium. Mobilities are lower than usually found for bulk germanium. All of the films made by thermal dissociation of GeH_4 were p type at room temperature. A region of conductivity with an activation energy of 0.72 electron volts was found in one film at temperatures above 600°C. At this temperature the Hall effect drops sharply to zero, and the mobility varies as $\sim T^{-1}$ in this temperature range. The magnetoresistance effect of these films was found to be much smaller than that of bulk germanium. At liquid nitrogen temperature, a change in resistance of only 0.01 percent was detectable using a field of 6700 gauss.

* This work was supported by Signal Corps contract.

P3. Infrared Absorption in p-Type Germanium.* W. Kaiser, R. J. Collins, and H. Y. Fan, *Purdue University.*—The absorption in p-type germanium after subtracting the lattice bands does not show the same wavelength dependence as in n-type. At room temperature there are two weak absorption peaks[1] at 2200 cm^{-1} and 3500 cm^{-1} and a sharp rise[2] at 1800 cm^{-1} to a high absorption which remains constant out to 310 cm^{-1}. The absorption is on the average an order of magnitude higher than that in n-type samples of comparable carrier concentration. Results for samples between 0.07 and 0.85 ohm-cm can be normalized to a single curve. The absorption is approximately proportional to the carrier concentration. At 77°K, instead of the two bands at 2200 cm^{-1} and 3500 cm^{-1}, one sharp band with a peak at 2700 cm^{-1} was observed. The absorption at the peak is comparable with the two peaks observed at room temperature but falls to negligible values on either side. After the steep rise at 1800 cm^{-1} the absorption exceeds the room temperature curve and reaches a maximum between 400 cm^{-1} and 330 cm^{-1}. These observations suggest an overlapping of bands within the valence band.

* Work supported by Signal Corps.
[1] H. B. Briggs and R. C. Fletcher, Phys. Rev. **87**, 1130 (1952).
[2] R. J. Collins and H. Y. Fan, Purdue Semiconductor Research Progress Report, June 30, 1952.

P4. Infrared Absorption in n-Type Germanium.* R. J. Collins and H. Y. Fan, *Purdue University.*—Infrared absorption in n-type germanium has been investigated in the region 2 to 110 microns.[1] After subtracting the lattice bands[2] the absorption obtained increases with wavelength approximately as λ^3. For samples ranging from 0.006 to 0.1 ohm-cm, the absorption seems to be proportional to the carrier concentration rather than to the ratio of carrier concentration to mobility as predicted by theory. The magnitude of absorption coefficient is two orders of magnitude higher than that given by theoretical calculation. For the temperature range where the carrier concentration remains essentially constant the absorption seems to vary as the reciprocal of the mobility. For the intrinsic range the shape of the absorption *vs* wavelength curve is qualitatively a superposition of n-type and p-type curves as expected. The data taken at different temperatures can be normalized to a single curve. The semilog plot of the normalization factor against $1/T$ has a slope corresponding to a 0.71-ev energy gap.

* Work supported by Signal Corps.
[1] Measurements beyond 40 microns were made with the facilities at the University of Michigan through the courtesy of Dr. G. B. B. M. Sutherland.
[2] R. J. Collins and H. Y. Fan, Phys. Rev. **86**, 648 (1952).

P5. Photoconductivity and Carrier Traps in Germanium.* H. A. Gebbie, M. Nisenoff, and H. Y. Fan, *Purdue University.*—Photoconductivity in germanium has a maximum near the absorption edge. At room temperature results on both n- and p-type samples can be explained simply by excitation, recombination, and motion of electrons and holes. Good agreement is found for the values of minority carrier lifetime deduced from the variation of photoresponse with applied field and distance of illuminated area from electrodes, as well as from the time constant of rise and decay. For different samples the response is proportional to the lifetime. At 77°K the response can be divided into a fast and a slow component. The former varies linearly with radiation intensity, being faster and correspondingly smaller than the room temperature effect. This means a smaller lifetime at the lower temperature. The slow component saturates with increasing radiation intensity (I) according to $I/(I+\text{const})$. The rise becomes faster with increasing intensity while the decay remains unchanged. These observations show the presence of traps for excited minority carriers, the concentration and energy levels of which have been determined. Normal electron-hole recombination cannot however be mainly determines by these traps.

* Work supported by Signal Corps contract.

P6. Dislocations in Low Angle Boundaries in Germanium Single Crystals. F. L. Vogel, W. G. Pfann, H. E. Corey, and E. E. Thomas, *Bell Telephone Laboratories.*—Convincing evidence that certain lineage boundaries in nearly perfect germanium single crystals consist of arrays of parallel edge dislocations has been obtained by microscopic and x-ray measurements. The boundaries are revealed by etching as a series of regularly-spaced conical pits when viewed in planes normal to the growth direction and are invisible when viewed in planes parallel to the growth direction. Precision x-ray measurements at individual boundaries show that such boundaries separate highly perfect regions differing in orientation by a rotation about the growth axis of the order of one minute. The measured pit-spacings agree well with the spacings D between dislocations calculated from the orientation differences θ on the basis of Burgers model[1] for a low angle boundary, in which $D=b/\theta$, where b is the lattice translation vector. These findings strongly suggest that the pits are sites of edge dislocations.

[1] J. M. Burgers, Proc. Phys. Soc. (London) **52**, 23 (1940).

P7. Theory of Thermoelectric Power in Semiconductors.* V. A. Johnson and K. Lark-Horovitz, *Purdue University.*—The thermoelectric power Q of a classical semiconductor is found by obtaining the Thomson coefficient from electric and thermal current densities and integrating the Thomson relation. For an energy independent mean free path, the result is

$$Q=-(2k/e)\tanh z+(1/eT)(\zeta+\tfrac{1}{2}E_G)-(E_G/2eT)\tanh z,$$

where $z=\zeta/(kT)+E_G/(2kT)+\frac{1}{2}\ln(cm_e^{\frac{1}{2}}/m_h^{\frac{1}{2}})$, ζ denotes the Fermil level, E_G the forbidden band width, c the ratio of electron to hole mobiiity, and m_e and m_h the electron and hole effective masses. This expression reduces to the special forms obtained earlier.[1] The maximum error introduced by an approximation used in integration appears in the intrinsic range and is given by $(3k/4e)\ln(m_h/m_e)$ about 10 microvolts/deg in germanium. Information about the temperature dependence of E_G is obtained by applying this equation to high temperature Q data. At low temperatures the theory must be modified to consider energy dependence of mean free path, sample degeneracy, and breakdown of the Boltzmann-Lorentz development of the scattering process. Theoretical results will be compared with measurements.[2]

* Supported by a Signal Corps contract.
[1] V. A. Johnson and K. Lark-Horovitz, Phys. Rev. **69**, 259 (1946).
[2] H. P. R. Frederikse, Phys. Rev. **86**, 674 (1952).

P8. Electrical Conduction and Thermoelectric Power in Thorium Oxide Crystals. O. A. WEINREICH AND W. E. DANFORTH, *Bartol Research Foundation.*—The conductivity and thermoelectric power of homogeneous crystalline specimens of thorium oxide are being measured in different gas atmospheres and in vacuum. Conduction in hydrogen is relatively stable and is accompanied by electrolytic discoloration. In oxygen, conductivity is higher, increases markedly with flow of current and is not accompanied by visible electrolytic deposits. In all cases where a change is made from an oxygen atmosphere to a non-oxygen atmosphere (or vacuum) the conductivity decreases. One, therefore, speculates that the material is a p-type conductor when in oxygen and in the temperature range concerned (700°–1000°C). This is corroborated by the polarity of the Seebeck effect. In vacuum at higher temperatures evidence points to n-type conduction. Data regarding the variation of thermoelectric power with temperature in an oxygen atmosphere yield energy-gap valves in fair agreement with those obtained from electrical conductivity. Using the simplest semiconductor theory with present data, the calculated density of impurity centers is unreasonably high. However, it is to be expected that, under the circumstances, the impurity density will vary with temperature. An attempt to take this into account mathematically is in progress.

P9. Thick $p-n$ Junctions in Germanium.* RALPH BRAY AND F. VAN DER MAESEN,† *Purdue University.*—In single crystal Ge samples, we have found $p-n$ barrier regions of such thickness (~0.05 cm) as to permit probe determination of the potential distribution at low reverse bias and operation of a rectifying point contact *inside the barrier*. From the potential distribution one may estimate the space charge in the barrier, its variation with reverse voltage, and consequently the capacitance. This capacitance and the barrier thickness are relatively insensitive to applied voltage for one such barrier. A new three-terminal device has been constructed involving the interaction of the biased $p-n$ junction and a separately biased, n-type rectifying point contact made *inside the* $p-n$ *barrier*. For instance, the point contact circuit may operate in a normal, low forward resistance state, or in a very high resistance state, depending on relative magnitudes of point contact forward voltage and reverse bias on $p-n$ junction. The switching from one stage to the other is accompanied by a negative resistance region. The critical switching voltages are dependent on the position of the point inside the barrier and on illumination.

* Work supported by Signal Corps contract.
† Present address: Phillips Research Laboratory, Eindhoven, Holland.

P10. On Noise in $p-n$ Junction Rectifiers and Transistors. I Theory. RICHARD L. PETRITZ, *U. S. Naval Ordnance Laboratory and Catholic University.*—The problem of the noise resulting from concentration fluctuations of the minority carrier in $p-n$ junction rectifiers and transistors, as formulated and solved with a lumped parameter approximation[1] has now been solved without this approximation. Our result for $G_p(\Delta I_{ss}^2)$ is

$$G_p(\Delta I_{ss}^2)=\frac{4kT|z|^2}{R_p}\left\{\frac{e^{-qV_0/kT}+(z+z^*)}{(z+z^*)(z+z^*+1)}+\frac{e^{qV_0/kT}}{F^{z+z^*}}\int_0^F\frac{y^{z+z^*-1}}{(1+y)}dy\right\},$$

where $F=[\exp(qV_0/kT)-1]$, $z=(1+i\omega\tau_p)^{\frac{1}{2}}$; other symbols are defined in reference 1. $G_n(\Delta I_{ss}^2)$ is of similar form. For $\omega\tau_p<1$ the expression simplifies, and the available noise power is $\geq kT$ for all bias values; clearing up an anomaly in our approximate solution (reference 1, Eq. 63). Further studies of the noise resulting from fluctuations in the local lattice temperature show that the parameter h, in Eqs. 6 and 8 of reference 2, is essentially an average diffusion length of the minority carriers.

[1] Richard L. Petritz, Proc. Inst. Radio Engrs. **40**, 1440 (1952).
[2] Richard L. Petritz, Phys. Rev. **87**, 535 (1952).

P11. On Noise in $p-n$ Junction Rectifiers. II Experiment. FRANCES L. LUMMIS AND RICHARD L. PETRITZ, *U. S. Naval Ordnance Laboratory.*—Measurements of the absolute magnitude and spectrum of noise in $p-n$ junction rectifiers were made over the frequency range 15 cps to 600 kcps with different values of reverse dc bias and load resistance (R_L). The spectrum of the noise power across R_L can be fitted by an equation of the form $G(e^2, R_L)=A/[1+(2\pi f\tau)^2]+B/f$. An attempt has been made to interpret these results in terms of the two mechanisms discussed in the above abstract. According to the theory, the electronic noise corresponds to the term $A/[1+(2\pi f\tau)^2]$ and the lattice temperature noise to the B/f term, the parameters A, B, and τ being evaluated by experiments not involving noise measurements (see abstract No. P11). We find that the theoretical expression for electronic noise is in reasonably good agreement with the $A/[1+(2\pi f\tau)^2]$ term, both in regard to absolute magnitude and spectrum over the range of bias and R_L values used. However, the theoretical expression for lattice noise, whole adequately fitting a $1/f$ law, over the range of frequencies investigated, is not of sufficient magnitude to account for the experimental data.

FRIDAY EVENING AT 7:00

Main Dining Hall, Duke Union

(G. B. PEGRAM presiding)

Banquet of the Americal Physical Society

After-dinner speakers: G. B. PEGRAM, P. M. GROSS, R. J. SEEGER, W. SHOCKLEY, and T. J. KILLIAN.

SATURDAY MORNING AT 10:00

Howell Hall

(HOWARD REISS presiding)

Division of Chemical Physics

Symposium on Nucleation Theory

Q1. Nucleation in Condensed Systems. DAVID TURNBULL, *General Electric Company.* (30 min.)

Q2. Nucleation of Solid-Solid Transitions. JOHN HOBSTETTER, *Bell Telephone Laboratories.* (30 min.)

Q3. Role of Nucleation-Theory in Crystal Growth. N. CABRERA, *University of Virginia.* (30 min.)

Q4. Time Lag in Spontaneous Nucleation Due to Non-Steady-State Effects. F. C. COLLINS, *Polytechnic Institute of Brooklyn.* (30 min.)

Division of High-Polymer Physics

Invited Paper

Q5. Statistical Mechanics of Polymer Chains in Solution. B. H. ZIMM, *General Electric Research Laboratory.* (30 min.)

SATURDAY MORNING AT 10:00

Bingham Hall

(V. A. JOHNSON presiding)

Strain and Stress; Theoretical Solid-State Physics

R1. The Strength of Solid Solution Alloys.—JOHN C. FISHER, *General Electric Company.*—Short range order in an alloy, by which is meant any short-range departure from randomness in the arrangement of atoms on lattice sites, must strengthen the alloy. The increment of strength due to short range order, or order-hardening as it will be called, results from the fact that the motion of a dislocation through such an ordered alloy changes the nearest-neighbor configuration of atoms across the slip plane, producing a more nearly random configuration of higher energy. If γ is the mean energy increase per square centimeter of interface produced by the passage of a single dislocation, and if b is the magnitude of the Burgers vector for the dislocation, the order-hardening is given by the expression $\tau_0 = \gamma/b$. For an interface with $\gamma \approx 20$ ergs/cm^2 the order-hardening is $\tau_0 \approx 10^9$ dynes/cm^2, or 15 000 psi.

R2. Strain and Crystallite Size in Experimental Iron Powders.* FRANK E. JAUMOT, JR., AND LEONARD MULDAWER, *Franklin Institute Laboratories.*—The strain and crystallite size present in an experimental iron powder produced by a carbonyl process (General Aniline and Film Company, designated P818) has been determined. Electron microscopic examination gave a mean particle diameter of about two microns. The method used to determine the strain and crystallite size has been described by Warren and Averbach.[1,2] Using a combination of Fe and Cu radiation, the shapes of five powder diffraction lines were obtained for the powder and for a well-annealed "standard." From a Fourier analysis of these lines, a line profile due only to strain and crystallite broadening was obtained. A curve of the Fourier coefficients of this line profile as a function of the order of the diffraction lines gave the crystallite size and strain directly.[2] The crystallite size given by the analysis was of the order of 120A, and the rms strain was computed to be approximately 10^{-2}. These values are in reasonable agreement with those found by Taylor[3] by a different method, for a similarly prepared powder.

* This work was supported in part by the U. S. Office of Naval Research.

[1] B. E. Warren and B. L. Averbach, J. Appl. Phys. **21**, 595 (1950).
[2] B. E. Warren and B. L. Averbach, J. Appl. Phys. **23**, 497 (1952).
[3] A. Taylor, Pittsburgh Conference on Diffraction, November 7, 1952.

R3. The Yield Point Strain. EDWARD W. HART, *General Electric Research Laboratory.*—The yield point phenomenon in metals has been ascribed[1] to the anchoring of dislocations by solute atoms. The yield stress is that stress which produces appreciable thermal nucleation of free moving segments of dislocations from the regions in which they are anchored. A Frank-Read source,[2] initially anchored, can be activated to produce a dislocation burst[3] even though its critical stress is greater than the applied stress, if the size of a critical nucleus is smaller than the length of the source. This latter condition is readily verified by use of a simplified model for anchoring, suggested by J. C. Fisher.[4] This process provides a basis for explanation of the size of the yield point strain, the apparently homogeneous nature of much of the yield strain, the subsequent initial increase in hardening rate, and dependence of the strain on crystal size.

[1] A. H. Cottrell, Rep. Conf. on Strength of Solids, Phys. Soc. London (1948).
[2] F. C. Frank and W. T. Read, Phys. Rev. **79**, 722 (1950).
[3] Fisher, Hart, and Pry, Phys. Rev. **87**, 958 (1952).
[4] Private communication.

R4. Change of Elastic Constants Resulting from Annealing of Cu and Al Cold Worked at −196°C.* E. C. CRITTENDEN, JR., AND H. DIECKAMP, *North American Aviation, Inc.*—The behavior of elastic constants after cold work or radiation

damage offers considerable promise as a tool for the identification of interstitial atoms in the presence of other imperfections. Interstitial atoms will probably increase the elastic moduli,[1] whereas vacancies and internal strain decrease the moduli. Preliminary observations have been made on Cu and Al wires treated so as to have a [111] fiber texture with the [111] fiber axis parallel to the wire axis. Since the shear modulus is isotropic for all directions in the (111) plane for cubic crystals, the modulus measured by torsion of such wires is a single crystal property. Such wires, 10 to 20 mils in diameter, were cold worked by twisting at −196°C to a surface strain of 0.5 and were then annealed by a series of 15-minute annealing pulses with a temperature increase of 25°C for each step up to room temperatures. All observations were made at −196°C between annealing pulses. The shear modulus can be observed to better than 5 parts in 10^4. The behavior of Cu and Al is very similar. After cold work the shear modulus had decreased about 10 percent. On annealing, the modulus recovered steadily throughout the range of −196°C to room temperature except in the region of −125°C for Al and −75°C for Cu where the modulus showed a slight decrease. This decrease suggests the loss of interstitial atoms during annealing.

* This report is based on studies conducted for the U. S. Atomic Energy Commission under contract AT-11-1-GEN-8.
[1] G. J. Dienes, Phys. Rev. **87**, 666 (1952).

R5. Theory of Initial Stress Strain Curves in Face-Centered Metals. J. S. KOEHLER, *University of Illinois.**—In an earlier paper[1] work-hardening by two mechanisms were considered: first, at small strains source hardening occurs, i.e., the longest free lengths of a dislocation generate and produce glide until they are locked by some process not yet understood. The hardening occurs because as the long dislocations are used more stress is required to make the short dislocations generate. At large strains the many dislocations present prevent additional dislocation motion; this is called interaction hardening. The temperature dependence of the source hardening in aluminum can be understood if it is assumed that all of the closely spaced glide lamellas found by electron microscopy in one slip band result from one source. The number of lamellas per band increases with increasing temperature. T. H. Blewitt[2] has found that source hardening in copper is the same at room temperature as it is at liquid nitrogen. This is consistent with C. S. Barrett's[3] observation that there exists only one glide lamella per slip band in copper at room temperature. The theory suggests that a search be made for multiple lamellas and stress strain curves dependent on temperature in copper crystals at elevated temperatures.

* Supported by the U. S. Office of Naval Research.
[1] J. S. Koehler, Phys. Rev. **86**, 52 (1952).
[2] T. H. Blewitt, see abstract this meeting.
[3] C. S. Barrett, Trans. Am. Inst. Mining Engrs. **156**, 62 (1944).

R6. X-Ray Measurements of Cold-Worked Alpha-Brass.* B. E. WARREN, B. L. AVERBACH, AND E. WAREKOIS, *M.I.T.*—Filings of 70–30 brass pressed into a briquet served as the cold-worked sample. Peak shapes were measured with a recording spectrometer using filtered CoKα. Fourier coefficients were determined and instrumental broadening corrected by the Stokes method. A log plot of the coefficients for the 111, 222 and the 200, 400 combinations gave particle sizes $L_{111}=180$A, $L_{100}=70$A, and slopes indicating appreciable distortion. Strip rolled to 98 percent reduction was used to get a strong (111) orientation and coefficients for (111), (222), (333) determined. The (333) points were above the (111), (222) line on the log plot indicating that an appreciable part of the particle size broadening is due to stacking faults. A small decrease in the (111), (200) peak separation and an increase in the (222), (400) separation was observed in agreement with Paterson's prediction for the effect of stacking faults. The distortion corresponds to a rms strain of 0.007. The results indicate that the x-ray broadening is due partly to distortion and partly to particle size, and that the particle size effect is largely due to stacking faults on the (111) planes at about every 25th plane.

* Sponsored by the U. S. Atomic Energy Commission.

R7. Comparison of Resistivity and Density Changes in Cold-Worked Brass. HERBERT I. FUSFELD, *Frankford Arsenal and Office of Ordnance Research.*—Experimental results have been obtained on the changes in resistivity of cold-worked brass with recovery at various annealing temperatures. All anneals were conducted below the recrystallization point. The curve shows certain maxima and minima. It is observed that the curve is similar to results obtained elsewhere on the changes in density of cold-worked brass as a function of annealing temperature. One curve may be transformed to the other by assuming that the underlying processes are identical, and are governed by an activation energy of approximately 19 000 calories per mole.

R8. Plastic Behavior of Polycrystalline Metals at Very High Strain Rates ($\sim 10^4$/sec). L. ZERNOW AND J. SIMON, *Aberdeen Proving Ground.*—The behavior of a variety of polycrystalline metals at strain rates of the order of 10^4/sec is being studied. These strain rates are achieved by the explosive collapse of the metal into a high velocity jet[1–4] along which a velocity gradient exists. Observation of the behavior of the metal under these conditions is accomplished by means of fractional microsecond flash radiography.[3,4] The face-centered cubic metals, copper, nickel, aluminum, and silver, have been found to deform plastically quite readily with relatively small differences in their comparative behavior. Body-centered cubic materials like iron have been observed to undergo early fracture, as have also, members of the close packed hexagonal family cobalt and zinc. These results are consistent with and constitute an extension of the observations of Kramer and Maddin[5] on single crystals of α-brass, aluminum, and β-brass. Factors modifying the normal behavior will be discussed.

[1] Birkhoff, MacDougal, Pugh, and Taylor, J. Appl. Phys. **19**, 563 (1948).
[2] Pugh, Eichelberger, and Rostocker, J. Appl. Phys. **23**, 532 (1952).
[3] J. C. Clark, Phys. Rev. **72**, 741 (1947).
[4] L. Zernow, Bull. Am. Phys. Soc. **27**, No. 6, 10 (1952).
[5] I. R. Kramer and R. Maddin, J. Metals **4**, 197 (1952).

R9. Lattice Vibrations in Graphite. HERBERT B. ROSENSTOCK, *U. S. Naval Research Laboratory.*—Gurney[1] justifies the assumption that, at low temperatures, the only vibrations that are excited in the graphite lattice are transverse ones propagated in the principal hexagonal crystal planes. On this assumption, the frequency distribution may be calculated exactly[2,3] for certain values of the force constants α, β, γ, for nearest, 2nd-nearest, and 3rd-nearest neighbors. The specific heat calculated from these "exact" distributions is slightly sensitive to the choice of β/α and γ/α, differing somewhat from the T^3 law predicted by Debye theory throughout the temperature range of interest here. Comparison with experiment[4] yields a numerical value for the parameter $\theta=\hbar\omega_{\max}/zk$, and from this the values of the force constants, which are related to $\omega_{\max}$, may be inferred. Numerical results will be given.

[1] R. W. GURNEY, Phys. Rev. **88**, 465 (1952).
[2] E. W. Montroll, J. Chem. Phys. **15**, 575 (1947).
[3] W. A. Bowers and H. B. Rosenstock, J. Chem. Phys. **18**, 1056 (1950).
[4] Esterman and Kirkland, as quoted in reference 1.

R10. Plasma Waves in Metals. P. A. WOLFF, *Bell Telephone Laboratories.*—The Hartree approximation is used to investigate the effect of the crystal lattice on plasma oscillations in metals. The plasma frequency is given by the formula $\omega^2=4\pi e^2 n_0\langle 1/m_z^*\rangle$, where n_0 is electron density and $\langle 1/m_z^*\rangle$ the average of the effective mass over filled states. For free electrons this equation reduces to that given by Bohm and Gross:[1] for insulators $\langle 1/m_z^*\rangle=0$ and there are no oscillations.

Interband transitions induced by the plasma waves cause frequency broadening and probably are responsible for the large widths observed in Cu, Ni, and Ag.[2] The matrix element for such a transition is the same as for optical absorption; *d*-electrons, being more numerous and more tightly bound contribute the major share of the transition probability.[3] This explains why plasma lines observed in Be and Al are much narrower than those seen in the metals mentioned above. A rough estimate of the frequency shift due to interband transitions is made and shown to be consistent with experiment.

[1] Bohm and Gross, Phys. Rev. **75**, 1851 (1949).
[2] G. Ruthemann, Ann. Physik **2**, 113 (1948); W. Long, Optik **3**, 233 (1948).
[3] The suggestion that *d*-electrons are mainly responsible for the broadening was first made by Conyers Herring.

R11. A New Treatment of Energy Bands. NORMAN ROSTOKER AND WALTER KOHN, *Carnegie Institute of Technology.*—The problem of finding the propagating electron wave functions of a crystal can be formulated as an integral equation, which leads to a stationary expression for the energy. If one employs only trial functions which satisfy the Schrödinger equation, the potential can be eliminated from this expression. The resulting secular equation depends only on the Green's function for the lattice under consideration and the logarithmic derivatives of the $s, p, d, \cdots$ etc., radial functions at the inscribed sphere of the atomic polyhedron. The Green's function is completely determined by the geometry of the crystal lattice while the logarithmic derivatives are determined by the ionic potential. Therefore, in this treatment, the effects of the type of lattice and of the ionic potential on the structure of the energy bands are clearly separated. The methods goes beyond the spherical approximation and takes into account the detailed shape of the atomic polyhedron. Preliminary results for lithium will be presented. We plan to apply this method next to transition metals.

R12. Brillouin Zone Structures of Alloys. Part I. Some Implications of Present Theories. E. I. SALKOVITZ AND A. I. SCHINDLER.—The changes occurring in the lattice parameters a and c and their ratio c/a in dilute magnesium solid solutions have been carefully studied by Hume-Rothery and Raynor[1] and others. The changes in the c/a ratio of these solutions have been interpreted by H. Jones[2] to be associated with a change in the Fermi energy arising from the distortion of the Brillouin zone: that is, these c/a changes are associated with an overlap which takes place at a given electron to atom ratio. This interpretation implies that an anomaly should exist in the conductivity *versus* concentration curve for these alloys. An indirect consequence should be the breakdown of Linde's and Matthiessin's rules. Indeed Linde's rule may be expected to be invalid on other grounds. The rule was based on dilute alpha-solutions of monovalent metals and has not been thoroughly checked for bivalent metals. It will be necessary to establish the dependence of the scattering probability upon alloying addition when c/a varies. These considerations also raise doubt concerning the validity of Matthiessin's rule.

[1] W. Hume-Rothery and G. V. Raynor, Proc. Roy. Soc. (London) **177**, 27 (1940); G. V. Raynor, *ibid.* **180**, 107 (1942); and R. S. Busk, Trans. Am. Inst. Mining Met. Engrs. **188**, 1460 (1950).
[2] H. Jones, Proc. Roy. Soc. (London) **A147**, 400 (1934); Physica **15**, 13 (1949); Phil. Mag. **41**, 663 (1950).

R13. Brillouin Zone Structures of Alloys. Part II. Hall Constant Data of Dilute Magnesium Alloys. A. I. SCHINDLER AND E. I. SALKOVITZ.—To explain the peculiar variation of the lattice parameters of dilute alpha-solutions of magnesium, H. Jones has postulated a Brillouin zone overlap at a certain electron to atom ratio. A direct consequence of this theory is that a significant effect should be found on the Hall constant when overlap occurs. In the application of the Jones' theory, other writers have tacitly assumed that the metals in column I of the periodic table have one valence electron, those in column II have 2, and those in column III, three electrons per atom. However, it is generally accepted that the valence of the solute is not necessarily equal to the number of outer electrons. An insight into the contribution of electrons to magnesium by the solute can be obtained from Hall data. If overlap occurs, the variation of Hall constant with solute concentration should be abrupt at overlap. As a test of these ideas, Hall data, using a technique described by Schindler and Pugh,[1] were obtained at room temperature on magnesium containing 0.8, 1.3 and 1.8 atomic percent aluminum and 0.1, 0.2, and 0.3 atomic percent silver. In both cases, the Hall constant decreased rapidly as a function of solute concentration with the variation in the silver approximately three times that of the variation in aluminum. These results will be discussed and an experimental program outlined.

[1] A. I. Schindler and E. M. Pugh, Phys. Rev. **89**, 295 (1953).

SATURDAY MORNING AT 10:00

Venable Hall

(NELSON FUSON presiding)

Infrared Spectroscopy

S1. A New Detector for the Infrared. S. MROZOWSKI, B. D. MCMICHAEL,* AND E. A. KMETKO, *University of Buffalo.*—In the process of condensation of aromatic molecules into large graphite planes, the energy gap between the filled and empty bands gradually decreases to zero, and the corresponding long-wave absorption edge moves from the visible into the infrared. By stopping the condensation process at a definite stage, substances with energy gaps as narrow as required can be produced. In this work the photoresponse of films made by heat-treating cellophane was investigated. A remarkable bolometric effect was found and also the presence of an internal photoeffect established. In general, the films with the best photoeffect showed a signal-to-noise ratio inferior to the PbS cells (by a factor of about 20 at 200 cycles.) However, the frequency response is good (checked only up to 2000 cycles), the maximum of sensitivity seems to be located in the infrared, and the long-wave limit coincides roughly with the absorption edge. By interposing another film with a shorter wavelength, absorption limit cells responding to a specified spectral region can be built. Cells with a sensitivity limit only up to about 5μ were obtained; the increasing conductivity of the films preventing a further extension into the infrared.

* Now at the Bell Aircraft Corporation, Niagara Falls, New York.

S2. An Infrared Analysis of the Associated O−H and O−D Stretching Vibrations of Simple Carboxylic Acids.* NELSON FUSON, MARIE-LOUISE JOSIEN, AND CONRADE C.

HINDS, *Fisk University.*—This paper reports a study of the "fine structure" of the associated hydroxyl group stretching vibration band of carboxylic acids, using a single beam infrared spectrometer equipped with a lithium fluoride prism. The compounds, studied in the vapor and/or solution state, included CF_3COOH, CF_3COOD, and CH_3COOD. Previously reported experimental results and interpretations[1] will be discussed in relation to the present findings, and a new explanation for the "fine structure" will be proposed.[2]

* This investigation has been supported by a Frederick Gardner Cottrell grant from the Research Corporation.
[1] V. M. Chulanovskii and P. D. Simova, Doklady Akad. Nauk. S.S.S.R. **68**, 1033 (1949); D. Hadzi and N. Sheppard, Boll. sci. facoltà chim. ind. univ. Bologna **10**, 25 (1952); M. Davies and J. C. Evans, J. Chem Phys. **20**, 342 (1952); and Fuson, Josien, Jones, and Lawson, J. Chem. Phys. **20**, 1627 (1952).
[2] M.-L. Josien and N. Fuson, Compt. rend. **235**, 1025 (1952).

S3. An Infrared Study of the Influence of Molecular Structure on the Carbonyl Band in Polycyclic Quinones.* MARIE-LOUISE JOSIEN, NELSON FUSON, AND ESSIE M. SHELTON, *Fisk University.*—A study of the position of the infrared absorption associated with the carbonyl bond vibration in over one hundred quinones[1-3] leads to some interesting correlations between the C=O frequency and other measures of molecular structure such as oxidation-reduction potential, bond order, index of free valence, Hammett's function, and the geometrical form of the molecule. Certain hydroxy-substituted quinones show spectral anomalies which do not seem to fit into the usual category of hydrogen bonded compounds.

* This investigation was supported by a research grant from the National Cancer Institute, United States Public Health Service.
[1] M.-L. Josien and N. Fuson, Bull. soc. chim. France **19**, 389 (1952).
[2] Josien, Fuson, Lebas, and Gregory, J. Chem. Phys. **21**, 331 (1953).
[3] Josien, Fuson, and Pearson, Compt. rend. **235**, 1206 (1952).

S4. The Infrared Spectrum and Molecular Constants of Deuterium Bromide. F. L. KELLER AND A. H. NIELSEN, *University of Tennessee.*—High dispersion measurements have been made for the first time on the fundamental ($v=0\rightarrow1$), first overtone ($v=0\rightarrow2$), and second overtone ($v=0\rightarrow3$) infrared vibration bands of DBr. The fundamental was observed by using a 40-cm cell and pressures of 90–150 mm. The overtones required the use of a multiple reflection cell with a path of 17 meters and pressures of 240–460 mm. It was necessary to elminate strong atmospheric absorption in the region of each band. The isotopic splitting of the rotation lines was measured and molecular constants determined for both isotopic species, DBr^{79} and DBr^{81}. The principal constants for DBr^{79} are $\omega_e=1885.33$ cm^{-1}, $x_e\omega_e=22.73$ cm^{-1}, $y_e\omega_e=-0.0106$ cm^{-1}, $B_e=4.290_8$ cm^{-1}, $\alpha_e=0.083_9$ cm^{-1}, $D_e=0.000096_4$ cm^{-1}, $\beta=-2_3\times10^{-6}$ cm^{-1}. The principal constants for DBr^{81} are $\omega_e=1884.75$ cm^{-1}, $x_e\omega_e=22.72$ cm^{-1}, $y_e\omega_e=-0.0106$ cm^{-1}, $B_e=4.287_6$ cm^{-1}, $\alpha_e=0.083_8$ cm^{-1}, $D_e=0.000095_9$ cm^{-1}, $\beta=-2_2\times10^{-6}$ cm^{-1}. These values are in good agreement with constants obtained from recent measurements on the fundamental vibration of HBr by Thompson, Williams, and Callomon.[1]

[1] Thompson, Williams, and Callomon, at the Physical Chemistry Laboratory, Oxford (private communication).

S5. A Study of the Infrared Spectrum of the Amide Group. HARRY LETAW, JR.,* AND ARMIN H. GROPP, *University of Florida.*—Two assignments have been proposed for the very strong 1560 cm^{-1} band of the N-substituted amide group. Lenormant[1] has suggested its assignment to ν(C–N) and Richards and Thompson[2] have suggested δ(N–H). This investigation consisted of a study of the frequency shifts of this and other bands in the infrared spectra of several *n*-butyl- and N,N-dibutyl-ethanamides upon substitution of chlorine and fluorine in the 2-position. On the basis of these shifts and other properties of the band in question, observed in the spectra both of the pure compounds and of their CCl_4 solutions, it is concluded that the ν(C–N) assignment is correct. The apparent absence of the corresponding band from the spectrum of the N,N-disubstituted amide group is explained by the accidental degeneracy of ν(C=O) and ν(C–N).

* U. S. Atomic Energy Commission, Predoctoral Fellow. Now at the University of Illinois.
[1] H. Lenormant, Ann. chim. **5**, 459 (1950).
[2] R. E. Richards and H. W. Thompson, J. Chem. Soc. (London) 1248 (1947).

S6. The Infrared Absorption Spectrum of SO_2.* R. D. SHELTON, A. H. NIELSEN, AND W. H. FLETCHER, *University of Tennessee.*—The infrared absorption spectrum of SO_2 was recorded with a grating spectrometer from 470 cm^{-1} to 8000 cm^{-1} with path lengths up to 20 atmometers. Fifteen bands were observed. Band centers of ν_2, ν_1, ν_3, $\nu_2+\nu_3$, $2\nu_1$, $\nu_1+\nu_3$, $2\nu_3$, $2\nu_1+\nu_2$, $\nu_1+\nu_2+\nu_3$, $3\nu_1$, $2\nu_1+\nu_3$, $3\nu_3$, $3\nu_1+\nu_3$, and $\nu_1+3\nu_3$ have been assigned frequencies of 517.76, 1151.30, 1361.11, 1875.58, 2295.82, 2499.55, 2715.30, 2815.98, 3011.25, 3431.19, 3629.57, 4054.26, 4751.23, and 5165.64 cm^{-1}, respectively. The first five had been previously observed.[1] Combination relations based on a symmetric top approximation were applied to the Q branches of the a_1 type bands ν_1, ν_2, $2\nu_1$ and $2\nu_3$. These gave respective $(A''-B'')$ values of 1.7009, 1.6903, 1.7144, and 1.7044 cm^{-1}, and respective $(A'-B'-A''+B'')$ values of -0.00035, $+0.0370$, -0.0538, and -0.0367 cm^{-1}. Combination relations applied to ν_3 gave $B''=0.3023$ cm^{-1} and $(B'-B'')=-0.00010$ cm^{-1}. Using the B'' value from ν_3 and the average $A''-B''$ from above, $A''=2.0048$ cm^{-1} compared with $A''=2.0271$ cm^{-1} from microwave data.[2] Calculation of the harmonic and anharmonic constants gave $\omega_1^0=1155.62$, $\omega_3^0=1368.06$, $x_{11}=-3.95$, $x_{33}=-5.52$, $x_{13}=+1.20$, $x_{33}=-3.59$, $x_{13}=-13.52$.

* Supported by the U. S. Office of Ordnance Research.
[1] G. Herzberg, *Infrared and Raman Spectra of Polyatomic Molecules* (D. Van Nostrand Company, Inc., New York, 1945), p. 285.
[2] M. H. Sirvetz, J. Chem. Phys. **19**, 938 (1951).

S7. Infrared Grating Spectrum of CH_3CN Vapor. F. W. PARKER, A. H. NIELSEN, AND W. H. FLETCHER, *University of Tennessee.*—Although the microwave spectrum[1] and infrared prism spectrum[2] of CH_3CN have been investigated, high dispersion infrared measurements have not been reported, and spectral regions masked by atmospheric H_2O vapor and CO_2 have been inadequately studied. Using a prism-grating spectrograph and suitable absorbants for H_2O and CO_2, it has been possible to measure many bands under high resolution from 1.5–16 mu. The parallel band $\nu_4(a_1)$ at 920 cm^{-1} and perpendicular bands $\nu_7(e)$ and $\nu_8(e)$ at 1050 cm^{-1} and 3010 cm^{-1} have been well resolved, and partial resolution of the P and R branches of $2\nu_8(A_1)$ at 715 cm^{-1} has been achieved. A multiple reflection cell with path length of 20 meters was used with vapor pressures as high as 60 mm in a search for combination and overtone bands. Resolution of bands at 2100, 4000, 4400, and 5600–6100 cm^{-1} resulted. New bands have been found at 1800, 4160–4210, 4840, 5014, 5270, 5410, 5845, 5965, and 6135 cm^{-1}, some of which exhibit rotational structure.

[1] H. H. Nielsen, Phys. Rev. **77**, p. 130 (1950); Kessler, Ring, Trambarulo, and Gordy, Phys. Rev. **79**, 54 (1950).
[2] P. Venkateswarlu, J. Chem. Phys. **19**, p. 293 (1951).

S8. An Analysis of the Infrared Spectrum of CF_3COCl. ROBERT JAMES LOVELL, *Vanderbilt University.*—The spectrum of CF_3COCl has been recorded in the rocksalt region from two to fifteen microns. Eighteen bands were observed, of which six are thought to be fundamentals and twelve overtones and combinations. The molecule has at most one plane of symmetry, and, therefore, has been assigned to the C_s point

group. Of the fifteen possible fundamentals, ten are A' (vibrations parallel to the plane of symmetry) and five are A'' (vibrations perpendicular to the plane of symmetry). The selection rules for this group allow all vibrations (both fundamentals and overtones and combinations) to appear in the infrared region. Utilizing data from studies (made by the author) of the Raman and infrared spectra of the analog CF_3COBr and a knowledge of the characteristic group frequencies involved, an attempt is made to follow Morris[1] and Wilson and Wells[2] in assignment of the fundamentals and overtones and combinations present in the infrared spectrum of CF_3COCl.

[1] J. C. Morris, J. Chem. Phys. **11**, 230 (1943).
[2] E. B. Wilson, Jr., and A. J. Wells, J. Chem. Phys. **9**, 319 (1941).

S9. Raman Spectrum, Force Constants, and Calculated Thermodynamic Properties of Germanium Tetrafluoride. LAWRENCE K. AKERS AND ERNEST A. JONES, *Vanderbilt University.*—One fundamental frequency of the Raman spectrum of gaseous GeF_4, the symmetrical frequency ν_1, has been obtained. Using this and other previously reported fundamentals,[1] force constants using various potential functions have been calculated. The thermodynamic properties, heat content, free energy, heat capacity, and entropy have also been calculated using spectroscopic data and the usual harmonic oscillator, rigid rotator approximation. Calculations are for ideal gas at one atmosphere pressure for temperatures 100°–1000°K.

[1] P. G. H. Woltz and A. H. Nielsen, J. Chem. Phys. **20**, 307 (1952).

SATURDAY MORNING AT 10:00

Phillips Hall

(A. M. WEINBERG presiding)

Effects of Irradiation on Solids

T1. Additional Data on the Resistivity of Cu_3Au during Neutron Irradiation. HARVEY L. GLICK AND W. F. WITZIG, *Westinghouse Electric Corporation.*—A continuation has been made of work[1] dealing with neutron irradiation of Cu_3Au at 80°C±7C° within a graphite moderated nuclear reactor. The initially ordered specimen resistivity continued to increase to a value 60 percent above its initial value at 2×10^{20} neutrons/cm². The initially disordered specimen resistivity reached a minimum 7.5 percent below its initial value at 5×10^{19} nvt and increased thereafter to a value 4.2 percent below its initial value. A disordered specimen held at 80°C without neutron irradiation showed that the above effect was not produced by temperature alone. Similar specimens were irradiated at 140°C±10C°. At 4×10^{18} nvt, the resistivity of the initially ordered specimen dropped 6 percent, then increased slowly to a value 4 percent above its initial value at 1.4×10^{20} nvt. The resistivity of the initially disordered specimen dropped 12 percent in 4×10^{18} nvt, another 5 percent at 2.5×10^{19} nvt and then remained substantially constant. A disordered specimen held at 140°C without neutron irradiation suffered a resistivity drop of 4 percent in a day and then remained essentially constant. These results indicate that the effect of irradiation is dependent upon the temperature of the specimen.

[1] Glick, Brooks, Witzig, and Johnson, Phys. Rev. **87**, 1074 (1952).

T2. X-Ray and Metallurgical Studies on Neutron Irradiated Cu_3Au. R. H. FILLNOW, E. K. HALTEMAN, AND G. F. MECHLIN, *Westinghouse Electric Corporation.*—Metallurgical and x-ray diffraction studies have been made on samples of Cu_3Au irradiated as a part of the 80°C electrical resistivity experiment discussed in the previous paper. Vickers hardness has been determined on sets of disordered and ordered material both before and after irradiation. The hardness of the disordered material increased by 21 vhn from an initial value of 100 vhn after an exposure of 3×10^{20} nvt. The ordered material increased by 48 vhn from an initial value of 110 vhn for the same exposure. Photographs of microstructure have been made and will be discussed. X-ray diffraction patterns have been obtained from powdered material having simultaneously received the heat treatment given the electrical resistivity and metallurgical samples. Debye-Scherrer patterns were made in a 114-mm camera on extruded samples with a starch diluent. Visual examination of the pattern indicates essentially no change in the disordered material and a perceptible sharpening after irradiation on the ordered material. Studies of the long range order parameter indicate only a small decrease in long range order. Lattice parameter determinations show no significant alteration of parameter for the disordered material but a significant increase in parameter for the ordered material.

T3. The Effect of Fast Neutron Bombardment on Diffusion in Cu_3Au. R. R. COLTMAN AND T. H. BLEWITT, *Oak Ridge National Laboratory.*—Previous work has indicated that fast neutron irradiation increases the rate of ordering of Cu_3Au. Prior to neutron bombardment two Cu_3Au resistors with a degree of order corresponding to equilibrium at 376°C were annealed at 150°C for 100 hours without appreciably affecting the resistance. The samples were then irradiated in the ORNL graphite reactor at 150°C. One sample was exposed to a fast neutron flux of 1×10^{12} neutrons/cm² and the other to 2.5×10^{11} neutrons/cm²/sec. The resistance of the sample exposed to the lower flux approached a minimum approximately 25 percent lower than the original value with about half of the decrease occurring in the first 24 hours. The other sample behaved similarly, however, approached the minimum four times as fast. A third specimen was bombarded for one week at −160°C in a flux of 2×10^{10} neutrons/cm²/sec. At this temperature the sample apparently disordered as a small increase (0.6 percent) was observed. Subsequent annealing for 3.5 hours at −80°C produced no change in resistance. Annealing at 0°C, 100°C, and 150°C indicated a relaxation time of approximately 50 hours at 0°C, 25 minutes at 100°C, and 10 minutes at 150°C. A total decrease in resistance of 4.7 percent was observed.

T4. The Deformation of Copper Crystals at 78°K and 300°K. T. H. BLEWITT, J. K. REDMAN, AND F. A. SHERRILL, *Oak Ridge National Laboratory.*—Experiments were designed to study the phenomena of low temperature recovery of the electrical resistance in copper single crystals. Pairs of crystals were simultaneously grown by the Bridgman technique with identical orientation. One sample of each pair was deformed at 300°K and the other at 78°K. The data obtained from four pairs of crystals indicate that: 1. The critical shear stress is independent of temperature. 2. The rate of work hardening is

temperature independent for shear strains less than 0.20. For shear strains greater than this the rate of work hardening for samples deformed at 78°K is about twice that of their corresponding sample at 300°K. 3. No recovery of the electrical resistance (±0.1 percent) was observed for a 16-hour anneal at 300°K when the shear strain was less than 0.20. For shear strains greater than 0.20, however, a recovery occurs whose magnitude depends on the strain in excess of 0.20. 4. There is no apparent recovery of the hardness associated with the recovery of resistance, however, a definite yielding phenomena is observed. It would appear possible that one variety of defect capable of moving at 300°K to form Cottrell atmospheres is formed by sufficiently large deformations

T5. Some Deformation Characteristics of Reactor Irradiated Copper Single Crystals at 78°K and 300°K. R. E. JAMISON AND T. H. BLEWITT, *Oak Ridge National Laboratory.*—Characteristics thus far observed on extension of reactor irradiated pure copper single crystals appear to be strongly dependent on the deformation temperature. Pairs of samples of the same orientation and irradiation were extended, one at room temperature and the other at liquid nitrogen temperature. The critical shear stress is increased at the lower temperature while the initial rate of work-hardening is decreased in such a way that the stress-strain curve after a strain of about 0.20 is similar to the curve for unirradiated copper at 78°K. The room temperature curves are nearly coincident for the larger strains. Cross slip is not as distinct at 78°K, and the slip lines are more closely spaced and in smaller clusters than those formed at room temperature. At 78°K the irradiated crystals will sometimes break in brittle fracture, depending on the initial orientation. The brittle fractures are preceded by a series of audible clicks with accompanying releases of stress and formation of crevices in the crystal surface.

T6. Annealing of Bombardment Damage in Germanium: Theoretical. R. C. FLETCHER, W. L. BROWN, AND S. MACHLUP, *Bell Telephone Laboratories.*—On bombardment of germanium with electrons of more than 650 kev,[1] germanium atoms are displaced to interstitial positions. Part of the defects thus produced will anneal at room temperature, apparently monomolecularly.[1] The remainder can be annealed at higher temperatures, but this part of the annealing requires too great a range of time at a given temperature to be either monomolecular or bimolecular recombination. It is proposed that the complete annealing process can be divided into three stages. First, interstitials displaced only a short distance from their vacancies will recombine monomolecularly because of lattice distortion. Second, interstitials farther away from their vacancies will diffuse, some of them recombining but some escaping from the vicinity of their own vacancies. Third, interstitials which have escaped in the second stage will continue to diffuse and will eventually recombine bimolecularly with other vacancies than their own. Similar considerations apply if vacancies diffuse rather than interstitials. Calculation of the various stages of the annealing, including the appropriate temperature dependence, have been made for an isotropic medium and for a diamond-type lattice. These calculations show an annealing which covers the range of time observed.

[1] E. E. Klontz, Signal Corps Report, Purdue University, June, 1952.

T7. Annealing of Bombardment Damage in Germanium: Experimental. W. L. BROWN AND R. C. FLETCHER, *Bell Telephone Laboratories.*—The previous paper indicates that the annealing of bombardment-introduced defects in germanium above room temperature may be described by a simple diffusion theory. An interstitial atom moves in the crystal by jumping between nearest neighbor sites of the interstitial lattice. The mean jump time τ varies with temperature, T, according to $\tau = \nu_0^{-1} \exp E/kT$, where E is the energy hump between interstitial positions and ν_0 is approximately the lattice vibrational frequency. In the simple diffusion model, the extent of annealing depends only upon the total number of jump times no matter what the temperature. Five n-type samples with an initial room temperature conductivity about 1 mho/cm were given equal bombardments with 3-Mev electrons. Each sample was annealed at 100° temperature intervals for seventy minutes. The five were interlaced to cover the temperature range from 140 to 360°C in 20° intervals. The annealing curves at different temperatures can be made to overlap by adjustment of the time scales. On the resultant curve, the times corresponding to 10 percent and 90 percent of complete annealing are in the ratio of 10^6. From the factors arising in adjustment of the time scales, an activation energy of 1.8 ev is obtained.

T8. Effect of Neutron Irradiation on the Phase Change in Tin.* JEROME FLEEMAN, *Brookhaven National Laboratory.*—The β-phase of tin transforms into the α-phase at transition temperatures below −13°C. The rate of transformation is known to vary as a function of the temperature[1] having a maximum at roughly −30°C. We have initiated a study of the influence of irradiation on the transformation rate of this phase change. Annealed samples of tin 0.25 in.×0.75 in. and 20 mils thick have been exposed at and near liquid nitrogen temperatures in the Brookhaven pile for periods of one and two weeks. After removal from the pile they have been kept at liquid nitrogen temperature until the radioactivity has died down sufficiently to allow visual examination. These specimens have been compared with similar tin samples unirradiated. The latter show no evidence of transformation whereas the irradiated samples show evidence of the characteristic grey tin "pimple" indicating marked influence of the irradiation upon the transformation. Photographs of irradiated and unirradiated specimens will be shown.

* Work performed under the auspices of the U. S. Atomic Energy Commission.

[1] G. Tamman and K. L. Dreyer, Z. anorg. u. allgem. Chem. **199**, 97 (1931).

T9. Electron Mean Free Path of Damaged Copper in Terms of Electrical Resistivity and Thermoelectric Power.* G. W. RODEBACK AND W. P. EATHERLY, *North American Aviation, Inc.*—According to Sommerfeld's theory of metals, thermoelectric power involves the energy derivatives of the electron mean free paths of the two metals. Measurements of the thermoelectric power of an annealed—cold-worked copper thermocouple have been made from 4.2°K to 300°K, together with resistivity measurements over the same temperature range. From these data an attempt was made to determine the type of scattering introduced by the cold work. By Mathieson's rule the reciprocal mean free path of the cold-worked metal is the sum of the reciprocal mean free paths for the crystalline structure and for the cold-work damage. The former mean free path is assumed to vary with the square of the degeneracy energy while the latter is assumed to be independent of energy, representing the effect of isolated scattering centers. This plus the Sommerfeld expressions for resistivity and thermoelectric power result in the determination of the temperature and energy dependence of the mean free paths together with a relation for the energy which is independent of electron density or mass. The observed constancy within 3 percent of the energy (4.3 ev) and the fixed scattering term, from 120°K to 300°K, appears to verify the assumption of isolated scattering centers (for example, vacancies and/or interstitials).

* This report is based on studies conducted for the U. S. Atomic Energy Commission.

T10. Hardness Change in Cu Irradiated with 1.25-Mev Electrons.* C. E. DIXON AND C. J. MEECHAN, *North American Aviation, Inc.*—The primary effects of pile and cyclotron ir-

radiation in metals are[1] (1) the production of interstitials and vacancies and (2) the production of thermal spikes. The indentation hardness increases which have been observed as a result of such irradiations may be a consequence of (1) or (2) or both. It appears that thermal spike effects are negligible when the irradiation consists of 1-Mev electrons since no disordering was observed upon irradiating ordered Cu_3Au.[2] This result suggests the attractive possibility of using electron irradiation to isolate the effects of (1) from (2). A moderate electron bombardment (5×10^{18} electrons/cm^2) of annealed copper was carried out at about -20°C. Tukon hardness measurements made at room temperature showed a change in D.P.H. number from 44.3 to 47.7 kg/mm^2 between the non-irradiated and irradiated portions of the specimen, respectively. About half of this increase annealed out in 8 hours at 170°C. It is believed this indicates that either interstitials or vacancies can contribute to hardness changes.

* This report is based on studies conducted for the U. S. Atomic Energy Commission.
[1] F. Seitz, Phys. Today **5**, 6 (June, 1952).
[2] Dixon, Meechan, and Brinkman (to be published in Phil. Mag.).

T11. Displacement Energy for Radiation Damage in Copper. D. T. Eggen and M. J. Laubenstein, *North American Aviation.*—M. Mills[1] has proposed the measurement of the lattice displacement energy in crystals by electron bombardment. Following this theory, Klontz has measured the displacement energy in Ge to be about 30 ev[2] and Denney has measured that in a Cu-Fe alloy to be about 26.5 for the iron.[3] A target box was constructed so as to be an extension of the acceleration tube of the NAA statitron. Thin Cu specimens were mounted on a heavy copper plate which was immersed in liquid air during the irradiation and measurements. Electrical resistance measurements were made at various times during the irradiation. The rate of change of the resistance of the damaged sample was plotted for electron energies ranging from 0.45 to 1.0 Mev. These slopes were then plotted against the electron energy. The zero damage intercept occurs at an electron energy between 0.45 and 0.50 Mev (0.49 ± 0.02 Mev). This corresponds to a displacement energy in copper of about 25.0 ± 1.0 ev.

[1] M. M. Mills (personal communication).
[2] E. E. Klontz, Ph.D. thesis, Purdue University, June, 1952.
[3] J. Denney, Bull. Am. Phys. Soc. **27**, No. 6, 9 (1952).

T12. Low Temperature Fast Neutron Bombardment of Copper-Beryllium Alloy. J. W. Cleland, D. S. Billington, and J. H. Crawford, Jr., *Oak Ridge National Laboratory.*—Taylor and Murray[1] have investigated the behavior of electrical resistivity and hardness of a solution-quenched copper-beryllium alloy containing 2 percent Be under pile irradiation at ~300°K. They attribute the appreciable increase in hardness and resistivity to the formation of precipitate nuclei made possible by enhanced microdiffusion associated with radiation disordering. Such an enhancement has been demonstrated by Blewitt and Coltman[2] for the in-pile ordering of Cu_3Au. In order to check this proposed mechanism for copper-beryllium, solution-quenched samples have been irradiated consecutively at ~120°K and ~300°K. The increase in resistivity at 120°K for a given exposure in the graphite reactor is smaller by about a factor of four than that observed at 300°K. If a sample, bombarded for some period at ~120°K, is subsequently irradiated for a short period at or somewhat above 300°K, the total change in resistivity is approximately that which would be expected if the total irradiation were carried out at ~300°K. These results indicate that the greater portion of radiation induced resistance increase depends on a process, presumably microdiffusion, which involves thermal activation.

[1] W. E. Taylor and G. T. Murray, Oak Ridge National Laboratory Report No. ORNL 1323 (to be published in Acta Metallurgica).
[2] T. H. Blewitt and R. R. Coltman, Phys. Rev. **85**, 384 (1952).

T13. Nature of Radiation Damage in Diamond.* G. J. Dienes and D. A. Kleinman, *Brookhaven National Laboratory.*—Debye temperature measurements[1] on irradiated silicon indicate strongly that the damage in this crystal cannot be explained by the presence of vacancies and interstitials. A model of radiation damage, applicable to silicon and diamond, has been constructed to explain the above observation and stored energy and lattice parameter changes. The model is based on the known tendency of carbon and silicon to form structures with single and double bonds. Energetic recoil atoms rupture the covalent single bonds which then reform into a system of double and single bonds. Calculations on diamond, which successfully correlate stored energy and lattice expansion with radiation dosage indicate that: (a) each fast neutron collision produces an isolated disordered region, (b) these regions are about 45A in diameter and contain about 10^4 atoms, (c) these regions are mechanically weak due to the rupture of bonds and may be considered as holes in the diamond. The predicted decrease in the elastic constants of diamond is of the same order of magnitude as found experimentally for silicon. In this model 10–100 times more atoms are involved than in the vacancy-interstitial picture.

* Under contract with the U. S. Atomic Energy Commission.
[1] Keesom, Lark-Horovitz, and Pearlman, Science **116**, 630 (1952).

T14. Irradiation Induced Photoconductivity in Magnesium Oxide.* Harold R. Day,† *University of Missouri.*—Photoconductivity in single crystals of magnesium oxide was measured by a dc method. The spectral distribution of photoconductivity is characterized by peaks at 1.2, 2.1, 3.7, and 4.8 ev. Irradiation of the crystals by ultraviolet light causes an enhancement of the photoconductivity subsequently measured in the 1.2- and 2.1-ev bands. The enhancement effect reaches a saturation level which is independent of the intensity of the ultraviolet light and which is a measure of the density of imperfections in the crystal lattice. The ultraviolet activated region can be displaced by an electric field in such a direction as to indicate that the charge carriers are holes in the valence band. Neutron irradiation of the crystals gives rise to a thermally unstable enhancement of photoconductivity throughout the spectrum and also causes an increase in the level of saturation of the ultraviolet activation. The latter increase is stable at room temperature and indicates that the neutron irradiation produces new lattice defects. This effect saturates with increasing neutron flux. The density of lattice defects can be estimated from the photoconductivity. An energy level model is proposed.

* Work supported in part by the U. S. Office of Naval Research and a grant from R. C. A.
† Now at General Electric Research Laboratory, Schenectady, New York.

SATURDAY MORNING AT 11:00

Library, Assembly Room

TA. Business Session of the Southeastern Section

SATURDAY MORNING AT 10:00

Business Administration

(F. SEITZ presiding)

Invited Papers in Solid-State Physics

U1. Studies of the Tensile Strengths and the Adhesion of Metals by Means of High Centrifugal Fields. J. W. BEAMS, *University of Virginia.* (30 min.)

U2. Theoretical and Experimental Studies of Electronic Phenomena in Graphite. W. P. EATHERLY, *North American Aviation.* (40 min.)

U3. The Minimum in Electrical Resistance of Metals at Low Temperatures. E. MENDOZA, *Carnegie Institute of Technology.* (30 min.)

Business Meeting of the Division of Solid-State Physics

SATURDAY AFTERNOON AT 2:00

Business Administration

(J. W. BEAMS presiding)

Invited Papers in Solid-State Physics

V1. Possibilities of X-Ray Small-Angle Scattering for Study of Crystal Imperfections. A. GUINIER, *Universite de Paris.* (30 min.)

V2. Theory of Conduction-Electron Spin Resonance. CHARLES KITTEL, *University of California.* (30 min.)

V3. Thermodynamics of Irreversible Processes. H. B. CALLEN, *University of Pennsylvania.* (35 min.)

V4. The 1952 NRC Conference on the Nature and Properties of Surfaces of Solids. HARVEY BROOKS, *Harvard University.* (25 min.)

SATURDAY AFTERNOON AT 2:00

Bingham Hall

(A. E. RUARK presiding)

X-Rays; Scattering; Theoretical Physics

W1. Determination of an X-Ray Spectrum from Absorption Measurements by Laplace Transformation.* JUDITH CASSIDY GURSKY AND P. K. S. WANG, *Vanderbilt University* — The attentuation of the beam from a 50-kv beryllium-window x-ray tube has been measured in aluminum and carbon. This information is used to determine the spectrum of the beam. The transmitted intensity I_x as a function of the absorber thickness x is given by[1]

$$\frac{I_x}{I_0}=\int_{\lambda_0}^{\infty} e^{-\mu(\lambda)x} f(\lambda)\,d\lambda,$$

where $f(\lambda)$ is the fractional intensity of the primary beam. $\mu(\lambda)$ being given, $f(\lambda)$ may be obtained by a simple change of variable if I_x/I_0 is known. The inverse Laplace transform of $(I_x/I_0)e^{\mu_0 x}$ leads directly to $f(\lambda)$ where μ_0 is the attenuation coefficient of the shortest wavelength λ_0. The practical problem lies in fitting an analytic expression to the experimental curve I_x/I_0 *vs* x. The spectra obtained from different fits and their comparison with the theory[2] will be presented.

* This work was supported, in part, by the U. S. Atomic Energy Commission.

[1] J. A. Greening, Proc. Phys. Soc. (London) **A63**, 1231 (1950).

[2] H. A. Kramers, Phil. Mag. **46**, 836 (1923).

W2. Second-Order Scattering Correction in Neutron and X-Ray Diffraction.* GEORGE H. VINEYARD,† *Brookhaven National Laboratory.*—A calculation has been made to estimate the multiple scattering correction needed in x-ray and neutron diffraction structure determinations. The sample is assumed to be a plane slab and to consist of small elements scattering with random phases. The intensity of n-fold scattered radiation may be expressed in terms of iterated integrals. Second-order scattering has been explicitly evaluated, with the aid of an approximation valid when the single scattering from each element is distributed nearly equally in a number of direc-

tions, as is usually the case with liquids and crystalline powders. Universal curves have been computed for several experimental arrangements. Some features which emerge are: (a) In all cases the ratio of 2nd-order to 1st-order scattering is proportional to the ratio scattering cross section/scattering plus absorption cross sections. For this reason multiple scattering is generally more important with neutrons than with x-rays. (b) In transmission arrangements the 2nd-order scattering is nearly isotropic for all scattering angles appreciably lower than 180°. (c) So long as 2nd-order scattering is small compared to 1st-order, 2nd-order is sufficiently representative of all multiple scattering.

* Under contract with the U. S. Atomic Energy Commission.
† On leave from the University of Missouri.

W3. Spin-Relativistic Effects in the Multiple Scattering of Electrons.* L. V. SPENCER AND C. H. BLANCHARD, *National Bureau of Standards.*—The slowly convergent Legendre polynomial series representing the angular distribution of electrons which have undergone multiple elastic scattering in traveling a given distance in a material has previously[1] been evaluated assuming a Rutherford single-scattering across section with a correction for screening at small angles; and, usually, using a small angle approximation. A new method[2] for summing Legendre polynomials permits evaluation taking account of the spin-relativistic corrections[3] to the Rutherford cross section and without small angle approximation. The results show that the spin-relativistic correction greatly improves the agreement of the theory (particularly at larger angles) with the experiment of Hanson *et al.*[4] for a thin gold foil at 15.7 Mev. The various effects other than elastic scattering (especially inelastic scattering and energy loss), and also the error involved in identifying foil thickness with pathlength will be discussed.

* Supported by the U. S. Office of Naval Research and the U. S. Atomic Energy Commission.
[1] Moliere, Z. Naturforsch. **3A**, 78 (1948). Snyder and Scott, Phys. Rev. **76**, 220 (1949).
[2] Spencer, Phys. Rev. (to be published).
[3] Feshbach, Phys. Rev. **88**, 295 (1952).
[4] Phys. Rev. **84**, 634 (1951).

W4. Energy Spectrum Resulting From Electron Slowing-Down.* U. FANO AND L. V. SPENCER, *National Bureau of Standards.*—Given a uniformly distributed source of electrons of energy E_0, we wish to calculate the flux $y(E_0, E)dE$ of electrons of energy E traversing a small unit spherical probe. The distribution of energy losses ϵ is very skew, with an ϵ^{-2} tail further extended by bremsstrahlung. This precludes a continuous-slowing-down model (according to which y is the reciprocal stopping power) as well as the direct integration which works for x-rays.[1] An analytical Landau-type treatment, valid at all E_0, yields

$$y(E_0, E) = (mv^2/2\pi NZe^4)\int_0^\infty du \exp(-u)\tan^{-1} \times \{\pi/\log[1.5262(E_0-E)/Q_{\min}u]\},$$

where the symbols have their standard meaning and $Q_{\min}$ is the effective minimum permissible recoil energy. The integral is essentially an average reciprocal stopping number with slowly varying value$\sim$0.1. The analytical treatment breaks down as E decreases, when departures from the assumptions of a constant $Q_{\min}$ and of an ϵ^{-2} tail can no longer be disregarded. Here one can switch to a numerical procedure, akin to that for x-rays, which takes into account analytically the singularity of the cross section for $\epsilon\sim 0$.

* Supported by the U. S. Office of Naval Research and the U. S. Atomic Energy Commission.
[1] P. R. Karr and J. C. Lamkin, Phys. Rev. **76**, 1843 (1949).

W5. Methods for Calculating Approximate Cross Sections for Electron-Scattering. WILLIAM J. BYATT, *University of Alabama* (introduced by Arthur E. Ruark).—In computing differential cross sections for electron scattering, either by the Born approximation or the much-improved method of Montroll, Hart, and Greenberg, it is very helpful to start with a simple closed formula for the potential of the scattering atom. The scattering of electrons by He, Ne, A, and Hg is discussed. The Hartree fields of these elements are represented analytically; and the differential cross section is considered for electron energies from 100 ev to 1 Mev. Extension of the method to intermediate atomic numbers is simple in principle, but actual application in this domain must await computation of a few Hartree potentials in the region Z equals 30 to 70.

W6. Nyquist and Einstein Relations Derived from a Scattering Model. STEFAN MACHLUP, *Bell Telephone Laboratories.*—The Nyquist relation between electrical conductivity and thermal (Johnson) noise spectral density, and the Einstein (-Nernst-Townsend) relation between mobility and diffusion coefficient are classically derived by thermodynamic reasoning (equipartition). Therefore any microscopic model of a conductor which permits calculation of these quantities must also lead to the proper relations between them. It was thought that verifying the relations for a particular model (scattering of electrons in a crystal) may help in gaining insight into the model. The model must, of course, be statistical: scattering (e.g., by lattice vibrations, impurities) is a random process. If interactions between electrons are neglected, a model is completely determined by specification of both (1) electron distribution function f and (2) transition proabilities. From the latter one obtains a relaxation time τ for each electron state. One finds that the electron mobility, the thermal noise spectrum, and the electron diffusion coefficient are all proportional to the same functional of f and τ, making their ratios obey the classical relations.

W7. Energy Exchange in Molecular Collisions. B. WIDOM* AND S. H. BAUER, *Cornell University.*—It is shown that the semiclassical theory[1] of inelastic molecular collisions is an adequate approximation to the quantum-mechanical theory[2] when the relative translational energy of the colliding molecules is much greater than the change in internal energy. The semiclassical theory, however, fails in the neighborhood of the threshold. The average cross section for de-excitation collisions between carbon-dioxide and water is known[3] to have a maximum at about 350°K; its falling at higher temperatures has hitherto been considered an anomaly. When applied to this system, the semiclassical theory yields an effective collision diameter which is indeed a monotonically decreasing function of the temperature, this behavior being a direct consequence of the mutual reactivity of these molecules. When corrected for the low energy failure of the theory, the calculated collision diameter must also fall at low temperatures. The results are then in qualitative accord with the experimental facts over the whole temperature range.

* Now at University of North Carolina.
[1] C. Zener, Phys. Rev. **38**, 277 (1931).
[2] C. Zener, Phys. Rev. **37**, 556 (1931).
[3] A. Eucken and L. Küchler, Physiks Z. **39**, 831 (1938).

W8. On the Energy-Momentum Tensor of the Electromagnetic Field Inside Matter. N. L. BALAZS, *Dublin Institute for Advanced Studies** (introduced by Eric Rodgers).—Two different energy-momentum tensors have been proposed to describe the electromagnetic field inside matter. Abraham suggested a symmetric tensor while Minkowski's tensor is nonsymmetric. With the aid of a thought-experiment it is shown here that only the symmetric tensor satisfies the momentum conservation and center-of-mass theorems simultaneously.

* Now at University of Alabama.

W9. Nuclear Shell Structure as a Many-Body Phenomenon.* INGRAM BLOCH AND YÜ-CHANG HSIEH, *Vanderbilt University.*—A nuclear Hamiltonian containing pairwise

Hooke's law interactions between the nucleons[1] provides a first approximation to many-body nuclear theory. The normal-mode oscillators obey a more restrictive exclusion principle than that which applies to individual nucleons. The ground-state energy of one set of oscillators depends on the number of neutrons present, while that of another set depends on the number of protons present. The magic numbers have not emerged from the simple Hamiltonian described, but may be derivable from a refined Hamiltonian.

* Assisted by the U. S. Army Office of Ordnance Research and by the Carnegie Foundation for the Advancement of Teaching.

[1] W. V. Houston, Phys. Rev. **47**, 942 (1935); **49**, 206 (1936). For other references, see H. Margenau and K. G. Carroll, Phys. Rev. **54**, 705 (1938).

W10. Magic Numbers and the Statistical Model of the Nucleus.* H. W. NEWSON, *Duke University*, AND E. MERZBACHER, *University of North Carolina*.—While the Fermi gas model of the nucleus is well known to predict the general features of energy level densities in fairly excited nuclei, particularly their dependence on excitation energy and particle number, it fails, of course, to describe such details as the observed increase in the average level spacing in compound nuclei near neutron magic numbers. In an attempt to incorporate some effects of shell structure into the scheme of individual particle energy levels, which the nucleons of the gas can occupy, a "semiconductor" model for the nucleus was considered. The following sequence of individual particle energy levels was assumed: A low-lying n-fold degenerate level, separated by an adjustable gap from the set of energy levels of a free particle confined to the nuclear volume, where, however, the levels immediately above the gap are as dense as those near the Fermi energy in the conventional model. Calculations for low temperatures were made, and the entropy *versus* excitation energy was plotted for various sizes of the gap. Several ways of correlating the variables in the model with characteristic nuclear quantities will be discussed in the light of the empirical evidence about level spacings.

* Under contract with the U. S. Atomic Energy Commission.

W11. On the Statistical Theory of Nuclear Reactions. BERNARD L. COHEN, *Oak Ridge National Laboratory*.—If Weisskopf's expression for the energy distribution, $N(E)$, of particles emitted from nuclear reactions which proceed via a compound nucleus is generalized by dropping his assumption that the sticking probability, η, for the inverse reaction is independent of energy, one obtains $1/\Sigma(E, E_0) = -\partial \log\eta/\partial E + 1/T(E_0-E)$ where $\Sigma = \{-\partial/\partial E(\log N(E)/E)\}^{-1}$, the slope of the energy spectrum as usually plotted. The following evidence is cited to show that the $-\partial \log\eta/\partial E$ term (hereafter (A)) is not negligible: (a) all observed neutron and proton ($E \gg$ Coulomb barrier) energy spectra curve away from the axis whereas assuming (A) $=0$ demands curvature toward the axis; (b) comparing these observed spectra shows that Σ is definitely not a function of (E_0-E) alone; (c) the values of (A) required to remove the large discrepancies between observed and calculated (n, p) and (n, α) cross sections are roughly consistent with those obtained from the experimental energy spectra. Assuming (A) not ignorable means that selection rules operate to make transitions to low-lying levels excessively probable. It also demands that if excited nuclei could be bombarded, sticking probabilities would not be unity as they are when ground-state nuclei are bombarded.

W12. The Energy-Momentum Tensor in General Stream Electrodynamics. M. AVRAMY MELVIN, *Florida State University*.—Unnecessary use of the canonical formalism may hinder insight into the structure of a theory. This is exhibited in recent discussions of the energy-momentum tensor in the "new classical electrodynamics," where the final symmetrized tensor turns out to be the same for both the first and second theories of Dirac. It is also the same for the more general stream theory discussed by the author. The simple reason for this sameness is that the form of the energy-momentum tensor does not depend at all upon the gauge conditions which characterize the different theories; this tensor is a consequence only of applying to a fine-grained stream of corpuscles of mass μ, charge ϵ, *specific* concentration N (i.e., number of corpuscles contained *in a unit comoving volume*), and continuous differentiable 4-velocity field $u^\alpha = dy^\alpha/ds$ (1) the Lorentz force law (L) for the individual corpuscles, and (2) the Maxwell equations: (M_1) expressing the vanishing of the cyclical divergence $\{A_{\alpha\beta,\gamma}+\text{cycl.}\}$ of the electromagnetic field $A_{\alpha\beta}$, and (M_2) equating the divergence $A^{\alpha\beta}{}_{,\beta}$ to the current density $N\epsilon u^\alpha$. The law of conservation of specific charge is as usual an identical consequence of (M_2). Assuming also $d\epsilon/ds=0$, we have also (M_2') the vanishing of $(Nu^\alpha)_{,\alpha}$. The total specific force density is obtained upon multiplying (L) by N. Integrating this by parts and using (M_2') gives: $(N\mu u_\alpha u^\beta)_{,\beta} = (A_{\alpha\beta}A^{\beta\gamma})_{,\gamma} - A^{\beta\gamma}A_{\alpha\beta,\gamma}$.

SATURDAY AFTERNOON AT 2:00

Venable Hall

(E. K. PLYLER presiding)

Ultraviolet Spectra; Theory of Molecular Structure; Mass Spectroscopy

X1. The Near Ultraviolet Absorption Spectrum of *p*-Difluorobenzene Vapor. C. DEWEY COOPER, *University of Georgia*.—The vapor absorption spectrum of *p*-difluorobenzene has been investigated in the 2900–2400A region with a Bausch and Lomb Littrow quartz spectrograph. Most of the bands are double with a separation of only 3 or 4 cm^{-1}. The 0,0 band is located at 36 843 cm^{-1}. Prominent bands on the violet side of this band are found to involve the excited state frequencies of 163, 409, 819, and 1250 cm^{-1}. Both the 819 and 1250 frequencies are found in progressions. Weak, temperature dependent bands on the red side of the 0,0 band are found to involve the ground-state frequencies of 247, 452, 860, and 1260 cm^{-1}. In the *p*-difluorobenzene spectrum the 0,0 band is shifted 1246 cm^{-1} toward the red relative to the calculated 0,0 band of benzene. This shift will be compared with similar shifts for other mono- and di-substituted benzenes.

X2. A Correlation of the Infrared and Ultraviolet Spectra of Associated Alcohols.* GLADYS A. ANSLOW AND IRENE S. WHITE, *Smith College*.—To aid the interpretation of the ultraviolet absorption in alcohols, ascribed to $OH^+\cdots O$ and $OH\cdots O$ association,[1] freshly distilled specimens, showing no impurities in the infrared, have been investigated in the 3μ region with a Perkin-Elmer double-beam spectrometer and in the ultraviolet with a Beckman spectrophotometer; recording spectra at numerous concentrations in carbon tetrachloride and isooctane, respectively. Changes in the ratio of polymer to dimer components in the infrared were paralleled by corre-

sponding changes in the ultraviolet. Values of the monomer fraction α measured in the infrared permit the calculation of the degree of association f and the polymer length, also a correlation with the concentration c.[3] Specimens which indicate $OH^+\cdots O$ association in the uv obey the $F(\alpha, f, c)$ equations for polymers, and those indicating $OH\cdots O$ association indicate dimer association. Specimens which appear to be mixtures show similar spectral irregularities at concentrations at which monomerization proceeds rapidly.

* Supported by the U. S. Office of Naval Research and by the Research Corporation.
[1] Gladys A. Anslow *et al.*, Faraday Soc. Disc. No. 9, 299 (1950); Phys. Rev. **88**, 154 (1952).
[3] R. Me ke, Faraday Soc. Disc. No. 9, 161 (1950).

X3. The Near Ultraviolet Vapor Spectrum of Thianaphthene. R. C. HECKMAN* AND H. SPONER, *Duke University.*—The near ultraviolet vapor spectrum of thianaphthene has been photographed using the large and medium Hilger quartz spectrographs. The spectrum arises from two, possibly three electronic transitions. The 0,0 bands for these transitions have been assigned the frequencies 34 060 cm^{-1} (2935.2A), 38 300 cm^{-1} (2610A) [or possibly 38 240 cm^{-1} (2614A)] and tentatively 43 070 cm^{-1} (2320A). The first system exhibits sharp vibrational bands while bands in the other systems are diffuse. Correlations of vibrational differences with Raman lines have been established, particularly in the sharp system. A comparison has been made of the observed spectrum with the electronic band systems of naphthalene in the near ultraviolet.

* Charles F. Kettering Foundation Fellow.

X4. Electronic Energy Levels of Molecular Oxygen.* ALVIN MECKLER,† *M.I.T.*—A configuration interaction study of the lower-lying electronic energy levels of molecular oxygen has been made. With the 1*s* and 2*s* shells kept filled, the remaining eight electrons were distributed among the twelve spin-orbitals arising from the 2*p* levels on each atom. The molecular orbitals were formed as symmetrical linear combinations of the atomic orbitals, simply for convenience. Inclusion of all configurations implies complete equivalence of all possible constructions of linear combinations. Out of the 495 many-electron determinants a group of nine states of $^3\Sigma_g^-$ character was set up and twelve of $^1\Sigma_g^+$ character. The interaction matrix of each block was computed and diagonalized (by electronic computer) yielding excellent results for the triplet ground state, not as accurate ones for the lowest singlet. The energies and wave functions for the lowest triplet and singlet were calculated and compared for various values of internuclear separation. The history of the molecule is therefore correctly traced from infinite separation inward, revealing the competition between the magnetic and nonmagnetic states and the deviation from the single configuration approximation.

* Supported by the U. S. Office of Naval Research.
† Now a staff member of Lincoln Laboratory, M.I.T.

X5. A Molecular Orbital Treatment of the Contribution of the π-electrons to the Electric Dipole Moments of Some Phenyl Halides.* R. H. KNIPE, *Duke University* (introduced by H. Sponer).—The contribution of the π-electrons to the electric dipole moments of some mono- and di-halogenated benzenes has been treated by the molecular orbital method without overlap. The influence of the additional π-orbital brought into the system upon substitution of the halogen is studied by introducing semi-empirical parameters. Using the known bond lengths, the approximate additivity rule has been verified numerically for a range of values of the halogen Coulomb integral.

* Supported by the U. S. Office of Naval Research.

X6. Application of the Thomas-Fermi Method to the Calculation of Certain Molecular Vibration Frequencies. W. A. BOWERS, *University of North Carolina.*—An attempt has been made to use the Thomas-Fermi method to calculate the frequency of the "breathing" vibrations of tetrahedral and octahedral molecules. This is done by an extension of the calculations of March,[1] who regarded the nuclei of the outer atoms as smeared out over a spherical surface and applied the Thomas-Fermi method to the resulting spherically symmetric problem. The energy can then be calculated, and has a minimum as a function of sphere radius; hence bond length and vibration frequency, or force constant, can be found. The force constants found in this way have been compared with the experimental data for a number of tetra-halide molecules; the agreement is poor, as March found in the case of bond lengths, if the actual nuclear charges are used. However, by assigning effective nuclear charges to the atoms, corresponding to compression of the inner shells into the nucleus, a reasonable correlation with the data can be obtained.

[1] N. H. March, Proc. Cambridge Phil. Soc. **48**, 665 (1952).

X7. Determination of Molecular Weight of Organic Compounds by Mass Spectrometry. JOHN R. SITES AND BERNARD L. STREHLER, *Oak Ridge National Laboratory.*—An investigation is being undertaken to determine the molecular weights of some organic compounds essential to luminescence in the firefly lantern extract. Data will be presented which were obtained during preliminary observations on riboflavin, luciferesceine, and luciferin. The molecular weights of these compounds are less than 400.

X8. Mass Spectrometer Analysis of UO_2F_2 in UF_4. RUSSELL BALDOCK, JOHN R. SITES, L. O. GILPATRICK, AND HOWARD E. CARR,* *Oak Ridge National Laboratory.*—A time integration method has been developed for the quantitative analysis of UO_2F_2 contamination in UF_4. Data are collected from a sample held at constant temperature in the mass spectrometer until the sample is completely used up.

* Consultant, Alabama Polytechnic Institute.

SATURDAY AFTERNOON AT 2:00

Howell Hall

(W. C. DUNLAP, JR., presiding)

Semiconductors, III

Y1. The Electrical Resistance of Graphite at Low Temperatures.* H. W. HEMSTREET AND J. M. REYNOLDS, *Louisiana State University.*—Measurements, previously reported,[1] on the resistance of polycrystalline graphite, have been repeated with greater precision to allow extrapolation of the resistance to absolute zero temperature. These measurements were made on two samples over a range of temperature from room temperature down to 1.35°K. The resistance was found to increase smoothly as the temperature was lowered to about 20°K. At this temperature the resistance begins to level off

until at 4°K it is virtually temperature independent at a value about double the room temperature resistance. Below 4°K the resistance seems to fall slightly. From 3.5°K to 1.35°K the drop is about 0.1 percent where the probable error of each point is 0.025 percent.

* Supported by the National Science Foundation.
[1] H. W. Hemstreet and J. M. Reynolds, Phys. Rev. **87**, 178 (1952).

Y2. Thermoelectric Power of Carbons.* E. E. LOEBNER, *University of Buffalo.*—The thermoelectric power of various soft carbons has been previously investigated by the author at room temperature as a function of the heat-treatment temperature H. In this work measurements were performed with an improved technique at three temperatures T (a) 88°K, (b) 308°K, and (c) 573°K. A single batch of carbon rods was used, rods being heat-treated to progressively higher temperatures and investigated after each heat-treatment. The thermoelectric power and electric resistivity of these rods were determined at the three temperatures and plotted as a function of H. Each of the three curves for the thermoelectric power exhibits a shallow minimum (around 1300°C of H) and a maximum. The position of the maximum varies with the temperature of the sample: (a) 2180°C, (b) 2080°C, (c) 1990°C of H. The total variation of change in the power from the minimum to maximum is roughly proportional to the absolute temperature T, thus indicating a metallic behavior of an unfilled energy band for carbons in the baked range ($1000°C < H < 2000°C$). All three resistivity curves show the well-known plateau:[1] the extent of the plateau varies with T, becoming shorter for higher T's, this being caused by a variation in the position of the high H end of the plateau.

* Supported in part by the U. S. Office of Naval Research.
[1] S. Mrozowski, Phys. Rev. **85**, 609 (1952) and **86**, 1056 (1952).

Y3. Electrical Properties of Indium Antimonide, InSb.* R. G. BRECKENRIDGE, W. R. HOSLER, AND W. OSHINSKY, *National Bureau of Standards.*—Measurements have been made of the electrical resistivity and Hall coefficient of indium antimonide, InSb, for a temperature range from liquid air to 200°C. This compound, whose physical properties strongly resemble germanium, has been prepared by the vacuum melting of high purity indium and antimony. The material was found to be a semiconductor with a low resistivity of the order of $10^{-2}\Omega$ cm at room temperature, a low activation energy for intrinsic conduction, *ca* 0.4 ev; and a high mobility of charge carriers, ca. 2.1×10^4 cm²/volt sec, for electrons at room temperature. It has been possible to prepare both n- and p-type samples by control of the composition of the melt. An analysis has been made of the temperature variation of the charge carrier densities and mobilities obtained from the resistivity and Hall coefficient data for both p and n type samples.

* This work was supported by the U. S. Office of Ordnance Research.

Y4. Thermally Unstable Disorder in p-type Ge Produced by Fast Neutron Bombardment. J. H. CRAWFORD, JR., J. W. CLELAND, D. K. HOLMES, AND J. C. PIGG, *Oak Ridge National Laboratory.*—A number of P type Ge samples have been irradiated at a variety of temperatures in the low temperature facility in the graphite reactor. The conductivity of P type Ge decreases with bombardment over the low temperature range investigated (−90°C to −160°C) at an initial rate which is about one-half that of N type material over the same temperature range. Warming the samples to room temperature and recooling indicates that a major portion of the disorder introduced below −90°C either anneals out or rearranges to a form which radically modifies the nature of the electronic energy levels associated with the disorder. Warm-up experiments also show that there are at least two types of thermally unstable disorder produced energy levels. Material bombarded below −140°C shows an additional decrease in conductivity on warm-up until the temperature rises to about −120°C, after which continued warming causes an increase in conductivity. Material irradiated above −140°C shows only a conductivity increase on warming. The disorder introduced above −140°C appears to anneal out or rearrange by a first-order process.

Y5. The Surface Tension of Liquid Silicon and Germanium. PAUL H. KECK AND WENDELL VAN HORN, *Signal Corps Engineering Laboratory.*—The surface tensions of liquid silicon and germanium were determined using the drop weight method. It was found to be 600 dynes/cm for germanium and 720 dynes/cm for silicon at their freezing points. The parachors of the group IVb elements as derived from surface tension measurements of the molten elements are compared with the atomic parachors calculated from compounds. The differences are interpreted as structural parachors which indicate that the bonding between neighboring atoms in the liquid state increase in nearly uniform steps from lead to germanium. Molten germanium and silicon have nearly the same structural parachor indicating similar structures which probably consist of tetrahedral groups of atoms.

Y6. Electrical Properties of Carbon Bisulfate Compounds. E. A. KMETKO, *University of Buffalo.*—The conductivity of graphite is known to be increased when bisulfate ions are introduced between the aromatic layers, this being due to formation of holes in the normally full π-band of graphite.[1] Results of an investigation of similar compounds using substances ranging from baked carbons to polycrystalline graphite will be reported. Baked carbons exhibit little change in conductivity and thermoelectric effect when bisulfate ions are introduced. Changes are increasingly larger for carbons heat-treated to higher temperature. For instance, the initial rate of change of resistance with ion concentration is for polycrystalline graphite (3000°C) 6 times greater than for a carbon baked to 1400°C. Baked carbons possess many traps on the crystallite boundaries (free carbon valencies)[2] which create large numbers of excess holes in the π-band of the pure material. Thus addition of a small number of extra holes by the formation of the compound changes only slightly the electronic properties of the substance. The number of traps is so large in baked carbons that the Fermi level is depressed below the inflection curve and the Hall coefficient is negative for these materials.

[1] G. R. Hennig, J. Chem. Phys. **19**, 922 (1951).
[2] S. Mrozowski, Phys. Rev. **85**, 609 (1952) and **86**, 1056 (1952).

Y7. Electrical Properties of the Compound Aluminum Antimony. R. K. WILLARDSON, A. C. BEER, AND A. E. MIDDLETON, *Battelle Memorial Institute.*—Preliminary investigations of the electrical properties of aluminum antimony indicate electrical characteristics somewhat similar to those reported for silicon with impurity additions. High purity aluminum and specially refined antimony* were reacted in approximately stoichiometric proportions to form the compound AlSb. The material was then processed to obtain specimens containing active impurities varying from approximately 0.5 percent to less than one part in ten million. Measurements were made of electrical resistivity, thermoelectric power, and Hall voltage over the temperature range from 90°K to 1200°K. Extrinsic conductivity of both n- and p-types was observed. The intrinsic conductivity indicated an energy band separation somewhat greater than that of silicon. The mobilities of the positive holes in the polycrystalline specimens of lower carrier density are given by $5\times10^5T^{-1}$ cm²/volt-second at the

higher temperatures where lattice scattering predominates. The effect of scattering by ionized impurities became significant at lower temperatures, the maximum of the mobility *versus* temperature curve occurring below room temperature.

* Supplied by Bradley Mining Company, San Francisco, California.

Y8. The Magnetoresistance Effect in InSb. M. TANENBAUM AND G. L. PEARSON, *Bell Telephone Laboratories.*—H. Welker[1] has shown that the compound indium antimonide is a semiconducting material having properties akin to the fourth column elements germanium and silicon and that it has unusually high electron and hole mobilities. The preparation of this compound in a highly purified form through the use of zone-melting techniques[2] will be described. Polycrystalline specimens of 0.03 ohm cm resistivity are obtained. These are *n*-type at room temperature and change to *p*-type near 175°K. Magnetoresistance measurements with H perpendicular to I give $\Delta\rho/\rho = 8\times10^{-9}H^2$ which corresponds to an electron mobility of 15 000 cm²/volt-sec. Welker has reported Hall mobilities as high as 25 000 cm²/volt-sec. The magnetoresistance effect approaches zero for H parallel to I thus indicating spherical energy surfaces. This is in contrast to measurements in *n*-type germanium where a nonspherical shape of the energy surface has been proposed[3] to explain the results.

[1] H. Welker, Z. Naturforsch. **7a**, 744 (1952).
[2] W. G. Pfann, J. Metals **4**, 747 (1952).
[3] W. Shockely, Phys. Rev. **78**, 173 (1950); Phys. Rev. **79**, 191 (1950).

Y9. Hall Mobility in Insulation Photoconductors.* ALFRED G. REDFIELD,† *University of Illinois.*—A technique has been developed for measurement of the electronic Hall mobility in insulating photoconductors which avoids difficulties caused by space charge effects and crystal nonuniformities. The crystal is illuminated by short bursts of light so that negligible space charge is built up during the time of illumination. The Hall electrodes are of unconventional design. Preliminary results on several diamonds between 100 and 300°K fail to give a unique value of the mobility, possibly because of variation in impurity content from diamond to diamond. The room temperature electronic Hall mobility in diamond is evidently in qualitative agreement with previous[1] Hall mobility measurements and much lower than the value of drift mobility obtained by Pearlstein and Sutton.[2]

* Partially supported by the U. S. Office of Naval Research.
† U. S. Atomic Energy Commission predoctoral fellow.
[1] C. C. Klick and R. J. Maurer, Phys. Rev. **81**, 124 (1951).
[2] E. A. Pearlstein and R. B. Sutton, Phys. Rev. **79**, 907 (1950).

Y10. Preparation of Gray Tin Filaments. A. W. EWALD, *Northwestern University.*—Filaments of gray tin suitable for direct electrical measurements have been prepared, and the specific conductivity and the temperature dependence of the conductivity have been determined. The method of preparation consists in drawing fine wires of pure metallic tin in an inert atmosphere by the Taylor process.[1] After dissolving away the glass envelopes, the filaments are inoculated with gray tin powder and stored at a reduced temperature to allow the transformation to proceed. Interrupting the transformation when short segments of the gray modification have been produced facilitates making electrical contact through the adjoining metallic portions. Electrical conductivity measurements on five samples ranging in diameter from 50 to 200 microns and in length from 1 to 3 mm have yielded the values: $(2.25\pm0.05)\times10^3\Omega^{-1}$ cm^{-1} for the conductivity at 0°C and (0.088 ± 0.002) ev for the activation energy determining the temperature dependence in the intrinsic range. These results are in satisfactory agreement with those of Busch, Wieland and Zoller[2] obtained by eddy current loss measurements on gray tin powder

[1] G. F. Taylor, Phys. Rev. **23**, 655 (1924).
[2] Busch, Wieland, and Zoller, Helv. Phys. Acta **24** (No. 1), 49 (1951).

SATURDAY AFTERNOON AT 2:00

Phillips Hall

(ERIC RODGERS presiding)

Solid-State Physics, Including Diffusion

(Papers Z1 to Z8 grouped together by request)

Z1. X-Ray Study of Graphitization. J. C. BOWMAN, *National Carbon Company* AND S. HAYES AND R. SMOLUCHOWSKI, *Carnegie Institute of Technology.*—The so-called carbons are highly imperfect structures which on annealing can be gradually transformed into graphites of various degrees of perfection. This process of graphitization in carbons, heated for very short time in the range between 1600 and 2000°C, has been studied by means of high resolution small angle x-ray scattering and by means of x-ray diffraction. In the range of angles between 10 and 30 minutes the small angle scattering indicates a total increase of about 40 percent in the number of particles in the range between 100 and 200A. This growth is accompanied by a substantial decrease of the number of small particles which scatter at higher angles. Diffraction patterns indicate a parallel increase in the average particle size in the *c*-direction from about 90A to 240A. A proposed mechanism of growth will be discussed.

Z2. Small Angle-X-Ray Scattering in Proton-Irradiated Diamond.* S. HAYES AND R. SMOLUCHOWSKI, *Carnegie Institute of Technology.*—Study of irradiation effects is particularly convenient in diamond because the high stability of the lattice minimizes annealing of the effects at room temperature. Natural uncut diamonds in form of thin plates, obtained through courtesy of the Koebel Diamond Tool Company, were irradiated by 360-Mev protons in the Carnegie Institute of Technology synchrocyclotron and the small angle x-ray scattering on irradiated and unirradiated crystals was compared by means of a high resolution instrument. Preliminary results indicate an appreciable increase of scattering in the range of angles between 10 and 30 minutes. No appreciable coloring was observed.

* Supported by a U. S. Atomic Energy Commission contract.

Z3. Changes in Conductivity of NaCl Produced by Bombardment with 360-Mev Protons.* E. A. PEARLSTEIN, *Carnegie Institute of Technology.*—Single crystals of NaCl, previously annealed in He at 650°C, have been irradiated with 360-Mev protons in the Carnegie Institute of Technology super synchrocyclotron. Amounts of bombardment were of the order of 10^{15}/cm². Large decreases in electrical conductivity were found, in agreement with the work of Nelson, Sproull,

and Caswell[1] on KCl. Much of this decrease annealed out at about 200°C in one hour. More annealing took place between 250°C and 300°C. No further annealing was observed up to about 470°C. After this annealing the conductivity measured between 100°C and 200°C was the same within 10 percent as in unirradiated crystals. The conductivity at higher temperatures could not be restored by annealing at temperatures up to about 470°C. Data will be presented on the magnitudes of conductivity and of irradiation. Calculations based on Seitz's work[2] indicate that each 360-Mev proton produces only about 3 sodium vacancies per cm of trajectory. This would lead one to believe that this flux of protons changes the conductivity mainly by producing ionization, except for the fact that the change does not completely anneal with regard to the temperature dependence of the conductivity.

* Supported by a U. S. Atomic Energy Commission contract.
[1] Nelson, Sproull, and Caswell, Bull. Am. Phys. Soc. **28**, No. 1 (1953).
[2] F. Seitz, Disc. Faraday Soc. No. 5, 271 (1949).

Z4. Density Change in Proton Irradiated Potassium Chloride.* W. J. LEIVO, *Carnegie Institute of Technology.*—Single crystals of potassium chloride were irradiated with about 10^{15} per cm² 360-Mev protons in the Carnegie Institute of Technology synchrocyclotron. The irradiation was fairly uniform as evidenced by color centers which were produced throughout the interior of the crystal. The change in density of the crystals upon irradiation was measured and it was found that the crystals decreased in density. This change in density was determined by observing the difference in suspension temperatures of the crystals when suspended in 1,3-dibromo-propane. To prevent burning of the crystals and contamination of the surface during irradiation, the crystals were enclosed in a thin-walled aluminum container which was filled with helium. An exposure of one hour in the proton beam produced a decrease in density of 5×10^{-6} g/cm³ which is large compared to theoretical expectations.

* Supported by a U. S. Atomic Energy Commission contract.

Z5. Mechanical Properties of Proton Irradiated Alkali Halides.* W. H. VAUGHAN, W. J. LEIVO, AND R. SMOLUCHOWSKI, *Carnegie Institute of Technology.*—The elastic and plastic behavior of single crystals of potassium chloride which were subjected to proton bombardment in the Carnegie Institute of Technology 360-Mev synchrocyclotron was determined by bending. The crystals were loaded at their midpoint while being freely supported at their ends and the maximum deflection as a function of the load was measured giving the Young's modulus and the elastic limit. Crystals which were irradiated for one hour in the cyclotron were compared with unirradiated crystals having the same dimensions. Preliminary results indicate an increase of Young's modulus. Hardness of irradiated and of unirradiated single crystals of KCl and of NaCl was measured by a Tukon tester which made indentations about 10^{-2} mm deep. Irradiation increased the hardness of the surface of the crystals (for NaCl from 16.3 to 36 while) the hardness of the inside of the crystals as measured on cleaved irradiated samples. Surface hardness increased with increasing beam intensity.

* Supported by a U. S. Atomic Energy Commission contract.

Z6. On Change of Metallic Conductivity Through Change in Thermal Scattering.* R. SMOLUCHOWSKI, *Carnegie Institute of Technology.*—In many changes of electrical conductivity observed in metals, the effect can be interpreted in terms of changed periodicity of the lattice or as a result of introduction of imperfections. The first occurs, for instance, in ordering phenomena, the latter in irradiation by nucleons. However, both these changes may be accompanied by a change in the vibration spectrum of the lattice and thus by a change in the thermal scattering of the conduction electrons. A rough estimate of these changes in ordering and in irradiation effects is given and the results compared with experimental data.

* Supported by a U. S. Atomic Energy Commission contract.

Z7. Anisotropy of Grain Boundary Diffusion.* L. COULING AND R. SMOLUCHOWSKI, *Carnegie Institute of Technology.*—As a result of a study of diffusion of silver and of zinc in grain boundaries of copper, a definite structure of these boundaries has been proposed.[1] In particular in grain boundaries between grains having one cubic direction in common and the angle θ between the other cubic directions varying from about 15 to 35 degrees the diffusion would occur along "rods" of distorted lattice caused by clustering of dislocations (or high concentration of vacancies). This would lead to an anisotropy of diffusion in various directions in the boundary. Diffusion in directions forming an angle $\varphi=0$, 45, and 90° with the common cubic direction has been measured using radioactive silver and an autoradiographic technique on bi-crystals of copper. Early indications of anisotropy of diffusion have been confirmed for the above-mentioned range of θ while for θ near 45° little or no anisotropy has been found in accord with the model of a uniform and isotropic grain boundary.

* Supported by a U. S. Atomic Energy Commission contract.
[1] R. Smoluchowski, Phys. Rev. **87**, 482 (1952).

Z8. Grain Boundary Self-Diffusion in Body-Centered Lattice.* C. W. HAYNES AND R. SMOLUCHOWSKI, *Carnegie Institute of Technology.*—Pronounced grain boundary diffusion was previously observed in face-centered cubic lattices in which the difference between the close-packed inside of the grain and the distorted grain boundary material is presumably large. In body-centered lattices, this difference would be expected to be much smaller. Bi-crystals were grown by means of the strain-anneal technique in iron containing about 3 percent silicon (to promote growth of large crystals). The relative orientation of the crystals was predetermined by Dunn's "seed" method.[1] The crystals had a common [110] direction and an angle $5°\leqslant\theta\leqslant86°$ between the axes in the (110) plane. The specimens were plated on one side with Fe^{55} to about 5×10^{5} cpm, diffused at various temperatures between 804°C and 827°C, and the depth of penetration of the radioactive isotope determined by autoradiography and by counting. The results indicate absence of measurable grain boundary diffusion at angles up to about $\theta=20$ degrees and an increasing boundary penetration up to $\theta=85$ degrees. There appears to be a cusp in the neighborhood of $\theta=45°$.

* Supported by a U. S. Atomic Energy Commission contract.
[1] C. G. Dunn, J. Metals **1**, 72 (1949).

Z9. Diffusion of Antimony in Silver.* E. SONDER, L. SLIFKIN, AND D. LAZARUS, *University of Illinois.*—As part of a general program of investigating diffusion of various neighboring elements into silver, diffusion coefficients for antimony into single crystals of 99.99 percent pure silver have been measured over a temperature range of 500 to 940°C using Sb^{124} as a tracer. A least squares calculation yields $D=0.19\exp(-38\,500/RT)$ cm²/sec. This is consistent with tentative values reported earlier and confirms the sharp disagreement with the data of Seith and Peretti, who obtained $D=5\times10^{-5}\exp(-21\,700/RT)$ cm²/sec.[1] Experiments concerning grain boundary diffusion for Sb^{124} into silver will also be discussed.

* Supported in part by the U. S. Atomic Energy Commission.
[1] Seith and Peretti, Z. Electrochem. **42**, 570 (1936).

Z10. Diffusion of Cadmium in Single Crystals of Silver.* T. TOMIZUKA, L. SLIFKIN, AND D. LAZARUS, *University of Illinois.*—As part of a program to obtain the dependence on atomic number of the diffusion in silver of neighboring elements, diffusion of cadmium 115 in 99.99 percent pure single

crystals of silver was measured. A thin wall beta-counter was employed for the immersion counting of a thin cylindrical layer of solution and the reproducibility thus obtained was satisfactory. Measurements at higher temperatures give a tentative value of 41 kcal/mole for the activation energy. This differs radically from the data of Seith and Peretti.[1] This will be compared with the activation energy of self-diffusion in silver[2] and with that of the diffusion of antimony in silver.[3]

* Supported in part by the U. S. Atomic Energy Commission.
[1] W. Seith and E. Peretti, Z. Elektrochem. **42**, 570 (1936).
[2] Slifkin, Lazarus, and Tomizuka, J. Appl. Phys. **23**, 1032 (1952).
[3] Slifkin, Lazarus, and Tomizuka, J. Appl. Phys. **23**, 1404 (1952).

Z11. The Influence of Impurities on Diffusion in Solids.* ALBERT W. OVERHAUSER, *University of Illinois.*—The elastic distortions introduced into a lattice by impurity atoms will modify the potential barriers over which atoms must jump during the diffusion process. A statistical distribution in barrier heights results which increases the average rate of diffusion by a factor e^{bf}, where f is the atomic fraction of impurity atoms and b is a constant. Diffusion by means of vacancies was assumed. The elastic strains about each impurity were estimated from the degree of misfit of the impurity atom. The change in barrier height at the saddle point due to a given distortion was assumed to be due to the change of the repulsive exchange potential of the nearest neighbors. A repulsive potential of the usual exponential type, fitted to the elastic constants, was used. An increase in the rate of self-diffusion has been observed for small amounts of Cu in Ag by Holloman and Turnbull, for Pb in Ag by Hoffman and Turnbull, for K^+ in NaCl by Etzel, and for interstitial Cu in Cu by the writer. The observed magnitudes for the coefficient b in each of the above cases are about 10, 10^2, $\frac{1}{2}\times10^3$, and 10^4, respectively, and agree with the computed values to a factor of two.

* This work was supported by the U. S. Atomic Energy Commission.

Z12. Activation Entropies for Diffusion Mechanisms.* H. B. HUNTINGTON, G. A. SHIRN, AND E. S. WAJDA, *Rensselaer Polytechnic Institute.*—For all diffusion mechanisms there are associated changes in the entropy associated with the occurrence of the activated complex that affect the diffusion coefficient as $\exp(\Delta S/k)$. An effort has been made to estimate these quantities from a simple atomic model considering only the changes in the vibration spectrum caused by the lattice defect during the diffusion jump. The calculation has been applied to a fcc metal with long range cohesive forces and close-range exponential repulsion between ions. The changes in the atomic vibrations can be considered as arising mainly from the central repulsive forces and their effect on the entropy is calculated from the basis of an Einstein model. These local effects are somewhat offset by the changes in the medium far from the defect where the condition for zero surface pressure affects the solition of the spherical elastic defect. For some defects ΔS is negative contrary to current thinking by some workers. For the particular case of an interstitial defect (using a repulsive force law fitted to the elastic data of copper) ΔS was about $-4.3k$. The negative result arises from the high density at the defect. For a vacancy defect with the same model ΔS is about $+1k$.

* Supported by the U. S. Atomic Energy Commission.

SUPPLEMENTARY PROGRAMME

SP1. A Versatile Radiation Oven.*† RICHARD B. BELSER, *Georgia Institute of Technology.*—The construction of an economical, high temperature, infrared oven consisting of a one-liter beaker, lined with a reflecting material, and a single 250-watt, infrared bulb has been previously described.[1] This oven has been developed further into a more versatile tool. The position of the axes of the beaker and the lamp with reference to a horizontal axis is of little importance in the oven's efficiency. By operation of the oven, with the beaker inverted over the lamp, the placing of samples to be heated is facilitated. The oven may be powered by a photoflood lamp or ultraviolet sun lamp as well. It thus offers intense fields of visible or ultraviolet radiation. By using a lamp with a hole drilled in its face the oven may be operated within a vacuum chamber. The heating efficiency is greater within the vacuum. A temperature of 725°C was reached within the oven with 135 volts across the lamp's filament. By use of this oven as a heating agent, without and within a vacuum, some interesting studies of the "aging" of thin metal films have been made.

* Supported by U. S. Army Signal Corps.
† To be given at the end of Session I if the Chairman rules that time permits.
[1] The Research Engineer, Georgia Institute of Technology, January, 1952, p. 9.

SP2. A Phase Transition in $ND_4D_2AsO_4$.*† B. C. FRAZER, *Brookhaven National Laboratory.*—It was shown by Matthias[1] that, as in the case of KD_2PO_4,[2] $ND_4D_2PO_4$ has a transition temperature about 90° higher than the undeuterated salt (an increase from 148°K to 242°K). The transition temperature for $NH_4H_2AsO_4$ is 216°K, which suggests that deuteration should shift the transition above room temperature. This has been confirmed by dielectric and optical studies. The transition temperature observed was 31°C. Thus the shattering or cracking which has usually interfered with investigations below the transition temperatures of the ammonium salts can be avoided, since $ND_4D_2AsO_4$ crystals can be grown at room temperature directly in the orthorhombic phase. The preferential axis of growth was identified optically and by x-rays as being what becomes the tetragonal C axis in the transition. Measurements were made in the laboratory of Dr. Ray Pepinsky at the Pennsylvania State College.

* Research carried out under the auspices of the U. S. Atomic Energy Commission.
† To be given at the end of Session E if the chairman rules that time permits.
[1] B. T. Matthias, Phys. Rev. **85**, 141 (1952).
[2] W. Bautle, Helv. Phys. Acta **15**, 373 (1942).

Author Index to Papers Presented at the North Carolina Meeting

Alfrey, Turner, Jr.—K1
Akers, Lawrence K. and Ernest A. Jones—S9
Amster, Adolph B. and Quentin Van Winkle—DB3
Anslow, Gladys A. and Irene S. White—X2
Balazs, N. L.—W8
Bal[illegible]ock, Russel, John R. Sites, L. O. Gilpatrick, and Howard E. Carr—X8
Barnett, C. F.—JA12
Barr, E. Scott—N3
Barr, T. A., Jr.—DB6
Beams, J. W.—U1
Beck, C. K.—M1
Becker, W. M. and K. Lark-Horovitz—P2
Belser, Richard B.—I11, SP1
Benedict, T. S. and W. Shockley—C2
Berlincourt, Ted G. and M. C. Steele—GA3
Bergstein, J. and R. D. Birkhoff—JA4
Berkowitz, A. E. and A. D. Franklin—B5
Bird, George R. and Richard C. Mockler—J7
Blewitt, T. H., J. K. Redman, and F. A. Sherrill—T4
Boch, A. L. and E. D. Hudson—JA7
Bloch, Ingram and Yü-Chang Hsieh—W9
Block, M. M., S. Passman, and W. W. Havens, Jr.—DA9
Bowen, Dwain B.—I3
Bowers, W. A.—X6
Bowman, J. C., S. Hays, and R. Smoluchowski—Z1
Boyer, R. F.—L2
Brabant, J. M., L. W. Cochran, and R. S. Caswell—DA5
Bray, Ralph and F. van der Maesen—P9
Breckenridge, R. G., W. R. Hosler, and W. Oshinsky—V3
Brooks, Harvey—V4
Brown, Alexander and F. P. Reding—L7
Brown, Frank B., Jr., and A. V. Masket—DA10
Brown, W. L. and R. C. Fletcher—T7
Bueche, A. M.—DB1
Bunn, C. W.—K4, L3
Burstein, E.—F5
Byatt, William J.—W5
Cabrera, N.—Q3
Callen, H. B.—V3
Campbell, W. H. and J. I. Hopkins—JA10
Carr, H. E.—D5
Chang, Hung-Chi—G9
Cleland, J. W., D. S. Billington, and J. H. Crawford, Jr.—T12
Cobbs, W. J., Jr., S. B. Cole, and R. L. Burton—L4
Cohen, Bernard L.—W11
Collins, F. C.—Q4
Collins, R. J. and H. Y. Fan—P4
Coltman, R. R. and T. H. Blewitt—T3
Conwell, Esther M.—C9
Cooper, C. Dewey—X1
Couling, L. and R. Smoluchowski—Z7
Cox, J. T., P. B. Peyton, Jr., and Walter Gordy—J6
Crawford, George W.—G6
Crawford, J. H., Jr., J. W. Cleland, D. K. Holmes, and J. C. Pigg—Y4
Crittenden, E. C., Jr., and H. Dieckamp—R4
Croft, George T. and Foster C. Nix—E3
Dank, M. and H. B. Callen—O9
Davisson, J. W.—O3
Day, Harold R.—T14
deBretteville, A., Jr.—E7
Debye, Peter P.—C8
deCarvalho, H. G., V. Davis, and W. Tesh—JA13
Dienes, G. J. and D. A. Kleinman—T13
Dixon, C. E. and C. J. Meechan—T10
Dolecek, R. L.—GA4
Domenicali, C. A. and B. A. Boyd—I2
Donahoe, F. J.—E2
Dunlap, W. C., Jr.—C10
Eatherly, W. P.—U2
Eggen, D. T. and M. J. Laubenstein—T11
Erickson, R. A. and L. D. Roberts—GA9
Ehrlich, P. and N. J. DeLollis—GB7
Ewald, A. H.—G11
Ewald, A. W.—Y10
Fan, H. Y.—F3
Fano, U. and L. V. Spencer—W4
Ferry, John D., Lester D. Grandine, Jr., and Edwin R. Fitzgerald—GB3
Ferry, J. D.—GB9
Fillnow, R. H., E. K. Halteman, and G. F. Mechlin—T2
Fisher, John C.—A3, R1
Fitzgerald, Edwin R., Lester D. Grandine, Jr., and John D. Ferry—GB2
Fleeman, Jerome—T8
Fletcher, R. C., W. L. Brown, and S. Machlup—T6
Flory, P. J.—K2
Foner, Simon and Emerson M. Pugh—I4
Forster, J. H., H. Y. Fan, and K. Lark-Horovitz—P1
Franklin, A. D., R. B. Campbell, and J. A. Weinman—B4
Frazer, B. C.—SP2
Frazer, B. C. and Ray Pepinsky—E6
Fusfeld, Herbert I.—R7
Fuson, Nelson, Marie-Louise Josien, and Conrade C. Hinds—S2
Gardner, W. R. and G. C. Danielson—I1
Gebbie, H. A., M. Nisenoff, and H. Y. Fan—P5
Gibbons, J. H. and Henry W. Newson—DA3
Glick, Harvey L. and W. F. Witzig—T1
Goldowski, N.—N7
Good, W. M.—M5
Gordy, W. M.—D1
Graham, Irwin, David Pomeroy, W. C. McGarvey, and John G. Randall—G5
Green, Farno L.—JA6
Gross, E. P.—O4
Guinier, A.—V1
Gursky, Herbert, Barbara Winnemore, and D. A. Cowan—DA4
Gursky, Judith Cassidy and P. K. S. Wang—W1
Harrison, Sol E. and Herbert B. Callen—B3
Hart, Edward W.—R3
Hayes S. and R. Smoluchowski—Z2
Haynes, C. W. and R. Smoluchowski—Z8
Heckman, R. C. and H. Sponer—X3
Heikes, Robert R.—E1
Hemstreet, H. W. and J. M. Reynolds—V1
Henisch, H. K.—F1
Hereford, F. L.—M3
Hill, Robert M. and Walter Gordy—J4
Hobstetter—Q2
Huibregtse, E. J. and L. P. Hunter—C5
Hunter, L. P.—C4
Huntington, H. B., G. A. Shirn, and E. S. Wajda—Z12
Jamison, R. E. and T. H. Blewitt—T5
Jaumot, Frank E., Jr., and Leonard Muldawer—R2
Javan, A., G. Silvey, C. H. Townes, and A. V. Grosse—J8
Jenkins, G. L., L. W. Cochran, H. H. Givin, J. L. Ryan, T. M. Hahn, and B. D. Kern—DA7
Johnson, V. A. and K. Lark-Horovitz—P7
Jones, Royce J.—JA5
Josien, Marie-Louise, Nelson Fuson, and Essie M. Shelton—S3
Kaiser, W., R. J. Collins, and H. Y. Fan—P3
Keck, Paul H. and Wendell Van Horn—Y5
Keesom, P. H. and N. Pearlman—GA1
Keffer, Frederic—B6
Keller, F. L. and A. H. Nielsen—S4
Kerr, Robert J., Sherwood K. Haynes, and George R. Meneely—G3
Kikuchi, Ryoichi—B1
King, J. G. and V. Jaccarino—DA1
Kittel, Charles—H6, V2
Kmetko, E. A.—Y6
Knight, W. D.—B10
Knipe, R. H.—X5
Koehler, J. S.—R5
Lafferty, D. L., J. A. Biggerstaff, B. D. Kern, and T. M. Hahn—JA3
Lamphere, R. W.—DA8
Landauer, Rolf and John Swanson—C3
Lax, M. and E. Burstein—C11
Leaderman, Herbert—GB1
Lehovec, Kurt—O5
Leivo, W. J.—Z4
Letaw, Harry, Jr., and Armin H. Gropp—S5
Lewis, H. W.—GA5
Loebner, E. E.—Y2
Loh, H. Y. and Peter Cheo—I10
London, Fritz—D3
Lord, Norman W.—I8
Lovell, Robert James—S8
Lummis, Frances L. and Richard L. Petritz—P11
Machlup, Stefan—W6
Mador, I. L., J. J. Markham, and R. T. Platt, Jr.—H4
Mandelkern, Leo—K3
Mandeville, C. E. and H. O. Albrecht—H9
Mapother, D. E. and J. F. Cochran—GA7
Marcus, Paul M.—GA6
Markham, J. J., R. T. Platt, and I. L. Mador—H3
Marshall, Henry P. and Ernest Grunwald—G8
Martin, Donald C.—N8
Martin, J. A.—JA8
Maxwell, L. R., S. J. Pickart, and R. W. Hall—B7
McCay, M. S. and J. H. Coulliette—G2
McDonald, E. W. and D. C. Ralph—JA2
McGuire, T. R.—B8
Meckler, Alvin—X4
Melnick, Donald A. and Leo J. Neuringer—O11
Melvin, M. Avramy—W12

Mendoza, E.—U3
Miller, P. H.—F4
Mitchell, F. H.—N4
Mize, J. P. and D. J. Zaffarano—DA6
Mizushima Masataka—J3
Mockler, Richard C. and Walter Gordy—J1
Morris, L. W. and Hung-Chi Chang—G10
Morrison, Ray M. and M. S. McCay—N9
Mrozowski, S., B. D. McMichael, and E. A. Kmetko—S1
Newell, Gordon F.—O1
Newson, H. W. and E. Merzbacher—W10
Nichols, J. B.—L1
Nowick, A. S. and A. E. Roswell—I9
Osgood, T. H.—N1
Overhauser, Albert W.—Z11
Padden, F. J., H. Markowitz, and T. W. DeWitt—GB5
Palmatier, E. D.—DA11
Parker, F. W., A. H. Nielsen, and W. H. Fletcher—S7
Pearlstein, E. A.—Z3
Pepinsky, R. and P. F. Eiland—O8
Petritz, Richard L.—P10
Pinnick, H. T.—O7
Platt, R. T., Jr., I. L. Mador, and J. J. Markham—H5
Pomeroy, David—N2
Porter, P. T. and J. I. Hopkins—DA2
Portis, A. M. and A. F. Kip—B11
Pratt, G. W., Jr.—E4
Prince, M. B.—C6
Pringsheim, Peter—H10
Protzman, T. F., J. J. Gouza, and W. F. Bartoe—DB5
Read, W. T.—A2
Reboul, T. Todd—O10
Redfield, Alfred G.—Y9
Rice, O. K.—D4
Rider, John A.—G7
Ritland, H. N.—O6
Roberts, Donald E. and Leo Mandelkern—L6
Rodeback, G. W. and W. P. Eatherly—T9
Rosenstock, Herbert B.—R9
Rostoker, Norman and Walter Kohn—R11
Ruark, Arthur E.—N5
Salkovitz, E. I. and A. I. Schindler—R12
Sanville, W. W., Foster C. Nix, and Frank E. Jaumot, Jr.—I5
Sartain, Carl C.—N6
Schindler, A. I. and E. I. Salkovitz—R13
Sclar, N., E. Burstein, W. J. Turner, and J. W. Davisson—GA2
Seitz, F.—H1
Shaw, T. M. and J. J. Windle—GB8
Shaw, Wm. C., D. E. Hudson, and G. C. Danielson—C7
Shelton, R. D., A. H. Nielsen, and W. H. Fletcher—S6
Shirane, Gen and Ray Pepinsky—E5
Shockley, William—F2, O2
Shreckengost, R. C., D. C. Swanson, and J. W. Flowers—JA11
Simon, Albert—M4
Sites, John R. and Bernard L. Strehler—X7
Slater, J. C., H. Statz, and G. F. Koster—B2
Smith, Thor L.—GB6
Smith, William A. and Allen B. Scott—H7
Smoluchowski, R.—A1, Z6
Sonder, E., L. Slifkin, and D. Lazarus—Z9
Spencer, L. V. and C. H. Blanchard—W3
Sutcliffe, Charles H. and Frank E. Jaumot, Jr.—I6
Swanson, D. C.—JA1
Tanenbaum, M. and G. L. Pearson—V8
Taylor, G. R. and S. R. Darin—DB4
Teegarden, K. and R. J. Maurer—H8
Tipton, Isabel H., W. D. Foland, Franklin C. Bobb, and W. C. McCorkle—G4
Tomizuka, T., L. Slifkin, and D. Lazarus—Z10
Townes, C. H.—D2
Trambarulo, R., S. N. Ghosh, C. A. Burrus, Jr., and W. Gordy—J5
Trice, James B.—JA9
Turnbull, David—Q1
Vaughan, W. H., W. J. Leivo, and R. Smoluchowski—Z5
Venkateswarlu, Putcha, Richard C. Mockler, and Walter Gordy—J2
Vineyard, George H.—W2
Vogel, F. L., W. G. Pfann, H. E. Corey, and E. E. Thomas—P6
Wales, M.—DB2
Wangsness, Roald K.—B9
Wannier, Gregory H.—C1
Warren, B. E., B. L. Averbach, and E. Warekois—R6
Weinberg, A. M.—M2
Weinreich, O. A. and W. E. Danforth—P8
Wert, C. A.—I7
Westervelt, D. R.—H2
Widom, B. and S. H. Bauer—W7
Wildhack, W. A. and R. O. Smith—G1
Willardson, R. K., A. C. Beer, and A. E. Middleton—Y7
Wolff, P. A.—R10
Wood, Lawrence A.—L5
Zapas, L. J., S. L. Shufler, and T. W. DeWitt—GB4
Zernow, L. and J. Simon—R8
Zilsel, P. R.—GA8
Zimm, B. H.—Q5

CONTENTS

THE PHYSICAL REVIEW SECOND SERIES, VOLUME 91, NO. 1 JULY 1, 1953

Simultaneous Measurement of Ionization and Attachment Coefficients . . . . . Melvin A. Harrison and Ronald Geballe 1

Conductivity of Thin Films in a Longitudinal Magnetic Field . . . . . Ernst Kunsigsberg 8

Angular Aberrations in Sector Shaped Electromagnetic Lenses for Focusing Beams of Charged Particles . . . . . Edgar G. Johnson and Alfred O. Nier 10

Specific Heat Discontinuity in Antiferromagnets and Ferrites . . Louis N. Howard and J. Samuel Smart 17

Hall Effects of the Cobalt Nickel Alloys and of Armco Iron . . . . Simon Foner and Emerson M. Pugh 20

Some Magnetic Properties of Gadolinium Metal . . . . . J. F. Elliott, S. Legvold, and F. H. Spedding 26

Matrix Elements of Spin-Spin Interaction . . . . . Frederick R. Innes 31

Correlation Energy in the Ground State of He I . Louis C. Green, Marjorie M. Mulder, and Paul C. Milner 35

Mass Surfaces . . . . . Alex E. S. Green and Nicholas A. Engler 40

Discontinuities in the Nuclear Mass Surface . . . . . Alex E. S. Green and David F. Edwards 46

Parameters for the Slow Neutron Resonance in Rhodium . . . . . V. L. Sailor 53

Photoprotons from Mo^{100} and Mo^{92} . . . . . W. A. Butler and G. M. Almy 58

Total Neutron Cross Sections of Chlorine and Carbon . R. M. Kiehn, Clark Goodman, and K. F. Hansen 66

Disintegration of Sr^{85} and Y^{85m} . . . . . D. P. Ames, M. E. Bunker, L. M. Langer, and B. M. Sorenson 68

Gallium-64 . . . . . Bernard L. Cohen 74

Nuclear Levels in Ce^{142} . . . . . J. M. Cork, J. M. LeBlanc, W. H. Nester, and M. K. Brice 76

Decay of As^{170m} . . . . . J. W. Mihelich and A. de-Shalit 78

Nuclear Magnetic Resonance in Thallium Compounds . . . . . H. S. Gutowsky and B. R. McGarvey 81

Calculation of the Half-Widths of One-Body Resonances . . . . . John L. Johnson and J. L. McHale 87

Interaction of 14-Mev Neutrons with Protons and Deuterons . J. C. Allred, A. H. Armstrong, and L. Rosen 90

Elastic Scattering of Protons and Neutrons by Deuterons . . . . . R. S. Christian and J. L. Gammel 100

Matrix Elements of β-Decay in jj Coupling . . . . . Igal Talmi 122

Thermal Neutron-Proton Capture . . . S. P. Harris, C. O. Muehlhause, D. Rose, H. P. Schroeder, G. E. Thomas, Jr., and S. Wexler 125

Unusual $\pi-\mu$ Decays in Photographic Emulsions . . . . . W. F. Fry 130

Diffusion Cloud-Chamber Study of Pion Interactions in Hydrogen and Helium . . . . . E. C. Fowler, W. B. Fowler, R. P. Shutt, A. M. Thorndike, and W. L. Whittemore 135

Nuclear Photoelectron Production . . . . . Israel Reif 150

Angular Distribution of Pions Scattered by Hydrogen . . . . . H. L. Anderson, E. Fermi, R. Martin, and D. E. Nagle 155

Consequences of Charge Independence for Nuclear Reactions Involving Photons . . . . . Murray Gell-Mann and Valentine L. Telegdi 169

WKB-Type Approximation to the Schrödinger Equation . . . . . S. C. Miller, Jr., and R. H. Good, Jr. 174

Generalized Statistical Mechanics and the Onsager Relations . Peter G. Bergmann and Alice C. Thomson 180

Exchange Scattering in a Three-Body Problem . . . . . Harry E. Moses 185

(continued on cover three)

LANCASTER PRESS, INC., LANCASTER, PA.